Advanced Clinical Pharmacy – Research, Development and Practical Applications 2

Dimitrios Lamprou *Editor*

Nano- and Microfabrication Techniques in Drug Delivery

Recent Developments and Future Prospects

Springer

Advanced Clinical Pharmacy – Research, Development and Practical Applications

Volume 2

Series Editor

Rhiannon Braund, University of Otago, Dunedin, New Zealand

This exciting new book series incorporates new areas of research and development with practical approaches and is designed to aid pharmacists up-skill in various new and traditional areas of practice that are applicable, but not limited to, hospital-based care, as well as incorporating the more advanced aspects of community-based care.

Advanced Clinical Pharmacy aims to publish titles that help intermediate level pharmacists see what further areas of practice need to be incorporated in to their skill set, as well as provide guidance on areas of expertise that they may wish to focus on for more advanced practice in the future. It also provides more advanced pharmacists with a tool for ensuring they are current and up-to-date in a wider range of topics, as well as in their chosen area of expertise. Additionally, it may provide newly registered pharmacists with guidance on what areas of practice they may aspire to work in.

The series will provide more comprehensive information that is also more focused than is typically found in traditional clinical pharmacy text books (which cover all topics in a single volume and typically cover a topic in one or two chapters). It will allow pharmacists to select topics that are more applicable to their individual areas of work, as well as areas that in the future they may wish to work in. Each volume will provide a summary of the main theory that underpins the topic, but will then move on to advanced information including areas of current research, clinical applications, case studies, practical tips, and common pitfalls. It will also look at future directions and also, where applicable, hints for the independent practitioner – in preparation for the advancement of pharmacists as more independent health professionals.

Titles in the series can be monographs (up to 3 authors) or edited volumes, ranging from 200-500 pages per volume. Each title will be published as ebook as well as in hard bound print format.

This series will be of interest to a wide readership, ranging from intermediate level pharmacists, with experience of 3 to 5 years post-registration (for a bachelor's degree) or experience of 2 to 3 years (for a PharmD), through to more advanced/ senior clinical pharmacists. It is hoped that the information would also be of interest to pharmacists working in community-based care, who wish to increase their knowledge and skill, as well as hospital-based pharmacists.

The series may also be useful as educational tools for the teaching of pharmacists involved in both formal post-graduate education as well as more ad hoc workplace based programmes – however, different titles in the series may be more suitable for this than others.

Unique features

· Offers readers the ability to select the topics that are of interest to them and focus on their area of work/expertise

· Provides the salient points of the background theory but then quickly moves on to more advanced knowledge that contains both current research as well as practical information in the context of cases (but not limited to case scenarios)

Dimitrios Lamprou
Editor

Nano- and Microfabrication Techniques in Drug Delivery

Recent Developments and Future Prospects

Springer

Editor
Dimitrios Lamprou
School of Pharmacy
Queen's University Belfast
Belfast, UK

ISSN 2524-5325 ISSN 2524-5333 (electronic)
Advanced Clinical Pharmacy – Research, Development and Practical Applications
ISBN 978-3-031-26907-3 ISBN 978-3-031-26908-0 (eBook)
https://doi.org/10.1007/978-3-031-26908-0

This Springer imprint is published by the registered company Springer Nature Switzerland AG
The registered company address is: Gewerbestrasse 11, 6330 Cham, Switzerland

Preface

New drug molecules (e.g. peptides and proteins) have been developed in recent years as a result of the advances in drug design and technologies. The inability to deliver these molecules at well-defined dosing regimens continues to be a major obstacle. As a result, novel materials and manufacturing processes are being developed to address the complications in the development and distribution of biopharmaceuticals and pharmaceuticals. Nano- and microfabrication techniques are aiming to create systems that can be used for personalized medicine, be tailored to the needs of patients, and teach traditional medications new tricks. Researchers can now create objects with micrometric resolutions, thanks to new technologies and their increasing resolution.

The book is organized in a logical sequence, starting with information on materials and current field, including restrictions on producing various pharmaceutical products. Polymers, and especially electroactive and conducting polymers, substances combining plasticity with the conductivity associated with metals, can be used for a variety of drug delivery and tissue engineering applications. These polymers can be used for applications, such as the manufacturing of films, for the preparation of components of composite or nanocomposite materials that are used in many of the technologies discussed in this book and, of course, in the manufacturing of nanoparticles and hydrogels. From there, the book moves on to the classification of advanced technologies, using recent examples and future perspectives on a variety of conventional and novel nano- and microfabrication techniques.

The first few chapters of the book cover the electrohydrodynamic processes, such as solution and melt electrospinning, for the manufacturing of degraded scaffolds that can be used for oral or transdermal administration. These technologies offer a method for the preparation of fibers with fast dissolving administration, which offers more obvious therapeutic advantages, and scaffolds that can be used for different applications in the biomedical and pharmaceutical fields, including in tissue regeneration and drug delivery. The fundamentals of spray drying, a continuous manufacturing process, are also discussed in the book, by providing a critical

presentation of different cases, such as drug, polymer, and carbohydrate optimizations that provided precisely timed or delayed targeted delivery.

The second part of the book focuses on additive manufacturing (3D printing and 4D Printing) technologies, a promising set of technologies for the manufacturing of drug delivery systems and medical implants. 3D printing has been developed for the manufacturing of dosage forms and drug delivery systems with excellent applications in personalized medicine. A major advantage of the additive manufacturing technologies is the ability to manufacture systems of various shapes and sizes and the ability to use Food and Drug Administration (FDA)-approved polymers for such applications. The book consists of different chapters that cover the main techniques used in the pharmaceutical field, such as Vat photopolymerization (e.g. stereolithography and digital light processing), semi-solid extrusion for the development of dosage forms for special patient groups, and binder-jetting powder bed printing. 3D printing can also use data obtained from nuclear magnetic resonance imaging or computed tomography in order to prepare personalized medications, including for cancer treatment, for the delivery of molecules with precise control. 3D printing structures have shown promise for biomedical applications but have lagged behind due to their inability to accurately mimic dynamic human tissue, and here is where 4D printing a breakthrough method that integrates "time" into the traditional concept of 3D printing to address the dynamic healing and regeneration of human tissues has been used and discussed in the book.

However, we cannot miss the discussion of traditional methods such as lithography and micro-moulding techniques. The application of lithography, adapted from the semiconductor industry to pharmaceuticals, has solved many issues that will be discussed in the book, which enabled innovative drug delivery systems and devices for advanced disease treatment and diagnosis. On the other hand, micro-moulding has been used in the plastic and food industry for a long time; however, it is a relatively new technique for the pharmaceutical industry; therefore, the future of the method in this field has also been discussed.

There are many factors that ensure that nanoparticles are superior to conventional methods of treatment. These include the ability to bypass biological barriers, different pharmacokinetic profiles, and precise delivery to target tissues. Therefore, different technologies such as microfluidics for the manufacturing of nanoparticles, nanofludics for drug screening, and supercritical fluids for encapsulation have been discussed together with the clinical trial area.

The reader is provided with a comprehensive understanding of this quickly expanding area of new technologies, through a focus on different examples and materials used to prepare these systems. Applied topics like R&D and production of healthcare products that have been significantly impacted by new scientific and technological advancements, which emphasize the need to update the regulatory framework in order to remove current regulatory barriers for high-innovation products and to guarantee adequate quality standards capable of protecting public health, have also been covered.

We hope that the chapters covered in this book will be helpful and provide new directions in your research.

Belfast, UK Dimitrios Lamprou

About the Book

Description: New materials and manufacturing techniques are evolving with the potential to address the challenges associated with the manufacture of medicinal products that will teach new tricks to old drugs. Nano- and microfabrication techniques include manufacturing methods such as additive manufacturing, lithography, micro-moulding, spray drying, and lab-on-a-chip, among many others. The increasing resolution of new techniques allows researchers to produce objects with micrometric resolutions. The book follows a consecutive order, beginning with a background in the current field and limitations in the manufacturing of different pharmaceutical products, moving on to the classification of each method by providing recent examples, and future prospective on a variety of traditional and new nano- and microfabrication techniques. The book focuses on the materials used to prepare these systems and their biocompatibility, including applied topics such as clinical applications and regulatory aspects, offering the reader a holistic view of this rapidly growing field.

Key Features

- Brings together technical, clinical, regulatory, and industrial perspectives for a complete overview of nano/microfabrication techniques for the manufacturing of pharmaceutical systems.
- Reviews the recent advances in the area, provides future prospective, and includes the potential clinical applications of these technologies.
- Appeals to a broad readership, including materials scientists, pharmaceutical and chemical engineers, clinicians, and regulatory experts.

Readership: Researchers in industry and academia working on nano/microfabrication techniques, across a broad selection of fields including pharmaceuticals, chemical engineering, and materials science. Advanced students in these areas will also find the proposed book very useful for their studies due to the increasing importance of the covered technologies for a variety of applications. Clinicians and regulatory experts will also find this book very interesting.

Contents

About the Editor

Dimitrios Lamprou (Ph.D., MBA) is Professor (Chair) of Biofabrication and Advanced Manufacturing at Queen's University Belfast. Prof Lamprou's lab is applying nano- and microfabrication techniques in the manufacturing of drug delivery systems, medical devices, and implants. He has trained in multidisciplinary areas and worked in projects across disciplines and in first-class laboratories in a number of countries. To date, he has over 150 peer-reviewed publications in leading international journals and over 350 conference abstracts and has over 150 Oral Talks in the area of nano/microfabrication.

Chapter 1
Conducting Polymers as Drug Release Systems

James R. Smith

Abstract Conducting polymers, also known as electroactive polymers and intrinsically conducting polymers (ICPs), are materials that combine the conductivity associated with metals with the processability of plastics. Examples include polypyrrole, polythiophene, polyaniline and poly(3,4-ethylenedioxythiophene). This chapter introduces the field of ICPs and reviews examples from recent literature concerning their use in drug delivery systems, which generally fall into five main categories, where the ICP is a simple film (typically deposited electrochemically); part of a composite material; included in nanocomposite materials; in the form of nanoparticles; and in the form of a hydrogel/conducting hydrogel. The switchable nature of ICPs, while providing conductivity and biocompatibility, puts these materials in a unique position in the field of drug delivery. The review period is from 2017 to the present (early–2022).

Keywords Conducting polymers · Polypyrrole · Polythiophene · Polyaniline · PEDOT · Drug delivery

Abbreviations

AISI	American Iron and Steel Institute
APS	Ammonium persulfate
BCNU	*N*,*N*′-bis(2-chloroethyl)-*N*-nitrosourea (carmustine)
cRGD	Arg-Gly-Asp peptide ligand
CPH	Conducting polymer hydrogel
CV	Cyclic voltammetry
DOX	Doxorubicin
DS	Dodecyl sulphate

J. R. Smith (✉)
School of Pharmacy and Biomedical Sciences, University of Portsmouth, Portsmouth, UK
e-mail: james.smith@port.ac.uk

D. Lamprou (ed.), *Nano- and Microfabrication Techniques in Drug Delivery*,
Advanced Clinical Pharmacy – Research, Development and Practical Applications 2,
https://doi.org/10.1007/978-3-031-26908-0_1

FU	Fucoidan
Glu	Glutamate
GM	Gentamicin
HeLa	Human cervix epithelioid carcinoma
HER2/neu	Human epidermal growth factor receptor 2
HPANI	Hollow mesoporous polyaniline
ICPs	Intrinsically conducting polymers
LD	Levodopa
Lu	Leucovorin
MAPLE	Matrix-assisted pulsed laser evaporation
NDs	Nanodiamonds
NIR	Near-infrared radiation
NIR-PTT	Near-infrared radiation photothermal therapy
NPs	Nanoparticles
NPX	Naproxen, sodium salt
pTS-Na	Sodium *p*-toluenesulfonate
PA	Polyacetylene
PANI	Polyaniline
PC	Pectin
PDA	Polydopamine
PEDOT	Poly(3,4-ethylenedioxythiophene)
PEG	Polyethylene glycol
PNIPAm	Poly(*N*-isopropylacrylamide)
PPy	Polypyrrole
PTh	Polythiophene
PTT	Photothermal therapy
PVA	Polyvinyl alcohol
RPM	Rapamycin
SCE	Saturated calomel electrode
SIM	Simvastatin
Tc	Tetracycline, hydrochloride salt
TERM	Thermosensitive electro-responsive mucogel

1.1 Introduction

Conducting polymers are an exciting class of electronic materials since they combine conductivity associated with metals with the processability, corrosion resistance and lightweight properties of polymers (Kaner and MacDiarmid 1988). The term intrinsically conducting polymers (ICPs), also known as electroactive polymers, are the main subclass of conducting polymers (Ouyang 2021). ICPs are distinct from other types of conducting polymers in that they conduct electricity in their own right and are not, for example, conventional polymers containing carbon black or other conducting additives (Costa et al. 2011).

ICPs are finding applications for many diverse fields, which have received recent reviews: these include battery materials (Xiang et al. 2021), electromagnetic shielding (Maruthi et al. 2021), electrochromic displays (Mortimer et al. 2006), molecular electronics (Xu et al. 2021), chemical sensors (Liu et al. 2022), biosensors (Zamani et al. 2019), biomaterial scaffolds (Talikowska et al. 2019) and drug delivery (Olvera and Monaghan 2021).

The purpose of this chapter is to provide a brief introduction to ICPs and to review their recent applications in the field of drug delivery. The review covers the period from 2017 to 2022.

1.1.1 Intrinsically Conducting Polymers

Interest in ICPs began in the 1970s when polyacetylene (PA) received both theoretical and experimental attention (Chiang et al. 1977).

1.1.1.1 Polyacetylene

Structurally, PA is the simplest ICP, consisting of a backbone of alternating carbon-to-carbon single and double bonds (Fig. 1.1) (Etemad et al. 1982). This conjugated system of electrons is the basis of the observed conductivity. However, it was shown that the conductivity of the pristine polymer, a semiconductor, could be improved by over 15 orders of magnitude with oxidising agents, such as iodine (10^5 S cm^{-1}; Naarmann and Theophilou 1987).

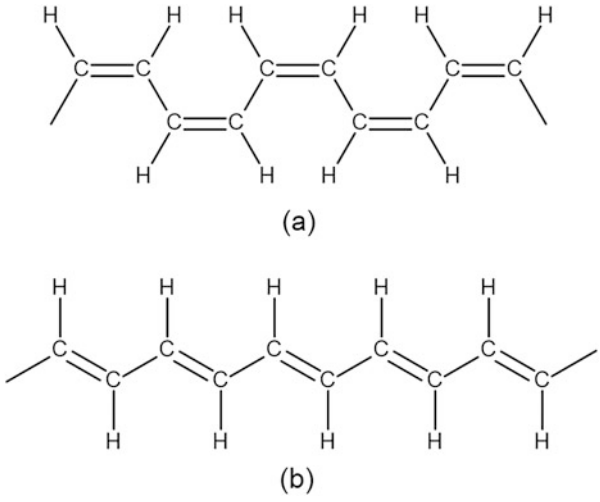

Fig. 1.1 Idealised structures of *(Z)*- (**a**) and *(E)*-polyacetylene (**b**)

The ‘Shirakawa’ type of PA, synthesised via the Ziegler-Natta polymerisation of acetylene (Shirakawa and Ikeda 1971; Ito et al. 1974), is formed as two isomers, *(E)* and *(Z)*, the more conducting and thermally stable of which is the *(E)*-form. The ratio of *(E)* and *(Z)* isomers depend on the reaction temperature, solvent and catalyst type. Varying the catalyst concentration enables PA to be formed as a powder, thin film or gel (Seeger 1982).

The Naarmann process is a modified Shirakawa method used to make PA, leading to vastly improved environmental stability and higher conductivity (Naarmann and Theophilou 1987). For example, PA prepared from the Shirakawa method and exposed to the air results in formation of carbonyl, hydroxyl and epoxide groups, which also disrupt the conjugated π-electron system, required for high conductivity.

A noticeable process to improve the intractability problems of PA has been a method developed at the University of Durham (Bott et al. 1986): ‘Durham polyacetylene’ applies a stress to a precursor polymer during heat treatment to orient polymer chains. When chemically doped, using bromine, iodine or arsenic pentafluoride, similar conductivities to those of Shirakawa PA were produced.

1.1.1.2 Polyheterocycles as ICPs

PA was the starting point for the development of a number of other ICPs. The discovery that free-standing films of polypyrrole (PPy) could be obtained from the electropolymerisation of pyrrole was a significant development (Diaz et al. 1981). Subsequently, intensive research began in the synthesis of polyheterocyclic and polyaromatic ICPs (Waltman and Bargon 1986). These have included polythiophene (PTh) (Waltman et al. 1983); polyfuran (Tourillon and Garnier 1982); polyaniline (PANI) (Genies and Tsintavis 1985); polyazulene (Diaz et al. 1982); polyindole (Tourillon and Garnier 1982); poly(para-phenylene) (Satoh et al. 1985), as well as many substituted, multi-ring and polynuclear aromatic hydrocarbon systems; and poly(3,4-ethylenedioxythiophene) (PEDOT) (Sun et al. 2015), a polymer produced from a thiophene derivative, which has received much noticeable attention (Fig. 1.2).

All conducting polymers have a conjugated backbone (alternating single and double bonds) that is essential for conductivity and electroactivity; these aspects are outlined in the next section. A multitude of derivatised ICPs have been reported, where, for example, substituents have been added to the three-position of the thiophene ring, which affect the properties of these materials (Roncali 1992; Smith et al. 1994).

1.1.2 Mechanisms of Conductivity

Although ICPs require a conjugated backbone, this is insufficient alone for conductivity. These polymers need to be ‘doped’, which is the addition or removal of electrons (reduction and oxidation, respectively) from the chain to form charge

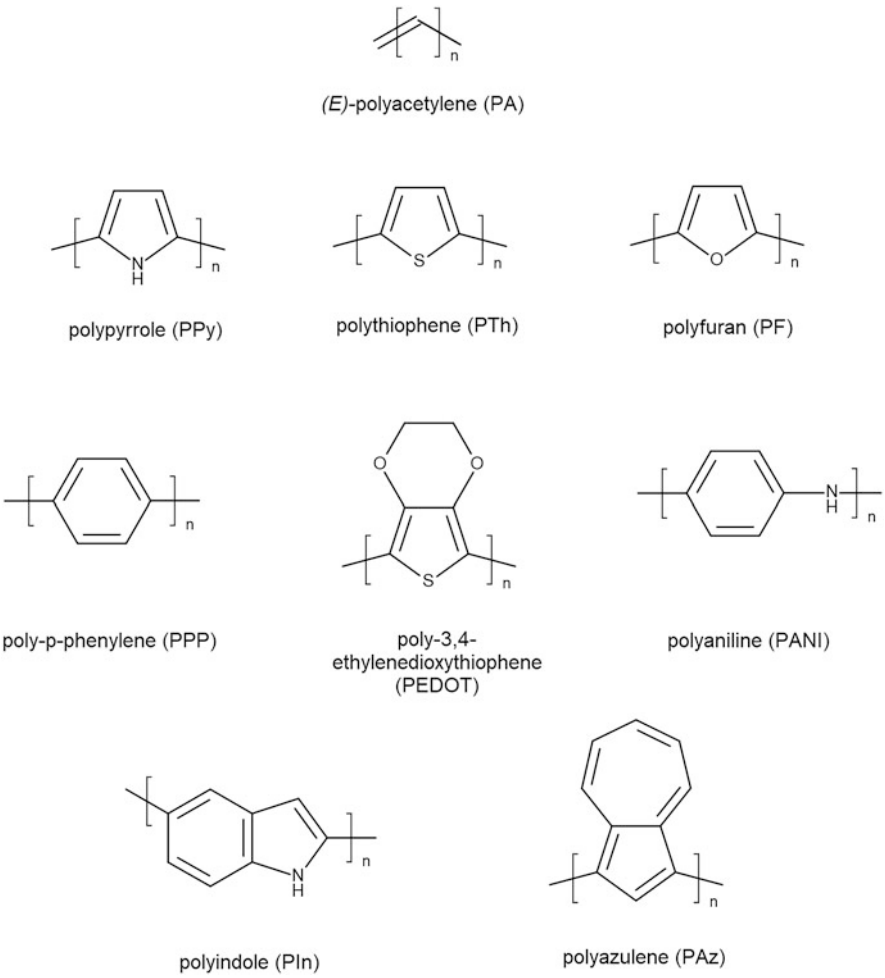

Fig. 1.2 Names and idealised structures of the most widely used ICPs

defects. For example, the energy gap (the band gap) between the highest occupied molecular orbital and lowest unoccupied molecular orbital in undoped (neutral) PPy is 3.16 eV but can be decreased to 1.4 eV upon oxidation to become a semiconductor (Namsheer and Rout 2021). When neutral PPy is oxidised, polaron and bipolaron charge carriers are formed; these are equivalent to radical cation and dication species (Fig. 1.3). In PPy, the polaron and bipolaron charge carriers are spread over about four monomer units (Bredas and Street 1985). An anion (A^-) is incorporated into the polymer to neutralise the positive charge on the backbone.

Conductivity is achieved through charge transfer along the polymer chain and also between chains and through different conjugated segments along the same chain by ‘electron hoping’. Conductivity is also influenced on a larger scale by

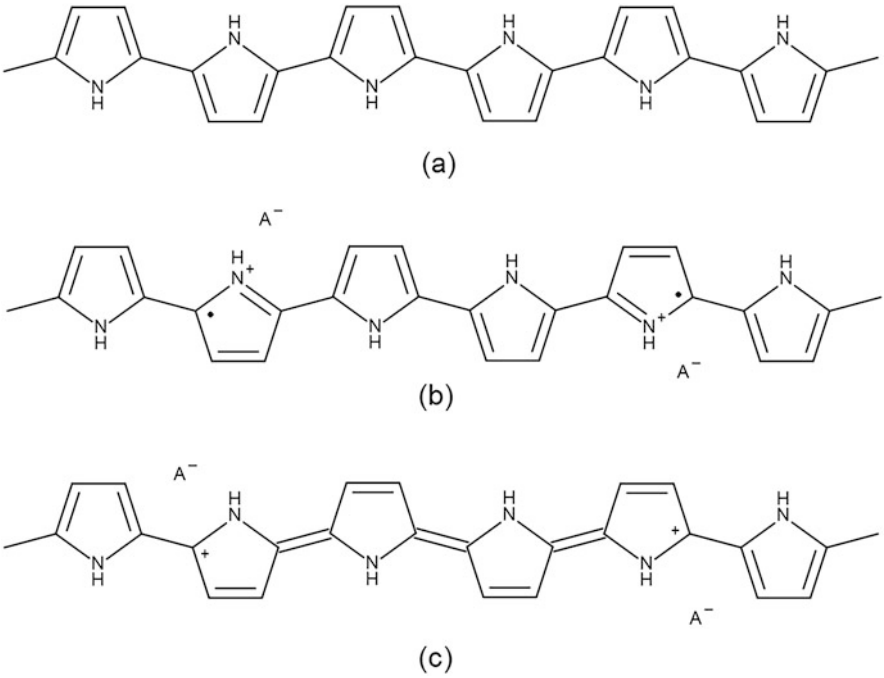

Fig. 1.3 Neutral (**a**) and doped PPy showing polaron (**b**, radical cation) and bipolaron (**c**, dication) charge carriers

morphological factors such as grain boundaries where electron transfer needs to take place (Qian and Qiu 1987).

1.1.3 Synthesis of ICPs

There are two main routes to synthesising ICPs: chemical and electrochemical, and these are next considered.

1.1.3.1 Chemical Polymerisation

ICPs can often be formed by oxidising the monomer chemically. For example, pyrrole can be polymerised in water using ferric chloride (Ayad 1994) or ammonium persulfate (APS) (Ferrero et al. 2006) as the oxidant. The first step in the mechanism is thought to be the formation of a monomeric radical cation which then either couples to neighbouring monomeric radical cations or a neutral monomer to form a dimer (Fig. 1.4); subsequent coupling steps involve oxidation of the dimer and

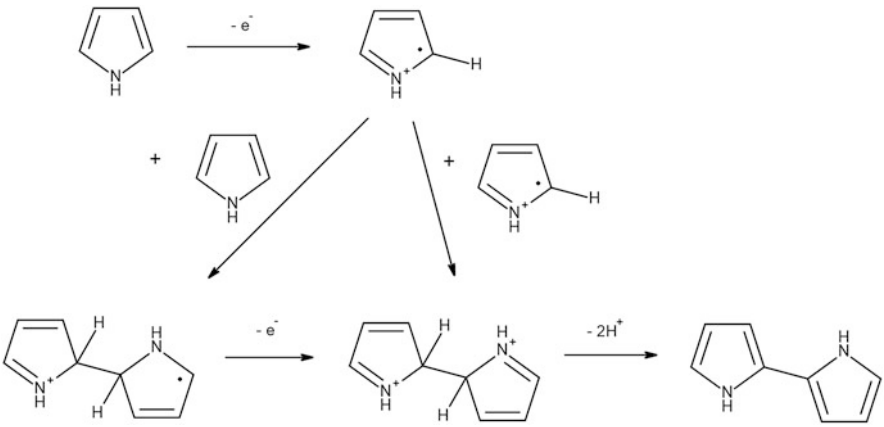

Fig. 1.4 Mechanism for the initial stages of the polymerisation of pyrrole to produce the dimer (2,2′-bipyrrole)

higher oligomers to form radical cations that too react with similarly charged or neutral oligomers (Tan and Ghandi 2013). Couplings via the three-position of the pyrrole/oligopyrrole ring can also occur, to a lesser extent initially during growth, although such couplings produce breaks in the conjugation length and hence lower conductivity (Smith et al. 1995a).

A number of ICP copolymers have also been produced, which have improved mechanical properties, solubility and processability (Jadoun et al. 2021).

1.1.3.2 Electrochemical Polymerisation

Electrochemical methods provide a convenient method for depositing ICP films in situ on electrode (often metallic) surfaces and hence eliminate the processability problems often encountered with chemically synthesised ICPs. The mechanism follows the same patterns as that described for chemically synthesised polymers. Electrooxidation reactions often take place in three-compartment electrochemical cells, either in aqueous or organic solvents, with a supporting electrolyte, the anion of which becomes incorporated into the film as the dopant. For example, PPy and PTh can be deposited on a Pt electrode by cycling the potential above the oxidation potential of the monomer in tetrabutylammonium tetrafluoroborate ($TBABF_4$) in acetonitrile (Roncali 1992), where the counterion (A^-) would be the BF_4^- ion. Electrochemical routes include cyclic voltammetry (CV, sweeping the potential between two potential limits) (Smith et al. 1995b), potentiometry (stepping and holding the potential above the monomer oxidation potential) and galvanostatic methods (constant current). Oligomers are oxidised at less anodic potentials than their corresponding monomers, and so polymers are produced at the same time as the monomer is oxidised to the radical cation. With CV, the polymers can be cycled

between oxidised (doped, conducting) and reduced (neutral, dedoped, insulating) states due to diffusion of the counterion into and out of the film to maintain electroneutrality (Genies et al. 1983). The nature of the counterion can influence the conductivity and properties of the ICP film (Hotta et al. 1983). Some ICPs, for example PA, can only be made via a chemical polymerisation route.

1.2 Methodology

The use of ICPs in the drug delivery literature part of this chapter was performed using Google Scholar, PubMed and ScienceDirect. Search terms used were *x* AND 'drug release', where *x* = polypyrrole, polyaniline, polythiophene and PEDOT. Inclusion criteria were publication in English language, research articles and full publication access; exclusion criteria were abstracts only; reviews; non-drug delivery applications of ICPs, such as sensors and biosensors; and non-subscribed journals at University of Portsmouth. A few papers were included where ICPs were being used or investigated as biomaterials, but where drug delivery was not a feature. This was to extend the discussion of the wide variety of uses of ICPs in biomedicine. The review presented in this chapter is not intended to be a full and exhaustive systematic review. The search period was limited to 2017 to 2022.

1.3 Drug Delivery Applications of ICPs

This section details recent studies where ICPs have been used in drug delivery. The ICPs PPy, PTh, PANI and PEDOT are considered in sequence, where appropriate.

1.3.1 ICP Films

The release of salicylate has been measured from electropolymerised PPy films, grown on AISI 316 L stainless steel under potentiostatic conditions (+0.8 V vs. Ag/AgCl), incorporating this drug (González et al. 2019). The usual globular topography of PPy changed to hollow rectangular microtubes when higher concentrations of sodium salicylate (0.5 M rather than 0.1 M) were used, increasing surface area and drug loading. The electrode could be reloaded (using CV) and was found be an effective against inhibiting albumin, indicative of anti-inflammatory action.

Ryan and Breslin reported the incorporation of dexamethasone during electropolymerisation at low potentials to produce PPy films (Ryan and Breslin 2018). Films were deposited on a PPy pre-layer, and controlled release of dexamethasone&spi2;(200 μg/cm^2 over 60 min) was observed on reduction of the

film (−0.9 V vs. SCE). This process took place with an influx of Na^+ ions to maintain electroneutrality, although this caused swelling and damage to the PPy film potentially limiting the use of this delivery system.

The same authors also realised that incorporating water insoluble drugs into PPy via electropolymerisation from aqueous solutions is not straightforward (Ryan and Breslin 2019). Sulindac and indomethacin (sodium salts of both), drugs with poor water solubilities, were incorporated into PPy on Pt from ethanol at 36 or 40 °C, respectively, in a solution of the monomer and tetrabutylammonium perchlorate under potentiostatic conditions (+0.9 V vs. Ag/Ag^+). Drug release studies were carried out in NaCl (0.1 M). Release at −0.10 V vs. SCE, which also included perchlorate ions, prevents the ingress of Na^+ ions from the release medium.

The drug anion saccharinate, a nonsteroidal anti-inflammatory, has been incorporated and released from a PANI film on a glassy carbon electrode (Shen et al. 2020). Electropolymerisation of anilinium saccharinate, which served as both the monomer and supporting electrolyte, in acetonitrile produced a self-doped polymer with a high degree of drug loading (33.5%). Release was under diffusion control with no applied potential but under anomalous transport mode under electrical stimulus.

PEDOT films loaded with naproxen (the Na salt, NPX) have been produced by electropolymerisation of the monomer (10 mM) in aqueous $LiClO_4$ or sodium dodecyl sulphate (DS, 0.1 M) on an Au electrochemical quartz crystal microbalance (Krukiewicz et al. 2018); cycling the potential between −0.5 and + 1.2 V vs. Ag/AgCl (25 cycles, 0.1 V/s) was used, followed by dedoping (holding the potential at −0.5 V vs. Ag/AgCl for 600 s) and drug loading during dedoping (+0.5 V vs. Ag/AgCl for 600 s in 0.1 M NPX). PEDOT-ClO_4-NPX has the highest drug loading and amount of NPX released, coinciding with greater anion (ClO_4^-) mobility; films made with the DS anion, however, showed more controlled NPX release.

The antibiotic tetracycline (the hydrochloride salt, Tc) was successfully incorporated in a PEDOT coating on Pt (Czerwinska-Główka et al. 2021); the potential was cycled from −0.9 to +1.27 V vs. Ag/AgCl (0.1 V/s, 25 cycles) in 3,4-ethylenedioxythiophene (10 mM) and Tc (0.5 to 50 M) in phosphate-buffered saline. A Tc concentration of 1 mM was found to be optimal for maximal drug loading. PEDOT-Tc compared with PEDOT without Tc showed enhanced antimicrobial (*E. coli*) activity, although PEDOT also showed an improvement compared to uncoated Pt. Smaller cell dimensions were observed on both coatings.

1.3.2 ICP Composites

Xie et al. produced polydopamine (PDA)-PPy microcapsule composite for on-demand drug delivery and electrical stimulation of cells (Xie et al. 2017). PDA and dexamethasone are incorporated into the structure during electropolymerisation. Cell affinity was afforded by PDA, while microstructure and electrical activity were introduced by the microcapsules.

PPy-pectin (PC) composites incorporating the antibiotic gentamicin (GM) have been electrodeposited onto TiNbZr using CV (Kumar et al. 2020). Films were produced by sweeping the potential (25 mV/s) from −100 to +1000 mV vs. SCE (10 cycles) in an aqueous solution containing 0.1 M pyrrole, 0.1 M oxalic acid and PC (5–20 wt%), with and without GM (5–20 wt%). PC, hydrogen-bonded to PPy, produced more homogeneous films, free from cracks, and showed a burst release of GM followed by more sustained release. PPy-20PC-10GM exhibited the lowest corrosion rate in simulated body fluid medium and the best antibacterial performance. Such composites show promise as coatings for orthopaedic implants.

A silver nanoparticle-PPy composite was produced in a single step by the in situ chemical oxidation of pyrrole (0.03 M) by silver nitrate (8.1×10^{-5} M) in the presence of (3-mercaptopropyl)trimethoxysilane (0.027 M) in ethanol (de Araújo Lima et al. 2021). The composite was found to exhibit low cytotoxicity towards non-tumoural cells but causes severe membrane damage to human cervix epithelioid carcinoma (HeLa) cells; good biocompatibility (low haemolytic activity) was also found.

Composite bone scaffolds comprised of PPy, gelatin (for cell attachment), hydroxyapatite (an inorganic bone component) and vancomycin-loaded mesoporous silica microparticles have been produced for prolonged drug delivery (Ezazi et al. 2018). A solvent casting method, involving PPy dispersed in water (0.26%w/v), was used to form the scaffolds. The PPy content was found to enhance electropolymerisation without being toxic to osteoblast cells; high mechanical strength and release of the antibiotic for 4 months was achieved.

1.3.3 ICP Nanocomposites

The anticancer drug leucovorin (Lu) has been incorporated into PPy via CV on a graphene oxide nanoribbons-modified glassy carbon electrode (Jalal et al. 2021). This high surface area substrate bearing allowed higher loading and slower release than with growth on PPy-Lu grown on glassy carbon electrodes alone.

Lincomycin, an antibiotic used to treat diseases caused by Gram-positive bacteria, has been incorporated into PANI with magnetite nanostructures (Popescu-Pelin et al. 2018). These biocompatible composite coatings, produced by matrix-assisted pulsed laser evaporation (MAPLE), for use as novel implantable devices showed resistance to *S. aureus*.

PANI-polyvinyl alcohol (PVA) composites containing Cu and Ni nanoparticles (NPs) have been developed to investigate their antibacterial and antifungal activities (Laourari et al. 2022). PANI was obtained by chemical polymerisation of the monomer with HCl as oxidant and mixed with PVA solution; different amounts of $CuCl_2$ and $NiCl_2$ were added to this solution, and films were produced after drying (48–72 h). Antibacterial (*E. coli*, *Klebsiella pneumoniae*, *Proteus* sp. and *S. aureus*) and antifungal (*Fusarium oxysporum f.* sp. *pisi*) activity was demonstrated.

A novel pH-sensitive biocompatible multifunctional nanocarrier was constructed from PANI, N-graphene quantum dots, Mn_3O_4 NPs and MgAl-layered double hydroxide for the release of doxorubicin (DOX) to breast cancer cells (Ahmadi-Kashani et al. 2020). PANI provided a higher degree of encapsulation and slower release behaviour, although a pH-triggered release was afforded in the low-pH extracellular tumour environment. Human breast cancer cells (MCF-7) were targeted, leaving normal cells unaffected.

1.3.4 ICP Nanoparticles

A combined chemo- and photothermal therapy (PTT) for cancer was developed using PPy as a photosensitiser (Nguyen et al. 2017). PPy NPs were loaded into trastuzumab-conjugated liposomes (LRPmAb), where the antibody selectively recognises the human epidermal growth factor receptor 2 (HER2/neu) for treating breast cancers (Fig. 1.5). The chemotherapeutic agent rapamycin was also loaded into the liposomes. Drug release was pH-dependent, and cells with high levels of HER2/neu showed higher uptake of nanoparticles, and when irradiated by near-infrared radiation (NIR, 808 nm), significant inhibition of the breast cancer cells was observed.

The use of PPy NPs as agents in NIR-PTT was further exploited in developing a therapy for lung cancer (Lu et al. 2021). PPy NPs were coated using fucoidan (FU), a

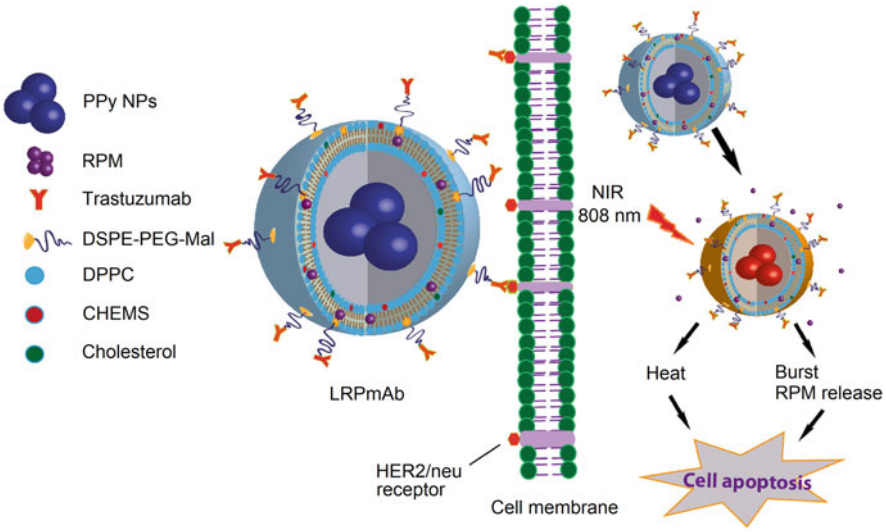

Fig. 1.5 Schematic of HER2-targeted trastuzumab conjugated liposomes for co-delivery of PPy-rapamycin (RPM) for combined photochemotherapy; DPPC = 1,2-dihexadecanoyl-sn-glycero-3-phosphocholine, CHEMS = cholesteryl hemisuccinate (Nguyen et al. 2017)

polysaccharide that has a high binding affinity for P-selectin which is overexpressed in lung cancer cells; FU also kills cancer cells via a number of mechanisms, including increased reactive oxygen species production. Cancer cells (human non-small cell lung carcinoma, H460) and tumour growth were inhibited.

PPy-ZnO nanoconjugates have been prepared and tested against *Acanthamoeba castellanii*, a pathogen that can cause a rare but fatal infection of the central nervous system and blindness (Acanthamoeba keratitis) (Mansur et al. 2022). Chemically synthesised PPy (using pyrrole and $FeCl_3$) was added to a ZnO solution and the mixture sonicated using a probe sonicator and the composite vacuum dried (60 °C). Dose-response antiamoebic effects were demonstrated and thought to be due to cell membrane damage, although the mechanism needs to be further investigated.

A bentonite (clay)-PPy-ZnO nanocomposite containing silver ions for use as an antibacterial and anticorrosive coating for carbon steel has been investigated (Jlassi et al. 2020). The material was formed via a photopolymerisation procedure involving the purified clay (amino-modified), pyrrole, ZnO and $AgNO_3$ as a photosensitiser. A reduction in *E. coli* growth by ca. 86% was noted.

Electrospun poly(ε-caprolactone) nanofibres containing PANI-coated TiO_2 NPs and loaded with simvastatin (SIM) have been studied for use in bone regeneration (Rezk et al. 2020). Although SIM is best known as an antihyperlipidemic drug, it has also shown promise as a bone regeneration drug (increasing expression of a bone growth factor). The PANI-TiO_2 NPs increased fibre diameters, increased hydrophilicity and modified the release of SIM, showing good promise for their use in controlled delivery.

NPs containing cisplatin, photosensitiser chlorin e6 and PANI have been studied for use in cancer NIR-PTT (You et al. 2019). The NPs had cyclic Arg-Gly-Asp (cRGD) peptide ligand at their surface that showed a high affinity for αvβ3/αvβ5 integrin receptors overexpressed on several types of cancer cells (e.g. glioma and breast). Upon NIR treatment, cisplatin was released in the cytoplasm of the targeted breast cancer (MCF-7) cells.

NIR-PTT has also been the theme for the development of hollow mesoporous PANI (HPANI) NPs encapsulating a very high loading of DOX (37.5%, Fig. 1.6) (Zhang et al. 2021). The NPs were polyethylene glycol (PEG)-modified to improve water dispersibility and bioavailability. The NPs exhibited low toxicity and good biocompatibility but, once activated, showed very good cancer cell-killing ability of A549 human lung cancer cells.

1.3.5 ICP Hydrogels

ICPs combined with hydrogels have combined electrical conductivity with the mechanical properties of swollen hydrogels to form conducting polymer hydrogels (CPHs) (Inal et al. 2018). These materials also overcome the limitation of delivering a restricted drug payload as with some early ICP films incorporating various drugs (Zinger and Miller 1984). In addition, the potential difference applied to trigger drug

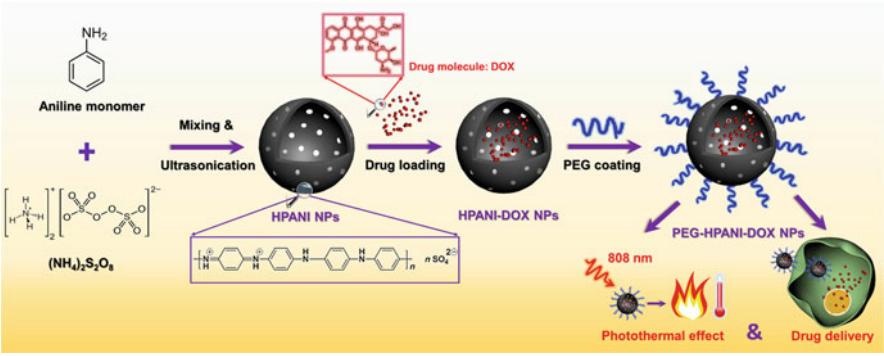

Fig. 1.6 Schematic of the fabrication of PEG-HPANI-DOX NPs as drug carriers with high drug payload and robust photothermal capability (Zhang et al. 2021)

release from some ICP films can lead to fracture and coting delamination (Wei et al. 2015). A number of recent CPH systems, extensively reviewed elsewhere (Zhao et al. 2017), are summarised in this section.

A novel CPH based on PPy doped with glutamate (Glu) within a gelatin methacrylate (GelMA) hydrogel has been formed and investigated (Bansal et al. 2022). GelMA was photolithographically patterned and covalently bound to an Au electrode surface via a cysteamine ($NH_2(CH_2)_2SH$) self-assembled monolayer. After soaking in a pyrrole-Glu solution for 6 h, the electrode was held at +0.9 V vs. Ag/AgCl until a charge of 1500 mC/cm^2 had passed, resulting in the formation of the GelMA/PPy/Glu CPH. A fivefold increase of Glu was observed upon electrical stimulation (−0.6 V) compared to passive release (no electrical stimulation). The CPH was stable and cytocompatible (undifferentiated human neuroblastoma cells, SH-SY5Y) and showed great promise for use in bioelectronic treatment of neurological disorders. Untypical of many CPHs, the ICP component in this system penetrated the entire volume of the hydrogel. Consequentially, a large reservoir of Glu could be delivered via electrical stimulation.

Levodopa (LD), a metabolic precursor of dopamine, is the gold standard oral drug for the management of Parkinson's disease, although it has many shortcomings, not least its short half-life (1 h) and dyskinesia side effect (involuntary movements) (Lakouraj et al. 2021). To overcome these issues, an LD-imprinted hydrogel (based on sodium alginate) was prepared and subsequently modified with PPy (Lakouraj et al. 2021). In vitro release of LD in acid and basic media was 60 and 80%, respectively, after 160 h. The amphiphilic hydrogel provided protection of LD due to the antioxidant properties of PPy; the hydrogel was also non-cytotoxic (human fibroblast cells).

Conductive hybrid hydrogels were formed by heating the thermally sensitive poly (*N*-isopropylacrylamide) (PNIPAm) to remove water and placing it in an HCl solution of either pyrrole or aniline; $Fe(NO_3)_3$ and APS, respectively, were then added to effect chemical polymerisation (Deng et al. 2018). PNIPAm/PPy/Fe_3O_4

magnetic responsive hybrid cryogels were similarly prepared. These cytocompatible (L929 fibroblasts) materials showed temperature-, light- and magnetic-dependent switching behaviour offering stimuli-responsive electronic properties in drug delivery.

Injectable conductive hydrogels have been formed by mixing a solution of chitosan-graft-PANI (chitosan and aniline mixed with APS) with oxidised dextran (a cross-linker) under physiological conditions (Qu et al. 2018). Hydrogels loaded with amoxicillin or ibuprofen (model drugs) were produced by adding these drugs to the solutions before gelation. The injectable conductive hydrogels showed antibacterial activity, cytocompatibility and drug release properties triggered by electrical stimulation and pH.

A novel biocompatible and biodegradable thermosensitive electro-responsive mucogel (TERM) loaded with a bionanocomposite has been investigated as 'nose-to-brain' delivery system activated via an electrical response (Akilo et al. 2019). The bionanocomposite consisted of chitosan, hydroxypropyl methylcellulose (for sustained drug release), pluronic F127 (a thermosensitive polymer) and PANI, in turn loaded with carmustine (BCNU)-Nano-co-Plex (and bioactive agent). Effective release of nanoparticles upon electrical stimulation was demonstrated.

A PANI derivative, poly(2-ethylaniline), was synthesised and embedded in a dextran hydrogel together with diclofenac (a model anionic drug) to investigate the materials used as a transdermal drug delivery system (Paradee et al. 2021). Release of the drug was in the absence, and presence of an applied electric potential was studied and the release mechanism determined. In the former case, either diffusion control or Fickian diffusion was noted, whereas under an applied field, a combination of Fickian and matrix swelling behaviour was found. The diffusion coefficient was increased by two orders of magnitude under an applied potential mainly due to electrorepulsion of charges.

1.4 Other Biomedical Applications

In carrying out this literature review, a few notable ICP systems were found that present interesting applications in the biomedical field, albeit that do not rely on drug release. These are included below.

A further type of PANI NP fabricated for NIR-PTT has been formed from nanodiamonds (NDs) (Ahn et al. 2019). PANI was formed by chemical polymerisation on to amine-modified NDs, forming NPs smaller and more spherical than would have been the case in the absence of this substrate; cellular uptake was therefore increased. Viability of HeLa cells treated with these NPs decreased by $<20\%$.

Xu et al. produced a PEDOT CPH based on carboxymethyl chitosan for use in neural tissue engineering applications (Xu et al. 2018). PEDOT was chemically polymerised in situ, and optimal conditions were investigated using different concentrations of APS, sodium *p*-toluenesulfonate (pTS-Na) and the monomer

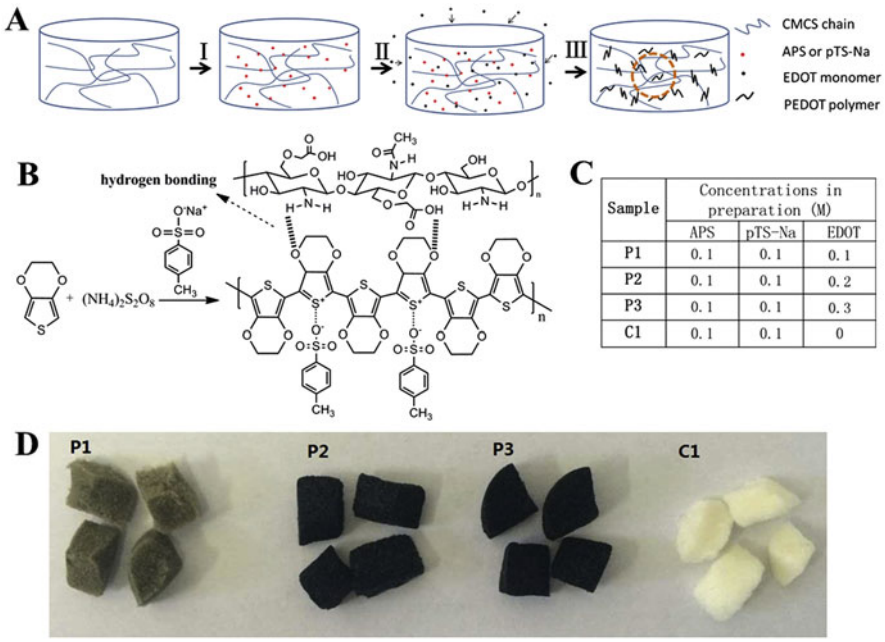

Sample	Concentrations in preparation (M)		
	APS	pTS-Na	EDOT
P1	0.1	0.1	0.1
P2	0.1	0.1	0.2
P3	0.1	0.1	0.3
C1	0.1	0.1	0

Fig. 1.7 Schematic of the fabrication of a PEDOT CPHs based on carboxymethyl chitosan (CMCS) for use in neural tissue engineering applications; (**a**) fabrication process; (**b**) chemical polymerisation process; (**c**) composition parameters to produce the various polymers (P1–P3; C1 = control); and (**d**) photographs of resultant CPHs (Xu et al. 2018)

(Fig. 1.7). PEDOT increased the mechanical strength, introduced conductivity and retained biocompatibility.

The use of ICPs has also been reported in a recent review on biomedical applications of polymer coatings (Smith et al. 2022).

1.5 Conclusions

ICPs are showing great promise in the field of drug delivery. These materials are being used in a number of ways including simple films (mostly electrochemically deposited), in composite and nanocomposite materials, in the form of nanoparticles and as hydrogels/conducting hydrogels. In many of these applications, the switchable nature of these materials opens a way forward where other conventional polymeric systems have not proved as successful.

Disclosure Statement No potential conflict of interest was reported by the author.

References

Ahmadi-Kashani M, Dehghani H, Zarrabi A (2020) A biocompatible nanoplatform formed by MgAl-layered double hydroxide modified Mn_3O_4/N-graphene quantum dot conjugated-polyaniline for pH-triggered release of doxorubicin. Mater Sci Eng C 114:111055. https://doi.org/10.1016/j.msec.2020.111055

Ahn GY, Yun TH, Park J, Lee MJ, Choi I, Ryu T-K, Na K, Choi S-W (2019) Polyaniline-grafted nanodiamonds for efficient photothermal tumor therapy. Colloids Surf B Biointerfaces 180: 273–280. https://doi.org/10.1016/j.colsurfb.2019.04.063

Akilo OD, Kumar P, Choonara YE, du Toit LC, Pradeep P, Modi G, Pillaya V (2019) In situ thermo-co-electroresponsive mucogel for controlled release of bioactive agent. Int J Pharm 559: 255–270. https://doi.org/10.1016/j.ijpharm.2019.01.044

de Araújo Lima EM, Holanda VN, Ratkovski GP, da Silva WV, do Nascimento PH, de Figueiredo RCBQ, de Melo CP (2021) A new biocompatible silver/polypyrrole composite with in vitro antitumor activity. Mater Sci Eng C 128:112314. https://doi.org/10.1016/j.msec.2021.112314

Ayad MM (1994) Influence of HCl on polypyrrole films prepared chemically from ferric chloride. J Polym Sci A Polym Chem 32:9–14. https://doi.org/10.1002/pola.1994.080320102

Bansal M, Raos B, Aqrawe Z, Wu Z, Svirskis S (2022) An interpenetrating and patternable conducting polymer hydrogel for electrically stimulated release of glutamate. Acta Biomater 137:124–135. https://doi.org/10.1016/j.actbio.2021.10.010

Bott DC, Brown CS, Chai CK, Walker NS, Feast WJ, Foot PJS, Calvert PD, Billingham NC, Friend RH (1986) Durham poly acetylene: preparation and properties of the unoriented material. Synth Met 14:245–269. https://doi.org/10.1016/0379-6779(86)90039-1

Bredas JL, Street GB (1985) Polarons, bipolarons, and solitons in conducting polymers. Acc Chem Res 18:309–315. https://doi.org/10.1021/ar00118a005

Chiang CK, Fincher CR, Park YW, Heeger AJ, Shirakawa H, Louis EJ, Gau SC, MacDiarmid AG (1977) Electrical conductivity in doped polyacetylene. Phys Rev Lett 39(17):1098–1101. https://doi.org/10.1103/PhysRevLett.39.1098

Costa LC, Chakki A, Achour ME, Graça MPF (2011) PTCR effect in carbon black/copolymer composites. Phys B: Cond Mat 406:245–249. https://doi.org/10.1016/j.physb.2010.10.056

Czerwinska-Główka D, Przystaś W, Zabłocka-Godlewska W, Student S, Cwalina B, Łapkowski M, Krukiewicz K (2021) Electrically-responsive antimicrobial coatings based on a tetracycline-loaded poly(3,4-ethylenedioxythiophene) matrix. Mater Sci Eng C 123:112017. https://doi.org/10.1016/j.msec.2021.112017

Deng Z, Guo Y, Ma PX, Guo B (2018) Rapid thermal responsive conductive hybrid cryogels with shape memory properties, photothermal properties and pressure dependent conductivity. J Colloid Interface Sci 526:281–294. https://doi.org/10.1016/j.jcis.2018.04.093

Diaz AF, Castillo J, Kanazawa KK, Logan JA, Salmon M, Fajardo O (1982) Conducting poly-*N*-alkylpyrrole polymer films. J Electroanal Chem 133:233–239. https://doi.org/10.1016/0368-1874(82)85140-X

Diaz AF, Castillo JI, Logan JA, Lee W-Y (1981) Electrochemistry of conducting polypyrrole films. J Electroanal Chem 129:115–132. https://doi.org/10.1016/S0022-0728(81)80008-3

Etemad S, Heeger AJ, MacDiarmid AG (1982) Polyacetylene, $(CH)_x$: the prototype conducting polymer. Annu Rev Phys Chem 33:443–469. https://www.annualreviews.org/doi/pdf/10.1146/annurev.pc.33.100182.002303

Ezazi NZ, Shahbazi M-A, Shatalin YV, Nadal E, Mäkilä E, Salonen J, Kemell M, Correia A, Hirvonen J, Santos HA (2018) Conductive vancomycin-loaded mesoporous silica polypyrrole-based scaffolds for bone regeneration. Int J Pharm 536:241–250. https://doi.org/10.1016/j.ijpharm.2017.11.065

Ferrero F, Napoli L, Tonin C, Varesano A (2006) Pyrrole chemical polymerization on textiles: kinetics and operating conditions. J Appl Polym Sci 102:4121–4126. https://doi.org/10.1002/app.24149

Genies EM, Bidan G, Diaz AF (1983) Spectroelectrochemical study of polypyrrole films. J Electroanal Chem 149:101–113. https://doi.org/10.1016/S0022-0728(83)80561-0

Genies EM, Tsintavis C (1985) Redox mechanism and electrochemical behaviour or polyaniline deposits. J Electroanal Chem 195:109–128. https://doi.org/10.1016/0022-0728(85)80009-7

González MB, Brugnoni LI, Saidman SB (2019) Salicylate release from a polypyrrole matrix. Mater Today Commun 18:119–123. https://doi.org/10.1016/j.mtcomm.2018.11.012

Hotta S, Hosaka T, Shimotsuma W (1983) Electrochemical preparation of a polythienylene film and a polypyrrole film containing AsF_6 groups. Synth Met 6:319–320. https://doi.org/10.1016/0379-6779(83)90187-X

Inal S, Rivnay J, Suiu A-O, Malliaras GG, McCulloch I (2018) Conjugated polymers in bioelectronics. Acc Chem Res 51:1368–1376. https://doi.org/10.1021/acs.accounts.7b00624

Ito Y, Shirakawa H, Ikeda S (1974) Simultaneous polymerization and formation of polyacetylene film on the surface of concentrated soluble Ziegler-type catalyst solution. J Polym Sci Polym Chem 12:11–20. https://doi.org/10.1002/pol.1974.170120102

Jadoun S, Rathore DS, Riaz U, Chauhan NPS (2021) Tailoring of conducting polymers via copolymerization – a review. Eur Polym J 155:110561. https://doi.org/10.1016/j.eurpolymj.2021.110561

Jalal NR, Madrakian T, Afkhami A, Ghoorchian A (2021) Graphene oxide nanoribbons/polypyrrole nanocomposite film: controlled release of leucovorin by electrical stimulation. Electrochim Acta 370:137806. https://doi.org/10.1016/j.electacta.2021.137806

Jlassi K, Sliem MH, Benslimane FM, Eltai NO, Abdullah AM (2020) Design of hybrid clay/polypyrrole decorated with silver and zinc oxide nanoparticles for anticorrosive and antibacterial applications. Progr Org Coatings 149:105918. https://doi.org/10.1016/j.porgcoat.2020.105918

Kaner RB, MacDiarmid AG (1988) Plastics that conduct electricity. Sci Am 258:106–111. https://www.jstor.org/stable/24988985

Krukiewicz K, Kruk A, Turczyn R (2018) Evaluation of drug loading capacity and release characteristics of PEDOT/naproxen system: effect of doping ions. Electrochim Acta 289:218–227. https://doi.org/10.1016/j.electacta.2018.09.011

Kumar AM, Adesina AY, Hussein MA, Umoren SA, Ramakrishna S, Saravanan S (2020) Preparation and characterization of Pectin/Polypyrrole based multifunctional coatings on TiNbZr alloy for orthopaedic applications. Carbohydr Polym 242:116285. https://doi.org/10.1016/j.carbpol.2020.116285

Lakouraj MM, Rezaei M, Hasantabar V (2021) Synthesis, characterization and in-vitro prolonged release of L-DOPA using a novel amphiphilic hydrogel based on sodium alginate-polypyrrole. Int J Biol Macromol 193:609–618. https://doi.org/10.1016/j.ijbiomac.2021.10.171

Laourari I, Lakhdari N, Belgherbi O, Medjili C, Berkani M, Vasseghian Y, Golzadeh N, Lakhdari D (2022) Antimicrobial and antifungal properties of NiCu-PANI/PVA quaternary nanocomposite synthesized by chemical oxidative polymerization of polyaniline. Chemosphere 291:132696. https://doi.org/10.1016/j.chemosphere.2021.132696

Liu X, Zheng W, Kumar R, Kumar M, Zhang J (2022) Conducting polymer-based nanostructures for gas sensors. Coord Chem Rev 462:214517. https://doi.org/10.1016/j.ccr.2022.214517

Lu K-Y, Jheng P-R, Lu L-S, Rethi L, Mi F-L, Chuang E-Y (2021) Enhanced anticancer effect of ROS-boosted photothermal therapy by using fucoidan-coated polypyrrole nanoparticles. Int J Biol Macromol 166:98–107. https://doi.org/10.1016/j.ijbiomac.2020.10.091

Mansur FA, Sridewi N, Anwar A, Anwar A, Shahabuddin S (2022) Polypyrrole-conjugated zinc oxide nanoparticle as antiamoebic drugs against Acanthamoeba castellanii. Mater Today 62:7077. https://doi.org/10.1016/j.matpr.2022.01.150

Maruthi N, Faisal M, Raghavendra N (2021) Conducting polymer based composites as efficient EMI shielding materials: a comprehensive review and future prospects. Synth Met 272:116664. https://doi.org/10.1016/j.synthmet.2020.116664

Mortimer RJ, Dyer AL, Reynolds JR (2006) Electrochromic organic and polymeric materials for display applications. Displays 27:2–18. https://doi.org/10.1016/j.displa.2005.03.003

Naarmann H, Theophilou N (1987) New process for the production of metal-like, stable polyacetylene. Synth Met 22:1–8. https://doi.org/10.1016/0379-6779(87)90564-9

Namsheer K, Rout CS (2021) Conducting polymers: a comprehensive review on recent advances in synthesis, properties and applications. RSC Adv 11:5659–5697. https://doi.org/10.1039/d0ra07800j

Nguyen HT, Tran TH, Thapa RK, Phung CD, Shin BS, Jeong J-H, Cho H-G, Yong CS, Kim JO (2017) Targeted co-delivery of polypyrrole and rapamycin by trastuzumab-conjugated liposomes for combined chemo-photothermal therapy. Int J Pharm 527:61–71. https://doi.org/10.1016/j.ijpharm.2017.05.034

Olvera D, Monaghan MG (2021) Electroactive material-based biosensors for detection and drug delivery. Adv Drug Deliv Rev 170:396–424. https://doi.org/10.1016/j.addr.2020.09.011

Ouyang J (2021) Application of intrinsically conducting polymers in flexible electronics. SmartMat 2:263–285. https://doi.org/10.1002/smm2.1059

Paradee N, Thanokiang J, Sirivat A (2021) Conductive poly(2-ethylaniline) dextran-based hydrogels for electrically controlled diclofenac release. Mater Sci Eng C 118:111346. https://doi.org/10.1016/j.msec.2020.111346

Popescu-Pelin G, Fufă O, Popescu RC, Savu D, Socol M, Zgură I, Holban AM, Vasile BŞ, Grumezescu V, Socol G (2018) Lincomycin–embedded PANI–based coatings for biomedical applications. Appl Surf Sci 455:653–666. https://doi.org/10.1016/j.apsusc.2018.06.016

Qian R, Qiu J (1987) Electrochemically prepared polypyrroles from aqueous solutions. Polym J 19:157–172. https://doi.org/10.1295/polymj.19.157

Qu J, Zhao X, Ma PX, Guo B (2018) Injectable antibacterial conductive hydrogels with dual response to an electric field and pH for localized "smart" drug release. Acta Biomater 72:55–69. https://doi.org/10.1016/j.actbio.2018.03.018

Rezk AI, Bhattarai DP, Park J, Park CH, Kim CS (2020) Polyaniline-coated titanium oxide nanoparticles and simvastatin-loaded poly(ε-caprolactone) composite nanofibers scaffold for bone tissue regeneration application. Colloids Surf B: Biointerfaces 192:111007. https://doi.org/10.1016/j.colsurfb.2020.111007

Roncali J (1992) Conjugated poly(thiophenes): synthesis, functionalization and applications. Chem Rev 92:711–738. https://doi.org/10.1021/cr00012a009

Ryan EM, Breslin CB (2018) Formation of polypyrrole with dexamethasone as a dopant: its cation and anion exchange properties. J Electroanal Chem 824:188–194. https://doi.org/10.1016/j.jelechem.2018.07.052

Ryan EM, Breslin CB (2019) The incorporation of drug molecules with poor water solubility into polypyrrole as dopants: indomethacin and sulindac. Electrochim Acta 296:848–855. https://doi.org/10.1016/j.electacta.2018.11.107

Satoh M, Kaneto K, Yoshino K (1985) Electrochemistry preparation of high quality poly (p-phenylene) film. J Chem Soc Chem Commun:1629–1630. https://doi.org/10.1039/C39850001629

Seeger K (1982) The morphology and structure of highly conducting polymers. Angew Makromol Chem 109:227–251. https://doi.org/10.1002/apmc.1982.051090116

Shen L, Gao N, Huang X (2020) Synthesis, characterization and electropolymerization of functionalized organic salteanilinium saccharinate and electrochemically controlled release of saccharinate anions. Electrochim Acta 329:135142. https://doi.org/10.1016/j.electacta.2019.135142

Shirakawa H, Ikeda S (1971) Infrared spectra of poly(acetylene). Polym J 2:231–244. https://www.nature.com/articles/pj197128

Smith JR, Campbell SA, Ratcliffe NM, Dunleavy M (1994) Polyheterocycles containing alkene spacer linkages part I. synthesis and electropolymerization of 3-styrylthiophenes. Synth Met 63:233–243. https://doi.org/10.1016/0379-6779(94)90234-8

Smith JR, Campbell SA, Walsh FC (1995b) Cyclic voltammetry at metal electrodes. Trans IMF 73:72. https://doi.org/10.1080/00202967.1995.11871062

Smith JR, Cox PA, Campbell SA, Ratcliffe NM (1995a) Application of density functional theory in the synthesis of electroactive polymers. J Chem Soc Faraday Trans 91:2331–2338. https://doi.org/10.1039/FT9959102331

Smith JR, Lamprou DA, Larson C, Upson SJ (2022) Biomedical applications of polymer and ceramic coatings: a review of recent developments. Trans IMF 100(1):25–35. https://doi.org/10.1080/00202967.2021.2004744

Sun K, Zhang S, Li P, Xia Y, Zhang X, Du D, Isikgor FH, Ouyang J (2015) Review on application of PEDOTs and PEDOT:PSS in energy conversion and storage devices. J Mater Sci Mater Electron 26:4438–4462. https://doi.org/10.1007/s10854-015-2895-5

Talikowska M, Fu X, Lisak G (2019) Application of conducting polymers to wound care and skin tissue engineering: a review. Biosens Bioelectron 135:50–63. https://doi.org/10.1016/j.bios.2019.04.001

Tan Y, Ghandi K (2013) Kinetics and mechanism of pyrrole chemical polymerization. Synth Met 175:183–191. https://doi.org/10.1016/j.synthmet.2013.05.014

Tourillon G, Garnier F (1982) New electrochemically generated organic conducting polymers. J Electroanal Chem 135:173–178. https://doi.org/10.1016/0022-0728(82)90015-8

Waltman RJ, Bargon J (1986) Electrically conducting polymers: a review of the electropolymerization reaction, of the effects of chemical structure on polymer film properties, and of applications towards technology. Can J Chem 64:76–95. https://doi.org/10.1139/v86-015

Waltman RJ, Bargon J, Diaz AF (1983) Electrochemical studies of some conducting polythiophene films. J Phys Chem 87:1459–1463. https://doi.org/10.1021/j100231a035

Wei B, Liu J, Ouyang L, Kuo C-C, Martin DC (2015) Significant enhancement of PEDOT thin film adhesion to inorganic solid substrates with EDOT-acid. ACS Appl Mater Interfaces 7(28):15388–15394. https://doi.org/10.1021/acsami.5b03350

Xiang H, Deng N, Zhao H, Wang X, Wei L, Wang M, Bowen C, Kang W (2021) A review on electronically conducting polymers for lithium-sulfur battery and lithium-selenium battery: progress and prospects. J Energy Chem 58:523–556. https://doi.org/10.1016/j.jechem.2020.10.029

Xie C, Li P, Han L, Wang Z, Zhou T, Deng W, Wang K, Lu X (2017) Electroresponsive and cell-affinitive polydopamine/polypyrrole composite microcapsules with a dual-function of on-demand drug delivery and cell stimulation for electrical therapy. NPG Asia Mater 9:e358. https://doi.org/10.1038/am.2017.16

Xu C, Guan S, Wang S, Gong W, Liu T, Ma X, Sun C (2018) Biodegradable and electroconductive poly(3,4-ethylenedioxythiophene)/carboxymethyl chitosan hydrogels for neural tissue engineering. Mater Sci Eng C 84:32–43. https://doi.org/10.1016/j.msec.2017.11.032

Xu S, Shi X-L, Dargusch M, Di C, Zou J, Chen Z-G (2021) Conducting polymer-based flexible thermoelectric materials and devices: from mechanisms to applications. Prog Mater Sci 121:100840. https://doi.org/10.1016/j.pmatsci.2021.100840

You C, Gao Z, Wang M, Wu H, An P, Wang S, Sun Y, Sun B, Zhang X (2019) Cisplatin and Ce6 loaded polyaniline nanoparticles: An efficient near-infrared light mediated synergistic therapeutic agent. Mater Sci Eng C 95:183–191. https://doi.org/10.1016/j.msec.2018.03.031

Zamani FG, Moulahoum H, Ak M, Demirkol DO, Timur S (2019) Current trends in the development of conducting polymers-based biosensors. TrAC Trends Anal Chem 118:264–276. https://doi.org/10.1016/j.trac.2019.05.031

Zhang Y, Fang F, Chen Y, Li M, Li L, Li W, Zhang J (2021) Hollow mesoporous polyaniline nanoparticles with high drug payload and robust photothermal capability for cancer combination therapy. Chin J Chem Eng 38:221–228. https://doi.org/10.1016/j.cjche.2021.03.011

Zhao F, Shi Y, Pan L, Yu G (2017) Multifunctional nanostructured conductive polymer gels: synthesis, properties, and applications. Acc Chem Res 50:1734–1743. https://doi.org/10.1021/acs.accounts.7b00191

Zinger B, Miller LL (1984) Timed release of chemicals from polypyrrole films. J Am Chem Soc 106(22):6861–6863. https://doi.org/10.1021/ja00334a076

Chapter 2
Electrospinning for Drug Delivery Applications

Luis Jesús Villarreal-Gómez and Graciela Lizeth Pérez-González

Abstract Electrospun nanofibers have gained importance in drug delivery applications thanks to their diverse properties such as biocompatibility, biodegradability, adequate mechanical properties, and high surface area, among others. Drug delivery systems are getting crucial to avoid or diminish secondary effects and improve the targeting of the administered drugs incrementing its effectivity. Hence, the objective of this book chapter is to discuss the current reported electrospun nanofibers that were proposed as drug carriers; moreover description of properties, polymers used, pharmaceutical drugs loaded, and targeted tissues are discussed. From all administration routes, oral administration is the most studied followed by transdermal, due to the nature of the electrospun fibers to degrade and create a tridimensional scaffold with malleable properties. On the other hand, fast dissolving administration is the most recommended strategy for the use of nanofibers, where more evident therapeutics benefits can be appreciated. Still studies of the effectivity of the nanofibers as drug carriers and comparison with traditional administration are needed.

Keywords Administration routes · Drug delivery · Electrospinning · Nanofibers

2.1 Introduction

Currently, pharmaceutical drugs are available in the market in different presentations such as tablets, syrups, and injections that the patients swallow and chew or are injected administering specific concentrations of the medical compound. However, kids and patients with specific conditions have still difficulty in obtaining the recommended doses through these administration routes and medical presentations (Dahmash et al. 2021; He et al. 2021; Özakar and Özakar 2021; Mehdi et al. 2021).

L. J. Villarreal-Gómez (✉) · G. L. Pérez-González
Facultad de Ciencias de la Ingeniería y Tecnología, Universidad Autónoma de Baja California, Tijuana, Baja California, Mexico
e-mail: luis.villarreal@uabc.edu.mx; perez.graciela@uabc.edu.mx

D. Lamprou (ed.), *Nano- and Microfabrication Techniques in Drug Delivery*,
Advanced Clinical Pharmacy – Research, Development and Practical Applications 2,
https://doi.org/10.1007/978-3-031-26908-0_2

Until now, oral administration has been the preferred administration route for its easiness of administration (Gao et al. 2022; Wang et al. 2021; Xu et al. 2022).

Electrospun nanofibers are polymeric-based structures that possess a diverse set of properties that makes them interesting to be used as drug delivery systems (Torres-Martínez et al. 2018); between these properties, it can be included in biocompatibility (Vass et al. 2020; Villarreal-Gómez et al. 2014), biodegradability (Birer and Acartürk 2021; Pacheco et al. 2021), high surface area (Badgar and Prokisch 2021; Zhang et al. 2021), adequate mechanical properties (Kopp et al. 2020; Huang et al. 2021), highly customizable fiber diameter and structure (Pérez-González et al. 2019; Mohammadinejad et al. 2021), excellent porosity connectivity (Rampichová et al. 2018; Yan et al. 2020), ease of handling (Sóti et al. 2016; Liu et al. 2018), functionalization (Niemczyk-Soczynska et al. 2020; Chen et al. 2021), and the ability to encapsulation of a diversity of bioactive molecules (Dumitriu et al. 2021; Toprak et al. 2021).

For all the above, this chapter discusses the electrospun nanofiber properties applied as drug delivery systems and some characteristics of the main polymers used, describing their advantages and disadvantages as well as the different administration routes reported (oral, vaginal, transdermal, ocular, rectal, and nasal). Some electrospinning strategies are also compared.

2.2 Electrospinning and Drug Incorporation Techniques

Electrospinning is a diverse method that has gained interest through the years; the objective of this technique is to fabricate fibers or particles in the nanoscale range (Villarreal-Gómez et al. 2016), creating a tridimensional scaffold that has desired properties with potential use in drug delivery systems such as the large surface area, where this property permits a high drug loading capacity in a reduced volume range (Luraghi et al. 2021), low cost (Velasco-Barraza et al. 2016), and adaptability (Luraghi et al. 2021).

The electrospinning technique uses a high-voltage electrical field that charges a polymer solution breaking its surface tension when injected with a specific rate; this polymer is attracted to a conductive collector creating a liquid jet yielding nanofibers (~10 to 1000 nm) where the solvent evaporates in the air (Villarreal-Gómez et al. 2016) (Fig. 2.1).

Figure 2.1 illustrated a standard electrospinning technique; in this method, a high voltage is applied and a polymer solution is fed, creating the Taylor cone phenomenon, that is, the initial form of the fibers; for that, the applied voltage produces charge movement in the polymer liquid, which stretches the pendant drop, and a spherical shape is created by surface tension. When the electrostatic repulsion of the charged polymer liquid overwhelms the surface tension, a conical shape known as the Taylor cone appears, and the jet is originated at the cone tip. Because both the applied voltage and feed rate affect the formation of the Taylor cone, the two parameters must be balanced to form a steady jet. If the polymer liquid is adequately

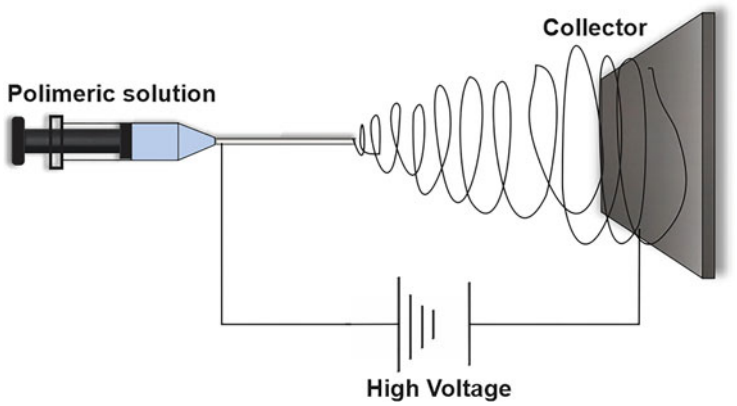

Fig. 2.1 Electrospinning technique setup based on (Torres-Martínez et al. 2019)

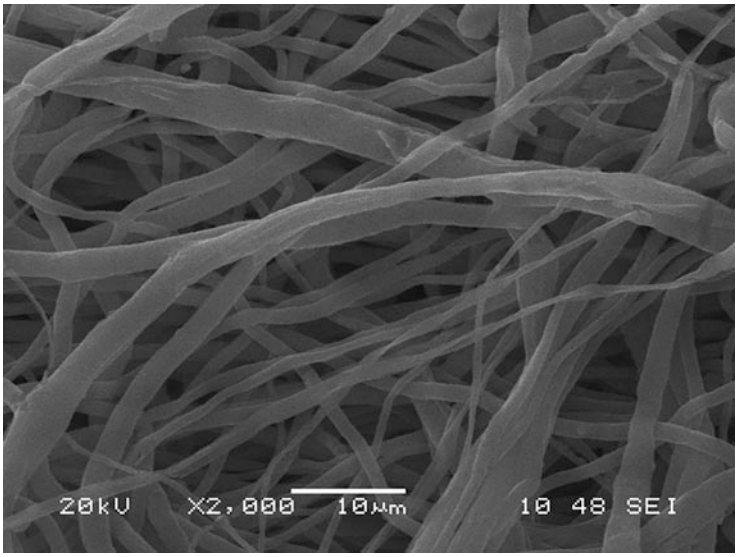

Fig. 2.2 Functionalized poly(caprolactone) electrospun fibers (2000× of amplification)

cohesive, a steady jet emerges from the Taylor cone, allowing the polymer chains to stretch and form a uniform filament. In this process, the solvent vaporizes, resulting in the stirring of the filament (Badgar and Prokisch 2021). Fibers are then placed over a grounded metallic collector, which is commonly placed at an optimal distance. Fibers are often distributed randomly throughout the collection process. In certain circumstances, a single piece of aluminum foil can be used to collect the fibers in a random distribution (Fig. 2.2).

There are different types of electrospinning techniques that help to incorporate bioactive molecules or drugs into the fibers or over their surface (Torres-Martínez

et al. 2019). The objective is to release the loaded drug at the target zone through the polymeric degradation of the fibers controlling its delivery rate depending on the polymer used (Uhljar et al. 2021).

From the reported, electrospinning techniques can be listed as blending, coaxial, emulsion, and surface modification electrospinning; each of them has a different strategy for drug incorporation, and they are explained as follows:

2.2.1 Blending Electrospinning

Blending electrospinning is the most simple and easy method for the incorporation of bioactive compounds into polymeric nanofibers. This method consists of the direct blending of the pharmaceutical drug with the polymeric solution. The advantage of this strategy is that it improves the equilibrium between the mechanical and physicochemical characteristics of the functionalized resulting fibers. Moreover, it permits the adjusting of the proportion used in the bioactive component by altering the concentration added to the final solution (Tipduangta et al. 2016) (Fig. 2.3a).

One of the advantages of blending electrospinning is that is a one-step method because the loaded biomolecules or drug solution is dissolved or dispersed directly into the polymeric solution. In this method, it is important to choose correctly the polymeric matrix because its characteristics will determine the efficiency in the drug encapsulation, dispersion in/on the fibers, and delivery rate. It is reported that the equilibrium between hydrophilic and hydrophobic functional groups in all components of the system (drug, polymer, solvent) will improve the optimal functionalization of the resulting fibers (Moreira et al. 2021).

It's important to note that due to the hydrophobic properties of some polymers, lipophilic drugs are easier to dissolve and create a homogeneous solution and vice versa. Such is the case of the polyester's polymers, which are hydrophobic and interact very well with the hydrophobic drugs rifampicin and paclitaxel, and gelatin, poly (ethylene glycol), and poly (vinyl alcohol), which are hydrophilic polymers, can dissolve hydrophilic drugs such as doxorubicin (Nguyen et al. 2020).

The disadvantage of this method is that some metallic bioactive molecules tend to aggregate in the polymer solution and in the resulting fibers (Villarreal-Gómez et al. 2021). Moreover, with this process, pharmaceutical drugs that are insoluble in water cannot be encapsulated using hydrophilic polymers (Balusamy et al. 2020). To avoid this issue, cyclodextrins are used to improve the solubility of the insoluble drugs into the polymeric solution (Costoya et al. 2017).

2.2.2 Coaxial Electrospinning

Another alternative technique for drug incorporation using the electrospinning method is coaxial electrospinning. This method permits the manufacture of

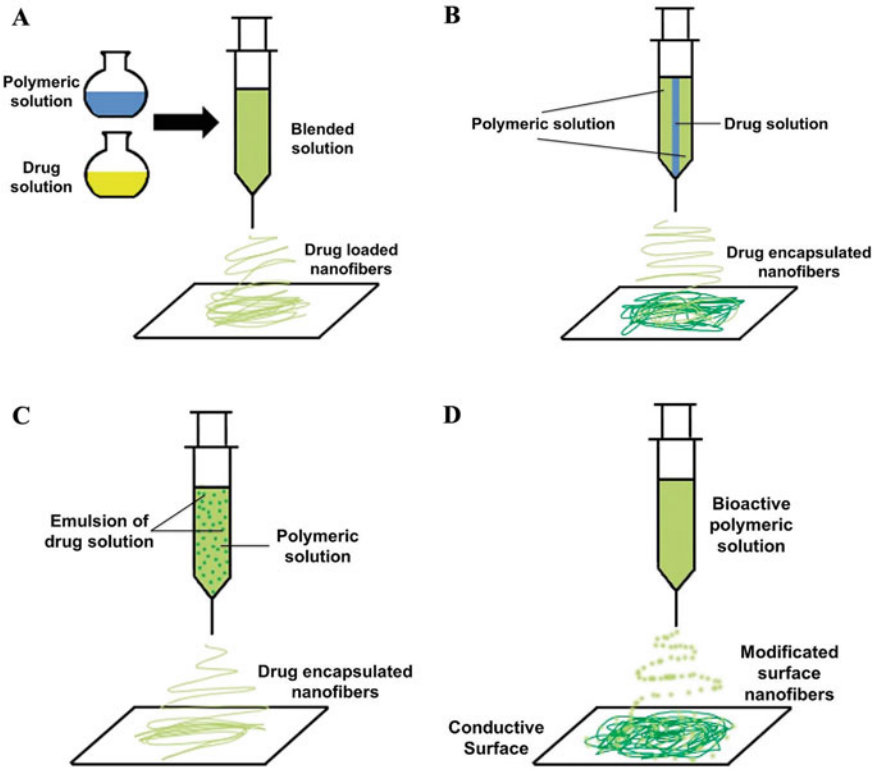

Fig. 2.3 Different electrospinning techniques: (**a**) blending electrospinning, (**b**) coaxial electrospinning, (**c**) emulsion electrospinning, (**d**) surface modification electrospinning

core-shell fibers (Fig. 2.3b) (Han and Steckl 2019), and it's useful for the load of molecules that are sensitive to environmental conditions such as proteins, growth factors, some antibiotics, and biological agents (Rafiei et al. 2020). The great advantage of this technique is that gives protection to the loaded molecules and remains intact until their delivery at the target zone (Lu et al. 2016; Uhljar et al. 2021).

For this technique, a special double coaxial needle is needed, which is usually made of two concentric standard needles and can be used to simultaneously infuse, electrospun, or 3D print up to two different materials (Rafiei et al. 2020).

Another advantage of the coaxial electrospinning method is augmenting the functionality of the bioactive molecules; by adding these molecules into the inner jet in the electrospinning process, the polymeric matrix gets at the outside of the fibers, protecting the biomolecule, helping with a sustained release of the drug, and allowing the bioability of unstable biological agents to be maintained (Zhang et al. 2012).

2.2.3 *Emulsion Electrospinning*

In the case of the emulsion electrospinning, this technique has been considered flexible in the choice of any drug to be encapsulated into the nanofibers (Fig. 2.3c) (Cornejo-Bravo et al. 2016). This method also permits the preparation of core-shell electrospun fibers, where under the influence of electrostatic forces, these core-sheath structures are formed due to the stretching and coalescence of polymeric emulsions (Zhang et al. 2021), but unlike coaxial electrospinning, this method is less expensive and efficient (Lu et al. 2016).

In this methodology, the oil phase is generated by the emulsion of the drug or aqueous bioactive molecules in the polymer solution followed by the electrospinning process. Also, the low molecular weight of the drugs is crucial for the optimal loading and fabrication of the core-shell fibers. The advantage of this strategy is the necessity of using a common solvent between polymer and drugs (Li et al. 2020).

Generally, the release profile of pharmaceuticals follows diffusion or degradation mechanisms depending on the dissolution or degradability of polymer structures.

2.2.4 *Surface Modification Electrospinning*

Finally, the surface of fabricated polymeric electrospun nanofibers can be modified externally by incorporating certain biomolecules that can camouflage the surface and change their biochemical properties (Fig. 2.3d). This strategy permits the avoidance of fast initial burst release and slow rate immobilization of the biological molecules. Moreover, it is possible to coat 3D surfaces with nanofibers such as microchips or organs on a chip technology (Yang et al. 2018).

2.3 Advantages and Disadvantages of Drug Loaded Electrospun Nanofibers

The main advantage of fibrous scaffolds for proposed drug delivery systems is that they possess a high surface-area-to-volume ratio, which can permit high dose load and promote the solubility of the drug in an aqueous environment, improving drug efficiency (Meng et al. 2011).

Not all polymers can be used for drug delivery systems; these polymers have to possess specific characteristics such as biocompatibility and biodegradability, permit drug loading, permit mass transfer, and respond to certain stimuli, among other characteristics (Cornejo-Bravo et al. 2016). Some examples of these polymers and their properties can be listed in the following Table 2.1:

Depending on their polymeric functional groups, antibiotics, anticancer agents, and biomolecules such as nucleic acids and proteins can be loaded (Dahmash et al.

Table 2.1 Most of the reported polymers which are used for electrospun fibers fabrication in drug delivery systems

Polymers	Advantages	Disadvantages	Ref.
Poly(caprolactone) (PCL)	Biodegradable, biocompatible, compatible with a range of other materials, FDA approved	Low melting point, resistance to water, slow degradation rate, poor mechanical properties, and low cell adhesion	Aguirre-Chagala et al. (2017)
Poly(vinyl alcohol) (PVA)	Bioadhesive, biodegradable, biocompatible, low tendency for protein adhesion, and low toxicity	Humidity reduces the polymer's tensile strength; slow biodegradation	Pérez-González et al. (2022)
Poly(vinyl pyrrolidone) (PVP)	Binder, FDA approved, excellent wetting properties, biocompatibility, low toxicity, adhesive characteristics, complexing stability, relatively inert behavior, and is resistant to thermal degradation	Certain allergic reactions, storage disease, subcutaneous granulomas, pulmonary vascularization, and reticuloendothelial system (RES) deposition, high hygroscopic nature which made it tough to store and handle, non-biodegradability in parenteral administration	Kurakula and Rao (2020) and Torres-Martínez et al. (2020)
Poly (N-isopropylacrylamide) (PNIPAM)	Mechanical strength, biocompatibility, biodegradability, multi-stimuli responsibility, higher drug loading	Low mechanical strength, limited drug loading capacity, and low biodegradability	Xu et al. (2020)
Poly(acrylic acid) (PAA)	Low toxicity, super hydrophilicity properties, biocompatibility, biodegradability characteristics	Poor mechanical properties, high solubility in water	Alhalawani et al. (2016)

2021), where surface morphology and structure of the polymeric nanofibers are key features for regulating the delivery rate and quantity of the drug. Also, the surface of the polymers can protect the bioactive loaded molecules from corrosion or degradation of the enzyme, water, or gastric acid, prolonging the effectivity of the pharmaceutical drug (Meng et al. 2011).

It is well known that the electrospinning technique is cost-effective and useful for fabricating long and continuous fibers with random and aligned distribution tailoring its mechanical properties (Villarreal-Gómez et al. 2016).

On the other hand, this technique needs the use of organic solvents and is not feasible to manipulate or reproduce the tridimensional structure and percentage of porosity (Cornejo-Bravo et al. 2016).

Another important concern of this technique is that environmental parameters such as temperature fluctuations and relative humidity affect directly the reproducibility and quality of the fibrous scaffolds and the optimal loading of the pharmaceutical drugs. Temperature, for example, disturbs the morphology of the resulting fibers and modifies the polymeric solution properties during the process, for example, a slight low temperature affects solvent evaporation rate, viscosity, and superficial tension, causing a slow jet solidification, affecting the stretching and elongation of the polymer. Slightly higher temperature decreases the viscosity and superficial tension affecting the optimal elongation and creation of the fibers (Rostamabadi et al. 2020). In the case of relative humidity, when it's high, the fibers get to experiment with a plasticizing effect, or the diameter of the fibers increments its thickness, because of the low potency of the electrostatic field that limits the stretching and elongation of the polymeric solution (Szewczyk and Stachewicz 2020). When the relative humidity decreases, fiber diameter is also reduced (Bavatharani et al. 2021).

Some other advantages and disadvantages of the discussed electrospinning methods are given in the following Table 2.2:

Table 2.2 Advantages and disadvantages of drug incorporation methods using electrospinning

Electrospinning technique	Advantages	Disadvantages	Ref.
Blending	• Improves physicochemical and mechanical properties of the drug-loaded fibers • Promotes the fabrication of controlled drug delivery systems • Permits the variation of bioactive molecule addition	• Not all bioactive molecules blend well with the polymeric matrix • Some bioactive molecules agglomerate in the polymeric solution	Tipduangta et al. (2016)
Coaxial	• Improves bioactive molecules' effectivity • Sensible bioactive molecules are protected by a polymeric shell and avoid direct contact with the environment	• Special syringe tip is needed (coaxial)	Han and Steckl (2019)
Emulsion	• Not necessary compatibility of solvents is required between polymers and drugs	• Not all bioactive molecules can create an emulsion system	Bardoňová et al. (2022)
Surface modification	• Inhibit the initial burst release phenomena • Avoid a brief release rate	• Not all polymers of drug can be used for this method	Palo et al. (2019)

2.4 Administration Routes of Drug-Loaded Electrospun Nanofibers

2.4.1 Oral Administration

The use of electrospun nanofibers as drug delivery for the oral cavity is the most reported due to its easy administration, effectivity, and ease to test (Dodero et al. 2021; Wang et al. 2021). This system is designed to be placed in the oral cavity for fast degradation in saliva before swallowing into the gastrointestinal tract (He et al. 2021). This type of administration is crucial for the effectiveness of this kind of delivery systems thanks to the intense vascularization in the buccal cavity. Most importantly, this oral administration provides an alternative route for patients that are sensitive to certain drugs that are administered in lesioned gastrointestinal tract or drugs that cause stomach distress (Dodero et al. 2021). Moreover, oral administration is especially useful for geriatric and pediatric patients (Gupta et al. 2021).

In this administration route, fast release is one of the desired factors that nanofibers improve, providing a release in seconds. This fast release and direct targeting of the blood torrent enhances drug availability by avoiding some initial steps in metabolism and absorption (He et al. 2021; Pacheco et al. 2021).

2.4.2 Vaginal Administration

For this administration route, fibrous scaffolds loaded with pharmaceutical drugs need to have the property to be mucoadhesive, because the release time needs to be prolonged due to the pathologies targeted in that area (Pérez-González et al. 2019).

Ball and Woodrow (2014) developed electrospun poly(vinyl pyrrolidone) and poly(ethylene oxide) nanofibers loaded with solid dispersions of maraviroc (antiretroviral agent) and evaluated their potential for the fast intravaginal pre-exposure prophylaxis of HIV. This proposed technology offers women options to protect themselves against sexual HIV transmission. Loaded nanofibers with maraviroc improve this drug solubility and permit drug retention for more than 15 min, requiring time for efficient drug bioactivity in the zone. The researchers showed that these water-soluble polymeric fibers release the bioactive component quickly upon contact with moisture.

Aggarwal et al. (2017) prepared poly(caprolactone)/chitosan electrospun nanofibers loaded with cisplatin for the treatment of cervical cancer. Developed functionalized nanofibers were evaluated as local chemotherapy in mice that were affected by cervical cancer. These nanofibers presented a sustained release pattern in about 1 month, and strong mucoadhesive samples were located in the vaginal mucosa in the cervix region of mice, showing great potential.

2.4.3 Transdermal Administration

In this administration route, the loaded drug is delivered locally, evading undesired drug spreading through the skin and other locations thanks to the excellent skin permeability. Electrospinning provides a drug delivery system that promotes drug solubility and sustained drug release kinetics (Shahriar et al. 2019). Nanofibers create a fibrous patch with excellent mechanical properties that can be manipulated by a regular patient with any medical knowledge (Toriello et al. 2020).

Khoshnevisan et al. (2018) discussed how cellulose acetate electrospun fibers can be functionalized with therapeutic agents with antimicrobial, antibacterial, antioxidant, systematic, and anti-inflammatory agents for transdermal delivery. This study affirmed that these modified fibers possess several interesting characteristics such as biodegradability, chemical persistence, biocompatibility, and thermal stability.

Moreover, Álvarez-Suárez et al. (2020) proposed electrospun fibers with sorbent prepared with AgNP as an effective wound dressing. Since skin burns and some ulcers are hard to treat thanks to their high risk of infection, electrospun nanofibers functionalized with antimicrobial agents have the potential to clean, protect, and avoid any infection. This research group prepared poly(ε-caprolactone)/poly (vinyl pyrrolidone) (PCL/PVP) electrospun fibers used in combination with Argovit™ silver nanoparticles (Ag-Si/Al_2O_3). Resulted fibers demonstrated effectivity against Gram-negative bacteria *Pseudomonas aeruginosa* and *Escherichia coli*, Gram-positive *Staphylococcus aureus*, and the fungal organism *Candida albicans*.

2.4.4 Ocular Administration

Another advantage of the electrospun nanofibers for drug delivery systems is that they can be adapted in hard zones like the ocular site. In a study, it was proposed an ophthalmic supplement composed of poly(vinyl pyrrolidone) (PVP)/hyaluronic acid (HA) nanofibers loaded with ferulic acid as an antioxidant (FA) and the peptide ε-polylysine (ε-PL) as an antimicrobial compound. These fibers resulted effectively against *Pseudomonas aeruginosa* and *Staphylococcus aureus* (Grimaudo et al. 2020).

One of the challenges of eye disease treatment is the limited residence time of the applied drug because most of the bioactive compounds just remain a few seconds. Göttel et al. (2020) proposed a dry form of drug delivery using electrospun nanofibers made of gellan gum/pullulan to guarantee a good fit to the eye anatomy, creating a fibrous system with the curvature of the eye lens.

Da Silva et al. (2019) tested the ocular biocompatibility of poly(ε-caprolactone) modified with dexamethasone acetate (PCL/DX) to target the ocular vitreous cavity for the treatment of retinal diseases. In that study ARPE-19 and MIO-M1 cells were used for cytotoxicity studies using the MTT assay. Moreover, SEM, FTIR, OCT, and in vivo studies were performed. The research group concluded that PCL/DX

nanofibers presented acceptable biocompatibility and safety in rodents' eyes and are optimal for dexamethasone delivery.

2.4.5 Rectal Administration

Rectal route administration is likely to be used in pediatrics because patients under 6 months are difficult to treat with other administration routes. Despite that, not much literature has been published on this route of administration, but the potential is that the electrospun fibers are clear. Using fibrous matrices with pharmaceutical drugs is especially useful in postoperative peritoneal effusions that are followed by pelvic/rectal surgery because, as mentioned before, nanofibers can be delivery systems that are biocompatible, biodegradable, and can permit a load of high doses of drugs (Shahriar et al. 2019).

Kondo et al. (2014) reported electrospun nanofibers prepared with synthetic material (PuraMatrix) for the treatment of lymphorrhea following pelvic surgery, demonstrating that the fibers are biocompatible and have an optimal biodegradation rate. The interesting part of this study is that researchers used 20 colorectal cancer patients who participated in clinical trials, and after 2–3 months, a significant reduction of cancer tissue was observed.

Moreover, Modgill et al. (2016) tested the permeability of poly(vinyl alcohol) (PVA) loaded with ciprofloxacin. The in vitro permeability assays showed the highest permeability of the drug in the rectal mucosa membrane. In the study, a successful controlled release was demonstrated.

2.4.6 Nasal Administration

Finally, nasal administration using nanofibers avoids poor absorption rate, promotes enzymatic activity, and prevents the acidic environment and first-pass metabolism that occurs in the liver. But administration in nasal tissues presented several issues such as poor retention time and a narrow adsorption window (Sofi et al. 2020). Because of that, Rivelli et al. (2021) proposed a fibrous delivery system of poly (lactic-co-glycolic acid) (PLGA) loaded with mometasone furoate for the treatment of chronic rhinosinusitis. Their results demonstrated that the drug was dispersed successfully in the polymeric matrix, showing sustained release in the nasal environment. Moreover, the grade of inflammation in the animal's mucosa that was treated with mometasone furoate-loaded nanofibers was lower than those that were not received.

Si et al. (2018) proposed a supramolecular peptide nanofiber as a platform for vaccines and immunotherapies, which promote an immune response in the lack of exogenous adjuvants without detectable inflammation. These nanofibers possess an influenza peptide epitope that generates higher antigen-specific CD^{8+} T cell

responses in lung draining lymph nodes. Compared to the subcutaneously applied nanofibers, the nasal route permitted a higher releasing of the epitope and provoked a persistent CD^{8+} T cell concentration in the lung, enhancing a faster immunological response at 6 weeks after vaccination.

Table 2.3 listed drug-loaded electrospun fibers and their intended administration routes as well as the characterization methods that were used.

2.5 Future Perspectives

Despite all the current work reported for electrospun nanofibers applied in drug delivery systems, where it can be seen in Fig. 2.4 how have been incrementing in the past 20 years, wherein 2019, was the year with more publications recorded in Pubmed (107 papers) (Fig. 2.4), most of the studies remain in the laboratory practice and just a few of them assesses clinical trials (Williams et al. 2012).

Maleki Dizaj et al. (2019) discussed that electrospun nanofibers containing antibacterial agents have been gaining great attention over the years. Among these, antimicrobial loaded agents include metal nanoparticles, antibiotics, triclosan, herbal extracts, quaternized ammonium compounds, graphene, and silver nanoparticles, among others. In this report, researchers clarify that all these agents were tested with in vitro studies. Because of this, in vivo clinical testing is still needed.

Necessary human equivalent doses still need to be tuned to generated electrospun fibers with adequate mechanical and biological properties that are loaded with specific doses of the pharmaceutical drug for a certain therapy. Another opportunity of study is the proposed different taste masking in order to avoid the bad taste of some drugs or polymers. In all these studies, still, biocompatibility, biodegradability, mechanical testing, in vivo efficacy, and pharmacokinetics must be studied. Future work must be focused on the biological response of the tissue, and clinical phases must be performed (Luraghi et al. 2021).

2.6 Conclusions

For all the things discussed, electrospinning is a promising technique for the fabrication of drug delivery systems applied in most of the administration routes such as oral, vaginal, transdermal, ocular, rectal, and nasal tissues. The unique qualities of these drug delivery systems include a large surface area, nanoporosity, high drug encapsulation, and fast disintegration and dissolution properties. The advantages and limitations of various synthetic polymers and natural polymer nanofibers are discussed in the context of producing target drug delivery systems. Also, the bioavailability can be enhanced by exploiting the hydrophilic nature of polymers and their ability to form hydrogen bonds with encapsulated drugs, resulting in uniform distribution of encapsulated molecules throughout the matrices

Table 2.3 Electrospun nanofibers loaded with pharmaceutical drug intended for drug delivery systems

Electrospun fibers	Pharmaceutical drugs	Administration route	Target health condition	Characterization assays	Ref.
Poly(ε-caprolactone) (PCL); poly (3-hydroxybutyric acid-co-3-hydroxyvaleric acid) (PHBV)	Metformin hydrochloride (MH); metoprolol tartrate (MPT)	Oral	(Type 2 diabetes) (control high blood sugar)	Morphology (SEM); surface and thermal properties; in vitro release studies; cytotoxicity using human mesenchymal stem cells	Hu et al. (2015)
Poly(vinyl alcohol) (PVA)	Phloretin	Oral	Oral cancer	XRD; DSC; wetting test; particle characterization of NF dispersion; in vitro release test; antiproliferation assay; apoptosis assay	Nam et al. (2017)
Gelatin	Ciprofloxacin/HP-β-CD inclusion complex	Oral	Bacterial infections	HNMR; FTIR; XRD; TGA; SEM; wetting test; computational methods	Aytac et al. (2019)
Pullulan/chitosan	Aspirin	Oral	Headache and fever	SEM; FTIR-ATR; XRD; TGA-DSC; DMTA; wetting test	Qin et al. (2019)
Poly(vinyl alcohol) and polyethylene oxide; poly(vinyl pyrrolidone) (PVP)	*Lactobacillus paracasei*	Oral	Probiotic	Rheological measurement; SEM; viability test; storage test; dissolution test	Hirscha et al. (2021)
Cellulose acetate phthalate (CAP)	Anti-HIV drug	Vaginal	VIH	ELISA; flow cytometry; molecular modeling	Thakkar and Misra (2017)
Poly(ethylene oxide) and polylactide	Cisplatin	Vaginal	Cervical cancers	SEM; contact angle; release profile; drug distribution; fluorescence; in vivo release and biodistribution	Zong et al. (2015)
Poly(L-lactide acid) (PLLA)	Fluconazole	Vaginal	Vaginal candidiasis	SEM; drug release; FTIR; antimycotic activity; pharmacokinetics studies	Kaur et al. (2016)
Poly(ε-caprolactone)/poly(vinyl pyrrolidone) (PCL/PVP)	Argovit™ silver nanoparticles (Ag-Si/Al_2O_3) sorbents	Transdermal	Skin burns and ulcers	SEM; FTIR; TGA; DSC; cytotoxicity assay; antimicrobial assay; degradation rate	Álvarez-Suárez et al. (2020)

(continued)

Table 2.3 (continued)

Electrospun fibers	Pharmaceutical drugs	Administration route	Target health condition	Characterization assays	Ref.
Chitosan-phospholipids	Curcumin, diclofenac, and vitamin B12	Transdermal	Inflammation	FTIR; DLS; degradation rate; cytotoxicity studies; fluorescence microscopy; release rate	Mendes et al. (2016)
Poly(vinyl pyrrolidone) (PVP)/hyaluronic acid (HA)	Ferulic acid (FA) and t ε-polylysine (ε-PL)	Ocular	Sclera/conjunctiva	SEM; release rate; antimicrobial activity; cytotoxicity studies	Grimaudo et al. (2020)
Gellan gum/pullulan	Fluorescein (as model)	Ocular	Eye diseases	Rheological studies; XRD; SEM	Göttel et al. (2020)
Poly(ε- caprolactone) (PCL)	Dexamethasone acetate	Ocular	Retinal diseases	FTIR; SEM; OCT; cytotoxicity studies; in vivo testing; release rate	Da Silva et al. (2019)
PuraMatrix	Peptide hydrogels	Rectal	Lymphorrhea following pelvic surgery	Clinical trials	Kondo et al. (2014)
Poly(vinyl alcohol) (PVA)	Ciprofloxacin	Rectal	Antimicrobial	SEM; DSC; drug entrapment efficiency; degree of swelling; solubility study; in vitro drug release studies; ex vivo permeability study	Modgill et al. (2016)
Poly(lactic-co-glycolic acid) (PLGA)	Mometasone furoate	Nasal	Chronic rhinosinusitis	SEM; TGA; XRD; DSC; release rate	Rivelli et al. (2021)
Supramolecular peptides	Influenza peptide epitope	Nasal	Influenza	TEM; in vivo release; influenza virus challenge; nanofiber uptake and presentation; evaluation of inflammation in the lung; IFN-γ ELISPOT assay; in vivo cytotoxicity assay; real-time quantitative PCR; tissue-resident T cell staining and flow cytometry	Si et al. (2018)

DLS diffraction light scattering, *DSC* differential scanning calorimetry, *DMTA* dynamic mechanical thermal analysis, *FTIR* Fourier transform infrared spectroscopy, *HNMR* hydrogen nuclear magnetic resonance, *OCT* optical coherence tomography, *SEM* scanning electron microscopy, *TEM* transmission electron microscopy, *TGA* thermogravimetric analysis, *XRD* X-ray diffraction

Fig. 2.4 Electrospun nanofibers applied for drug delivery system scientific papers included in PubMed (PubMed, 2022, accessed March 18, 2022)

and providing the formulation with rapid dissolution abilities. The electrospinning scale-up approach is based on the Taylor cone multiplication concept, which increases fiber productivity. In this manner, the number of liquid jets departing the solution can be increased, enabling production through either multiple nozzles or free surface technologies; all electrospinning variations pretend to optimize the loading condition of specific molecules with special requirements and conditions. Although much literature can be found, most of them still test these systems just for in vitro approaches. But in vivo and clinical trials are still poor.

References

Aggarwal U, Goyal AK, Rath G (2017) Development and characterization of the cisplatin loaded nanofibers for the treatment of cervical cancer. Mater Sci Eng C Mater Biol Appl 75:125–132. https://doi.org/10.1016/j.msec.2017.02.013

Aguirre-Chagala YE, Altuzar V, León-Sarabia E, Tinoco-Magaña JC, Yañez-Limón JM, Mendoza-Barrera C (2017) Physicochemical properties of polycaprolactone/collagen/elastin nanofibers fabricated by electrospinning. Mater Sci Eng C Mater Biol Appl 76:897–907. https://doi.org/10.1016/j.msec.2017.03.118

Alhalawani AMF, Curran DJ, Boyd D, Towler MR (2016) The role of poly (acrylic acid) in conventional glass polyalkenoate cements. J Polym Eng 36(3):221–237. https://doi.org/10.1515/polyeng-2015-0079

Álvarez-Suárez AS, Dastager SG, Bogdanchikova N, Grande D, Pestryakov A, García-Ramos JC, Pérez-González GL, Juárez-Moreno K, Toledano-Magaña Y, Smolentseva E, Paz-González JA, Popova T, Rachkovskaya L, Nimaev V, Kotlyarova A, Korolev M, Letyagin A, Villarreal-Gómez LJ (2020) Electrospun fibers and sorbents as a possible basis for effective composite wound dressings. Micromachines (Basel) 11(4):441. https://doi.org/10.3390/mi11040441

Aytac Z, Ipek S, Erol I, Durgun E, Uyar T (2019) Fast-dissolving electrospun gelatin nanofibers encapsulating ciprofloxacin/cyclodextrin inclusion complex. Colloids Surf B: Biointerfaces 178:129–136. https://doi.org/10.1016/j.colsurfb.2019.02.059

Badgar K, Prokisch J (2021) Elemental selenium enriched nanofiber production. Molecules 26(21):6457. https://doi.org/10.3390/molecules26216457

Ball C, Woodrow KA (2014) Electrospun solid dispersions of Maraviroc for rapid intravaginal preexposure prophylaxis of HIV. Antimicrob Agents Chemother 58(8):4855–4865. https://doi.org/10.1128/AAC.02564-14

Balusamy B, Celebioglu A, Senthamizhan A, Uyar T (2020) Progress in the design and development of "fast-dissolving" electrospun nanofibers-based drug delivery systems-a systematic review. J Control Re2lease 326:482–509. https://doi.org/10.1016/j.jconrel.2020.07.038

Bardoňová L, Kotzianová A, Skuhrovcová K, Židek O, Vágnerová H, Kulhánek J, Hanová T, Knor M, Starigazdová J, Mamulová Kutláková K, Velebný V (2022) Effects of emulsion, dispersion, and blend electrospinning on hyaluronic acid nanofibers with incorporated antiseptics. Int J Biol Macromol 194:726–735. https://doi.org/10.1016/j.ijbiomac.2021.11.118

Bavatharani C, Chokkiah B, Eswaran M, Wabaidur SM, Alothman ZB, Al-Sheetan KM, AL-Anazy M, Ragupathy D (2021) Electrospinning technique for production of polyaniline nanocomposites/nanofibres for multi-functional applications: a review. Synth Met 271:116609. https://doi.org/10.1016/j.synthmet.2020.116609

Birer M, Acartürk F (2021) Electrospun orally disintegrating film formulation of telmisartan. Pharm Dev Technol 26(6):661–672. https://doi.org/10.1080/10837450.2021.1916031

Chen W, Zheng D, Chen Y, Ruan H, Zhang Y, Chen X, Shen H, Deng L, Cui W, Chen H (2021) Electrospun fibers improving cellular respiration via mitochondrial protection. Small 17(46): e2104012. https://doi.org/10.1002/smll.202104012

Cornejo-Bravo JM, Villarreal-Gómez LJ, Serrano A (2016) Electrospinning for drug delivery systems: drug incorporation techniques. In: Haider S, Haider A (eds) Electrospinning - material, techniques, and biomedical applications. IntechOpen, London. https://doi.org/10.5772/65939

Costoya A, Concheiro A, Alvarez-Lorenzo C (2017) Electrospun fibers of cyclodextrins and poly (cyclodextrins). Molecules 22(2):230. https://doi.org/10.3390/molecules22020230

Da Silva GR, Lima TH, Fernandes-Cunha GM, Oréfice RL, Da Silva-Cunha A, Zhao M, Behar-Cohen F (2019) Ocular biocompatibility of dexamethasone acetate loaded poly(ε-caprolactone) nanofibers. Eur J Pharm Biopharm 142:20–30. https://doi.org/10.1016/j.ejpb.2019.05.010

Dahmash EZ, Iyire A, Alyami HS (2021) Development of orally dissolving films for pediatric-centric administration of anti-epileptic drug topiramate–a design of experiments (DoE) study. Saudi Pharm J 29(7):635–647. https://doi.org/10.1016/j.jsps.2021.04.025

Dodero A, Schlatter G, Hébraud A, Vicini S, Castellano M (2021) Polymer-free cyclodextrin and natural polymer-cyclodextrin electrospun nanofibers: a comprehensive review on current applications and future perspectives. Carbohydr Polym 264:118042. https://doi.org/10.1016/j.carbpol.2021.118042

Dumitriu RP, Stoleru E, Mitchell GR, Vasile C, Brebu M (2021) Bioactive electrospun fibers of poly (ε-caprolactone) incorporating α-tocopherol for food packaging applications. Molecules 26(18):5498. https://doi.org/10.3390/molecules26185498

Gao S, Li X, Yang G, Feng W, Zong L, Zhao L, Ye F, Fu Y (2022) Antibacterial perillaldehyde/hydroxypropyl-γ-cyclodextrin inclusion complex electrospun polymer-free nanofiber: improved water solubility, thermostability, and antioxidant activity. Ind Crop Prod 176: 114300. https://doi.org/10.1016/j.indcrop.2021.114300

Göttel B, de Souza E, Silva JM, Santos de Oliveira C, Syrowatka F, Fiorentzis M, Viestenz A, Viestenz A, Mäder K (2020) Electrospun nanofibers - a promising solid in-situ gelling alternative for ocular drug delivery. Eur J Pharm Biopharm 146:125–132. https://doi.org/10.1016/j.ejpb.2019.11.012

Grimaudo MA, Concheiro A, Alvarez-Lorenzo C (2020) Crosslinked hyaluronan electrospun nanofibers for ferulic acid ocular delivery. Pharmaceutics 12(3):274. https://doi.org/10.3390/pharmaceutics12030274

Gupta MS, Kumar TP, Gowda DV (2021) Orodispersible films: conception to quality by design. Adv Drug Deliv Rev 178:113983. https://doi.org/10.1016/j.addr.2021.113983

Han D, Steckl AJ (2019) Coaxial electrospinning formation of complex polymer fibers and their applications. ChemPlusChem 84(10):1453–1497. https://doi.org/10.1002/cplu.201900281

He M, Zhu L, Yang N, Li H, Yang Q (2021) Recent advances of oral film as platform for drug delivery. Int J Pharm 604:120759. https://doi.org/10.1016/j.ijpharm.2021.120759

Hirscha E, Pantea E, Vass P, Domján J, Molnár M, Suhajda Á, Adnersen SK, Vigh T, Verreck G, Morosi GJ, Nagy ZK (2021) Probiotic bacteria stabilized in orally dissolving nanofibers prepared by high-speed electrospinning. Food Bioprod Process 128:84–94. https://doi.org/10.1016/j.fbp.2021.04.016

Hu J, Prabhakaran MP, Tian L, Ding X, Ramakrishna S (2015) Drug-loaded emulsion electrospun nanofibers: characterization, drug release and *in vitro* biocompatibility. RSC Adv 5(21): 100256–100267. https://doi.org/10.1039/C5RA18535A

Huang A, Liu F, Cui Z, Wang H, Song X, Geng L, Wang H, Peng X (2021) Novel PTFE/CNT composite nanofiber membranes with enhanced mechanical, crystalline, conductive, and dielectric properties fabricated by emulsion electrospinning and sintering. Compos Sci Technol 214: 108980. https://doi.org/10.1016/j.compscitech.2021.108980

Kaur R, Garg T, Goyal AK, Rath G (2016) Development, optimization and evaluation of electrospun nanofibers: tool for targeted vaginal delivery of antimicrobials against urinary tract infections. Curr Drug Deliv 13(5):754–763. https://doi.org/10.2174/1567201812666150212123348

Khoshnevisan K, Maleki H, Samadian H, Shahsavari S, Sarrafzadeh MH, Larijani B, Dorkoosh FA, Haghpanah V, Khorramizadeh MR (2018) Cellulose acetate electrospun nanofibers for drug delivery systems: applications and recent advances. Carbohydr Polym 198:131–141. https://doi.org/10.1016/j.carbpol.2018.06.072

Kondo Y, Nagasaka T, Kobayashi S, Kobayashi N, Fujiwara T (2014) Management of peritoneal effusion by sealing with a self-assembling nanofiber polypeptide following pelvic surgery. Hepatogastroenterology 61:49–353. http://ousar.lib.okayama-u.ac.jp/metadata/51449

Kopp A, Smeets R, Gosau M, Kröger N, Fuest S, Köpf M, Kruse M, Krieger J, Rutkowski R, Henningsen A, Burg S (2020) Effect of process parameters on additive-free electrospinning of regenerated silk fibroin nonwovens. Bioact Mater 5(2):241–252. https://doi.org/10.1016/j.bioactmat.2020.01.010

Kurakula M, Rao G (2020) Pharmaceutical assessment of polyvinylpyrrolidone (PVP): as excipient from conventional to controlled delivery systems with a spotlight on COVID-19 inhibition. J Drug Deliv Sci Technol 60:102046. https://doi.org/10.1016/j.jddst.2020.102046

Li J, Pan H, Ye Q, Shi C, Zhang X, Pan WS (2020) Carvedilol-loaded polyvinylpyrrolidone electrospun nanofiber film for sublingual delivery. J Drug Deliv Sci Technol 58:101726. https://doi.org/10.1016/j.jddst.2020.101726

Liu H, Zhou Z, Lin H, Wu J, Ginn B, Choi JS, Jiang X, Chung L, Elisseeff JH, Yiu S, Mao HQ (2018) Synthetic nanofiber-reinforced amniotic membrane via interfacial bonding. ACS Appl Mater Interfaces 10(17):14559–14569. https://doi.org/10.1021/acsami.8b03087

Lu Y, Huang J, Yu G, Cardenas R, Wei S, Wujcik EK, Guo Z (2016) Coaxial electrospun fibers: applications in drug delivery and tissue engineering. Wiley Interdiscip Rev Nanomed Nanobiotechnol 8(5):654–677. https://doi.org/10.1002/wnan.1391

Luraghi A, Peri F, Moroni L (2021) Electrospinning for drug delivery applications: a review. J Control Release 334:463–484. https://doi.org/10.1016/j.jconrel.2021.03.033

Maleki Dizaj S, Sharifi S, Jahangiri A (2019) Electrospun nanofibers as versatile platform in antimicrobial delivery: current state and perspectives. Pharm Dev Technol 24(10):1187–1199. https://doi.org/10.1080/10837450.2019.1656238

Mehdi M, Hussain S, Gao BB, Shah KA, Mahar FK, Yousif M, Hussain S, Ahmed F (2021) Fabrication and characterization of rizatriptan loaded pullulan nanofibers as oral fast-dissolving drug system. Mater Res Express 8(5):055404. https://doi.org/10.1088/2053-1591/abff0b

Mendes AC, Gorzelanny C, Halter N, Schneider SW, Chronakis IS (2016) Hybrid electrospun chitosan-phospholipids nanofibers for transdermal drug delivery. Int J Pharm 510(1):48–56. https://doi.org/10.1016/j.ijpharm.2016.06.016

Meng ZX, Xu XX, Zheng W, Zhou HM, Li L, Zheng YF, Lou X (2011) Preparation and characterization of electrospun PLGA gelatin nanofibers as a potential drug delivery system. Colloids Surf B: Biointerfaces 84(1):97–102. https://doi.org/10.1016/j.colsurfb.2010.12.022

Modgill V, Garg T, Goyal AK, Rath G (2016) Permeability study of ciprofloxacin from ultra-thin nanofibrous film through various mucosal membranes. Artif Cells Nanomed Biotechnol 44(1): 122–127. https://doi.org/10.3109/21691401.2014.924007

Mohammadinejad R, Madamsetty VS, Kumar A, Verzandeh M, Dehshahri A, Zarrabi A, Sharififar F, Mahammadi M, Fahimipour A, Ramakrishna S (2021) Electrospun nanocarriers

for delivering natural products for cancer therapy. Trends Food Sci Technol 118:887–904. https://doi.org/10.1016/j.tifs.2021.10.007

Moreira A, Lawson D, Onyekuru L, Dziemidowicz K, Angkawinitwong U, Costa PF, Radacsi N, Williams GR (2021) Protein encapsulation by electrospinning and electrospraying. J Control Release 329:1172–1197. https://doi.org/10.1016/j.jconrel.2020.10.046

Nam S, Lee SY, Cho HJ (2017) Phloretin-loaded fast dissolving nanofibers for the locoregional therapy of oral squamous cell carcinoma. J Colloid Interface Sci 508:112–120. https://doi.org/10.1016/j.jcis.2017.08.030

Nguyen J, Stwodah RM, Vasey CL, Rabatin BE, Atherton B, D'Angelo PA, Swana KW, Tang C (2020) Thermochromic fibers via electrospinning. Polymers (Basel) 12(4):842. https://doi.org/10.3390/polym12040842

Niemczyk-Soczynska B, Gradys A, Sajkiewicz P (2020) Hydrophilic surface functionalization of electrospun nanofibrous scaffolds in tissue engineering. Polymers (Basel) 12(11):2636. https://doi.org/10.3390/polym12112636

Özakar RS, Özakar E (2021) Current overview of oral thin films. Turk J Pharm Sci 18(1):111–121. https://doi.org/10.4274/tjps.galenos.2020.76390

Pacheco MS, Barbieri D, da Silva CF, de Moraes MA (2021) A review on orally disintegrating films (ODFs) made from natural polymers such as pullulan, maltodextrin, starch, and others. Int J Biol Macromol 178:504–513. https://doi.org/10.1016/j.ijbiomac.2021.02.180

Palo M, Rönkönharju S, Tiirik K, Viidik L, Sandler N, Kogermann K (2019) Bi-layered polymer carriers with surface modification by electrospinning for potential wound care applications. Pharmaceutics 11(12):678. https://doi.org/10.3390/pharmaceutics11120678

Pérez-González GL, Cornejo-Bravo JM, Vera-Graciano R, Adan-López ES, Villarreal-Gómez LJ (2022) Development, characterization, and *in vitro* evaluation of adhesive fibrous mat for mucosal propranolol delivery. E-Polymers 22(1):58–68. https://doi.org/10.1515/epoly-2022-0002

Pérez-González GL, Villarreal-Gómez LJ, Serrano-Medina A, Torres-Martínez EJ, Cornejo-Bravo JM (2019) Mucoadhesive electrospun nanofibers for drug delivery systems: applications of polymers and the parameters' roles. Int J Nanomedicine 14:5271–5285. https://doi.org/10.2147/IJN.S193328

Qin ZY, Jia XW, Liu Q, Kong BH, Wang H (2019) Fast dissolving oral films for drug delivery prepared from chitosan/pullulan electrospinning nanofibers. Int J Biol Macromol 137:224–231. https://doi.org/10.1016/j.ijbiomac.2019.06.224

Rafiei M, Jooybar E, Abdekhodaie MJ, Alvi M (2020) Construction of 3D fibrous PCL scaffolds by coaxial electrospinning for protein delivery. Mater Sci Eng C Mater Biol Appl 113:110913. https://doi.org/10.1016/j.msec.2020.110913

Rampichová M, Košťáková Kuželová E, Filová E, Chvojka J, Šafka J, Pelcl M, Daňková J, Prosecká E, Buzgo M, Plencner M, Lukáš D, Amler E (2018) Composite 3D printed scaffold with structured electrospun nanofibers promotes chondrocyte adhesion and infiltration. Cell Adh Migr 12(3):271–285. https://doi.org/10.1080/19336918.2017.1385713

Rivelli GG, Perez AC, Silva PHR, Gomes ECL, Moreira CPS, Tamashiro E, Valera FCP, Anselmo-Lima WT, Pianetti GA, Silva-Cunha A (2021) Biodegradable electrospun nanofibers: a new approach for rhinosinusitis treatment. Eur J Pharm Sci 163:105852. https://doi.org/10.1016/j.ejps.2021.105852

Rostamabadi H, Assadpour E, Tabarestani HS, Falsafi SR, Jafari SM (2020) Electrospinning approach for nanoencapsulation of bioactive compounds; recent advances and innovations. Trends Food Sci Technol 100:190–209. https://doi.org/10.1016/j.tifs.2020.04.012

Shahriar SMS, Mondal J, Hasan MN, Revuri V, Lee DY, Lee YK (2019) Electrospinning nanofibers for therapeutics delivery. Nanomaterials (Basel) 9(4):532. https://doi.org/10.3390/nano9040532

Si Y, Wen Y, Kelly SH, Chong AS, Collier JH (2018) Intranasal delivery of adjuvant-free peptide nanofibers elicits resident CD8+ T cell responses. J Control Release 282:120–130. https://doi.org/10.1016/j.jconrel.2018.04.031

Sofi HS, Abdal-Hay A, Ivanovski S, Zhang YS, Sheikh FA (2020) Electrospun nanofibers for the delivery of active drugs through nasal, oral and vaginal mucosa: current status and future perspectives. Mater Sci Eng C Mater Biol Appl 111:110756. https://doi.org/10.1016/j.msec.2020.110756

Sóti PL, Weiser D, Vigh T, Nagy ZK, Poppe L, Marosi G (2016) Electrospun polylactic acid and polyvinyl alcohol fibers as efficient and stable nanomaterials for immobilization of lipases. Bioprocess Biosyst Eng 39(3):449–459. https://doi.org/10.1007/s00449-015-1528-y

Szewczyk PK, Stachewicz U (2020) The impact of relative humidity on electrospun polymer fibers: from structural changes to fiber morphology. Adv Colloid Interf Sci 286:102315. https://doi.org/10.1016/j.cis.2020.102315

Thakkar S, Misra M (2017) Electrospun polymeric nanofibers: new horizons in drug delivery. Eur J Pharm Sci 107:148–167. https://doi.org/10.1016/j.ejps.2017.07.001

Tipduangta P, Belton P, Fábián L, Wang LY, Tang H, Eddleston M, Qi S (2016) Electrospun polymer blend nanofibers for tunable drug delivery: the role of transformative phase separation on controlling the release rate. Mol Pharm 13(1):25–39. https://doi.org/10.1021/acs.molpharmaceut.5b00359

Toprak Ö, Topuz B, Monsef YA, Oto Ç, Orhan K, Karakeçili A (2021) BMP-6 carrying metal organic framework-embedded in bioresorbable electrospun fibers for enhanced bone regeneration. Mater Sci Eng C Mater Biol Appl 120:111738. https://doi.org/10.1016/j.msec.2020.111738

Toriello M, Afsari M, Shon HK, Tijing LD (2020) Progress on the fabrication and application of electrospun nanofiber composites. Membranes (Basel) 10(9):204. https://doi.org/10.3390/membranes10090204

Torres-Martínez EJ, Cornejo-Bravo JM, Serrano-Medina A, Pérez-González GL, Villarreal-Gómez LJ (2018) A summary of electrospun nanofibers as drug delivery system: drugs loaded and biopolymers used as matrices. Curr Drug Deliv 15:1360–1374. https://doi.org/10.2174/1567201815666180723114326

Torres-Martínez EJ, Pérez-González GL, Serrano-Medina A, Grande D, Vera-Graziano R, Cornejo-Bravo JM, Villarreal-Gómez LJ (2019) Drugs loaded into electrospun polymeric nanofibers for delivery. J Pharm Pharm Sci 22(1):313–331. https://doi.org/10.18433/jpps29674

Torres-Martínez EJ, Vera-Graziano R, Cervantes-Uc J, Bogdanchikova N, Olivas-Sarabia A, Valdez-Castro R, Serrano-Medina A, Iglesias A, Pérez-González G, Cornejo-Bravo J, Villarreal-Gómez L (2020) Preparation and characterization of electrospun fibrous scaffolds of either PVA or PVP for fast release of sildenafil citrate. E-Polymers 20(1):746–758. https://doi.org/10.1515/epoly-2020-0070

Uhljar LÉ, Kan SY, Radecsi N, Koutsos V, Szabó-Révész P, Ambrus R (2021) *In vitro* drug release, permeability, and structural test of ciprofloxacin-loaded nanofibers. Pharmaceutics 13(4):556. https://doi.org/10.3390/pharmaceutics13040556

Vass P, Szabó E, Domokos A, Hirsch E, Galata D, Farkas B, Démuth B, Andersen SK, Vigh T, Verreck G, Marosi G, Nagy ZK (2020) Scale-up of electrospinning technology: applications in the pharmaceutical industry. Wiley Interdiscip Rev Nanomed Nanobiotechnol 12(4):e1611. https://doi.org/10.1002/wnan.1611

Velasco-Barraza RD, Álvarez-Suárez AS, Villarreal-Gómez LJ, Páz-González JA, Iglesias AL, Vera-Graziano R (2016) Designing a low-cost electrospinning device for practical learning in a bioengineering biomaterials course. Rev Mex Ing Biomed 37(1):7–16. https://doi.org/10.17488/RMIB.37.1.1

Villarreal-Gómez LJ, Cornejo-Bravo JM, Vera-Graziano R, Grande D (2016) Electrospinning as a powerful technique for biomedical applications: a critically selected survey. J Biomater Sci Polym Ed 27(2):157–176. https://doi.org/10.1080/09205063.2015.1116885

Villarreal-Gómez LJ, Pérez-González GL, Bogdanchikova N, Pestryakov A, Nimaev V, Soloveva A, Cornejo-Bravo JM, Toledaño-Magaña Y (2021) Antimicrobial effect of electrospun nanofibers loaded with silver nanoparticles: influence of Ag incorporation method. J Nanomater 2021:e9920755. https://doi.org/10.1155/2021/9920755

Villarreal-Gómez LJ, Vera-Graziano R, Vega-Rios MR, Pineda-Camacho JL, Mier-Maldonado PA, Almanza-Reyes H, Mier-Maldonado PA, Cornejo-Bravo JM (2014) Biocompatibility evaluation of electrospun scaffolds of poly(L-lactide) with pure and grafted hydroxyapatite. J Mex Chem Soc 58:435–443. http://www.scielo.org.mx/scielo.php?script=sci_arttext&pid=S1870-249X2014000400010&lng=es&tlng=en

Wang Y, Deng Z, Wang X, Shi Y, Lu Y, Fang S, Liang X (2021) Formononetin/methyl-β-cyclodextrin inclusion complex incorporated into electrospun polyvinyl-alcohol nanofibers: enhanced water solubility and oral fast-dissolving property. Int J Pharm 603:120696. https://doi.org/10.1016/j.ijpharm.2021.120696

Williams GR, Chatterton NP, Nazir T, Yu DG, Zhu LM, Branford-White CJ (2012) Electrospun nanofibers in drug delivery: recent developments and perspectives. Ther Deliv 3(4):515–533. https://doi.org/10.4155/tde.12.17

Xu C, Ma J, Wang W, Liu Z, Gu L, Qian L, Hou J, Jiang Z (2022) Preparation of pectin-based nanofibers encapsulating *Lactobacillus rhamnosus* 1.0320 by electrospinning. Food Hydrocoll 124:107216. https://doi.org/10.1016/j.foodhyd.2021.107216

Xu X, Liu Y, Fu W, Yao M, Ding Z, Xuan J, Li D, Wang S, Xia Y, Cao M (2020) Poly(N-isopropylacrylamide)-based thermoresponsive composite hydrogels for biomedical applications. Polymers 12(3):580. https://doi.org/10.3390/polym12030580

Yan W, Miao D, Babar AA, Zhao J, Jia Y, Ding B, Wang X (2020) Multi-scaled interconnected inter- and intra-fiber porous janus membranes for enhanced directional moisture transport. J Colloid Interface Sci 565:426–435. https://doi.org/10.1016/j.jcis.2020.01.063

Yang X, Li K, Zhang X, Liu C, Guo B, Wen W, Gao X (2018) Nanofiber membrane supported lung-on-a-chip microdevice for anti-cancer drug testing. Lab Chip 18(3):486–495. https://doi.org/10.1039/c7lc01224a

Zhang L, Huang J, Si T, Xu RX (2012) Coaxial electrospray of microparticles and nanoparticles for biomedical applications. Expert Rev Med Devices 9(6):595–612. https://doi.org/10.1586/erd.12.58

Zhang X, Xie L, Wang X, Shao Z, Kong B (2021) Electrospinning super-assembly of ultrathin fibers from single- to multi-Taylor cone sites. Appl Mater Today 26:101272. https://doi.org/10.1016/j.apmt.2021.101272

Zong S, Wang X, Yang Y, Wu W, Li H, Ma Y, Lin W, Sun T, Huang Y, Xie Z, Yue Y, Liu S, Jing X (2015) The use of cisplatin-loaded mucoadhesive nanofibers for local chemotherapy of cervical cancers in mice. Eur J Pharm Biopharm 93:127–135. https://doi.org/10.1016/j.ejpb.2015.03.029

Chapter 3
Melt Electrospinning and Electrowriting for Pharmaceutical and Biomedical Applications

María del Carmen De Lama-Odría, Luis J. del Valle, and Jordi Puiggalí

Abstract Melt electrospinning and electrowriting are eco-friendly and solvent-free processes able to produce fibrous membranes for different industrial applications. These processes have clear advantages over conventional solution electrospinning but have also different challenges that still need to be solved. This chapter starts with a brief presentation of melt electrospinning techniques with the explanation of essential parameters that allow to control the process. Attention is also given to the effect caused by the incorporation of additives together with the benefits caused by blending and composite preparations. Nevertheless, the main goal corresponds to the explanation and discussion of scaffolds with interest in the biomedical/pharmaceutical fields, covering both tissue regeneration and drug delivery applications.

Keywords Melt electrospinning · Melt electrowriting · Tissue regeneration · Drug delivery · Scaffolds · Porous membranes · Micro and nanofibers

3.1 Introduction

An exponential growth of the research field concerning the development of scaffolds for tissue engineering has been produced in the two last decades. This scientific production has shined a light on four fundamental requirements that scaffolds have to satisfy: form, function, formation, and fixation. Briefly, form refers to the 3D

M. del C. De Lama-Odría
Departament d'Enginyeria Química, Universitat Politècnica de Catalunya, EEBE, Barcelona, Spain
e-mail: maria.de.lama@upc.edu

L. J. del Valle · J. Puiggalí (✉)
Departament d'Enginyeria Química, Universitat Politècnica de Catalunya, EEBE, Barcelona, Spain

Barcelona Research Center in Multiscale Science and Engineering, Universitat Politècnica de Catalunya, Barcelona, Spain
e-mail: luis.javier.del.valle@upc.edu; jordi.puiggali@upc.edu

D. Lamprou (ed.), *Nano- and Microfabrication Techniques in Drug Delivery*,
Advanced Clinical Pharmacy – Research, Development and Practical Applications 2,
https://doi.org/10.1007/978-3-031-26908-0_3

defect in the target tissue that the scaffold must initially fill. Function means that the scaffold can support the mechanical demands. The formation fundament implies that the scaffold can deliver factors that will promote tissue regeneration and that can act as an appropriate mass-transport environment. Finally, fixation describes the simplicity of the scaffold implantation and attachment to the surrounding tissue margins of the defect (Hollister 2009).

Based on the explained fundaments, polymeric materials are normally selected for scaffold designs because of their biocompatibility, their tunability, and the possibility of developing 3D constructs with the desired shape and capability to reflect the tissue structure and the metabolic demand. The same trend is evidenced in the pharmaceutical research. While new bio-therapeutic agents like proteins, peptides, and nucleic acids are still employed, the polymeric materials are being carefully chosen to optimize the delivery systems, protect the active molecules from degradations, establish a specific release rate, and even attempt the design of scaffolds that can trigger a drug release based on environmental changes, such as pH, oxidation, or enzyme concentration (Davoodi et al. 2018).

In this scenario, electrospinning has been widely used for the elaboration of pharmaceutical systems and scaffolds for biomedical applications (Lian and Meng 2017a). Among the variety of electrospinning techniques, melt electrospinning (MES) presents a series of advantages. Thus, the absence of solvents reduces the production cost as post-processing of scaffolds for their extraction is not required (Brown et al. 2016). The lack of organic solvents also represents a biological advantage as biocompatibility can be expected. Moreover, three-dimensional nanofibrous structures with a range of pore sizes can be created, optimizing cell invasion and vascularization of the tissue (Lokmic and Mitchell 2008).

In order to improve the control of the fiber deposition in a micron to submicron level, MES can be further developed into melt electrospinning writing (MEW). Like fused deposition modeling, scaffolds are predesigned with a computer software and then produced by electrospinning in a layer-by-layer manner. However, unlike additive techniques, a continuous flow of the extrusion material is required during printing. A high level of design that allows full control of crosshatch, gradient porosity, and tubular configuration is not feasible. The improvement of the software will approach the MEW technique to the clinic, enabling the production of patient-specific scaffold configurations (Paxton et al. 2020).

Drug loading and release are also benefited from these techniques. First, the loading of water-poor soluble molecules can be achieved (Lian and Meng 2017a). Second, during the release, the burst effect can be prevented, and the rate can be decreased (Bachs-Herrera et al. 2021). Furthermore, MES and MEW facilitate changes in the geometry and architecture of the delivery systems, making a transition from release profiles controlled by diffusion mechanism, degradation of the polymeric particles, or surface erosion to a tunable profile (Davoodi et al. 2018).

The main goal of the present review is to describe the recent advances in the application of MES and MEW for the elaboration of scaffolds for tissue regeneration and pharmaceutical systems. Simultaneously, the limitations of the techniques in each field and the potential methods to overcome them are summarized in detail as their effects in the produced scaffolds are described.

3.2 Melt Electrospinning Parameters and Methodologies

Conventional electrospinning is based on the application of a high electrical field to a polymer solution droplet that is continuously feed to the end of a capillary tube (e.g., a hypodermic needle with blunt tip). The electrostatic repulsion between surface charges can overcome the surface tension and lead to a Taylor cone and the ejection of a jet toward a grounded target (collector). Multiple filaments are formed from the jet as a consequence of radial charge repulsion, and finally after solvent evaporation, ultrathin fibers can be obtained. The process has a mass transfer step and gives rise to scaffolds constituted by tightly packed layers of fibers. Porosity is mainly restricted to the surface of deposited scaffolds, a feature that appears as a serious limitation for a subsequent cell growth. Great efforts are consequently being addressed to modify the conventional process and get real 3D structures having interconnected pores (i.e., multilayered assembly, template-assisted electrospinning, incorporation of porogen agents, and combination of electrospinning with 3D technologies) (Chainani et al. 2013; Sun et al. 2014; Kim et al. 2008; Sampath Kumar et al. 2018).

MES is a similar process, but in this case, the polymer solution droplets are changed by molten polymer drops. Main differences concern to the high viscosity of the melt, the fact that heat transfer is a fundamental step (Fig. 3.1a), and the requirements for a heat supply to melt the polymer, and a fast cool of the formed jet. Main advantages correspond to the absence of toxic solvents, the great possibility to generate porous 3D structures as a consequence of the usual high diameter of the generated fibers, and the spongy texture of the final scaffold. Nevertheless, the technique is limited by a potential thermal degradation and the difficulty to get an accurate control over morphology (Bachs-Herrera et al. 2021; Brown et al. 2016; Zhang et al. 2016). MEW combines MES with additive manufacturing since the electrospun fibers are deposited onto the collector according to computer-aided designs (Castilho et al. 2017) (Fig. 3.1b, c).

Temperature, applied voltage, flow rate, tip-to-collector distance, and spinneret diameter are the most important parameters that influence MES (Góra et al. 2011; Lyons et al. 2004). Temperature is usually chosen between 10 and 30 °C above the melting point of the polymer. Cautions are necessary to avoid degradation, being in some cases essential in the presence of additives. Applied voltage usually varies between 7 kV and 50 kV and must be selected according to the viscosity and conductivity of the polymer melt. Voltage influences a higher volume of molten polymer drawn from the tip, a higher stretching, and a higher production of secondary jets. Therefore, both the increase and decrease in the fiber diameter can be expected depending on the predominant effect. Flow rate is directly proportional to the fiber diameter and usually ranges between 5 μL/h and 9 mL/h. Tip-to-collector distance has a great relevance for the ability to stretch the polymer and to provide enough time for cooling/solidifying the molted fibers. Fiber diameter decreases when the spinneret hole becomes smaller, but the high viscosity of the molten polymer is a great challenge for the use of small orifices.

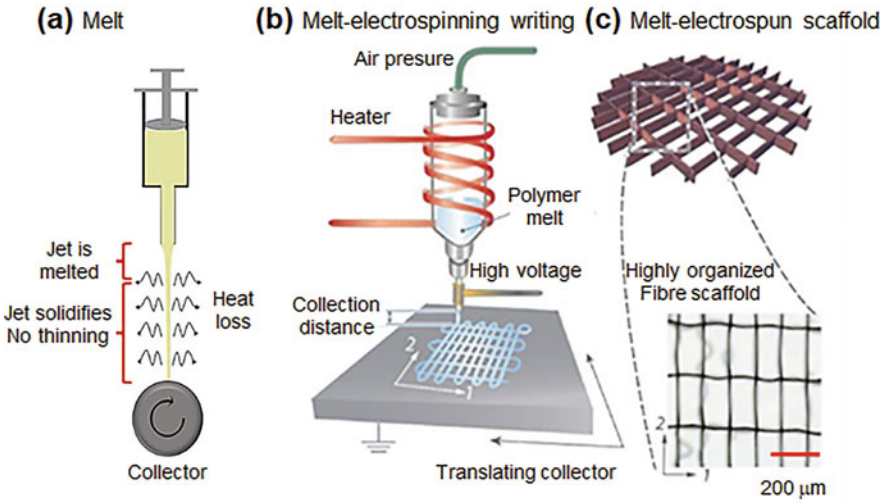

Fig. 3.1 (**a**) Schematics of melt electrospinning showing the heat transfer process (adapted from Morikawa et al. 2019). (**b**) Melt electrowriting showing principal components (dispensing unit; electrical heating system; high-voltage source electrode; and computer-assisted collector plate) and (**c**) schematic of a melt electrospun fiber scaffold (adapted from Castilho et al. 2017)

Figure 3.2 shows different configurations of the MES process. These affect devices that are able to dispense the melt flow (e.g., syringe pumps, air pressure systems, screw extruders and mechanical feed), to initiate the jet (e.g., needle, needleless, gas-assisted and laser), and to heat the sample (e.g., electric system, circulating fluid and even laser).

3.3 Additives for Melt Electrospinning

The use of additives in MES is highly important to overcome different challenges associated with the process: high viscosity of the melt, low electrical conductivity, and high temperature setup. Main studies have been focused on polypropylene due to its high use and great difficulty to get thin (usual diameter are close to 20 μm) and continuous fibers (Nayak et al. 2012). Polyethylene glycol (PEG) and poly(dimethyl siloxane) (PDMS) have been revealed as good additives to reduce viscosity. On the other hand, ionic salts like sodium oleate (SO) and NaCl improve the electrical conductivity in such a way that diameters of 371 and 310 nm could be attained with the incorporation of 7 wt.% and 5 wt.%, respectively (Nayak et al. 2012).

Stearates of mono and divalent metals have been employed to render an effective but moderate diameter decrease (1–5 μm) (Malakhov et al. 2018). Again, these compounds were able to decrease melt viscosity and increase conductivity, being the lower diameter attained with the sodium stearate (SS). Positive and negative ions

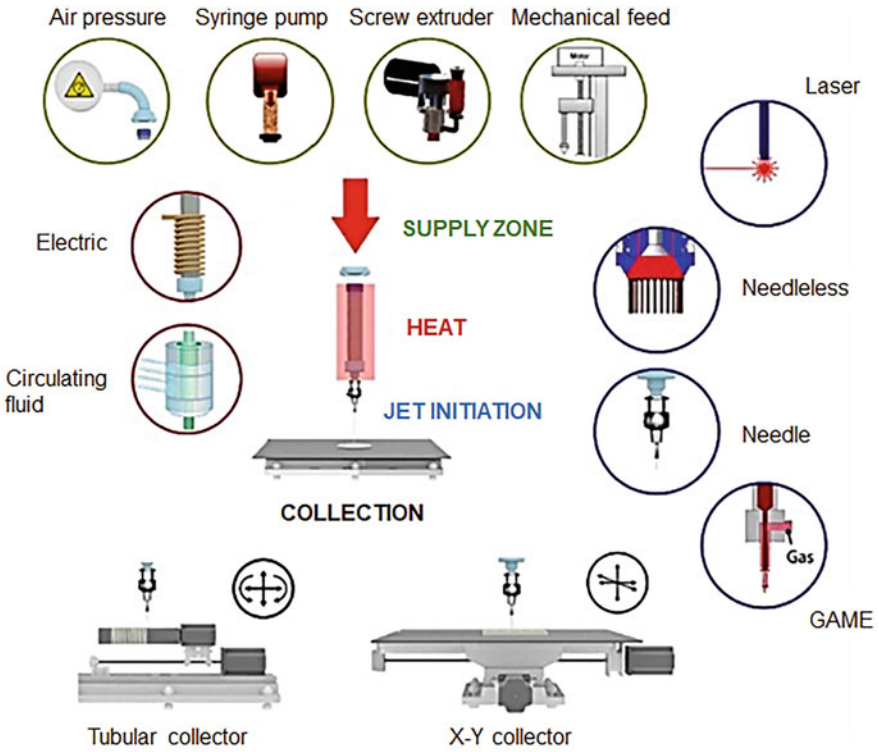

Fig. 3.2 Schematics of various systems for dispensing the melt flow, heating, and initiating the jet. Copyright 2016 Elsevier (Brown et al. 2016)

migrated to opposite directions and gave rise to a strong electric force in the direction of the applied field that facilitated the stretching of the fiber. Diameters as low as 210 nm were attained when an appropriate combination of Irgastat® P, a usual antistatic additive that increases conductivity, SS, and propylene was incorporated (Daenicke et al. 2019). Low molecular weight plasticizers like di-2-ethylhexyl terephthalate were found effective to reduce viscosity of polymethyl methacrylate (PMMA) (i.e., a decrease from 34.0 to 19.7 μm was observed with the incorporation of 40 wt-% of DOTP, a value that could be decreased to 4 μm with the incorporation of KCl) (Wang and Zheng 2009).

Poly(ε-caprolactone) (PCL) is an example of a polymer widely employed for biomedical applications. MES appears as an ideal technique in order to avoid organic and not fully biocompatible solvents that are usually required for solution electrospinning as a consequence of the high polymer hydrophobicity. PCL melt electrospun fibers have quite large diameters (i.e., close to 23 μm) (Piyasin et al. 2019), and consequently the addition of conductive salts is usually required. Logically, these are limited to avoid toxic effects, and specifically NaCl has been mainly used. Thus, diameters close to 3 μm could be attained after the addition of 8 wt.% of

the salt, although a disruption of fiber continuity was also observed. NaCl and SS have also been revealed effective to decrease the fiber diameter of polylactide (PLA), the most commercial bio-based and biodegradable polymer (Koenig et al. 2020).

3.4 Melt Electrospun Nanocomposites and Blends

MES is a suitable technique for the preparation of nanocomposites, but so far it has had limited applications, which mainly concern photothermal conversion systems (i.e., conversion of absorbed light energy to thermal energy, lithium-ion battery separators, and wastewater purification) (Li et al. 2017; Pan et al. 2018; Karahaliloglu et al. 2014). Other significant works differentiated by the type of the incorporated nanoparticles can be mentioned. Incorporation of silica nanoparticles to polyethylene terephthalate provided fibers with excellent mechanical properties and good and chemical thermal stability together with high dye ability (Zhang et al. 2008). Nanohydroxyapatite (nHAp) has successfully been incorporated in melt electrospun poly(L-lactic acid) (PLLA) fibers leading to an increase of hydrophilicity and diameters close to 4.5 μm (Li et al. 2012). PCL/nHAp scaffolds have been directly prepared by a hand-held MES apparatus (Abdal-hay et al. 2018). Membranes based on PCL and Fe_3O_4 magnetic nanoparticles have also been directly deposited onto the surface of tumor tissues for hyperthermia treatment (Fig. 3.3) (Hu et al. 2020). Incorporation of montmorillonites to electrospun nylon 6 fibers allowed to increase the resulting Young modulus by a factor of 2 and a significant increase of conductivity by a factor of 4 (Malakhov et al. 2016).

Polymer blending is an efficient way to tune properties and in general to improve the final performance of a material. Usually, blends are immiscible, and, consequently, processing becomes complex due to the different viscoelastic behavior of the involved components (Van Puyvelde et al. 2008). Unfortunately, scarce works have been addressed to the comprehension of the MES of polymer blends. Interesting studied systems correspond to blends of PCL and PEG-*b*-PCL (Van Puyvelde et al. 2008) and PLA/PEG (Haroosh and Dong 2015; Nazari and Garmabi 2018). Phase separation could render core/shell fibrous morphologies depending on component and specific composition as reported for blends of isotactic polypropylene (i-PP) and the styrene-acrylonitrile copolymer (Cao et al. 2013).

3.5 General Applications of Melt Electrospinning

Several applications of MES deserve to be briefly commented in addition to the biomedical applications that will then be explained later. Food packaging and filtration and separation processes are probably the areas where MES have a higher potential.

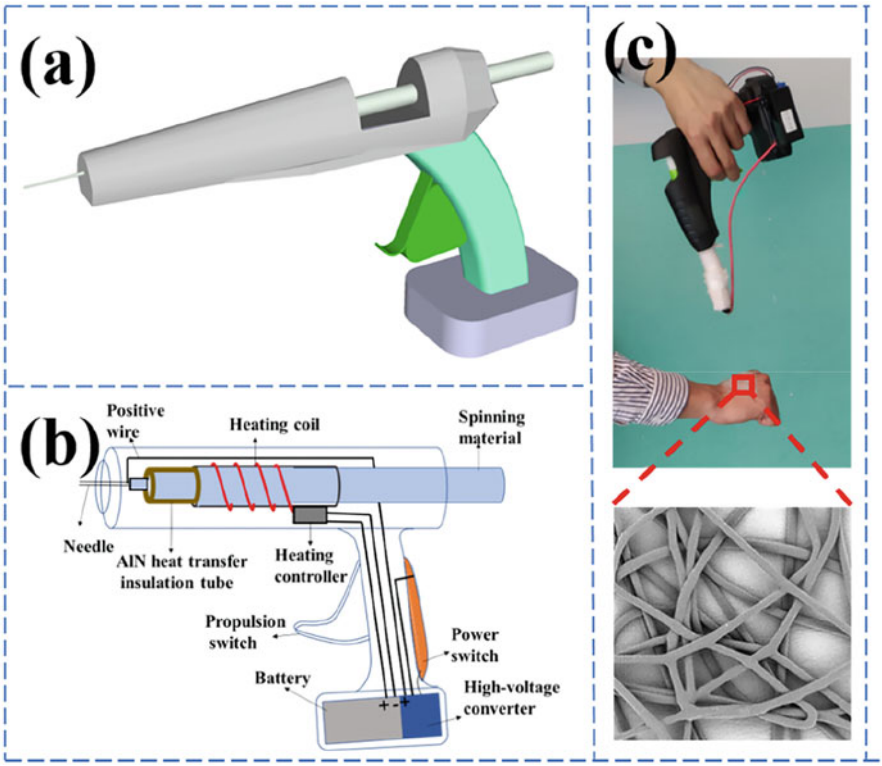

Fig. 3.3 Schemes showing a hand-held melt electrospinning apparatus (**a**, **b**), in situ deposition, and typical electrospun scaffold (**c**). Copyright 2020 Elsevier (Hu et al. 2020)

MES is able to load easily active agents that can be released as a response to environmental conditions. In this way, active (i.e., by incorporating compounds able to control moisture, to enhance barrier properties, to act as oxygen scavengers, or to provide antimicrobial and antifungal properties) and smart (i.e., compounds able to act as temperature sensors) packaging systems can be developed (Arkoun et al. 2018; Randazzo et al. 2018). Phenolic compounds (i.e., carnosol, rosmanol, epirosmanol, or rosmadiphenol) have been widely employed due to their antimicrobial characteristics, and in particular, PCL electrospun fibers loaded with extracts from rosemary plant have been successfully developed (Bhullar et al. 2015).

Nowadays, the use of nanofibrous membranes appears highly interesting for filtration processes due to their high surface energy, porous structure, and capacity to control porous dimensions and correct mechanical performance (Sahay et al. 2011). MES offer clear advantages with respect to solution electrospinning since the high consumption of toxic solvents and the derived problems with waste management can be completely avoided. In this way, gas-assisted MES has been found of high interest for industrial filtration due to its higher performance compared

to traditional systems (Watanabe et al. 2011). Membranes constituted by polyamides (e.g., nylon 12 and block polyether amides) appeared of high interest for the filtration of suspended particles in the air (Buivydiene et al. 2019). Melt electrospun polyphenylene sulfide (PPS) nanofiber membranes appeared as efficient systems for high temperature dedusting (An et al. 2018).

3.6 Use of Melt Electrospinning and Melt Electrowriting in the Pharmaceutical Field

In the last decade, the production of drug carriers based on melt electrospun polymeric material has increased as the existence of different formulations can improve drug loading, facilitate drug delivery, and enable a controlled and sustained release (Mehta et al. 2021). As an example, Davachi et al. elaborated a PLA/starch/PCL/triclosan scaffold using nanohydroxyapatite (nHAp) as an additive. A 3 wt.% addition of the calcium phosphate improved the hydrolytic degradation, the hydrophilicity, the antibacterial activity, and the drug release profile of the construct (Davachi et al. 2017).

Alongside the aforementioned benefits, polymeric matrices also allow the encapsulation or entrapment of poorly soluble active pharmaceutical ingredients (APIs). In detail, drugs with low solubility are presented in a crystalline form in which the strong intermolecular bonds lead to a low solubility. Conversion to the amorphous form of the active by using a proper solvent makes possible the mixture of this solution with a hydrophilic polymer. Solvent-based electrospinning techniques are normally used afterwards to produce fibers that will increase the surface area to dissolution media volume ratio, improving the release of the amorphous drug molecules as colloidal particles (Laitinen et al. 2013; Mehta et al. 2021; Huang and Dai 2014). It has been recently demonstrated that the preparation of API-loaded polymer fibers is also feasible by MES. For this purpose, melt homogenized drug-polymer mixtures can be elaborated before feeding them into the MES equipment. In this case, working temperatures over the drug melting point and the fast cooling of the melts favor the amorphization, enabling the preparation of drug amorphous solid dispersions (ASDs) (Nagy et al. 2013). Based on this principle, Nagy et al. produced melt electrospun fibers of EUDRAGIT® E with 20% carvedilol, a molecule with poor water solubility. They demonstrated a fast release of the drug from the cationic copolymer matrices (Nagy et al. 2013). In this line, Cao et al. developed a PLLA/polyhydroxybutyrate (PHB) system to deliver different concentrations of dipyridamole (DPD), an antithrombotic and antithrombogenic drug. A short time delivery system was created with this formulation, and, interestingly, DPD addition reduced the melting temperature of the composite (Cao et al. 2018). The same year, Semjonov et al. reported the incorporation of indomethacin, a nonsteroidal anti-inflammatory drug (NSAID), into a Soluplus® scaffold. They also confirmed an ASD with a chemical stability of the drug (Semjonov et al. 2018).

Another water poor-soluble drug frequently used in biomedicine is ciprofloxacin. He et al. reported its successful incorporation into PCL/PEG constructs by MEW. The incorporation of PEG into the fiber mats, fabricated to deliver the antibiotic during dermal regeneration, not only functions as plasticizer of PCL but also changed the release profile of the antibiotic due to the hydrophilic nature of the polymer (He et al. 2019).

MES and MEW have also emerged as an alternative technique to produce scaffolds for long-term drug delivery in targeted antitumoral therapy. As an example, Lian and Meng elaborated curcumin-loaded melt electrospun PCL fibers that showed a smoother surface and a larger amount of drug in amorphous state inside the fibers when compared to solution electrospun fibers. The higher crystallinity character of the fibers allowed a low release rate of curcumin without the burst phase evidenced with the solution electrospun matrices (Lian and Meng 2017b). The same research group developed daunorubicin hydrochloride-PCL membranes for a localized tumoral therapy. They tested different drug concentrations and noted that, despite the formation of aggregates with higher concentrations that lead to uniform distribution of the hydrophilic drug, daunorubicin could still be encapsulated in the hydrophobic polymer matrix and exhibited a slow-release rate with no burst effect (Lian and Meng 2017a).

MES can also be used to elaborate magnetic fibrous membranes for magnetic hyperthermia, a recent tumor treatment method proposed to by applied alongside chemotherapy and radiotherapy. The principle of this method is the sensitivity demonstrated by tumoral cells to temperatures ranging from 41 to 45 °C. As mentioned in Sect. 3.4, Hu et al. developed a PCL/Fe_3O_4 fiber membrane by MES and using a handheld apparatus for easy access in the medical field. They obtained a fibrous mat composed of uniform fibers with a diameter of 4–17 μm. The Fe_3O_4 nanoparticles were successfully incorporated and dispersed in the fibers. Additionally, the magnetic composite fiber membrane had excellent heating efficiency and thermal cycling characteristics. There was a fast conversion of the alternating magnetic field energy into thermal energy, and, as an advantage of incorporating the nanoparticles in PCL fibers, a repeatable heating with no decreased heating efficiency was registered (Hu et al. 2020).

Despite the advantages offered by MES and MEW, thermosensitive drugs and most biomolecules (such as proteins, polysaccharides, and nuclei acids) cannot be treated by this method (Lian and Meng 2017b). In this situation, thermosensitive drugs could be incorporated into fibers by surface immobilization after the spinning process, but the release profile would depend on strong noncovalent bonding between the polymer and the drug. Thus, the release rate might not adapt to the therapeutical purposes (Luraghi et al. 2021). A recent approach to avoid APIs degradation in MES and MEW is the use of plasticizers to decrease the intermolecular forces between polymer chains, resulting in a reduced melting and glass transition temperature of the polymer, a reduced elastic modulus, and a decreased viscosity of the melt, while preventing the active pharmaceutical molecule degradation (Bachs-Herrera et al. 2021; Semjonov et al. 2018). Table 3.1 summarizes the additives so far reported to reduce working temperatures of polymers during the elaboration of scaffold with pharmaceutical purposes.

Table 3.1 Additives to reduce the melting point of selected thermoplastic for pharmaceutical scaffolds design

Polymer	Additive/ method	Effects in produced scaffold	Reference
PLA	Sucrose fatty acid esters (SE)	Increased flowability of PLA melt ensuring a decreased diameter of fibers: PLA-SE (average of 1.5 μm) vs. PLA (average of 6.4 μm)	Zhao et al. (2012)
PVPVA64	PEG (Mw: 1500 and 3000 Da)	The addition of the drug carvedilol (CAR) dropped PVPVA64 viscosity, but not enough to reach the desired viscosity in MES at 145 °C. PVPVA64/10% CAR/15% PEG 3000 formulation exhibited the right viscosity. The fiber diameters varied from 30 μm to 60 μm. Fast CAR release at neutral pH was observed	Balogh et al. (2015)
Soluplus®[a]	Water	Reduced processing temperature, fiber diameter at microscale, amorphization of drug, and fast dissolution of drug from the mesh (30 min)	Semjonov et al. (2018)

[a]Polyvinyl caprolactam-polyvinyl acetate-polyethylene glycol graft copolymer. PEG, polyethylene glycol; PLA, polylactic acid; PVPVA64, vinylpyrrolidone-vinyl acetate copolymer

Hybridization of MES and electrospray has also emerged as an alternative for scaffold loading of thermosensitive APIs. Considering this approach, Bock et al. created a microparticle protein delivery system. The PCL scaffold elaborated by MES was electrosprayed with a solution of dichloromethane and 10 wt/v.% BSA-loaded poly(lactic-*co*-glycolic acid) (PLGA) microparticles, with a BSA concentration of 1 wt.%. Since PLGA degrades rapidly in PBS, a burst liberation of BSA from the composite was evidenced after 10 days, followed by a slow-release rate until 110 days of experiment. Mouse osteoblast precursor cell line MC3T3-E1 was used to test cell viability and infiltration. After 1 day of assay, there was a uniform cell infiltration, and after 9 and 18 days of control, no cytotoxic effect was detected (Bock et al. 2014).

3.7 Use of Melt Electrospinning and Melt Electrowriting in Tissue Engineering and Regenerative Medicine

Advancements in biomedical scaffolds design have led to a significant development of an array of polymeric fibrous structures based on electrospinning techniques. As temporary tissue substitutes, electrospun scaffolds are expected to provide a microenvironment for cell adhesion, migration, proliferation, and differentiation (Bachs-Herrera et al. 2021). Nevertheless, the production of nanoscale fibers with solvent electrospinning (SES) that limit cell migration is shifting the researcher's interest toward MES and MEW. The objective is to increase the pore size and offer a three-dimensional structure for cell growth (Kim et al. 2015). Based on these techniques, scaffolds for bone, cardiac, vascular, neuronal, skin tissue, kidney tubular tissue (van

Genderen et al. 2021), and corneal stromal tissue regeneration (Gao et al. 2021) have been developed in the last 20 years.

In this section, the biological fundaments for tissue regeneration and the current advances in scaffold elaboration by MES and MEW in the biomedical fields are revised. Similarly, the properties of the most used polymers in regenerative medicine are summarized.

3.7.1 Biological, Physiological, and Morphological Considerations for Scaffold Design

As part of the optimization of the mechanical and biological properties of melt electrospun and melt electrowritten scaffolds, the pore configuration is a relevant component of the fabrication. Paxton et al. produced tubular scaffolds of 3 and 16 mm in diameter, 40 mm in length, 10 layers, and pore areas of 0.5 and 1 mm^2. Regarding the laydown angles, they considered values of 90°, 50°, and 20° in order to determine the influence of these patterns in the cellular activity. MC3T3-E1 cells were then seeded onto the scaffold. There was found a more uncontrolled cell bridging in the structures with laydown angles of 20° and 50°, regardless of the alignment. Moreover, the non-aligned scaffolds exhibited a higher cellular infiltration due to the varying pore sizes (0.33 mm^2 to 0.02 mm^2) that reduced the bridging time of cells across the scaffolds (Fig. 3.4) (Paxton et al. 2020).

Other important factors in tissue engineering are the attenuation of the pro-inflammatory response and the promotion of macrophage polarization from the M1 to the M2 phenotype. This has an immunomodulatory function and releases anti-inflammatory cytokines, which contribute to vascularization while preventing the formation of fibrous tissue. To achieve this, recent reports demonstrated that the functionalization of fibers with extracellular matrix (ECM) proteins or loading with anti-inflammatory molecules (i.e., dexamethasone, IL-4, IL-10) can generate an immunomodulating scaffold. A different strategy is to modify the material stiffness, surface roughness, or microstructure. Regarding the physical and morphological changes, it was reported that softer structures can reduced the release of pro-inflammatory factors (Tylek et al. 2020). Similarly, porous structures influence the macrophage infiltration and polarization to the healing phenotype (Bryers et al. 2012). Further studies are necessary to understand the effect of other design parameters in the cell activity.

As MES/MEW parameters must be adjusted to meet the target tissue needs, the physiological and morphological characteristics of the most frequently studied tissues in regenerative medicine are also summarized in this section.

Bone Tissue The main structural components are the cortical bone and the cancellous bone. The first possesses an outer surface covered by the periosteum. In this tissue there are blood vessels, nerve fibers, and an osteogenic niche that act as a source of bone-forming cells (Baldwin et al. 2017). Additionally, the cortical bone is

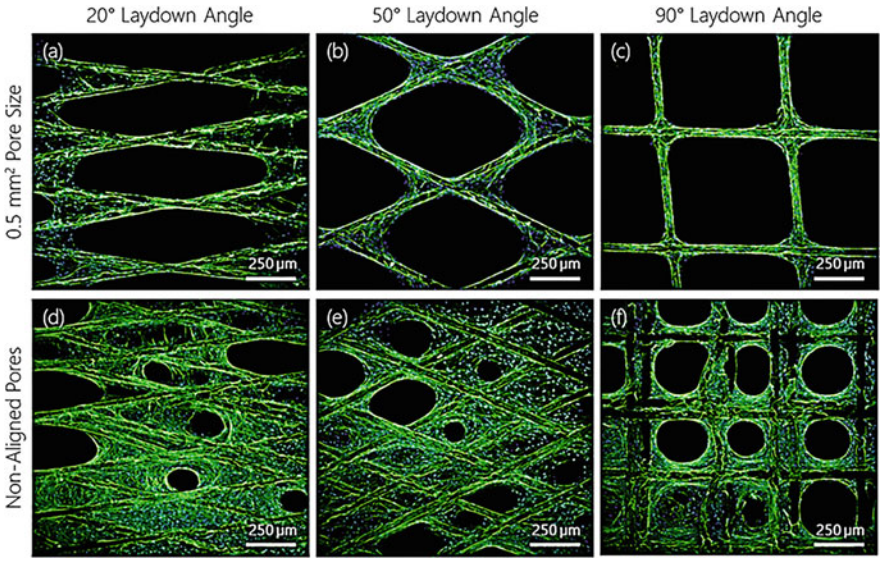

Fig. 3.4 DAPI/phalloidin-stained MC3T3-E1 cells cultured for 21 days on PCL scaffolds with (**a**–**c**) 0.5 mm^2 and (**d**–**f**) non-aligned pores where fibers in consecutive layers were not programmed to stack on top of each other using the proposed software, fabricated at 20°, 50°, and 90° laydown angle. Copyright 2020 Elsevier (Paxton et al. 2020)

characterized by an osteonal structure, and it can maintain and recover the elastic properties after deformation, enhancing the mechanical support of bone to external load (Abbasi et al. 2020). In the case of the cancellous bone, it has a plate- and rod-like trabecular structure (Hollister 2009). It is formed by osteoblasts, bone-forming cells, and ECM proteins (osteopontin, fibronectin, vitronectin, neural cadherin) that promote the hematopoietic stem cell growth (Muerza-Cascante et al. 2017).

Bone vascularization guarantees a high metabolic activity, a high permeability, and diffusivity coefficients. It has been demonstrated that high partial pressure of oxygen (PO_2) values (21%) condition the bone matrix by osteoblast and bone marrow stromal cell differentiation (Hollister 2009; Utting et al. 2006). The mechanical properties of this tissue are complex but often modeled as linear elastic materials with anisotropic Hooke's constants (attributed to cortical and cancellous bone morphology). Other important biological fundaments to be considered are the osteoconductivity (bone cell migration for matrix deposition), the osteoinductivity (process for the recruitment and transformation of immature cells into preosteoblasts), and the osseointegration (Hollister 2009; Albrektsson and Johansson 2001).

The reported ideal scaffold conditions for regeneration of this tissue include a pore size between 100 and 400 µm with a square pore geometry that can promote osteoblast and endosteal cell growth (Bachs-Herrera et al. 2021; Muerza-Cascante et al. 2017). Gradient pore size structures can also provide better conditions for regeneration, and inclusion of calcium phosphates (CaP and HAp) in the matrix can be considered to improve osteoconductivity (Abbasi et al. 2020; Hollister 2009).

Cartilage and Tendons Tendons are formed by collagen triple helices (mostly collagen type I and regions of α-helices that provide the elastomeric character) assembled into fibrils. Fibril bundles form fibers that constitute the tendon fascicle and that are covered by the endotenon. Multiple fascicles are surrounded by epitenon to form the tendon tissue. The main cells in this tissue are the tenocytes (Bachs-Herrera et al. 2021). Tendon and ligaments show a nonlinear, tensile stress-strain behavior (Hochleitner et al. 2018).

Cartilage is a tissue that lacks lymphatic system and nerves. It counts with low vascularization and metabolic activity. The ECM of articular cartilage is formed by collagen (mostly type II), proteoglycans (mainly aggrecan), fibronectin, cartilage oligomeric matrix protein, and smaller proteoglycans (Bachs-Herrera et al. 2021). The cells found in this tissue are the chondrocytes. Those located in the superficial zone express the chondrogenic markers SOX9 and the superficial ones express zone protein (SZP) for joint lubrication. Chondrocytes in deeper zones express aggrecan and collagen for compression resistance (Hollister 2009; Qiao et al. 2021). The compressive and tensile strength of cartilage depends on the interaction between the highly negatively charged proteoglycans and collagen type II fibrils (Bachs-Herrera et al. 2021). In the subchondral bone zone, there is a high alkaline phosphatase (ALP) and OCN concentration by osteocytes required for mechanical support of the osteochondral tissue. The collagen fibers organize tangentially and orderly in the superficial zone for axial load distribution (Qiao et al. 2021). Low PO_2 increases the expression of cartilage matrix genes and cell lineage maintenance by chondrocytes (Hollister 2009).

Cardiac Tissue The heart is a complex organ composed of atrial cardiomyocytes, ventricular cardiomyocytes, fibroblasts, endothelial cells, pericytes, smooth muscle cells, immune cells (myeloid and lymphoid), adipocytes, mesothelial cells, and neuronal cells. An intrinsic electrophysiological system works to propagate the electrical impulses from the sinoatrial node to the atrioventricular node and along Purkinje fibers to the apex to begin the contraction (Litviňuková et al. 2020). Artificially regenerated cardiomyocytes must be oriented on the material surface to resist directional forces in the healing tissue. Simultaneously, the new myocardial cells must be aligned to existing cells. Undirected restructuring of fibrin networks leads to malformed myocardium architectures. Materials with electrical properties like the native cardiac environment can be selected (i.e., conductive carbon and gold nanowires) to improve cardiomyocyte contraction and myoblast differentiation (Kaiser and Coulombe 2015).

Skin The three main structural layers are epidermis, dermis, and hypodermis. Epidermis can be divided in stratum corneum (corneocytes are found here), stratum lucidum, stratum granulosum, stratum spinosum, and stratum basale. Other cells found in this layer are keratinocytes, Langerhans, melanocytes, Merkel-Ranvier cells, and inflammatory cells. Fibroblasts, macrophages, and adipocytes are located in the dermis. For guided tissue regeneration, 5 μm pore size has been reported to improve neovascularization, while 5–15 μm and 20–125 μm pore sizes have been associated to a better fibroblast ingrowth and dermal repair, respectively.

Angiogenesis has been determined as the rate-limiting step for skin regeneration, so scaffolds must be designed to enhance new vessel formation (Rahmati et al. 2020).

3.7.2 *Frequently Used Polymers for the Application of MES and MEW in Biomedicine*

One of the limiting aspects of MES and MEW in biomedical and pharmaceutical research is that the high processing temperatures shorten the list of thermostable and water-soluble polymers that can be selected for the melt (Semjonov et al. 2018).

Among the FDA-approved thermoplastic polymers, PCL is an aliphatic polyester often selected for MES/MEW because its high hydrophobicity forces the use of toxic solvents when employing other techniques (Bachs-Herrera et al. 2021). Additionally, its low melting point (around 60 °C), high flexibility, slow degradation rate (2–3 years), biodegradability, and the fact that the degradation products can be metabolized by the cells in the citric acid cycle make it a good selection for biomedical applications (He et al. 2019; Lanaro et al. 2018). Nevertheless, its application can be conditioned by its high elongation and low modulus and the plasticizing effect and modulus reduction observed after hydration (Davachi et al. 2017; Hochleitner et al. 2018).

PLA is a semicrystalline thermoplastic polymer (i.e., melting point and glass transition temperature are around 178 ° C and 60 °C, respectively) with a high tensile strength and high Young's modulus. However, it is a very brittle material with a short degradation time (i.e., 3–6 months after hydrolysis) and a hydrophobic character that lowers cellular attachment. For these reasons, PLA is usually blended or copolymerized (Davachi et al. 2017; Lanaro et al. 2018). The same approach applies to PLGA, a glycolic acid and lactic acid copolymer that, although is commonly used in MES/MEW due to its good biocompatibility and fast biodegradability, have some disadvantages derived to the easy fiber deformation due to creep (Kim et al. 2010; Hochleitner et al. 2018).

Finally, PEG is a polymer with high hydrophilicity often included in the scaffold design as plasticizer of other polymers, to reduce fiber diameter, to decrease working temperature, or to improve drug release (He et al. 2019; Yoon et al. 2013).

3.7.3 *Advances in MES/MEW Scaffold Design According to Target Tissue*

3.7.3.1 MES/ MEW for Bone Regeneration

To date, the predilect polymer for bone regeneration studies applying MES has been PCL. Zaiss et al. manufactured PCL scaffolds with pore geometries of 0°/90° and 0°/60°/120° and a CaP coating. The fiber average diameter and pore size were 15 μm and 250–300 μm, respectively. In vitro studies with ovine osteoblast indicated cell

proliferation, ECM formation, and a sustained cell viability after 20 and 40 days of assay (Zaiss et al. 2016).

MEW has also been selected for generating scaffolds for bone tissue engineering. Brown et al. conducted an in vitro study with melt electrospun PCL fibers that were directly deposited onto a cylindrical rotating cylinder. This scaffold supported the growth of primary human osteoblasts, primary mouse osteoblast, and human mesothelial cells. They also managed to obtain 20 μm fibers by combining an electrostatic drawing with further mechanical drawing associated to the winding process (Brown et al. 2012).

In 2018, Abdal-hay et al. presented a novel PCL/nHAp fibrous scaffold that provided a favorable microenvironment for human osteoblasts infiltration and growth. This was in part attributed to the orderly stacked fibers with a 0–90° pattern and to the presence of nHAps that facilitated a more homogeneous distribution of cells. The nanoparticle addition also increased the roughness of the surface and the diameters of fibers from an average of 10.79 μm in plain PCL scaffolds to 16.84 and 20.26 μm for 3 and 7% wt nHAp formulations, respectively (Abdal-hay et al. 2018).

Fuchs et al. went a step further and used MEW to develop a multilayered membrane for guided regeneration of oral bone and mucosal tissue. For this purpose, two surface layers with individualized geometries (see Sect. 3.7.1 for reference of ideal pore shape) were elaborated with PCL and connected by one bacteria-tight core membrane. As a result, they evidenced a good viability and proliferation of osteoblasts, keratinocytes, and fibroblasts (Fuchs et al. 2019).

MEW has also been used to create 3D models that mimic the endosteal microenvironment. Muerza-Cascante et al. reported the use of a MEW PCL scaffold as a model to compare the suitability of primary human osteoblasts (hOBs) and placenta-derived mesenchymal stem cells (plMSCs) to form a structure similar to the human endosteum. For this purpose, they stacked ten layers of fibers in a 40×40 mm^2 and a 0–90° deposition pattern. The 5×5 mm^2 cut samples were later employed for biological testing. It was observed that hOBs secreted an ECM with deposition of endosteal proteins (i.e., fibronectin and vitronectin) under osteogenic conditions. These cells also expressed osteocalcin when the scaffolds were coated with calcium phosphate. Finally, the 3D co-culture of the hOB cells with primary human hematopoietic stem cells demonstrated the migration, growth, and expansion of the latest in the tissue-engineered endosteal microenvironment (Muerza-Cascante et al. 2017).

Notwithstanding the promising results so far presented in vitro, only few studies have demonstrated the osteoconductive capacity of melt electrowritten scaffolds in vivo. Baldwin et al. aimed to close this gap by preforming studies in a mouse orthotopic xenograft model. They fabricated a PCL tubular multiphasic scaffold characterized by the combined seeding of bone marrow mesenchymal stem cells and HUVECs to mirror the vascular and osteogenic niche in native periosteum. Immunohistochemistry showed blood vessel growth, maturation, and connection to the host vasculature (Fig. 3.5) (Baldwin et al. 2017).

Finally, Abbasi et al. performed in vivo studies in a rodent calvarial defect model. They based the PCL scaffold design in previous studies by the group that demonstrated that gradient pore size structures can simulate the transition from cortical to

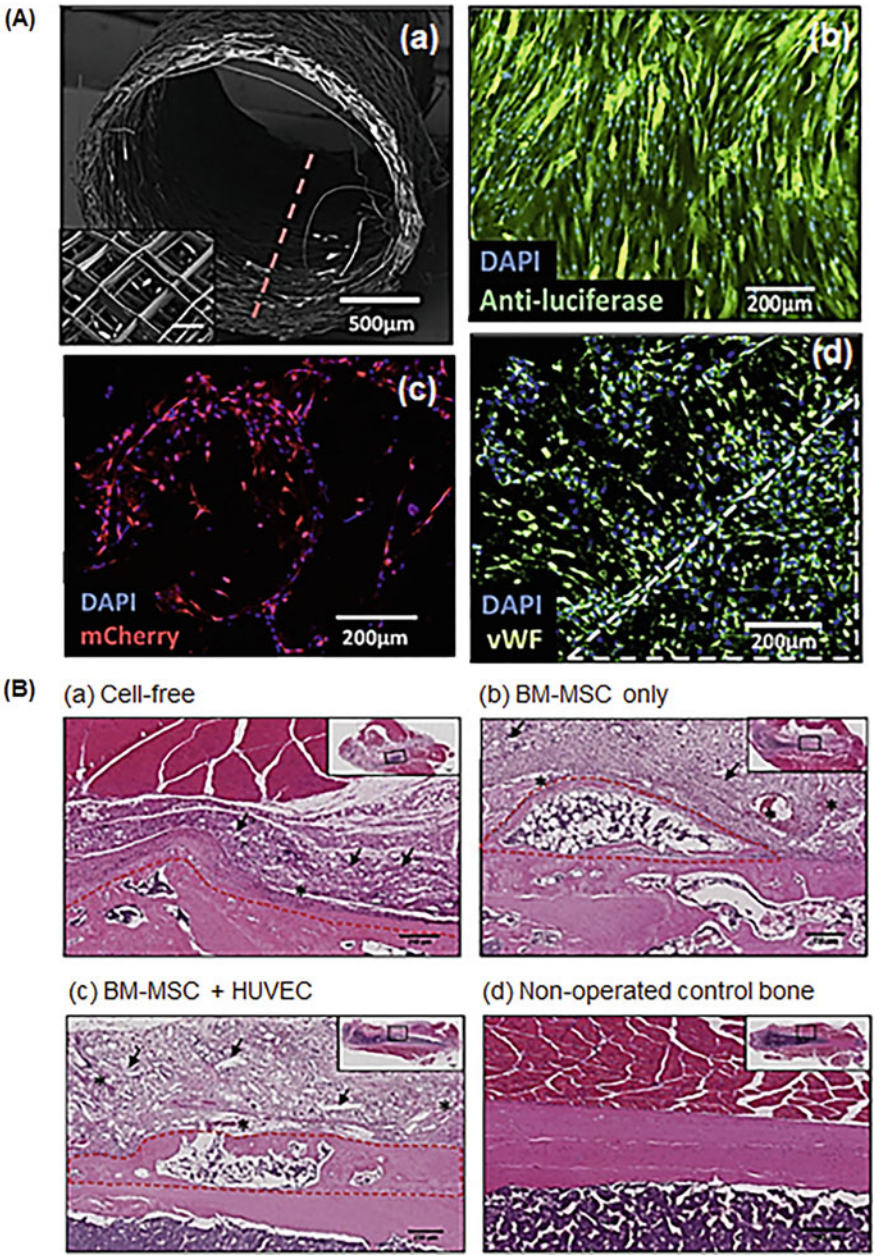

Fig. 3.5 (**A**) Characteristics of the periosteal constructs: (**a**) SEM micrograph of melt electrospun fibers in the PCL tubular scaffold (inset magnification of a longitudinal cut (*red dashed line*)); (**b**) immunofluorescence of 2D fixed BM-MSC luciferase-labeled cells; (**c**) projection of z-stack images by confocal laser microscopy showing at day 7 the formation of capillary networks by HUVECs cells; and (**d**) immunofluorescence for the endothelial marker in the star-PEG heparin hydrogel layer. (**B**) Representative sections (H&E staining) of control and periosteal construct experimental groups at day 30 of in vivo study. Newly formed bone in the tissue-engineered periosteum constructs (*dashed red lines*), the presence of the PCL fibers (*arrows*), and blood vessels (*) are indicated (bar = 250 µm). Copyright 2016 Elsevier (Baldwin et al. 2017)

cancellous bone. Therefore, there was an improved mechanical integrity and osteoblast cell differentiation toward osteogenic lineage (Abbasi et al. 2020). The new five constructs were all coated with calcium phosphate and created with pores of 250 μm and 500 μm, 500 μm with 50% fiber offset, trilayer 250–500-750 μm gradient (larger pore exposed to the dura mater), or 750–500-250 μm gradient. Results showed an enhancement of the tensile properties, increased formation of bone, the highest bone volume, and the highest intensity of the osteocalcin marker with the 250–500–750 μm gradient scaffold (Abbasi et al. 2020).

3.7.3.2 MES/MEW for Tissue Engineering of Neocartilage, Tendons, Ligaments, and Muscle

In recent years, fibrous networks have been introduced in the scaffolds designed for cartilage regeneration as a reinforcement of soft matrices. Albeit the increased compressive modulus of the constructs, the fibers are usually arranged in a limited architectural position, leading to a low interconnected porosity. To tackle this drawback, MES and MEW have been recently used (Bas et al. 2017). Bas et al. aimed to emulate the viscoelasticity and stress relaxation of articular cartilage by designing a hydrogel with poly(ethylene glycol)/heparin (Speg/Hep) and reinforced with a PCL fibrous network produced via MEW. The constructs exhibited good mechanical properties. Simultaneously, the negatively charged proteoglycan matrix favored the human articular chondrocytes viability, leading to neocartilage formation when testing in vitro (Bas et al. 2017).

Research for the development of scaffolds that resemble the crimped collagenous fibrils in tendons and ligaments has also been performed. Hochleitner et al. tried to recapitulate the nonlinear biomechanics of these connective tissues with a melt electrowritten scaffold. They used a copolymer of PCL and acryloyl carbonate p (CL-*co*-AC) for this objective. The biomimetic constructs showed a high tensile strength, elasticity, and creep resistance. Assays preformed with murine cells demonstrated the cytocompatibility of the aligned and crimpled elastomeric scaffolds. Human mesenchymal stem cells were also capable to adhere to the constructs (Hochleitner et al. 2018).

Scaffolds for tissue regenerations of lesioned articular cartilage and subchondral bone require more complex structures with lubrication properties and able to reconstruct the osteochondral defect with anisotropic tissue inductivity. Qiao et al. presented in 2021 a scaffold based on poly(ε-caprolactone)-block-poly (ethylene glycol)-block-poly(ε-caprolactone) (PCL-b-PEG-b-PCL, PCEC) fibers fabricated via MEW. Variations of collagen architecture in native osteochondral tissue were considered for fiber orientation and spacing. Simultaneously, a gelatin methacrylamide hydrogel loaded with rabbit bone-derived mesenchymal cells and PLGA microspheres incorporating growth factors were created. These structures were UV-crosslinked to the triblock polymer networks for structural reinforcement (Fig. 3.6a–c). In vitro analysis of osteochondral regeneration revealed the induction of mesenchymal cell differentiation to chondrogenic and osteogenic lineages and

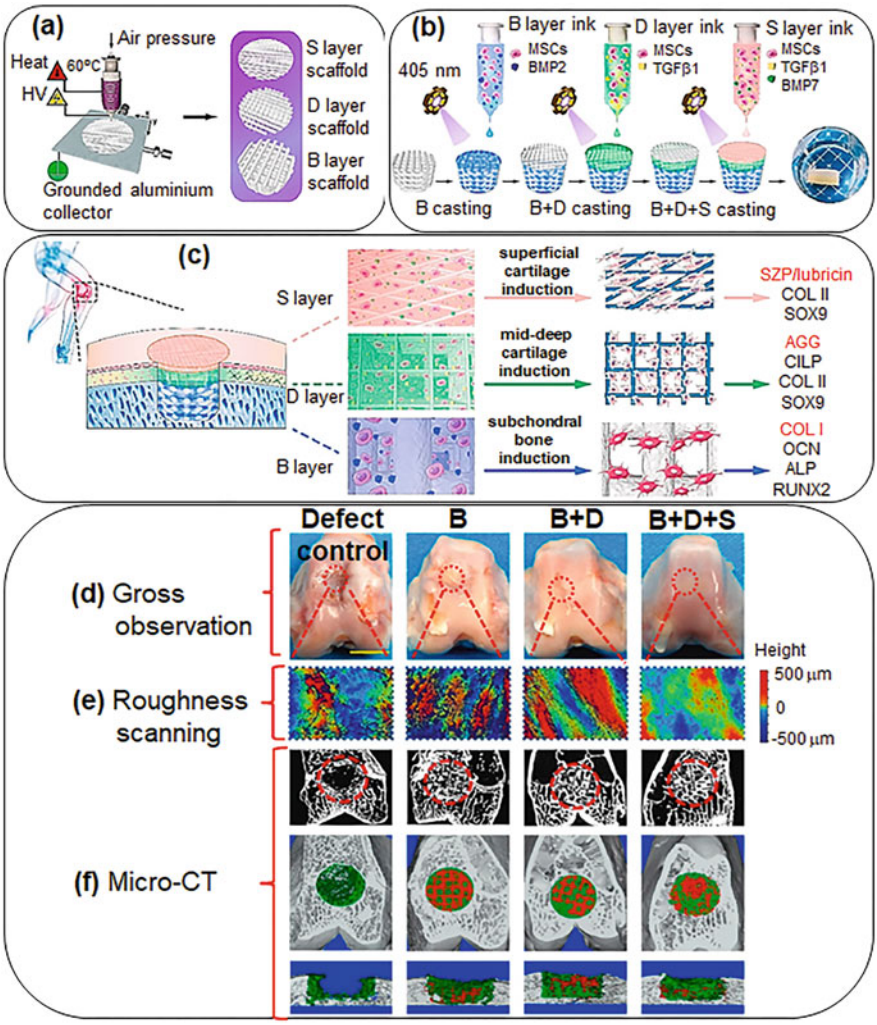

Fig. 3.6 Design of a three-layered fiber-hydrogel construct: (**a**) MEW of the PCL fiber networks (S, D, and B layers), (**b**) construction of the integrated trilayered by UV-assisted technique, (**c**) illustration for application of the trilayered scaffold in layer-specific osteochondral tissue induction and regeneration, (**d**–**f**) the trilayered constructs promoted the regeneration of osteochondral tissues in a rabbit osteochondral defect model when compared to monolayered (B) and bilayered (B + D) groups, (**d**) defect repair at 24 weeks post-surgery, (**e**) surface topography of the repaired cartilage by optical profilometer, (**f**) 2D projection images and 3D reconstruction (transverse and sagittal view) of bone repair at 24 weeks post-surgery (*off-white color* for primary bone, *green color* for regenerated bone, and red color for implanted scaffold). Copyright 2020 Elsevier (Qiao et al., 2021)

matrix accumulation. In vivo studies showed cartilage and subchondral bone regeneration (Fig. 3.6d–f) (Qiao et al. 2021).

MEW can be combined with other techniques to improve the biomimicry of the scaffolds for muscle regeneration. As an example, Uribe-Gomez et al. fabricated a shape-changing bilayered scaffold by combining a 3D printed hyaluronic acid hydrogel and a melt electrowritten PCL-polyurethane elastomer. The scaffold was able to undergo a controlled shape transformation (Uribe-Gomez et al. 2021).

3.7.3.3 MES/MEW for Cardiac and Vascular Tissue Engineering

Different attempts have been made to elaborate scaffolds for cardiac tissue regeneration. From a biomimicry perspective, the main obstacles for a successful regeneration are the achievement of a construct that will allow vascularization and that will present a fiber-organized structure that simulates the mechanical environment of cardiac tissue (Bachs-Herrera et al. 2021; Castilho et al. 2017). The reported diffusion limit of oxygen and nutrients is between 150 and 200 μm within tissues, so a correct vascularization of the scaffolds could prevent necrosis (Bachs-Herrera et al. 2021). To circumvent these issues, MES and MEW are two techniques that can help to improve the scaffold design to stimulate cell retention and guided cardiac cell growth (Castilho et al. 2017).

Liao et al. fabricated a bilayered scaffold to promote tissue growth at the interface between the myocardium and a suture-less inflow cannula designed to allow an off-bypass implantation of left ventricular assist devices. In detail, the scaffold consisted of a silicone base layer that mimics the seal and a melt electrospun PCL scaffold as a tissue integration layer. When tested with human foreskin fibroblasts for 14 days, no cytotoxic effects or morphological changes were detected, and a better cell proliferation rate was observed compared to the control on silicone sheets (Liao et al. 2018).

In other heart tissue engineering studies, a scaffold made with a blend of poly (hydroxymethylglycolide-*co*-ε-caprolactone) and PCL (pHMGCL/PCL) via MEW was designed by Castilho et al. Even though there was uniformity of the pores, the rectangular-shaped construct promoted the alignment of the embedded cardiac progenitor cells along the scaffold long axis. Moreover, the survival rate was of 99.9% after 7 days. From the mechanical aspect, the scaffold behavior approximated the properties of the native myocardial tissue (Castilho et al. 2017).

To improve the construct design and applications, Castilho et al. later tailored a PCL ultra-stretchable microfiber scaffold with a hexagonal microstructure via MEW. The construct, designed as a treatment for ischemic heart disease and heart failure, exhibited a large biaxial deformation and delivered up to 40 times more elastic energy when compared to previously developed scaffolds. For the in vitro assays, they encapsulated induced pluripotent stem cell-derived cardiomyocytes in a collagen-based hydrogel and seeded them on the scaffold. The results demonstrated a 1.5-fold increased beating rate, improved cell alignment and maturation, and sarcomere content. In vivo experiments in a porcine model indicated a shape

recovery after the epicardial delivery of the scaffold into the porcine beating heart (Castilho et al. 2018).

There have also been recent approaches to elaborate scaffolds that mimic the heart valves via MEW. As an example, Saidy et al. developed a PCL scaffold that simulates the crimped structure of natural collagen and that could support tissue remodeling, growth, and the creation of ECM. The latest were demonstrated by seeding human umbilical cord vein smooth muscle cells on the scaffold. The constructs also displayed tensile J-shaped stress/strain curves, anisotropy, and viscoelastic properties of native valve leaflets (Saidy et al. 2019).

3.7.3.4 MES/MEW for Wound Dressing Fiber Mats

The purpose of wound dressings is the coverage of open wounds and the simultaneous controlled release of drugs that can prevent the infection of the affected tissue. As the two main pathogens of wound infections are the gram-positive *Staphylococcus* and the gram-negative *Pseudomonas* bacteria, antibiotics that have low minimal inhibitory concentrations for both are usually selected (i.e., ciprofloxacin) (Jannesari et al. 2011).

The elaboration of wound dressing with polymeric materials can prolong the drug entrapment in the carrier, decrease the frequency of drug replacements, and reduce the release rate as the drug must diffuse in the polymeric systems or its release gets conditioned by the polymer degradation. Furthermore, polymer fiber mats possess a high absorbability, hemostatic properties, semipermeability for cell migration, and the potential for no scars (He et al. 2019).

As already demonstrated, MES PCL scaffolds favor the infiltration and growth of the most frequently used cell models in skin regeneration research, such as mouse embryo fibroblasts BALB/3T3 clone A31 (CCL-163) and human adult low calcium temperature (HaCat) keratinocytes. Hence, PCL makes a suitable thermoplastic polymer for wound dressing designs (Gazzarri et al. 2013).

Farrugia et al. employed MES in a direct writing mode to manufacture a PCL porous scaffold for dermal fibroblast infiltration. Fibers were 7.5 ± 1.6 μm in diameter and with an interfiber distance average of 46 ± 22 μm. Dermal fibroblasts were subsequently seeded onto the surface, and cellular infiltration was assessed 14 days later. Cells were observed throughout and underneath the scaffold. Immunohistochemistry confirmed the presence of the dermal ECM proteins collagen type I and fibronectin (Farrugia et al. 2013).

Hacker et al. developed a thermoplastic polyurethane (TPU) scaffold, modified with PEG and functionalized with silver nanoparticles (nAgs) to improve the wettability and antimicrobial properties of the system. The obtained fibrous network presented an average fiber diameter of 4.89 ± 0.94 μm with a successful incorporation of nAgs onto the surface. The antibacterial activity was demonstrated against *Staphylococcus aureus* and *Escherichia coli*. Cell viability and proliferation assays were performed with the mouse fibroblast cell line L929, and the TPU/PEG/nAgs mats did not show a cytotoxic effect (Hacker et al. 2014).

As aforementioned, He et al. fabricated PCL matrices modified with PEG to improve hydrophilicity and obtain a higher release of ciprofloxacin. The fiber mats were prepared with different geometries by MEW. PEG: PCL *w/w* percentages ranged from 5 to 15%, and the hydrophilicity of the mats increased proportionally to the PEG content. The drug release profiles with PEG changed from a non-Fickian diffusion into Fickian diffusion. The geometric structure also conditioned the release behavior (He et al. 2019).

Hewitt et al. tested the same material for wound dressing elaboration via MEW. They aimed to evaluate the potential of lactoferrin (LF) and whey protein (WP), two bioactive milk proteins, as additive in PCL scaffolds to improve its biological activity in deep tissue dermal regeneration. A high porosity, low degradation, and rapid protein release was evidenced for the tested matrices. Even though WP/PCL formulations showed lower mechanical strength that makes it more suitable for soft tissue regeneration, both types of constructs enhanced tissue regeneration when tested with HaCat keratinocytes and neonatal human dermal fibroblast for 21 days (Hewitt et al. 2019).

3.7.3.5 MES/MEW for Neural Regeneration and Stimulation

New MEW based, flexible, and highly conductive scaffolds are being proposed for neurological recovery. Wang et al. elaborated a PCL scaffold with a micro-grid pattern and a sputter-coated nanolayer of gold. The resultant scaffolds exhibited a higher Young's modulus, tensile strength, and elongation. Immunofluorescence staining and fluorescence imaging were used to evaluate the neural differentiation of PC12 cells under electrical stimulation. Results showed that neurites grew along the frame (Wang et al. 2020). The growth of this electroactive neural cell line on melt electrowritten PCL scaffolds was also observed by Zhang et al. The topographical pattern of the scaffold was subsequently optimized by sequential addition of graphene oxide nanosheets and rGO/graphitic carbon nitride (g-C_3N_4) nanoparticles (Fig. 3.7) (Zhang et al. 2020).

3.7.3.6 MES/MEW Applications in Dentistry

Periodontal disease is a pathology that affects gingiva, periodontal ligament, the alveolar bone, and the cementum. The accumulation of bacteria and activation of inflammatory response lead to the loss of the support tissue and, ultimately, the tooth. To date, the standards for repairing periodontal bone defects are the autografts and allografts that have considerable limitations due to the donor scarcity and the immunogenic response, respectively. To circumvent this problem, MES/MEW alternative is being proposed for guided bone regeneration scaffolds (GBR). Recently, Dubey et al. produced a hydrogel reinforced with melt electrowritten PCL mesh to be used as GBR scaffolds in periodontal disease. The gelatin methacryloyl hydrogel was loaded with amorphous magnesium phosphate (AMP)

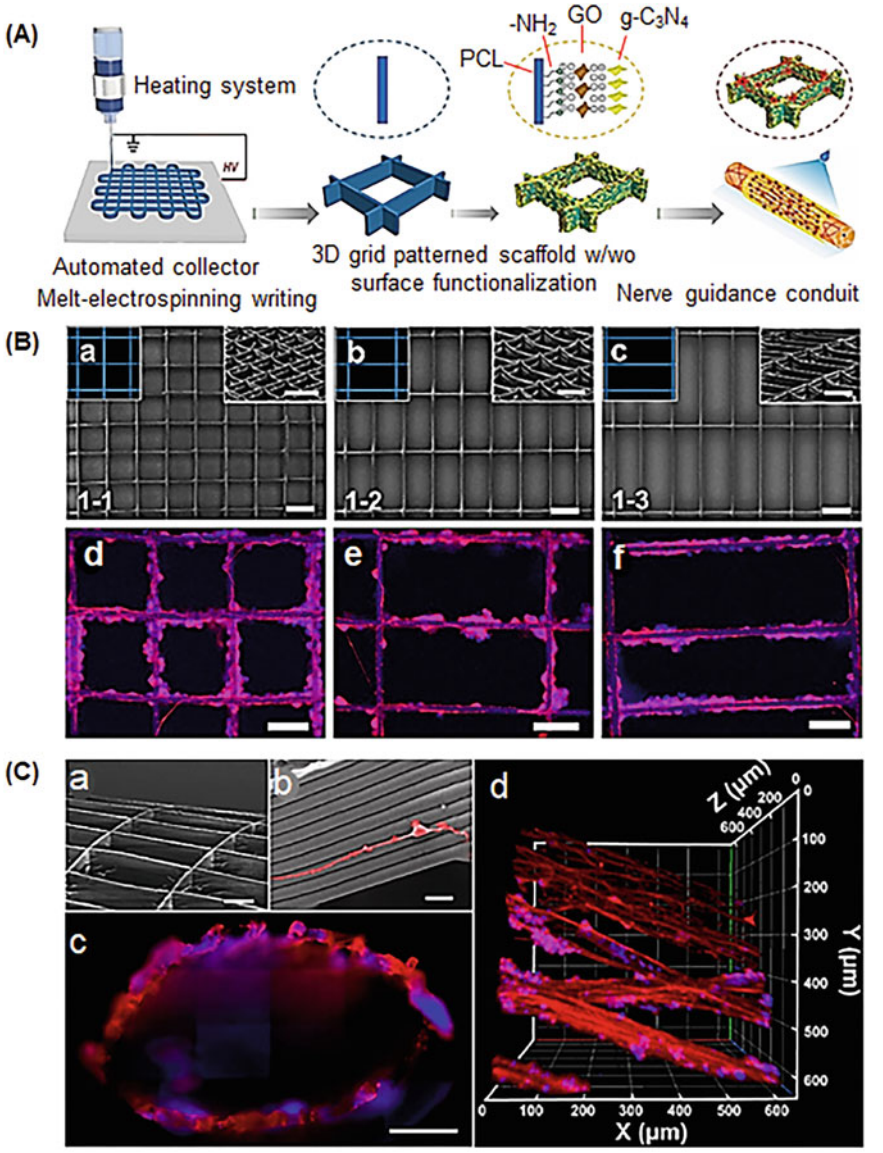

Fig. 3.7 (**A**) Scheme of 3D polymeric grid-patterned scaffolds with neuro guidance conduits. (**B**) SEM images (scale bar: 200 μm) of melt electrowritten PCL scaffolds with square pattern 1–1 (**a**), 1–2 (**b**), and 1–3 (**c**) rectangular patterns (side views are shown in the insets). (**d**–**f**) Immunofluorescence images (scale bar: 100 μm) of PC12 cells after differentiation for 7 days in the mentioned scaffolds. (**C**) SEM images of a nerve conduit (one to two rectangular pattern) (**a**), PC12 cells (**b**) (pseudo-color red) cultured on the conduit after 14 days of differentiation, immunofluorescence images of PC12 cells after 14 days differentiation on conduit showing a top view (scale bar: 1 mm) (**c**), and a 3D reconstruction on the luminal surface of the conduit (**d**). Copyright 2020 Elsevier (Zhang et al. 2020)

to help control the mechanical properties of the hydrogel and to proportionate osteogenic properties. Stiffness of the construct was significantly enhanced by PCL fibers. It was concluded that the reinforcement could be modulated by the number of PCL meshes added to the hydrogel and by the concentration of the calcium phosphate. The PCL fiber mesh also delayed the hydrogel degradation, and, in clinical application, this would prevent soft tissue invasion. Cellular response was significantly higher with the PCL/hydrogel construct, which was evidenced by a higher mineralization, osteogenic gene expression, and in vivo bone formation (Dubey et al. 2020). A similar approach was presented by Daghrery et al., but they replaced the AMP with a fluorinated calcium phosphate (F/CaP) coating and a different strand spacing. A significant increase in human-derived periodontal ligament stem cells and the upregulation of osteogenic genes were observed. The presence of F/CaP gave a minor antimicrobial character against *Porphyromonas gingivalis*. In vivo experiments showed periodontal tissue regeneration with the implants in a fenestration defect in rodents (Daghrery et al. 2021).

3.7.3.7 MES/MEW for In Vitro Physiology Studies and In Vivo Models of Disease

In the field of neurophysiology, one of the limitations of network electrophysiology and neurophysiological mechanisms research is the lack of 3D models. Normally, 2D neural networks are grown onto rigid substrates that do not simulate the cell morphology, the cell-to-cell interaction, or the neuritic outgrowth in all directions (Frega et al. 2015). To better emulate this complex microenvironment, Schaefer et al. proposed a 3D electrophysiology model in which Matrigel was reinforced by a series of scaffolds produced via MEW. Glycine receptor-transfected Ltk-11 mouse fibroblasts were considered for the electrophysiology tests. The cell line selection was based on the scientific evidence that the inhibitory glycine receptor is a ligand-gated ion channel that undergoes conformational changes after glycine binding, leading to the channel pore opening. The MEW PCL construct had an average thickness of 141.4 ± 5.7 μm and was obtained by the continuous deposition of 9.7 ± 0.2 μm diameter fibers. The pore geometry was square with tested spacings of 100, 200, and 400 μm. They examined that the mechanical properties of the constructs were evaluated with and without the Matrigel. Results indicated that the scaffolds without Matrigel had similar mechanical behaviors but the 400 μm pore size matrix was difficult to handle when Matrigel was added. In the bioassays, similar Ltk-11 viability percentages were obtained when cells were grown in the 3D MEW/Matrigel construct when compared to the 2D model. An evaluation 9 days after seeding demonstrated cell colonization across the MEW scaffold/Matrigel independently of the pore size. Regarding the electrophysiological recordings, small changes in glycine-induced currents and potency were registered, but they did not interfere with the measurements. These results open the possibility of developing MEW scaffolds for the in vitro studies of neurophysiology and pathological mechanisms (Schaefer et al. 2019).

Models for cancer metastasis research can be developed by MEW too. Thibaudeau et al. sought to model breast cancer bone metastasis in a melt electrospun PCL tubular scaffold seeded with primary human osteoblastic (hOB) cells and recombinant human bone morphogenic protein-7. A fiber thickness of 30 μm and a fiber spacing of 0.5 mm were selected for the scaffold that was implanted subcutaneously in non-obese diabetic/severe combined immunodeficient mice after 7 days of hOB seeding. The construct allowed the formation of a morphologically intact organ bone. The newly formed structure was humanized with human bone cells and human-derived matrix proteins. The dissemination of luciferase-expressing human breast cancer cell lines to the bone ossicles in question proved the metastasis with a clear osteolysis in the recently formed bone tissue. The results demonstrated the potential of the model for breast cancer metastasis in the bone (Thibaudeau et al. 2014).

3.7.3.8 Future of MES/MEW in Translational Medicine

As MES/MEW techniques keep evolving, the transition to patient-specific biofabrication is possible. In this scenario, routinely acquired magnetic resonance images could provide the necessary data for 3D customized scaffold design. As an example of this new medicine translational approach, Paxton et al. fabricated a patient-specific scaffold for an ear cartilage and femur defect case studies (Paxton et al. 2020).

3.8 Conclusions

Melt electrospinning and electrowriting are highly powerful techniques to get porous membranes with a controlled design and architecture. Capacity to work with a large number of polymers including blends and composites allows a great control on final properties, surface characteristics, biodegradability, and cellular responses. Furthermore, extraction of one component in the blend fibers gives a clear opportunity to develop hollow fiber morphologies. Advantages of these solvent-free processes are also related to the reduced processing costs and decreased toxicity of derived materials. Nevertheless, some challenges still exist providing some limitations for an optimum application in the biomedical field: (a) fiber diameters are usually larger than those required for simulating the ECM matrix, (b) processed polymers usually render a hydrophobic surface that is difficult for cell attachment and protein adsorption, (c) materials usually display higher stiffness and lower elasticity than human tissues, and (d) potential polymer degradation can take place during the melting process. New promising strategies have been developed by incorporating additives, cell-laden hydrogels, heat-sensitive molecules, and bioactive molecules as well as trying to combine these electrospinning processes with other additive manufacturing techniques in order to favor polymer functionalization and improve mechanical

properties of derived multiphasic composites. Surfaces of materials can also be improved for cell interaction using plasma treatment or coating with calcium phosphates.

References

Abbasi N, Ivanovski S, Gulati K et al (2020) Role of offset and gradient architectures of 3-D melt electrowritten scaffold on differentiation and mineralization of osteoblasts. Biomater Res 24:2. https://doi.org/10.1186/s40824-019-0180-z

Abdal-hay A, Abbasi N, Gwiazda M et al (2018) Novel polycaprolactone/hydroxyapatite nanocomposite fibrous scaffolds by direct melt-electrospinning writing. Eur Polym J 105: 257–264. https://doi.org/10.1016/j.eurpolymj.2018.05.034

Albrektsson T, Johansson C (2001) Osteoinduction, osteoconduction and osseointegration. Eur Spine J 10:S96–S10. https://doi.org/10.1007/s005860100282

An Y, Yu S, Li S et al (2018) Melt-electrospinning of Polyphenylene sulfide. Fibers Polym 19: 2507–2513. https://doi.org/10.1007/s12221-018-8619-8

Arkoun M, Ardila N, Heuzey M-C, Ajji A (2018) Chitosan-based structures/coatings with antibacterial properties. In: Handbook of antimicrobial coatings. Elsevier, Amsterdam, pp 357–389. https://doi.org/10.1016/B978-0-12-811982-2.00017-2

Bachs-Herrera A, Yousefzade O, del Valle LJ, Puiggali J (2021) Melt electrospinning of polymers: blends, nanocomposites, additives and applications. Appl Sci 11:1808. https://doi.org/10.3390/app11041808

Baldwin JG, Wagner F, Martine LC et al (2017) Periosteum tissue engineering in an orthotopic in vivo platform. Biomaterials 121:193–204. https://doi.org/10.1016/j.biomaterials.2016.11.016

Balogh A, Farkas B, Faragó K et al (2015) Melt-blown and electrospun drug-loaded polymer fiber Mats for dissolution enhancement: a comparative study. J Pharm Sci 104:1767–1776. https://doi.org/10.1002/jps.24399

Bas O, De-Juan-Pardo E, Meinert C et al (2017) Biofabricated soft network composites for cartilage tissue engineering. Biofabrication 9:025014. https://doi.org/10.1088/1758-5090/aa6b15

Bhullar SK, Kaya B, Jun MB-G (2015) Development of bioactive packaging structure using melt electrospinning. J Polym Environ 23:416–423. https://doi.org/10.1007/s10924-015-0713-z

Bock N, Woodruff MA, Roland S et al (2014) Composites for delivery of therapeutics: combining melt electrospun scaffolds with loaded electrosprayed microparticles. Macromol Biosci 14:202–214. https://doi.org/10.1002/mabi.201300276

Brown TD, Dalton PD, Hutmacher DW (2016) Melt electrospinning today: An opportune time for an emerging polymer process. Prog Polym Sci 56:116–166. https://doi.org/10.1016/j.progpolymsci.2016.01.001

Brown TD, Slotosch A, Thibaudeau L et al (2012) Design and fabrication of tubular scaffolds via direct writing in a melt electrospinning mode. Biointerphases 7:13. https://doi.org/10.1007/s13758-011-0013-7

Bryers JD, Giachelli CM, Ratner BD (2012) Engineering biomaterials to integrate and heal: the biocompatibility paradigm shifts. Biotechnol Bioeng 109(8):1898–1911. https://doi.org/10.1002/bit.24559

Buivydiene D, Krugly E, Ciuzas D et al (2019) Formation and characterisation of airfilter material printed by melt electrospinning. J Aerosol Sci 131:48–63. https://doi.org/10.1016/j.jaerosci.2019.03.003

Cao K, Liu Y, Olkhov AA et al (2018) PLLA-PHB fiber membranes obtained by solvent-free electrospinning for short-time drug delivery. Drug Deliv Transl Res 8:291–302. https://doi.org/10.1007/s13346-017-0463-7

Cao L, Dong M, Zhang A et al (2013) Morphologies and crystal structures of styrene-acrylonitrile/isotactic polypropylene ultrafine fibers fabricated by melt electrospinning. Polym Eng Sci 53:2674–2682. https://doi.org/10.1002/pen.23515

Castilho M, Feyen D, Flandes-Iparraguirre M et al (2017) Melt electrospinning writing of poly-hydroxymethylglycolide-co-ε-caprolactone-based scaffolds for cardiac tissue engineering. Adv Healthc Mater 6:1700311. https://doi.org/10.1002/adhm.201700311

Castilho M, van Mil A, Maher M et al (2018) Melt electrowriting allows tailored microstructural and mechanical design of scaffolds to advance functional human myocardial tissue formation. Adv Funct Mater 28:1803151. https://doi.org/10.1002/adfm.201803151

Chainani A, Hippensteel KJ, Kishan A et al (2013) Multilayered electrospun scaffolds for tendon tissue engineering. Tissue Eng Part A 19:2594–2604. https://doi.org/10.1089/ten.TEA.2013.0165

Daenicke J, Lämmlein M, Steinhübl F, Schubert DW (2019) Revealing key parameters to minimize the diameter of polypropylene fibers produced in the melt electrospinning process. E-Polymers 19:330–340. https://doi.org/10.1515/epoly-2019-0034

Daghrery A, Ferreira JA, de Souza IJ et al (2021) A highly ordered, nanostructured fluorinated CaP-coated melt electrowritten scaffold for periodontal tissue regeneration. Adv Healthc Mater 10:2101152. https://doi.org/10.1002/adhm.202101152

Davachi SM, Shiroud Heidari B, Hejazi I et al (2017) Interface modified polylactic acid/starch/poly ε-caprolactone antibacterial nanocomposite blends for medical applications. Carbohydr Polym 155:336–344. https://doi.org/10.1016/j.carbpol.2016.08.037

Davoodi P, Yeng LY, Xu Q et al (2018) Drug delivery systems for programmed and on-demand release. Adv Drug Deliv Rev 132:104–138. https://doi.org/10.1016/j.addr.2018.07.002

Dubey N, Ferreira JA, Daghrery A et al (2020) Highly tunable bioactive fiber-reinforced hydrogel for guided bone regeneration. Acta Biomater 113:164–176. https://doi.org/10.1016/j.actbio.2020.06.011

Farrugia BL, Brown TD, Zee U et al (2013) Dermal fibroblast infiltration of poly(ε-caprolactone) scaffolds fabricated by melt electrospinning in a direct writing mode. Biofabrication 5:025001. https://doi.org/10.1088/1758-5082/5/2/025001

Frega M, Tedesco M, Massobrio P (2015) Network dynamics of 3D engineered neuronal cultures: a new experimental model for in-vitro electrophysiology. Sci Rep 4:5489. https://doi.org/10.1038/srep05489

Fuchs A, Youssef A, Seher A et al (2019) A new multilayered membrane for tissue engineering of oral hard- and soft tissue by means of melt electrospinning writing and film casting – an in vitro study. J Craniomaxillofac Surg 47:695–703. https://doi.org/10.1016/j.jcms.2019.01.043

Gao Q, Xie J, Salero E et al (2021) Tissue engineering of corneal stroma via melt electrowriting. J Tissue Eng Regen Med 15:841–851. https://doi.org/10.1002/term.3235

Gazzarri M, Bartoli C, Mota C et al (2013) Fibrous star poly(ε-caprolactone) melt-electrospun scaffolds for wound healing applications. J Bioact Compat Polym 28:492–507. https://doi.org/10.1177/0883911513494625

van Genderen AM, Jansen K, Kristen M et al (2021) Topographic guidance in melt-electrowritten tubular scaffolds enhances engineered kidney tubule performance. Front Bioeng Biotechnol 18:617364. https://doi.org/10.3389/fbioe.2020.617364

Góra A, Sahay R, Thavasi V, Ramakrishna S (2011) Melt-electrospun fibers for advances in biomedical engineering, clean energy, filtration, and separation. Polym Rev 51:265–287. https://doi.org/10.1080/15583724.2011.594196

Hacker C, Karahaliloglu Z, Seide G et al (2014) Functionally modified, melt-electrospun thermoplastic polyurethane mats for wound-dressing applications. J Appl Polym Sci 131:40132. https://doi.org/10.1002/app.40132

Haroosh HJ, Dong Y (2015) 4-Electrospun poly(lactic acid) (PLA): poly(ε-caprolactone) (PCL)/halloysite nanotube (HNT) composite fibers: synthesis and characterization. In: Dong Y, Umer R, Lau AK-T (eds) Fillers and reinforcements for advanced nanocomposites. Woodhead

Publishing, Sawston/Cambridge, pp 59–80. https://doi.org/10.1016/B978-0-08-100079-3.00004-1

He F-L, Deng X, Zhou Y-Q et al (2019) Controlled release of antibiotics from poly-ε-caprolactone/polyethylene glycol wound dressing fabricated by direct-writing melt electrospinning. Polym Adv Technol 30:425–434. https://doi.org/10.1002/pat.4481

Hewitt E, Mros S, Mcconnell M et al (2019) Melt-electrowriting with novel milk protein/PCL biomaterials for skin regeneration. Biomed Mater 14:055013. https://doi.org/10.1088/1748-605X/ab3344

Hochleitner G, Chen F, Blum C et al (2018) Melt electrowriting below the critical translation speed to fabricate crimped elastomer scaffolds with non-linear extension behaviour mimicking that of ligaments and tendons. Acta Biomater 72:110–120. https://doi.org/10.1016/j.actbio.2018.03.023

Hollister SJ (2009) Scaffold design and manufacturing: from concept to clinic. Adv Mater 21:3330–3342. https://doi.org/10.1002/adma.200802977

Hu P-Y, Zhao Y-T, Zhang J et al (2020) In situ melt electrospun polycaprolactone/Fe3O4 nanofibers for magnetic hyperthermia. Mater Sci Eng C 110:110708. https://doi.org/10.1016/j.msec.2020.110708

Huang Y, Dai W-G (2014) Fundamental aspects of solid dispersion technology for poorly soluble drugs. Acta Pharm Sin B 4:18–25. https://doi.org/10.1016/j.apsb.2013.11.001

Jannesari M, Varshosaz J, Morshed M, Zamani M (2011) Composite poly(vinyl alcohol)/poly(vinyl acetate) electrospun nanofibrous mats as a novel wound dressing matrix for controlled release of drugs. Int J Nanomedicine 6:993–1003. https://doi.org/10.2147/IJN.S17595

Kaiser NJ, Coulombe K (2015) Physiologically inspired cardiac scaffolds for tailored in vivo function and heart regeneration. Biomed Mater 10:034003. https://doi.org/10.1088/1748-6041/10/3/034003

Karahaliloglu Z, Hacker C, Demirbilek M et al (2014) Photocatalytic performance of melt-electrospun polypropylene fabric decorated with TiO2 nanoparticles. J Nanopart Res 16:2615. https://doi.org/10.1007/s11051-014-2615-8

Kim BS, Park KE, Kim MH et al (2015) Effect of nanofiber content on bone regeneration of silk fibroin/poly(ε-caprolactone) nano/microfibrous composite scaffolds. Int J Nanomedicine 9:485–502. https://doi.org/10.2147/IJN.S72730

Kim SJ, Jang DH, Park WH, Min B-M et al (2010) Fabrication and characterization of 3-dimensional PLGA nanofiber/microfiber composite scaffolds. Polymer 51:1320–1327. https://doi.org/10.1016/j.polymer.2010.01.025

Kim TG, Chung HJ, Park TG (2008) Macroporous and nanofibrous hyaluronic acid/collagen hybrid scaffold fabricated by concurrent electrospinning and deposition/leaching of salt particles. Acta Biomater 4:611–1619. https://doi.org/10.1016/j.actbio.2008.06.008

Koenig K, Hermanns S, Ellerkmann J et al (2020) The effect of additives and process parameters on the pilot-scale manufacturing of polylactic acid sub-microfibers by melt electrospinning. Text Res J 90:1948–1961. https://doi.org/10.1177/0040517520904019

Laitinen R, Löbmann K, Strachan CJ et al (2013) Emerging trends in the stabilization of amorphous drugs. Int J Pharm 453:65–79. https://doi.org/10.1016/j.ijpharm.2012.04.066

Lanaro M, Booth L, Powell SK, Woodruff MA (2018) Electrofluidodynamic technologies for biomaterials and medical devices. In: Guarino V, Ambrosio L (eds) Electrofluidodynamic technologies (EFDTs) for biomaterials and medical devices. Elsevier, Cambridge, pp 37–69. https://doi.org/10.1016/B978-0-08-101745-6.00003-7

Li R, Zhang L, Shi L et al (2017) MXene Ti3C2: an effective 2D light-to-heat conversion material. ACS Nano 11:3752–3759. https://doi.org/10.1021/acsnano.6b08415

Li X, Liu H, Wang J, Li C (2012) Preparation and characterization of PLLA/nHA nonwoven mats via laser melt electrospinning. Mater Lett 73:103–106. https://doi.org/10.1016/j.matlet.2011.12.108

Lian H, Meng Z (2017a) Melt electrospinning of daunorubicin hydrochloride-loaded poly (-ε-caprolactone) fibrous membrane for tumor therapy. Bioact Mater 2:96–100. https://doi.org/10.1016/j.msec.2017.02.024

Lian H, Meng Z (2017b) Melt electrospinning vs. solution electrospinning: a comparative study of drug-loaded poly (ε-caprolactone) fibres. Mater Sci Eng 74:117–123. https://doi.org/10.1016/j.msec.2017.02.024

Liao S, Theodoropoulos C, Blackwood K et al (2018) Melt electrospun bilayered scaffolds for tissue integration of a suture-less inflow cannula for rotary blood pumps. Artif Organs 42:E43–E54. https://doi.org/10.1111/aor.13018

Litviňuková M, Talavera-López C, Maatz H et al (2020) Cells of the adult human heart. Nature 588:466–472. https://doi.org/10.1038/s41586-020-2797-4

Lokmic Z, Mitchell GM (2008) Engineering the microcirculation. Tissue Eng Part B Rev 14:87–103. https://doi.org/10.1089/teb.2007.0299

Luraghi A, Peri F, Moroni L (2021) Electrospinning for drug delivery applications: a review. J Control Release 334:463–484. https://doi.org/10.1016/j.jconrel.2021.03.033

Lyons J, Li C, Ko F (2004) Melt-electrospinning part I: processing parameters and geometric properties. Polymers 45:7597–7603. https://doi.org/10.1016/j.polymer.2004.08.071

Malakhov SN, Bakirov AV, Dmitryakov PV, Chvalun SN (2016) Nanocomposite nonwoven materials based on polyamide-6 and montmorillonite, prepared by electrospinning of the polymer melt. Russ J Appl Chem 89:165–172. https://doi.org/10.1134/S1070427216010262

Malakhov SN, Belousov SI, Orekhov AS, Chvalun SN (2018) Electrospinning of nonwoven fabrics from polypropylene melt with additions of stearates of divalent metals. Fibre Chem 50:27–32. https://doi.org/10.1007/s10692-018-9922-2

Mehta P, Rasekh M, Patel M et al (2021) Recent applications of electrical, centrifugal, and pressurised emerging technologies for fibrous structure engineering in drug delivery, regenerative medicine and theranostics. Adv Drug Deliv Rev 175:113823. https://doi.org/10.1016/j.addr.2021.05.033

Morikawa K, Vashisth A, Grimme CJ et al (2019) Wire melt electrospinning of thin polymeric fibers via strong electrostatic field gradients. Macromol Mater Eng 304:1800417. https://doi.org/10.1002/mame.201800417

Muerza-Cascante ML, Shokoohmand A, Khosrotehrani K et al (2017) Endosteal-like extracellular matrix expression on melt electrospun written scaffolds. Acta Biomater 52:145–158. https://doi.org/10.1016/j.actbio.2016.12.040

Nagy ZK, Balogh A, Drávavölgyi G et al (2013) Solvent-free melt electrospinning for preparation of fast dissolving drug delivery system and comparison with solvent-based electrospun and melt extruded systems. J Pharm Sci 102:508–517. https://doi.org/10.1002/jps.23374

Nayak R, Padhye R, Kyratzis IL et al (2012) Effect of viscosity and electrical conductivity on the morphology and fiber diameter in melt electrospinning of polypropylene. Text Res J 83:606–617. https://doi.org/10.1177/0040517512458347

Nazari T, Garmabi H (2018) The effects of processing parameters on the morphology of PLA/PEG melt electrospun fibers. Polym Int 67:178–188. https://doi.org/10.1002/pi.5486

Pan J-L, Zhang Z, Zhang H et al (2018) Ultrathin and strong electrospun porous fiber separator. ACS Appl Energy Mater 1:4794–4803. https://doi.org/10.1021/acsaem.8b00855

Paxton NC, Lanaro M, Arixin B et al (2020) Design tools for patient specific and highly controlled melt electrowritten scaffolds. J Mech Behav Biomed Mater 105:103695. https://doi.org/10.1016/j.jmbbm.2020.103695

Piyasin P, Yensano R, Pinitsoontorn S (2019) Size-controllable melt-electrospun polycaprolactone (PCL) fibers with a sodium chloride additive. Polymers (Basel) 11:1768. https://doi.org/10.3390/polym11111768

Qiao Z, Lian M, Han Y et al (2021) Bioinspired stratified electrowritten fiber-reinforced hydrogel constructs with layer-specific induction capacity for functional osteochondral regeneration. Biomaterials 266:120385. https://doi.org/10.1016/j.biomaterials.2020.120385

Rahmati M, Blaker JJ, Lyngstadaas SP et al (2020) Designing multigradient biomaterials for skin regeneration. Mater Today Adv 5:100051. https://doi.org/10.1016/j.mtadv.2019.100051

Randazzo W, Fabra MJ, Falcó I (2018) Polymers and biopolymers with antiviral activity: potential applications for improving food safety. Compr Rev Food Sci Food Saf 17:754–768. https://doi.org/10.1111/1541-4337.12349

Sahay R, Thavasi V, Ramakrishna S (2011) Design modifications in electrospinning setup for advanced applications. J Nanomater 2011:1–17. https://doi.org/10.1155/2011/317673

Saidy NT, Wolf F, Bas O et al (2019) Biologically inspired scaffolds for heart valve tissue engineering via melt electrowriting. Small 15:1900873. https://doi.org/10.1002/smll.201900873

Sampath Kumar TS, Yogeshwar Chakrapani V (2018) Electrospun 3D scaffolds for tissue regeneration. In: Chun H, Park C, Kwon I, Khang G (eds) Cutting-edge enabling technologies for regenerative medicine, Advances in experimental medicine and biology, vol 1078. Springer, Singapore, pp 29–47. https://doi.org/10.1007/978-981-13-0950-2_3

Schaefer N, Janzen D, Bkiri E et al (2019) 3D Electrophysiological measurements on cells embedded within fiber-reinforced Matrigel. Adv Healthc Mater 8:1801226. https://doi.org/10.1002/adhm.201801226

Semjonov K, Lust A, Kogermann K et al (2018) Melt-electrospinning as a method to improve the dissolution and physical stability of a poorly water-soluble drug. Eur J Pharm Sci 121:260–268. https://doi.org/10.1016/j.ejps.2018.06.004

Sun B, Li J, Liu W et al (2014) Fabrication and characterization of mineralized P(LLA-CL)/SF three-dimensional nanoyarn scaffolds. Iran Polym J 24:29–40. https://doi.org/10.1007/s13726-014-0297-9

Thibaudeau L, Taubenberger A, Holzapfel B et al (2014) A tissue-engineered humanized xenograft model of human breast cancer metastasis to bone. Dis Model Mech 7:299–309. https://doi.org/10.1242/dmm.014076

Tylek T, Blum C, Hrynevich A et al (2020) Precisely defined fiber scaffolds with 40 μm porosity induce elongation driven M2-like polarization of human macrophages. Biofabrication 12:025007. https://doi.org/10.1088/1758-5090/ab5f4e

Uribe-Gomez J, Posada-Murcia SA et al (2021) Shape-morphing fibrous hydrogel/elastomer bilayers fabricated by a combination of 3D printing and melt electrowriting for muscle tissue regeneration. ACS Appl Bio Mater 4:1720–1730. https://doi.org/10.1021/acsabm.0c01495

Utting JC, Robins SP, Brandao-Burch A et al (2006) Hypoxia inhibits the growth, differentiation and bone-forming capacity of rat osteoblasts. Exp Cell Res 312:1693–1702. https://doi.org/10.1016/j.yexcr.2006.02.007

Van Puyvelde P, Vananroye A, Cardinaels R, Moldenaers P (2008) Review on morphology development of immiscible blends in confined shear flow. Polymer 49:5363–5372. https://doi.org/10.1016/j.polymer.2008.08.055

Wang X-F, Zheng M-H (2009) Melt-electrospinning of PMMA. Chin J Polym Sci 28:45–53. https://doi.org/10.1007/s10118-010-8208-9

Wang Y, Zhang Y, Zhang Z et al (2020) An injectable high-conductive bimaterial scaffold for neural stimulation. Colloids Surf B Biointerfaces 195:111210. https://doi.org/10.1016/j.colsurfb.2020.111210

Watanabe K, Hochleitner B-S, Kim I-S (2011) Development of polypropylene nanofiber production system. Polym Rev 51:288–308. https://doi.org/10.1080/15583724.2011.594195

Yoon YI, Park KE, Lee SJ, Park WH (2013) Fabrication of microfibrous and nano-/microfibrous scaffolds: melt and hybrid electrospinning and surface modification of poly(L-lactic acid) with plasticizer. Biomed Res Int 2013:1–10. https://doi.org/10.1155/2013/309048

Zaiss S, Brown T, Reichert J, Berner A (2016) Poly(ε-caprolactone) scaffolds fabricated by melt electrospinning for bone tissue engineering. Materials (Basel) 9:232. https://doi.org/10.3390/ma9040232

Zhang L-H, Duan X-P, Yan X et al (2016) Recent advances in melt electrospinning. RSC Adv 6: 53400–53414. https://doi.org/10.1039/C6RA09558E

Zhang X, Tian X, Zheng J et al (2008) Relationship between microstructure and tensile properties of PET/silica nanocomposite fibers. J Macromol Sci B 47:368–377. https://doi.org/10.1080/00222340701849277

Zhang Z, Lindh M, Wang Z et al (2020) 3D anisotropic photocatalytic architectures as bioactive nerve guidance conduits for peripheral neural regeneration. Biomaterials 253:120108. https://doi.org/10.1016/j.biomaterials.2020.120108

Zhao FW, Liu Y, Ding YM et al (2012) Effect of plasticizer and load on melt electrospinning of PLA. Key Eng Mater 501:32–36. https://doi.org/10.4028/www.scientific.net/KEM.501.32

Chapter 4
Pharmaceutical Spray Drying

Ioannis Partheniadis, Nizar Al-Zoubi, and Ioannis Nikolakakis

Abstract Spray drying is a continuous manufacturing process that requires the use of a small number of excipients and offers great flexibility to formulation scientists due to the easy operation and scale-up. Although the direct interest of its application is for solubility improvement, other areas such as drug compatibility, especially for formulations with high drug dosing and controlled release delivery, can equally benefit by optimizing the co-spray-dried composition and operation variables. Application for solidification of biological agents is another attractive opportunity which is unfortunately slow-progressing due to the lack of understanding of physicochemical stability in the presence of excipients. Drug formulations as dry powders for inhalation are another important area for the application of spray drying which is not dealt with here. In this chapter, the basic principles of spray drying are presented followed by a critical presentation of cases where improvement of mechanical behaviour was achieved by co-processing with polymers. Next, cases where optimized drug/polymer/carbohydrate combinations succeeded in providing fine-tuned prolonged or delayed targeted delivery are presented. Finally, studies of co-spray drying aqueous dispersions with biologicals reporting in vitro release, maintenance of biological activity, and in vivo performance are discussed.

Keywords Oral dosage forms · Direct compression · Aqueous polymeric dispersions

I. Partheniadis · I. Nikolakakis (✉)
Department of Pharmaceutical Technology, School of Pharmacy, Faculty of Health Sciences, Aristotle University of Thessaloniki, Thessaloniki, Greece
e-mail: ioanpart@pharm.auth.gr; yannikos@pharm.auth.gr

N. Al-Zoubi
Department of Pharmaceutics and Pharmaceutical Technology, Faculty of Pharmaceutical Sciences, The Hashemite University, Zarqa, Jordan
e-mail: nzoubi@hu.edu.jo

D. Lamprou (ed.), *Nano- and Microfabrication Techniques in Drug Delivery*,
Advanced Clinical Pharmacy – Research, Development and Practical Applications 2,
https://doi.org/10.1007/978-3-031-26908-0_4

4.1 Introduction

Spray drying is a well-established technique with a long history of use in the food and chemical industry. The use of spray drying in the pharmaceutical industry dates to the early twentieth century when it was used for drying blood. Since then, it has been employed for various pharmaceutical applications including formation of amorphous solid dispersions, encapsulation of drugs and essential oils, and spray drying of bioactive agents (i.e., proteins, vaccines, DNA, antibodies) (Partheniadis et al. 2017; Vehring et al. 2020). It has been extensively used to produce compressible powdered drug compositions, inhalations, and taste-masked, sustained-, or targeted-release preparations (Al-Zoubi et al. 2021a; Al-Zoubi et al. 2022; Malamatari et al. 2020). It is capable of producing powders with particle size ~~ranging~~ from nanometers to micrometers depending on the dimensions of the drying chamber, and by careful selection of the type and composition of the sprayed liquid and of the operating conditions, it is possible to control the particle size, shape, density, flowability, crystallinity, and product dispersibility (Littringer et al. 2013; Vehring 2008). Additionally, spray drying can be used for both particle engineering and crystal engineering, and it is easily scalable (Poozesh and Bilgili 2019).

4.2 Spray Drying Process and Process Parameters

Spray drying is a single-step manufacturing process where a liquid feed is converted to a dried particulate form (Fig. 4.1). The main principles behind the process are the atomization of liquid feed into fine droplets and the evaporation of the solvent by means of a hot drying gas. The process follows four steps: liquid feedstock

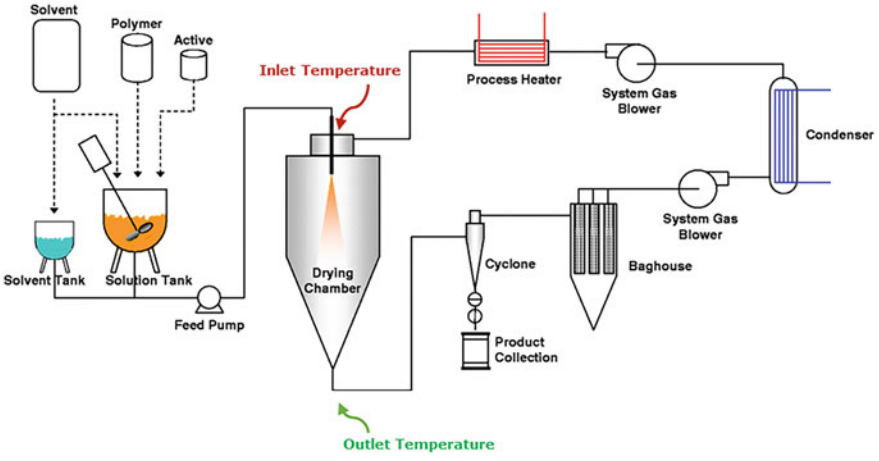

Fig. 4.1 Schematic representation of spray dryer instrumentation based on (Dobry et al. 2009)

preparation, atomization of the feed into a spray through a nozzle and contact with the hot drying gas, particle formation by evaporative mass transfer of the liquid from the droplet into the drying gas, and, lastly, separation of the dried product from the gas (Masters 1991).

4.2.1 Feedstock Preparation

The liquid feed should be of relatively low viscosity to be pumpable. It can be a solution, suspension, or emulsion of the drug(s), excipient(s), and solvent or solvent mixture. The type and composition of feedstock are chosen taking into account the solubility of the drug and the target product characteristics. In the case of emulsions and suspensions, the stability of the liquid feed is important as it is associated with the homogeneity of the spray-dried product and the operation of the dryer (e.g., nozzle blockage).

For spray drying colloidal systems, the size of dispersed phase should be smaller than the nozzle orifice to avoid clogging. Also, the dispersed phase particles should be approximately one order of magnitude smaller than the droplets to assure consistent composition of the spray-dried particles (Vehring et al. 2020). Increase of solids concentration in the liquid feed can result in larger particles with higher effective particle density (Elversson and Millqvist-Fureby 2005). For example, Cheow et al. (2010) reported that spray drying silica NPs at pH <7 and $<$ 1% w/w feed concentration resulted in particles with small aerodynamic diameter ($\sim$ 3 μm) and monodisperse size distribution while processing of higher feed concentrations led to higher particle size and multimodal size distribution (Cheow et al. 2010).

4.2.2 Atomization

In this step, the liquid feed is broken up into fine droplets with the use of a nozzle. Different types of atomizers are available for development of commercial pharmaceutical applications (two-fluid or pneumatic, hydraulic pressure, rotary disk atomizer, and ultrasonic nozzles). The two-fluid nozzles are commonly used in the pharmaceutical industry due to their suitability for small-scale plants and the formation of small size droplets compared to other types of atomizers. During the process, atomization occurs by rapid expansion of the supplied gas, mixed with the liquid feed either inside the nozzle body (internal mixing) or at its tip (external mixing). The velocity of the gas is much higher than that of the liquid at the orifice and provides the work required to create the large surface area of the spray. A detailed study on spray drying and atomization using a two-fluid nozzle for the production of inhalable particles can be found elsewhere (Kemp et al. 2013).

4.2.3 *Drying*

This is the step of solvent evaporation, which is a coupled heat and mass transfer process. The driving force is the difference between the solvent vapour pressure in the droplet and its partial pressure in the gas phase. The drying kinetics of droplets containing suspended nanoparticles can be divided into two stages. A constant rate period comprising solvent evaporation from the droplet surface results in a constant rate of decreasing diameter. This is followed by a falling rate period starting at the critical moisture content, where the solvent from the droplet interior cannot keep the entire surface saturated, resulting in the formation of a shell by deposition of solid matter at the liquid-air interface. During this stage, evaporation continues through the pores of the shell until equilibrium moisture content is reached, signifying the end of drying (Fig. 4.2) (Mezhericher et al. 2010; Osman et al. 2017).

Particle formation can be described by two dimensionless parameters: the Peclet number (*Pe*) and the initial saturation of excipients. Pe represents the rate of liquid evaporation from the drying droplet relative to the diffusion rate of dissolved or nano-dispersed phase towards the centre of the drying droplet (Eq. 4.1) (Tsapis et al. 2002).

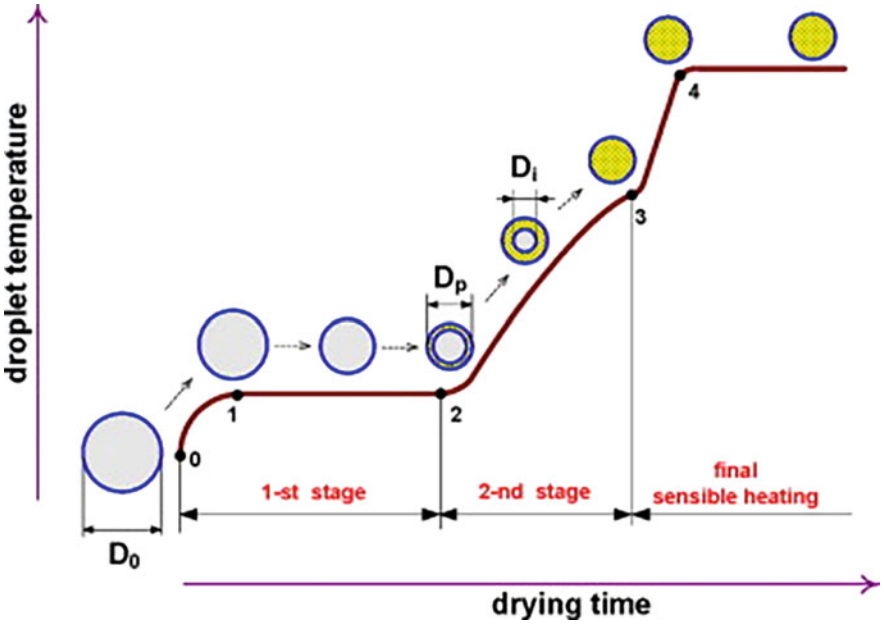

Fig. 4.2 Drying kinetics. The time interval between 0 and 1 corresponds to droplet initial heating, period 1–2 to droplet evaporation period, period 2–3 to second drying stage, and period 3–4 to particle heating up to equilibrium with the surrounding drying agent (D_0, initial diameter; D_p, particle diameter; D_i, internal diameter) based on (Mezhericher et al. 2010)

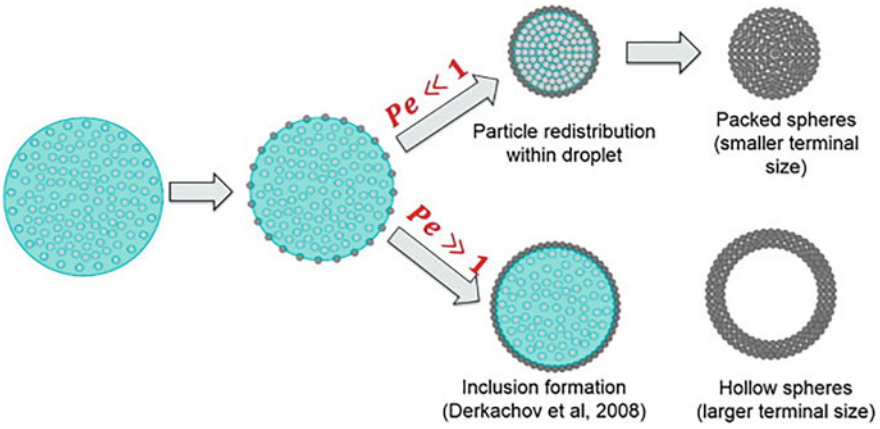

Fig. 4.3 Drying of droplets containing particles of low (≪1) and high (≫1) Peclet number based on (Wei et al. 2016)

$$Pe = R^2/\tau_d D \tag{4.1}$$

R is the droplet radius, D the diffusion coefficient, and τ_d the drying time. High Pe means accumulation of dispersed phase at the surface and shrinkage. From Eq. (4.1) appears that the drying temperature and solvent type which affect the rate of evaporation, on one hand, and the particle size and solubility of dispersed solid phase that affect diffusivity control the Pe value.

For low $Pe \gg 1$, diffusion is faster or of the same order with the radial velocity of the receding droplet surface, and the dispersed phase is evenly distributed in the droplet during evaporation, resulting in spherical particle agglomerates of rough or smooth surface depending on the size of crystallites. For $Pe \ll 1$, the particles have insufficient time to diffuse, and they accumulate at the liquid-air interface. As evaporation continues through the crust, hollow or doughnut shape particles are formed (Fig. 4.3) (Vehring 2008; Wei et al. 2016). Viscoelastic material behaviour leads to the formation of a flexible surface skin in the late stages of drying, causing localized collapse and surface cavities (Torge et al. 2017). The morphology of the spray-dried particles was found to depend on the size and concentration of the suspended particles as well as the initial droplet volume. Osman et al. (2017) reported that suspensions containing NPs exhibit low Pe due to high diffusion rate and upon drying form a spherical shell with irregular surfaces (Osman et al. 2017). Conversely, suspensions containing microparticles with high Pe number, upon drying, tend to form a surface crust that collapses at the late drying stages resulting in particles with half apricot-like shape. Spray-dried solutions of the water-soluble mannitol produce spherical and smooth particles due to the low hygroscopicity of the sugar and its high melting point allowing fast drying with high nucleation rate and nanocrystal formation (Littringer et al. 2013).

4.2.4 Separation

The separation of the dry particles from the gas stream is the final step of the process. Excess liquid is first condensed at the bottom of the drying chamber. The dry particles continue their route following the gas stream and are collected in vessels using cyclones with the action of centrifugal forces. Standard cyclones have low efficiency for collecting particles smaller than 2 μm which has led to the use of cyclones with improved design and altered dimensions (Fig. 4.4) which give higher production yields of the high-cost biopharmaceuticals (Maa et al. 1998). Use of an 'improved', narrow cyclone was found to increase the production yield of amorphous trehalose (Maury et al. 2005). Also, production of inhalable particles by spray

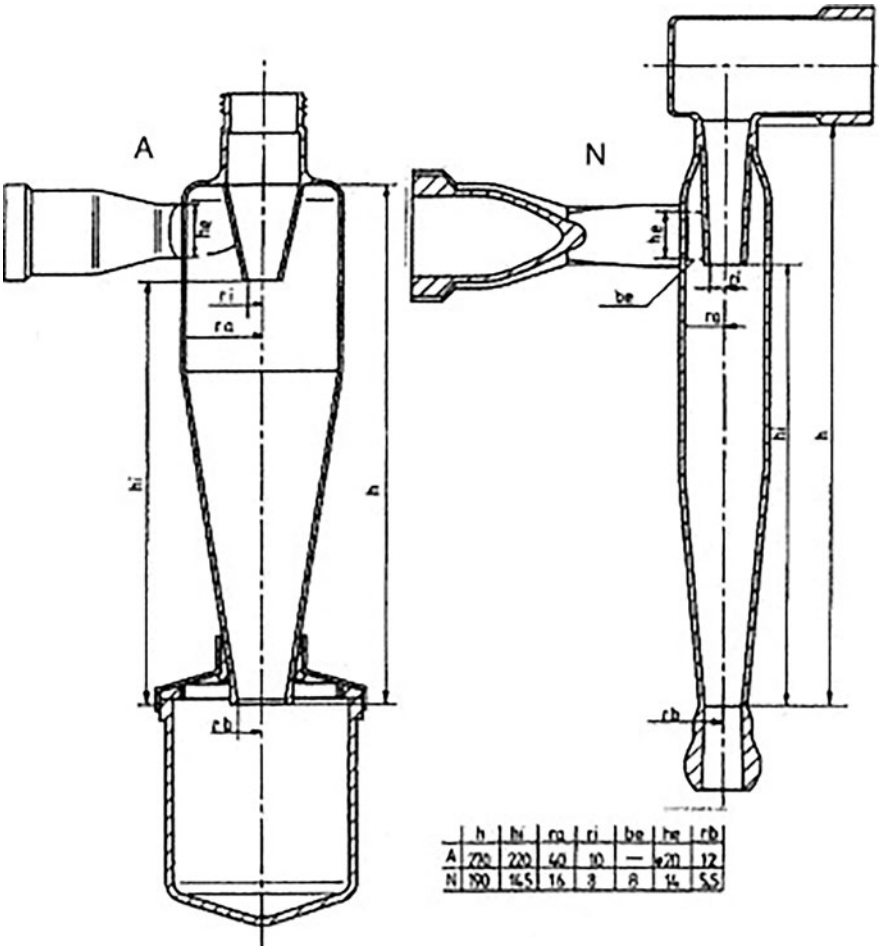

	h	hi	ra	ri	be	he	rb
A	720	220	40	10	—	≈20	12
N	390	165	16	8	8	14	5.5

Fig. 4.4 Design of a standard Buchi cyclone (left) and an improved cyclone (right) based on (Maury et al. 2005)

drying using the Buchi B-290 equipped with the standard cyclone resulted in about 13% product recovery, whereas spray drying of the same materials using the high-efficiency cyclone delivered product yields of 50–70% (Kemp et al. 2016).

4.3 Particle Engineering for Direct Compression

Spray drying has been particularly important for enhancing the compression of poorly compressible high-dose drugs. Although the majority of the studies report combinations of drugs with auxiliaries, there are some studies reporting spray drying of a solution of drug alone, aiming for compression improvement via changes in the solid state, particle size, shape, and intraparticle porosity. The main investigations of drugs spray-dried alone or with excipients are summarized in Table 4.1.

Studies on spray drying acetazolamide and chlorothiazide drugs or their salts alone resulted in nanoparticulate-based microparticles composed of amorphous nanoparticles or nanocrystals with improved tabletability mainly due to the increased specific surface area (Paluch et al. 2012; Paluch et al. 2013) or due to amorphization (Di Martino et al. 2001).

Co-spray drying of metformin hydrochloride, naproxen and its sodium salt, paracetamol, ibuprofen, and cimetidine with hydrophilic polymers and polysaccharides has been reported (Al-Zoubi et al. 2017; Barot et al. 2010; Gonnissen et al. 2008a; Gonnissen et al. 2007; Gonnissen et al. 2008b; Joshi et al. 2010; McDonagh et al. 2020; Rathod et al. 2019; Vanhoorne et al. 2016). Co-spray drying paracetamol with carbohydrates gave different outcome depending on the carbohydrate compound. Mannitol and maltodextrin enhanced compactability, while erythritol increased packability and flowability (Gonnissen et al. 2007). The product was directly compressible after blending with a small proportion of ~5% crospovidone (Gonnissen et al. 2008a; Gonnissen et al. 2008b). Similarly, ibuprofen and cimetidine benefited by co-spray drying with polysaccharides which resulted in improved powder flowability and compactibility.

Different inlet feed solvent compositions of paracetamol with lactose were explored by increasing the soluble fraction of lactose in the feed. This increase resulted in more intimate mixing in the spray-dried product and greater compressibility and tabletability (McDonagh et al. 2020). Further improvement of paracetamol properties was achieved by co-spray drying with mannitol (20%) and PVP (5%). Strong tablets with low friability were obtained which was attributed to the coating of paracetamol crystals with these two excipients. Furthermore, improvement of cefuroxime axetil compressibility was achieved by co-spray drying a slurry of drug with chitosan chlorhydrate/mannitol (1:1) in isopropanol (Rathod et al. 2019). Co-spray drying celecoxib-PVP-meglumine ternary mixture produced amorphous celecoxib which survived devitrification after compaction (Joshi et al. 2010).

High-dose drugs with poor compactibility have also benefited from co-spray drying. Solutions of the high dosing (500–800 mg/tablet), poorly compatible metformin HCl with 2% PVP K30 resulted in a product of excellent flowability and

Table 4.1 Studies for direct compression of drugs spray-dried alone or co-spray-dried with excipients based on (Al-Zoubi et al. 2021a)

Drug	Nominal amount per tablet (mg)	Additive(s)	Additives nominal percentage (%)	Functional property alterations related to improvement of direct compression	Reference
Spray-dried drugs					
Acetazolamide	250	n.a.	0	Formation of mixture of polymorphs I and II More isodiametric microparticles Reduced elastic recovery Higher tensile strength	Di Martino et al. (2001)
Chlorothiazide	250–500	n.a.	0		Paluch et al. (2012)
Chlorothiazide sodium		n.a.	0	Higher specific surface area and superior tabletability of nanoparticulate microparticles obtained by spray drying	Paluch et al. (2013)
Chlorothiazide potassium		n.a.	0	Higher specific surface area and superior tabletability of nanoparticulate microparticles obtained by spray drying	Paluch et al. (2013)
Co-spray-dried drug excipients					
Celecoxib	50–400	PVP Meglumine	30	High degree of amorphization, more isodiametric microparticles, lower Carr's index, lower angle of repose, lower Hausner's ratio, higher mass flow rate, lower yield pressure (Heckel), higher compactability and tabletability	Joshi et al. (2010)
Cefuroxime axetil	125–500	Mannitol Chitosan chlorhydrate	50	Lower yield pressure (Heckel)	Rathod et al. (2019)

(continued)

Table 4.1 (continued)

Drug	Nominal amount per tablet (mg)	Additive(s)	Additives nominal percentage (%)	Functional property alterations related to improvement of direct compression	Reference
Metformin HCl	500–1000	PVP	0–3	Disruption of the crystal lattice, more isodiametric microparticles	Barot et al. (2010)
Metformin HCl	500–1000	PVP Copovidone HPMC Sodium alginate Sodium CMC	0–5	Reduced crystallinity, more isodiametric microparticles, reduced elastic recovery, higher compactability, tabletability, higher work of compaction	Al-Zoubi et al. (2017)
Naproxen	250–500	HPMC	5	Reduced crystallinity, more isodiametric particles, higher compactability and tabletability	Al-Zoubi et al. (2021b)
Naproxen sodium	275–550	HPMC	5	Increased dihydrate content, more isodiametric particles, higher compactability and tabletability	Al-Zoubi et al. (2021b))
Paracetamol	325–650	Erythritol Maltodextrin Mannitol	50.8	Improved flowability and compactability; prevented capping and lamination	Gonnissen et al. (2007)
Paracetamol	325–650	Erythritol Mannitol Maltodextrin Crospovidone Colloidal silicon dioxide Polysorbate 80	30–58.1	Improved flowability and compactability, production of an RTC mixture	Gonnissen et al. (2008a, 2008b)
Ibuprofen	200–800	Mannitol Erythritol Maltodextrin Crospovidone Colloidal silicon dioxide Polysorbate 80	25–55	Improved flowability and compactability, production of an RTC mixture	Gonnissen et al. (2008b)

(continued)

Table 4.1 (continued)

Drug	Nominal amount per tablet (mg)	Additive(s)	Additives nominal percentage (%)	Functional property alterations related to improvement of direct compression	Reference
Cimetidine	200–400	Mannitol Erythritol Maltodextrin Kollidon_cl Colloidal silicon dioxide Polysorbate 80	30–55	Improved flowability and compactability	Gonnissen et al. (2008b)
Paracetamol	325–650	Lactose	50	Improved compressibility and compactability, lower yield pressure	McDonagh et al. (2020)
Paracetamol	325–650	Mannitol	20–25	Improved tabletability and decreased friability	Vanhoorne et al. (2016)
		PVP	0–5		

compressibility. Furthermore, co-spray drying metformin HCl with five hydrophilic polymers (HPMC, PVP, copovidone, sodium alginate, and carmellose sodium) resulted in increased amorphous drug content associated with increased deformability and reduced ejectability but only when anionic polymers were used, which could make ionic interactions with the positively charged ammonium group of the drug (Al-Zoubi et al. 2017). Naproxen and naproxen sodium are also high-dose drugs with problematic compaction. Their co-processing with HPMC led to reduced crystallinity of naproxen and higher content of dihydrate naproxen sodium. After blending with ~5% auxiliaries, tablets with superior mechanical properties were obtained compared to unprocessed or spray-dried alone drug powders.

In conclusion, due to the poor solubility of synthetic drugs coming out of throughput screening, formulations of new drugs tend to contain high doses comprising a large proportion of the tablet weight. The same is the case with many drugs such as nonsteroidal anti-inflammatories and pain killers that have been in the market for a long time (Bergström et al. 2007). As a consequence, the compaction characteristics of the drugs govern the mechanical behaviour of such formulations, since the drugs are present in levels above 25–30% which is the percolation limit. This points to the importance of the processing benefits on compactibility obtained by co-spray drying. These benefits are attributed partly to amorphization of the drug but mainly to the porous structure of the spray-dried particles enhanced by the use of spray drying auxiliaries such as sugars and by the binder action of the polymers present.

4.4 Particle Engineering for Controlled Release Using Aqueous Polymeric Dispersions

Aqueous dispersions of water-insoluble polymers (APDs) traditionally employed for coating tablets and multiparticulates can be co-spray-dried with drugs dissolved or suspended in them. Their advantages are as follows: avoid use of hazardous organic solvents, easy processability due to their low viscosity, adjustable polymer content, commercial availability, and short processing time (Felton and Porter 2013; Lecomte et al. 2004; Yang and Craig 2020). Co-spray drug/APD produces composite microparticles that may be formulated as a matrix system to deliver a modified release product, thus circumventing the risk of film rupture (Al-Zoubi et al. 2019; Al-Zoubi et al. 2021a; Jedinger et al. 2014), or as a multiparticulate system (MUPS) suitable for oral disintegrating tablets (Kim et al. 2014; Lazzari et al. 2018; Mizumoto et al. 2008; Wei et al. 2013) and films (Wasilewska et al. 2020). They have also been investigated for delivery via the skin through transdermal (Arici et al. 2014; Brniak et al. 2015), subcutaneous injection (Arici et al. 2014), and microneedle systems (Akalkotkar et al. 2015). Although feasible, formulations targeting the nasal, rectal, and vaginal routes are still understudied. The applications of co-spray drying with APDs in the cited articles are classified into four categories based on the primary objective: (i) prolonged release (PR), (ii) delayed release (DR), (iii) protection of biological drugs, and (iv) taste masking. The studies are listed in Tables 4.2, 4.3, and 4.4.

4.4.1 Prolonged Release

The application of APD in the formulation of prolonged release matrix-type dosage forms by co-spray drying attracts interest for several reasons: the polymer in the APDs is in colloidal nanosized form, increasing tortuosity and drug percolation threshold compared to large particles (Agrawal et al. 2003; Crowley et al. 2004; Millán et al. 1998; Obeidat and Alzoubi 2014); co-spray drying results in intimate drug-polymer mixing (Al-Zoubi et al. 2011; Chen et al. 2008); and co-spray-dried mixtures are more compressible (Sakhnini et al. 2015) resulting in low matrix porosity and more effective release control. APDs that have been studied for prolonged release by co-spraying with drugs are ethylcellulose-based dispersions (Aquacoat® ECD and Surelease®) followed by methacrylate-based (Eudragit® RS 30 D, Eudragit® NE 30 D, and Eudragit® RL 30 D). The release studies were related to agglomerates and microparticles (Arici et al. 2014; Kasashima et al. 2016; Kulkarni et al. 2013; Liu et al. 2013b; Nova et al. 2019; Rattes and Oliveira 2007; Souza and Oliveira 2012), matrix tablets (Al-Zoubi et al. 2016; Kulvanich et al. 2002; Takeuchi et al. 1989; Thakare and Singh 2006), or both (Al-Zoubi et al. 2008; Garekani et al. 2015; Garekani et al. 2013; Wei et al. 2013). In vivo studies

Table 4.2 Studies on co-spray drying of drugs with aqueous polymer dispersions for prolonged release based on (Al-Zoubi et al. 2022)

APD	Co-spray-dried excipients	Model drug	Particle size (μm)	Presentation	Reference
Eudragit® E 30D	Colloidal silicon dioxide	Theophylline	10.0–30.0	Matrix tablets	Takeuchi et al. (1989)
Eudragit® RS 30D	n.a.	Chlorpheniramine maleate	n.a.	Matrix tablets	Guo and Bodmeier (1997)
		Ibuprofen			
		Naproxen			
Surelease®	PVP Lactose Colloidal silicon dioxide	Theophylline	5–20	Matrix tablets	Kulvanich et al. (2002)
Eudragit® NE 30D	Talc Colloidal silicon dioxide	Diclofenac sodium	10.5–12.9	Matrix tablets	Thakare and Singh (2006)
Eudragit® RS 30D	Propylene glycol Talc Colloidal silicon dioxide Titanium dioxide	Diclofenac sodium	9.1–24.5[c]	Microparticles	Rattes and Oliveira (2007)
Surelease®			10.4–19.0		
Kollicoat® SR 30D	n.a.	Buspirone HCl	2–20[a]	Matrix tablets	Al-Zoubi et al. (2008)
Eudragit® RS 30D					
Eudragit® RS 30D	Propylene glycol Titanium dioxide	Ketoprofen	25.6 ± 1.8[b]	Microparticles	Souza and Oliveira (2012)
Eudragit® RS 30D	n.a.	Theophylline	38–46[b]	Matrix tablets	Garekani et al. (2013)
n.a.	Eudragit® RSPO[d]		32–43[b]		
Eudragit® RS 30D	Talc Colloidal silicon dioxide	Metformin HCl	4.55–6.61	Microparticles	Kulkarni et al. (2013)
Eudragit® RL 30D			4.39–6.77		
Surelease®			4.41–6.53		
Eudragit® NE	Lactose	Vitamin B12	70.65–100.55[c]	Microparticles	Liu et al. (2013b)
	Silica nanoparticles		98.10–114.81		

(continued)

Table 4.2 (continued)

APD	Co-spray-dried excipients	Model drug	Particle size (μm)	Presentation	Reference
Eudragit® RS 30D	PEG 6000 Starch 1500®	Ketoprofen	n.a.	Orally disintegrating tablets	Wei et al. (2013)
Aquacoat® ECD	Triethyl citrate Colloidal silicon dioxide	Naproxen	10.8–14.7	Transdermal drug delivery system	Arici et al. (2014)
Surelease®	n.a.	Theophylline	3–40[c]	Matrix tablets	Garekani et al. (2015)
n.a.	Ethocel 20 cps[d]		1–25		
Kollicoat® SR 30D	PVP	Diltiazem HCl	9.68–23.14	Matrix tablets	Al-Zoubi et al. (2016)
Aquacoat® ECD	Triethyl citrate	Mirabegron	<200	Microparticles	Kasashima et al. (2016)
Surelease®	Pectin	L-alanyl-L-glutamine dipeptide	1.77–2.52	Microparticles	Nova et al. (2019)

[a]The mean particle size was not measured nor reported. This estimate is based on SEM images presented
[b]Reported for optimized formulation
[c]A range was reported based on optical microscopy, and it varies as per individual formulation
[d]Polymer was dissolved in organic solvent(s)

supplemented in vitro results have also been reported (Kasashima et al. 2016; Nova et al. 2019; Wei et al. 2013).

A *proof-of-concept* study compared co-spray-dried mirabegron lauryl sulphate (LS) salt/complex microparticles with the corresponding salt/complex solution. Encapsulation by co-spray drying mirabegron lauryl sulphate (LS) salt/complex in ethylcellulose with Aquacoat® ECD gave a sustained-release oral suspension with low Cmax and peak-trough fluctuation with slower release than the non-encapsulated lauryl sulphate salt/complex. Studies in dogs confirmed the sustained-release profile of the suspension (Kasashima et al. 2016). Further studies reported that important formulation parameters impacting prolonged release were the type of APD (Al-Zoubi et al. 2008; Kulkarni et al. 2013; Rattes and Oliveira 2007), the drug solubility (Guo and Bodmeier 1997), the addition and percentage of co-excipients (Al-Zoubi et al. 2016; Kulvanich et al. 2002; Liu et al. 2013b; Nova et al. 2019), and the polymer/drug (P:D) ratio (Al-Zoubi et al. 2008; Guo and Bodmeier 1997; Kasashima et al. 2016; Kulvanich et al. 2002; Takeuchi et al. 1989; Thakare and Singh 2006). In particular, release of diclofenac sodium co-spray-dried with Surelease® aqueous dispersion was slower than Eudragit® RS 30 D. Particle size of uncompacted microparticles also affected release (Rattes and Oliveira 2007). Feed flow rate was the important process parameter (Rattes and Oliveira 2007). Microparticles prepared at high feeding rate gave slow release due to the larger size of the resulting microparticles (Rattes and Oliveira 2007).

Table 4.3 Studies on co-spray drying of drugs with aqueous polymer dispersions for delayed drug release based on (Al-Zoubi et al. 2022)

APD	Co-spray-dried excipients	Model drug	Particle size (μm)	Presentation	Reference
Eudragit® L 30D	PEG 6000 Colloidal silicon dioxide	Theophylline	10.0–30.0	Matrix tablets	Takeuchi et al. (1989)
Eudragit® L100–55					
Eudragit® L 30D	PEG 6000 Colloidal silicon dioxide Soluble starch Lactose	Diclofenac sodium	3.0–12.0[a]	Enteric tablets	Lin and Kao (1991)
n.a	Eudragit® S 100[b]	Pantoprazole sodium sesquihydrate	9.1 (span 1.55)	Microparticles	Colomé et al. (2007)
Eudragit® RS 30D	n.a.		10.9 (span 1.69)		
Eudragit® RS 30D	Eudragit® S 100[b]		53.5 (span 3.60)		
Eudragit® L 30D-55	n.a.	Vitamin B12	75.06–90.17[c]	Microparticles	Liu et al. (2013a)
	Eudragit® NE 30D		83.26–90.56		
	TEOS		91.01–94.37		
Eudragit® L 30D-55	Citric acid	Losartan potassium	1.3–7.3[d]	Microparticles	Jankowski et al. (2014)
	Triethyl citrate				
Eudragit® FS 30D	Zein Gantrez® AN119	Curcumin	10.2–25.6[c]	Microparticles	Blanco-García et al. (2017)
Eudragit® FS 30D	n.a.	S-nitrosoglutathione glutathione	5.0–7.0	Microparticles	Shah et al. (2017)
Eudragit® L 30D-55	Triethyl citrate	Furosemide	11.4–33.0	Microparticles	Ostróżka-Cieślik et al. (2018)

[a]The mean particle size was not measured nor reported. This estimate is based on SEM images presented
[b]Polymer was dissolved in organic solvent(s)
[c]A range was reported based on optical microscopy, and it varies as per individual formulation
[d]Reported for optimized formulation

Table 4.4 Studies on co-spray drying of drugs with aqueous polymer dispersions for protection/delivery of biological drugs based on (Al-Zoubi et al. 2022)

APD	Co-spray-dried excipients	Model drug	Particle size (μm)	Presentation	Reference
HPMCAS-MF Aquacoat® ECD	Magnesium stearate	*Actinobacillus pleuropneumoniae* antigens	2 – 25[a]	Microparticles for oral vaccine	Liao et al. (2001))
AQOAT® Aquacoat® ECD	Magnesium stearate	*Actinobacillus pleuropneumoniae* antigens	5.00–30.00	Microparticles for peroral vaccine	Liao et al. (2003))
Eudragit® L30D-55	Talc Glycerol	*Mycoplasma hyopneumoniae* antigens	n.a.	Microparticles for oral vaccine	Lin et al. (2003))
HPMCAS-MF	n.a.	*Escherichia coli* antigen	3.00–30.0[c]	Microparticles for oral vaccine	Liao et al. (2004))
Aquacoat® ECD	n.a.				
n.a.	Ethylcellulose[d] Aqualon™ ECN7, ECN14, ECN22, ECN50, ECN100				
Aquacoat® ECD AQOAT®	Bovine serum albumin	Extracellular antigen from B16 melanoma cells	2.55–5.50	Microparticles for oral vaccine	Lai and D'Souza (2007))
Eudragit® L100-55	n.a.	Bromophenol blue-loaded bovine serum albumin	2.48–8.74[b]	Enteric coated microparticles	Bejugam et al. (2008))
Eudragit® L30D-55, FS30D	n.a.	*Vibrio cholerae*	2.67–3.41	Microparticles for oral vaccine	Año et al. (2011))
Aquacoat® ECD AQOAT®	n.a.	Bovine serum albumin	0.63–1.40	Microparticles for transdermal vaccine	Bhowmik et al. (2011))
AQOAT® Eudragit® FS 30D	Chitosan glycol Trehalose Fluorescein isothiocyanate-albumin	Whole cell lysate	0.35–2.00	Microparticles for oral vaccine	Akalkotkar et al. (2012))

(continued)

Table 4.4 (continued)

APD	Co-spray-dried excipients	Model drug	Particle size (μm)	Presentation	Reference
Eudragit® FS 30D AQOAT®	β-Cyclodextrin Trehalose Tween 20	HBs antigen	0.63–1.40	Microparticles for oral vaccine	Bhowmik et al. (2012))
Aquacoat® ECD AQOAT®	β-Cyclodextrin Trehalose Tween 20	Whole cell lysate (4T07 antigen)	1.0–4.0	Microparticles for oral vaccine	Chablani et al. (2012a))
Eudragit® FS 30D AQOAT®	Chitosan glycol Trehalose Bovine serum albumin	Fluorescein isothiocyanate-albumin	1.53	Microparticles for oral vaccine	Chablani et al. (2012b))
AQOAT® Aquacoat® ECD	Bovine serum albumin	Whole cell lysate	0.47–2.03	Microparticles for oral vaccine	D'Souza et al. (2012))
AQOAT® Eudragit® FS 30D	Chitosan glycol	Mouse serum albumin	1.55–2.05	Microparticles for transdermal/subcutaneous vaccine	Tawde et al. (2012))
Eudragit® L30D-55	n.a.	*Vibrio cholerae*	8.87 ± 0.04	Microparticles for oral vaccine	Pastor et al. (2013))
	Sodium alginate		8.92 ± 0.03		
	Carbopol®		7.64 ± 1.20		
Eudragit® L30D-55	Sodium alginate	*Vibrio cholerae*	7.55 ± 0.25[c]	Gastro-resistant microparticles	López et al. (2014))
	n.a.		8.93 ± 0.01		
Aquacoat® CPD	Sodium alginate	*Vibrio cholerae*	6.05–6.50	Microparticles for oral vaccine	Patil-Gadhe and Pokharkar (2014))

Aquacoat® ECD AQOAT®	β-Cyclodextrin	Insulin	0.5–1.2	Microparticles for oral delivery	D'Souza et al. (2015))
Aquacoat® ECD AQOAT®	β-Cyclodextrin Trehalose Tween 20	Whole cell lysate (4 T07 antigen)	1.0–4.0	Microparticles for skin vaccine	Chablani et al. (2019))

[a]The mean particle size was not measured nor reported. This estimate is based on SEM images presented
[b]Reported for optimized formulation
[c]A range was reported based on optical microscopy, and it varies as per individual formulation
[d]Polymer was dissolved in organic solvent(s)

Comparison of Eudragit® RS 30 D, Eudragit® RL 30 D, and Surelease® APDs on the controlled release of the water-soluble metformin hydrochloride showed that prolongation and best control were achieved from microparticles prepared by co-spray drying the drug with Eudragit® RS 30 D at P/D ratio (11:1) (Kulkarni et al. 2013). The release from non-compacted buspirone HCl agglomerated particles obtained by co-spray drying with Kollicoat® SR 30 D or Eudragit® RS 30 D decreased with increasing P/D, but the APD type had no significant influence. However, the release from matrix tablets of microparticles of drug co-spray-dried with Kollicoat® SR 30 D was slower than Eudragit® RS 30 D, due to the plasticity of the PVP present in Kollicoat® and its binding action (Al-Zoubi et al. 2008).

Hydrophilic additives such as lactose (Kulvanich et al. 2002; Liu et al. 2013b) and pectin (Nova et al. 2019) increase drug release rate from APD-based matrices. Lactose and CSD nanoparticles have been used as additives to Eudragit® NE 30 D to modify the release of vitamin B12. Lactose is distributed in the matrix resulting in faster release by enhancing polymeric matrix swelling, whereas CSD remains at the microparticle surface causing erosion and initial burst release. Prolonged release of diclofenac sodium from tablets prepared by compaction of drug/Eudragit® NE 30 D co-spray-dried microparticles at P/D 1.2:1 ratio was achieved. Adding CSD at about one third of polymer reduced tackiness and improved the yield of spray drying without affecting release (Thakare and Singh 2006). In a further study (Kulvanich et al. 2002), addition of 5–10% PVP decreased the release rate of theophylline from matrix tablets prepared from drug microparticles co-spray-dried with Surelease®. This was ascribed to reduced porosity by filling of the pores with polymer leading to enhanced interparticle bonding, mechanical strength, and ultimately lower diffusion rate.

Slower release was obtained by co-spray drying diltiazem HCl with Kollicoat® SR 30 D compared with physical mixture of drug with Kollidon® SR powder (Al-Zoubi et al. 2016). This was ascribed to the lower PVP content in Kollicoat® SR 30 D dispersion compared to Kollidon® SR powder (9% and 19%, respectively). Also, the co-spray-dried particles compressed better than the PM giving stronger tablets. Addition of PVP K30 to microparticles increased the drug release from the tablets. L-alanyl-l-glutamine (AGP) sustained-release microparticles were prepared by co-spray drying with Surelease® and pectin. Increasing pectin content and the pH of the dissolution medium improved the release. This result was supplemented by in vivo studies. By adjusting the Surelease/pectin ratio, the desired in vitro release and in vivo activity could be achieved. Comparison of theophylline microparticles of theophylline co-spray-dried with APDs of Eudragit® RS 30 D (Garekani et al. 2013) and Surelease (Garekani et al. 2015), with ethanolic (96%) drug solutions co-spray-dried with the same polymers, showed that the release from microparticles from organic solutions and their compacted matrices was slower compared to the release from the APD-based microparticles and compacted matrices. Also, the release was slower from matrices than from microparticles (Garekani et al. 2015; Garekani et al. 2013).

Most studies progress the co-spray-dried powder into matrix tablets. There are however studies on other dosage forms. Sustained-release oral suspension of

mirabegron lauryl sulfate (LS) salt/complex was prepared (Kasashima et al. 2016). Oral disintegrating tablet of co-spray-dried ketoprofen with Eudragit® RS 30 D, starch® 1500, and PEG 6000 provides sustained release for about 24 h after an initial rapid (30 s) disintegration (Wei et al. 2013). The sustained-release action was also seen in in vivo studies in beagles, and there was an in vitro-in vivo correlation. Overall, the release profiles of compacted co-spray-dried microparticle matrices follow Fickian diffusion (Al-Zoubi et al. 2016; Kulvanich et al. 2002; Takeuchi et al. 1989), which is common for insoluble polymer matrices with negligible erosion. Addition of hydrophilic excipients shift release towards zero-order kinetics (Al-Zoubi et al. 2016; Thakare and Singh 2006). On the other hand, release from microparticles was reported to follow anomalous transport (Nova et al. 2019).

In conclusion, the above-cited works show that use of selected additives at the right drug/polymer/additive proportions can provide fine-tuning of the release profiles of drugs. The type of the APD, the particle size of the spray-dried powders which is influenced by the feeding rate, and the nozzle characteristics should be optimized according to the target product. Finally, it is important that the spray-dried product should retain its release characteristics after incorporation into a final dosage form. This will necessitate the use of auxiliaries such as disintegrants to enable rapid redispersibility in the case of a tablet form, or addition of agents for viscosity enhancing, pH control, and taste improvement in the case of oral suspensions.

4.4.2 Delayed Release

Co-spray drying of drugs with APDs has been employed for delaying release until the drug reaches the distal part of the GIT, thus offering improved efficacy and reduced side effects over conventional delivery systems. There are not many articles published in this area. In Table 4.3 six of these articles are for targeting specific parts of the GIT using Eudragit® L 30 D 55 (dissolves above pH 5.5 and targets the duodenum), Eudragit® L 30 D (dissolves above pH 6.0 and targets the jejunum), and Eudragit® FS 30 D (dissolves above pH 7.0 and targets the ileum and colon). Two studies had a dual purpose, i.e., to provide targeting besides sustained release. These systems combine matrix-forming excipients (Eudragit® RS 30 D, NE 30 D, silicates) with enteric and pH-sensitive methacrylic polymers (Eudragit® L 30 D 55, L 30 D, FS 30 D, Eudragit® S100).

Theophylline enteric and sustained-release tablets prepared by co-spray drying with Eudragit® L30 D or L100-55 provided complete enteric release with polymer/drug ratio 3:1 (Takeuchi et al. 1989). In parallel, tablets with 2–40% E 30 D showed sustained release, independently of the pH of the dissolution media. The controlled release property was attributed to the homogeneity of the polymeric matrix formed by spray drying and subsequent compression. Another dual-purpose study involved preparation of pantoprazole-loaded microparticles by co-spray drying the drug with the combination of the enteric Eudragit® S100 with the sustained-release Eudragit® RS 30 D dispersion (Colomé et al. 2007). This combination provided good

gastroprotection. Orally administered microparticles were able to protect the rat stomach against ulceration induced by ethanol.

Sodium diclofenac enteric-coated microcapsules were prepared by co-spray drying with Eudragit® L 30 D followed by blending with microcrystalline cellulose (Neocel®) and pregelatinized starch (flostarch®). The last additives improved the flow properties of the spray-dried powder. Both the spray-dried powder and the corresponding tablets provided enteric release (Lin and Kao 1991). Homogeneous microencapsulates of vitamin B12 were prepared via microfluidic co-spray drying with Eudragit® L 30 D 55 (Liu et al. 2013a). Addition of hydrolysed tetraethoxysilane yielded a rigid porous interpenetrating network, while incorporation of Eudragit® NE formed a flexible dense entangled polymer network, which altered the swelling behaviour of Eudragit® L polymer and modified the release rates. Overall, uniform microparticles with almost completely encapsulated active ingredient and tailored controlled release enteric microparticles were made.

A microparticulate system of curcumin (CRM) intended to heal inflammations in the intestine was developed by Blanco-García et al. (Blanco-García et al. 2017). Microspheres based on zein (ZN) and methyl vinyl ether and maleic acid copolymer (PVMMA) were prepared by co-spray drying and coated with Eudragit® FS 30D. FTIR and DSC studies suggested the presence of a-helix structure for ZN which is stabilized by PVMMA or CRM by hydrogen bonding. Although encapsulation efficiency was high (89%) for ZN/PVMMA microspheres, coating with Eudragit® led to a decrease of 62%. Coating retained 20% of CRM within 6 h of release, and the anti-inflammatory activity of CRM-loaded microspheres was confirmed by using cell line RAW 264.7. In conclusion, the ZN/PVMMA microspheres present a serious alternative for delivering CRM to the intestine.

Glutathione (GSH) and S-nitrosoglutathione (GSNO) pH-sensitive microparticles were prepared by co-spray drying with Eudragit® FS 30 D (Shah et al. 2017). Fast release was reported at basic pH 7.4, sustained release at pH 6.8, but no release at acidic pHs of 1.2, 3.0, and 6.0. Optimal particle size and shape were obtained at inlet temperature 120 °C, pump rate 5 mL/min, and air flow 100%. Therefore, using Eudragit® FS 30 D as a gastro-resistant rate-controlling polymer, GSNO could be targeted to the colon for treatment of inflammatory bowel diseases including Crohn's disease. Microspheres of furosemide obtained by co-spray drying with Eudragit® L30 D 55 were prepared by Ostróżka-Cieślik et al. (Ostróżka-Cieślik et al. 2018). The optimized parameters were inlet temperature 140 °C, pump rate 10%, and aspiration 80%. Release from microspheres after 2 h in 0.1 HCl was only 28.68% FS, while the remaining drug was released within 30 min in pH 6.8 buffer. Allicin-rich extract phytosome (ArE-Ps) is encapsulated in Eudragit L 30D-55 by co-spray drying at three ArE-Ps:polymer ratios (1:1, 1:1.5, and 1:2) (Nining et al. 2021). No allicin release was noticed in acidic medium, whereas in phosphate buffer, release reached between 55.23 and 61.26% after 45 min confirming enteric release from the microparticles.

The results of the above studies show the potential of APDs for the formulation for targeted delivery dosage forms by delaying drug release using suitable commercial APDs in combination or with complimentary additives.

4.4.3 Protection and Delivery of Biological Drugs

Published research of co-spray-dried biologicals with APDs is principally oriented towards release requirements. Most studies published in the area of co-spray drying APDs with biologicals (Table 4.4) deal with the in vitro release, maintenance of biological activity, and in vivo performance. Less attention has been paid to the effects of processing parameters on product characteristics (Liao et al. 2001; Liao et al. 2004; Shastri et al. 2013). In some studies, the process is not fully described. Regarding the route of administration, the majority of the studies on biologicals in Table 4.4 (15 out of 22) report formulations of vaccine powders for oral administration, and the primary function of APDs was to prepare gastro-resistant microparticles and provide enteric release. For this reason, most studies utilized HPMCAS together with ethylcellulose (9 out of 22 studies) or with methacrylic acid copolymer (Eudragit® FS30D/ L30D-55) (5 out of 22 studies). Three studies (Akalkotkar et al. 2015; Bhowmik et al. 2011; Chablani et al. 2019) concern dermal application.

So far, contrary to the considerable amount of research that has been done, there are no commercial APD products aimed specifically for the protection of orally administered biological drugs such as vaccines, proteins, and enzymes. Of great importance for their long-term storage is that proteinous products are moisture-free. Freeze-drying has been applied for this purpose, but it is time and energy consuming as it requires a final breakdown step of the aggregated freeze-dried mass into powder (Haj-Ahmad et al. 2016). Moreover, denaturing of biologicals has been reported (Preston and Randolph 2021; Ziaee et al. 2019). For these reasons, spray drying could be an alternative for the production of moisture-free biologicals with good stability (Ziaee et al. 2019).

4.5 Conclusions

The numerous publications on the application of spray drying in the pharmaceutical field, the wide publicity of the potential of spray drying in the processing of pharmaceuticals via webinars and the press, as well as the recent investments of pharmaceutical companies in modern spray drying machinery emphasize the importance of this manufacturing platform in the formulation of pharmaceuticals. Although the direct interest is for solubility improvement, other areas can equally benefit from this process by optimizing co-spray-dried drug/polymer/auxiliaries combinations. The poor solubility of the new synthetic drugs leading to dose increase and the problematic tableting behaviour of high dosing anti-inflammatories and pain killers necessitate improvement of their compaction. Formulations targeting other routes such as nasal, rectal, and vaginal are feasible but understudied. Lack of understanding of physicochemical stability of biologicals in the presence of excipients has limited their spray dry processing and commercial manufacturing. Despite the considerable amount of research, there are no yet commercial APD

products aimed specifically for the protection of orally administered vaccines, proteins, and enzymes.

The results of the studies presented in this chapter show the potential of spray drying optimized drug/APD combinations for compactibility improvement and fine-tuned prolonged or targeted delayed release. The strength of spray drying as a formulation platform for pharmaceuticals lies in its facile scaling up from a few grams of highly priced biopharmaceuticals to hundreds of kilos of commercial product.

References

Agrawal AM, Neau SH, Bonate PL (2003) Wet granulation fine particle ethylcellulose tablets: effect of production variables and mathematical modeling of drug release. AAPS PharmSci 5: E13

Akalkotkar A, Chablani L, Tawde SA, D'Souza C, D'Souza MJ (2015) Development of a microparticulate prostate cancer vaccine and evaluating the effect of route of administration on its efficacy via the skin. J Microencapsul 32:281–289

Akalkotkar A, Tawde SA, Chablani L, D'Souza MJ (2012) Oral delivery of particulate prostate cancer vaccine: in vitro and in vivo evaluation. J Drug Target 20:338–346

Al-Zoubi N, AlKhatib HS, Bustanji Y, Aiedeh K, Malamataris S (2008) Sustained-release of buspirone HCl by co spray-drying with aqueous polymeric dispersions. Eur J Pharm Biopharm 69:735–742

Al-Zoubi N, Al-obaidi G, Tashtoush B, Malamataris S (2016) Sustained release of diltiazem HCl tableted after co-spray drying and physical mixing with PVAc and PVP. Drug Dev Ind Pharm 42:270–279

Al-Zoubi N, Al-Rusasi A, Sallam A-S (2019) Ethanol effect on acid resistance of selected enteric polymers. Pharm Dev Technol 24:24–34

Al-Zoubi N, Gharaibeh S, Aljaberi A, Nikolakakis I (2021a) Spray drying for direct compression of pharmaceuticals. Processes 9:267

Al-Zoubi N, Odeh F, Nikolakakis I (2017) Co-spray drying of metformin hydrochloride with polymers to improve compaction behavior. Powder Technol 307:163–174

Al-Zoubi N, Odeh F, Partheniadis I, Gharaibeh S, Nikolakakis I (2021b) Spray drying of naproxen and naproxen sodium for improved tableting and dissolution – physicochemical characterization and compression performance. Pharm Dev Technol 26:193–208

Al-Zoubi N, Partheniadis I, Aljaberi A, Nikolakakis I (2022) Co-spray drying drugs with aqueous polymer dispersions (APDs)—a systematic review. AAPS PharmSciTech 23:140

Al-Zoubi NM, AlKhatib HS, Obeidat WM (2011) Evaluation of hydrophilic matrix tablets based on Carbopol(®) 971P and low-viscosity sodium alginate for pH-independent controlled drug release. Drug Dev Ind Pharm 37:798–808

Año G, Esquisabel A, Pastor M, Talavera A, Cedré B, Fernández S, Sifontes S, Aranguren Y, Falero G, García L, Solís RL, Pedraz JL (2011) A new oral vaccine candidate based on the microencapsulation by spray-drying of inactivated Vibrio cholerae. Vaccine 29:5758–5764

Arici M, Topbas O, Karavana SY, Ertan G, Sariisik M, Ozturk C (2014) Preparation of naproxen–ethyl cellulose microparticles by spray-drying technique and their application to textile materials. J Microencapsul 31:654–666

Barot B, Parejiya P, Patel T, Parikh R, Gohel M (2010) Development of directly compressible metformin hydrochloride by the spray-drying technique. Acta Pharma 60:165–175

Bejugam NK, Uddin AN, Gayakwad SG, D'Souza MJ (2008) Formulation and evaluation of albumin microspheres and its enteric coating using a spray-dryer. J Microencapsul 25:577–583

Bergström CA, Wassvik CM, Johansson K, Hubatsch I (2007) Poorly soluble marketed drugs display solvation limited solubility. J Med Chem 50:5858–5862

Bhowmik T, D'Souza B, Shashidharamurthy R, Oettinger C, Selvaraj P, D'Souza MJ (2011) A novel microparticulate vaccine for melanoma cancer using transdermal delivery. J Microencapsul 28:294–300

Bhowmik T, D'Souza B, Uddin MN, D'Souza MJ (2012) Oral delivery of microparticles containing plasmid DNA encoding hepatitis-B surface antigen. J Drug Target 20:364–371

Blanco-García E, Otero-Espinar FJ, Blanco-Méndez J, Leiro-Vidal JM, Luzardo-Álvarez A (2017) Development and characterization of anti-inflammatory activity of curcumin-loaded biodegradable microspheres with potential use in intestinal inflammatory disorders. Int J Pharm 518:86–104

Brniak W, Maślak E, Jachowicz R (2015) Orodispersible films and tablets with prednisolone microparticles. Eur J Pharm Sci 75:81–90

Chablani L, Tawde SA, Akalkotkar A, D'Souza C, Selvaraj P, D'Souza MJ (2012a) Formulation and evaluation of a particulate oral breast cancer vaccine. J Pharm Sci 101:3661–3671

Chablani L, Tawde SA, Akalkotkar A, D'Souza MJ (2019) Evaluation of a particulate breast cancer vaccine delivered via skin. AAPS J 21:12

Chablani L, Tawde SA, D'Souza MJ (2012b) Spray-dried microparticles: a potential vehicle for oral delivery of vaccines. J Microencapsul 29:388–397

Chen R, Okamoto H, Danjo K (2008) Preparation of functional composite particles of salbutamol sulfate using a 4-fluid nozzle spray-drying technique. Chem Pharm Bull 56:254–259

Cheow WS, Li S, Hadinoto K (2010) Spray drying formulation of hollow spherical aggregates of silica nanoparticles by experimental design. Chem Eng Res Des 88:673–685

Colomé LM, Raffin RP, Jornada DS, Pohlmann AR, Guterres SS (2007) Pantoprazole-loaded Eudragit blended microparticles: preparation, characterization, in vitro gastro-resistance and in vivo anti-ulcer evaluation. J Drug Deliv Sci Technol 17:113–118

Crowley MM, Schroeder B, Fredersdorf A, Obara S, Talarico M, Kucera S, McGinity JW (2004) Physicochemical properties and mechanism of drug release from ethyl cellulose matrix tablets prepared by direct compression and hot-melt extrusion. Int J Pharm 269:509–522

D'Souza B, Bhowmik T, Shashidharamurthy R, Oettinger C, Selvaraj P, D'Souza M (2012) Oral microparticulate vaccine for melanoma using M-cell targeting. J Drug Target 20:166–173

D'Souza B, Bhowmik T, Uddin MN, Oettinger C, D'Souza M (2015) Development of β-cyclodextrin-based sustained release microparticles for oral insulin delivery. Drug Dev Ind Pharm 41:1288–1293

Di Martino P, Scoppa M, Joiris E, Palmieri GF, Andres C, Pourcelot Y, Martelli S (2001) The spray drying of acetazolamide as method to modify crystal properties and to improve compression behaviour. Int J Pharm 213:209–221

Dobry DE, Settell DM, Baumann JM, Ray RJ, Graham LJ, Beyerinck RA (2009) A model-based methodology for spray-drying process development. J Pharm Innov 4:133–142

Elversson J, Millqvist-Fureby A (2005) Particle size and density in spray drying—effects of carbohydrate properties. J Pharm Sci 94:2049–2060

Felton LA, Porter SC (2013) An update on pharmaceutical film coating for drug delivery. Expert Opin Drug Deliv 10:421–435

Garekani AH, Sedighi S, Sadeghi F (2015) Surelease or organic solution of ethylcellulose in preparation of sustained release theophylline micromatrices or matrices using spray drying technique. Pharm Dev Technol 20:204–210

Garekani HA, Moghaddam ZF, Sadeghi F (2013) Organic solution versus aqueous dispersion of Eudragit RS in preparation of sustained release microparticles of theophylline using spray drying. Colloids Surf B: Biointerfaces 108:374–379

Gonnissen Y, Gonçalves SIV, De Geest BG, Remon JP, Vervaet C (2008a) Process design applied to optimise a directly compressible powder produced via a continuous manufacturing process. Eur J Pharm Biopharm 68:760–770

Gonnissen Y, Remon JP, Vervaet C (2007) Development of directly compressible powders via co-spray drying. Eur J Pharm Biopharm 67:220–226

Gonnissen Y, Verhoeven E, Peeters E, Remon JP, Vervaet C (2008b) Coprocessing via spray drying as a formulation platform to improve the compactability of various drugs. Eur J Pharm Biopharm 69:320–334

Guo X, Bodmeier R (1997) Polymeric microparticles prepared by spray-drying a drug-containing, aqueous colloidal acrylic polymer dispersion, Eudragit RS30D. STP Pharm Sci 7:521–528

Haj-Ahmad RR, Mamayusupov M, Elkordy EA, Elkordy AA (2016) Influences of copolymers (Copovidone, Eudragit RL PO and Kollicoat MAE 30 DP) on stability and bioactivity of spray-dried and freeze-dried lysozyme. Drug Dev Ind Pharm 42:2086–2096

Jankowski A, Balwiarz R, Marciniak D, Lukowiec D, Plita J (2014) Influence of spray drying manufacturing parameters on quality of losartan potassium microspheres. Acta Pol Pharm 71: 833–841

Jedinger N, Khinast J, Roblegg E (2014) The design of controlled-release formulations resistant to alcohol-induced dose dumping – a review. Eur J Pharm Biopharm 87:217–226

Joshi AB, Patel S, Kaushal AM, Bansal AK (2010) Compaction studies of alternate solid forms of celecoxib. Adv Powder Technol 21:452–460

Kasashima Y, Uchida S, Yoshihara K, Yasuji T, Sako K, Namiki N (2016) Oral sustained-release suspension based on a lauryl sulfate salt/complex. Int J Pharm 515:677–683

Kemp IC, Hartwig T, Herdman R, Hamilton P, Bisten A, Bermingham S (2016) Spray drying with a two-fluid nozzle to produce fine particles: atomization, scale-up, and modeling. Dry Technol 34: 1243–1252

Kemp IC, Wadley R, Hartwig T, Cocchini U, See-Toh Y, Gorringe L, Fordham K, Ricard F (2013) Experimental study of spray drying and atomization with a two-fluid nozzle to produce inhalable particles. Dry Technol 31:930–941

Kim J-Y, An S-H, Rhee Y-S, Park C-W, Park E-S (2014) A comparative study between spray-drying and fluidized bed coating processes for the preparation of pramipexole controlled-release microparticles for orally disintegrating tablets. Dry Technol 32:935–945

Kulkarni NB, Wakte P, Naik J (2013) Metformin hydrochloride microparticles for oral controlled release: effect of formulation variables. Int J Pharm Pharm Sci 5:135–144

Kulvanich P, Leesawat P, Patomchaiviwat V (2002) Release characteristics of the matrices prepared from co-spray-dried powders of theophylline and ethylcellulose. Drug Dev Ind Pharm 28:727–739

Lai YH, D'Souza MJ (2007) Formulation and evaluation of an oral melanoma vaccine. J Microencapsul 24:235–252

Lazzari A, Kleinebudde P, Knop K (2018) Xanthan gum as a rate-controlling polymer for the development of alcohol resistant matrix tablets and mini-tablets. Int J Pharm 536:440–449

Lecomte F, Siepmann J, Walther M, MacRae RJ, Bodmeier R (2004) Polymer blends used for the coating of multiparticulates: comparison of aqueous and organic coating techniques. Pharm Res 21:882–890

Liao CW, Cheng IC, Yeh KS, Lin FY, Weng CN (2001) Release characteristics of microspheres prepared by co-spray drying Actinobacillus pleuropneumoniae antigens and aqueous ethyl-cellulose dispersion. J Microencapsul 18:285–297

Liao C-W, Chiou H-Y, Yeh K-S, Chen J-R, Weng C-N (2003) Oral immunization using formalin-inactivated Actinobacillus pleuropneumoniae antigens entrapped in microspheres with aqueous dispersion polymers prepared using a co-spray drying process. Prev Vet Med 61:1–15

Liao CW, Lin SH, Lin PY, Chiou HY, Chang WF, Weng CN (2004) Orally administrable enterotoxigenic Escherichia coli vaccine encapsulated by ethylcellulose powder dispersion. Appl Microbiol Biotechnol 65:295–300

Lin JH, Weng CN, Liao CW, Yeh KS, Pan MJ (2003) Protective effects of oral microencapsulated Mycoplasma hyopneumoniae vaccine prepared by co-spray drying method. J Vet Med Sci 65: 69–74

Lin SY, Kao YH (1991) Tablet formulation study of spray-dried sodium diclofenac enteric-coated microcapsules. Pharm Res 8:919–924
Littringer EM, Zellnitz S, Hammernik K, Adamer V, Friedl H, Urbanetz NA (2013) Spray drying of aqueous salbutamol sulfate solutions using the Nano Spray Dryer B-90—the impact of process parameters on particle size. Dry Technol 31:1346–1353
Liu W, Selomulya C, Chen XD (2013a) Design of polymeric microparticles for pH-responsive and time-sustained drug release. Biochem Eng J 81:177–186
Liu W, Wu WD, Selomulya C, Chen XD (2013b) On designing particulate carriers for encapsulation and controlled release applications. Powder Technol 236:188–196
López Y, Pastor M, Infante JF, Díaz D, Oliva R, Fernández S, Cedré B, Hernández T, Campos L, Esquisabel A, Pedraz JL, Perez V, Talavera A (2014) Repeated dose toxicity study of Vibrio cholerae-loaded gastro-resistant microparticles. J Microencapsul 31:86–92
Maa Y-F, Nguyen P-A, Sit K, Hsu CC (1998) Spray-drying performance of a bench-top spray dryer for protein aerosol powder preparation. Biotechnol Bioeng 60:301–309
Malamatari M, Charisi A, Malamataris S, Kachrimanis K, Nikolakakis I (2020) Spray drying for the preparation of nanoparticle-based drug formulations as dry powders for inhalation. Processes 8: 788
Masters K (1991) The spray drying handbook. Longman Scientific & Technical, New York, pp 329–556
Maury M, Murphy K, Kumar S, Shi L, Lee G (2005) Effects of process variables on the powder yield of spray-dried trehalose on a laboratory spray-dryer. Eur J Pharm Biopharm 59:565–573
McDonagh AF, Duff B, Brennan L, Tajber L (2020) The impact of the degree of intimate mixing on the compaction properties of materials produced by crystallo-co-spray drying. Eur J Pharm Sci 154:105505
Mezhericher M, Levy A, Borde I (2010) Spray drying modelling based on advanced droplet drying kinetics. Chem Eng Process Process Intensif 49:1205–1213
Millán M, Caraballo I, Rabasco AM (1998) The role of the drug/excipient particle size ratio in the percolation model for tablets. Pharm Res 15:216–220
Mizumoto T, Tamura T, Kawai H, Kajiyama A, Itai S (2008) Formulation design of taste-masked particles, including famotidine, for an oral fast-disintegrating dosage form. Chem Pharm Bull 56:530–535
Nining N, Srifiana Y, Fadlianty EM (2021) Preparation and characterization of enteric-coated delayed-release microsphere of phytosome loading allicin-rich extract. Int J Appl Pharm 13: 71–75
Nova MV, Nothnagel L, Thurn M, Travassos PB, Herculano LS, Bittencourt PRS, Novello CR, Bazotte RB, Wacker MG, Bruschi ML (2019) Development study of pectin/Surelease® solid microparticles for the delivery of L-alanyl-L-glutamine dipeptide. Food Hydrocoll 89:921–932
Obeidat WM, Alzoubi NM (2014) Controlled-release cellulose esters matrices for water-soluble diclofenac sodium: compression and dissolution studies. Pharmazie 69:96–103
Osman A, Goehring L, Patti A, Stitt H, Shokri N (2017) Fundamental investigation of the drying of solid suspensions. Ind Eng Chem Res 56:10506–10513
Ostróżka-Cieślik A, Sarecka-Hujar B, Krzykawski T, Karcz J, Banyś A, Jankowski A (2018) Application of selected diffractive and microscopic methods to evaluate the physical state of drug and morphology of microspheres obtained by spray drying of furosemide with Eudragit L30 D-55. Acta Pol Pharm 2018:759
Paluch KJ, Tajber L, Adamczyk B, Corrigan OI, Healy AM (2012) A novel approach to crystallisation of nanodispersible microparticles by spray drying for improved tabletability. Int J Pharm 436:873–876
Paluch KJ, Tajber L, Corrigan OI, Healy AM (2013) Impact of alternative solid state forms and specific surface area of high-dose, hydrophilic active pharmaceutical ingredients on tabletability. Mol Pharm 10:3628–3639
Partheniadis I, Karakasidou P, Vergkizi S, Nikolakakis I (2017) Spectroscopic examination and release of microencapsulated oregano essential oil. ADMET & DMPK 5:224–233

Pastor M, Esquisabel A, Talavera A, Año G, Fernández S, Cedré B, Infante JF, Callicó A, Pedraz JL (2013) An approach to a cold chain free oral cholera vaccine: in vitro and in vivo characterization of Vibrio cholerae gastro-resistant microparticles. Int J Pharm 448:247–258

Patil-Gadhe A, Pokharkar V (2014) Single step spray drying method to develop proliposomes for inhalation: a systematic study based on quality by design approach. Pulm Pharmacol Ther 27: 197–207

Poozesh S, Bilgili E (2019) Scale-up of pharmaceutical spray drying using scale-up rules: a review. Int J Pharm 562:271–292

Preston KB, Randolph TW (2021) Stability of lyophilized and spray dried vaccine formulations. Adv Drug Deliv Rev 171:50–61

Rathod P, Mori D, Parmar R, Soniwala M, Chavda J (2019) Co-processing of cefuroxime axetil by spray drying technique for improving compressibility and flow property. Drug Dev Ind Pharm 45:767–774

Rattes ALR, Oliveira WP (2007) Spray drying conditions and encapsulating composition effects on formation and properties of sodium diclofenac microparticles. Powder Technol 171:7–14

Sakhnini N, Al-Zoubi N, Al-Obaidi GH, Ardakani A (2015) Sustained release matrix tablets prepared from cospray dried mixtures with starch hydrophobic esters. Pharmazie 70:177–182

Shah SU, Socha M, Sejil C, Gibaud S (2017) Spray-dried microparticles of glutathione and S-nitrosoglutathione based on Eudragit® FS 30D polymer. Ann Pharm Fr 75:95–104

Shastri PN, Ubale RV, D'Souza MJ (2013) Implementation of mixture design for formulation of albumin containing enteric-coated spray-dried microparticles. Drug Dev Ind Pharm 39:164–175

Souza CRF, Oliveira WP (2012) Microencapsulation of ketoprofen in blends of acrylic resins by spray drying. Dry Technol 30:263–275

Takeuchi H, Handa T, Kawashima Y (1989) Controlled release theophylline tablet with acrylic polymers prepared by spray-drying technique in aqueous system. Drug Dev Ind Pharm 15: 1999–2016

Tawde SA, Chablani L, Akalkotkar A, D'Souza C, Chiriva-Internati M, Selvaraj P, D'Souza MJ (2012) Formulation and evaluation of oral microparticulate ovarian cancer vaccines. Vaccine 30:5675–5681

Thakare M, Singh KK (2006) Preparation and evaluation of diclofenac sodium controlled release tablets using spray-drying technology in aqueous system. Indian J Pharm Sci 68:530

Torge A, Grützmacher P, Mücklich F, Schneider M (2017) The influence of mannitol on morphology and disintegration of spray-dried nano-embedded microparticles. Eur J Pharm Sci 104:171–179

Tsapis N, Bennett D, Jackson B, Weitz DA, Edwards DA (2002) Trojan particles: large porous carriers of nanoparticles for drug delivery. Proc Natl Acad Sci U S A 99:12001–12005

Vanhoorne V, Van Bockstal PJ, Van Snick B, Peeters E, Monteyne T, Gomes P, De Beer T, Remon JP, Vervaet C (2016) Continuous manufacturing of delta mannitol by cospray drying with PVP. Int J Pharm 501:139–147

Vehring R (2008) Pharmaceutical particle engineering via spray drying. Pharm Res 25:999–1022

Vehring R, Snyder H, Lechuga-Ballesteros D (2020) Spray drying. In: Drying technologies for biotechnology and pharmaceutical applications. Wiley, Weinheim, pp 179–216

Wasilewska K, Ciosek-Skibińska P, Lenik J, Srčič S, Basa A, Winnicka K (2020) Utilization of ethylcellulose microparticles with rupatadine fumarate in designing orodispersible minitablets with taste masking effect. Materials (Basel) 13:2715

Wei Q, Yang F, Luan L (2013) Preparation and in vitro/in vivo evaluation of a ketoprofen orally disintegrating/sustained release tablet. Drug Dev Ind Pharm 39:928–934

Wei Y, Deng W, Chen R-H (2016) Effects of insoluble nano-particles on nanofluid droplet evaporation. Int J Heat Mass Transf 97:725–734

Yang Z, Craig DQM (2020) Monitoring film coalescence from aqueous polymeric dispersions using atomic force microscopy: surface topographic and nano-adhesion studies. Asian J Pharm Sci 15:104–111

Ziaee A, Albadarin AB, Padrela L, Femmer T, O'Reilly E, Walker G (2019) Spray drying of pharmaceuticals and biopharmaceuticals: critical parameters and experimental process optimization approaches. Eur J Pharm Sci 127:300–318

Chapter 5
Vat Photopolymerisation Additive Manufacturing for Pharmaceutical Applications

Atheer Awad, Xiaoyan Xu, Jun Jie Ong, Alvaro Goyanes, and Abdul W. Basit

Abstract Vat photopolymerisation three-dimensional (3D) printing is redefining manufacturing paradigms within the pharmaceutical and healthcare industries. Marked by its superb printing resolution and speed, this technology provides an advanced method for engineering patient-centred drug products and devices. In the future, it is foreseen that the combination of 3D printing with other digital health technologies could in fact give rise to a new healthcare model, involving transitioning from current treatment pathways towards personalised digital therapies. This chapter outlines the various vat photopolymerisation techniques, illustrating their unique applications for the fabrication of medicines and drug-laden devices. This is followed by a brief overview of the challenges and drawbacks associated with this printing system in context of its use within healthcare.

Keywords Stereolithography (SLA) · Digital light processing (DLP) · Continuous liquid interface production (CLIP) · Two-photon polymerisation (2PP) · Volumetric printing · Digital medicine production · Custom-made therapeutics and precision

A. Awad · X. Xu · J. J. Ong
UCL School of Pharmacy, University College London, London, UK
e-mail: atheer.awad.15@ucl.ac.uk; xiaoyan.xu.13@ucl.ac.uk; j.ong.17@ucl.ac.uk

A. Goyanes
UCL School of Pharmacy, University College London, London, UK

FabRx Ltd., Henwood House, Henwood, Ashford, Kent, UK

Departamento de Farmacología, Farmacia y Tecnología Farmacéutica, I+D Farma (GI-1645), Facultad de Farmacia, Materials institute (iMATUS) and Health Research Institute (IDIS), Universidade de Santiago de Compostela, Santiago de Compostela, Spain
e-mail: a.goyanes@fabrx.co.uk

A. W. Basit (✉)
UCL School of Pharmacy, University College London, London, UK

FabRx Ltd., Henwood House, Henwood, Ashford, Kent, UK
e-mail: a.basit@ucl.ac.uk

D. Lamprou (ed.), *Nano- and Microfabrication Techniques in Drug Delivery*,
Advanced Clinical Pharmacy – Research, Development and Practical Applications 2,
https://doi.org/10.1007/978-3-031-26908-0_5

medicine · 3D printed formulations and systems · On-demand dispensing and drug manufacturing · Customised dosage forms and drug-loaded medical devices

5.1 Introduction and History of Stereolithography

"Stereolithography" (SLA) is the oldest three-dimensional (3D) printing technology which was originated by Chuck Hull in 1984 (Hull 1984). The invention was defined as "*a method and apparatus for making solid objects by successively 'printing' thin layers of a curable material, e.g., an ultraviolet (UV) curable material one on top of the other*" (Hull 1984). Following the patenting of the technology in 1986, Hull founded 3D Systems, marking the commercialisation of the first 3D printers (Ligon et al. 2017). Currently, due to the presence of various technologies, 3D printing is generally referred to as a system for generating physical objects based on a 3D design obtained from a computer-aided design (CAD) software or an imaging technique (Seoane-Viaño et al. 2021; Awad et al. 2018).

Of the different 3D printing technologies, vat photopolymerisation (i.e. the category under which SLA 3D printing falls) has shown great potential for various applications owing to its high accuracy, greater printing resolution (e.g. 1 μm for microstereolithography vs. 100 μm for fused deposition modelling (FDM) (Gardan 2016; Awad et al. 2023)) and fast production speed compared to other 3D printing technologies (e.g. extrusion- or melting-based systems). Collectively, these features make this technology unique, permitting its use for creating intricate and complex objects at a fast rate (Vitale and Cabral 2016). Since its introduction, interest in the vat photopolymerisation technology has rapidly branched out into different fields, with the technology being leveraged in the aerospace (Joshi and Sheikh 2015), fashion (e.g. 3D printed shoes (Industry 2019) and jewellery (Wannarumon and Bohez 2004)), water filtration and automotive industries(Hegde et al. 2017) and even the medicine field (e.g. 3D printed patient-specific surgical tools, implants and tissue engineering scaffolds (Melchels et al. 2010; Yu et al. 2020; Lim et al. 2020; Li et al. 2020; Appuhamillage et al. 2019; Lee et al. 2020)).

This chapter will describe the principles underpinning the vat photopolymerisation process and outline examples of its potential for healthcare applications, including its use to create medical devices, novel drug delivery systems and oral dosage forms. This will be followed by an overview of the challenges faced with vat photopolymerisation in context of its use for the preparation of medicines and drug-loaded medical devices.

5.2 Theory of Vat Photopolymerisation

Photosensitive resins used in vat photopolymerisation typically comprise the two key reactive components: (a) a photoinitiator or photoinitiator system that decomposes upon light irradiation to give reactive species that initiates

photopolymerisation and (b) a reactive monomer that undergoes chain polymerisation in the presence of the generated reactive species. Resins may also contain a photoabsorber, which is a molecule that absorbs light to ensure selective polymerisation by increasing the light dose threshold for photopolymerisation, and nonreactive diluent molecules that serve to modify the viscosity of the resin. Broadly, there are two types of photocurable systems, categorised according to the type of photoinitiators used: radical and cationic systems. The choice of reactive monomers is in turn dependent on the photocurable system that is being used for 3D printing.

5.2.1 Radical Systems

The mechanism of radical photopolymerisation includes four principal steps of radical generation, initiation, propagation and termination. Upon light irradiation, photoinitiators or photoinitiator systems absorb photolytic energy that induces intramolecular bond cleavage to generate reactive radical fragments. The majority of commercially available radical photoinitiators, such as the family Irgacure® photoinitiators, undergo Norrish type I α-cleavage reaction upon light irradiation, whereby a $n \rightarrow \pi^*$ photoexcitation causes the homolysis of an aldehyde or ketone to form an acyl and an alkyl radical pairs (Ligon et al. 2017; Bagheri and Jin 2019). The wavelength and intensity of the incident light that can induce this photochemical reaction are dependent on the chemical structure of the photoinitiators. For instance, photoinitiators with relatively low energy $n \rightarrow \pi^*$ transitions, such as benzil ketals (e.g. Irgacure and Irgacure 651), absorb light in the UV range (350–360 nm), whilst phosphine oxides (such as TPO and BAPO) have the maximum of the $n \rightarrow \pi^*$ transitions shifted closer to the visible light region (~400 nm) as the phosphorus atom adjacent to the carbonyl group lowers the energy level of the π^* state (Ligon et al. 2017). Instead of a single photoinitiator species, two-component photoinitiator systems may also be used, whereby an uncleavable photoinitiator undergoes electron transfer reactions or hydrogen abstraction in the presence of a co-initiator to generate the reactive species (Fouassier and Jacques 2021). Examples of such systems include camphorquinone/amine pairs and triethanolamine/eosin-Y. Upon radical generation, the primary radicals attack monomers to form monomer radicals, which in turn react with other monomers to form polymer radical species. This process occurs repeatedly as the polymer chain grows, until termination occurs. Termination may occur through several mechanisms, such as through the combination of two active polymer chain ends or interacting with inhibitors such as molecular oxygen.

(Meth)acrylate monomers and oligomers are commonly used with radical photoinitiators in vat photopolymerisation 3D printing (Xu et al. 2021a). These photocurable resins may contain multifunctional monomers, such as di- or triacrylates, which enable the formation of cross-linked structures that confer greater structural integrity. Examples of (meth)acrylate monomers commonly used in pharmaceutical 3D printing include poly(ethylene glycol) diacrylate (PEGDA) and poly

(ethylene glycol) methacrylate (PEGMA). These may also be functionalised to confer unique properties, such as shape memory capabilities through urethane functionalisation (Wu et al. 2019; Zhao et al. 2018). A key limitation of (meth)acrylate-based photocurable systems is their tendency to undergo shrinkage during polymerisation, due to their low gel point which limits the flow of the remaining uncured resin (Bagheri and Jin 2019). Upon reaching the gelation point, the formation of new bonds aggravates the shrinkage stress. Strategies to mitigate this include the use of high molecular weight oligomeric acrylates (though the high viscosity necessitates additional modifications such as the application of heat), or the use of step growth polymerisation instead of chain growth polymerisation (Bagheri and Jin 2019).

Another class of monomers that is commonly used with radical photoinitiators are thiol-enes and thiol-ynes (Kharkar et al. 2016). Here, thiols react with reactive radicals to generate reactive thiyl radicals, donating a hydrogen atom in the process. These thiyl radicals then attack reactive C=C double bonds to initiate radical step-growth polymerisation. Their advantages over (meth)acrylate photocurable systems include lower shrinkage stress due to their relatively higher gel point and their relatively higher biocompatibility. However, the presence of the thiol group results in these systems having a bad smell and often having poor shelf life (Bagheri and Jin 2019). Additionally, objects formed may be soft due to the flexibility of thioether linkages.

5.2.2 *Cationic Systems*

Photoinitiators used in cationic photocurable systems are typically onium salts, also known as photoacid generators, which decompose upon UV light irradiation to produce reactive species including cations, radical cations and radical intermediates (Bagheri and Jin 2019). These reactive intermediates then react with monomer molecules to form a super acid HMX_n, which in turn initiates the polymerisation reaction (Fig. 5.1) (Crivello and Lam 1996). The reactivity of the cationic initiator is dependent on the nucleophilicity of the anion, whereby low nucleophilicity confers

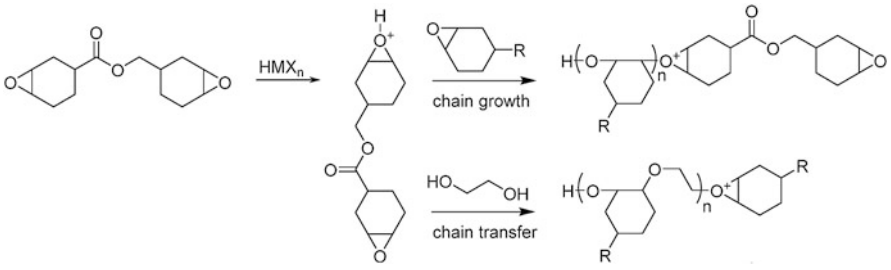

Fig. 5.1 Schematic showing the reaction steps of cationic chain growth of diepoxide monomers and chain transfer with diols. Reproduced with permission from (Ligon et al. 2017)

higher reactivity. Commonly used anions include (in increasing order of reactivity) borates, phosphates, arsenic and antimonates. Cationic photopolymerisation proceeds via chain growth mechanism, sharing similar principal steps of radical photopolymerisation of initiation, propagation and termination. The advantage of cationic curing is the absence of oxygen inhibition, which in turn enables "dark curing" where polymerisation continues in the absence of light to allow for a high degree of monomer conversion and low shrinkage (Sangermano et al. 2014). Monomers that are commonly used in cationic photocurable systems include epoxides, oxetanes, and vinyl ethers.

5.2.3 *Parameters Influencing Rate of Photopolymerisation*

The rate of photopolymerisation is influenced by numerous environment variables and by the properties of the components of the photocurable system. Foremost, as alluded to earlier, different photoinitiators possess different absorption spectra, therefore affecting the wavelength of light that induces photopolymerisation. Key intrinsic properties of the photoinitiator that impact photopolymerisation rate include the quantum yield Φ, which is the measure of the ratio of photon emission to photon absorption, and the molar extinction coefficient, which is the measure of how strongly the photoinitiator absorbs light at a defined wavelength. These physicochemical properties impact the amount of photolytic energy that is available per unit of irradiated light energy. Similarly, the intensity of the incident light also alters the rate of photopolymerisation, with a higher light intensity conferring greater amount of photolytic energy to accelerate photopolymerisation. The rate constants of the primary radicals towards the monomer also contribute to the interplay between the various parameters that influence photopolymerisation. The concentration of inhibitors, such as molecular oxygen, affects the propagation and termination rate constants, whereby higher levels of inhibitor molecules attenuate the rate of photopolymerisation. Finally, external environment factors, such as the viscosity and temperature of the system, also play a role in defining the rate of the photocuring process. Both factors influence the diffusion of reactive radicals and inhibitors, which in turn impacts the reaction rate, whereby a system that permits greater molecular mobility (i.e. high temperature, low viscosity) to the reactive species will photopolymerise at a faster rate. The effect of these variables on photopolymerisation may not be binary, as the overall rate of photopolymerisation is defined through the interplay between the photocurable components' intrinsic characteristics, the inhibitor properties and the numerous external factors.

5.3 Vat Photopolymerisation-Based 3D Printing Techniques

Vat photopolymerisation refers to any process in which a vat of photosensitive materials is solidified under light irradiation in a controlled manner. It is an umbrella term given to a range of approaches including SLA, digital light processing (DLP), continuous liquid interface production (CLIP), two-photon polymerisation (2PP) and volumetric printing, which will be briefly discussed in this section.

5.3.1 Stereolithography (SLA)

Commonly, the SLA 3D printer can be either bottom-up (Fig. 5.2a) or top-down (Fig. 5.2b). In bottom-up 3D printing, the object is cured on the platform by the laser which sits underneath the resin vat, whereas in the bottom-up approach, the laser source is positioned above the vat of resin and the build platform is lowered into the resin vat. Compared to the top-down approach, the bottom-up setup is more affordable with the advantage of using small build volume, hence easier to swap material. During the SLA printing process, the laser points at two mirror galvanometers, which direct the light to the correct coordinates to cure the first layer of resin on the build platform (Xu et al. 2021a). After this, the cured layer gets "peeled" off the surface of the resin tank, and the platform moves vertically along the z-axis to allow the fresh resin to redistribute. Then the platform lowers to recoat, thereby solidifying the second layer on top of the previous one. Subsequently, this process is repeated until a 3D object is fabricated.

5.3.2 Digital Light Processing (DLP)

DLP is another common vat photopolymerisation technique wherein a projector induces illumination of an entire layer at once to cure the resin (Fig. 5.2c). Compared to SLA where the laser beam moves from point to point to trace the printing pattern, DLP is considered to have a much faster printing speed (Bagheri and Jin 2019; Al Rashid et al. 2021). In DLP, a digital micromirror device (DMD) chip has several hundred thousand micromirrors which by changing orientation could generate the pattern onto the resin tank. Because the image of each layer is composed of square pixels, the rectangular shape of voxels causes a stepped effect on the curved edges, also known as the voxel effect (Formlabs 2020a). To achieve smooth surface finish of the final object, a post-processing step (e.g. sanding) is required.

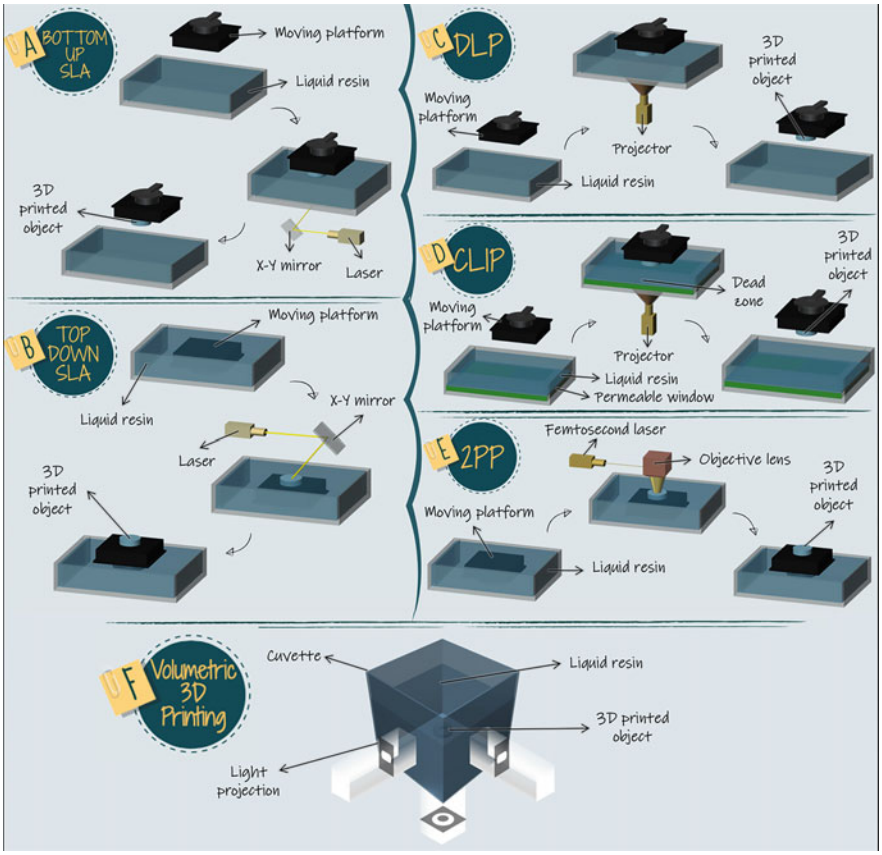

Fig. 5.2 Schematic representation of the (**a**) bottom-up SLA, (**b**) top-down SLA, (**c**) DLP, (**d**) CLIP, (**e**) 2PP, and (**f**) volumetric 3D printing technologies. Reprinted with permission from (Xu et al. 2021a)

5.3.3 Continuous Liquid Interface Production (CLIP)

In 2015, the CLIP (originally Continuous Liquid Interphase Printing) technology was invented by Joseph DeSimone and his co-workers (Tumbleston et al. 2015). The key to this fabrication method is the oxygen-permeable window, which creates a "dead zone" where photopolymerisation is inhibited between the printed parts and the liquid precursor (Fig. 5.2d). In this way, the solid object is drawn out of the resin at rates of hundreds of millimetres per hour, different from traditional SLA methods where stepwise layer formation is required (exposure and curing, separation, recoating and repositioning). Another notable characteristic of the CLIP technology is its ability to generate smooth surfaces for printed objects without slicing artefacts.

5.3.4 Two-Photon Polymerisation (2PP)

2PP has gained a huge interest due to its ability to create microstructures with extremely high resolution (less than 100 nm), making it well-suited for use in microdevices, microfluidics, and microphotonics (Xing et al. 2015; Faraji Rad et al. 2021). Common vat polymerisation techniques use single-photon polymerisation, which is a planar process where only one photon is absorbed by the photoinitiator to initiate polymerisation near the surface of the resin (Wu et al. 2006). Two-photon absorption (TPA), originally predicted by Maria Goeppert Mayer in her doctoral dissertation in 1931, is a nonlinear optical process based on the simultaneous absorption of two photons to excite the initiator from its ground state. The 2PP process is a TPA-based fabrication process where a titanium sapphire femtosecond laser (typically at 780 nm with a repetition rate of 80 MHz) is tightly focused by an objective lens onto the volume of the photosensitive resin (Fig. 5.2e) (Park et al. 2009). When the laser moves three-dimensionally, the solidification is initiated along the trace of the focus, enabling the fabrication of 3D microstructures.

5.3.5 Volumetric Printing

More recently, volumetric printing has been developed as a new fabrication paradigm that allows manufacturing of the entire 3D object within seconds (Shusteff et al. 2017; Kelly et al. 2019; Loterie et al. 2020; Bernal et al. 2019). This is achieved by irradiating the photosensitive liquid within a contained volume from different angles, in contrast to conventional layer-based printing methods that use a single angle (Fig. 5.2f). In general, there are two different volumetric printing approaches. The first type of volumetric printing is via tomographic reconstruction where a set of two-dimensional (2D) light patterns computed by a Radon transform is displayed in synchronisation with the rotating resin container (Kelly et al. 2019; Loterie et al. 2020). In the other type, three orthogonal beams generated from a single light beam by 45° prism mirrors are projected onto a photosensitive resin where the 3D structure is solidified through superposition of multiple 2D images (Shusteff et al. 2017).

5.4 Vat Photopolymerisation in Healthcare

Having shown high printing speed and accuracy, the vat photopolymerisation technologies have been abundantly investigated to create various forms of drug products with controlled or sustained release behaviours. Generally, with this technology the drug can be loaded in two ways: (a) by directly being incorporated into the liquid resin prior to printing or (b) by incorporating the drug into a blank device following its printing (Fig. 5.3) (Bloomquist et al. 2018). In the first scenario, the

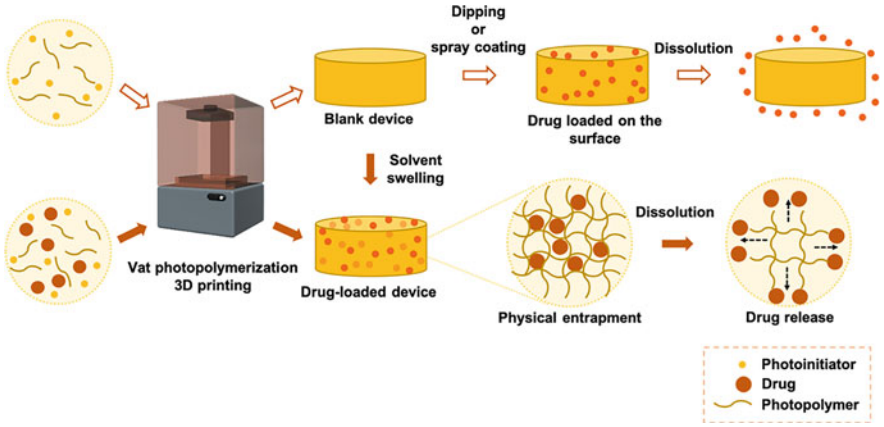

Fig. 5.3 Graphical illustration of the drug loading pathways of vat photopolymerisation 3D printing for healthcare applications. Reprinted with permission from (Xu et al. 2021a)

complete dissolution or homogenous dispersion of the active pharmaceutical ingredient (API) in a liquid resin mixture of a photoinitiator and a photopolymer is achieved through magnetic stirring at room temperature. Once the printing of the device is completed, the API becomes physically entrapped in the cross-linked polymeric network. After placing the device in a dissolution medium, the matrix swells, releasing the API through diffusion. Whilst this approach can achieve high drug loading, some APIs may be prone to degradation during or before the printing process. In this case, the alternative approach involving the use of blank devices can be used instead. Herein, the API is included into the device using a traditional drug loading technique (e.g. dipping or spray coating) or by placing the blank device in a concentrated drug solution, causing the device to swell and the drug being absorbed into the polymer network. Despite this approach being longer than the previous one, it enables maintaining the integrity of the drug pre-printing or during printing.

5.4.1 Oral Dosage Forms

Like most 3D printing technologies, the motivation behind the use of vat photopolymerisation for oral drug delivery is for the purpose of tailoring treatments to the individual needs of each patient. In this regard, various types of personalised oral dosage forms have been produced. The earliest study using vat photopolymerisation involved the use of SLA 3D printing to create torus-shaped paracetamol and 4-aminosalicylic acid (4-ASA) Printlets™ (i.e. 3D printed tablets) with modified release properties (Fig. 5.4a) (Wang et al. 2016a). The Printlets were fabricated using poly(ethylene glycol) diacrylate (PEGDA), wherein it was noticed that as the concentration of PEGDA increased, the Printlets exhibited a slower drug release rate. This behaviour was primarily linked to the higher degree of

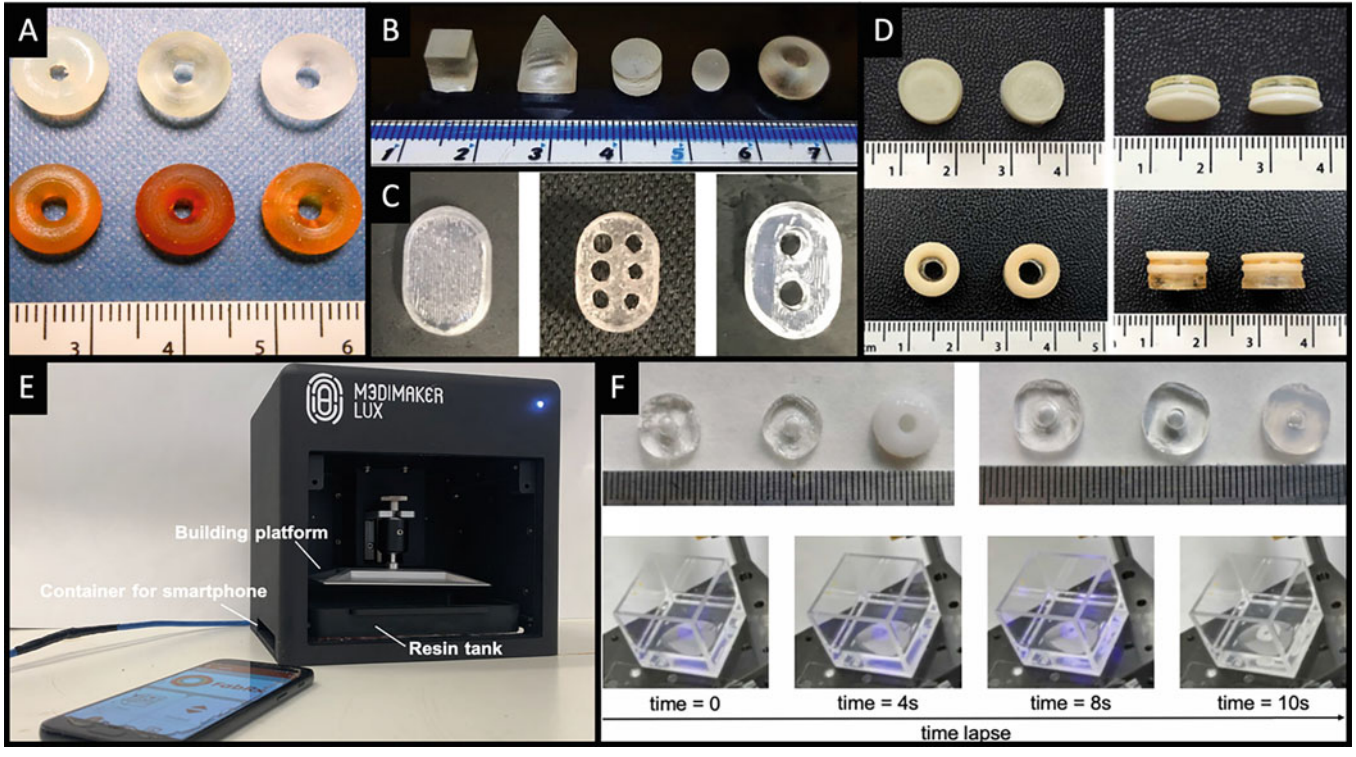

Fig. 5.4 (**a**) SLA torus Printlets containing (top) paracetamol and (bottom) 4-ASA (Wang et al. 2016a). (**b**) SLA Printlets with similar SA/V ratios (Martinez et al. 2018). (**c**) DLP Printlets containing (from left to right) no holes, six holes or two holes (Kadry et al. 2019). (**d**) SLA Polyprintlets with (top) cylinder and (bottom) ring shapes, incorporating (from top to bottom layer) naproxen, aspirin, paracetamol, caffeine, chloramphenicol and prednisolone (Robles-Martinez et al. 2019). (**e**) Image of a smartphone-based 3D printer alongside a smartphone (Xu et al. 2021b). (**f**) (top) Images of volumetric paracetamol Printlets containing (from left to right) 10, 35 and 65% water, with (left) water or (right) PEG 300 as a diluent. (bottom) Sequential view of the cuvette of the volumetric printer during a Printlet fabrication process (Rodríguez-Pombo et al. 2022). Images were reprinted with permission from their original sources

cross-linking in the presence of more PEGDA, reducing the molecular mobility in the Printlet core and slowing down the drug diffusion through the matrix. To control this effect, different excipients have been investigated, including water (Martinez et al. 2017), poly(caprolactone) triol (Healy et al. 2019), mannitol and sodium chloride (Krkobabić et al. 2019). It should be noted however that Printlets made of photocross-linkable materials (e.g. PEGDA and poly(ethylene glycol) dimethacrylate (PEGDMA)) do not degrade and are eliminated from the body intact. This may raise concerns for some patients by posing risks for potential intestinal blockage.

The drug release rate from Printlets can also be adjusted by altering their geometry. A study involving Printlets with different shapes has shown that those with analogous surface-area-to-volume (SA/V) ratio exhibit similar release behaviours (Fig. 5.4b) (Martinez et al. 2018). In another example, increasing the SA/V ratio of a torus Printlet has shown to accelerate the drug release. In a similar approach, it has been demonstrated that fine-tuning the number of perforations in a Printlet can be exploited to control the drug release rate (Fig. 5.7c) (Kadry et al. 2019; Karakurt et al. 2020).

Polypharmacy (i.e. simultaneous use of more than five medicines) has been a persistent concern for patients, resulting in high pill burden and affecting patients' adherence to treatments (Trenfield et al. 2019). To overcome these challenges, it has been proposed to fabricate polypills (i.e. single dosage forms incorporating multiple drugs) using vat photopolymerisation due to the technology's ability to distribute materials precisely and flexibly. This concept has been demonstrated using SLA 3D printing wherein Polyprintlets (i.e. 3D printed polypills) have been fabricated to include between four (e.g. atenolol, hydrochlorothiazide, irbesartan and amlodipine (Xu et al. 2020)) to six (e.g. naproxen, aspirin, paracetamol, caffeine, chloramphenicol and prednisolone (Robles-Martinez et al. 2019)) different APIs. Each drug was present in a separate layer of a cylindrical or ring-shaped formulation (Fig. 5.4d). To achieve this, the printer's software had to be modified, enabling the user to control the position of the building platform when the printing process was paused. With vat photopolymerisation, it is also possible to produce hydrogels for site-specific drug delivery purposes. As an example, DLP 3D printing was used to fabricate pH-responsive hydrogel tablets incorporating sulforhodamine B (Larush et al. 2017). As the pH increased, the tablets swelled to a higher extent, releasing the drug at a faster rate. Apart from directly printing dosage forms, the technology has been investigated for the fabrication of bespoke moulds. An example of such is the use of SLA 3D printing to create moulds for capsaicin candies indicated for oral ulcers (Jiang et al. 2019).

In a futuristic approach for producing customised dosage forms, a portable smartphone-activated 3D printer was developed and investigated (Xu et al. 2021b). The printer operates using the light from a smartphone's display, leading to the photopolymerisation of the liquid resin and forming the Printlets (Fig. 5.4e). The concept was demonstrated through the fabrication of warfarin Printlets using different resins and in various sizes and shapes (e.g. caplet, triangle, diamond, square, pentagon, torus and gyroid lattices). With the advancement in internet and

mobile sensing technologies, doctors can now remotely monitor their patients' medications and dosages based on their disease status or pain level. In the future, it is expected that the whole medical care process will be performed distantly. It is envisioned that patients will be sent electronic prescriptions of their personalised medicines directly to their smartphone app. Then they will have the choice of selecting their preferred oral dosage form shape and eventually print their own medications at the comfort of their homes.

More recently, volumetric 3D printing was investigated for its suitability for producing personalised Printlets (Fig. 5.4f) (Rodríguez-Pombo et al. 2022). With volumetric printing's ability to produce objects within a matter of a few seconds, the technology marked a major advancement in the field of on-demand dispensing. The findings of the study demonstrated that the drug release from the paracetamol-based Printlets can be fine-tuned by varying the monomer-to-diluent ratio in the photosensitive resin. A lower ratio resulted in a more rapid drug release, whereas high ratios have shown more sustained effects.

5.4.2 Microneedles

Vat photopolymerisation has been thoroughly explored for the fabrication of microneedles (MNs) for improved transdermal drug delivery (Economidou et al. 2018). MNs are miniaturised structures that can pierce through the stratum corneum barrier without reaching the nerve endings, facilitating drug delivery without inducing pain (Rzhevskiy et al. 2018). Although MNs can be fabricated using a wide range of materials (e.g. silicon, metal, glass and ceramic) (Donnelly et al. 2010), the polymeric-based ones are of particular interest for healthcare applications owing to their biocompatibility, biodegradability, strong mechanical properties and optical clarity. Whilst polymeric MNs are traditionally produced using casting or injection moulding (Luzuriaga et al. 2018), such methods can be complex, time- and resource-intensive, and limited to small-scale production. FDM 3D printing has been previously studied for the fabrication of MNs, but the absence of sharp tips in the resulting MNs has rendered it unsuitable for this application (Luzuriaga et al. 2018). Conversely, the use of vat photopolymerisation makes the MNs fabrication process a single-step, time- and cost-effective process resulting in high-resolution end products.

MNs with various shapes have been reported. As an example, pyramid- and cone-shaped MN patches were fabricated using SLA 3D printing and coated with insulin using inkjet printing (Fig. 5.5a) (Pere et al. 2018). The MN arrays were successfully inserted into porcine skin, with in vitro drug release studies showing 90–95% of insulin being released within 30 min. Subsequent in vivo animal studies comparing the activity of spear-shaped 3D printed MN arrays to subcutaneous injections have shown lower glucose levels with the printed MNs (Fig. 5.5b) (Economidou et al. 2019). In a similar approach, cisplatin (i.e. an anticancer drug) was added onto the surface of SLA 3D printed cross-shaped MN arrays (Fig. 5.5c) (Uddin et al. 2020).

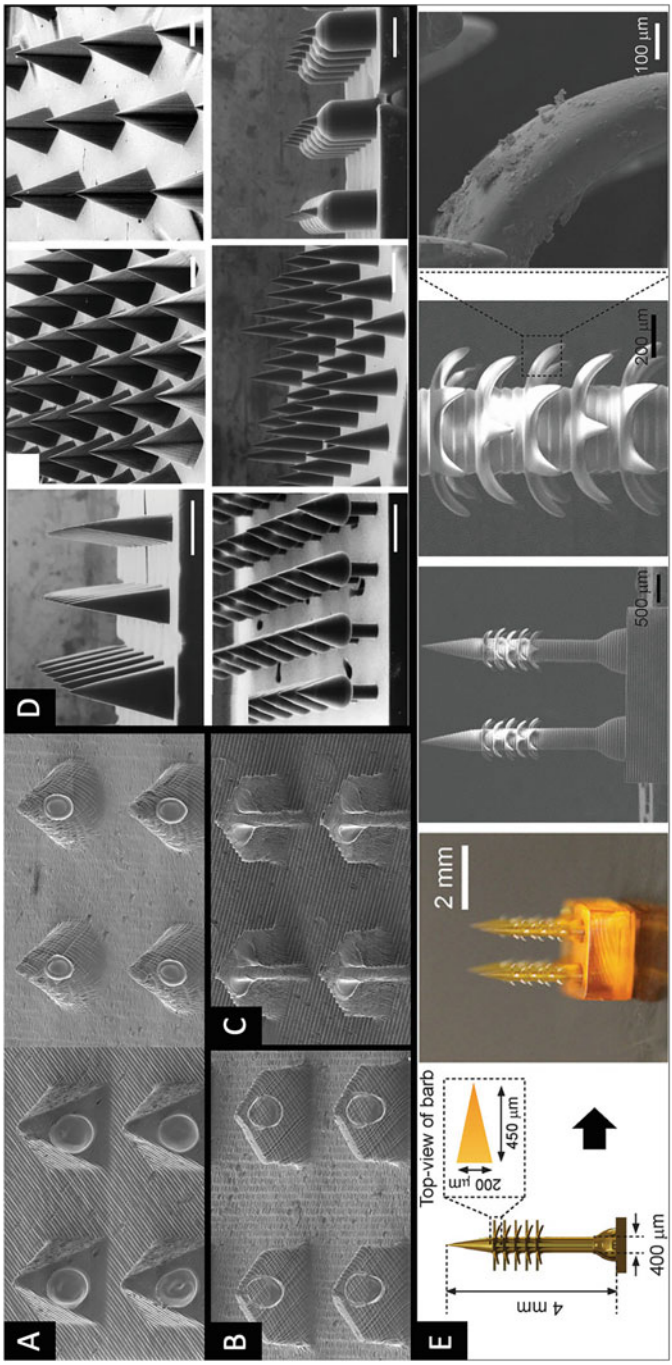

Fig. 5.5 (**a**) SLA 3D printed MNs with pyramid and cone-shaped design (Pere et al. 2018). (**b**) SLA 3D printed MNs with a spear-shaped design (Economidou et al. 2019). (**c**) SLA 3D printed MNs with cross-shaped design (Uddin et al. 2020). (**d**) CLIP 3D printed MNs of different shapes (Johnson et al. 2016). (**e**) 3D design, photographs and SEM images of SLA 4D printed MN array with backward-facing barbs (Han et al. 2020). Images were reprinted with permission from their original sources

In vitro studies have shown that cisplatin is quickly released within 1 h and in vivo findings in mice displayed significant anticancer activity with complete tumour regression.

Whilst in the aforementioned examples the drugs were incorporated onto the surface of the MNs following printing, it is also possible to load them in the resin mixture before printing. As an example, DLP 3D printed MN arrays were fabricated with 1–2% dacarbazine directly present in the poly(propylene fumarate) and diethyl fumarate solutions (Lu et al. 2015). In this example, the direct fabrication of drug-loaded MNs was simpler and more suited for achieving an extended drug release (e.g. over 5 weeks). In a different approach, the CLIP technology was used to fabricate MNs using various photopolymers and loaded with rhodamine B and fluorescein (Fig. 5.5d) (Johnson et al. 2016). It is worth noting here that of the different photopolymers investigated, polyacrylic acid was able to result in water-soluble MNs that are capable of completely releasing rhodamine within 30 min of their placement in a phosphate-buffered saline medium.

3D printing of personalised MN arrays directly onto curved structures has been also described using the DLP technology (Lim et al. 2017). Herein, the resulting MNs were able to completely contour the swollen exterior of a finger, guaranteeing the complete penetration into the skin and consequently an efficient drug delivery at the site of action. In particular, the skin treated with the MN finger splint has shown improved diclofenac diethylamine gel penetration compared to untreated skin. In a similar approach, it was demonstrated that tissue adhesion could be amplified using bioinspired MNs having rearward barbs (Fig. 5.5e) (Han et al. 2020).

5.4.3 Hearing Aids

Hearing aids constitute another unique example where vat photopolymerisation 3D printing is used to simplify the production of bespoke medical devices. Conventionally, the production timeline of patient-oriented hearing aids was averaged at 2–3 weeks (Udhayakumar and Pandiyarajan 2021). Nowadays, the complete process, starting from scanning and modelling all the way to 3D printing, requires less than 1 day (Dodziuk 2016). As such, currently, the majority (i.e. >99%) of custom-made hearing aids are produced through 3D printing (Banks 2013). An example of a company leading the way in this domain is EnvisionTEC which produces hearing aids on a large scale. At present, they are offering the choice from over 16 different biomedically approved materials with various properties (e.g. soft and hard materials, transparent skin coloured as well as ear moulds or shells) (EnvisionTEC 2020). More recently, the concept was even applied for drug-laden hearing devices for the treatment of ear infections (Vivero-Lopez et al. 2021).

5.4.4 Dental Applications

Within dentistry, vat photopolymerisation has been widely investigated for the creation of dental prosthetics and orthodontic treatments (Piedra-Cascón et al. 2020). This started in 2015 after the Dentca™ Denture Base II became the first "light-cured resin indicated for the fabrication and repair of full and partial removable dentures and baseplates" to be approved by the United States Food and Drug Administration (FDA) (United States Food and Drug Administration 2015). Nowadays, a broad selection of biocompatible resins is commercially available for a range of different dental applications (e.g. trays, drilling templates, dental models, temporary crowns and bridges and surgical guides) (Next Dent 2020; Formlabs 2020b). Compared with their counterparts produced using 3D printing technologies with limited resolutions (e.g. mouthguards made using FDM (Liang et al. 2018)), those fabricated using vat photopolymerisation have shown improved fitting, making them more comfortable for use by patients. Such applications are not limited to commercial resins; antimicrobial resins containing diurethane dimethacrylate (UDMA), glycerol dimethacrylate (GDMA) and quaternary ammonium methacrylate have also been suggested for use with SLA 3D printing for dental and orthopaedic purposes (Yue et al. 2015).

5.4.5 Ocular Applications

Vat photopolymerisation has also been applied within ophthalmology for the treatment of eye diseases. As an example, punctal plugs were developed using DLP 3D printing for the treatment of dry eye diseases (Xu et al. 2021c). The plugs were fabricated containing varying amounts of the API dexamethasone, wherein PEGDA and polyethylene glycol 400 (PEG 400) were used to produce a semi-interpenetrating network (semi-IPN). Compared to the current treatment involving the use of eye drops, the punctal plugs showed improved therapeutic efficacy, providing a sustained release of dexamethasone for up to 7 days. In another approach, DLP 3D printing was applied to produce personalised contact lenses with optical sensors for diagnosis (Alam et al. 2021). Similarly, contact lenses for colour vision deficiency (CVD) were also fabricated using masked SLA 3D printing (i.e. a type of SLA 3D printing system that uses an LCD panel to selectively block pixels and control the passage of light) (Alam et al. 2022). Herein, the lenses contained wavelength selective filtering dyes (e.g. Atto 565 and 488) which can accurately block the problematic wavelengths and improve vision for patients with red-green and blue-yellow forms of CVD.

5.4.6 *Medical Devices, Implants and Scaffolds*

One of the key applications of the vat photopolymerisation technologies is to create personalised drug-loaded devices, implants and scaffolds. An example of such includes patient-specific antiacne masks containing salicylic acid (Fig. 5.6a) (Goyanes et al. 2016). The nose-shaped devices produced using SLA 3D printing have shown superior printing resolution, enhanced drug loading and quicker drug diffusion rate compared to their FDM equivalents. In a different approach, the DLP technology was used to produce implants in various shapes (e.g. T-, ring-, U- and arc-shaped) for intrauterine drug delivery or as femoral cartilage and contact lenses (Fig. 5.6b) (Yang et al. 2020). Likewise, the CLIP technology was studied as a potential method for creating intravaginal rings containing hormones and microbicides (Janusziewicz et al. 2020). The concept involved controlling the drug release by changing the patterns (e.g. nodal, cylinder, dode and honeycomb) on the surface of the lattice ring structures (Fig. 5.6c). The CLIP technology has also been investigated as a novel method for generating biocompatible drug-laden scaffolds (Fig. 5.6d) (Bloomquist et al. 2018). To control the drug release properties, the 3D design of the scaffolds was fine-tuned (e.g. to obtain a faster drug release rate, a smaller unit cell was selected, and vice versa). Alternatively, the cross-link density and compositions of the polymers could be changed. In a similar approach, SLA 3D printing was studied for fabricating lidocaine-loaded devices for the treatment of severe bladder diseases (Xu et al. 2021d). The devices can be printed hollow or solid and could contain different drug concentrations (e.g. 10, 30 or 50%).

To achieve a more accurate and efficient targeted drug delivery, the concept of 2PP 3D printed microswimmers was proposed (Bozuyuk et al. 2018). These chitosan-based devices are directed to the site of action via magnetic propulsion after which a light stimulus is used to initiate the release of doxorubicin (i.e. a chemotherapeutic agent). In a different site-specific approach, microreservoir devices with an anchoring surface were produced using DLP 3D printing (Fig. 5.7) (Vaut et al. 2020). Due to their improved mucoadhesion to the intestinal mucosa (i.e. up to twofold in comparison with the control) and their ability to adhere in multiple orientations, the devices exhibit unidirectional drug release and consequently increased drug uptake.

5.5 Challenges

5.5.1 *Leaching of Unreacted Monomers*

At present, photoreactive monomers commonly used for pharmaceutical 3D printing are not recognised in the list of generally recognised as safe (GRAS) compounds. This is primarily due to the allergenicity and cytotoxicity of unreacted monomers (Oskui et al. 2016; Oesterreicher et al. 2016) that may leach out of the photocured

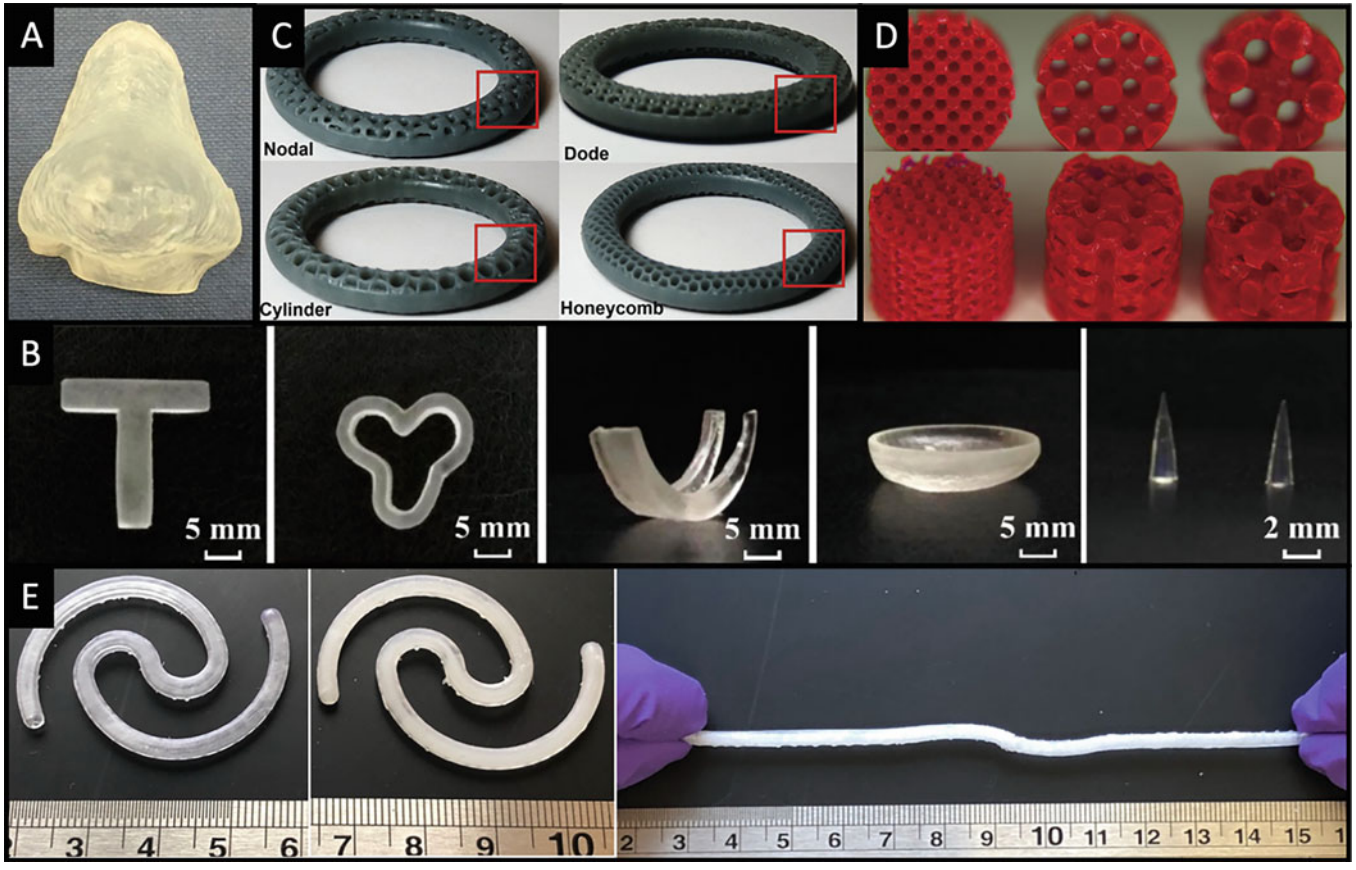

Fig. 5.6 (**a**) Image of an SLA 3D printed personalised nose-shaped patch containing salicylic acid (Goyanes et al. 2016). (**b**) DLP 3D printed T-, ring-, U-, arc- and needle-shaped implants (from left to right) (Yang et al. 2020). (**c**) Images of intravaginal rings fabricated using a urethane-methacrylate resin (UMA)

Fig. 5.6 (continued) prototyping resin and a silicone-based resin (SIL 30) with varying unit cell designs, including nodal, cylinder, dode and honeycomb, with the unit cell size kept constant at 3.80 mm and band parameters of height = 4.0 mm and thickness = 0.6 mm(Januszewicz et al. 2020). (**d**) Images of CLIP 3D printed model devices of (from left to right) 1, 2 and 3 mm unit cells loaded with rhodamine B as a surrogate drug (Bloomquist et al. 2018). (**e**) Images of an SLA 3D printed hollow bladder device (left) before and (middle) after filling with 10% drug loading mixture; and (right) the hollow 10% device under stretching (Xu et al. 2021d). Scale in cm. Images were reprinted with permission from their original sources

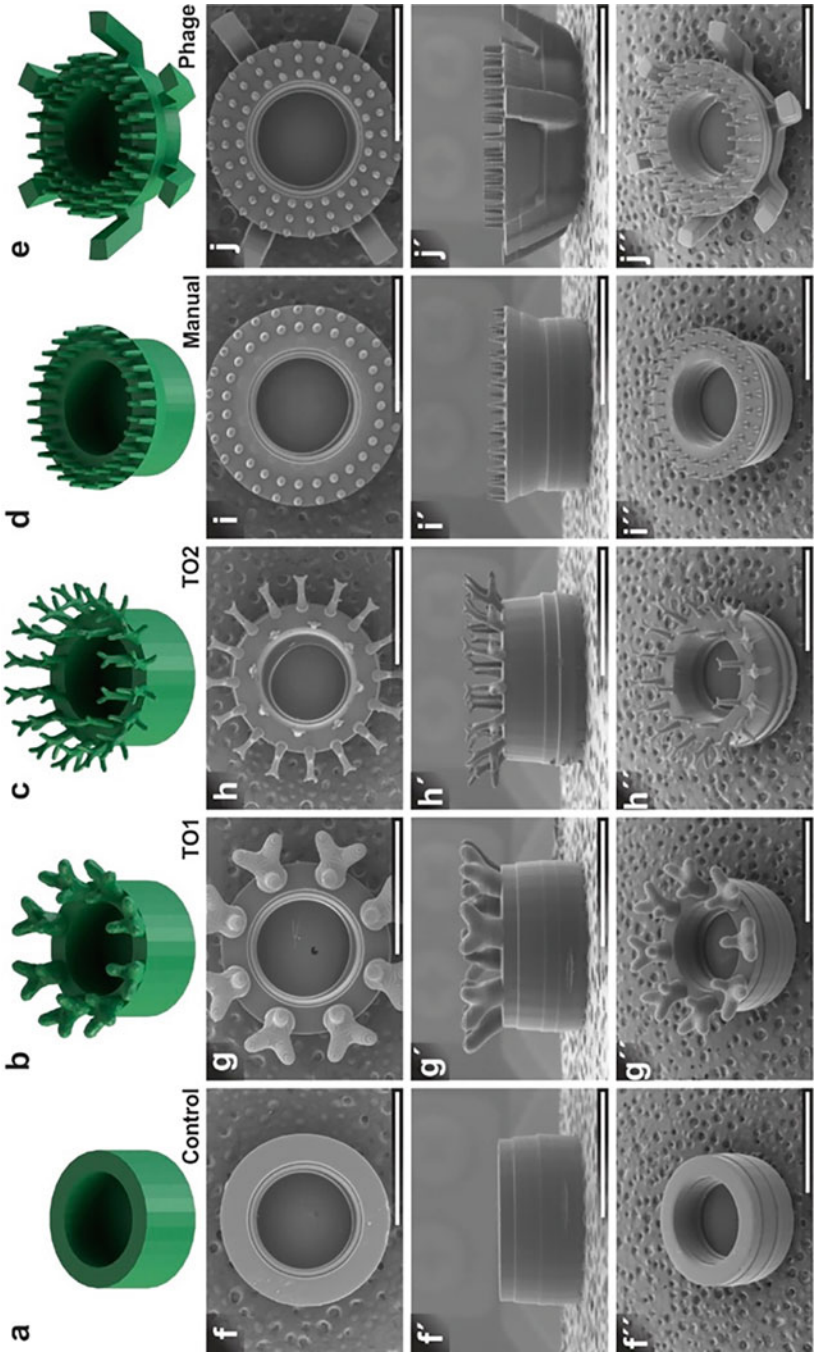

Fig. 5.7 **(a-e)** 3D designs and **(f-j)** SEM images of DLP 3D printed microreservoirs with various geometries, including (from left to right) a control specimen (control), design with large branching edge anchors (TO1), design with small branching edge anchors (TO2), design featuring overhang and straight anchor spikes (manual), and a bio-inspired phage-style design with straight anchor spikes, rounded bottom side and legs (phage), shown in **(f-j)** top, **(f′-j′)** side and **(f″-j″)** 45° views. Scale bars correspond to 2 mm. Reprinted with permission from (Vaut et al. 2020). Copyright © 2020 American Chemical Society

object. The leaching of unreacted monomers is a concern due to the relatively low rate of acrylate group conversion (typically 60–90%). Furthermore, the hydrolytic cleavage of (meth)acrylate bonds may result in the release of acrylic acid-containing moieties, which may decrease the pH of the local tissue environment and negatively impact biochemical and enzymatic processes (Bagheri and Jin 2019; Alifui-Segbaya et al. 2018). To mitigate this, vat photopolymerisation 3D printed objects undergo post-washing and post-curing. Isopropyl alcohol (IPA) is commonly used to wash-out uncured monomers, but it is highly volatile and flammable. Moreover, IPA can be easily absorbed orally, topically or through inhalation (due to its volatility) and may depress the central nervous system. Tripropylene glycol monomethyl ether has been proposed as a safe and non-flammable alternative but requires a long time to completely evaporate. Furthermore, there are concerns that the washing process may also inadvertently washout some of the loaded drug molecules, resulting in inaccurate drug loading and consequently attenuated clinical efficacy. 3D printed objects are also post-cured to increase the functional group conversion rate and reduce unreacted monomers. This involves placing the printed (and washed) object in an oven with UV light for a defined period. However, as cross-linking density increases relative to the curing period, drug release rate might be negatively impacted due to the increased resistance to diffusion out of the denser polymer matrix (Wang et al. 2016b; Kadry et al. 2019). Alternative strategies to remove unreacted monomers include supercritical fluid processing, whereby printed objects are treated with supercritical carbon dioxide (Popov et al. 2004), and high-temperature heating under nitrogen, which causes the sublimation of unreacted monomers (Inoue and Ikuta 2013).

5.5.2 Drug-Photopolymer Reaction

To produce a functional drug-loaded device, it is essential to ensure that the correct amount of API is incorporated chemically unchanged and that the API may be released. However, unexpected chemical reactions may occur between the drug and the reactive monomers and/or the photoinitiator. For instance, the reactive C=C double bonds in (meth)acrylate systems can undergo Michael addition with amine groups that are commonly found in APIs. This was observed in one study via Fourier transform infrared spectroscopy (FTIR) and nuclear magnetic resonance (NMR) spectroscopy, where a reaction between the diacrylate group of PEGDA and the primary amine group of amlodipine was noted (Xu et al. 2020). This might not be limited to (meth)acrylate systems, as thiol-ene photocurable systems also possess similar reactive alkene functional groups. It is also not yet possible to rule out other chemical reactions that might occur with more chemically complex APIs, such as biologic drugs. Therefore, further testing is required to assure the chemical integrity of APIs at the photocurable resin preparation stage as well as during and after photopolymerisation.

5.5.3 Unintended Temperature Increase

During the printing process, temperature may rise due to the heat generated by the exothermic photopolymerisation process and the heat transmitted from light sources (Lloyd et al. 1986; Hofmann et al. 2002). Moreover, although most vat photopolymerisation 3D printers operate at ambient temperatures, the long use of the printer may also possibly increase the temperature of the hardware, generating heat around the resin tank. This is particularly critical if thermolabile drugs or biological compounds were directly embedded in the printable resins (Goyanes et al. 2016). Nonetheless, as no drug degradation has been reported so far, photopolymerisation 3D printing is still considered as an appropriate technique for printing drug delivery systems containing thermosensitive drugs (Abdella et al. 2021).

5.5.4 Printing Optimisations

In powder bed-based 3D printing techniques, such as binder jetting and powder bed fusion, the powder particles act as the support material and allow the fabrication of overhanging or intricate structures (Awad et al. 2021a). On the contrary, it may be challenging to print such objects using vat photopolymerisation 3D printing, resulting in their warping or collapsing during the printing process. Thus, it is essential to correctly orient objects and include support structures to minimise the overhung area, which inevitably increases material costs and labour time due to the need for removing the supports (Xu et al. 2021a; Holt et al. 2019).

Another important consideration is when printing parts with internal voids (e.g. microfluidic channels or hollow microneedles), whereby the trapped uncured resin within the hollow cavity could absorb light during the printing of subsequent layers, causing it to solidify and block the space (Gong et al. 2015). To avoid this situation, the void areas should be properly designed for a given resin, and it is necessary to rinse the parts immediately after the printing process with an appropriate solvent before the post-curing step.

5.5.5 Regulatory Challenges

Whilst the FDA has cleared a number of biocompatible resins for dental applications (e.g. for use in surgical guides, retainers, aligners or as denture bases), to date, none have been approved for biological or pharmaceutical use (Ng et al. 2020). Moreover, current FDA guidelines are based on mass production of medicines, making them unsuitable for personalised treatments (Zema et al. 2017). Although the FDA issued a guidance on technical considerations for medical devices manufactured using

additive manufacturing/3D printing in 2017 (US Food and Drug Administration 2017), it did not cover aspects concerning 3D printed products with biological, cellular or tissue-based origins or content. Hence, regulatory bodies must issue a guidance that is specific for 3D printed drug products, covering all their technical requirements (e.g. material stability, hardware and software processing parameters as well as final product quality control) that need to be considered and validated prior to regulatory approval.

Despite manufacturers working towards this aim, it may be challenging for them to satisfy the requirements of different regulatory agencies (e.g. FDA and European Medicines Agency (EMA)), especially in the absence of an international concordance in the regulatory decision-making. Therefore, there is a need for regular engagement and collaboration between various regulatory agencies to facilitate this and reduce the burden on manufacturers. Furthermore, it is necessary for these conversations to involve different pharmaceutical stakeholders, allowing for discussions that can bring this technology a step closer to clinical use and implementation.

5.6 Conclusion

With its high feature resolution and superior surface finishing, the vat photopolymerisation 3D printing technology is making significant progress within the healthcare industry. In particular, it is simplifying the production process of drug-loaded products and devices having unique structures and functional designs. This empowers clinicians to fabricate patient-specific medicines with improved efficacy and reduced side effects. Due to the digital nature of the technology, it could be combined with novel digital principles (e.g. four-dimensional (4D) printing, biosensors and artificial intelligence (Abdalla et al. 2023; Melocchi et al. 2019a; Melocchi et al. 2019b; Trenfield et al. 2022; Awad et al. 2021b; Muñiz Castro et al. 2021)), enabling the creation of Printlets with advanced therapeutic action for the treatment of complex medical conditions. With that in mind, the potential of vat photopolymerisation to transform the healthcare sector should not be overlooked, and instead, efforts should be made to help progress and embrace these technologies to provide patients with better treatments.

References

Abdella S et al (2021) 3D printing of Thermo-sensitive drugs. Pharmaceutics 13(9):1524

Abdalla Y et al (2023) Machine learning using Multi-Modal Data Predicts the Production of Selective Laser Sintered 3D Printed Drug Products. Int J Pharm 633:122628

Al Rashid A et al (2021) Vat photopolymerization of polymers and polymer composites: processes and applications. Addit Manuf 47:102279

Alam F et al (2021) 3D printed contact lenses. ACS Biomater Sci Eng 7(2):794–803

Alam F et al (2022) 3D printed contact lenses for the management of color blindness. Addit Manuf 49:102464
Alifui-Segbaya F et al (2018) Toxicological assessment of additively manufactured methacrylates for medical devices in dentistry. Acta Biomater 78:64–77
Appuhamillage GA et al (2019) 110th anniversary: vat Photopolymerization-based additive manufacturing: current trends and future directions in materials design. Ind Eng Chem Res 58(33):15109–15118
Awad A, Gaisford S, Basit AW (2018) Fused deposition modelling: advances in engineering and medicine. In: Basit AW, Gaisford S (eds) 3D printing of pharmaceuticals. Springer International Publishing, Cham, pp 107–132
Awad A et al (2021a) Advances in powder bed fusion 3D printing in drug delivery and healthcare. Adv Drug Deliv Rev 174:406-424
Awad A et al (2021b) Connected healthcare: improving patient care using digital health technologies. Adv Drug Deliv Rev 178:113958
Awad A et al (2023) A Review of State-of-the-Art on Enabling Additive Manufacturing Processes for Precision Medicine. J Manuf Sci Eng 145(1):010802
Bagheri A, Jin J (2019) Photopolymerization in 3D printing. ACS Appl Polym Mater 1(4):593–611
Banks J (2013) Adding value in additive manufacturing: researchers in the United Kingdom and Europe look to 3D printing for customization. IEEE Pulse 4(6):22–26
Bernal PN et al (2019) Volumetric bioprinting of complex living-tissue constructs within seconds. Adv Mater 31(42):1904209
Bloomquist CJ et al (2018) Controlling release from 3D printed medical devices using CLIP and drug-loaded liquid resins. J Control Release 278:9–23
Bozuyuk U et al (2018) Light-triggered drug release from 3D-printed magnetic chitosan microswimmers. ACS Nano 12(9):9617–9625
Crivello JV, Lam JHW (1996) Photoinitiated cationic polymerization with triarylsulfonium salts. J Polym Sci A Polym Chem 34(16):3231–3253
Dodziuk H (2016) Applications of 3D printing in healthcare. Kardiochirurgia i torakochirurgia polska= Polish J Cardio-Thoracic Surg 13(3):283
Donnelly RF, Singh TRR, Woolfson AD (2010) Microneedle-based drug delivery systems: microfabrication, drug delivery, and safety. Drug Deliv 17(4):187–207
Economidou SN, Lamprou DA, Douroumis D (2018) 3D printing applications for transdermal drug delivery. Int J Pharm 544(2):415–424
Economidou SN et al (2019) 3D printed microneedle patches using stereolithography (SLA) for intradermal insulin delivery. Mater Sci Eng C 102:743–755
EnvisionTEC (2020) The Top Choice for 3D Printed Hearing Aids, Inner-Ear Devices. [cited 2020 21st June]; Available from: https://envisiontec.com/3d-printing-industries/medical/hearing-aid/
Faraji Rad Z, Prewett PD, Davies GJ (2021) High-resolution two-photon polymerization: the most versatile technique for the fabrication of microneedle arrays. Microsyst Nanoeng 7(1):1–17
Formlabs (2020a) SLA vs. DLP: Guide To Resin 3D Printers. [cited 2020 31st Mar]; Available from: https://formlabs.com/uk/blog/resin-3d-printer-comparison-sla-vs-dlp/
Formlabs (2020b) High-Accuracy 3D Printing Materials for dental labs and practices. [cited 2020 18th June]. Available from: https://dental.formlabs.com/uk/materials/
Fouassier J-P, Jacques L (2021) Two-component radical photoinitiators, in Photoinitiators: Structures, Reactivity and Applications in Polymerization. John Wiley & Sons, pp 117–197
Gardan J (2016) Additive manufacturing technologies: state of the art and trends. Int J Prod Res 54(10):3118–3132
Gong H et al (2015) Optical approach to resin formulation for 3D printed microfluidics. RSC Adv 5(129):106621–106632
Goyanes A et al (2016) 3D scanning and 3D printing as innovative technologies for fabricating personalized topical drug delivery systems. J Control Release 234:41–48
Han D et al (2020) 4D printing of a bioinspired microneedle Array with backward-facing barbs for enhanced tissue adhesion. Adv Funct Mater 30(11):1909197

Healy AV et al (2019) Additive manufacturing of personalized pharmaceutical dosage forms via Stereolithography. Pharmaceutics 11(12):645
Hegde M et al (2017) 3D printing all-aromatic polyimides using mask-projection stereolithography: processing the nonprocessable. Adv Mater 29(31):1701240
Hofmann N, Hugo B, Klaiber B (2002) Effect of irradiation type (LED or QTH) on photo-activated composite shrinkage strain kinetics, temperature rise, and hardness. Eur J Oral Sci 110(6): 471–479
Holt C et al (2019) Construction 3D printing. In: 3D concrete printing technology. Elsevier, pp 349–370
Hull CW (1984) Apparatus for production of three-dimensional objects by stereolithography. United States Patent, Appl., No. 638905, Filed
Industry DP (2019) Adidas to release a new version of 3D printed shoe, Alphaedge 4D. [cited 2020 3rd Apr]; Available from: https://3dprintingindustry.com/news/adidas-to-release-a-new-version-of-3d-printed-shoe-alphaedge-4d-155578/
Inoue Y, Ikuta K (2013) Detoxification of the Photocurable polymer by heat treatment for Microstereolithography. Procedia CIRP 5:115–118
Janusziewicz R et al (2020) Design and characterization of a novel series of geometrically complex intravaginal rings with digital light synthesis. Adv Mater Technol 5:2000261
Jiang H et al (2019) 3D printed mold-based capsaicin candy for the treatment of oral ulcer. Int J Pharm 568:118517
Johnson AR et al (2016) Single-step fabrication of computationally designed microneedles by continuous liquid interface production. PLoS One 11(9):e0162518
Joshi SC, Sheikh AA (2015) 3D printing in aerospace and its long-term sustainability. Virtual Phys Prototyping 10(4):175–185
Kadry H et al (2019) Digital light processing (DLP) 3D-printing technology and photoreactive polymers in fabrication of modified-release tablets. Eur J Pharm Sci 135:60–67
Karakurt I et al (2020) Stereolithography (SLA) 3D printing of ascorbic acid loaded hydrogels: a controlled release study. Int J Pharm 584:119428
Kelly BE et al (2019) Volumetric additive manufacturing via tomographic reconstruction. Science 363(6431):1075–1079
Kharkar PM et al (2016) Thiol–ene click hydrogels for therapeutic delivery. ACS Biomater Sci Eng 2(2):165–179
Krkobabić M et al (2019) Hydrophilic excipients in digital light processing (DLP) printing of sustained release tablets: impact on internal structure and drug dissolution rate. Int J Pharm 572: 118790
Larush L et al (2017) 3D printing of responsive hydrogels for drug-delivery systems. J 3D Printing Med 1(4):219–229
Lee M et al (2020) Guiding lights: tissue bioprinting using Photoactivated materials. Chem Rev 120:10950
Li W et al (2020) Recent advances in formulating and processing biomaterial inks for vat polymerization-based 3D printing. Adv Healthc Mater 9:2000156
Liang K et al (2018) 3D printing of a wearable personalized oral delivery device: a first-in-human study. Sci Adv 4(5):eaat2544
Ligon SC et al (2017) Polymers for 3D printing and customized additive manufacturing. Chem Rev 117(15):10212–10290
Lim KS et al (2020) Fundamentals and applications of photo-cross-linking in bioprinting. Chem Rev 120:10662
Lim SH, Ng JY, Kang L (2017) Three-dimensional printing of a microneedle array on personalized curved surfaces for dual-pronged treatment of trigger finger. Biofabrication 9(1):015010
Lloyd C, Joshi A, McGlynn E (1986) Temperature rises produced by light sources and composites during curing. Dent Mater 2(4):170–174
Loterie D, Delrot P, Moser C (2020) High-resolution tomographic volumetric additive manufacturing. Nat Commun 11(1):1–6

Lu Y et al (2015) Microstereolithography and characterization of poly(propylene fumarate)-based drug-loaded microneedle arrays. Biofabrication 7(4):045001
Luzuriaga MA et al (2018) Biodegradable 3D printed polymer microneedles for transdermal drug delivery. Lab Chip 18(8):1223–1230
Martinez PR et al (2017) Fabrication of drug-loaded hydrogels with stereolithographic 3D printing. Int J Pharm 532(1):313–317
Martinez PR et al (2018) Influence of geometry on the drug release profiles of stereolithographic (SLA) 3D-printed tablets. AAPS PharmSciTech 19(8):3355–3361
Melchels FP, Feijen J, Grijpma DW (2010) A review on stereolithography and its applications in biomedical engineering. Biomaterials 31(24):6121–6130
Melocchi A et al (2019a) Retentive device for intravesical drug delivery based on water-induced shape memory response of poly(vinyl alcohol): design concept and 4D printing feasibility. Int J Pharm 559:299–311
Melocchi A et al (2019b) Expandable drug delivery system for gastric retention based on shape memory polymers: development via 4D printing and extrusion. Int J Pharm 571:118700
Muñiz Castro B et al (2021) Machine learning predicts 3D printing performance of over 900 drug delivery systems. J Control Release 337:530–545
Next Dent (2020) Leading dental materials for 3D printing. [cited 2020 18th June]; Available from: https://nextdent.com/
Ng WL et al (2020) Vat polymerization-based bioprinting—process, materials, applications and regulatory challenges. Biofabrication 12(2):022001
Oesterreicher A et al (2016) Tough and degradable photopolymers derived from alkyne monomers for 3D printing of biomedical materials. Polym Chem 7(32):5169–5180
Oskui SM et al (2016) Assessing and reducing the toxicity of 3D-printed parts. Environ Sci Technol Lett 3(1):1–6
Park SH, Yang DY, Lee KS (2009) Two-photon stereolithography for realizing ultraprecise three-dimensional nano/microdevices. Laser Photonics Rev 3(1–2):1–11
Pere CPP et al (2018) 3D printed microneedles for insulin skin delivery. Int J Pharm 544(2): 425–432
Piedra-Cascón W et al (2020) A vat-polymerized 3-dimensionally printed dual-material occlusal device: a dental technique. J Prosthet Dent 26(3):271–275
Popov VK et al (2004) Laser stereolithography and supercritical fluid processing for custom-designed implant fabrication. J Mater Sci Mater Med 15(2):123–128
Robles-Martinez P et al (2019) 3D printing of a multi-layered Polypill containing six drugs using a novel stereolithographic method. Pharmaceutics 11(6):274
Rodríguez-Pombo L et al (2022) Volumetric 3D printing for rapid production of medicines. Addit Manuf 52:102673
Rzhevskiy AS et al (2018) Microneedles as the technique of drug delivery enhancement in diverse organs and tissues. J Control Release 270:184–202
Sangermano M, Razza N, Crivello JV (2014) Cationic UV-curing: technology and applications. Macromol Mater Eng 299(7):775–793
Seoane-Viaño I et al (2021) Translating 3D printed pharmaceuticals: from hype to real-world clinical applications. Adv Drug Deliv Rev 174:553–575
Shusteff M et al (2017) One-step volumetric additive manufacturing of complex polymer structures. Sci Adv 3(12):eaao5496
Trenfield SJ et al (2019) Shaping the future: recent advances of 3D printing in drug delivery and healthcare. Expert Opin Drug Deliv 16(10):1081–1094
Trenfield SJ et al (2022) Advancing pharmacy and healthcare with virtual digital technologies. Adv Drug Deliv Rev 182:114098
Tumbleston JR et al (2015) Continuous liquid interface production of 3D objects. Science 347(6228):1349–1352
Uddin MJ et al (2020) 3D printed microneedles for anticancer therapy of skin tumours. Mater Sci Eng C 107:110248

Udhayakumar SSP, Pandiyarajan R (2021) Additive manufacturing for customized hearing aid parts production: an empirical study. J Chin Inst Eng 44(7):704–717
United States Food and Drug Administration (2015) Approval premarket notification: dentca denture base. 510 (k) Number K143033. [cited 2020 13th Apr]; Available from: https://www.accessdata.fda.gov/cdrh_docs/pdf14/K143033.pdf
United States Food and Drug Administration (2017) Technical Considerations for Additive Manufactured Medical Devices - Guidance for Industry and Food and Drug Administration Staff. [cited 2020 20th Dec]; Available from: https://www.fda.gov/downloads/MedicalDevices/DeviceRegulationandGuidance/GuidanceDocuments/UCM499809.pdf
Vaut L et al (2020) 3D printing of reservoir devices for Oral drug delivery: from concept to functionality through design improvement for enhanced Mucoadhesion. ACS Biomater Sci Eng 6(4):2478–2486
Vitale A, Cabral JT (2016) Frontal conversion and uniformity in 3D printing by photopolymerisation. Materials 9(9):760
Vivero-Lopez M et al (2021) Anti-biofilm multi drug-loaded 3D printed hearing aids. Mater Sci Eng C 119:111606
Wang J et al (2016a) Stereolithographic (SLA) 3D printing of oral modified-release dosage forms. Int J Pharm 503(1–2):207–212
Wang J et al (2016b) Stereolithographic (SLA) 3D printing of oral modified-release dosage forms. Int J Pharm 503(1):207–212
Wannarumon S, Bohez EL (2004) Rapid prototyping and tooling technology in jewelry CAD. Comput Aided Design Appl 1(1–4):569–575
Wu H et al (2019) Four-dimensional printing of a novel acrylate-based shape memory polymer using digital light processing. Mater Des 171:107704
Wu S, Serbin J, Gu M (2006) Two-photon polymerisation for three-dimensional micro-fabrication. J Photochem Photobiol A Chem 181(1):1–11
Xing J-F, Zheng M-L, Duan X-M (2015) Two-photon polymerization microfabrication of hydrogels: an advanced 3D printing technology for tissue engineering and drug delivery. Chem Soc Rev 44(15):5031–5039
Xu X et al (2020) Stereolithography (SLA) 3D printing of an antihypertensive polyprintlet: case study of an unexpected photopolymer-drug reaction. Addit Manuf 33:101071
Xu X et al (2021a) Vat photopolymerization 3D printing for advanced drug delivery and medical device applications. J Control Release 329:743–757
Xu X et al (2021b) Smartphone-enabled 3D printing of medicines. Int J Pharm 609:121199
Xu X et al (2021c) 3D printed Punctal plugs for controlled ocular drug delivery. Pharmaceutics 13(9):1421
Xu X et al (2021d) Stereolithography (SLA) 3D printing of a bladder device for intravesical drug delivery. Mater Sci Eng C Mater Biol Appl 120:111773
Yang Y et al (2020) Printability of external and internal structures based on digital light processing 3D printing technique. Pharmaceutics 12(3):207
Yu C et al (2020) Photopolymerizable biomaterials and light-based 3D printing strategies for biomedical applications. Chem Rev 120(19):10695–10743
Yue J et al (2015) 3D-Printable antimicrobial composite resins. Adv Funct Mater 25(43): 6756–6767
Zema L et al (2017) Three-dimensional printing of medicinal products and the challenge of personalized therapy. J Pharm Sci 106(7):1697–1705
Zhao T et al (2018) 4D printing of shape memory polyurethane via stereolithography. Eur Polym J 101:120–126

Chapter 6
Semi-solid Extrusion 3D Printing for the Development of Dosage Forms for Special Patient Groups

Angelos Gkaragkounis and Dimitrios G. Fatouros

Abstract The current availability of dosage forms for patients with special requirements, such as pediatrics, is low while often leading to poor acceptability and inadequate treatment adherence. As a result, unlicensed and off-labeled preparations are common, exposing patients to unpredictable risks. During the last years, there is an obvious momentum for drug development tailored to such patient groups, with 3D printing being at the forefront of research in this area. In this context, semi-solid extrusion 3D printing, with the unique capability of additive manufacturing without requiring extreme temperatures, is paving the way toward personalized medicine, point-of-care fabrication upon demand, and digitalization of the pharmaceutical industry.

Keywords 3D printing · Semi-solid extrusion · Personalized medicine · Special groups · Patient compliance

Abbreviations

3DP	Three-dimensional Printing
API	Active Pharmaceutical Ingredient
CAD	Computer-Aided Design
CMC	Carboxymethylcellulose
FDA	Food and Drug Administration
FDM	Fused Deposition Modelling
HPC	Hydroxypropyl Cellulose
HPMC	Hydroxypropyl Methylcellulose
LEV	Levetiracetam

A. Gkaragkounis · D. G. Fatouros (✉)
Laboratory of Pharmaceutical Technology, Department of Pharmacy, School of Health Sciences, Aristotle University of Thessaloniki, Thessaloniki, Greece
e-mail: dfatouro@pharm.auth.gr

D. Lamprou (ed.), *Nano- and Microfabrication Techniques in Drug Delivery*, Advanced Clinical Pharmacy – Research, Development and Practical Applications 2,
https://doi.org/10.1007/978-3-031-26908-0_6

MSUD	Maple Syrup Urine Disease
ODF	Orodispersible Film
ODT	Orodispersible Tablet
PLGA	Poly Lactic-co-Glycolic Acid
PS	Pregelatinized Starch
PVA	Polyvinyl Alcohol
PVP	Polyvinyl Pyrrolidone
QbD	Quality by Design
SPG	Special Patient Group
SSE	Semi-Solid Extrusion

6.1 Introduction

Medication adherence is the cornerstone of a successful therapeutic plan, yet, special populations, such as pediatrics, require special management in drug delivery. Currently, conventional medicines monopolize the pharmaceutical market leaving little space for adjustment and personalization or forcing the adaptation of unlicensed, off-labeled, and extemporaneous handling in order to complement the scarcity of commercially available appropriate dosage forms. This type of empirical preparation may often lead to dose inaccuracy and variations, exposing the patient to unpredictable safety risks (Karavasili et al. 2021).

Following the adoption of additive manufacturing in the pharmaceutical world and the growing demand for patient-centric medicines, the "one size fits all" approach seems to have been overcome, as three-dimensional printing (3DP) and pharmacoprinting enable the preparation of novel dosage forms as per individual patient's health requirements (Goyanes et al. 2017). There is already one pharmaceutical 3DP product (Spritam®—Aprecia Pharmaceuticals) that has entered the market while Triastek Inc. has granted permission by the United States Food and Drug Administration (FDA) to begin clinical trials for another two 3D printed products ("Triastek, Inc-Triastek Receives FDA IND Clearance for 3D Printed Product of Blockbuster Molecule," n.d.).Fused Deposition Modelling(FDM) 3DP has been extensively studied during the last years for the manufacturing of dosage forms, often tailored toward the needs of special patient groups (SPG). For instance, 3D printed "candy-like" pediatric tablets with enhanced palatability have been fabricated in different shapes (heart, ring, lion, etc.) providing the opportunity for involvement of sensitive patients, like children, in the design process and therefore improve the acceptability of the final product and their overall healthcare experience (Scoutaris et al. 2018). Recently, dosage forms for people with visual impairment were developed as FDM 3DP was used for the fabrication of intraoral films, enhanced with haptic identifiers of Braille-encoded texts about the treatment regimens (Eleftheriadis and Fatouros 2021). Food scientists are also approaching food

customization using 3DP techniques, especially semi-solid extrusion (SSE) 3DP (Le-Bail et al. 2020; Singhal et al. 2020).

SSE 3DP is based on extrusion of paste- or gel-like materials through a syringe or a cartridge and their deposition in sequential layers generating 3D objects. Generally, this technology is ruled by most of the main parameters that affect 3DP, starting with the design of a 3D model using a computer-aided design (CAD) software. Extrusion can be carried out by means of a pneumatic, mechanical, or solenoid-based system either at room temperature or heating might be applied until the feeding material reaches a viscosity low enough to be extruded through the nozzle with the desired flow. During printing, nozzle diameter, travel speed, and extrusion rate are some of the key considerations for optimizing the method. Upon extrusion, the material hardens, usually by a post-processing step of drying, cooling, solvent-treating, or photopolymerization, allowing the subsequent tiers to be supported by the underneath ones, producing the final product or dosage form (Seoane-Viaño et al. 2021a).

Through SSE 3DP, low-temperature extrusion can be achieved enabling the production of dosage forms of materials, shapes, and properties that could not be replicated with the classical pharmaceutical methods or other printing technologies, offering new opportunities for medical individualization. Therefore, it has lately drawn researchers' attention, especially for pediatric drug delivery. The current article explores the applications of SSE 3DP during the development of pharmaceutical products for drug delivery in special patient groups (SPG).

6.2 Semi-solid Extrusion 3D Printing in Pharmaceutical Production

SSE 3DP has been used for the production of drug delivery platforms since 2012, when dexamethasone was encapsulated in a Poly Lactic-co-Glycolic Acid (PLGA): Polyvinyl alcohol (PVA) matrix producing a system with a two-stage drug release profile, over a 4-month period (Rattanakit et al. 2012). This technology has also been used for the fabrication of tablets with defined release profiles containing one or multiple APIs (polypill) (Khaled et al. 2014, 2015a, 2015b). The use of SSE 3DP offers the great advantage of creating complex dosage forms avoiding the harsh conditions (e.g., very high temperature) of other printing techniques, such as FDM, enabling printing of sensitive, and thermolabile materials (Abdella et al. 2021; Goyanes et al. 2015). Furthermore, the relatively simple setup combined with pre-loaded cartridges make SSE a great candidate for meeting regulations' requirements and application for point-of-care treatment.

6.2.1 *Semi-solid Extrusion 3D Printing of Dosage Forms for Special Patient Groups*

6.2.1.1 Tablets

To date, the only one commercially available 3DP medicinal product is Spritam ® which is the brand name for levetiracetam tablets developed and manufactured using the Binder Jet 3DP method. Levetiracetam (LEV) is an anticonvulsant which is very often used for the treatment of seizures in adults and children (4 years of age or older) with epilepsy. However, prescription of an appropriate dose for a patient is an extremely complicated and individualized process, as it depends on body weight, age, health level, and phase of treatment. The major advantage of 3DP, especially SSE, is dose flexibility and production upon demand. Within this context, there are many studies that aim to develop 3DP dosage forms with the feasibility of dose regulation while being appropriate for sensitive groups, like children and the elderly. For instance, rapid release cylindrical tablets of LEV with excellent mechanical properties have been prepared using croscarmellose sodium, carboxymethylcellulose (CMC) sodium, and polyvinylpyrrolidone (PVP), as excipients. The API content was modified by manipulating the model's volume through three different patterns: a) modifying the height of the design by varying the number of printed layers, b) varying the diameter using a constant height, c) synchronously regulating both the diameter and the height. In all cases, a linear relationship between tablet mass and volume was observed, while the release profile was dependent on the surface area/mass ratio (Cui et al. 2019).

Some patients often endure discomfort when swallowing large dosage forms, often leading to rejection. Therefore, formulations that enable the production of high-dose products with an easy-to-swallow size are necessary. SSE 3DP has been used for the fabrication of high drug loading (96%) LEV tablets using hydroxypropyl cellulose (HPC) as a binder and croscarmellose sodium as the disintegrant. A lattice structure was used in three geometrical shapes (cylinder, torus, and oval) enabling control of the drug release profiles by varying lattice cell size and hence, infill percentage. The high drug loading enabled printing of approximately 600 mg tablets without exceeding 12 mm in diameter, significantly smaller than the commercial 3DP LEV tablets (20.03 ± 0.08 mm). While all tablets showed more than 85% drug release within 15 min, torus tablets with 50% infill achieved an optimum drug release of 97.45% within 2 min (Cui et al. 2020).

The use of organic solvents, like ethanol, acetone, and dimethyl sulfoxide (DMSO), is sometimes inevitable in SSE in order to prevent nozzle clogging or to achieve adequate dissolving, restricting the use of such dosage forms from some patients, especially pediatrics, for which, the European Pharmacopoeia requires absence of such solvents in the final dosage form. Nevertheless, 3DP formulations comprising LEV have been prepared using only water as a solvent and applying a drying step after printing. Polyvinyl alcohol-polyethylene glycol graft copolymer

was used as a hydrophilic matrix with rapid disintegration and immediate release characteristics. However, the size of the tablets might not be suitable for the younger pediatric subgroups (El Aita et al. 2020). In addition, a mixture of polyvinyl acetate/polyvinylpyrrolidone copolymer (PVAc-PVP), hydroxypropyl methylcellulose (HPMC), and highly dispersed silicon dioxide (SiO_2) was found to be a feasible polymer matrix for achieving sustained release. Storage of the formulation for up to 5 days did not affect its solid state, printing, or dissolution properties demonstrating the suitability of this technology for a quick response upon demand using a large batch of feeding material (Aita et al. 2020).

The availability of medicinal products of appropriate strength for every patient would contribute to limiting the use of rough preparations, such as pill breaking. Tablets containing furosemide (2 or 10 mg) or sildenafil (4 mg) for pediatric populations have been developed using Gelucire 48/16 as an excipient and a heated piston-driven SSE 3D printer, aiming to shorten the gap in the market for pediatric products comprising these APIs. The dosage forms were tested for their appropriateness to be analyzed according to European Pharmacopoeia protocols as well as their compliance with regulatory requirements (Lafeber et al. 2021).

6.2.1.2 Chewable Formulations

Candy-like chewable formulations have been introduced as a means to overcome swallowing difficulties and taste aversion of the conventional oral dosage forms. The acceptability of 3DP chewable tablets of isoleucine, prepared at a hospital setting by SSE 3DP, has been recently investigated among four pediatric patients (aged between 3 and 16 years) suffering from maple syrup urine disease (MSUD). Excipients used to prepare the formulations include sucrose, pectin, maltodextrin, water, flavorings, and colorants. Printlets, which varied in color and flavor, were well tolerated and accepted by children, who also showed specific color and flavor preferences (Goyanes et al. 2019). In another study, dosage forms, each one printed with a different 3DP technique, were visually assessed by 368 children (aged 4–11 years), according to their preferences. Although the initial perception about the SSE printlets was not desirable compared to other techniques, most of the participants changed their minds once they were aware that the SSE printlets were chewable, highlighting the popularity of that kind of dosage forms in the pediatric population (Januskaite et al. 2020).

Edible excipients are gaining popularity toward the development of age-appropriate dosage forms. For example, pediatric friendly chocolate-based 3DP formulations with desirable mouthfeel properties have been developed for the administration of both hydrophilic (paracetamol) and lipophilic (ibuprofen) APIs with a rapid and high-release profile in simulated salivary fluid. Printing in various designs enabled accurate dose adjustment and potentially a more engaging role for the pediatric patient, aiming to improve their healthcare experience and hence,

therapeutic outcome (Karavasili et al. 2020). Starch-based 3DP dosage forms of isoniazid have been developed as a cost-effective platform for drug delivery in children suffering from latent tuberculosis infection. SSE was conducted at room temperature while the products indicated soft textures comparable to food textures well accepted by children (e.g., fruit or potato puree). Drug diffusion from printed tablets was rapid with ca. 70% of ISO being released within the first 5 min and almost total drug release achieved within 45 min (Chatzitaki et al. 2021). Drug administration combined with a daily habit, like eating breakfast, is a promising method for overcoming treatment adherence barriers. Nevertheless, mixing with foods or drinks is a common practice for drug administration, especially in young children. In this framework, cereal-based 3D printed medications comprising paracetamol or ibuprofen, have been fabricated with SSE and tested in vitro for their behavior during coadministration with full-fat and low-fat milk. Release of ibuprofen in simulated fluids was found to be affected by the fat content of milk (Karavasili et al. 2022).

Similarly, gummy-like formulations are another approach in printed medicine tailored to children. Ranitidine HCl has been incorporated in various matrices of hydrocolloids or other gelling agents (corn starch, carrageenan, xanthan gum, gelatin) and palatability enhancers. The drug-loaded gummies ("drugmies") had an appealing appearance with homogenous, bright color, similar to commercial ones, while the drug release rate was inversely proportional to starch content(Herrada-Manchón et al. 2020). Gummy drug formulations comprising the antiepileptic drug lamotrigine have also been developed with gelatin, HPMC, reduced syrup, and water as excipients and printed in various shapes and colors by using an air-assisted extrusion 3D bioprinter. The dosage forms showed remarkable strength, mainly influenced by gelatin concentration, while dissolution tests showed 85% drug release within 15 minutes (Tagami et al. 2021).

Embedded 3DP is an emerging additive manufacturing method where semi-solid materials are been extruded in a solidifying liquid matrix. In this context, pediatric chewable Lego™-like dosage forms with dual drug loading have been developed. The embedded extrusion paste was a locust bean gum solution comprising either 28% w/w ibuprofen or 40% w/w paracetamol. A mixture of water:glycerol:gelatin (45:25:30 w/w) was used as a thermo-responsive embedding medium. In an one-step printing process, the embedded phase was printed into a warm (75 °C) embedding phase and then left to cool down and solidify. A multi-step printing method has also been tested, according to which, printing of pastes is being conducted on casted semi-solid gelatin or embedding solution and then is covered with liquid gelatin or embedding solution and left to solidify. Despite their difference in solubility, both APIs showed similar release rates due to the slow dissolution of locust bean gum which forms a gel in the embedded phase (Rycerz et al. 2019) (Fig. 6.1).

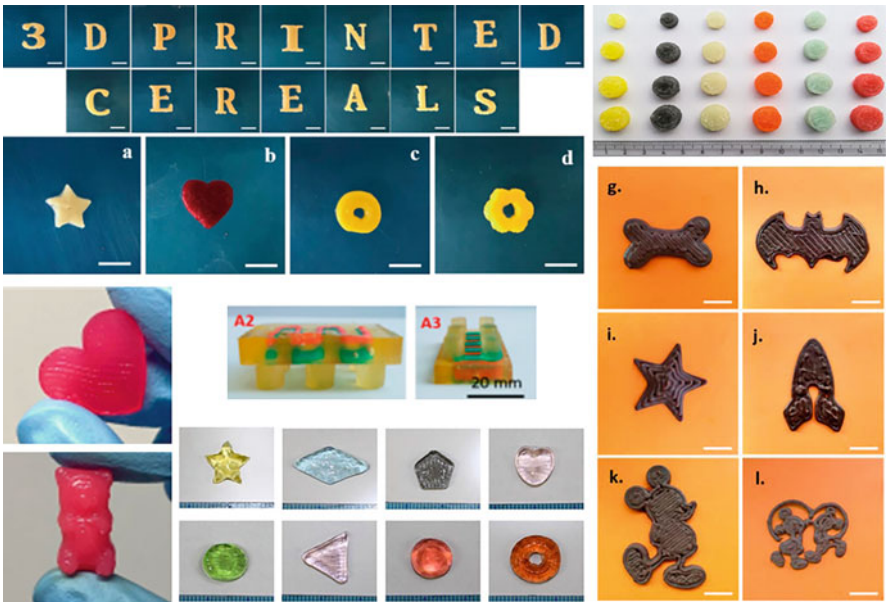

Fig. 6.1 3D printed chewable dosage forms; cereal-based (upper-left) (Karavasili et al. 2022); dosage forms with various colors and flavors (upper-right) (Goyanes et al. 2019); gummy dosage forms (lower-left) (Herrada-Manchón et al. 2020); LegoTM-shaped dosage forms (center) (Rycerz et al. 2019); gelatin-based gummy dosage forms (lower-middle) (Tagami et al. 2021); chocolate-based dosage forms (lower-right) (Karavasili et al. 2020)

6.2.1.3 Orodispersible Formulations

Orodispersible films (ODFs) are polymeric thin film strips that rapidly dissolve upon contact with saliva and consequently, they have been widely used for administration to dysphagic patients. Individualized levocetirizine hydrochloride ODFs have been printed in pediatric and adult doses using SSE 3DP. The inks were prepared with HPMC as the film-forming polymer, pregelatinized starch (PS) as the filling agent, maltitol, and sucralose as the flavoring agents, at an HPMC:API:PS:mannitol: sucralose ratio of 64:10:10:15:1. The films showed preferable flexibility and wetting characteristics while the API was completely released in vitro in 2 mins (Yan et al. 2020). Latest advancements in 3DP ODF research include the development of a toolbox of characterization techniques with the aim of enabling the design, reformulation, and quality control of films with the desired palatability and acceptability attributes (Desai et al. 2022).

Optimizing critical parameters of the 3DP process is of paramount importance for the quality of the final customized products as well as their approval by authorities. During the development of 3DP pediatric orodispersible tablets (ODTs) comprising hydrochlorothiazide, a Quality by Design (QbD) approach was adopted, especially for the optimization of the first printed layer. Hence, various materials were used as

the printing surface (printing bed), different first-layer heights, infill patterns, and number of perimeters were tested. Banana flavoring essence was also added to mask the bitter taste of the API. With the appropriate parameters applied, small orodispersible tablets (4.62 mm × 1.90 mm) with a high drug loading (>40.4% w/w) were produced (Eduardo et al. 2021).

Three-dimensional printing is not the only one alternative to tablet compression process. Molding is another technique with the potential for production in a hospital environment. In a comparative study, hydrochlorothiazide ODTs were fabricated either by SSE 3DP or by molding. Generally, the results indicated acceptable characteristics for both formulations however, the molded tablets lacked content uniformity. In contrast, high drug-loaded 3DP ODTs with good quality attributes passed all the recommended pharmacopoeia tests (Suárez-González et al. 2021).

6.2.1.4 Suppositories

Although the oral is the most popular route of administration, 3DP technology has also been used for the fabrication of rectal suppositories for the treatment of ulcerative colitis. Suppositories may often be uncomfortable for some patients while age-appropriate doses are required. Hence, SSE has been applied in order to regulate the shape and size of tacrolimus suppositories. The API was dissolved in Gelucire 44/14 or Gelucire 48/16 while coconut oil was employed as a plasticizer. The suppositories would solidify in less than 1 min after printing so, there was no need for refrigeration or other solidifying steps. The Gelucire 44/14 suppositories had a faster disintegration time but slower drug release rate than the ones with Gelucire 48–16 (Seoane-Viaño et al. 2021b).

6.3 Conclusions

SSE 3DP is a cost-effective method that has the potential to reform healthcare and lead the pharmaceutical industry to a novel, decentralized manufacturing process. Its versatility for the fabrication of individualized dosage forms in various shapes and sizes, combined with a relatively simple set up and easy handling during operation, make SSE 3DP a great candidate for point-of-care treatment and on-demand medicine preparation. Disposable syringes and printing at room temperature are key characteristics for meeting the regulatory requirements. Recently, this technology has shown its potential for producing drug delivery systems for special patient groups with special requirements, such as age-appropriate dosage forms, paving the way for more personalized therapeutic protocols, with increased adherence, acceptability, and therefore, treatment (Table 6.1).

Table 6.1 Dosage forms for special patient groups fabricated with semi-solid extrusion 3D printing

Dosage form	API (% w/w)	Excipients	Properties	References
Tablets	Levetiracetam (93%)	Croscarmellose Na, CMC-Na, PVP	Rapid drug release. Three modifying-the-dose patterns.	(Cui et al. 2019)
	Levetiracetam (96%)	Croscarmellose Na, HPC	High drug loading and rapid drug release.	(Cui et al. 2020)
	Levetiracetam (47.1%)	PVA/PEG copolymer	Rapid drug release. Absence of organic solvents.	(El Aita et al. 2020)
	Levetiracetam (23.4%)	PVA/PVP copolymer, HPMC, SiO_2	Sustained drug release. Absence of organic solvents. Stability after 5 days.	(Aita et al. 2020)
	Furosemide (2–10 mg/tablet)or sildenafil(4 mg/tablet)	Gelucire 48/16, polysorbate 80	Compliance with European pharmacopoeia requirements.	(Lafeber et al. 2021)
Chewable formulations	Isoleucine (14.4%)	Sucrose, pectin, maltodextrin, water, flavorings, colorants	Good acceptability by 4 children. Blood drug levels were in target range. Preferable compared to other printed dosage forms.	(Goyanes et al. 2019; Januskaite et al. 2020)
	Paracetamol (2.29%) or ibuprofen(1.96%)	Bitter chocolate, corn syrup	Rapid drug release in simulated saliva fluid. Both hydrophilic and lipophilic APIs can be incorporated.	(Karavasili et al. 2020)
	Isoniazid (7.95%)	Starch	Rapid drug release. Soft texture.	(Chatzitaki et al. 2021)
	Paracetamol (0.83%) & ibuprofen (0.33%)	Cereals	Easy to combine with eating habits. Food-dependent drug release. Both hydrophilic and lipophilic APIs can be incorporated.	(Karavasili et al. 2022)
	Ranitidine (14.6%)	Corn starch, carrageenan, xanthan gum, gelatine, liquid sweetener, strawberry essence, food coloring	Drug release rate was inversely proportional to starch content.	(Herrada-Manchón et al. 2020)
	Lamotrigine (0.17–0.36%)	Gelatin, HPMC, reduced syrup	Rapid drug release.	(Tagami et al. 2021)
	Paracetamol (16–77 mg/dosage form) & ibuprofen (12–76 mg/dosage form)	Glycerol, gelatin, locust bean, colorants	Both hydrophilic and lipophilic APIs can be incorporated with similar release rate.	(Rycerz et al. 2019)

(continued)

Table 6.1 (continued)

Dosage form	API (% w/w)	Excipients	Properties	References
Orodispersible films	Levocetirizine (1,25–5 mg/film)	HPMC, PS, maltitol, sucralose	Rapid drug release	(Yan et al. 2020)
Orodispersible tablets	Hydrochlorothiazide (40.4%)	Lactose monohydrate, PVP, croscarmellose, banana flavoring	Small size, high drug loading, rapid dis-integration, meet pharmacopoeia requirements.	(Eduardo et al. 2021; Suárez-González et al. 2021)
Suppositories	Tacroolimus (0.12%)	Gelucire 44/14, Gelucire 44/16, coconut oil	Self-supported lipid-based suppositories.	(Seoane-Viaño et al. 2021b)

References

Abdella S, Youssef SH, Afinjuomo F, Song Y, Fouladian P, Upton R, Garg S (2021) 3D printing of thermo-sensitive drugs. Pharmaceutics 13:1524. https://doi.org/10.3390/pharmaceutics13091524

Aita IE, Breitkreutz J, Quodbach J (2020) Investigation of semi-solid formulations for 3D printing of drugs after prolonged storage to mimic real-life applications. Eur J Pharm Sci 146:105266. https://doi.org/10.1016/j.ejps.2020.105266

Chatzitaki A-T, Mystiridou E, Bouropoulos N, Ritzoulis C, Karavasili C, Fatouros DG (2021) Semi-solid extrusion 3D printing of starch-based soft dosage forms for the treatment of paediatric latent tuberculosis infection. J Pharm Pharmacol 74:1498. https://doi.org/10.1093/jpp/rgab121

Cui M, Li Y, Wang S, Chai Y, Lou J, Chen F, Li Q, Pan W, Ding P (2019) Exploration and preparation of a dose-flexible regulation system for Levetiracetam tablets via novel semi-solid extrusion three-dimensional printing. J Pharm Sci 108:977–986. https://doi.org/10.1016/j.xphs.2018.10.001

Cui M, Pan H, Fang D, Qiao S, Wang S, Pan W (2020) Fabrication of high drug loading levetiracetam tablets using semi-solid extrusion 3D printing. J Drug Deliv Sci Technol 57:101683. https://doi.org/10.1016/j.jddst.2020.101683

Desai N, Masen M, Cann P, Hanson B, Tuleu C, Orlu M (2022) Modernising Orodispersible film characterisation to improve palatability and acceptability using a toolbox of techniques. Pharmaceutics 14:732. https://doi.org/10.3390/pharmaceutics14040732

Eduardo D-T, Ana S-E, José BF (2021) A micro-extrusion 3D printing platform for fabrication of orodispersible printlets for pediatric use. Int J Pharm 605:120854. https://doi.org/10.1016/j.ijpharm.2021.120854

El Aita I, Rahman J, Breitkreutz J, Quodbach J (2020) 3D-printing with precise layer-wise dose adjustments for paediatric use via pressure-assisted microsyringe printing. Eur J Pharm Biopharm 157:59. https://doi.org/10.1016/j.ejpb.2020.09.012

Eleftheriadis GK, Fatouros D (2021) Haptic evaluation of 3D-printed braille-encoded intraoral films. Eur J Pharmaceut Sci 157:105605. https://doi.org/10.1016/j.ejps.2020.105605

Goyanes A, Buanz ABM, Hatton GB, Gaisford S, Basit AW (2015) 3D printing of modified-release aminosalicylate (4-ASA and 5-ASA) tablets. Eur J Pharm Biopharm 89:157–162. https://doi.org/10.1016/j.ejpb.2014.12.003

Goyanes A, Madla CM, Umerji A, Duran Piñeiro G, Giraldez Montero JM, Lamas Diaz MJ, Gonzalez Barcia M, Taherali F, Sánchez-Pintos P, Couce M-L, Gaisford S, Basit AW (2019) Automated therapy preparation of isoleucine formulations using 3D printing for the treatment of MSUD: first single-Centre, prospective, crossover study in patients. Int J Pharm 567:118497. https://doi.org/10.1016/j.ijpharm.2019.118497

Goyanes A, Scarpa M, Kamlow M, Gaisford S, Basit AW, Orlu M (2017) Patient acceptability of 3D printed medicines. Int J Pharm 530:71–78. https://doi.org/10.1016/j.ijpharm.2017.07.064

Herrada-Manchón H, Rodríguez-González D, Alejandro Fernández M, Suñé-Pou M, Pérez-Lozano P, García-Montoya E, Aguilar E (2020) 3D printed gummies: personalized drug dosage in a safe and appealing way. Int J Pharm 587:119687. https://doi.org/10.1016/j.ijpharm.2020.119687

Januskaite P, Xu X, Ranmal SR, Gaisford S, Basit AW, Tuleu C, Goyanes A (2020) I spy with my little eye: a Paediatric visual preferences survey of 3D printed tablets. Pharmaceutics 12:1100. https://doi.org/10.3390/pharmaceutics12111100

Karavasili C, Gkaragkounis A, Fatouros DG (2021) Patent landscape of pediatric-friendly oral dosage forms and administration devices. Expert Opin Ther Pat 31:663–686. https://doi.org/10.1080/13543776.2021.1893691

Karavasili C, Gkaragkounis A, Moschakis T, Ritzoulis C, Fatouros DG (2020) Pediatric-friendly chocolate-based dosage forms for the oral administration of both hydrophilic and lipophilic drugs fabricated with extrusion-based 3D printing. Eur J Pharm Sci 105291:105291. https://doi.org/10.1016/j.ejps.2020.105291

Karavasili C, Zgouro P, Manousi N, Lazaridou A, Zacharis CK, Bouropoulos N, Moschakis T, Fatouros DG (2022) Cereal-based 3D printed dosage forms for drug administration during breakfast in pediatric patients within a hospital setting. JPharmSci 0:2562. https://doi.org/10.1016/j.xphs.2022.04.013

Khaled SA, Burley JC, Alexander MR, Roberts CJ (2014) Desktop 3D printing of controlled release pharmaceutical bilayer tablets. Int J Pharm 461:105–111. https://doi.org/10.1016/j.ijpharm.2013.11.021

Khaled SA, Burley JC, Alexander MR, Yang J, Roberts CJ (2015a) 3D printing of five-in-one dose combination polypill with defined immediate and sustained release profiles. J Control Release 217:308–314. https://doi.org/10.1016/j.jconrel.2015.09.028

Khaled SA, Burley JC, Alexander MR, Yang J, Roberts CJ (2015b) 3D printing of tablets containing multiple drugs with defined release profiles. Int J Pharm., The potential for 2D and 3D Printing to Pharmaceutical Development 494, 494:643–650. https://doi.org/10.1016/j.ijpharm.2015.07.067

Lafeber I, Tichem JM, Ouwerkerk N, van Unen AD, van Uitert JJD, Bijleveld-Olierook HCM, Kweekel DM, Zaal WM, Le Brun PPH, Guchelaar HJ, Schimmel KJM (2021) 3D printed furosemide and sildenafil tablets: innovative production and quality control. Int J Pharm 603:120694. https://doi.org/10.1016/j.ijpharm.2021.120694

Le-Bail A, Maniglia BC, Le-Bail P (2020) Recent advances and future perspective in additive manufacturing of foods based on 3D printing. Curr Opin Food Sci Food Eng Proc 35:54–64. https://doi.org/10.1016/j.cofs.2020.01.009

Rattanakit P, Moulton SE, Santiago KS, Liawruangrath S, Wallace GG (2012) Extrusion printed polymer structures: a facile and versatile approach to tailored drug delivery platforms. Int J Pharm 422:254–263. https://doi.org/10.1016/j.ijpharm.2011.11.007

Rycerz K, Stepien KA, Czapiewska M, Arafat BT, Habashy R, Isreb A, Peak M, Alhnan MA (2019) Embedded 3D printing of novel bespoke soft dosage form concept for pediatrics. Pharmaceutics 11:630. https://doi.org/10.3390/pharmaceutics11120630

Scoutaris N, Ross SA, Douroumis D (2018) 3D printed "Starmix" drug loaded dosage forms for Paediatric applications. Pharm Res 35:34. https://doi.org/10.1007/s11095-017-2284-2

Seoane-Viaño I, Januskaite P, Alvarez-Lorenzo C, Basit AW, Goyanes A (2021a) Semi-solid extrusion 3D printing in drug delivery and biomedicine: personalised solutions for healthcare challenges. J Control Release 332:367–389. https://doi.org/10.1016/j.jconrel.2021.02.027

Seoane-Viaño I, Ong JJ, Luzardo-Álvarez A, González-Barcia M, Basit AW, Otero-Espinar FJ, Goyanes A (2021b) 3D printed tacrolimus suppositories for the treatment of ulcerative colitis. Asian J Pharmaceut Sci 16:110–119. https://doi.org/10.1016/j.ajps.2020.06.003

Singhal S, Rasane P, Kaur S, Garba U, Bankar A, Singh J, Gupta N (2020) 3D food printing: paving way towards novel foods. An Acad Bras Ciênc 92:e20180737. https://doi.org/10.1590/0001-3765202020180737

Suárez-González J, Magariños-Triviño M, Díaz-Torres E, Cáceres-Pérez AR, Santoveña-Estévez A, Fariña JB (2021) Individualized orodispersible pediatric dosage forms obtained by molding and semi-solid extrusion by 3D printing: a comparative study for hydrochlorothiazide. J Drug Deliv Sci Technol 66:102884. https://doi.org/10.1016/j.jddst.2021.102884

Tagami T, Ito E, Kida R, Hirose K, Noda T, Ozeki T (2021) 3D printing of gummy drug formulations composed of gelatin and an HPMC-based hydrogel for pediatric use. Int J Pharm 594:120118. https://doi.org/10.1016/j.ijpharm.2020.120118

Triastek, Inc-Triastek Receives FDA IND Clearance for 3D Printed Product of Blockbuster Molecule [WWW Document], n.d.. URL https://www.triastek.com/detail/22.html. Accessed 26 April 2022

Yan T-T, Lv Z-F, Tian P, Lin M-M, Lin W, Huang S-Y, Chen Y-Z (2020) Semi-solid extrusion 3D printing ODFs: an individual drug delivery system for small scale pharmacy. Drug Dev Ind Pharm 46:531–538. https://doi.org/10.1080/03639045.2020.1734018

Chapter 7
Binder Jetting Powder Bed 3D Printing for the Fabrication of Drug Delivery System

Naseem A. Charoo, Eman M. Mohamed, Mathew Kuttolamadom, Mansoor A. Khan, and Ziyaur Rahman

Abstract FDA approval of Spritam® and investigational new drug clearance of another drug candidate T19 have generated huge interest in 3D printing (3DP) technology and its application to pharmaceutical manufacturing. The technology is still evolving as more knowledge is gathered to understand the impact of raw material on printed delivery system/dosage forms (printlets) and scalability of the technology. Binder jetting 3DP is a subject of discussion in this chapter. Key aspects of the process which are relevant to pharmaceutical application are reviewed. Process features including post-processing steps, critical raw material attributes, quality control, defects and challenges, and applications are discussed.

Keywords 3D printing · Binder-Jetting · Printhead · Excipients · Quality control · Quality defects · Regulatory landscape · Emerging Technology Program

N. A. Charoo
Succor Pharma Solutions, 216- Laboratory Complex, Dubai Science Park, Dubai, UAE

Centric Compounding LLC, 216- Laboratory Complex, Dubai Science Park, Dubai, UAE

E. M. Mohamed
Irma Lerma Rangel School of Pharmacy, Texas A&M Health Science Center, Texas A&M University, College Station, TX, USA

Department of Pharmaceutics, Faculty of Pharmacy, Beni-Suef University, Beni-Suef, Egypt

M. Kuttolamadom
College of Engineering, Texas A&M University, College Station, TX, USA

M. A. Khan · Z. Rahman (✉)
Irma Lerma Rangel School of Pharmacy, Texas A&M Health Science Center, Texas A&M University, College Station, TX, USA
e-mail: rahman_76@tamu.edu

D. Lamprou (ed.), *Nano- and Microfabrication Techniques in Drug Delivery*,
Advanced Clinical Pharmacy – Research, Development and Practical Applications 2,
https://doi.org/10.1007/978-3-031-26908-0_7

7.1 Introduction

3D printing (3DP) is defined as "Fabrication of objects through the deposition of a material using a print head, nozzle, or another printer technology" (ISO/ASTM 2021). The material is deposited layer by layer to create an object. Deposition of material can be accomplished by a variety of methods including welding, extrusion, curing, and inkjet (Rahman et al. 2018a; Beg et al. 2020). Deposition methods define the techniques, specific applications, and limitations. Welding, extrusion, and curing use heat to fuse material to create an object. Example of technique that relies on heat is fused deposition modeling (FDM) (Gottschalk et al. 2022). The techniques that use laser light to selectively cure liquid oligomer and sinter and fuse powder material are stereolithography and selective laser sintering, respectively (Charoo et al. 2020; Triacca et al. 2022). Liquid solvent or polymer binder solution/dispersion is selectively sprayed to glue powder material in the binder jetting (BJ) (Kozakiewicz-Latała et al. 2022). Each of the techniques has its own nuances with regard to raw material requirements and properties imparted to the printed object (Rahman et al. 2018a). In comparison with other methods, BJ offers many potential advantages such as the following: virtually any powdered raw material can be printed, and it has relatively high build rate (100 nozzle printhead can create parts up to 200 cm^3/min) and suitable for heat- and light-sensitive drugs/polymers since building takes place at room temperature with minimal heat exposure during post-processing and recycling potential of unprinted/support powder. Only limitations are post-processing requirements to remove the solvent, and it cannot be used to process drugs/excipients that degrade in the presence of water/solvent (Bai and Williams 2015; Ziaee and Crane 2019; Mostafaei et al. 2021).

3DP techniques are widely employed in prototype and commercial manufacturing by various industries including biomedical industries (medical devices and drug delivery systems) (Giannatsis and Dedoussis 2009; Guo and Leu 2013; Dawood et al. 2015). FDA has also approved number of such products, e.g., orthopedic and cranial implants, surgical instruments, dental restorations such as crowns, and external prosthetics. In comparison with medical devices, only one printed dosage form (delivery system/printlet) Spritam® containing levetiracetam has been approved (Rahman et al. 2018a; Charoo et al. 2020). Recently, FDA cleared IND (Investigational New Drug) application for T19 drug candidate manufactured by 3DP (Everett 2021). Manufacturing of medical devices is quite different from the delivery system as the devices are mostly printed using one component (polymer, ceramic, or metal). Printing of drug delivery system requires multicomponent formulation (drug, excipients, polymer, processing aids). Nevertheless, compared to traditional pharmaceutical manufacturing methods, lesser number of processing steps is involved and probably requires a lesser number of excipients in 3DP. The techniques have potential applications in printing personalized medications especially for pediatric and geriatric population which offer many advantages over existing manufacturing methods. It imparts unique features such as high porosity to the printlets that can disperse in the mouth in a matter of seconds, without even

consuming a sip of water, a feature desired for patients with difficulty in chewing or swallowing. The printlets containing multiple drug candidates can be printed that would potentially reduce adverse reactions due to polypharmacy and at the same time increase compliance. 3DP is not constrained by the geometry and design. Literally any complex geometries can be printed with the drug release modulation capability to meet the patient needs (Rahman et al. 2019; Charoo et al. 2020). This book chapter reviews key features of the BJ process with regard to its application in printing the printlets.

7.2 Process Description

Emanuel Sachs and coworkers of the Massachusetts Institute of Technology patented BJ in 1993, which was later commercialized by ZCorp Inc. (Sachs et al. 1992; Sachs et al. 1994; Ziaee and Crane 2019). This technology is also referred as powder bed inkjet printing. BJ process is akin to a wet granulation process, a commonly used process in tablets/capsules manufacturing. ASTM F2792 defines binder jetting as "an additive manufacturing process in which a liquid bonding agent is selectively deposited to join powder materials (ASTM 2012)". The printing process comprises of three main components, i.e., powder bed/reservoir, binder solution, and a build platform (Fig. 7.1). The process involves the following steps, namely, printing (green), drying, and depowdering. In printing stage, reservoir powder is spread as a uniform thin layer on the build platform with the help of a counter-clock rotating roller spread. This is followed by jetting of binder solution or dispersion/solvent as a

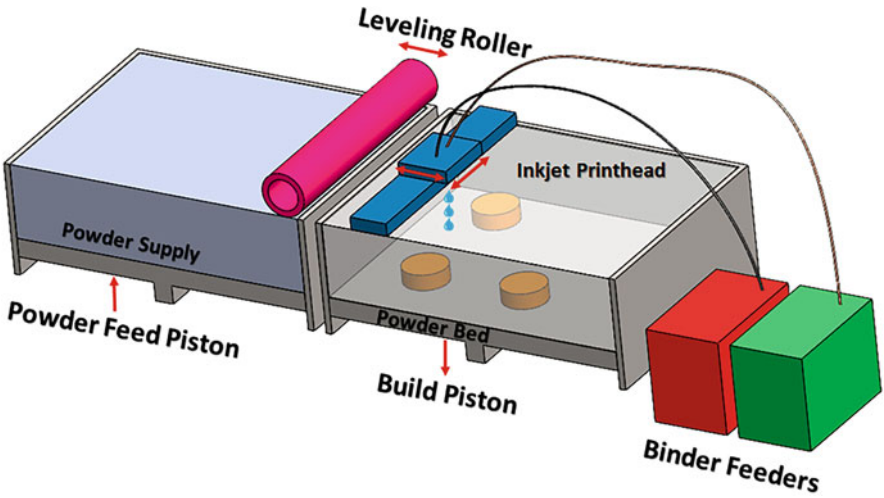

Fig. 7.1 Binder jetting 3D printing process

fine mist (minute droplet size) onto the defined printing area of first layer. The process is guided by the image file from the computer. The role of the binder solution is to bind powder particles in order to develop a 3DP structure. Optionally, an electrical heater passes over the printed layer to partially dry the printed layer and prepare for the subsequent layering process. After binder deposition and partial drying, the build platform lowers down to a one-layer thickness in preparation of printing of the next layer. Powder is again spread on the build platform followed by a binder jetting process. In this fashion an object is created layer by layer until the desired printlet is obtained. The unprinted powder on build platform around the printlets provides necessary support during the printing process. The green printlets does not have enough mechanical strength to maintain the shape and design. In drying stage, green printed printlets are dried to remove the solvent from the binder. The printer has either in-built heater to dry the printed printlets, or printed powder bed is dried in an oven at suitable temperature based on the properties and stability of the formulation. Depowdering stage involves separating the dried printlets from the loose powder that can be done manually or sieving (Ziaee and Crane 2019; Mostafaei et al. 2021).

The process may comprise of other post-processing steps after depowdering such as heat sintering and polymerization with light. These steps are performed to improve additional mechanical properties, control drug release, etc. For example, the printlets fabricated with Polyox™ polymer when sintered above 70 °C result in melting of Polyox™ polymer, fusion, and bond formation between the particles. This process dramatically enhances the mechanical properties of the delivery system. Some commercially available products use this concept to manufacture abuse deterrent formulations to deter abuser from abuse of opioid drug products (Barakh Ali et al. 2020; Dharani et al. 2020). The printlets fabricated using binder that polymerize in UV light can be post-processed in the UV chamber to increase mechanical strength and provide sustained release characteristics (Wilts et al. 2019).

7.3 Components of Printing Process

The printing process involves integration of printer and raw materials. The process involves the following components:

- Printhead
- Drug
- Excipients
- Binder
- Solvent

7.3.1 Printheads

Printhead is the most important component of the BJ printer. Two types of printheads, i.e., drop on demand (DoD) and continuous jet (CJ) printheads, are commonly employed in binder jet printing. They differ in the generation and deposition mechanism of binder droplets (Salehi et al. 2018; Mostafaei et al. 2021).

7.3.1.1 Drop-on-Demand Printheads

In drop-on-demand (DoD) printhead, individual drops are produced based on the demand. DoD technology is simple, is cost effective, and produces printlets with high precision. The breakup behavior of droplets is important for resolution and is influenced by the surface tension, viscosity, and droplet velocity. The size of the droplets can be controlled with high accuracy in DoD, and less waste is generated. Based on the mechanism with which drops are ejected from the printhead, DoD is further categorized into piezoelectric and thermal inkjet printheads (Sachs et al. 1992; Rahman et al. 2018a).

Piezoelectric Printheads

The piezoelectric heads work on the principle of generating pressure waves inside the printhead chamber. The pressure is generated by the change in physical dimensions of the piezoelectric element (actuator) upon receiving the electric signal (Fig. 7.2a). The pressure waves are responsible for jetting of binder solution through the nozzle. After this cycle, piezoelectric element returns back to its actual shape, followed by reloading of the nozzle with the binder, and is ready for next cycle (Rahmati 2009). The advantages of piezoelectric printheads are that they operate at low temperature and use less volatile and biocompatible fluids. The handling of a low viscosity binder is challenging with a piezoelectric printhead, as chances of leakage and mist formation during printing increase (Pond 2000; Kwon and Kim 2007).

Thermal Printheads

In thermal printheads, heating element (resistors in close proximity to the binder) causes vaporization of the binder (bubble formation) that creates a positive pressure resulting in the jetting of the binder during printing due to pressure difference. Vaporized liquid should dissolve quickly; otherwise, defective printlets may form due to a discontinuous supply of the binder (Fig. 7.2b). Compared to piezoelectric printheads, thermal printheads have higher print speed and lower cost. Drawbacks with this method are thermal exposure of binder (especially temperature-sensitive

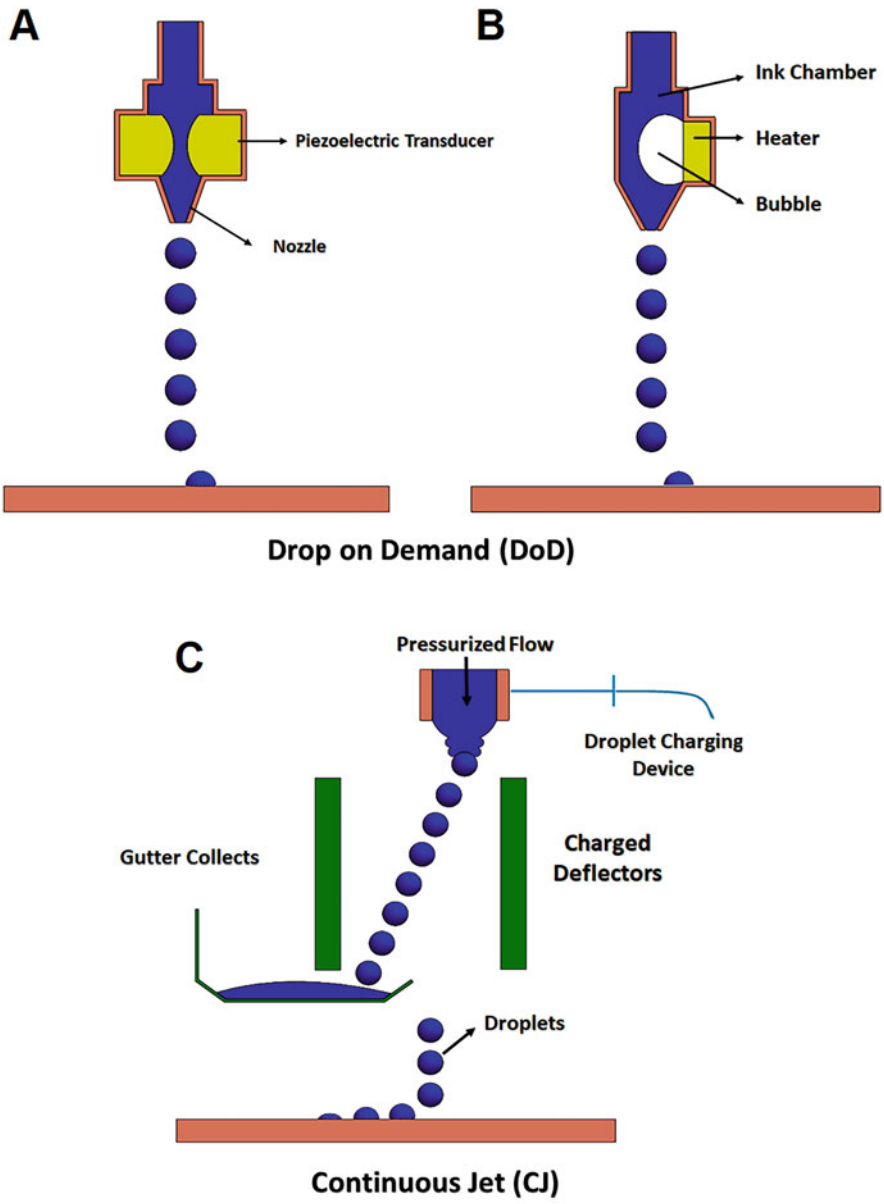

Fig. 7.2 (**a**) Piezoelectric and (**b**) thermal drop-on-demand printheads and (**c**) continuous jet printhead

drug and polymer), low droplet directionality, and non-uniform droplet size (Pond 2000; Kwon and Kim 2007; Murphy and Atala 2014). Notwithstanding this, thermal printheads are more suitable for aqueous-based binder formulation, while piezoelectric binder is preferred for organic solvents (Rahman et al. 2018a).

7.3.1.2 Continuous Jet Printheads

CJ printheads generate binder droplets continuously and use pressure to drive liquid binder toward the nozzle. The vibration of the nozzle breaks the binder liquid stream into uniform-sized droplets that are subsequently ejected out of the nozzle (Fig. 7.2c). Due to the continuous droplet generation mechanism, the wastage of binder liquid is more in CJ (Salehi et al. 2018). However, the printing rate is generally higher in CJ compared to DoD printheads which is advantageous as it prevents clogging of nozzles. The important feature that these printheads have is a proportional deflection mechanism (charged deflector at the nozzle tip) such that the drops are deflected toward waste chamber when printhead is not depositing the binder onto the powder. The deflected binder can be recycled or reused after verifying that previous processing steps have not adversely impacted critical material attributes. CJ printheads offer many advantages such as better size control of overlapping layers, control over binder leakage, and slower traverse speed (Sachs et al. 1993; Pond 2000).

7.3.2 Drugs

Drug candidate must be compatible with the excipients, binder, and solvent system. Formal drug excipients compatibility studies can be performed to screen and select the excipients for the formulation. Another important feature is stability requirement of the drug. Since the process involves solvent, drugs that hydrolyze or degrade by other mechanism are not good candidates for BJ process. For a drug substance known to be unstable in aqueous system, nonaqueous solvents or hydro-organic solvent can be used to inhibit or reduce chemical degradation. Both hydrophilic and hydrophobic drugs can be printed into printlets. Some hydrophilic and hydrophobic drugs that have been fabricated into printlets include quinapril hydrochloride, clotrimazole, paracetamol, ibuprofen, naproxen, famotidine, flufenamic acid (Kozakiewicz-Latała et al. 2022), levetiracetam and pyridoxine hydrochloride (Hong et al. 2021), acetaminophen (Wilts et al. 2019), naproxen (Acosta-Vélez et al. 2018), etc.

7.3.3 Excipients

Depending upon the dose of the drug and other characteristics of the printlets, excipients can form minor or major components of the formulation. Essentially, they perform the same function in the printlets as they do in traditionally manufactured dosage forms. Excipients are classified based on their specific function such as diluent, binder, disintegrants, flavoring agent, etc. Excipients have to meet

certain requirements in terms of safety and toxicity. FDA lists approved excipients in drug products in the Inactive Ingredient Database (FDA-IIG 2022). Similarly, excipients can be from "Generally Regarded as Safe category" (FDA-GRAS 2022). Using new excipients for printlets intended for human use would require safety and toxicity assessment (FDA 2005).

BJ process is similar to wet granulation process used to prepare granules either for compression into tablets or filling into hard gelatin capsules. In wet granulation, solvent(s) or binder solution/dispersion is gradually added to the powder mixture. Wet granulation is performed to increase particle size, density, and flow property and/or improve content uniformity and assay (Rahman et al. 2015). Excipients used in wet granulation can also be used in BJ process. Drug can be either added to the powder mixture (for high strength/dose medication), or it can be added to binder solution/solvent provided it is soluble. For low-dose drugs, it is recommended to dissolve the drug in a binder solution to meet content uniformity and assay specifications of the pharmacopeia. Insoluble drugs if dispersed in binder solution should be suspended in the colloidal particulate form. FDA-approved printlets (Spritam®) are prepared by BJ process and contain excipients such as colloidal silicon dioxide, glycerin, mannitol, microcrystalline cellulose, polysorbate 20, povidone, sucralose, butylated hydroxyanisole, and natural and artificial spearmint flavor. While mannitol, microcrystalline cellulose, colloidal silicon dioxide, sucralose, and butylated hydroxyanisole function as a diluent, disintegrant, flow promotor, sweetener, and preservative, respectively (Spritam®-FDA 2015), glycerin and polysorbate 20 are possibly part of the binder system as drug is highly soluble in water. Glycerin also acts as a humectant and retards drying of the binder and thus prevents clogging of printhead during printing. Polysorbate lowers the surface tension of the binder system. Furthermore, Spritam® is a high-dose printlet (250–1250 mg levetiracetam). It is highly possible that the drug is part of powder mixture and contributed significantly in providing the skeleton to the printlets.

Following excipients were investigated for designing various drug delivery systems.

- Polyethylene oxide, polyvinylpyrrolidone (PVP K30), lactose, mannitol, maltitol, maltodextrin, Kollidon SR, Eudragit® E100, Eudragit® RLPO, ethyl cellulose, and hydroxypropyl methylcellulose (E50) have been investigated for designing sustained released, delayed released, and rapidly dispersible tablets by BJ (Wu et al. 1996; Lee et al. 2003; Wang et al. 2006; Yu et al. 2007; Yu et al. 2009a; Yu et al. 2009b).
- Lactose monohydrate, PVP K25, Tween 20, ethyl cellulose, sodium dodecyl sulfate, methylcellulose, and hydroxypropyl methylcellulose (4000, 100,000 cps) were investigated for immediate release printlets of hydrophobic drugs (Kozakiewicz-Latała et al. 2022).
- Various sugars (D-sucrose, lactose, dextrin), pregelatinized starch, MCC, mannitol, sorbitol, HPMC, sodium carboxymethyl cellulose, ethyl cellulose, PVP, and polyethylene glycol (PEG) 4000 were investigated for immediate release printlets (Tian et al. 2019).

- Mannitol, MCC, PVP, sucralose, and colloidal silicone dioxide were used in the development of complex and multicompartment dispersible printable of combination drugs (Hong et al. 2021).
- Lactose, confectioners' sugar, and silica were used to design immediate release tablet using UV curable binder (Wilts et al. 2019).

7.3.4 Binder System

Binder performs the critical function of holding the formulation components during the printing process and maintains the 3D shape post-processing. It should possess adequate rheology characteristics, must be chemically compatible with other components, sufficiently wet the powder bed, and demonstrate good binding strength. The solvent used as a vehicle should have a high boiling point and be noncorrosive to printhead. Binder system usually consists of solvent, humectant, surfactant, and polymer or polyols. Insoluble particles if present in the binder must be milled to the colloidal range to prevent sedimentation and clogging of the printhead. Additionally, sedimentation would lead to content non-uniformity and other quality issues (Rahman et al. 2019; Mostafaei et al. 2021).

Solvent for the binder is selected based on the solubility of polymer, and drug, compatibility, safety, and toxicity. The International Council for Harmonization (ICH) classifies the solvents into three categories based on their safety profile. In pharmaceutical manufacturing, class 3 is preferred, class 1 is to be avoided due to toxicity, and use of class 2 is to be limited (ICH 2021). Aqueous solvents are preferred over organic solvents (ethanol, acetone, isopropanol, etc.); however, organic solvents/hydro-organic solvent may have to be used out of necessity for solubility and stability reasons. However, printhead should be compatible with organic solvents as not all BJ printers are suitable for printing with organic solvent-based binder system. Typically, polymer binder is dissolved/dispersed in the solvent. Low viscosity/molecular weight grade polymer in low concentration in aqueous-based solution/dispersion is used to control the viscosity. Concentrated aqueous solution/dispersion cannot be handled by the printhead of the BJ due to variability in spraying and clogging. However, organic solvents offer an advantage that higher polymer percentage can be used (Rahman et al. 2019; Tian et al. 2019; Mostafaei et al. 2021). Liquid polymer binder solution binds the particles by filling the interstitial spaces between the powder particles in each layer. In BJ processes where binder is added to the powder mixture (in-bed binders) directly and later activated by spraying solvent, polymer swells up and binds the powder layers. In the latter approach (in-bed binders), polymer binders can be used in higher concentration. In-bed binder processes would need optimization of solvent spray rate and also polymer amount necessary to achieve adequate binding. Over-swelling of the polymer should be controlled as it can interfere with spreading of subsequent layer of the powder. On the other hand, under-swelling of the polymer can produce quality defects such as delamination. Thus, regardless of the way binder is added, its

concentration in the formulation is critical for producing printlets of desired mechanical strength, disintegration, and dissolution. Although high binder concentration can produce mechanically strong printlets, it can prolong disintegration time and slow drug release (Rahman et al. 2019). Polymers used as binders are polylactic acid, polycaprolactone, polyvinylpyrrolidone (K17, K25, and K30 grades) ethyl cellulose, methylcellulose, hydroxypropyl methylcellulose (4000, 100,000 cps), sodium carboxymethyl cellulose, PEG 4000, and photocurable poly(ethylene glycol) (Wu et al. 1996; Lee et al. 2003; Wang et al. 2006; Yu et al. 2007; Yu et al. 2009a; Yu et al. 2009b; Acosta-Vélez et al. 2018; Tian et al. 2019). Other components that may be part of the formulation composition are humectants such as glycerin, propylene glycol, etc. They are added to the binder system to prevent drying and clogging of the printhead opening. Glycerin was used as a humectant in Spritam®. It is not unusual to add a small percentage of surfactants to the binder system to control surface tension and to ensure smooth spraying of the binder system. Tween 20 and sodium dodecyl sulfate have been commonly used (Spritam®-FDA 2015; Rahman et al. 2019; Kozakiewicz-Latała et al. 2022).

In the case of DOD printheads, generation of drops takes place by jet breakup of binder solution. Surface tension and viscosity play important role in controlling breakup patterns of binder solution and also determine the stability of droplets. The desired viscosity and surface tension of binder solution/dispersion are 1.6–5.99 mPa. S and 25.7–52 mN/m, respectively (Buanz et al. 2011; Pardeike et al. 2011; Sandler et al. 2011; Genina et al. 2012; Lee et al. 2012; Genina et al. 2013; Raijada et al. 2013). While the main drop is formed, satellite droplets are also generated simultaneously. Merger of satellite drops with the main drop prior to reaching powder bed results in the formation of stable droplet (Mostafaei et al. 2021). Failure to produce stable drop may cause generation of large satellite drops, or even no drop will be formed resulting in decrease in print resolution. Highly viscous solutions would require a higher ejection pressure that can lead to uneven jetting and clogging and consequent increase in the temperature of printhead. On the other hand, low viscous liquids can generate satellite drops behind main drops that may impact the deposition of binder on the powder bed, thereby producing non-uniformity in printlets. At high viscosity and surface tension, the required binder-powder interaction may not occur which can result in production of mechanically fragile printlets. Surface tension can be reduced by adding surface-active agents like Tween 80. Polyols can also be utilized to modify the viscosity of the binder solution (Rahman et al. 2019).

7.3.4.1 Viscosity and Surface Tension

Viscosity and surface tension are important properties of the liquid binder system. Liquid binder behavior is defined by the Weber number (W_e) which is related to surface tension, and Reynolds (R_e) number is related to the viscosity. Both properties can be defined by the following equations (Dini et al. 2019):

Reynolds number, R_e

$$R_e = \frac{\rho dV}{\eta} = \frac{\text{Inertial forces}}{\text{Viscous forces}}$$

Weber number, W_e

$$W_e = \frac{\rho dV^2}{\gamma} = \frac{\text{Inertial forces}}{\text{Surace forces}}$$

where ρ is the density of liquid (Kg/m^3), γ is the surface tension (N/m), η is the dynamic viscosity of liquid (Ns/m^2), d is the diameter of droplets of the nozzle head (m), and V is the velocity of flow speed (m/s).

Jettability of a binder system through an inkjet nozzle is measured by Ohnesorge number (Oh) (Derby 2010). It is defined by using the following equation:

$$Oh = \frac{\sqrt{W_e}}{R_e} = \frac{\eta}{\sqrt{\gamma \rho d}}$$

It is a dimensionless number that correlates viscous forces to surface forces between the binder and particle surface. It is related to the dimension of droplets, jets, and liquid but is independent of the velocity. Oh should be between 0.1 and 1 for a successful BJ process. The binder is considered non-jettable when Oh$<$0.1. The values Oh$>$1 imply high viscosity that prevents droplet separation from the liquid (Derby 2010). Another parameter "Z," which is reciprocal of the Ohnesorge number, is also used to define binder wettability:

$$Z = \frac{1}{Oh}$$

For binder wettability, the Z value should be between 1 and 10. Z values $<$1 (viscous force predominate) or $>$10 (continuous column ejected behind main drop) would provide an early indication of printing defects that are likely to be encountered (Fig. 7.3) (Duineveld et al. 2001). The binder splashing can also happen during printing. It is related to velocity, density, and volume of the droplets. Binder splashing affects surface finish. Weber number is related to splashing by the following equation:

$$f(R) = {W_e}^{1/2} {R_e}^{1/4}$$

where *f(R)* function is a surface roughness. Weber number should be 50 for smooth and flat surface without producing any splashing (Song and Nur 2004).

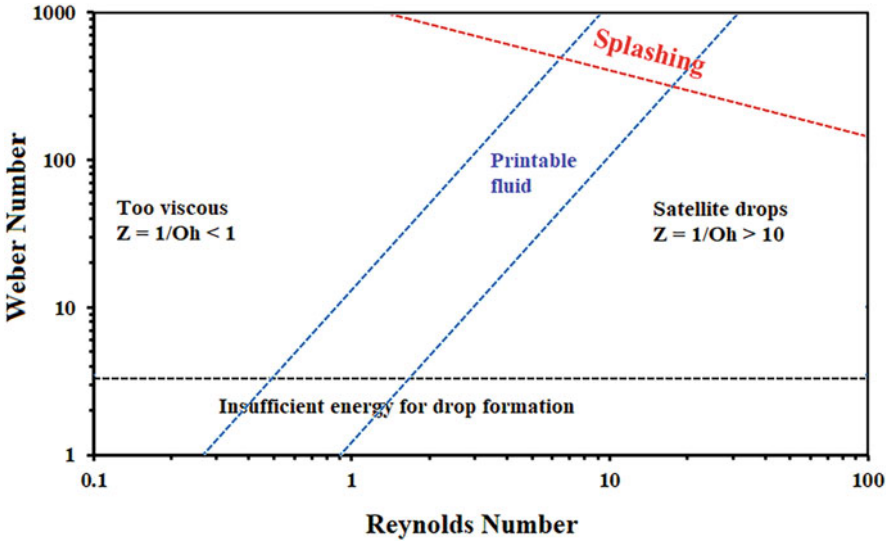

Fig. 7.3 Printable zone of binder solution/dispersion based on the Weber and Reynolds numbers

7.3.5 Powder Bed: Liquid Binder Solution/Solvent Interactions

Interactions between binder/solvent and powder bed are determined by their intrinsic properties such as viscosity, surface tension, liquid powder contact angle, etc. Furthermore, the depth of interactions is determined by size, shape, and material of powder and binder properties such a solvent, composition, velocity, etc. It is reported that interaction depth is higher in irregularly shaped particles compared to spherical particles primarily due to higher interlocking between angular particles (Parab et al. 2019). Various steps are involved in the formation of printlets including deposition of binder solution onto the powder bed surface (impacts) in a pattern controlled by the 3D design, wetting and spreading of the binder, and penetration within the powder bed (Fan 1996; Lv et al. 2019). Initially, the jetted solvent/binder wets the top layer of the powder bed followed by spreading of the binder which is assisted by the kinetic energy of the droplets forming liquid bridges connecting adjacent particles. The binder starts penetrating into loose powder beneath the surface. This is facilitated by capillary force; however, droplet gravity has negligible effect during this step due to its low mass/volume. At this stage powder layer may get saturated with the binder depending on the binder spray rate and amount. This results in the formation of agglomerates (granules) surrounded by a loose powder bed. The granules continue to form as the binder hits the powder surface. The impinging drops simultaneously facilitate bond formation between granules across

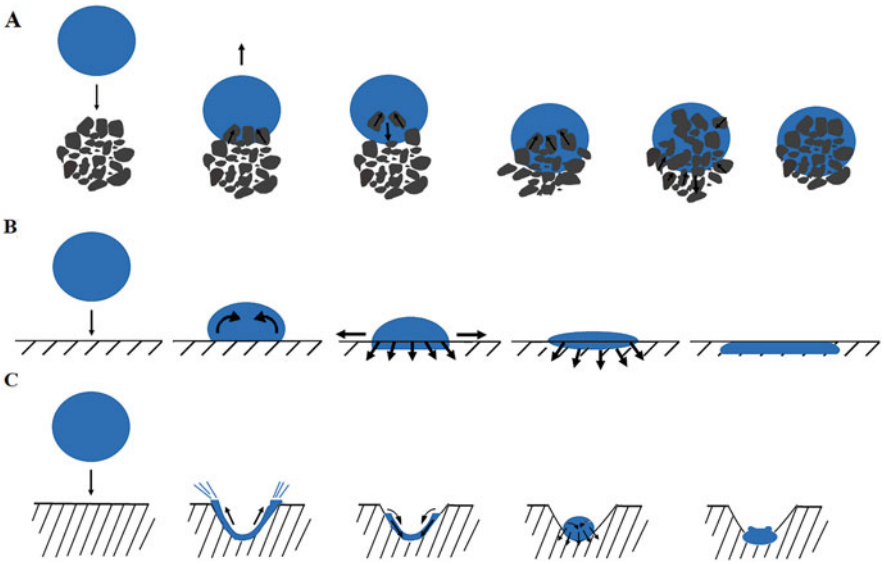

Fig. 7.4 Mechanism of granule formation mechanisms by (**a**) tunneling, (**b**) spreading, and (**c**) crater formation

each layer, and finally layers are sewn layer by layer to form printlets (Miyanaji et al. 2018).

Various mechanisms are involved in granule formation such as tunneling, spreading, and crater formation. Tunneling is observed in fine and cohesive powders in which binder droplets incompletely penetrate the loose powder in all directions, resulting in formation of spherical granules with some protrusions (Fig. 7.4a). Coarse, free-flowing powders form granules by crater or spreading formation depending on velocity of binder/solvent droplets. Spreading of binder droplets at slow speed results in the formation of granules that are flat disks (Fig. 7.4b). In contrast, the high velocity of binder droplets forms the crater over the powder bed. The droplets pick up particles before retracting and then penetrate into the powder bed, forming rounder granules than those formed by spreading (Fig. 7.4c) (Emady et al. 2011; Emady et al. 2013). Modified granular bond number (Bo_g) has been proposed to distinguish the mechanism responsible for granule formation. It is derived by dividing capillary force with gravity force acting on a particle. At $Bo_g < 65{,}000$, spreading/crater mechanism dominate, whereas $Bo_g > 65{,}000$ tunneling is likely to be the main mechanism of granule formation (Emady et al. 2013).

The most important aspect of interactions between binder/solvent and powder bed is wettability as it determines spreadability and penetration depth. Binder starts spreading and penetrating the powder as soon as it touches the powder bed (Fig. 7.5). Thus, contact angle between powder bed and binder is dynamic as advancing (lateral spread) and receding (vertical penetration) the powder bed. The

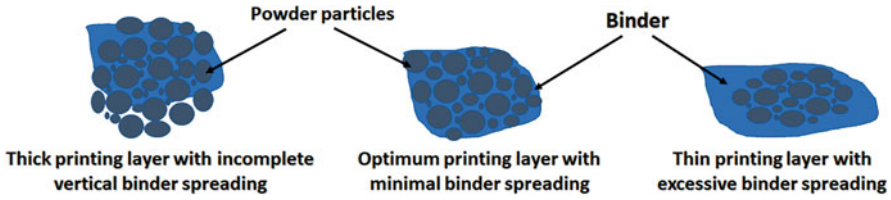

Fig. 7.5 Effect of binder spread of powder layer thickness

dynamic contact angle can be calculated using the following equations (Bai et al. 2019):

$$C_{\mathrm{a}} = \frac{\eta V}{\gamma}$$

$$\cos\theta_d - \cos\theta = \sqrt[a]{C_a}$$

where C_a is the capillary pressure.

Both cohesive and adhesive forces take part in powder-binder interaction (Mostafaei et al. 2021). The total amount of binder required to print a particular formulation is measured by binder saturation level (Vaezi and Chua 2011). Binder saturation is the ratio of binder to air volume in the prespecified powder layer. The saturation level has to be adequate for printing printlets with desired mechanical strength and other critical quality attributes. Higher saturation level than required may cause excess binder to flow out of the printing area, whereas inadequate saturation level can impact mechanical strength of the printlets. Saturation level depends on the powder bed density, diameter of the printed object, and powder layer thickness. Higher capillary pressure at initial saturation level can increase the penetration of binder. By controlling the bed porosity, optimal penetration ratio could be obtained which in turn can increase the geometrical accuracy of printlets. Binder saturation of 70% is considered optimum for achieving maximum densification of printlets. The morphological features of the agglomerates including shape can help to estimate the mechanical strength and the shape of printlets and guide in optimizing printing process parameters to obtain printlets of specific mechanical strength and shape (Shrestha and Manogharan 2017).

During liquid binder/solvent and powder bed interactions, drug and other components may also solubilize and consequently may change to different polymorphic form. During solvent removal step, drug substance may transform into an amorphous form or different crystalline form. This transformation may impact dissolution. During shelf life or exposure to high temperature and humidity, amorphous drug may revert back to the stable crystalline form that can decrease drug dissolution remarkably for poorly soluble drugs (Rahman et al. 2014; Rahman et al. 2015).

7.4 Interaction of Process Parameters and Material Attributes

Quality and performance of printlets are affected by BJ process parameters and material attributes. It is important to understand the impact of these variables on the CQAs of the printlets and control the critical parameters to ensure consistency in quality and performance.

7.4.1 Process Parameters

BJ printer parameters such as type of printhead, droplet line spacing, spray rate, powder spread rate, drying temperature and power, type of dryer, roller, etc. may impact quality and performance of the printlets (Rahman et al. 2018a; Rahman et al. 2019; Mostafaei et al. 2021).

7.4.1.1 Powder Spread Speed

The majority of the BJ printers use a counter rotating roller to spread the powder over the building platform. Readily flowing powder can be fed from gravity-fed hopper bin, whereas force-feeding/induction mechanism is needed for powder with undesirable characteristics. In some printers, powder reservoir is present next to the building platform, and roller feeds the powder from reservoir to build a platform. After the powder is deposited on the surface, roller spreads the powder on to the powder bed and compacts it lightly to produce a reasonably dense powder bed with smooth and homogenous surface. Speed of recoat (mm/s, the speed at which the hopper traverses while dispensing powder onto the bed), oscillator (rpm, the frequency at which the dispensing mechanism oscillates), roller (rpm, the rotational speed of the roller, if used), and roller traverse (mm/s, the speed the roller moves across the bed as it rotates) are the major factors in determining overall powder spread speed (Heywood 1993; Jimenez et al. 2019). Roller rotation rate and traverse speed generally do not influence powder-packing properties unless roller vibrates (Ziaee and Crane 2019). However, roller traverse speed determines the roller speed to spread the powder on the bed. Roller traverse speed varies from 0.1 to 16 mm/s. The speed should be optimized to increase accuracy and eliminate defects in the powder bed and final printlets. Lower speed can lead to inhomogeneous powder bed and delamination in final printlets while faster speed may increase the powder layer defect formation such as powder bed displacement and cracking. The higher speeds are likely to increase the friction between powder bed and roller as well as the friction among the particles (Heywood 1993; Jimenez et al. 2019; Mostafaei et al. 2021).

7.4.1.2 Layer Thickness

Layer thickness is the powder bed height along the z-axis which is constructed during printing. It is influenced by particle size, density, flowability, and cohesion between powder particles. It is selected based on particle size distribution of the powder mixture and is typically greater than the biggest particle size. It ranges from 30 to 300 μm. It determines packing bed density, mechanical strength, resolution, binder penetration/saturation, and quality attributes of printlets. Thinner layers produce denser, mechanically strong and high surface resolution printlets with less weight variability. Moreover, thinner layers also mitigate stepping stair and post-processing shrinkage defects (Ziaee and Crane 2019; Mostafaei et al. 2021). The binder droplets can easily reach the previously printed thin layers. Additionally, in the case of thin layers, binder spreads in the lateral direction freely. However, lateral spread of the binder beyond the design boundary may impact the composition of unprinted powder. On the other hand, lower binder saturation ratio results in less lateral spread of the binder, especially in thick layers that may impact the mechanical strength of the final printlets (Fig. 7.5). In one study, it was noticed that by reducing the layer thickness from 200 to 50 μm, an increase in tensile strength of 30% could be achieved possibly due to the change in density with layer thickness (Vaezi and Chua 2011; Sen et al. 2021). Since thinner layers produce mechanically strong printlets, disintegration time may show significant increase that can impact dissolution characteristics, especially for biopharmaceutical classification system class II and IV drugs. Manufacturing time of the printlets utilizing thin layers is comparatively longer than thick layers (Ziaee and Crane 2019, Mostafaei et al. 2021).

7.4.1.3 Printing Speed

Printing speed is determined by the binder spray rate and powder spread speed. Higher binder spraying rate can reduce printing time remarkably. However, high speed may affect the printing resolution or accuracy of fabricated printlets shape (Sen et al. 2021). Furthermore, the high speed may not provide adequate time for evaporation of binder solution from the pre-printed layer prior to the printing of next layer that may increase surface roughness, decrease dimensional accuracy, or even cause smudging of the pre-printed layer during the printing process. Consequently, the fabricated printlets will exhibit poor mechanical integrity and reduced reproducibility (Myers et al. 2021).

7.4.1.4 Droplet/Line Spacing

Droplet-to-droplet distance, line spacing (Fig. 7.6), and printhead speed affect printing pattern and droplet landing position of the binder, binder/solvent distribution, dimensional accuracy, and resolution (Lanzetta and Sachs 2003). Binder/

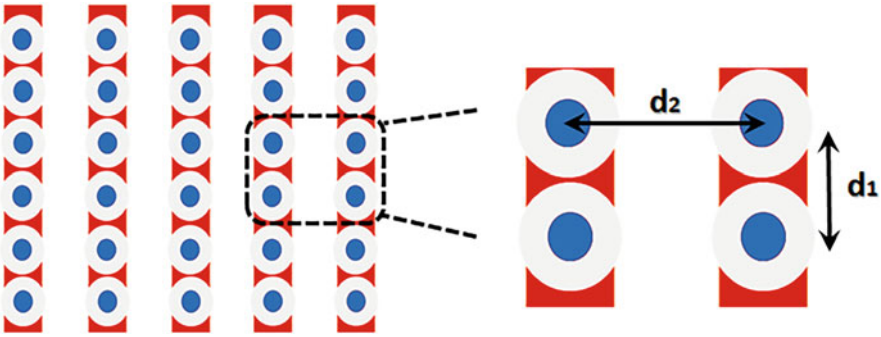

Fig. 7.6 The printhead nozzle droplet spacing

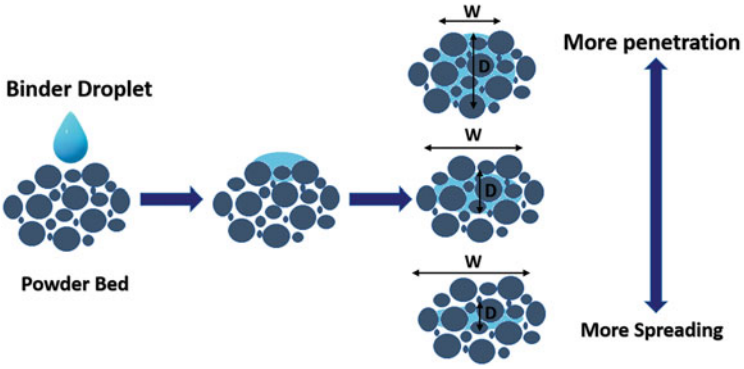

Fig. 7.7 Binder droplet penetration in a bed of powder

solvent droplets migrate to powder bed due to capillary pressure or gravity and continue till equilibrium is achieved. Depth of penetration and binder/solvent spread depend on powder bed and binder properties (Fig. 7.7) (Basaran 2002). Generally, less line spacing is desired as overlapped lines would ensure the adequate spread and penetration of the binder/solvent. Cramped line spacing, however, tends to increase the printing time and also increases the risk of powder bed saturation and bleeding (Colton et al. 2021).

7.4.1.5 Orientation of Printlets

Printing orientation in binder jetting is related to layer stacking and part build orientation. The layer stacking orientation refers to the orientation of the part being printed with respect to the powder stacking direction by the roller (i.e., z-axis). The build orientation indicates the alignment of the parts being printed with respect to the x-, y-, and z-axes of the build platform. The orientation of the

printed printlets during printing process can have an effect on the porosity and the mechanical strength of printed objects. Non-uniform dispensing of the powder and binder solution with inappropriate printing direction can cause variation in mechanical strength between printlets and even within the same printlet with zones of varying mechanical properties. The problem is exasperated at higher printing speeds leading to uneven distribution of raw material and decrease in printing accuracy. The accuracy of final printlets shape increases when the print build plane is parallel to printing. Surface finish of the final printlets is also influenced by the orientation (Sen 2020; Mostafaei et al. 2021).

7.4.1.6 Binder Saturation

Saturation refers to the pore volume of powder bed that is filled with the binder solution or solvent. It depends on the type of printhead employed (fixed droplet volume printheads or adjustable droplet volume printheads), powder bed properties (such as porosity, wettability), and layer thickness. Binder saturation (S) can be estimated using the following equation:

$$S = \frac{100 \times V}{\left(1 - \left(\frac{PR}{100}\right)\right) \times X \times Y \times Z}$$

where V—Volume of binder per drop (pL)

PR—Packing rate (%)

X and Y—Spacing between binder droplets (μm)

Z—Layer thickness (μm)

Jetted solvent or binder solution over the powder bed can spread into interstitial voids in both vertical and lateral directions. Higher contact angle decreases infiltration of the binder. Powder-packing properties, solubility characteristics, and wettability determine the type of solvent and binder to be used and desired binder saturation level and volume. In fact, powder layer thickness drives the saturation level. Thick and densely packed layers can accommodate higher binder saturation levels compared to porous and thinner layers. Inadequate saturation of powder layer can lead to poor bonding between particles and between layers, resulting in delamination and highly porous printlets. On the other hand, oversaturation may cause particles to stick to the roller and produce inhomogeneous powder bed and rough surface with dimensional inaccuracy. Oversaturation can also cause lateral flow of binder called bleeding, resulting in printing of large and uneven printlets. Saturation should be optimized to attain printlets of sufficient mechanical strength and free from the defects (Sen 2020, Mostafaei et al. 2021).

7.4.1.7 Drying Temperature, Power, and Time

Powder bed is subjected to heat cycle after every spraying phase during the printing process resulting in partial drying of the printed layer. The extent of drying is influenced by various factors, including solvent type and binder (polymer) (whether present in the powder mixture or the solvent), binder saturation level (binder spraying rate), and composition, wettability, thermal conductivity, surface area, permeability, and packing density of the powder. Factors related to heater such as drying temperature and power consumption assume high importance since they control the drying time of the liquid binder and thus control deformation, shrinkage, dimensional accuracy, and surface finish of the green part during the build cycle. Lower drying temperature during the build cycle can impact dimensional accuracy and surface finish. On the other hand, high temperature increases drying rate that may lead to higher deformation, delamination, and shrinkage. Controlling in-process drying is important as it will restrict the vertical penetration of the binder to the newly spread powder layer only and enhance the saturation level and accuracy. Moreover, it also prevents lateral spread of the binder. Insufficient drying related to low temperature or drying time may cause the binder to penetrate beyond the thickness of powder layer. Consequently, dimensionally inaccurate printlets with unacceptable mechanical properties will be produced. On the other hand, excessive in-process drying may reduce interlayer bonding as low amount of residual liquid is available on the dried layer on which new powder layer is to be spread. As a consequence, loss of mechanical strength ensues (Zhou et al. 2015; Chen and Zhao 2016; Mostafaei et al. 2021). Drying temperature can also have an impact on amorphous and crystalline content, disintegration, and dissolution of the printlets. Drying performed at high temperature for a short duration may prove advantageous in terms of retaining amorphous form during the printing process as time available may not be sufficient to trigger crystallization. On the other hand, slow temperature at low temperature tends to cause crystallization of amorphous drug molecules (Rahman et al. 2014; Rahman et al. 2015; Rahman et al. 2019).

7.4.2 Material Attributes

The powder forms the building block of printlets. Therefore, selection of material attributes (drug, excipients, polymer, solvent) with appropriate physicochemical properties and deposition mechanism is essential for fabricating a quality printlet. Critical material attributes that assume high importance include particle size, shape, density, flowability, wettability, solubility, dissolution, and crystallinity (Rahman et al. 2019; Mostafaei et al. 2021; Sen et al. 2021).

7.4.2.1 Particle Shape

Particle shape influences wettability (binder penetration) and flow properties. Spherical shape powder has better flow property and wettability compared to irregularly shaped particles (Bai and Williams 2015). Most of pharmaceutical components are available in irregular shapes. Although irregular shape particles can reduce segregation potential, at the same time, they can prove detrimental to the powder flow due to mechanical interlocking. Moreover, interlocking can increase interparticle friction, especially during flow that can reduce pack density. Often, such components with irregular shape are milled to remove the impact of shape on flow. One way to overcome the impact of inadequate flow during printing is to use spray-dried excipients which show excellent flow properties and produce printlets with good tensile strength. Dry coating of excipients with glidants such as silica can also improve the powder flow. During mixing operations, prolonged mixing time enhances the efficiency of the mixing process of powder containing irregular-shaped particles. Irregular particles have a high number of bonding points and crystal defects that can facilitate formation of strong bonds (Miyanaji et al. 2016).

7.4.2.2 Particle Size Distribution

Particle size distribution (PSD) influences bulk density, flow properties, packing properties, cohesion and adhesion, binder saturation and layer thickness, resolution, and surface finish of the printlets. Particle size also wields a strong influence on the penetration of binder. Wetting of the powder by binder is additionally dependent on hydrophilicity of the powder and viscosity and surface tension of the binder. Time needed for the binder to penetrate the powder increases with PSD. Furthermore, small particles create macro voids within the powder bed due to aggregation of finer particles that further increase the binder penetration time. On the other hand, powder with uniform PSD has better and complete binder penetration (Zou et al. 2011; Zhou et al. 2014). Poorly penetrated and wetted powder will delaminate easily and show poor mechanical strength. Hence, the binder system should be selected according to the hydrophilicity of the powder. Consideration should also be given to the fact that powder which is wetted to a higher level will have poor resolution and excess binder may seep in the lateral and vertical direction of the powder bed resulting in printing defects (Hogekamp and Pohl 2004).

Powder mixture with components having similar size, shape, and density would show high mixing efficiency. In contrast, particle size difference between the components of powder bed can induce percolative segregation resulting in drug non-uniformity within the same manufactured batch. The segregation potential is increased further by the high density of smaller particles. It is therefore desirable that the particle size distribution be controlled within a narrow range to ensure CQAs of the printlets are met consistently during printing. A powder bed with an average particle size <100 μm generally exhibits higher interparticle forces than

gravitational forces which reduces the tendency for segregation. Other parameters contributing to interparticle forces are the moisture content, consolidation, and geometric interlocking between powder components. Notwithstanding above, small particle size powder exhibits poor flow characteristics that can reduce the resolution remarkably leading to quality defects. On the other hand, powders which are highly flowable produce powder beds with insufficient stability. Optimum flow is, therefore, essential for spreading powder uniformly as a thin layer on the build platform (Vaezi and Chua 2011; Farzadi et al. 2014; Asadi-Eydivand et al. 2016).

The surface finish of the printed printlets is also impacted by the particle size of the powder. Smaller powder size produces printlets with better surface finish and also decreases the minimum layer thickness. Higher surface area of finer particles facilitates bonding to the high degree. Physical integrity of the printlets would increase at higher bed packing density. However, fine powders are more sensitive to environmental conditions and show poor flow properties during handling and feeding process (Lanzetta and Sachs 2003).

7.4.2.3 Packing Density

Packing density is the density of deposited layers. It affects shrinkage and mechanical and other quality properties of the printlets. Higher packing density is likely to yield printlets with higher mechanical strength, longer disintegration, and possibly slow dissolution due to reduction in interparticle voids (Fig. 7.8) (Ziegelmeier et al. 2015). Packing density is influenced by properties of formulation components such as morphology, PSD, interparticle forces, powder flowability, roller speed, and layer thickness. A powder with broad PSD exhibits better packing density compared to narrow PSD powder. For bigger size particles, packing density is a function of PSD and morphology. However, in the case of smaller particles (fine particles), higher interparticle forces may negatively impact packing density (Sohn and Moreland 1968; Mostafaei et al. 2019).

The theoretical packing density of mono-sized spherical particles is about 60% of the true density. An effective densification of 50% is desirable for fabricated printlets. The printlets of good mechanical strength can be manufactured close to the tap density of the powder (Mostafaei et al. 2021). Multimodal powder is an effective strategy to increase packing density where a mixture of coarse and fine powders is used. Coarse particles ensure flowability while fine powders fill the void between large particles. However, ratio of coarse to fine particles should be

Fig. 7.8 Schematic presentation of binder penetration within homogeneously and heterogeneously distributed powder beds

optimized to maximized packing density. The ratio of 7:1 to 10:1 of coarse to fine particles are proposed for maximum packing density (German 1992; Karapatis et al. 1999). Theoretical packing density can be calculated from the below equation (German 1992):

$$f_M = f_L + (1 - f_L) f_S$$

where

f_M—Maximum packing density
f_L—Large powder fractional packing density
f_S—Small powder fractional packing density

The type of printlets may also influence the required packing density. For instance, high packing density may not be desired for orodispersible or orally disintegrating tablets. However, high packing density is required for sustained release printlets (Sen et al. 2021).

7.4.2.4 Flowability

Powder flow is an important parameter for the printing process to ensure consistent deposition over the building platform. Optimum flow enables the roller to spread thin and homogenous layer over the powder bed. Good flowable powders have a consistent bed packing density, resolution, dimensional accuracy, and content uniformity compared to poorly flowable powder. In contrast, poor powder flow leads to non-uniform powder spread, weight variation, quality defects, etc. Flowability is affected by PSD, morphology, temperature, and humidity. Higher packing density is observed in more spherical/regular particles due to their better flow (Slotwinski et al. 2014). Irregular-shaped particles exhibit poor flowability due to higher interparticle adhesion caused by mechanical interlocking of angular particles (Chan and Page 1997). In general, small particles exhibit poor flowability owing to formation of agglomerates. The cutoff limit of particle size for improved flowability has been reported as >21.8 μm. The powder with mean particle size below 21.8 μm has been shown to exhibit poor flow and generating defective printlets (Smith and Midha 1997; Schade et al. 2014). Flow property can be increased by flow promotor such as colloidal silicon dioxide, magnesium stearate, and talc. However, low concentration of flow promotor should be used as these are hydrophobic ingredients that may prolong disintegration time and decrease dissolution (Rahman et al. 2018a; Rahman et al. 2019).

7.5 Quality Control

The quality control activities pertaining to printlets can be categorized into the following stages: data control (3D CAD models and process data), raw material control, visual manufacturing control, and post-processing control. In traditional pharmaceutical manufacturing that involves multiple discrete steps, quality is monitored at each step before moving to the next step. This is not practical in 3DP since printlet is fabricated in a single step. Process analytical technology tools can be very useful in controlling and maintaining the quality of the printlets. Near-infrared and Raman spectroscopy can be mounted to monitor the chemical and physical changes in the printlets as well as the support powder. These tools can provide useful information on the individual layers that can be correlated with formulation and process variables. However, a challenge remains in mounting the probe since the process is dynamic and thickness of printlets changes during manufacturing (Zidan et al. 2010; Rahman et al. 2013; Rahman et al. 2019).

The uniqueness of the 3D printing process demands a slightly different approach to quality control of the finished product than conventional dosage forms (Budzik et al. 2021). The universal tests description, identification, assay, and impurities apply to all dosage forms including printlets (ICH, Q. A 2000). Additionally, dissolution test, disintegration test, hardness, friability, uniformity of dosage units, water content/residual solvent, microbial limits, antimicrobial preservative content, and antioxidant preservative content should be part of quality controls tests of finished printlets. The printlets have internal structure that can be correlated with formulation and process variables. Internal structure such as porosity, surface area, etc. can be measured using X-ray microcomputer tomography and a surface area analyzer. It may be difficult to measure hardness of printlets (mechanically weak) with tablet hardness tester as the 3DP process is devoid of compression step. Texture analyzer can be used to measure mechanical strength of the printlets. The recycled material also needs to be subjected to quality control tests to determine its suitability for reuse (Barakh Ali et al. 2019; Mohamed et al. 2020; Hamed et al. 2021).

7.6 Quality Defects

Not thoroughly understanding process and formulation variables and lack of adequate tools to monitor and control the process may lead to the manufacturing of defective printlets. These defects may be cosmetic in nature with little or no effect on the CQAs. On the other hand, defect such as weight variation and delamination may directly impact CQAs and the performance of printlets.

7.6.1 Coffee Stain Defect

Drying of isolated binder droplets leaves a characteristics ring deposit near the initial contact line of sessile drop. This inhomogeneous deposition is known as coffee ring or coffee stain. The drying is faster near the contact line as compared to the center of the drop due to lower fluid column (Deegan et al. 2000; Dou et al. 2011). As the drying proceeds, there is a radial migration of liquid from center of drop to contact line (which is pinned) bringing with it solute and particulate matter. Consequently, after drying, the solute and particulates deposit at the contact line. The coffee stain can be eliminated by controlling the fluid movement and preventing outward flow. A surface tension gradient of even 10^{-4} J/m^2 is adequate to prevent coffee staining by opposing the radial flow. Solvent mixtures have been shown to be effective in preventing coffee staining (Soltman and Subramanian 2008; Derby 2015).

7.6.2 Staircase Effect/Layer Shifting

When printed new layer does not align with the previously printed layers, it results in off-center geometry that resembles a staircase. This occurs due to powder bed movement during printing. Powder is usually spread by a shear force that may cause the printed layer to move or crack during printing. This can be reduced by decreasing layer thickness, particle size distribution, and controlling saturation level (Rahman et al. 2018a; Rahman et al. 2019).

7.6.3 Delamination

Insufficient binder/solvent (low binder saturation) will not produce adequate bonding between powder particles and between adjacent layers and consequently can cause delamination during the post-processing stage. High drying temperature or pronged heating time during printing process may leave a very low amount of residual binder/solvent available on the dried surface on which new powder layer is to be spread and therefore can lead to loss of interlayer strength. Another reason for delamination is low binder saturation. Oversaturation can result in extra powder particles sticking to printlets, thereby producing rough surfaced printlets with dimensional inaccuracies. Delamination can be corrected by optimizing the binder composition, solvent, saturation level, and temperature during printing (Rahman et al. 2018a; Mostafaei et al. 2021).

7.6.4 Weight Variation

Variation of weight may lead to variation in drug content in the printlets (assay and uniformity of dosage units) and also impact drug dissolution. Factors such as wide particle size distribution, powder segregation, unstable powder flow rate, faster roller speed, etc. are known to cause weight variability among printlets. Weight variation can be minimized by controlling drug and excipient attributes and process parameters (Rahman et al. 2018a; Charoo et al. 2020).

7.6.5 Shrinkage

Excipients and polymer may swell up during solvent spraying especially if the binder is part of powder mixture. Unfavorable drying conditions (high drying temperature and prolonged drying time) of printlets cause shrinkage of the printlets due to solidification of binder and evaporation of the solvent. Shrinkage can be minimized by using excipients that do not swell or dissolve by the binder/solvent (Rahman et al. 2019).

7.7 Challenges in Binder Jetting

7.7.1 Solvent Sensitivity

BJ process is ideal to prepare printlets of thermally unstable drugs (degrade above 50–60 °C). However, it is not suitable for drugs/excipients that undergo water- or solvent-mediated degradation and transformation such as hydrolysis, disproportionation, polymorphic transformation, etc. (Patel et al. 2015; Rahman et al. 2018b; Yang et al. 2019). Water can be replaced by organic solvents such as ethanol and isopropanol if the formulation components are sensitive to the aqueous system. However, the compatibility of printhead with the solvents employed should be checked (Rahman et al. 2019).

7.7.2 Thermal Stability

Drying is an essential post-processing step to remove residual solvents and enhance the mechanical strength of printlets (Bhattacharjee and Srivastava 2020). Although binder jetting does not involve extreme thermal exposure, temperature as high as 50 °C may still be required to rid the product of the residual solvent. Thermally sensitive drugs and excipients may pose challenge even when drying is performed

above 50 °C. For products containing thermally sensitive drug or excipients, air drying or vacuum drying at low temperature can be employed (Rahman et al. 2019; Charoo et al. 2020).

7.7.3 Powder Recycling and Wastage

A significant portion of powder may remain unbound after printing. The processing may impact critical material attributes and may also cause compositional changes, rendering powder incapable to produce printlets that meet its CQAs. Evaluating unused powder after printing by itself involves significant analytical work to assess the quality attributes of powder. Generation of high wastage and analysis of recycled powder makes this process less economical. Likewise, a high percentage of binder solution or dispersion may be left unused that needs to be evaluated for its further use (Rahman et al. 2018a; Rahman et al. 2019).

7.7.4 Polymorphic Transformation

There is a high probability that processes in which drug is a part of the binder system may be maintained in the amorphous state after printing. The process parameters including binder system may alter polymorphic composition of the system. Moreover, during post-processing drying, exposure to high temperature may cause a transition of less stable amorphous form to stable crystalline form that can impact dissolution and hence the clinical performance of the printlets, especially for formulations containing low soluble drugs (Rahman et al. 2019).

7.8 Evolving Regulatory Landscape

In general, regulatory paradigm does not change with a manufacturing method of drug product. Whether the drug product is manufactured by traditional manufacturing method, continuous or additive methods, regulatory pathway does not change. For example, regulatory pathway for new drug products is either 505(b)(1) or 505(b)(2) new drug application, and 505j regulatory pathway for abbreviated new drug application (generics) (Rahman et al. 2018a, Rahman et al. 2019). Spritam® was approved under 505(b)(2) regulatory pathway (Spritam®-FDA 2015). Generic drug products of Spritam® will have to be submitted under 505j. Furthermore, FDA does not emphasize on the manufacturing method for generic product as long as sponsors demonstrate consistency in product quality, pharmaceutical equivalence, and bioequivalence with reference listed drug product. For example, generic version of Spritam® does not need to be manufactured by BJ or any additive manufacturing

method. As per the regulation, the sponsor of generic product has to demonstrate pharmaceutical equivalency and bioequivalence with Spritam®. To encourage use of novel technology in drug product manufacturing including 3D printing, FDA/CDER has established "Emerging Technology Program (ETP)" to guide sponsors in identifying and resolving potential technical and regulatory challenges (FDA 2017a). Recently, a Chinese pharmaceutical company has received Investigational New Drug (IND) clearance for its 3D printed drug product "T19" under ETP (Everett 2021). There is a growing trend to deploy 3DP in printing personalized medicines in hospitals or pharmacies. For filling prescriptions using 3DP, pharmacies and hospitals are exempted from Sect. 501(a)(2)(B) (concerning cGMP requirements), Sect. 502(f)(1) (concerning the labeling of drugs with adequate directions for use), and Sect. 505 (concerning the approval of drugs under new drug applications or abbreviated new drug applications) of Food, Drug, and Cosmetic Act (FD&C) (145). However, these facilities should meet the criteria for exceptions laid out in 501(a)(2)(B), 502(f)(1), and 505 of the FD&C Act (Rahman et al. 2018a, Rahman et al. 2019).

Similar to drug product registration pathway, current regulatory paradigm can be used for approval of medical devices by the binder jetting process. The current regulatory pathway comprises premarket notification 510(k) or premarket approval (FDA 2020). Moreover, FDA issued guidelines for medical devices manufactured by 3D printing method (FDA 2017b.). BJ has been used in point of care (POC) in fabricating devices in the hospital or similar clinical setting. POC provides rapid and agile production of devices, including but not limited to patient-matched devices and anatomical models for surgical planning. Recently issued guidance for 3DP in POC for medical devices categorizes POC as medical device production system (MDPS) which is covered under FD&C Act since it is intended for medical purpose (FDA 2022).

7.9 Applications of Binder Jetting

7.9.1 Amorphous Delivery System

Amorphous solid dispersion is a commonly used technique to increase the dissolution rate of poorly soluble drugs. Indomethacin is a poorly soluble drug indicated for the treatment of rheumatoid arthritis, osteoarthritis, ankylosing spondylitis, degenerative joint disease of the hip, acute musculoskeletal disorders, gout, and pain associated with dysmenorrhea. To increase the dissolution of indomethacin, dose flexible ink of the drug with PVP and arginine was printed as film. The solvent system comprised of propylene glycol and dimethyl sulfoxide. The drug substance was present in the film in an amorphous state. Almost 90% of the drug was released from printlets in 20 min. Furthermore, the amorphous system was stable for 6 months at room temperature (Wickström et al. 2015). Similarly, an ethanolic solution of naproxen-PVP was printed on the film of chitosan and hydroxypropyl methylcellulose. Crystalline drug was converted to amorphous form on printing. The drug

dissolution was almost 80% in 60 min (Hsu et al. 2013). In another similar study, an amorphous solid dispersion of felodipine was prepared using PVP in ethanol-dimethyl sulfoxide to increase boiling point of the solvent system and thus prevent clogging of the nozzle. The drug dissolution increased with an increase in polymer loading (Scoutaris et al. 2011).

7.9.2 Fast Disintegrating and Dispersible Printlets

Orally disintegrating tablets (ODT) should disintegrate in 30 seconds or less, and weight of the tablet is limited to 500 mg (FDA 2008), suggesting that ODTs can be prepared for only low-dose drugs owing to limitations in traditional manufacturing methods. ODT is preferred by geriatric and pediatric patients. The printlets produced using BJ are highly porous that disintegrate and dissolve rapidly upon contact with the gastrointestinal fluids. Spritam® is a high-dose (250–1250 mg) printlets with DT of 11 s. This feat is difficult to achieve with currently available traditional manufacturing techniques (Spritam®FD Alabel).

Fast disintegrating highly porous tablets of acetaminophen were prepared by depositing binder solution onto selected regions. The powder particles were loosely bound together by weak forces to maintain the printlets integrity. The tablets showed hardness of 54.5 N/cm^2 and friability of 0.92%, disintegration time of 21.8 seconds, and wetting time of 51.7 seconds. More than 97% drug was released in 2 min (Yu et al. 2009). Similarly, a multicompartment (three-layer nested structure) dispersible tablet of levetiracetam-pyridoxine hydrochloride was prepared by BJ. Tablets showed loose interior and tight exterior characteristics that ensured adequate mechanical properties and at the same time enabled tablets to disintegrate quickly. Pyridoxine being photosensitive was jetted into the middle layer that protected it from degradation. A micro drug system developed to adjust the number of printed layers can enable deposition of low drug doses (Hong et al. 2021).

7.9.3 Sustained Drug Release Delivery System

3D printing provides an opportunity to deliver drugs for bone engineering applications. The adsorption and desorption kinetics of vancomycin, ofloxacin, and tetracycline onto microporous bioceramics (hydroxyapatite, brushite, and monetite) was studied in a low-temperature 3D powder printing process. The adsorption of these antibiotics showed a linear relationship with the drug concentration in the immersion solution. On the other hand, immersion time exhibited a nonlinear correlation with the amount of drug adsorbed. The vancomycin and ofloxacin devices released drug within 1–2 days, and tetracycline device exhibited much slower drug release with 25% drug released in 5 days of immersion. When polylactic acid/polyglycolic acid

polymers were used in the drug solution matrix, the release kinetics was further sustained (Gbureck et al. 2007).

In another study, tricalcium phosphate scaffolds were fabricated by infiltration with biodegradable, poly(D,L-lactide-co-glycolide) (PLGA) and biomolecule (fluorescein isothiocyanate-labeled bovine serum albumin) utilizing BJ process with the purpose to provide sustained drug release. The PLGA has been shown to degrade within 3 months approximately. The device exhibited two phase release profiles. The initial burst drug release was followed by first-order release kinetics. The release profile assumes importance in bone reconstruction as initial high drug concentration can prove beneficial in angiogenesis and the sustained drug release component may facilitate stabilization of freshly formed vessels and osteoinduction (Cornelsen et al. 2013).

Low-temperature binder jet process has also been explored to deliver temperature-sensitive drug candidates. In one such study, vancomycin, heparin, and rhBMP-2 fabricated using ink jet 3D printing allowed preservation of biological activity and spatial distribution of drugs within the printed device. Drug release could be modulated to zero order with the use of hydroxypropyl methyl cellulose or chitosan hydrochloride (Vorndran et al. 2010). Inzana et al. further modified the process and used a low acidity binder solution to fabricate rifampin- and vancomycin-laden calcium phosphate scaffolds for treating implant-associated *Staphylococcus aureus* bone infection (Inzana et al. 2015).

7.9.4 Microparticles

Monodisperse microparticle delivery system can be printed using BJ. A piezoelectric inkjet was used to deposit sodium alginate aqueous solutions containing rhodamine R6G dye onto calcium chloride surfaces in order to create uniform size calcium alginate microcapsules. The drug release was modulated by particle size. The drug release was faster in 20 μm compared to 30 μm microparticles (Desai et al. 2010). BJ can also be used to fabricate core-shell microparticles. For instance, core-shell microparticles were fabricated out of alginate, carrageenan, linseed oil, and sodium alginate, including lipid-in-water, water-in-lipid, and water-in-water particles (ten Cate et al. 2010). In another study, piezoelectric inkjet printer was used to prepare monodisperse 60 μm diameter PLGA microspheres containing paclitaxel. The drug loading was >68%. Sustained release for approximately 50 days, with over 80% of the drug released, was obtained with microspheres (Radulescu et al. 2003).

7.9.5 Printing of Printlets: QR Code

BJ printer can be used to print personalized medicines. Edible printlets of haloperidol in the form of a quick response (QR) code were printed on porous substrate of

hydroxypropyl methylcellulose and mesoporous fumed silica. The drug ink consisted of haloperidol, lactic acid, and ethanol. The printed pattern contained the drug with encoded information relevant to the patient and/or healthcare professionals. The mechanical properties of the substrate were not impacted by printing, and no significant edge bleeding was noticed. The actual drug content in the printlets was in accordance with the encoded drug content. The printlets could be read by smartphone even when they were stored in harsh conditions indicating that this approach can be very useful in providing safe and patient-friendly drug products (Edinger et al. 2018).

7.9.6 Active Ink-Based Formulations

Oral salbutamol films were fabricated by thermal ink jetting using modified Hewlett-Packard printer in which cartridge was modified to accommodate the aqueous drug solution instead of ink. The drug was deposited onto an oral film made of potato starch. The drug losses arise as a result of erosion of the printed layer and within BP limits for tablets and oral syrups (Buanz et al. 2011). Similarly, propylene glycol-water solution of paracetamol, caffeine, and theophylline was printed on uncoated paper, coated paper, and polyethylene terephthalate for dose flexibility purpose (Sandler et al. 2011). In another study, a water-based ink formulation with adequate jetting properties was developed with the purpose to provide a framework for formulation development of water-soluble drugs. Tablets were printed on polyethylene terephthalate films, and solvent evaporation was carried out in ambient conditions. The printed tablets released drug rapidly. The method provides an opportunity to avoid the use of toxic solvents (Cader et al. 2019).

7.10 Summary

3D printing manufacturing processes including BJ have unlimited possibility of fabricating personalized printlets. However, interplay of process parameters and formulation components need to be understood, monitored, and controlled to fabricate a quality printlets free from defects. For regularity submission of drug approval or devices, current regulatory paradigm can be used. Deployment of BJ in manufacturing printlets in pharmacy or hospital does not require oversight of FDA.

References

Acosta-Vélez GF, Zhu TZ, Linsley CS, Wu BM (2018) Photocurable poly(ethylene glycol) as a bioink for the inkjet 3D pharming of hydrophobic drugs. Int J Pharm 546(1–2):145–153

Asadi-Eydivand M, Solati-Hashjin M, Farzad A, Abu Osman NA (2016) Effect of technical parameters on porous structure and strength of 3D printed calcium sulfate prototypes. Robot Comput Integr Manuf 37:57–67

ASTM I (2012) Standard Terminology for Additive Manufacturing Technologies, in ASTM. F2792-12a

Bai Y, Williams CB (2015) An exploration of binder jetting of copper. Rapid Prototyp J 21(2): 177–185

Bai Y, Wall C, Pham H, Esker A, Williams CB (2019) Characterizing binder-powder interaction in binder jetting additive manufacturing via sessile drop goniometry. J Manufact Sci Eng Trans Asme 141(1):011005

Barakh Ali SF, Dharani S, Afrooz H, Mohamed EM, Cook P, Khan MA, Rahman Z (2020) Development of abuse-deterrent formulations using sucrose acetate Isobutyrate. AAPS PharmSciTech 21(3):99

Barakh Ali SF, Mohamed EM, Ozkan T, Kuttolamadom MA, Khan MA, Asadi A, Rahman Z (2019) Understanding the effects of formulation and process variables on the printlets quality manufactured by selective laser sintering 3D printing. Int J Pharm 570:118651

Basaran OA (2002) Small-scale free surface flows with breakup: drop formation and emerging applications. AICHE J 48(9):1842–1848

Beg S, Almalki WH, Malik A, Farhan M, Aatif M, Rahman Z, Alruwaili NK, Alrobaian M, Tarique M, Rahman M (2020) 3D printing for drug delivery and biomedical applications. Drug Discov Today 25(9):1668–1681

Bhattacharjee D, Srivastava V (2020) Aspects of 3D printed drugs. J Med Eng Technol 44(8): 472–480

Buanz AB, Saunders MH, Basit AW, Gaisford S (2011) Preparation of personalized-dose salbutamol sulphate oral films with thermal ink-jet printing. Pharm Res 28(10):2386–2392

Budzik G, Woźniak J, Paszkiewicz A, Przeszłowski Ł, Dziubek T, Dębski M (2021) Methodology for the quality control process of additive manufacturing products made of polymer materials. Materials (Basel) 14(9):2202

Cader HK, Rance GA, Alexander MR, Gonçalves AD, Roberts CJ, Tuck CJ, Wildman RD (2019) Water-based 3D inkjet printing of an oral pharmaceutical dosage form. Int J Pharm 564:359–368

ten Cate AT, Pieterse G, Eversdijk J, Brouwers LA, Craenmehr EG, van Ee RJ, Rijfers A, Papen-Botterhuis NE, Houben RJ, van Bommel KJ (2010) Novel encapsulation technology for the preparation of core-shell microparticles. J Control Release 148(1):e8–e9

Chan LCY, Page NW (1997) Particle fractal and load effects on internal friction in powders. Powder Technol 90(3):259–266

Charoo NA, Barakh Ali SF, Mohamed EM, Kuttolamadom MA, Ozkan T, Khan MA, Rahman Z (2020) Selective laser sintering 3D printing - an overview of the technology and pharmaceutical applications. Drug Dev Ind Pharm 46(6):869–877

Chen H, Zhao YF (2016) Process parameters optimization for improving surface quality and manufacturing accuracy of binder jetting additive manufacturing process. Rapid Prototyp J 22(3):527–538

Colton, T, Liechty J, McLean A, Crane N (2021). Influence of drop velocity and droplet spacing on the equilibrium saturation level in binder jetting. Preprint

Cornelsen M, Petersen S, Dietsch K, Rudolph A, Schmitz K, Sternberg K, Seitz H (2013) Infiltration of 3D printed tricalciumphosphate scaffolds with biodegradable polymers and biomolecules for local drug delivery. Biomed Tech (Berl) 58(Suppl):1

Dawood A, Marti Marti B, Sauret-Jackson V, Darwood A (2015) 3D printing in dentistry. Br Dent J 219(11):521–529

Deegan RD, Bakajin O, Dupont TF, Huber G, Nagel SR, Witten TA (2000) Contact line deposits in an evaporating drop. Phys Rev E Stat Phys Plasmas Fluids Relat Interdiscip Topics 62(1 Pt B):756–765

Derby B (2010) Inkjet Printing of Functional and Structural Materials: Fluid Property Requirements, Feature Stability, and Resolution. Ann Rev Mater Res 40:395–414. D. R. Clarke, M. Ruhle and F. Zok.

Derby B (2015) Additive manufacture of ceramics components by inkjet printing. Engineering 1(1): 113–123

Desai S, Perkins J, Harrison BS, Sankar J (2010) Understanding release kinetics of biopolymer drug delivery microcapsules for biomedical applications. Mat Sci Eng B-Adv Funct Solid-State Mat 168(1–3):127–131

Dharani S, Barakh Ali SF, Afrooz H, Mohamed EM, Cook P, Khan MA, Rahman Z (2020) Development of methamphetamine abuse-deterrent formulations using sucrose acetate Isobutyrate. J Pharm Sci 109(3):1338–1346

Dini F, Ghaffari SA, Jafar J, Rezaie H, Shiri M (2019) A review of binder jet process parameters; powder, binder, printing and sintering condition. Metal Powder Rep 75(2):95–100

Dou R, Wang T, Guo Y, Derby B (2011) InkJet printing of zirconia: coffee staining and line stability. J Am Ceram Soc 94:3787–3792

Duineveld PC, de Kok MA, Buechel M, Sempel AH, Mutsaers KAH, van de Weijer P, Camps IGJ, van den Biggelaar TJM, Rubingh J, Haskal EI (2001) Ink-jet printing of polymer light-emitting devices. In: Conference on organic light-emitting materials and devices V, San Diego, CA

Edinger M, Bar-Shalom D, Sandler N, Rantanen J, Genina N (2018) QR encoded smart oral dosage forms by inkjet printing. Int J Pharm 536(1):138–145

Emady HN, Kayrak-Talay D, Litster JD (2013) Modeling the granule formation mechanism from single drop impact on a powder bed. J Colloid Interface Sci 393:369–376

Emady HN, Kayrak-Talay D, Schwerin WC, Litster JD (2011) Granule formation mechanisms and morphology from single drop impact on powder beds. Powder Technol 212(1):69–79

Everett (2021) Triastek receives FDA IND clearance for 3d printed drug to treat rheumatoid arthritis. from https://3dprintingindustry.com/news/triastek-receives-fda-ind-clearance-for-3d-printed-drug-to-treat-rheumatoid-arthritis-184159/

Fan T (1996) Droplet-powder impact interaction in three dimensional printing. PhD

Farzadi A, Solati-Hashjin M, Asadi-Eydivand M, Abu Osman NA (2014) Effect of layer thickness and printing orientation on mechanical properties and dimensional accuracy of 3D printed porous samples for bone tissue engineering. PLoS One 9(9):e108252

FDA. (2005) FDA guidance for industry. Nonclinical Studies for the Safety Evaluation of Pharmaceutical Excipients

FDA (2008) FDA guidance for industry - orally disintegrating tablets

FDA (2017a) FDA guidance for industry - advancement of emerging technology applications for pharmaceutical innovation and modernization

FDA (2017b) FDA guidance for industry - technical considerations for additive manufactured medical devices

FDA (2020) FDA - Overview of device regulation. from https://www.fda.gov/medical-devices/device-advice-comprehensive-regulatory-assistance/overview-device-regulation

FDA (2022) FDA - discussion paper: 3d printing medical devices at the point of care. from https://www.fda.gov/media/154729/download

FDA-GRAS (2022) FDA data of generally recognized as safe

FDA-IIG (2022) FDA inactive ingredient database

Gbureck U, Vorndran E, Müller FA, Barralet JE (2007) Low temperature direct 3D printed bioceramics and biocomposites as drug release matrices. J Control Release 122(2):173–180

Genina N, Fors D, Palo M, Peltonen J, Sandler N (2013) Behavior of printable formulations of loperamide and caffeine on different substrates--effect of print density in inkjet printing. Int J Pharm 453(2):488–497

Genina N, Fors D, Vakili H, Ihalainen P, Pohjala L, Ehlers H, Kassamakov I, Haeggström E, Vuorela P, Peltonen J, Sandler N (2012) Tailoring controlled-release oral dosage forms by combining inkjet and flexographic printing techniques. Eur J Pharm Sci 47(3):615–623

German RM (1992) Prediction of sintered density for bimodal powder mixtures. Metallurgical Trans Phys Metallurgy Mater Sci 23(5):1455–1465
Giannatsis J, Dedoussis V (2009) Additive fabrication technologies applied to medicine and health care: a review. Int J Adv Manuf Technol 40(1–2):116–127
Gottschalk N, Quodbach J, Elia AG, Hess F, Bogdahn M (2022) Determination of feed forces to improve process understanding of fused deposition modeling 3D printing and to ensure mass conformity of printed solid oral dosage forms. Int J Pharm 614:121416
Guo N, Leu MC (2013) Additive manufacturing: technology, applications and research needs. Front Mech Eng 8(3):215–243
Hamed R, Mohamed EM, Rahman Z, Khan MA (2021) 3D-printing of lopinavir printlets by selective laser sintering and quantification of crystalline fraction by XRPD-chemometric models. Int J Pharm 592:120059
Heywood B (1993) The design and manufacture of a powder deposition system for a large powder bed on a three dimensional printer. B.S., Massachusetts Institute of Technology
Hogekamp S, Pohl M (2004) Methods for characterizing wetting and dispersing of powder. Chemie Ingenieur Technik 76(4):385–390
Hong X, Han X, Li X, Li J, Wang Z, Zheng A (2021) Binder jet 3D printing of compound LEV-PN dispersible tablets: an innovative approach for fabricating drug systems with multicompartmental structures. Pharmaceutics 13(11):1780
Hsu HY, Toth SJ, Simpson GJ, Taylor LS, Harris MT (2013) Effect of substrates on naproxen-polyvinylpyrrolidone solid dispersions formed via the drop printing technique. J Pharm Sci 102(2):638–648
ICH (2021) ICH harmonized guidelines - Impurities: guideline for residual solvents Q3C(R8)
ICH, Q. A (2000) International conference on harmonisation; guidance on Q6A specifications: test procedures and acceptance criteria for new drug substances and new drug products: chemical substances. Notice Fed Regist 65:83041–83063
Inzana JA, Trombetta RP, Schwarz EM, Kates SL, Awad HA (2015) 3D printed bioceramics for dual antibiotic delivery to treat implant-associated bone infection. Eur Cell Mater 30:232–247
ISO/ASTM (2021) Additive manufacturing — General principles — Fundamentals and vocabulary. Retrieved 31 Mar 2022
Jimenez EM, Ding DM, Su LS, Joshi AR, Singh A, Reeja-Jayan B, Beuth J (2019) Parametric analysis to quantify process input influence on the printed densities of binder jetted alumina ceramics. Addit Manuf 30:100864
Karapatis NP, Egger G, Gygax PE, Glardon R (1999) Optimization of powder layer density in selective laser sintering. In: 10th solid freeform fabrication symposium (SFF). Univ Texas, Austin, TX
Kozakiewicz-Latała M, Nartowski KP, Dominik A, Malec K, Gołkowska AM, Złocińska A, Rusińska M, Szymczyk-Ziółkowska P, Ziółkowski G, Górniak A, Karolewicz B (2022) Binder jetting 3D printing of challenging medicines: from low dose tablets to hydrophobic molecules. Eur J Pharm Biopharm 170:144–159
Kwon KS, Kim W (2007) A waveform design method for high-speed inkjet printing based on self-sensing measurement. Sensors Actuat Phys 140(1):75–83
Lanzetta M, Sachs E (2003) Improved surface finish in 3D printing using bimodal powder distribution. Rapid Prototyp J 9(3):157–166
Lee BK, Yun YH, Choi JS, Choi YC, Kim JD, Cho YW (2012) Fabrication of drug-loaded polymer microparticles with arbitrary geometries using a piezoelectric inkjet printing system. Int J Pharm 427(2):305–310
Lee KJ, Kang A, Delfino JJ, West TG, Chetty D, Monkhouse DC, Yoo J (2003) Evaluation of critical formulation factors in the development of a rapidly dispersing captopril oral dosage form. Drug Dev Ind Pharm 29(9):967–979
Lv XY, Ye F, Cheng LF, Fan SW, Liu YS (2019) Binder jetting of ceramics: powders, binders, printing parameters, equipment, and post-treatment. Ceram Int 45(10):12609–12624

Miyanaji H, Orth M, Akbar JM, Yang L (2018) Process development for green part printing using binder jetting additive manufacturing. Front Mech Eng 13(4):504–512
Miyanaji H, Zhang SS, Lassell A, Zandinejad A, Yang L (2016) Process development of porcelain ceramic material with binder jetting process for dental applications. JOM 68(3):831–841
Mohamed EM, Barakh Ali SF, Rahman Z, Dharani S, Ozkan T, Kuttolamadom MA, Khan MA (2020) Formulation optimization of selective laser sintering 3D-printed tablets of clindamycin palmitate hydrochloride by response surface methodology. AAPS PharmSciTech 21(6):232
Mostafaei A, De Vecchis PR, Nettleship I, Chmielus M (2019) Effect of powder size distribution on densification and microstructural evolution of binder-jet 3D-printed alloy 625. Mater Des 162: 375–383
Mostafaei A, Elliott AM, Barnes JE, Li FZ, Tan WD, Cramer CL, Nandwana P, Chmielus M (2021) Binder jet 3D printing?Process parameters, materials, properties, modeling, and challenges*. Prog Mater Sci 119:100707
Murphy SV, Atala A (2014) 3D bioprinting of tissues and organs. Nat Biotechnol 32(8):773–785
Myers K., Paterson A, Iizuka T, Klein A. (2021) The effect of print speed on surface roughness and density uniformity of parts produced using binder jet 3D printing. Preprints: 2021010459
Parab ND, Barnes JE, Zhao C, Cunningham RW, Fezzaa K, Rollett AD, Sun T (2019) Real time observation of binder jetting printing process using high-speed X-ray imaging. Sci Rep 9(1): 2499
Pardeike J, Strohmeier DM, Schrödl N, Voura C, Gruber M, Khinast JG, Zimmer A (2011) Nanosuspensions as advanced printing ink for accurate dosing of poorly soluble drugs in personalized medicines. Int J Pharm 420(1):93–100
Patel P, Dave A, Vasava A, Patel P (2015) Formulation and characterization of sustained release dosage form of moisture sensitive drug. Int J Pharm Investig 5(2):92–100
Pond SF (2000) Inkjet technology and product development strategies. Torrey Pines Research
Radulescu D, Schwade N, Wawro D (2003) Uniform paclitaxel-loaded biodegradable microspheres manufactured by ink-jet technology. In: Winter Symposium and 11th International Symposium on Recent Advances in Drug Delivery Systems
Rahman Z, Barakh Ali SF, Ozkan T, Charoo NA, Reddy IK, Khan MA (2018a) Additive manufacturing with 3D printing: Progress from bench to bedside. AAPS J 20(6):101
Rahman Z, Charoo NA, Kuttolamadom M, Asadi A, Khan MA (2019) Printing of personalized medication using binder jetting 3D printer. In: Precision medicine for investigators, practitioners and providers. F. S. Faintuch J, Elsevier Science
Rahman Z, Dharani S, Barakh Ali SF, Afrooz H, Reddy IK, Khan MA (2018b) Effect of processing parameters and controlled environment storage on the disproportionation and dissolution of extended-release capsule of phenytoin sodium. Int J Pharm 550(1–2):290–299
Rahman Z, Korang-Yeboah M, Siddiqui A, Mohammad A, Khan MA (2015) Understanding effect of formulation and manufacturing variables on the critical quality attributes of warfarin sodium product. Int J Pharm 495(1):19–30
Rahman Z, Siddiqui A, Bykadi S, Khan MA (2014) Determination of tacrolimus crystalline fraction in the commercial immediate release amorphous solid dispersion products by a standardized X-ray powder diffraction method with chemometrics. Int J Pharm 475(1–2):462–470
Rahman Z, Siddiqui A, Khan MA (2013) Characterization of a nonribosomal peptide antibiotic solid dispersion formulation by process analytical technologies sensors. J Pharm Sci 102(12): 4337–4346
Rahmati S (2009) Piezo-electric head application in a new 3D printing design. Rapid Prototyp J 15(3):187–191
Raijada D, Genina N, Fors D, Wisaeus E, Peltonen J, Rantanen J, Sandler N (2013) A step toward development of printable dosage forms for poorly soluble drugs. J Pharm Sci 102(10): 3694–3704
Sachs E, Cima M, Williams P, Brancazio D, Cornie J (1992) 3-dimensional printing - rapid tooling and prototypes directly from A cad model. J Eng Ind Trans ASME 114(4):481–488
Sachs E, Haggerty JS, Cima MJ, Williams PA (1993) Three-dimensional printing techniques. U.-S. Patent and Trademark Office, Washington, DC

Sachs E, Haggerty JS, Cima MJ, Williams PA (1994) Three-dimensional printing techniques. M. I. O. Technology. US. 5340656

Salehi M, Gupta M, Maleksaeedi S, Sharon NML (2018) Overview of additive manufacturing processes for metals. In: Inkjet Based 3d Additive Manufacturing of Metals, vol 20. Materials Research Forum LLC, pp 1–21

Sandler N, Määttänen A, Ihalainen P, Kronberg L, Meierjohann A, Viitala T, Peltonen J (2011) Inkjet printing of drug substances and use of porous substrates-towards individualized dosing. J Pharm Sci 100(8):3386–3395

Schade C, Murphy T, Hoeganaes (2014) Development of atomized powders for additive manufacturing. Mater Sci 1:02.15–02.25

Scoutaris N, Alexander MR, Gellert PR, Roberts CJ (2011) Inkjet printing as a novel medicine formulation technique. J Control Release 156(2):179–185

Sen K (2020) A mechanistic understanding of binder-jet based 3D printing process PhD

Sen K, Mehta T, Sansare S, Sharifi L, Ma AWK, Chaudhuri B (2021) Pharmaceutical applications of powder-based binder jet 3D printing process - A review. Adv Drug Deliv Rev 177:113943

Shrestha S, Manogharan G (2017) Optimization of binder jetting using Taguchi method. JOM 69(3):491–497

Slotwinski JA, Garboczi EJ, Stutzman PE, Ferraris CF, Watson SS, Peltz MA (2014) Characterization of metal powders used for additive manufacturing. J Res Natl Inst Stand Technol 119: 460–493

Smith LN, Midha PS (1997) Computer simulation of morphology and packing behaviour of irregular particles, for predicting apparent powder densities. Comput Mater Sci 7(4):377–383

Sohn HY, Moreland C (1968) The effect of particle size distribution on packing density. Can J Chem Eng 46(3):162–167

Soltman D, Subramanian V (2008) Inkjet-printed line morphologies and temperature control of the coffee ring effect. Langmuir 24(5):2224–2231

Song JH, Nur HM (2004) Defects and prevention in ceramic components fabricated by inkjet printing. J Mater Process Technol 155:1286–1292

Spritam®-FDA. (2015). FDA - Spritam® Chemistry review, 2015. Retrieved 03/31/2022, from https://www.accessdata.fda.gov/drugsatfda_docs/nda/2015/207958Orig1s000ChemR.pdf

Spritam®FDA label. from https://www.accessdata.fda.gov/drugsatfda_docs/label/2017/207958s004lbl.pdf

Tian P, Yang F, Yu LP, Lin MM, Lin W, Lin QF, Lv ZF, Huang SY, Chen YZ (2019) Applications of excipients in the field of 3D printed pharmaceuticals. Drug Dev Ind Pharm 45(6):905–913

Triacca A, Pitzanti G, Mathew E, Conti B, Dorati R, Lamprou DA (2022) Stereolithography 3D printed implants: A preliminary investigation as potential local drug delivery systems to the ear. Int J Pharm 616:121529

Vaezi M, Chua CK (2011) Effects of layer thickness and binder saturation level parameters on 3D printing process. Int J Adv Manuf Technol 53(1–4):275–284

Vorndran E, Klammert U, Ewald A, Barralet JE, Gbureck U (2010) Simultaneous immobilization of bioactives during 3D powder printing of bioceramic drug-release matrices. Adv Funct Mater 20(10):1585–1591

Wang CC, Tejwani Motwani MR, Roach WJ, Kay JL, Yoo J, Surprenant HL, Monkhouse DC, Pryor TJ (2006) Development of near zero-order release dosage forms using three-dimensional printing (3-DP) technology. Drug Dev Ind Pharm 32(3):367–376

Wickström H, Palo M, Rijckaert K, Kolakovic R, Nyman JO, Määttänen A, Ihalainen P, Peltonen J, Genina N, de Beer T, Löbmann K, Rades T, Sandler N (2015) Improvement of dissolution rate of indomethacin by inkjet printing. Eur J Pharm Sci 75:91–100

Wilts EM, Ma D, Bai Y, Williams CB, Long TE (2019) Comparison of linear and 4-arm star poly (vinyl pyrrolidone) for aqueous binder jetting additive manufacturing of personalized dosage tablets. ACS Appl Mater Interfaces 11(27):23938–23947

Wu BM, Borland SW, Giordano RA, Cima LG, Sachs EM, Cima MJ (1996) Solid free-form fabrication of drug delivery devices. J Control Release 40(1–2):77–87

Yang Q, Yuan F, Xu L, Yan Q, Yang Y, Wu D, Guo F, Yang G (2019) An update of moisture barrier coating for drug delivery. Pharmaceutics 11(9):436

Yu DG, Branford-White C, Ma ZH, Zhu LM, Li XY, Yang XL (2009b) Novel drug delivery devices for providing linear release profiles fabricated by 3DP. Int J Pharm 370(1–2):160–166

Yu DG, Branford-White C, Yang YC, Zhu LM, Welbeck EW, Yang XL (2009a) A novel fast disintegrating tablet fabricated by three-dimensional printing. Drug Dev Ind Pharm 35(12): 1530–1536

Yu DG, Shen XX, Branford-White C, Zhu LM, White K, Yang XL (2009) Novel oral fast-disintegrating drug delivery devices with predefined inner structure fabricated by three-dimensional printing. J Pharm Pharmacol 61(3):323–329

Yu DG, Yang XL, Huang WD, Liu J, Wang YG, Xu H (2007) Tablets with material gradients fabricated by three-dimensional printing. J Pharm Sci 96(9):2446–2456

Zhou YHW, Tang YL, Hoff T, Garon M, Zhao FY (2015) The verification of the mechanical properties of binder jetting manufactured parts by instrumented indentation testing. In: 43rd north American manufacturing research conference, NAMRC 43, vol 1, Charlotte, NC, p 327

Zhou Z, Buchanan F, Mitchell C, Dunne N (2014) Printability of calcium phosphate: calcium sulfate powders for the application of tissue engineered bone scaffolds using the 3D printing technique. Mater Sci Eng C Mater Biol Appl 38:1–10

Ziaee M, Crane NB (2019) Binder jetting: A review of process, materials, and methods. Addit Manuf 28:781–801

Zidan AS, Rahman Z, Khan MA (2010) Online monitoring of PLGA microparticles formation using Lasentec focused beam reflectance (FBRM) and particle video microscope (PVM). AAPS J 12(3):254–262

Ziegelmeier S, Christou P, Wollecke F, Tuck C, Goodridge R, Hague R, Krampe E, Wintermantel E (2015) An experimental study into the effects of bulk and flow behaviour of laser sintering polymer powders on resulting part properties. J Mater Process Technol 215:239–250

Zou RP, Gan ML, Yu AB (2011) Prediction of the porosity of multi-component mixtures of cohesive and non-cohesive particles. Chem Eng Sci 66(20):4711–4721

Chapter 8
3D Printing for Localized Cancer Therapy

Mahmood Razzaghi, Amir Seyfoori, and Mohsen Akbari

Abstract Treating cancers is challenging due to tumor heterogeneity and off-target toxicities of existing therapeutics. Hundreds of genetic variations associated with human disease have been identified that contribute to the disparate treatment responses seen among individual patients. Additionally, lack of efficacy because of dose-limiting toxicities is another major bottleneck in developing effective drugs for cancer treatment. To remedy these challenges, personalized treatment strategies combined with localized drug delivery platforms offer a promising approach. Notably, localized delivery of chemotherapeutics reduces systemic adverse effects, prevents dose-limiting toxicities, and enables effective chemotherapeutic treatment. To this end, three-dimensional (3D) printing of materials is a viable route for manufacturing personalized drug delivery systems with precise control over spatiotemporal drug distribution. This chapter will overview the various 3D-printed therapeutics currently being used for localized cancer treatment.

M. Razzaghi
Laboratory for Innovations in Micro Engineering (LiME), Department of Mechanical Engineering, University of Victoria, Victoria, BC, Canada

A. Seyfoori
Laboratory for Innovations in Micro Engineering (LiME), Department of Mechanical Engineering, University of Victoria, Victoria, BC, Canada

Center for Advanced Materials and Related Technologies, University of Victoria, Victoria, BC, Canada

M. Akbari (✉)
Laboratory for Innovations in Micro Engineering (LiME), Department of Mechanical Engineering, University of Victoria, Victoria, BC, Canada

Center for Advanced Materials and Related Technologies, University of Victoria, Victoria, BC, Canada

Biotechnology Center, Silesian University of Technology, Gliwice, Poland

Terasaki Institute for Biomedical Innovation, Los Angeles, CA, USA
e-mail: makbari@uvic.ca

D. Lamprou (ed.), *Nano- and Microfabrication Techniques in Drug Delivery*,
Advanced Clinical Pharmacy – Research, Development and Practical Applications 2,
https://doi.org/10.1007/978-3-031-26908-0_8

Keywords 3D printing · Cancer · Localized drug delivery · 3D bioprinting · Tumor · Anticancer delivery

Abbreviations

3D	Three-dimensional
ABS	Acrylonitrile butadiene styrene
CAD	Computer-aided design
CMC	Carboxymethyl cellulose sodium
CSBT	Conformal superficial brachytherapy
CT	Computerized tomography
DLP	Digital light processing
DNA	Deoxyribonucleic acid
E-jet	Electrohydrodynamic jet
FDM	Fused deposition modeling
GelMA	Gelatin methacryloyl
GO	Graphene oxide
MN	Microneedle
MNA	Microneedle arrays
NIR	Near-infrared
PCL	Polycaprolactone
PLA	Polylactic acid
PLGA	Poly(lactic-co-glycolic acid)
PLLA	Poly(L-lactic acid)
PPF	Poly(propylene fumarate)
PTX	Paclitaxel
rBMSCs	Rat bone marrow mesenchymal stem cells
ROS	Reactive oxygen species
SEM	Scanning electron microscopy
SLA	Stereolithography
SLS	Selective laser sintering
TMZ	Temozolomide
TNF	Tumor necrosis factor
TRAIL	Tumor necrosis factor-related apoptosis-inducing ligand
UV	Ultraviolet
UV-LED	Ultraviolet light-emitting diodes

8.1 Introduction

Cancer is one of the main causes of death worldwide (Rebecca et al. 2017; Bakhtiar et al. 2018). Solid tumors are difficult to treat because of tumor heterogeneity that varies among patients, many physical, chemical, and biological barriers against drug diffusion, and the presence of multidrug-resistant cells. Surgery followed by systemic delivery of drugs is the standard of care for treating many solid tumors (Findlay-Shirras et al. 2018; Gooch and Schnabel 2019; Veronesi et al. 1993; Regine et al. 2011; Hui et al. 2009). However, systemic drug delivery has many adverse effects. Oral therapeutics have disadvantages, including digestive system discomfort, possible breaking down by the digestion environment, and intestinal bacteria, which can decrease the absorbed amount of the drug and cause an unavoidable delay in the drug efficacy (Zhou et al. 2022). Orally taken drugs should be absorbed into the bloodstream from the intestines, but it undergoes some loss because of the metabolism in the gastrointestinal tract (Shaikh et al. 2019; Homayun et al. 2019). Also, both oral and injectable systemic drug delivery routes are not appropriate for emergency cases because of the steps they need to reach the tumor site. Localized therapy, delivering drugs directly to the tumor site with or without delivery vehicles, is an alternative approach to mitigate some of the shortcomings of systemic therapy (Reithofer et al. 2014; Conde et al. 2016). Notably, in localized therapy, off-target medication toxicity is restricted to the tumor region, with little effect on healthy tissues nearby (Yang et al. 2018a; Yang et al. 2016). Furthermore, the medication release rate can be adjusted during localized chemotherapy to attain sustained release. As a consequence, maintaining drug levels at the target location inside the therapeutic window between minimum effective and minimum toxic concentrations becomes more likely (Lee and Yeo 2015). High local drug concentrations, less systemic toxicity, and longer drug exposure are all advantages of localized drug administration. Beyond its usage as primary tumor treatment, it has shown promise as a postoperative adjuvant therapy for preventing local cancer recurrence, which is a remarkable cause of patient relapse and mortality (Exner and Saidel 2008). Due to the existence of physiological barriers like blood-brain barrier, which hinders effective treatment with typical systemic chemotherapy, localized chemotherapy shows particular potential as a therapeutic option for solid cancers such as brain tumors (Juratli et al. 2013).

Cancer therapy is difficult due to tumor heterogeneity, requiring personalized medication to improve cancer treatment. Fabricating personalized medications is a difficult process involving accuracy and precision to make an ideal personalized treatment. 3D printing, a well-established method recognized for its accuracy, is used to precisely create the personalization required in personalized treatment (Bhuskute et al. 2022). Numerous 3D printing methods have shown their potential to provide cancer-specific therapies for various tumor types (Uddin et al. 2020; Lu et al. 2015; Monshi et al. 2020; Yang et al. 2020; Ma et al. 2018; Maher et al. 2017). Improved treatment efficiency is ensured by custom-designed 3D-printed devices and dosage forms (Bhuskute et al. 2022). 3D-printed therapeutic implants have

revolutionized personalized medication by allowing for more design freedom and are a far better fit than traditional implants, resulting in improved patient healthcare outcomes (Serrano et al. 2018).

8.2 Why 3D Printing?

3D printing allows for rapid prototyping of complex structures with precise control over their geometry, form, size, and mechanical and biological properties (Bhuskute et al. 2022; Shafiee 2020; Roopavath and Kalaskar 2017; Lancellotta et al. 2019). 3D printing has been extensively used in medicine as well as other fields, including aerospace, automotive, education, and art (Haleem and Javaid 2019; Chia and Wu 2015). It took several decades from when 3D printing was first introduced in the late 1980s until it has found applications in medicine (Serrano et al. 2018). Doctors and researchers are using 3D printing to develop novel ways to generate human-like constructs, prosthetics, wearable electronics, and implants (Bakhtiar et al. 2018; Huang et al. 2019). 3D printing technology has recently drawn much attention for cancer therapy due to its ability to produce pills or drug-eluting implants with drug dosages tailored to each patient's needs. 3D printing combined with stem cell technology has been used to regenerate massive tissue losses caused by surgical tumor removals. In this approach, the magnetic resonance imaging (MRI) and computerized tomography (CT) images taken from patients are converted into 3D digital computer-aided design (CAD) models, which are later used to generate 3D scaffolds using biological materials (Chae et al. 2014; Haleem and Javaid 2018). Sophisticated scaffolds are printed layer by layer, resulting in a 3D physical product that can fill the tumor cavity while delivering therapeutics to remove cancer residues and induce tissue regeneration. 3D printing promises to benefit physicians and patients in terms of patient-specific, tailored therapy (Choi and Kim 2015). Its popularity is growing since it can produce personalized products rapidly. It fits the goal of customized therapy, which requires a customized, individual treatment strategy for each patient (Bakhtiar et al. 2018; Serrano et al. 2018). As the concept of personalized medicine gains traction, it is important to demonstrate an approach that is easy to understand, flexible in terms of adding minute customization features, and cost-effective (Tan et al. 2020). Personalized medicine might include adjusting parameters such as dosages, release durations, release profiles, medication combinations, patient-specific device/implant production, and more. Due to the simplicity of collecting and modifying minor elements using CAD software, 3D printing is an appropriate approach for the production of personalized medicine (Bhuskute et al. 2022).

8.3 3D Printing Techniques

In the process of 3D printing, materials are added layer by layer in order to produce constructions based on CAD 3D models. The development of 3D printing has taken decades, during which time several innovative approaches to 3D printing have been used in a variety of applications and sectors (Guo and Leu 2013; Parandoush and Lin 2017). Different precise 3D bioprinting techniques could be classified into four categories: (a) inkjet (Yang et al. 2020; Qiao et al. 2019), (b) microextrusion (Monshi et al. 2020; Chen et al. 2012; Chen et al. 2015), (c) laser assisted (Rimann et al. 2016), and (d) stereolithographic (Uddin et al. 2020; Wang et al. 2020a; Pedde et al. 2017). Figure 8.1 depicts the process of these four 3D bioprinting methods schematically.

In inkjet printing, droplets of prepolymer solutions are jetted in a predetermined pattern onto the build platform. The deposited components are subsequently polymerized using various cross-linking techniques. The primary advantages of inkjet bioprinting include rapid printing, adequate spatial resolution, cost-effectiveness, and the ability to control the concentration gradient of any element in printed materials. In addition, the modification of commercially available inkjet printers into 3D inkjet bioprinters is a cost-effective approach used by several laboratories to manufacture tissue structures (Cui et al. 2014). Inkjet bioprinting, on the other hand, poses various problems, including a limited range of printable material viscosities,

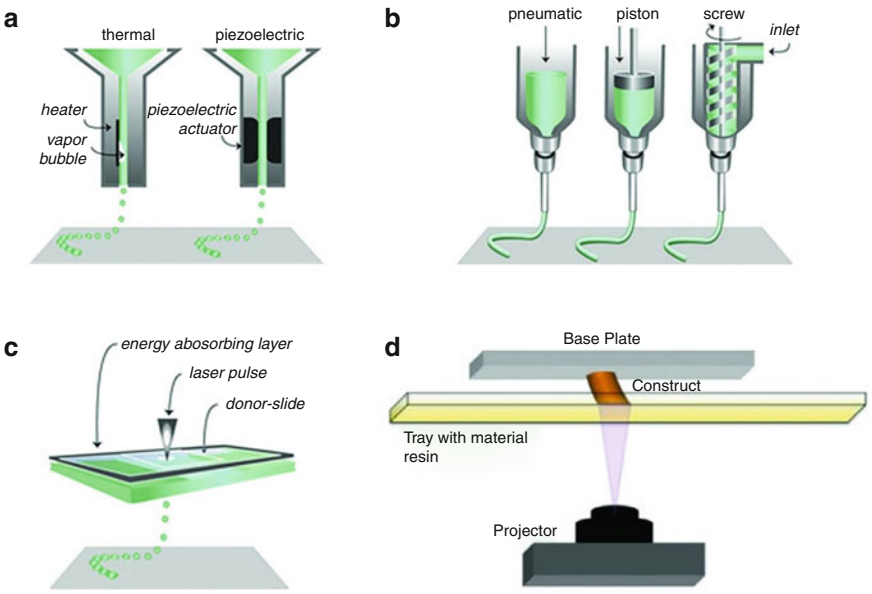

Fig. 8.1 Schematic illustration of the process of four 3D bioprinting methods: (**a**) inkjet, (**b**) microextrusion, (**c**) stereolithography, and (**d**) laser assisted. Reprinted with permission from Wiley-VCH: Advanced Materials (Pedde et al. 2017), copyright 2017

the ejection of only liquid phase materials, difficulty with cross-linking, and a limitation to thin structures owing to a discrete flow (Wang et al. 2015). Depending on the gelation process, excessive thermal stress during thermal deposition and the possibility of cell lysis during high-frequency piezoelectric actuation may significantly affect the survival and function of cells and biological materials (Xu et al. 2005). Moreover, inkjet bioprinting is limited to solutions with decreased cell densities in order to prevent nozzle clogging, increase droplet formation, and preserve cell viability in printed structures (Pedde et al. 2017).

Electrohydrodynamic (E-jet) 3D printing, as one of inkjet printing methods, has been designed to create synthetic biopolymer high-resolution structures by controlling the movement of the collecting substrate. This method of printing is based on "pulling" force as opposed to "pushing" force, presenting the unique advantage of high resolution (Li et al. 2020). The E-jet method generates the fluid flows needed for ink delivery to the substrate using electric fields (Park et al. 2007). A voltage is applied between the nozzle and a conducting plate to initiate ink flow from the nozzle tip. The ink is forced toward the metal-coated nozzle tip by the syringe pump's back pressure. The electric field causes the mobile ions or charged solutes of the ink to accumulate near to the surface of the meniscus. Due to the Coulomb repulsion between solute particles, the circular meniscus transforms into a Taylor cone. Under the influence of a sufficiently high electric field, the applied voltage above the critical voltage required to form a Taylor cone, the electrostatic stresses overcome the surface tension, resulting in the ejection of ink droplets from the cone (Kwon et al. 2021). Microextrusion uses an air-pressure controller, a piston-assisted system, or a screw-assisted mechanism to push out biomaterials for continuous layer-by-layer bioprinting. During the microextrusion process, the size and shape of the deposited material can be controlled by changing either the flow rate or the pressure that is used. For structural integrity, materials that are dispensed are cross-linked either at the same time or after they are extruded. This kind of printing can print the materials with high viscosity (Pedde et al. 2017).

Fused deposition modeling (FDM), as one of the microextrusion methods, deposits a thread of molten material using a moving head. The material used in FDM is often a plastic filament, which is deposited onto a substrate using a movable head. The material is heated inside the head to a temperature just over its melting point, extruded via a nozzle onto a substrate, and then cooled until it solidifies and creates a layer. Utilizing a multi-nozzle system in which each nozzle deposits a distinct material to build things with new characteristics has been a recent development in research (Guo and Leu 2013).

Laser-assisted bioprinting is usually conducted with laser-induced forward transfer, a technique that was first made to put patterns on a substrate made of metals and other inorganic materials. Laser-based bioprinters are made up of three parts: (1) a laser source that makes a pulsed laser beam; (2) a ribbon with a laser-transparent supporting layer (donor slide), a laser-absorbent layer, and the material to be deposited; and (3) a substrate that the material is deposited on it (Pedde et al. 2017).

Selective laser sintering (SLS) is a laser-assisted 3D printing process that uses a laser beam to selectively fuse and sinter particles by scanning cross-sections on the

surface of a powder bed layer by layer to make a 3D object based on a CAD model. After each cross-section is scanned, the powder bed is lowered by one layer thickness, a new layer of material is put on top, and the process is repeated until the part is made. SLS can use a wide range of powder materials like wax, polymers, polymer/glass composites, polymer/metal powders, metals, and ceramics to make 3D-printed parts (Guo and Leu 2013).

Stereolithography (SLA), which was the first commercially accessible 3D printing method, creates constructs by the selective exposure of a resin vat to ultraviolet (UV) light, solidifying a liquid photosensitive resin. In this method, the CAD 3D model is sliced into layers, and each layer is then scanned by UV light to cure the resin in each cross-section selectively. After completing a layer, the platform descends by the thickness of one layer. Then, a resin-filled blade re-coats the cross-section of the component with a single layer of new resin. The succeeding layer is subsequently scanned while adhering to the preceding layer (Guo and Leu 2013). Since there is no risk of cell lysis caused by nozzle shear when using the SLA process, which does not include the use of nozzles, it is possible to print encapsulated cells at high densities. However, modern SLA-based bioprinters still face a number of issues related with UV light sources, which have the potential to damage cell DNA (Pedde et al. 2017).

8.4 Different Types of Localized Cancer Therapy

Every year at least 4.2 million individuals pass away within the first 30 days after undergoing surgery, as reported by the Global Health Research Unit of the National Institutes of Health (Nepogodiev et al. 2019). As a result, it is critical to plan and create effective postsurgery therapy. Localized therapy may be a promising treatment option for local tumor residual and recurrence in which off-target drug toxicity is confined to the tumor location, with little impact on healthy tissues in the vicinity (Reithofer et al. 2014; Conde et al. 2016; Yang et al. 2018a; Yang et al. 2016). The following section highlights the application of localized therapy for delivering various therapeutic payloads.

8.4.1 Chemotherapy

Chemotherapy is a cancer treatment that involves the administration of one or more anticancer medications (chemotherapeutic agents) as part of standardized chemotherapy protocol. Chemotherapy is the basis of many cancer treatments at various stages of the disease (Alfarouk et al. 2015). Chemotherapy for cancer treatment was first used over 50 years ago in the clinic. Although this kind of therapy has been beneficial in treating some cancers, such as certain leukemias, it has been less successful in treating common epithelial malignancies of the breast, colon, and

lung (Johnstone et al. 2002). Localized chemotherapy has been used for the treatment of some cancers such as bone cancer (Wang et al. 2020a) and breast cancer (Qiao et al. 2019).

8.4.2 Immunotherapy

Immunotherapy is a method for treating cancer that uses the body's immune system to prevent, control, or eradicate the disease. Immunotherapy for cancer has fewer and less severe side effects than conventional chemotherapy. Immune checkpoint inhibitors, monoclonal antibodies, cancer vaccines, and other nonspecific immunotherapies such as cytokines are the most common kinds of immunotherapy now utilized to treat cancer (Baudino and T. 2015). Immunotherapy has been studied for the localized treatment of some cancers such as carcinoma (Hui et al. 2009).

8.4.3 Gene Therapy

In general, gene therapy involves treating an underlying disease by introducing a normal form of a damaged or missing gene (Das et al. 2015). Gene therapy, which involves replacing a damaged gene with a functional, healthy copy of that gene, may be a more successful cancer treatment than chemotherapy, which can be inefficient and cause nonspecific harm. To make vectors/transgenes safer and more effective, a variety of new genetic techniques are being developed. Gene expression may now be tailored in a tissue- and organ-specific way using cutting-edge delivery methods (Das et al. 2015).

8.4.4 Hyperthermia

The simultaneous or continuous delivery of heat therapy for tumor treatment is referred to as hyperthermia or thermotherapy. Therapeutic hyperthermia is a method in which tissues are heated to a higher temperature, usually between 41 °C and 45 °C (Alfarouk et al. 2015). Hyperthermia has been used for the localized treatment of cancer in combination with other methods of cancer therapy (Rao and Deng 2010; Zhang et al. 2014).

8.4.5 Brachytherapy

Brachytherapy is a complex and operator-dependent radiation therapy that involves inserting a radioactive substance into the patient's body. A problem of brachytherapy is finding the target tumor volume and delivering it to irregular surfaces, which may be solved by utilizing 3D-printed customized models (Bhuskute et al. 2022).

8.5 3D-Printed Devices for Localized Cancer Therapy

For localized cancer treatment, several dosage forms such as implants, scaffolds, microneedles (MNs), drug delivery patches with varied delivery profiles, and custom-made templates have been studied (Patil et al. 2020). Hereafter some of them are reviewed.

8.5.1 3D-Printed Microneedles for Localized Cancer Therapy

The oral administration of most of the chemodrugs has many disadvantages, including various digestive system discomforts, possible breaking down by the digestion environment and intestinal bacteria, loss of the gastrointestinal tract's metabolism, and delay in absorption (Zhou et al. 2022; Shaikh et al. 2019; Homayun et al. 2019). Syringe injection also has some other major disadvantages, like inflammation and infection risk at the injection site, the incidence of pain and anxiety, difficulty administering for children or specific locations, and the inability to infuse a small quantity of medication (Shaikh et al. 2019; Dugam et al. 2021; Lee et al. 2015). Microneedles are an alternative to traditional oral and syringe injection drug delivery systems, and they have outstanding characteristics, including painless penetration, minimal invasiveness, mild inflammation, and sustained treatment efficacy. Also, they don't need professional staff to apply them (Mdanda et al. 2021). Although MNs are primarily used for drug delivery through the skin, they have recently been used to deliver drugs to other tissues like the brain (Wang et al. 2022).

8.5.1.1 Types of Microneedles

MNs can be classified based on their different factors such as material, the mechanism of action, application type, morphology, external structure, and delivery method (Khan et al. 2021). Based on their mechanism of working and drug delivery method, MNs are classified into five classes: solid, coated, hollow, dissolvable, and hydrogel based (Parhi and Supriya 2019).

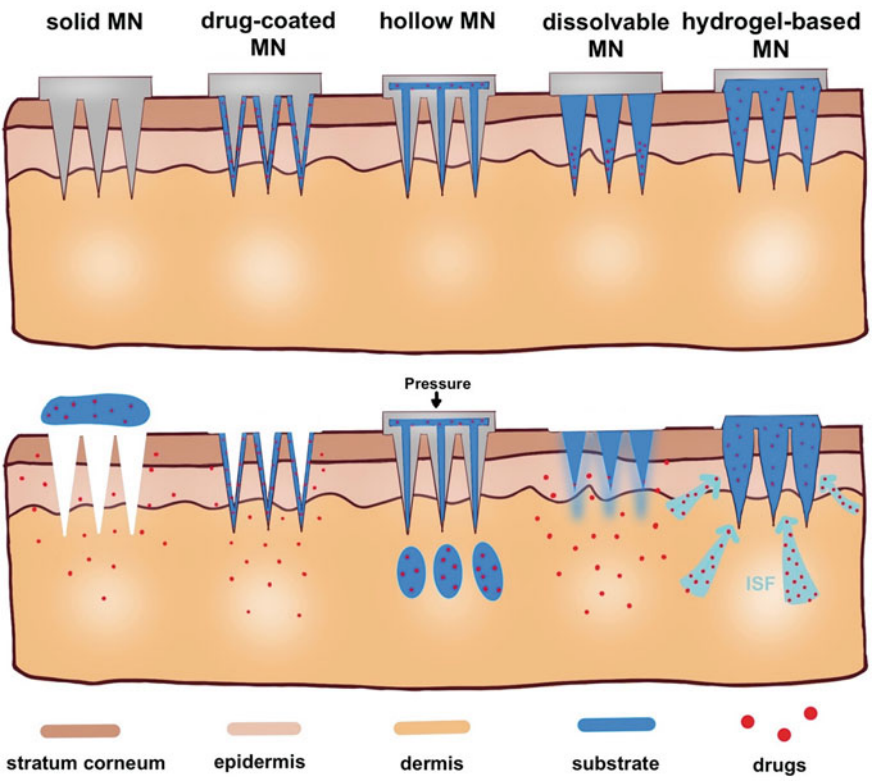

Fig. 8.2 Different types of MNs based on their mechanism of working and drug delivery method. Reprinted with permission from MDPI: Molecules (Xu et al. 2021), copyright 2021

Solid MNs are designed to make micropores in the skin to bypass the stratum corneum (SC) layer and to help in delivering the medication to the epidermis layer (Parhi and Supriya 2019). After forming micropores, the medication can be applied to the micropores to distribute to all body parts (Yang et al. 2019). Coated MNs have two main functions, including piercing the skin and delivering the desired medication coated on the surface of the MN (Yang et al. 2019). Hollow MNs consist of a drug reservoir with a hollow core in the center of the needle and are mainly intended to administer a comparatively large dose of medication (Parhi and Supriya 2019). Dissolvable MNs are degraded after insertion into the body tissue to allow the medication to enter and release it (Rejinold et al. 2016; Arya et al. 2017). Hydrogel-based MNs are the newest type of MNs. They are made from cross-linked hydrogels. When they are inserted into the skin, they readily take up tissue fluid because of the nature of the hydrophilic hydrogels and generate microchannels or pathways within the needle through which the drug can diffuse into microcirculation (Turner et al. 2021). Classification of MNs based on their working mechanism and drug delivery method is shown in Fig. 8.2 (Xu et al. 2021).

8.5.1.2 Materials of Microneedles

MNs have been fabricated from different materials, including metals such as titanium (Li et al. 2017); stainless steel (Jung et al. 2017; Vinayakumar et al. 2016; Rajabi et al. 2016); silicon (Lee et al. 2015; Pennathur et al. 2020); ceramics (Boks et al. 2015); biodegradable polymers such as polylactic acid (PLA) (Nguyen et al. 2019), poly(lactic-co-glycolic acid) (PLGA) (He et al. 2020), and polyglycolic acid (PGA) (Chen et al. 2020); non-degradable polymers like photolithographic epoxy (Stavrinidis et al. 2016); and hydrogels. Generally, MN materials should have adequate mechanical properties to pierce the target tissue (Dharadhar et al. 2019). Non-dissolving MNs should be inert and biocompatible without causing an immune response. In contrast, the material used to fabricate the coated and dissolving MNs should generally be biocompatible and water soluble. Additionally, it should dissolve or disintegrate in the body without inducing toxicity. Material and the incorporated drug should be able to keep the specifications of the MNs unchanged during manufacturing, storage, and transportation (Jung and Jin 2021). The characteristics of some well-known materials used in MNs are described below.

Silicon is still the most common MN material because it has adequate rigidity that facilitates skin penetration (Rad et al. 2021; Hoang et al. 2015). Silicon MNs with sharp tips and lengths of 100 μm or even smaller can be precisely fabricated using the deep-reactive ion etching process (Li et al. 2019). It can be a safety risk when the silicon MN breaks from the skin and fragments remain in the tissue. Silicon has also been employed in reverse master molds apart from solid MNs (Lutton et al. 2015).

Polymers are important materials for using localized drug delivery for cancer therapy. Recently, multiple studies have investigated the role of polymeric MNs, including dissolvable and hydrogel-based types, in drug delivery applications (Stavrinidis et al. 2016; Hao et al. 2017). Polymeric materials have received more interest due to their biocompatibility, high mechanical properties, low material cost, biodegradability, and comparatively low fabrication cost (Rad et al. 2021; Prausnitz 2017). Dissolving or hydrogel/swellable MNs have been fabricated with different types of polymers like hydroxypropyl methylcellulose (Kim et al. 2016), hyaluronic acid (Du et al. 2019), CMC (Mistilis et al. 2015), polyvinylpyrrolidone (Caffarel-Salvador et al. 2015; Tang et al. 2018; Tas et al. 2017), PLGA (Lutton et al. 2015), and poly(methyl vinyl ether co-maleic acid) (Parhi and Supriya 2019). Hydrogels have good mechanical properties in their dry state, which allows them to be inserted into the skin while keeping their structure in the swollen state and remaining intact during removal (Wang et al. 2017a).

8.5.1.3 3D Printing Methods of Microneedles

Improvements in printing resolution, feature precision, and the availability of low-price raw materials for printing have enabled 3D printing to fabricate different types of MNs (Ogundele and Okafor 2017; Park et al. 2019; Economidou et al. 2018;

Dabbagh et al. 2020). 3D printing techniques can fabricate more sophisticated and more complicated MN structures than conventional methods (Han et al. 2020). MNs with various structures can be made using 3D printing technology in a single step so the 3D printer's high resolution ensures accurate forming of the arrays of MNs can be formed in detail (Pere et al. 2018).

MNs have been manufactured using different 3D printing methods, including digital light processing (DLP), high-precision stereolithography (SLA), and FDM methods (Johnson and Procopio 2019; Luzuriaga et al. 2018; Economidou et al. 2021). In a study to treat skin cancer, first, a type of polymeric MN was fabricated using the SLA 3D printing process, and then the drug (cisplatin) was coated on the needles using inkjet printing (Uddin et al. 2020).

3D printing could also be employed to fabricate MNs by manufacturing master molds (Dabbagh et al. 2020; Balmert et al. 2020). These methods are appropriate for the fabrication of microneedle arrays (MNAs) in high quantities with a diverse range of materials (Tejavibulya et al. 2019). However, to modify the geometry of mold-based MNAs, the whole fabrication process of the mold must be repeated (Dabbagh et al. 2020).

8.5.1.4 Localized Cancer Therapy Using Microneedles

MNAs can effectively deliver chemotherapeutic drugs to cancer growth sites, reducing leakage into the systemic circulation and surrounding tissues and avoiding unwanted side effects (Mojeiko et al. 2019). MNA technology may help with disease treatment by allowing patients to self-administer injections without pain (Yang et al. 2019). Multiple medications could be inserted within the MNAs individually or simultaneously with a well-controlled release profile with both the drug type and on-demand dosage (Wang et al. 2020b).

MNs offer new possibilities for transdermal drug delivery in situations where the skin is the preferred delivery route (Uddin et al. 2020; Lu et al. 2015). Uddin et al. (2020) developed a unique 3D-printed polymeric MNA for improved cisplatin delivery to A-431 epidermoid skin tumors. They employed Class I biocompatible resin as the MNA material, and the MNAs were fabricated by SLA, followed by inkjet dispensing of the cisplatin drug on the surface of the needles (Fig. 8.3). SLA 3D printing was optimized to improve the mechanical properties of MNA. Tomography analysis revealed that 3D-printed microneedles had a high piercing capability, in which up to 80% of MNA's height is penetrated in the skin samples. Franz diffusion cell experiments demonstrated rapid cisplatin release rates of 80–90% within 1 h, while in vivo tests with Balb/c nude mice revealed adequate cisplatin permeabilization with strong anticancer efficacy and tumor regression. The results showed that transdermal delivery of anticancer medications using 3D-printed MNAs holds great promise for cancer therapy (Uddin et al. 2020). This innovative MN architecture allows for delivering different quantities using a single drug delivery system. The combination of stereolithographic 3D printing and inkjet coating of MNs produces precise and repeatable arrays of microneedles as well as good

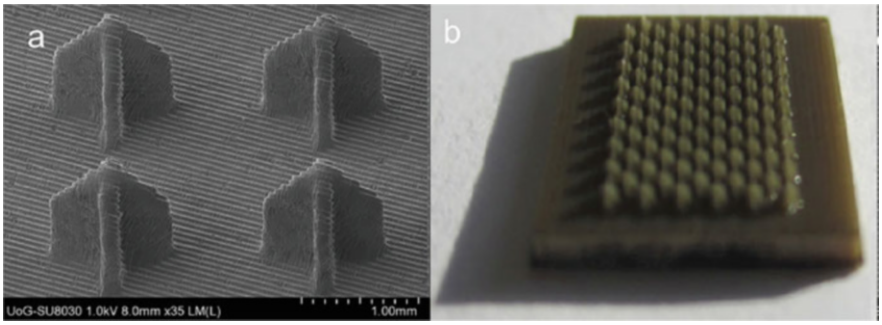

Fig. 8.3 (**a**) SEM and (**b**) optical image of 3D-printed MNA for localized skin cancer therapy. Reprinted with permission from Elsevier: Materials Science and Engineering: (**c**) (Uddin et al. 2020), copyright 2020

coatings with desired drug amounts and no material losses that can be readily scaled up.

In another research, multi-material microstereolithography (μSL) was used to manufacture drug-loaded MNAs for transdermal administration of a chemotherapeutic medicament. Poly(propylene fumarate) (PPF) MNs were precisely oriented on the same polymeric substrate in these arrays. The mechanical properties of micro arrays were enhanced by controlling the viscosity of the PPF. Prior to cross-linking, two separate loadings of dacarbazine, which is often used to treat skin cancer, were uniformly added to the printing material. The failure force was substantially more than the predicted skin insertion force according to compression test findings and characterization. Moreover, release kinetics results revealed that the dacarbazine drug can be delivered at a controlled rate for 5 weeks. The findings suggested that these drug-loaded MNAs can be used to treat skin carcinomas. Increased loading may change the amount of drug released, but modifying the molecular weight of PPF is required to change the release profile. The findings indicated that microstereolithography might be a useful approach for fabricating transdermal drug release devices with good structural stability (Lu et al. 2015).

MNAs have also been employed for localized cancer therapy, in which the applied MNAs have not been directly 3D printed, and 3D printing was employed to create a mold, which was then used to fabricate the final MNA (Monshi et al. 2020).

8.5.2 3D-Printed Scaffolds for Localized Cancer Therapy

Over the past decades, 3D printing/bioprinting has also shown a great promise for fabricating scaffolds for different applications from tissue engineering to cancer therapy. Recently, 3D-printed scaffolds have been used in several studies for the localized treatment of solid tumors. One of the applications of 3D-printed scaffolds

for localized cancer therapy is using them for bone cancer treatment (Monshi et al. 2020; Yang et al. 2020; Zhang et al. 2014; Wang et al. 2017b; Ahangar et al. 2018; Ma et al. 2016; Fu et al. 2020). Chemotherapy and surgery are two of the most common treatments for bone cancer. The problem in treating bone tumors is repairing the huge bone defects caused by surgery while also killing any remaining tumor cells (Yang et al. 2020). The use of scaffolds for bone tissue engineering has a promising effect on overcoming the significant bone defect caused by surgical resection of bone cancer (Yang et al. 2020; Ma et al. 2018; Ahangar et al. 2018; Suleman et al. 2021) so that chemotherapeutic drugs are effectively delivered to cancer cells using 3D-printed scaffolds (Agila and Poornima 2015). Natural polymers such as gelatin, alginate, collagen, and chitosan, as well as synthetic polymers such as polycaprolactone (PCL), polyurethane, polylacticacid, and polyvinyl alcohol, could be used for this application. Also, bioceramics like calcium silicate, calcium phosphate, and bioglass might be used for bone regeneration (Suleman et al. 2021). The spine is the most frequent location of bone metastasis, which may occur due to prostate, lung, or breast cancer. Porous 3D-printed scaffolds might be an appropriate way to deliver chemotherapeutics to tumor resection areas in a patient-specific manner.

3D printing was used to manufacture Fe-$CaSiO_3$ composite scaffolds. The fabricated scaffolds had a high compressive strength, which allowed them to offer enough mechanical support to bone cortical defects. Synergistic photothermal and reactive oxygen species (ROS) treatments showed an improved tumor therapeutic effect in vitro and in vivo. It was shown that incorporating $CaSiO_3$ in the composite scaffolds improved degradation, stimulated rat bone marrow mesenchymal stem cells (rBMSCs) proliferation and differentiation, and enhanced bone formation in vivo. The outcomes demonstrated that such high-compressive-strength Fe-$CaSiO_3$ scaffolds might be used as adaptable and effective biomaterials for the regeneration of cortical bone defects and the treatment of bone cancer. Figure 8.4a shows the illustration of the fabrication of Fe-$CaSiO_3$ composite scaffolds and their bioapplication (Ma et al. 2018).

The simultaneous removal of tumor tissues and regeneration of bone defects is a critical clinical problem in treating malignant bone tumors, and bifunctional 3D scaffolds that serve in both tumor therapy and tissue regeneration are anticipated to fulfill this demand. A type of scaffold was fabricated by integrating a 3D printing approach with a hydrothermal process. In this research, MoS_2 nanosheets were formed in situ on the strut surface of bioceramic scaffolds during the hydrothermal process, enabling them for photothermal therapy. The temperature of the scaffolds rapidly increased under near-infrared (NIR) irradiation and was efficiently regulated by altering the MoS_2 concentration, scaffold sizes, and laser power densities. The photothermal temperature reduced the viability of osteosarcoma and breast cancer cells while also inhibiting tumor progression in vivo. Furthermore, the scaffolds aided bone mesenchymal stem cell adhesion, proliferation, and osteogenic differentiation and stimulated bone regeneration in vivo. The research results showed that this bifunctional scaffold is capable of tumor treatment while promoting bone formation, making it a viable therapeutic method for treating tumor-induced bone

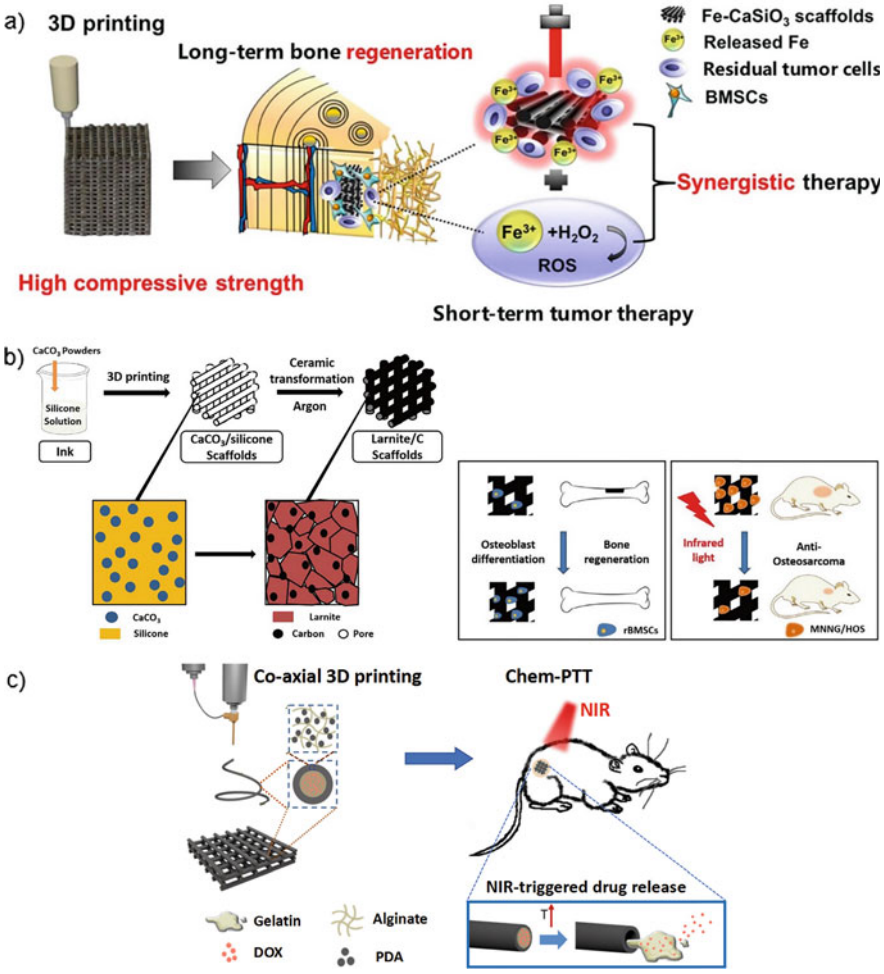

Fig. 8.4 Illustration of (**a**) the fabrication of Fe-$CaSiO_3$ composite scaffolds for the treatment of bone cancer (reprinted with permission from Nature: NPG Asia Materials (Ma et al. 2018)), (**b**) the carbon-embedding larnite scaffold manufacturing process and its applications in tumor treatment and bone regeneration (reprinted with permission from Elsevier: Chemical Engineering Journal (Fu et al. 2020)), and (**c**) co-axial 3D printing of core-shell fibers/scaffolds for localized cancer therapy (reprinted with permission from Elsevier: International Journal of Pharmaceutics (Wei et al. 2020))

defects. The akermanite scaffolds with well-designed morphology appeared white, while the color of MoS_2-modified akermanite changed from light to dark black, and more MoS_2 nanosheets or nanoflowers were growing on the strut surface of akermanite scaffolds with the increase of the concentrations of Mo and S sources in the hydrothermal reaction solutions (Wang et al. 2017b).

In another study, Fu et al. (Fu et al. 2020) used 3D printing of silicone resin loaded with $CaCO_3$ filler and high-temperature treatment in an inert environment to make porous free carbon-embedding larnite scaffolds. The produced scaffolds featured consistent interconnecting macropores with a good photothermal effect, killing human osteosarcoma cells and slowing tumor progression in nude mice. Furthermore, the carbon-embedding larnite scaffolds could induce new bone formation in critical-sized rat calvarial defects by stimulating the expression of an osteogenesis-related gene in rBMSCs. This study found that combining 3D printing with a polymer-derived ceramics method might produce multifunctional bioceramic scaffolds, which could be useful in the treatment of tumor-associated bone defects. The fabrication process of the carbon-embedding larnite scaffolds and their functions for tumor treatment and bone regeneration are shown schematically in Fig. 8.4b (Fu et al. 2020).

3D-printed scaffolds have been used for localized therapy of residual breast cancer and to prevent local recurrence following surgery (Qiao et al. 2019; Wei et al. 2020; Luo et al. 2019; Mirani et al. 2019). The drug delivery system based on 3D-printed scaffolds allows for a lower medication dose, which leads to a higher effect on human breast cancer cell apoptosis and tumor growth inhibition (Qiao et al. 2019). Although risks such as high local recurrence of cancer and loss of breast tissues threaten patients' survival and quality of life following surgery, surgical removal and neoadjuvant therapy remain the most common therapeutic strategy for treating most breast cancer.

Luo et al. (Luo et al. 2019) used 3D printing to manufacture a bifunctional scaffold made of dopamine-modified alginate and polydopamine (PDA) for treating breast cancer and filling the cavity, resulting in tissue repair. The Alg-PDA scaffold also enhanced the attachment and proliferation of normal breast epithelial cells by having a comparable mechanical property to that of normal breast tissues. Magnetic resonance and photoacoustic dual-modality imaging were also used to monitor the Alg-PDA scaffold's in vivo performance. This scaffold has an individually created structure with macropores, a strong photothermal effect, and improved cell proliferation capacity and could be used to treat breast cancer and restore tissue after surgery (Luo et al. 2019).

Wei et al. (Wei et al. 2020) developed a simple method to fabricate core-shell hydrogel fibers/scaffolds with controlled drug delivery and designed structures to manage residual breast cancer cells and prevent local recurrence following surgery. The designed hydrogel comprised a combination of PDA and concentrated alginate inks as the shell layer and drug-loaded temperature-sensitive hydrogels as the core component. Drug-loaded temperature-sensitive hydrogels were co-injected and 3D printed into core-shell hydrogel fibers and scaffolds. Under NIR irradiation, PDA raised the temperature of core-shell fibers, resulting in the gel-sol transition of the core gels and, subsequently, drug release from the loosened hydrogel network. The photothermal action and the released medications can eliminate cancer effectively. After an NIR-induced reversible sol-gel transition, the drug was released from the core hydrogels. The fabricated core/shell scaffolds with on-demand NIR-triggered

drug release properties would be appealing options for filling the cavity of breast tissues after surgical resection of cancer, offering a therapeutic effect for remaining and recurring cancer. In Fig. 8.4c, a schematic illustration of co-axial 3D printing of core-shell fibers/scaffolds for targeted cancer therapy is shown (Wei et al. 2020).

8.5.3 3D-Printed Meshes and Patches for Localized Cancer Therapy

Drug-loaded meshes have been investigated to deliver anticancer medications to the brain (Mirani et al. 2019; Hosseinzadeh et al. 2019). These results revealed that drug-loaded meshes manufactured using 3D printing technology had the potential to open up new avenues for treating brain tumors. This would help patients who suffer from this awful ailment and increase their chances of survival. This localized medication administration allows for a lower drug dose and fewer side effects (Mirani et al. 2019). Drugs could be loaded into these devices for sustained release over an extended period at the tumor site and placed in the immediate proximity of tumors through surgery instead of frequent intravenous injections of nanocarriers or frequent oral administration of cancer therapy (Exner and Saidel 2008; Hosseinzadeh et al. 2019; Yi et al. 2016; Yang et al. 2018b; Wolinsky et al. 2012; Wei and Liu 2017; Chew and Danti 2017).

The mesh or patch's flexibility enables them to be adjusted to each patient's tumor location (Hosseinzadeh et al. 2019; Yi et al. 2016). Additionally, these devices may be loaded with a combination of therapeutics (Yi et al. 2016). The biodegradability of the devices may eliminate the need for a second surgery to remove the device after the drugs have been released completely. The ability to control drug release by modifying the surface area was proven using 3D printing of porous patches with various shapes (Yi et al. 2016). Additionally, magnetic hyperthermia is another capability that could be applied to the tumor location using the modified 3D-printed patches with magnetic nanoparticles (Yang et al. 2018b). Hosseinzadeh et al. (Hosseinzadeh et al. 2019) introduced a novel therapy for glioblastoma that used a 3D-printed hydrogel-based mesh loaded with temozolomide (TMZ)-releasing microparticles that could deliver TMZ to the tumor site over several weeks. The mesh's cytotoxic effects on glioblastoma cells were assessed in vitro by examining at the degrees of DNA breakage, autophagic activity, and mitochondrial damage. The mesh, as compared to free TMZ, causes much more sensitivity to the drug by sustaining autophagic activity and producing higher levels of mitochondrial damage. The research outcomes showed that sustained TMZ treatment can reduce chemoresistance to TMZ, which develops in glioblastoma cells after systemic administration of the medication owing to autophagy activation. Figure 8.5 shows the schematic of the fabrication process of the mesh as well as the image of the fabricated part (Hosseinzadeh et al. 2019).

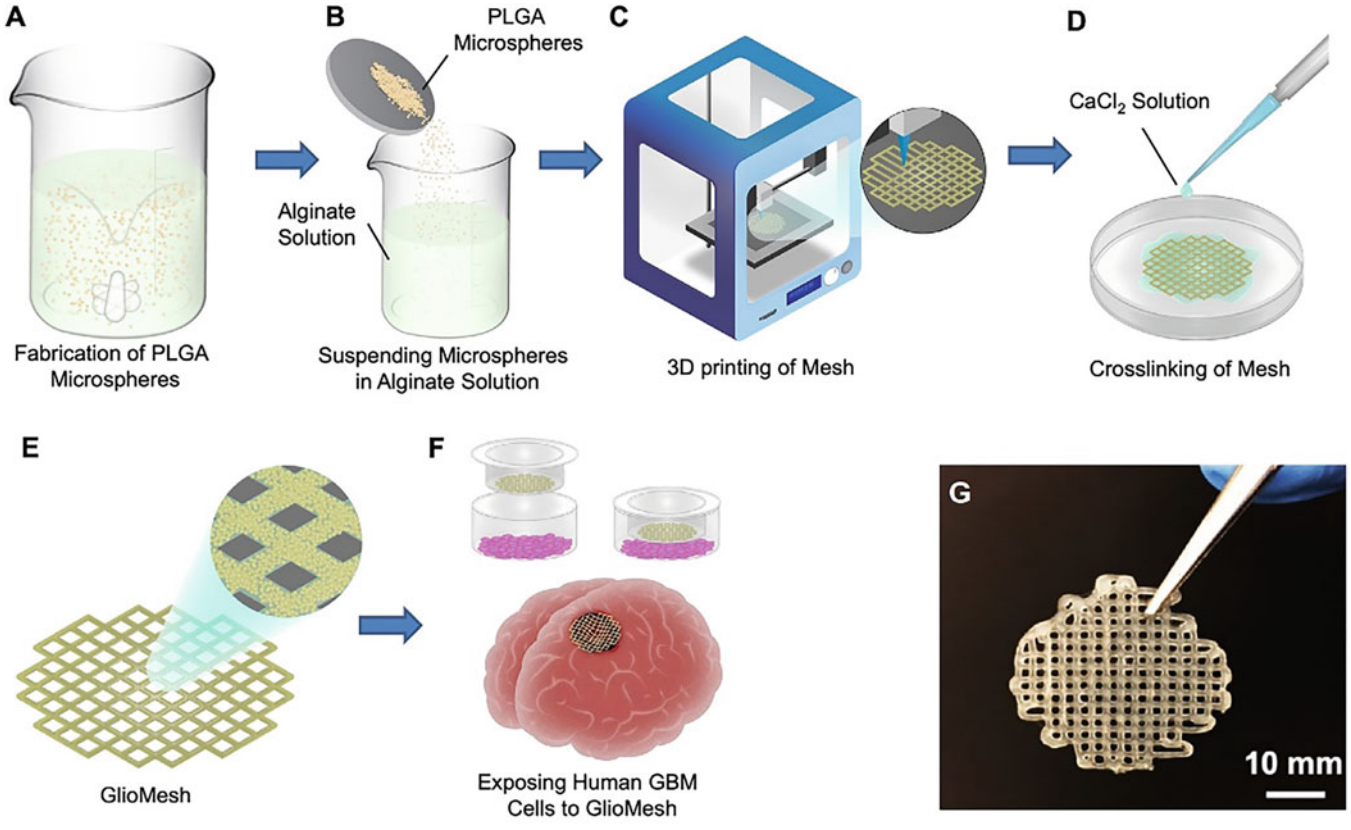

Fig. 8.5 (**a**–**f**) Illustration of the fabrication process of the mesh for localized therapy of glioblastoma. (**g**) Image of the fabricated mesh. Reprinted with permission from Wiley: Advanced Therapeutics (Hosseinzadeh et al. 2019), copyright 2019

In the other study, implantable 3D-bioprinted hydrogel patches containing nanomedicine were fabricated by Liu et al. (Liu et al. 2020) as a potential personalized cancer therapy. A semi-solid extrusion-type 3D bioprinter was used to print hydrogel-based patches using a UV-curable bioink, under UV-LED. They focused on the printer ink's composition, semi-synthesized fish gelatin methacryloyl (F-GelMA) derived from cold fish gelatin, which included the major component. The inclusion of carboxymethyl cellulose sodium (CMC), a pharmaceutical excipient, significantly enhanced the low viscosity of F-GelMA owing to its low melting point. As a model nanomedicine, PEGylated liposomal doxorubicin (DOX) was introduced into the hydrogel, and liposome stability following photopolymerization was assessed. The inclusion of CMC slowed the growth of the particles. A 3D bioprinter was used to create three different types of 3D-designed patches (cylinder, torus, and gridlines). The geometry of the 3D-printed patches and the UV-LED exposure time influenced drug release (Liu et al. 2020).

8.5.4 3D-Printed Implants for Localized Cancer Therapy

Drug-loaded implants have attracted great attention in cancer treatment because of their precise delivery of drugs into cancer tissues (Yang et al. 2020). They offer various advantages, including reduced drug administration frequency, less systemic toxicity, and improved delivery effectiveness (Yang et al. 2020). Yang et al. *(*Yang et al. 2020*)* developed a precise drug delivery system for orthotopic breast cancer treatment that may decrease breast tumor development and prevent lung metastasis when combined chemotherapy is used. 3D-printed PLGA implants were used to immobilize 5-fluorouracil and NVP-BEZ235. The implanted scaffolds considerably decreased therapeutic doses and guaranteed curative drug levels near tumor locations for a long time while minimizing drug exposure to normal tissues. Furthermore, long-term drug release was achieved, possibly permitting one-time implantation and significantly decreasing drug delivery frequency. The findings revealed that this drug-loaded implant has significant antitumor potential, potentially opening the way for precise, effective, and safe cancer treatments.

Through a series of in vivo anti-osteosarcoma experiments following clinical procedures, Wang et al. (Wang et al. 2020a) revealed that local chemotherapy with the assistance of the as-prepared PLLA implant had anti-osteosarcoma effectiveness superior to standard chemotherapy. Individual local chemotherapy, multidrug administration, long-term sustainable drug release, and non-reoperation in osteosarcoma treatment might all be achieved with their suggested 3D-printed drug delivery system. Their research paved the way for using 3D printing to treat osteosarcomas and helped guide future clinical trials. Other cancers' local chemotherapy may be customized using the same approaches and ideas. Figure 8.6 depicts their process schematically (Wang et al. 2020a).

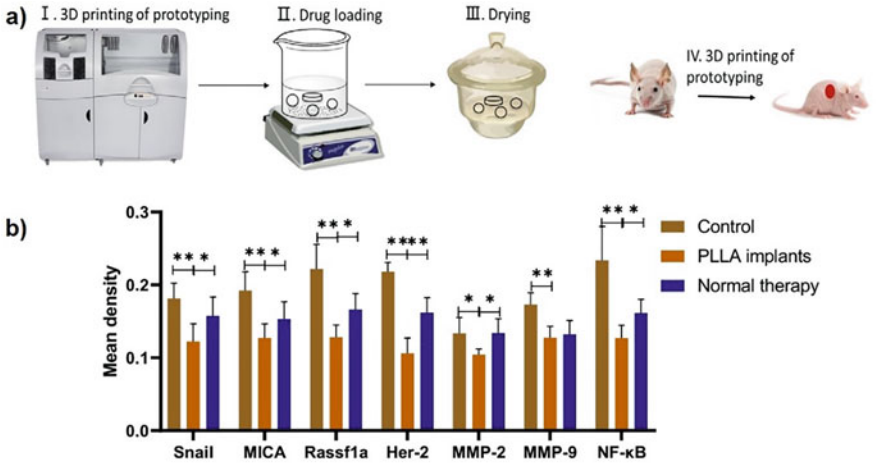

Fig. 8.6 (**a**) Schematic illustration of 3D-printed PLLA implant for anti-osteosarcoma application, (**b**) comparative results of mean density analysis of the tissues around the tumor site for the treatment using PLLA implants and normal therapy. Reprinted with permission from Elsevier: Materials & Design (Wang et al. 2020a)

Maher et al. (2017) demonstrated a novel form of localized drug-releasing titanium implant with improved biointegration and drug release capabilities, which might provide a high concentration of anticancer drugs locally to treat bone cancers. The implants were made by 3D printing of Ti alloy and then anodizing it featuring unique micro (particles) and nano (tubular arrays) surface topography. They used two kinds of anticancer drugs, doxorubicin and apoptosis-inducing ligand (Apo2L/TRAIL), to show their improved bone osseointegration and drug loading characteristics.

In vitro testing revealed high anticancer activity against cancer cells, indicating that their developed drug-releasing implants may be employed for targeted chemotherapy and fracture support in treating primary and secondary bone cancers (Maher et al. 2017).

Breast cancer patients with localized combination chemotherapy were investigated using 3D-printed implants. The findings revealed that implanted scaffolds might deliver drugs for a long time, reducing necessary medication doses and ensuring curative drug levels around tumor sites for a long time while minimizing drug exposure to normal tissues (Yang et al. 2020).

Patients with inoperable esophageal cancers are being treated with palliation therapy for dysphagia utilizing esophageal stents (Lin et al. 2019). 3D-printed stents as one type of implant have been investigated for the localized treatment of esophageal cancers (Lin et al. 2019; Fouladian et al. 2020).

Incorporating anticancer therapeutics into endoluminal stents is a potential technique for providing sustained release of anticancer therapies to malignant esophageal tissues while also extending stent retention and relieving dysphagia. The findings of

the studies indicated that 3D printing is a viable method for producing personalized drug-loaded stents; nevertheless, more research is necessary to understand the ideal geometrical and mechanical characteristics as well as drug release profiles in vivo (Fouladian et al. 2020).

To solve the issues like esophageal tumor ingrowth and stent migration into the stomach, a tubular, flexible polymer stent with spirals was designed. The parameters of the spirals were computationally optimized by using a finite element analysis. A 3D printing technique then printed the designed polymer stents with optimized spirals. The self-expansion and anti-migration properties of the printed stent were characterized in an ex vivo normal porcine esophagus. The results showed that the 3D-printed flexible polymer stent with designed structures potentially has promising potential to treat inoperable esophageal malignancies potentially (Lin et al. 2019).

Polymeric (Wang et al. 2020a) and metallic (Maher et al. 2017) 3D-printed implants have been studied to deliver therapeutics locally to treat bone cancer. An extrusion-based 3D-printed core-shell-shaped implant comprising a hydrogel network exhibited controlled drug delivery to treat and prevent breast cancer recurrence by undergoing gel-sol transition when exposed to NIR light, which provided additional control over breast cancer management (Wei et al. 2020).

A 3D-printed implant was tested for removing remaining glioblastoma cells after surgery. This implant was 3D printed to fit into the tumor cavity and releases an oncolytic virus-inspired DNA nanocomplex that kills glioblastoma cells by inducing apoptosis. Meanwhile, a 3D-engineered subcutaneous glioblastoma xenograft was produced to resemble mice's resection tumor cavity. The implant was successfully inserted into the glioblastoma resection cavity, delaying tumor recurrence and greatly extending overall life. This research showed that a conformal implant that releases oncolytic DNA nanocomplexes may be used to treat glioblastoma (Yang et al. 2017).

The use of 3D printing to produce complicated objects has been extensively shown. This technology has the potential to be useful in the manufacture of internal human body components. Bhavsar (Bhavsar and Prakash 2020) developed an approach in which CT scan data was utilized to fabricate a 3D model, with the cancerous area excised using CAD software. A 3D printer was used to create the defect-free portion, which was then compared to normal bone structure. Osteosarcoma is linked to certain genetic mutations, illnesses, and radiation exposure. It is an arbitrary disease that may attack anybody at any time. As a result, when cancer has not progressed, this form of implantation may be quite beneficial. This study employed CAD software to remove malignant areas of the skull and create an STL file that could be used to 3D print an implant. There has been a case when 3D printing was used to conduct cranioplasty. The neurosurgeon must spend a substantial amount of time molding and sculpting the implant, whether it is made of acrylic, titanium, or bone graft, to suit the patient's skull, which takes more than 6 hours. Because the patient's tissue is exposed to various toxins in the environment throughout the process, the longer the surgery takes, the greater the risk of infection. In instances with osteosarcoma in the skull, a similar procedure may be done. Mineralized collagen and hydroxyapatite, for example, have estrogenic action and may

guide bone repair. However, constructing bony scaffolds with these materials is very challenging, and the mechanical strength of this artificial bone is insufficient to offer adequate support at human load-bearing areas. The titanium implants are expensive because they are difficult to shape, cast, and mill. As a result, 3D printing provides an affordable alternative to traditional implants that is also a speedier option, particularly for bone cancer patients, whose treatment is costly, and this may help them decrease their financial load (Bhavsar and Prakash 2020).

8.5.5 *Other 3D-Printed Devices for Localized Cancer Therapy*

Other 3D-printed devices like prosthesis (Hao et al. 2021), tablet (Salmoria et al. 2017), and disc (Cho et al. 2019) have been used for the localized treatment of cancers. A 3D-printed prosthesis containing paclitaxel (PTX) and doxorubicin microspheres was assessed to prevent tumor recurrence and metastasis after breast-conserving surgery (Hao et al. 2021). In vitro drug release experiments revealed that the 3D-printed prosthesis loaded with therapeutic microspheres could continuously release the therapeutics for more than 3 weeks, reducing cancer recurrence while causing minimal adverse effects.

A 3D-printed drug-loaded tablet was evaluated for localized release of medication on the tumor region with potential improvement for cartilage cancer treatments (Salmoria et al. 2017). The printed tablets initially showed a rapid drug release due to the hydrophilic character of fluorouracil. After implantation, a high initial drug concentration locally in the cancer cells is a desirable profile (Salmoria et al. 2017).

Nanogels are biocompatible materials that can deliver several drugs locally. Cho et al. (Cho et al. 2019) revealed that nanogel discs containing PTX and rapamycin could be accurately constructed using 3D printing technology. Premature gelation during storage and the first burst release of the drugs in the dissolving media were avoided using 3D-printed nanogel disc rounds containing PTX and rapamycin. 3D-printed nanogel discs successfully delivered PTX and rapamycin intraperitoneally in ES-2-luc ovarian cancer-bearing xenograft mice in vivo. The treated xenograft mice were also demonstrated to be therapeutically efficacious and capable of avoiding postsurgical peritoneal adhesions. The easy fabrication of a poloxamer 407 nanogel disc containing PTX and rapamycin was made possible through 3D printing. Easy handling, effective peritoneal administration of drugs, avoidance of postsurgical peritoneal adhesion, and increased survival of ovarian cancer-bearing xenograft mice were all made possible by 3D-printed discs delivering drugs. To minimize hepatic toxicity, PTX and rapamycin administered simultaneously through a nanogel disc in vivo might be adjusted to lower quantities (Cho et al. 2019).

Skin cancer is the most common kind of cancer in the United States. When surgery is not feasible or surgical margins are insufficient, radiation treatment,

especially high-dose-rate (HDR) brachytherapy, is an effective type of cancer management. Treatment of superficial skin malignancies on uneven areas, such as the nose, lips, and ears, may be difficult. Chmura et al. (Chmura et al. 2019) developed a novel conformal superficial brachytherapy (CSBT) device prototype to enhance patient-specific treatment for complex locations in order to solve this problem. The device was mounted on an automated remote after-loader, limiting radiation exposure to operating employees and giving a novel conformal surface radiation treatment approach. The target treatment area was planned using a CT scan of a Rando phantom. A hexagonal lattice array of retractable rods with radioactive seeds deposited at the tip of each rod makes up the CSBT device. A single linear actuator inserted a 3D-printed conformal shape insert with a hexagonal array of cylindrical projections of various lengths into the rods. To fit to the patient's skin, the rods were displaced. This device design allows radiation delivery to complicated targets by using commonly accessible beta-emitting radionuclides like Yttrium-90 or Strontium-90. This device offered a safe and cost-effective method of enhancing radiation delivery to complicated treatment areas (Chmura et al. 2019).

Carrier geometry is an important factor in drug delivery systems because it affects drug release rate and interactions with cells and tissues. Anticancer agents in nanoparticulate form with customized dose requirements printed as a bio-adhesive film by inkjet printing maintained their anticancer activity even after being used as a printing ink (Varan et al. 2019). A magnetic sponge cylinder with a 3D-printed reservoir exhibited on-demand, localized delivery of 5-fluorouracil as triggered by varying strengths of magnetic fields applied using an external device, enabling long-term, efficient carcinogenic cell inhibition. On-demand delivery is ensured as a higher drug dose is released upon applying a higher magnetic field and vice versa (Shi et al. 2020).

8.6 Summary

Table 8.1 shows summary information of some 3D-printed devices that have been used for localized cancer therapy.

Despite much research in 3D printing for localized cancer therapy, this new treatment approach still requires more time to be researched, developed, and properly translated into the clinic.

3D printing presents multiple advantages related to the production of personalized medicine and especially its application in invasive and hard-to-treat diseases such as cancer. Tumor heterogeneity caused by various factors brings a huge hurdle in designing a standard treatment for cancer. Personalized medicine that analyzes and considers factors such as lifestyle differences, environmental changes, and patient's responses to illness contributing to tumor heterogeneity is becoming the new future of cancer medicine. 3D printing techniques like bioprinting rightly provide the precision, accuracy, and detail required in personalized medicine. 3D bioprinting and personalized medicine are the future of cancer medicine, yet their

Table 8.1 Summary of different 3D-printed devices for localized cancer therapy

Device	Application (type of cancer)	3D printing method	Device material	Delivered drug(s)	Ref.
Microneedle	Skin cancer	SLA	Class I biocompatible resin	Cisplatin (coated using inkjet printing)	(Uddin et al. 2020)
Microneedle	Skin cancer	μSL	PPF	Dacarbazine	(Lu et al. 2015)
Scaffold	Bone cancer	Extrusion-based	Fe-$CaSiO_3$	ROS	(Ma et al. 2018)
Scaffold	Bone cancer	FDM	Electroconductive PLA	–	(Monshi et al. 2020)
Scaffold	Bone cancer	Combining a 3D printing technique with a hydro-thermal method	MoS_2 modified akermanite	–	(Wang et al. 2017b)
Scaffold	Bone cancer	FDM	PCL/chitosan/ clay/β-tricalcium phosphate	Doxorubicin	(Chen et al. 2012)
Scaffold	Bone cancer	Extrusion based	Fe_3O_4 nanoparticles containing mesoporous bio-active glass/PCL	Doxorubicin hydrochloride	(Zhang et al. 2014)
Scaffold	Bone cancer	Not mentioned	$Ca_7Si_2P_2O_{16}$ bioceramic	–	(Ma et al. 2016)
Scaffold	Bone cancer	Extrusion based	Silicone resin loaded with $CaCO_3$ filler	–	(Fu et al. 2020)
Scaffold	Breast cancer	E-jet	PLGA	Doxorubicin and cisplatin simultaneously	(Qiao et al. 2019)
Scaffold	Breast cancer	Extrusion based	Dopamine-modified alginate and PDA	–	(Luo et al. 2019)
Scaffold	Breast cancer	Extrusion-based	Polydopamine/alginate	Doxorubicin hydrochloride	(Wei et al. 2020)
Scaffold	Bone metastases secondary to prostate cancer	Extrusion based	PLA, ABS, polyvinyl alcohol (PVA)	Doxorubicin	(Ahangar et al. 2018)
Scaffold	Cancer	Extrusion based	Graphene oxide (GO)/PCL composite	Doxorubicin and TNF-related apopto-sis-inducing ligand (TRAIL)	(Agila and Poornima 2015)
Mesh	Glioblastoma	Microextrusion	Alginate hydrogel	TMZ	(Hosseinzadeh et al. 2019)

Mesh	Glioblastoma		Alginate-GelMA hydrogel	All-trans retinoic acid	(Mirani et al. 2019)
Patch	Pancreatic cancer	Extrusion based	PLGA, PCL, PLGA/PCL	5-Fluorouracil	(Yi et al. 2016)
Patch	Cancer	Extrusion based	Fish gelatin methacryloyl +carboxymethyl cellulose sodium	Doxorubicin	(Liu et al. 2020)
Implant	Lung cancer and glioma	FDM	PCL	siRNA and doxorubicin	(Chen et al. 2015)
Implant	Breast cancer	E-jet	PLGA/5-fluorouracil/NVP-BEZ235	5-Fluorouracil/NVP-BEZ235	(Yang et al. 2020)
Implant	Osteosarcomas	SLA	PLLA	Methotrexate, doxorubicin, ifosfamide, and cisplatin	(Wang et al. 2020a)
Implant	Osteosarcomas	Selective laser sintering (SLS)	Titanium alloy	Doxorubicin and apoptosis-inducing ligand	(Maher et al. 2017)
Implant	Bone cancer	–	–	–	(Bhavsar and Prakash 2020)
Implant	Glioblastoma			–	(Yang et al. 2017)
Stent	Esophageal cancers	FDM	Polyurethane	5-Fluorouracil	(Fouladian et al. 2020)
Stent	Esophageal cancers	Extrusion based	Thermoplastic polyurethane (TPU), PLA		(Lin et al. 2019)
Prosthesis	Breast cancer	Extrusion based		PTX and doxorubicin	(Hao et al. 2021)
Bio-adhesive film	Cervical cancer	Inkjet printing	PEG-PCL	PTX-cyclodextrin complex, cidofovir	(Varan et al. 2019)
Reservoir	Cancer	FDM	PLA	5-fluorouracil	(Shi et al. 2020)
Tablet	Cartilage cancer	SLS	PCL	Fluorouracil	(Salmoria et al. 2017)
Nanogel disc	Ovarian cancer	FDM	Poly(ethylene oxide)-b-poly (propylene oxide)-b-poly (ethylene oxide)	PTX and rapamycin	(Cho et al. 2019)
Brachytherapy device	Skin cancer	Extrusion based/SLA	Different materials	–	(Chmura et al. 2019)

production and delivery remain challenging due to the complexity of designing exact tailor-made models and products. The technological and material challenges prevail and require further understanding of material and technique compatibility. Variations in such experimental studies require in-depth understanding and detailed research to obtain a validated outcome. Rewarding applications of 3D-printed personalized medicine in diagnosis, treatment, reconstruction, and tissue regeneration in the case of brain, kidney, breast, thyroid, bone, and liver cancers are critical. The complexity of tumor location and complications in delivering efficient chemotherapy to irregular surfaces using traditional ways highlight the importance of 3D-printed personalized medicine for cancer. Factors such as cost, time, quality aspects, regulatory approvals, and patient compliance and acceptance play a crucial role in establishing 3D printing personalized medicine for cancer treatment (Vaz and Kumar 2021). It is concluded that these technological advances need holistically driven, detailed applicative research to achieve a successful bed-to-bench transition.

Acknowledgments The authors would like to thank the Natural Sciences and Engineering Research Council of Canada (NSERC) for their financial support.

References

Agila S, Poornima J (2015, July) Magnetically controlled nano-composite based 3D printed cell scaffolds as targeted drug delivery systems for cancer therapy. In: 2015 IEEE 15th international conference on nanotechnology (IEEE-NANO). IEEE, pp 1058–1061. https://doi.org/10.1109/NANO.2015.7388803

Ahangar P, Akoury E, Ramirez Garcia Luna AS, Nour A, Weber MH, Rosenzweig DH (2018) Nanoporous 3D-printed scaffolds for local doxorubicin delivery in bone metastases secondary to prostate cancer. *Materials 11*(9):1485. https://doi.org/10.3390/ma11091485

Alfarouk KO, Stock CM, Taylor S, Walsh M, Muddathir AK, Verduzco D et al (2015) Resistance to cancer chemotherapy: failure in drug response from ADME to P-gp. Cancer Cell Int 15(1):1–13. https://doi.org/10.1186/s12935-015-0221-1

Arya J, Henry S, Kalluri H, McAllister DV, Pewin WP, Prausnitz MR (2017) Tolerability, usability and acceptability of dissolving microneedle patch administration in human subjects. Biomaterials 128:1–7. https://doi.org/10.1016/j.biomaterials.2017.02.040

Bakhtiar SM, Butt HA, Zeb S, Quddusi DM, Gul S, Dilshad E (2018) 3D printing technologies and their applications in biomedical science. In: Omics technologies and bio-engineering. Academic Press, pp 167–189. https://doi.org/10.1016/B978-0-12-804659-3.00010-5

Balmert SC, Carey CD, Falo GD, Sethi SK, Erdos G, Korkmaz E, Falo LD Jr (2020) Dissolving undercut microneedle arrays for multicomponent cutaneous vaccination. J Control Release 317:336–346. https://doi.org/10.1016/j.jconrel.2019.11.023

Baudino TA (2015) Targeted cancer therapy: the next generation of cancer treatment. Curr Drug Discov Technol 12(1):3–20. https://doi.org/10.2174/1570163812666150602144310

Bhavsar T, Prakash S (2020) 3D-printing of skull bone from CT scan data. Mater Today Proc 28:2447–2451. https://doi.org/10.1016/j.matpr.2020.04.789

Bhuskute H, Shende P, Prabhakar B (2022) 3D printed personalized medicine for cancer: applications for betterment of diagnosis, prognosis and treatment. *AAPS PharmSciTech* 23(1):1–12. https://doi.org/10.1208/s12249-021-02153-0

Boks MA, Unger WW, Engels S, Ambrosini M, van Kooyk Y, Luttge R (2015) Controlled release of a model vaccine by nanoporous ceramic microneedle arrays. Int J Pharm 491(1–2):375–383. https://doi.org/10.1016/j.ijpharm.2015.06.025

Caffarel-Salvador E, Tuan-Mahmood TM, McElnay JC, McCarthy HO, Mooney K, Woolfson AD, Donnelly RF (2015) Potential of hydrogel-forming and dissolving microneedles for use in paediatric populations. Int J Pharm 489(1–2):158–169. https://doi.org/10.1016/j.ijpharm.2015.04.076

Chae MP, Hunter-Smith DJ, Spychal RT, Rozen WM (2014) 3D volumetric analysis for planning breast reconstructive surgery. Breast Cancer Res Treat 146(2):457–460. https://doi.org/10.1007/s10549-014-3028-1

Chen M, Andersen MØ, Dillschneider P, Chang CC, Gao S, Le DQ et al (2015) Co-delivery of siRNA and doxorubicin to cancer cells from additively manufactured implants. RSC Adv 5(123):101718–101725. https://doi.org/10.1039/C5RA23748C

Chen M, Le DQ, Hein S, Li P, Nygaard JV, Kassem M et al (2012) Fabrication and characterization of a rapid prototyped tissue engineering scaffold with embedded multicomponent matrix for controlled drug release. Int J Nanomedicine 7:4285. https://doi.org/10.2147/IJN.S33083

Chen MC, Chen CS, Wu YW, Yang YY (2020) Poly-γ-glutamate microneedles as transdermal immunomodulators for ameliorating atopic dermatitis-like skin lesions in Nc/Nga mice. Acta Biomater 114:183–192. https://doi.org/10.1016/j.actbio.2020.07.029

Chew SA, Danti S (2017) Biomaterial-based implantable devices for cancer therapy. Adv Healthc Mater 6. https://doi.org/10.1002/adhm.201600766

Chia HN, Wu BM (2015) Recent advances in 3D printing of biomaterials. J Biol Eng 9(1):1–14. https://doi.org/10.1186/s13036-015-0001-4

Chmura J, Erdman A, Ehler E, Lawrence J, Wilke CT, Rogers B, Ferreira C (2019) Novel design and development of a 3D-printed conformal superficial brachytherapy device for the treatment of non-melanoma skin cancer and keloids. 3D Printing Med 5(1):1–6. https://doi.org/10.1186/s41205-019-0045-z

Cho H, Jammalamadaka U, Tappa K, Egbulefu C, Prior J, Tang R, Achilefu S (2019) 3D printing of poloxamer 407 nanogel discs and their applications in adjuvant ovarian cancer therapy. Mol Pharm 16(2):552–560. https://doi.org/10.1021/acs.molpharmaceut.8b00836

Choi JW, Kim N (2015) Clinical application of three-dimensional printing technology in craniofacial plastic surgery. Arch Plast Surg 42(3):267. https://doi.org/10.5999/aps.2015.42.3.267

Conde J, Oliva N, Zhang Y, Artzi N (2016) Local triple-combination therapy results in tumour regression and prevents recurrence in a colon cancer model. Nat Mater 15(10):1128–1138. https://doi.org/10.1038/nmat4707

Cui X, Gao G, Yonezawa T, Dai G (2014) Human cartilage tissue fabrication using three-dimensional inkjet printing technology. JoVE J Visual Exp 88:e51294. https://doi.org/10.3791/51294

Dabbagh SR, Sarabi MR, Rahbarghazi R, Sokullu E, Yetisen AK, Tasoglu S (2020) 3D-printed microneedles in biomedical applications. Iscience 102012:102012. https://doi.org/10.1016/j.isci.2020.102012

Das SK, Menezes ME, Bhatia S, Wang XY, Emdad L, Sarkar D, Fisher PB (2015) Gene therapies for cancer: strategies, challenges and successes. J Cell Physiol 230(2):259–271. https://doi.org/10.1002/jcp.24791

Dharadhar S, Majumdar A, Dhoble S, Patravale V (2019) Microneedles for transdermal drug delivery: a systematic review. Drug Dev Ind Pharm 45(2):188–201. https://doi.org/10.1080/03639045.2018.1539497

Du H, Liu P, Zhu J, Lan J, Li Y, Zhang L et al (2019) Hyaluronic acid-based dissolving microneedle patch loaded with methotrexate for improved treatment of psoriasis. ACS Appl Mater Interfaces 11(46):43588–43598. https://doi.org/10.1021/acsami.9b15668

Dugam S, Tade R, Dhole R, Nangare S (2021) Emerging era of microneedle array for pharmaceutical and biomedical applications: recent advances and toxicological perspectives. Future J Pharmaceut Sci 7(1):1–26. https://doi.org/10.1186/s43094-020-00176-1

Economidou SN, Lamprou DA, Douroumis D (2018) 3D printing applications for transdermal drug delivery. Int J Pharm 544(2):415–424. https://doi.org/10.1016/j.ijpharm.2018.01.031

Economidou SN, Uddin MJ, Marques MJ, Douroumis D, Sow WT, Li H et al (2021) A novel 3D printed hollow microneedle microelectromechanical system for controlled, personalized transdermal drug delivery. Addit Manuf 38:101815. https://doi.org/10.1016/j.addma.2020.101815

Exner AA, Saidel GM (2008) Drug-eluting polymer implants in cancer therapy. Expert Opin Drug Deliv 5(7):775–788. https://doi.org/10.1517/17425247.5.7.775

Findlay-Shirras LJ, Outbih O, Muzyka CN, Galloway K, Hebbard PC, Nashed M (2018) Predictors of residual disease after breast conservation surgery. Ann Surg Oncol 25(7):1936–1942. https://doi.org/10.1245/s10434-018-6454-1

Fouladian P, Kohlhagen J, Arafat M, Afinjuomo F, Workman N, Abuhelwa AY et al (2020) Three-dimensional printed 5-fluorouracil eluting polyurethane stents for the treatment of oesophageal cancers. Biomater Sci 8(23):6625–6636. https://doi.org/10.1039/D0BM01355B

Fu S, Hu H, Chen J, Zhu Y, Zhao S (2020) Silicone resin derived larnite/C scaffolds via 3D printing for potential tumor therapy and bone regeneration. Chem Eng J 382:122928. https://doi.org/10.1016/j.cej.2019.122928

Gooch JC, Schnabel F (2019) Locoregional recurrence of breast cancer. In: Clinical algorithms in general surgery. Springer, Cham, pp 97–100. https://doi.org/10.1007/978-3-319-98497-1_26

Guo N, Leu MC (2013) Additive manufacturing: technology, applications and research needs. Front Mech Eng 8(3):215–243. https://doi.org/10.1007/s11465-013-0248-8

Haleem A, Javaid M (2018) Role of CT and MRI in the design and development of orthopaedic model using additive manufacturing. J Clin Orthopaedics Trauma 9(3):213–217. https://doi.org/10.1016/j.jcot.2018.07.002

Haleem A, Javaid M (2019) Polyether ether ketone (PEEK) and its 3D printed implants applications in medical field: an overview. Clin Epidemiol Global Health 7(4):571–577. https://doi.org/10.1016/j.cegh.2019.01.003

Han D, Morde RS, Mariani S, La Mattina AA, Vignali E, Yang C et al (2020) 4D printing of a bioinspired microneedle array with backward-facing barbs for enhanced tissue adhesion. Adv Funct Mater 30(11):1909197. https://doi.org/10.1002/adfm.201909197

Hao W, Zheng Z, Zhu L, Pang L, Ma J, Zhu S et al (2021) 3D printing-based drug-loaded implanted prosthesis to prevent breast cancer recurrence post-conserving surgery. Asian J Pharmaceut Sci 16(1):86–96. https://doi.org/10.1016/j.ajps.2020.06.002

Hao Y, Li W, Zhou X, Yang F, Qian Z (2017) Microneedles-based transdermal drug delivery systems: a review. J Biomed Nanotechnol 13(12):1581–1597. https://doi.org/10.1166/jbn.2017.2474

He M, Yang G, Zhao X, Zhang S, Gao Y (2020) Intradermal implantable PLGA microneedles for etonogestrel sustained release. J Pharm Sci 109(6):1958–1966. https://doi.org/10.1016/j.xphs.2020.02.009

Hoang MT, Ita KB, Bair DA (2015) Solid microneedles for transdermal delivery of amantadine hydrochloride and pramipexole dihydrochloride. Pharmaceutics 7(4):379–396. https://doi.org/10.3390/pharmaceutics7040379

Homayun B, Lin X, Choi HJ (2019) Challenges and recent progress in oral drug delivery systems for biopharmaceuticals. Pharmaceutics 11(3):129. https://doi.org/10.3390/pharmaceutics11030129

Hosseinzadeh R, Mirani B, Pagan E, Mirzaaghaei S, Nasimian A, Kawalec P et al (2019) A drug-eluting 3D-printed mesh (GlioMesh) for management of glioblastoma. Adv Therapeut 2(11):1900113. https://doi.org/10.1002/adtp.201900113

Huang X, Liu Z, Wang X, Li XD, Cheng K, Zhou Y, Jiang XB (2019) A small 3D-printing model of macroadenomas for endoscopic endonasal surgery. Pituitary 22(1):46–53. https://doi.org/10.1007/s11102-018-0927-x

Hui D, Qiang L, Jian W, Ti Z, Da-Lu K (2009) A randomized, controlled trial of postoperative adjuvant cytokine-induced killer cells immunotherapy after radical resection of hepatocellular carcinoma. Dig Liver Dis 41(1):36–41. https://doi.org/10.1016/j.dld.2008.04.007

Johnson AR, Procopio AT (2019) Low cost additive manufacturing of microneedle masters. 3D Printing Med 5(1):1–10. https://doi.org/10.1186/s41205-019-0039-x

Johnstone RW, Ruefli AA, Lowe SW (2002) Apoptosis: a link between cancer genetics and chemotherapy. Cell 108(2):153–164. https://doi.org/10.1016/S0092-8674(02)00625-6

Jung D, Rejinold NS, Kwak JE, Park SH, Kim YC (2017) Nano-patterning of a stainless steel microneedle surface to improve the dip-coating efficiency of a DNA vaccine and its immune response. Colloids Surf B: Biointerfaces 159:54–61. https://doi.org/10.1016/j.colsurfb.2017.07.059

Jung JH, Jin SG (2021) Microneedle for transdermal drug delivery: current trends and fabrication. J Pharm Investig 1-15:503. https://doi.org/10.1007/s40005-021-00512-4

Juratli TA, Schackert G, Krex D (2013) Current status of local therapy in malignant gliomas—a clinical review of three selected approaches. Pharmacol Ther 139(3):341–358. https://doi.org/10.1016/j.pharmthera.2013.05.003

Khan S, Hasan A, Attar F, Babadaei MMN, Zeinabad HA, Salehi M et al (2021) Diagnostic and drug release systems based on microneedle arrays in breast cancer therapy. J Control Release 338:341. https://doi.org/10.1016/j.jconrel.2021.08.036

Kim JY, Han MR, Kim YH, Shin SW, Nam SY, Park JH (2016) Tip-loaded dissolving microneedles for transdermal delivery of donepezil hydrochloride for treatment of Alzheimer's disease. Eur J Pharm Biopharm 105:148–155. https://doi.org/10.1016/j.ejpb.2016.06.006

Kwon HJ, Hong J, Nam SY, Choi HH, Li X, Jeong YJ, Kim SH (2021) Overview of recent progress in electrohydrodynamic jet printing in practical printed electronics: focus on variety of printable materials for each component. Mater Adv 2:5593. https://doi.org/10.1038/nmat1974

Lancellotta V, Pagano S, Tagliaferri L, Piergentini M, Ricci A, Montecchiani S et al (2019) Individual 3-dimensional printed mold for treating hard palate carcinoma with brachytherapy: a clinical report. J Prosthet Dent 121(4):690–693. https://doi.org/10.1016/j.prosdent.2018.06.016

Lee HJ, Son Y, Kim D, Kim YK, Choi N, Yoon ES, Cho IJ (2015) A new thin silicon microneedle with an embedded microchannel for deep brain drug infusion. Sensors Actuators B Chem 209:413–422. https://doi.org/10.1016/j.snb.2014.11.132

Lee JH, Yeo Y (2015) Controlled drug release from pharmaceutical nanocarriers. Chem Eng Sci 125:75–84. https://doi.org/10.1016/j.ces.2014.08.046

Li J, Liu B, Zhou Y, Chen Z, Jiang L, Yuan W, Liang L (2017) Fabrication of a Ti porous microneedle array by metal injection molding for transdermal drug delivery. PLoS One 12(2):e0172043. https://doi.org/10.1371/journal.pone.0172043

Li K, Wang D, Zhao K, Song K, Liang J (2020) Electrohydrodynamic jet 3D printing of PCL/PVP composite scaffold for cell culture. Talanta 211:120750. https://doi.org/10.1016/j.talanta.2020.120750

Li Y, Zhang H, Yang R, Laffitte Y, Schmill U, Hu W et al (2019) Fabrication of sharp silicon hollow microneedles by deep-reactive ion etching towards minimally invasive diagnostics. Microsyst Nanoeng 5(1):1–11. https://doi.org/10.1038/s41378-019-0077-y

Lin M, Firoozi N, Tsai CT, Wallace MB, Kang Y (2019) 3D-printed flexible polymer stents for potential applications in inoperable esophageal malignancies. Acta Biomater 83:119–129. https://doi.org/10.1016/j.actbio.2018.10.035

Liu J, Tagami T, Ozeki T (2020) Fabrication of 3D-printed fish-gelatin-based polymer hydrogel patches for local delivery of PEGylated liposomal doxorubicin. Mar Drugs 18(6):325. https://doi.org/10.3390/md18060325

Lu Y, Mantha SN, Crowder DC, Chinchilla S, Shah KN, Yun YH et al (2015) Microstereolithography and characterization of poly (propylene fumarate)-based drug-loaded microneedle arrays. Biofabrication 7(4):045001. https://doi.org/10.1088/1758-5090/7/4/045001

Luo Y, Wei X, Wan Y, Lin X, Wang Z, Huang P (2019) 3D printing of hydrogel scaffolds for future application in photothermal therapy of breast cancer and tissue repair. Acta Biomater 92:37–47. https://doi.org/10.1016/j.actbio.2019.05.039

Lutton RE, Larrañeta E, Kearney MC, Boyd P, Woolfson AD, Donnelly RF (2015) A novel scalable manufacturing process for the production of hydrogel-forming microneedle arrays. Int J Pharm 494(1):417–429. https://doi.org/10.1016/j.ijpharm.2015.08.049

Luzuriaga MA, Berry DR, Reagan JC, Smaldone RA, Gassensmith JJ (2018) Biodegradable 3D printed polymer microneedles for transdermal drug delivery. Lab Chip 18(8):1223–1230. https://doi.org/10.1039/C8LC00098K

Ma H, Li T, Huan Z, Zhang M, Yang Z, Wang J et al (2018) 3D printing of high-strength bioscaffolds for the synergistic treatment of bone cancer. NPG Asia Mater 10(4):31–44. https://doi.org/10.1038/s41427-018-0015-8

Ma H, Luo J, Sun Z, Xia L, Shi M, Liu M et al (2016) 3D printing of biomaterials with mussel-inspired nanostructures for tumor therapy and tissue regeneration. Biomaterials 111:138–148. https://doi.org/10.1016/j.biomaterials.2016.10.005

Maher S et al (2017) Engineering of micro- to nanostructured 3D-printed drug-releasing titanium implants for enhanced osseointegration and localized delivery of anticancer drugs. ACS Appl Mater Interfaces 9(35):29562–29570. https://doi.org/10.1021/acsami.7b09916

Mdanda S, Ubanako P, Kondiah PP, Kumar P, Choonara YE (2021) Recent advances in microneedle platforms for transdermal drug delivery technologies. Polymers 13(15):2405. https://doi.org/10.3390/polym13152405

Mirani B, Pagan E, Shojaei S, Duchscherer J, Toyota BD, Ghavami S, Akbari M (2019) A 3D bioprinted hydrogel mesh loaded with all-trans retinoic acid for treatment of glioblastoma. Eur J Pharmacol 854:201–212. https://doi.org/10.1016/j.ejphar.2019.04.007

Mistilis MJ, Bommarius AS, Prausnitz MR (2015) Development of a thermostable microneedle patch for influenza vaccination. J Pharm Sci 104(2):740–749. https://doi.org/10.1002/jps.24283

Mojeiko G, de Brito M, Salata GC, Lopes LB (2019) Combination of microneedles and microemulsions to increase celecoxib topical delivery for potential application in chemoprevention of breast cancer. Int J Pharm 560:365–376. https://doi.org/10.1016/j.ijpharm.2019.02.011

Monshi M, Esmaeili S, Kolooshani A, Moghadas BK, Saber-Samandari S, Khandan A (2020) A novel three-dimensional printing of electroconductive scaffolds for bone cancer therapy application. Nanomed J 7(2):138–148. https://doi.org/10.22038/nmj.2020.07.007

Nepogodiev D, Martin J, Biccard B, Makupe A, Bhangu A, Ademuyiwa A et al (2019) Global burden of postoperative death. Lancet 393(10170):401. https://doi.org/10.1016/S0140-6736(18)33139-8

Nguyen TT, Choi JA, Kim JS, Park H, Yang E, Lee WJ et al (2019) Skin immunization with third-generation hepatitis B surface antigen using microneedles. Vaccine 37(40):5954–5961. https://doi.org/10.1016/j.vaccine.2019.08.036

Ogundele M, Okafor HK (2017) Transdermal drug delivery: microneedles, their fabrication and current trends in delivery methods. J Pharmaceut Res Int 1-14:1. https://doi.org/10.9734/JPRI/2017/36164

Parandoush P, Lin D (2017) A review on additive manufacturing of polymer-fiber composites. Compos Struct 182:36–53. https://doi.org/10.1016/j.compstruct.2017.08.088

Parhi R, Supriya ND (2019) Review of microneedle based transdermal drug delivery systems. Int J Pharmaceut Sci Nanotechnol *12*(3):4511–4523. https://doi.org/10.37285/ijpsn.2019.12.3.1

Park BJ, Choi HJ, Moon SJ, Kim SJ, Bajracharya R, Min JY, Han HK (2019) Pharmaceutical applications of 3D printing technology: current understanding and future perspectives. J Pharm Investig 49(6):575–585. https://doi.org/10.1007/s40005-018-00414-y

Park JU, Hardy M, Kang SJ, Barton K, Adair K, Lee CY et al (2007) High-resolution electrohydrodynamic jet printing. Nat Mater 6(10):782–789. https://doi.org/10.1038/nmat1974

Patil A, Narvenker R, Prabhakar B, Shende P (2020) Strategic consideration for effective chemotherapeutic transportation via transpapillary route in breast cancer. Int J Pharm 586:119563. https://doi.org/10.1016/j.ijpharm.2020.119563

Pedde RD, Mirani B, Navaei A, Styan T, Wong S, Mehrali M et al (2017) Emerging biofabrication strategies for engineering complex tissue constructs. Adv Mater 29(19):1606061. https://doi.org/10.1002/adma.201606061

Pennathur S, Kim H, Wang B, Queenan BN, Huber D (2020) 896-P: putting the pieces together: building a nonenzymatic wearable glucose sensor using silicon microneedle arrays. Diabetes 69 (Supplement_1). https://doi.org/10.2337/db20-896-P

Pere CPP, Economidou SN, Lall G, Ziraud C, Boateng JS, Alexander BD et al (2018) 3D printed microneedles for insulin skin delivery. Int J Pharm 544(2):425–432. https://doi.org/10.1016/j.ijpharm.2018.03.031

Prausnitz MR (2017) Engineering microneedle patches for vaccination and drug delivery to skin. Ann Rev Chem Biomol Eng 8:177–200. https://doi.org/10.1146/annurev-chembioeng-060816-101514

Qiao X, Yang Y, Huang R, Shi X, Chen H, Wang J et al (2019) E-jet 3D-printed scaffolds as sustained multi-drug delivery vehicles in breast cancer therapy. Pharm Res 36(12):1–16. https://doi.org/10.1007/s11095-019-2687-3

Rad ZF, Prewett PD, Davies GJ (2021) An overview of microneedle applications, materials, and fabrication methods. Beilstein J Nanotechnol 12(1):1034–1046. https://doi.org/10.3762/bjnano.12.77

Rajabi M, Roxhed N, Shafagh RZ, Haraldson T, Fischer AC, Wijngaart WVD et al (2016) Flexible and stretchable microneedle patches with integrated rigid stainless steel microneedles for transdermal biointerfacing. PLoS One 11(12):e0166330. https://doi.org/10.1371/journal.pone.0166330

Rao W, Deng ZS (2010) A review of hyperthermia combined with radiotherapy/chemotherapy on malignant tumors. *Critical reviews™*. Biomed Eng 38(1):101. https://doi.org/10.1615/CritRevBiomedEng.v38.i1.80

Rebecca L, Siegel M, Kimberly D, Miller MPH, Ahmedin Jemal DVM (2017) Cancer statistics. Ca Cancer J Clin 67(27):7–30. https://doi.org/10.3322/caac.21387

Regine WF, Winter KA, Abrams R, Safran H, Hoffman JP, Konski A et al (2011) Fluorouracil-based chemoradiation with either gemcitabine or fluorouracil chemotherapy after resection of pancreatic adenocarcinoma: 5-year analysis of the US intergroup/RTOG 9704 phase III trial. Ann Surg Oncol 18(5):1319–1326. https://doi.org/10.1245/s10434-011-1630-6

Reithofer MR, Chan KH, Lakshmanan A, Lam DH, Mishra A, Gopalan B et al (2014) Ligation of anti-cancer drugs to self-assembling ultrashort peptides by click chemistry for localized therapy. Chem Sci 5(2):625–630. https://doi.org/10.1039/C3SC51930A

Rejinold NS, Shin JH, Seok HY, Kim YC (2016) Biomedical applications of microneedles in therapeutics: recent advancements and implications in drug delivery. Expert Opin Drug Deliv 13(1):109–131. https://doi.org/10.1517/17425247.2016.1115835

Rimann M, Bono E, Annaheim H, Bleisch M, Graf-Hausner U (2016) Standardized 3D bioprinting of soft tissue models with human primary cells. J Lab Automation 21(4):496–509. https://doi.org/10.1177/2211068214567146

Roopavath UK, Kalaskar DM (2017) Introduction to 3D printing in medicine. In: In *3D printing in medicine*. Woodhead Publishing, pp 1–20. https://doi.org/10.1016/B978-0-08-100717-4.00001-6

Salmoria GV, Vieira FE, Ghizoni GB, Marques MS, Kanis LA (2017) 3D printing of PCL/fluorouracil tablets by selective laser sintering: properties of implantable drug delivery for cartilage cancer treatment. Drugs 4(6). https://doi.org/10.15761/ROM.1000121

Serrano DR, Terres MC, Lalatsa A (2018) Applications of 3D printing in cancer. J 3D Printing Med 2(3):115–127. https://doi.org/10.2217/3dp-2018-0007

Shafiee A (2020) Design and fabrication of three-dimensional printed scaffolds for cancer precision medicine. Tissue Eng Part A 26(5–6):305–317. https://doi.org/10.1089/ten.tea.2019.0278

Shaikh S, Bhan N, Rodrigues FC, Dathathri E, De S, Thakur G (2019) Microneedle platform for biomedical applications. In: Bioelectronics and medical devices. Woodhead Publishing, pp 421–441. https://doi.org/10.1016/B978-0-08-102420-1.00023-6

Shi K, Aviles-Espinosa R, Rendon-Morales E, Woodbine L, Maniruzzaman M, Nokhodchi A (2020) Novel 3D printed device with integrated macroscale magnetic field triggerable anti-cancer drug delivery system. Colloids Surf B: Biointerfaces 192:111068. https://doi.org/10.1016/j.colsurfb.2020.111068

Stavrinidis G, Michelakis K, Kontomitrou V, Giannakakis G, Sevrisarianos M, Sevrisarianos G et al (2016) SU-8 microneedles based dry electrodes for electroencephalogram. Microelectron Eng 159:114–120. https://doi.org/10.1016/j.mee.2016.02.062

Suleman A, Kondiah PP, Mabrouk M, Choonara YE (2021) The application of 3D-printing and nanotechnology for the targeted treatment of osteosarcoma. Front Mater 8:668834. https://doi.org/10.3389/fmats.2021.668834

Tan YJN, Yong WP, Kochhar JS, Khanolkar J, Yao X, Sun Y et al (2020) On-demand fully customizable drug tablets via 3D printing technology for personalized medicine. J Control Release 322:42–52. https://doi.org/10.1016/j.jconrel.2020.02.046

Tang J, Wang J, Huang K, Ye Y, Su T, Qiao L et al (2018) Cardiac cell–integrated microneedle patch for treating myocardial infarction. Sci Adv 4(11):eaat9365. https://doi.org/10.1126/sciadv.aat9365

Tas C, Joyce JC, Nguyen HX, Eangoor P, Knaack JS, Banga AK, Prausnitz MR (2017) Dihydroergotamine mesylate-loaded dissolving microneedle patch made of polyvinylpyrrolidone for management of acute migraine therapy. J Control Release 268:159–165. https://doi.org/10.1016/j.jconrel.2017.10.021

Veronesi U, Luini A, Del Vecchio M, Greco M, Galimberti V, Merson M et al (1993) Radiotherapy after breast-preserving surgery in women with localized cancer of the breast. N Engl J Med 328(22):1587–1591. https://doi.org/10.1056/NEJM199306033282202

Zhou X, Li B, Guo M, Peng W, Wang D, Guo Q et al (2022) Microneedle patch based on molecular motor as a spatio-temporal controllable dosing strategy of L-DOPA for Parkinson's disease. Chem Eng J 427:131555. https://doi.org/10.1016/j.cej.2021.131555

Yang Y, Wang X, Yang F, Wang L, Wu D (2018a) Highly elastic and ultratough hybrid ionic–covalent hydrogels with tunable structures and mechanics. Adv Mater 30(18):1707071. https://doi.org/10.1002/adma.201707071

Yang Y, Wang X, Yang F, Shen H, Wu D (2016) A universal soaking strategy to convert composite hydrogels into extremely tough and rapidly recoverable double-network hydrogels. Adv Mater 28(33):7178–7184. https://doi.org/10.1002/adma.201601742

Uddin MJ, Scoutaris N, Economidou SN, Giraud C, Chowdhry BZ, Donnelly RF, Douroumis D (2020) 3D printed microneedles for anticancer therapy of skin tumours. Mater Sci Eng C 107:110248. https://doi.org/10.1016/j.msec.2019.110248

Yang Y, Qiao X, Huang R, Chen H, Shi X, Wang J et al (2020) E-jet 3D printed drug delivery implants to inhibit growth and metastasis of orthotopic breast cancer. Biomaterials 230:119618. https://doi.org/10.1016/j.biomaterials.2019.119618

Wang Y, Sun L, Mei Z, Zhang F, He M, Fletcher C et al (2020a) 3D printed biodegradable implants as an individualized drug delivery system for local chemotherapy of osteosarcoma. Mater Des 186:108336. https://doi.org/10.1016/j.matdes.2019.108336

Wang Z, Abdulla R, Parker B, Samanipour R, Ghosh S, Kim K (2015) A simple and high-resolution stereolithography-based 3D bioprinting system using visible light crosslinkable bioinks. Biofabrication 7(4):045009. https://doi.org/10.1088/1758-5090/7/4/045009

Xu T, Jin J, Gregory C, Hickman JJ, Boland T (2005) Inkjet printing of viable mammalian cells. Biomaterials 26(1):93–99. https://doi.org/10.1016/j.biomaterials.2004.04.011

Zhang J, Zhao S, Zhu M, Zhu Y, Zhang Y, Liu Z, Zhang C (2014) 3D-printed magnetic Fe 3 O 4/MBG/PCL composite scaffolds with multifunctionality of bone regeneration, local anticancer drug delivery and hyperthermia. J Mater Chem B 2(43):7583–7595. https://doi.org/10.1039/C4TB01063A

Wang Z, Yang Z, Jiang J, Shi Z, Mao Y, Qin N, Tao TH (2022) Silk microneedle patch capable of on-demand multidrug delivery to the brain for glioblastoma treatment. Adv Mater 34(1):2106606. https://doi.org/10.1002/adma.202106606

Yang J, Liu X, Fu Y, Song Y (2019) Recent advances of microneedles for biomedical applications: drug delivery and beyond. Acta Pharm Sin B 9(3):469–483. https://doi.org/10.1016/j.apsb.2019.03.007

Turner JG, White LR, Estrela P, Leese HS (2021) Hydrogel-forming microneedles: current advancements and future trends. Macromol Biosci 21(2):2000307. https://doi.org/10.1002/mabi.202000307

Xu J, Xu D, Xuan X, He H (2021) Advances of microneedles in biomedical applications. Molecules 26(19):5912. https://doi.org/10.3390/molecules26195912

Vinayakumar KB, Kulkarni PG, Nayak MM, Dinesh NS, Hegde GM, Ramachandra SG, Rajanna K (2016) A hollow stainless steel microneedle array to deliver insulin to a diabetic rat. J Micromech Microeng 26(6):065013. https://doi.org/10.1088/0960-1317/26/6/065013

Wang M, Hu L, Xu C (2017a) Recent advances in the design of polymeric microneedles for transdermal drug delivery and biosensing. Lab Chip 17(8):1373–1387. https://doi.org/10.1039/C7LC00016B

Tejavibulya N, Colburn DA, Marcogliese FA, Yang KA, Guo V, Chowdhury S et al (2019) Hydrogel microfilaments toward intradermal health monitoring. Iscience 21:328–340. https://doi.org/10.1016/j.isci.2019.10.036

Wang Z, Han R, Shi Z, Mao Y, Tao TH, Qin N (2020b, January) Heterogeneous and multifunctional silk microneedles for in situ treatment of brain glioma. In: *2020 IEEE 33rd International Conference on Micro Electro Mechanical Systems (MEMS)*. IEEE, pp 369–371. https://doi.org/10.1109/MEMS46641.2020.9056316

Wang X, Li T, Ma H, Zhai D, Jiang C, Chang J et al (2017b) A 3D-printed scaffold with MoS2 nanosheets for tumor therapy and tissue regeneration. NPG Asia Mater 9(4):e376–e376. https://doi.org/10.1038/am.2017.47

Wei X, Liu C, Wang Z, Luo Y (2020) 3D printed core-shell hydrogel fiber scaffolds with NIR-triggered drug release for localized therapy of breast cancer. Int J Pharm 580:119219. https://doi.org/10.1016/j.ijpharm.2020.119219

Yi HG, Choi YJ, Kang KS, Hong JM, Pati RG, Park MN et al (2016) A 3D-printed local drug delivery patch for pancreatic cancer growth suppression. J Control Release 238:231–241. https://doi.org/10.1016/j.jconrel.2016.06.015

Yang Y, Tong C, Zhong J, Huang R, Tan W, Tan Z (2018b) An effective thermal therapy against cancer using an E-jet 3D-printing method to prepare implantable magnetocaloric mats. J Biomed Mater Res B Appl Biomater 106(5):1827–1841. https://doi.org/10.1002/jbm.b.33992

Wolinsky JB, Colson YL, Grinstaff MW (2012) Local drug delivery strategies for cancer treatment: gels, nanoparticles, polymeric films, rods, and wafers. J Control Release 159(1):14–26. https://doi.org/10.1016/j.jconrel.2011.11.031

Wei J, Liu B (eds) (2017) Personalized management of gastric cancer: translational and precision medicine. Springer

Yang Y, Du T, Zhang J, Kang T, Luo L, Tao J et al (2017) A 3D-engineered conformal implant releases DNA nanocomplexs for eradicating the postsurgery residual glioblastoma. Adv Sci 4(8):1600491. https://doi.org/10.1002/advs.201600491

Varan C et al (2019) Mechanical characterization and ex vivo evaluation of anticancer and antiviral drug printed bioadhesive film for the treatment of cervical cancer. Eur J Pharm Sci 130:114–123. https://doi.org/10.1016/j.ejps.2019.01.030

Vaz VM, Kumar L (2021) 3D printing as a promising tool in personalized medicine. AAPS PharmSciTech 22(1):1–20. https://doi.org/10.1208/s12249-020-01905-8

Chapter 9
4D Printing in Pharmaceutics and Biomedical Applications

Moqaddaseh Afzali Naniz, Mohsen Askari, Ali Zolfagharian, and Mahdi Bodaghi

Abstract 3D printing (3DP) has made significant advancements in the past decade in the fabrication of complex objects that are based on biomaterials. Although 3D-printed constructs were promising for biomedical applications, they fell short due to their inability to accurately mimic dynamic human tissues. 4D printing (4DP) is a breakthrough delivery system that integrates "time" into the conventional concept of 3DP to address the dynamic healing and regeneration of human tissues. In that way, additive manufacturing (AM) goes from 3DP to 4DP and implicates the use of stimuli-responsive materials. With its ability to create a wide range of useful biomedical products, 4DP has become an important tool in biomedical engineering. The purpose of this chapter is to present the concept of 4D bioprinting and the recent developments in smart materials, which can be actuated by different stimuli and can be used to develop biomimicry materials and structures with significant implications for pharmaceutics and biomedical research, as well as perspectives for the future.

Keywords 4D printing · Biomedical applications · Pharmaceutics · Tissue engineering · Medical devices · Soft robotics

9.1 Introduction

In recent years, three-dimensional printing (3DP) has made it possible to manufacture customized biomedical devices, such as stents (Morrison et al. 2015; Park et al. 2015), implants (Agarwal et al. 2021a; Li et al. 2016; Agarwal et al. 2021b; Okolie et al. 2020; Genova et al. 2020; Javaid and Haleem 2020), prosthetics (Manero et al.

M. A. Naniz · M. Askari · M. Bodaghi (✉)
Department of Engineering, School of Science and Technology, Nottingham Trent University, Nottingham, UK
e-mail: mahdi.bodaghi@ntu.ac.uk

A. Zolfagharian
School of Engineering, Deakin University, Geelong, VIC, Australia

D. Lamprou (ed.), *Nano- and Microfabrication Techniques in Drug Delivery*, Advanced Clinical Pharmacy – Research, Development and Practical Applications 2,
https://doi.org/10.1007/978-3-031-26908-0_9

2019; Park et al. 2019), and surgical tools (Lee Ventola 2014), with unprecedented spatial resolution and design freedom. 3D bioprinting takes advantage of traditional 3DP technologies to build biomaterials (Topuz et al. 2018; Liu et al. 2019a; Shapira et al. 2020). Utilizing 3D bioprinting techniques, bioinks (typically composed of biomaterials, living cells, or bioactive molecules) are printed as scaffolds that can regenerate target tissues containing functions (such as cell growth and proliferation) (Chen 2019; Rider et al. 2018). Medical devices, drugs, and tissues can all be customized and personalized with the help of 3DP. In addition, it is faster and less expensive than traditional manufacturing methods (Ng et al. 2017; Murphy and Atala 2014).

Some biomedical applications require dynamic shape change, which is not feasible for conventional 3DP technologies (Lu et al. 2013). Although 3D-printed structures can be created with biomaterials and living cells, they cannot match native tissue dynamics and cannot meet functional requirements (Tamay et al. 2019; Gao et al. 2016). Biological tissues are dynamic and constantly changing in shape and properties, requiring more complex fabrication techniques (Kuang et al. 2019; Polley et al. 2019). Four-dimensional printing (4DP) fulfills this need by adding the fourth dimension of time to 3D space (Wu et al. 2018a; Chalissery et al. 2022). Having time combined with 3D-printed biomaterials and bioinks enables the production of biomimetic tissues from the printed constructs to be pre-programmed to achieve more native-like results (Ionov 2013; Inverardi et al. 2020). A new path has opened up for biomedical engineering with 4DP. It has been widely used in various academic fields and industries, including biomedicine (Ong et al. 2018; An et al. 2016; Khoo et al. 2015). The 4D bioprinting technique allows for the creation of dynamic structures that change shape and function depending on stimuli (Khalid et al. 2022).

Smart designs and smart materials are necessary components for 4DP in order to achieve stimuli-responsive behaviors. As for smart designs, 4D-printed structures must be pre-programmed in computer-aided design (CAD) carefully by anticipating the time-dependent deformation of 3D objects (Choi et al. 2015; Miao et al. 2017). Materials that respond to external stimuli to change their geometry or properties are defined as smart materials (Khoo et al. 2015). Stimuli can be in the form of temperature, moisture, pH, light, pressure, or magnetic field. A variety of smart materials have been used for 4DP, including shape memory metal alloys, shape memory polymers (SMPs), stimuli-responsive hydrogels, dielectric elastomers, and smart nanocomposites (Miao et al. 2017; Champeau et al. 2020; Zhao et al. 2015).

4D bioprinting is seen as the next-generation printing technique capable of fabricating tissue-like shapes, but its limitations remain. Due to the difficulty of developing smart biomedical materials containing living cells for printing, reports on 4D bioprinting have been limited. Though only a few studies have been published in this field, it is clear that it offers some of the most exciting opportunities in biofabrication (Leist and Zhou 2016; Sydney Gladman et al. 2016; Bajpai et al. 2020; Stroganov et al. 2018; Bakarich et al. 2015; Yang et al. 2019; Suntornnond et al. 2017).

Here, we provide a comprehensive overview of 4DP and its potential applications in tissue engineering, medical devices, soft robotics, and drug delivery systems. We discuss challenges and future developments for 4DP in biomedical engineering, as well as possible future developments. By reading this chapter, readers can gain a more in-depth understanding of 4DP's current position as well as its potential future directions. A list of recent applications of 4DP is given in Table 9.1.

9.2 Tissue Engineering

Cell-based therapies and bioactive and porous materials are used in tissue engineering and regenerative medicine (TERM) to replace or restore damaged tissues and organs (Khademhosseini and Langer 2016). There are three elements of tissue engineering: matrix (scaffold), cells (stem cells or primary lineages), and signals (mechanical, physical, electrical, and/or molecules such as proteins and peptides) (Saska et al. 2021). It is essential that the morphology and chemical composition of the matrix be analogous to the extracellular matrix (ECM), as this leads to greater cell proliferation and differentiation (Agarwal et al. 2019). Pore size and porosity rate directly influence tissue formation inside 3D scaffolds during tissue restoration. In order to promote angiogenesis, these properties are essential (Karageorgiou and Kaplan 2005). Human tissues are highly plastic and non-static and can adapt to changes in the body dynamically. 3D-printed structures could have specific shapes, architectures, or cells, but they cannot demonstrate dynamic processes. As a result, 4D bioprinting meets the biomedicine requirement (Yang et al. 2020a).

Cell-laden scaffolds and seeded scaffolds are different types of tissue scaffolds. Tissue scaffolds are manufactured by embedding 4D inks, filaments made from biomaterials, or a combination of biomaterials (Gungor-Ozkerim et al. 2018), which encapsulate cells with growth factors or load cells after fabrication (Ionov 2018). A scaffold containing cells can be created by combining bioinks with biocompatible materials. Cell-seeded scaffolds can be easily made by printing, washing, and then topically treating printed constructs with growth factors or cells. This methodology is advantageous because it allows printing on synthetic plastic polymers (Gungor-Ozkerim et al. 2018). In comparison to conventional 4DP materials, several requirements are necessary for utilizing 4D materials in biomedical applications: (1) providing proper printing temperatures that do not exceed physiological temperatures for encapsulating cells or for in vivo applications; (2) suitable conditions for cross-linking or gelation in case cells are encapsulated; (3) materials with non-toxic and biocompatible components, and (4) an appropriate environment to promote cell attachment and proliferation in tissue regeneration (Wang et al. 2021a).

Hydrogels (Zhao et al. 2021) and SMPs are the most commonly used materials in 4D bioprinting. In order to create shape-morphing biomedical devices, several SMPs have been explored (Wang et al. 2017a; Zarek et al. 2017; Miao et al. 2016a; Hendrikson et al. 2017). Published research on 4D bioprinting explores the possibility of printing 3D structures using living cells that utilize a variety of natural

Table 9.1 Overview of 4D printing applications in pharmaceutics and biomedical applications

Applications	Stimuli	Printing techniques[a]	Materials[b]	Cells[c]	References
3D cell culture, histological study	Temperature	PμSL	PEGDA and bisphenol A ethoxylate dimethacrylate	Human neural progenitor cell	Yang et al. (2020c)
3D cell culture (neural)	Temperature	FDM, SLA, replica molding and imprinting	PVA (microstructured mold preparation), PMMA (microwell imprinting mold) BDE, PBE, and DA (4D ink)	Mouse NSCs	Miao et al. (2020)
Vascular tissue engineering	Water	Extrusion	Alg-MA, HA-MA	D1 cells	Kirillova et al. (2017)
Vascular tissue engineering, stent	Temperature	Extrusion	PGDA	–	Zhang et al. (2021a)
Cardiac tissue engineering	Temperature	PSTS	SOEA	Human MSCs	Miao et al. (2018b)
Cardiac tissue engineering	Water (solvent-induced stress relaxation)	SLA	GelMA and PEGDA	Human (iPSC-CMs), human MSCs, HUVECs	Cui et al. (2020b)
Cardiac tissue engineering	NIR-induced photothermal effects	DLP and replica molding	PEGDA (mold preparation), BDE, PBE, DA, and graphene nanoplatelets (4D ink)	Human (iPSC-CMs), human MSCs, HUVECs	Wang et al. (2021b)
Neural tissue engineering	Temperature and NIR-induced photothermal effects	FDM, extrusion, and replica molding	PVA (mold preparation), BDE, PBE, DA, and graphene nanoplatelets (4D ink)	Mouse NSCs	Cui et al. (2019)
Neural tissue engineering	Solvent (water/ethanol), temperature	SLA	SOEA (with/without graphene)	Human MSCs	Miao et al. (2018a)
Neural tissue engineering, drug release	Magnetoelectric	DLP	4-Hydroxybutyl acrylate, urethane–polyethylene glycol–polypropylene glycol, and electro-magnetized carbon porous nanocookies	PC12 cells	Fang et al. (2020)

Bone/cartilage tissue engineering	Water	Extrusion	Oxidized Alg-MA	NIH-3T3 cells, human adipose-derived stem cells	Lee et al. (2021)
Bone tissue engineering	Water, pH, Calcium ions	Extrusion	Oxidized Alg-MA and GelMA	Human MSCs	Ding et al. (2022)
Bone tissue engineering	Temperature	LTDM	Polyurethane, superparamagnetic iron oxide nanoparticles (combined with gelatin or PEO)	Human MSCs	Wang et al. (2018c)
Bone tissue engineering	NIR-induced photothermal effects	Extrusion	BPNS, β-TCP, and p(DLLA-TMC)	Rat MSCs	Wang et al. (2020)
Bone tissue engineering	Temperature	DLP	Poly(propylene fumarate)	–	Le Fer and Becker (2020)
Bone tissue engineering	Water, temperature	DLP	PCLDA-2000 and PCLDA-10000 (micropatterned SMP layer) HEA, PCLDA-2000, and SPMA (hydrogel layer)	Rat MSCs	You et al. (2021)
Bone tissue engineering	Thrombin, alkaline phosphatase	DLP	PEGDA (700)	NIH-3T3 cells	Devillard et al. (2018)
Bone tissue engineering	Temperature	Extrusion	Castor oil and PCL triol	Human MSCs	Miao et al. (2016b)
Trachea tissue engineering	Magnetic field	Extrusion	PLA, Fe_3O_4 nanoparticles	–	Zhao et al. (2019)
Trachea tissue engineering	Water and NaCl	DLP	Sil-MA	Human/rabbit chondrocytes and TBSCs	Kim et al. (2020)
Muscle tissue engineering	Temperature	FDM	PCL triol and poly(hexamethylene diisocyanate)-coated PCL	Human MSCs	Miao et al. (2019)
Muscle tissue engineering	Calcium ions	Extrusion, MEW	Alg-MA and PCL	C2C12 cells	Constante et al. (2021)

(continued)

Table 9.1 (continued)

Applications	Stimuli	Printing techniques[a]	Materials[b]	Cells[c]	References
Muscle tissue engineering	Water	Extrusion, MEW	HA-MA and PCL–polyurethane	C2C12 cells	Uribe-Gomez et al. (2021)
Tissue engineering	Water	Inkjet	GelMA (top layer) Carboxylated GelMA (bottom layer) PEI/HA/Alg/Alg-gelatin (sacrificial layer)	HUVEC	Cui et al. (2020a)
Tissue engineering	NIR-induced photothermal effects	Extrusion	Alg and polydopamine (for shape morphing) Alg and GelMA (for cell encapsulation)	293T HEK cells	Luo et al. (2019)
Tissue engineering	Temperature	SLA	SOEA	Human MSCs	Miao et al. (2016a)
Tissue engineering	Temperature	Extrusion	Collagen conjugated-polyether urethane (MM3520)	Human MSCs	Hendrikson et al. (2017)
Tissue engineering	Temperature	Extrusion	pAAm, pNIPAAm, Alg, and sugar particles	–	Ko et al. (2020)
Tissue engineering, medical applications	Water, temperature	SLA	HBC-MA	–	Seo et al. (2020)
Tissue engineering, biomedical devices	Temperature	Inkjet	Agarose, pAAm, and LAPONITE®	–	Guo et al. (2018)
Tissue engineering, biomedical devices (origami based)	Temperature	Extrusion	PLA	–	Langford et al. (2021)
Tissue engineering, soft robotics, biomedical actuators	Water	SLA	PEGDA, HEMA, SPMA, AUD, and MEO2MA	–	Ji et al. (2019)
Surgical suture, self-expandable stents/scaffolds	Temperature	DIW	PLMC	–	Wan et al. (2019)

Self-deployable stents	Temperature	FDM	Polyurethane	–	Bodaghi and Liao (2019)
Tubular stents and grippers	Temperature	3D multi-material printing	SMPs (TangoBlackPlus™, VeroWhitePlus™), a hydrophilic gel known as Sup705	–	Bodaghi et al. (2016)
Suture-less sealant clips	Temperature	Extrusion	RS and PHBV	–	Bittolo Bon et al. (2021)
Intravascular stents	Temperature	DIW	PLA, benzophenone, and Fe_3O_4 nanoparticles	–	Wei et al. (2017)
Endoluminal devices	Temperature	SLA	PCL-MA	–	Zarek et al. (2017)
Left atrial appendage occluder	Temperature, magnetic field	FDM	PLA and Fe_3O_4 nanoparticles	–	Lin et al. (2021)
Biomedical devices, soft robotics	Magnetic field	Extrusion	PDMS, dibutyl phthalate, fumed silica, and NdFeB nanoparticles	–	Zhang et al. (2021c)
Wearable assistive devices	Magnetic field	SLS	Nylon and ferrofluid	–	Ploszajski et al. (2019)
Elbow protective devices	Temperature	FDM	Unsaturated PLA–PCL copolymer	–	Cheng et al. (2020)
Vascular repair devices	Temperature	DIW	PCL, AUD, and n-butyl acrylate (with/without silica nanoparticles)	–	Kuang et al. (2018)
Biomedical engineering, soft robotics	Temperature	DIW	pAAM and pNIPAM, LAPONITE® XLG	–	Liu et al. (2019b)
Biomedical engineering, soft robotics	Temperature	Extrusion	Fe_3O_4 nanoparticles Alg, $CaCl_2$	–	Simińska-Stanny et al. (2022)
Biomedical devices, drug delivery	Water, temperature	Extrusion	Polyurethane elastomer (swellable and non-swellable) and polyethylene (heat shrinkable)	–	Song et al. (2020)

(continued)

Table 9.1 (continued)

Applications	Stimuli	Printing techniques[a]	Materials[b]	Cells[c]	References
Biomedical engineering, on-demand microparticle capture and release	pH	FsLDW	AAc, pNIPAAm and PVP	–	Hu et al. (2020)
Biomedical devices, soft robotics, drug delivery	Temperature, pH, enzyme	DIW	Pickering emulsion gels BSA-MA + pNIPAAm (thermo-sensitive ink), BSA-MA + p (DMAEMA) (pH-sensitive ink), BSA-MA + F127 (enzyme-sensitive ink)	–	Narupai et al. (2021)
Drug delivery (barbed microneedles)	Desolvation and drying	PμSLA	PEGDA	–	Han et al. (2020a)
Drug delivery (retentive intravesical devices)	Water	FDM	PVA and glycerol	–	Melocchi et al. (2019b)
Drug delivery (hydrogels)	Ionic cross-linking (calcium and carbonate ions)	Extrusion	F127DA and Alg	–	Wang et al. (2018b)

[a] PμSLA: projection micro stereolithography; FDM: fused deposition modelling; SLA: stereolithography; PSTS: photolithographic-stereolithographic-tandem strategy; DLP: Digital Light Processing; LTDM: low-temperature deposition manufacturing; DIW: direct ink writing; MEW: melt electrowriting; SLS: selective laser sintering; FsLDW: femtosecond laser direct writing

[b] PEGDA: poly(ethylene glycol) diacrylate; PVA: polyvinyl alcohol; PMMA: polymethyl methacrylate; BDE: bisphenol A diglycidyl ether; PBE: poly (propylene glycol) bis(2-aminopropyl ether); DA: decylamine; Alg-MA: alginate methacrylate; HA-MA: methacrylated hyaluronic acid; PGDA: poly(glycerol dodecanoate) acrylate; SOEA: soybean oil epoxidized acrylate; GelMA: gelatin-methacryloyl; PEO: poly(ethylene oxide); BPNS: black phosphorus nanosheets; β-TCP: β-tricalcium phosphate; p(DLLA-TMC): poly(lactic acid-co-trimethylene carbonate); HEA: hydroxyethylacrylate; PCL: poly(-ε-caprolactone); Sil-MA: methacrylated silk; HA: hyaluronic acid; PEI: polyethyleneimine; pAAM: polyacrylamide; pNIPAM: poly(N-isopropylacrylamide); HBC-MA: hydroxybutyl methacrylated chitosan; HEMA: hydroxyethyl methacrylate; SPMA: sulfopropyl methacrylate potassium; AUD: aliphatic urethane diacrylate; MEO2MA: (2-methoxyethoxy) ethyl methacrylate; PLMC: poly($_{D,L}$-lactide-*co*-trimethylene carbonate); RS: regenerated silk; PHBV: poly

(3-hydroxybutyrate-*co*-3-hydroxyvalerate); PLA: poly(lactic acid); PDMS: polydimethylsiloxane; PVP: polyvinylpyrrolidone; AAc: Acrylic acid; MA-BSA: methacrylated bovine serum albumin; F127DA: pluronic F127 diacrylate macromer; $CaCl_2$: calcium chloride

[c] NSCs: neuronal stem cells; MSCs: mesenchymal stem cells; Human (iPSC-CMs): Human-induced pluripotent stem cell-derived cardiomyocytes; HUVECs: human umbilical vein endothelial cells; TBSCs: trophoblast stem cells; HEK: human embryonic kidney

hydrogels, which can be controlled to achieve proportional cross-linking degrees across different thicknesses or planes of these 3D structures (Kirillova et al. 2017; Kim et al. 2020; Luo et al. 2019). Besides shape-changing constructs, functionally changing structures are also expected to attain distinct functions like natural tissues after fabrication. Several studies have demonstrated the development of 3D-printed organoids and spheroids (Brassard et al. 2021; Goulart et al. 2020; Skylar-Scott et al. 2019). A few studies in the literature deal with cells as stimuli or as smart materials (Kuribayashi-Shigetomi et al. 2012). The shape of 3D cell-laden constructs could be controlled by different patterns, intervals, and joints of cell-seeded microplates in a procedure called cell origami.

9.2.1 Bone Tissue Regeneration

As well as the impressive progress made in the above applications, 4DP has also been shown to be effective in regenerating bone tissue (Yang et al. 2020a). Bone repair was an early application of 3DP in tissue engineering. A promising strategy for treating critical-sized bone defects is bone tissue engineering using scaffolds (Wen et al. 2017; Gupta et al. 2021). Due to the complexity of irregular bone defects, a customized scaffold may be difficult to fit directly into irregular defects (Zhang et al. 2014). This may require additional surgery after the implant has been placed. 4DP has revealed an emerging application for producing bone tissue scaffolds with the ability to adapt dynamically to the irregular areas of the defect. This will facilitate personalized bone regeneration. To be specific, their shape memory properties enable them to reshape themselves to exactly match defects in the host (Wan et al. 2020). Among the advantages of 4D-printed bone scaffolds is their adaptability to minimally invasive surgery and their ability to fit irregularly shaped defects (Shakibania et al. 2021).

According to literature review (Wan et al. 2020), 4D-printed bone tissues can be fabricated by three main methods: (1) injectable thermosensitive hydrogels: the hydrogel can be injected into irregular defects and transformed into gel under body temperature (Demirtaş et al. 2017; Nafee et al. 2018); (2) shape-changing mechanism: a 3D-printed biomimetic scaffold changes its size to fit the void space, enabling personalized bone regeneration (Miao et al. 2016a, b; Zhang et al. 2019); and (3) creating a bio-inspired microenvironment: using 4D-printed biomimetic scaffolds with modified architecture, the osteogenesis of stem cells can be stimulated, which enhances the formation of new bone tissue (Jacob et al. 2018; Tandon et al. 2018; Kang et al. 2018).

You et al. developed a dual stimulus-responsive SMP to induce macroscopic swelling and microscopic heat changes (You et al. 2021). With a digital light processing (DLP) printer, they fabricated the static flat surface, static micro-pillar surface, and static cell culturing surface (Fig. 9.1a). Cytoskeletons spread continuously on dynamic surfaces according to the study. A 4D-printed membrane regulates multiscale structural deformation in vivo by combining SMP and hydrogel. With the

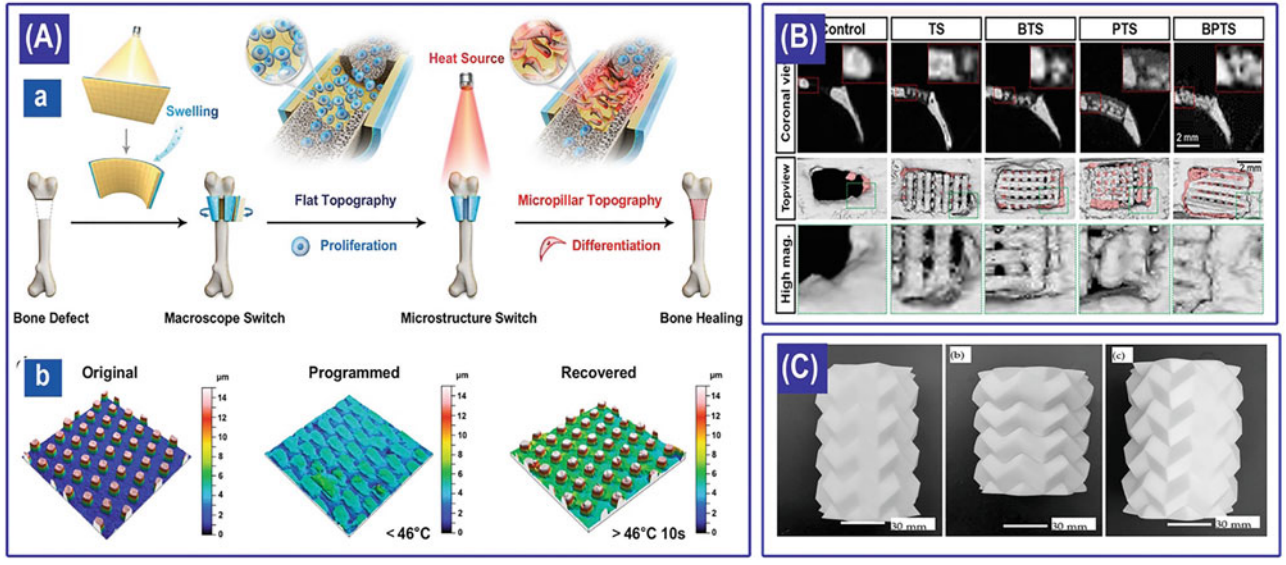

Fig. 9.1 4D-printed bone tissue scaffolds: (**A**) 4D-printed multi-responsive membrane for accelerated in vivo bone healing through remote regulation of stem cell fate. (a) The schematic illustration of a 4D-printed bilayer membrane. (b) Images of the original, programmed, and recovered surface topography captured with a laser confocal scanning microscope (LCSM). Reproduced from You et al. (2021) with permission from Wiley-VCH GmbH, © 2021. (**B**) 4D-printed photothermal-responsive reconfigurable scaffolds for reconstructing critical-size bone defects of irregular forms. μ-CT images of regenerated cranial bone defects from a top and coronal view; new bone tissue is indicated with pink color. Reproduced from Wang et al. (2020) with permission from IOP Publishing, © 2020. (**C**) 4D-printed origami scaffolds for minimally invasive surgeries. (a) As-printed herringbone tessellation origami (b) after compression and (c) after recovery. Reproduced from Langford et al. (2021) with permission from MDPI, © 2020

SMP layer, topography changes at the microscale occurred instantly, and the layered hydrogel allowed for macrofitting of defects with complex geometries.

Cryogenic 3DP is one of the most advantageous fabrication techniques. This is because it provides scaffolds with a hierarchically porous structure, strong mechanical properties, and high initial loading levels (Wang et al. 2017b). Using this technology, shape memory bone scaffolds were constructed, containing biodegradable photothermal and osteoinductive agents that work similarly to bone morphogenetic protein-2 and promote osteogenic differentiation and bone formation in vitro and in vivo (Wang et al. 2020). When exposed to NIR, the scaffold morphed to match the irregular shape of the defect. After implantation into cranial bone defect cavities, shape memory scaffolds fit well inside irregular cavities (Fig. 9.1b).

Wang et al. recently fabricated NIR-induced photothermal-responsive shape memory scaffolds in open configurations using extrusion printing (Lai et al. 2021a). Using NIR reduces the scaffold's elastic modulus, allowing it to adopt a temporary closed shape, which could then be fixed by cooling the scaffold. Therefore, the closed structure would facilitate minimally invasive and rapid implantation. During implantation, NIR was applied a second time to ensure a precise fit on irregular bone defects. A precise fit into rat cranial defects showed improved bone regeneration in vivo.

Biomedical fields can benefit greatly from origami structures due to their ability to expand from minimal to larger volumes, making them ideal for developing surgical tools and devices (Ahmed et al. 2021). With the help of origami structures, Langford et al. developed biomedical scaffolds with high shape recovery rates (Langford et al. 2021). Fused deposition modelling (FDM) was used to create origami structures with herringbone tessellation and an internal cancellous bone core. Based on deformability tests, the scaffolds recovered 96% of their original shape (Fig. 9.1c).

Microvasculature and nerve networks in the substitute are major challenges in large bone graft substitute engineering (Barabaschi et al. 2015). Several methods of fabricating microvascular constructs using 4D techniques have been proposed. Mouse mesenchymal stem cells (MSCs) have been combined with methacrylate alginate and hyaluronic acid hybrid hydrogels to fabricate hollow, self-folding tubes with diameters comparable to those of the smallest blood vessels (Kirillova et al. 2017). In addition, through the entrapment of enzymes in the 4D hydrogel during the bioprinting process, localized and pre-programmed calcification can occur, and fibrin biofilms can be formed. In this study, vascularized alveolar bone constructs were created by combining bone-like structures with blood vessels (Devillard et al. 2018). By co-immobilizing these enzymes, bioinspired constructs that have multiple functions can be created. As the first technology to demonstrate the fabrication of such multifunctional, 4D-printed constructs, this is potentially useful for treating complex bone problems.

9.2.2 Neural and Brain Tissue Regeneration

Neurotrauma (including brain damage) and neurological diseases (e.g., strokes, Alzheimer's disease, Parkinson's disease, multiple sclerosis, and Huntington's disease) cause damaged nerves that are difficult to regenerate. The distinct advantage of 3D-bioprinted scaffolds over other neuroregenerative treatment strategies is their ability to be customized. In other words, they mirror the architecture of biological in vivo systems (Lee et al. 2018; Yoo et al. 2020). Here, we will demonstrate how 4D-printed neural scaffolds, such as dynamic self-enturbulation and seamless integration, can be used for neural tissue engineering.

Wang et al. demonstrated the first thermally responsive brain model based on photothermal graphene (Cui et al. 2019). NIR irradiation returned the scaffold to its folded original shape after a short-term flat shape. Due to their conductive and optoelectronic properties, the neural stem cell-laden constructs were superior to pure epoxy scaffolds in terms of growth and differentiation (Fig. 9.2a). Miao et al. developed a temperature-sensitive nerve guidance conduit using stereolithography (SLA) (Miao et al. 2018a). The developed nerve conduct performed well in 4D shape transformation to provide minimally invasive and in situ shape activation, as shown in Fig. 9.2b. A 4D-printed construct's ability to dynamically and seamlessly integrate with a damaged nerve showed that it had the potential for regeneration of neural tissue.

The same research team has developed a 4D programmable medium for culturing neural stem cells (NSCs) by integrating printing and imprinting techniques, as illustrated in Fig. 9.2c (Miao et al. 2020). The 4D culture substrate shows a time-dependent self-morphing procedure that is crucial in controlling NSC behavior and in improving neuronal differentiation. As opposed to other tissue scaffolds or biomedical devices, 4D nerve grafts require no large-scale or complex shaping. It takes only one step from the plane to the conduit. Therefore, it should be more widely available commercially in the future.

Additionally, electrically responsive biomaterials have shown remarkable potential for regenerating nerve tissue with 4D bioprinting. Miao's research group has demonstrated a versatile graphene hybrid 4D-printed architecture exhibiting multiple regeneration capabilities, such as chemical cues, chemical guidance, and seamless integration (Esworthy et al. 2019).

9.2.3 Vascular Regeneration

Fabricating functional tissues via 3DP, i.e., vascularization, is a considerable challenge that can be met by 4D bioprinting. Using self-folding polymers, it is possible to fabricate blood vessels that can enclose blood cells, which deform after being wet to form tubes (Patel et al. 2017). SMPs and photo-cross-linked hydrogels can be used to manufacture multiple self-folding structures through 4D bioprinting (Jamal et al.

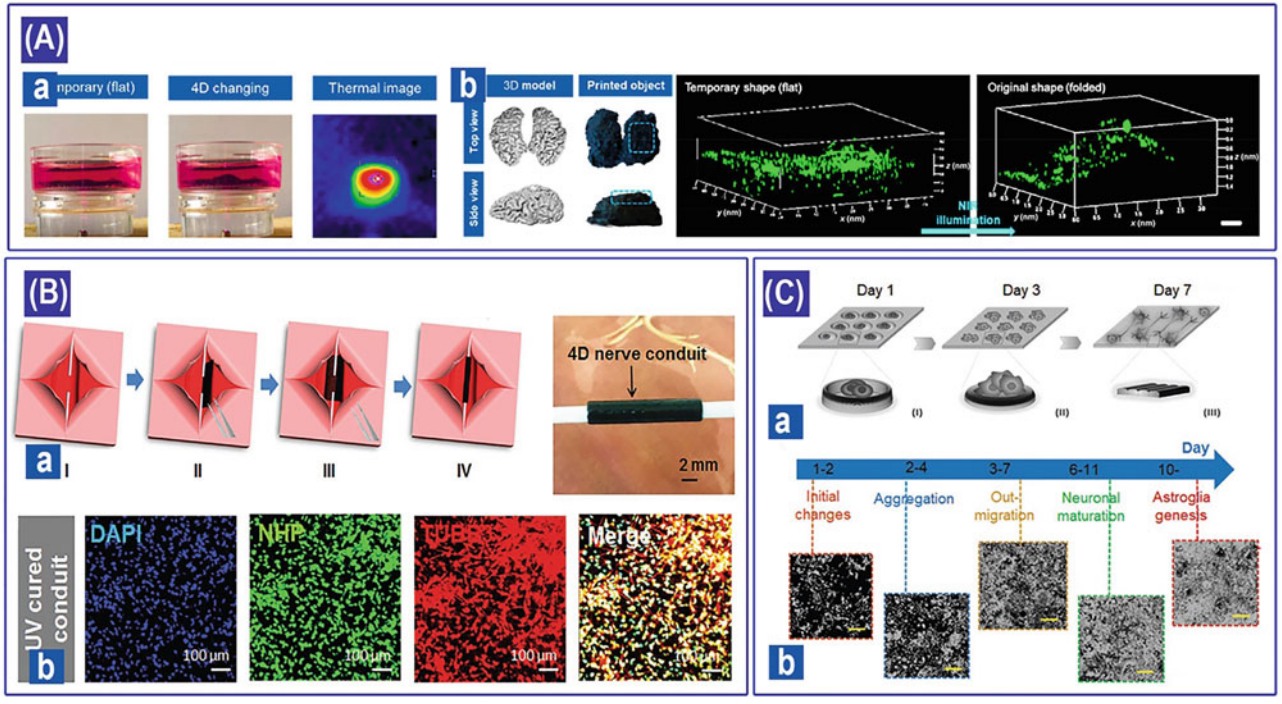

Fig. 9.2 4D-printed neural and brain tissues. (**A**) NIR-responsive 4D-printed brain construct. (a) Under NIR illumination, brain structures are transformed from a temporary flat shape to their original folded shape. A photothermal effect is visible on the thermal image. (b) Distribution of GFP-NSCs in 4D-printed brain constructs when the flat shape of the construct changed to a folded shape. Reproduced from Cui et al. (2019) with permission from Springer Nature. (**B**) Stereolithographic 4D bioprinting of multi-responsive structures for neural engineering. (a) "Thermomechanical programming" shape memory features facilitate temporary opening and fixing of a closed conduit in order to facilitate surgical insertion. (b) ND1, NSE, and NGN2 gene expression was higher in 4D-printed samples than in control sample. Reproduced from Miao et al. (2018a) with permission from WILEY-VCH Verlag GmbH & Co. KGaA, Weinheim, © 2018. (**C**)

A novel 4D neural scaffold fabrication technique with a time-dependent topographic transformation. The platform was used to modulate extracellular microenvironments from early NSC aggregation to highly aligned axons for NSC differentiation. (a) Illustration of the time-dependent cell patterning process during 7 days of culture, (b) Illustration of the time-dependent differentiation behavior of NSCs, demonstrating the different stages of RA-induced in vitro neural differentiation of NSCs (microscopic images), and the biological features (the expression of neurogenic markers) in the differentiated NSCs after 14 days of culture. Reproduced from Miao et al. (2020) with permission from WILEY-VCH Verlag GmbH & Co. KGaA, Weinheim, © 2020

2013). By controlling the photo-cross-linking degree, 4D-bioprinted hydrogels can be shaped into microvascular scaffolds with diameters of 20–500 m (Kirillova et al. 2017; Kim et al. 2020; Zhang et al. 2020). Additionally, vascular structures can be made in small or large diameters and can fold into a hollow 3D tube from a flat 2D shape. As the printed planar SMP scaffold is heated to human body temperature, it self-folds into a vascular scaffold with a diameter of several micrometers to several centimeters. This permits cell spread evenly, which is difficult to do with 3DP (Lai et al. 2020).

The use of GelMa as the upper layer with a low swelling rate (34%), and its carboxylated form (Gel-COOH-MA) as the bottom layer with a high swelling rate (59%), resulted in the micropatterns folding upon exposure to water (Cui et al. 2020a). As a result of the sacrificial layer, self-folding microtubes replicating human blood vessels can be initiated at a specific time. Additionally, the sacrificial layer enabled the cultivation of human umbilical vein endothelial cells (HUVECs) during the early stages of experiments.

A hybrid method using extrusion bioprinting and melt electrowriting was used by Constante et al. to produce multilayer scroll-like scaffolds with anisotropic topography (Constante et al. 2021). Combining these techniques and materials allows for flexible, adaptive, multi-scale, multi-material constructions that self-fold when inflated. By adjusting calcium ion concentration, media composition, and geometrical shape of the structure, they were able to control shape morphing. 4D-printed scaffolds successfully promoted and aligned C2C12 myoblasts.

9.2.4 Cardiac Patches

A cardiac patch is a bioengineered scaffold used to treat heart problems. Infarcted areas are mechanically strengthened and deficiencies are eliminated by this technique (Azhar et al. 2019). In order to successfully fix to the surface of the heart, cardiac scaffolds/patches must be curved and aligned (Wang et al. 2021a). 4DP has the capability of fabricating curved surfaces that are physiologically relevant and incorporate dynamic mechanical stimulation, which is not the case with 3DP for cardiovascular regeneration (Askari et al. 2021; Budharaju et al. 2021).

Micropatterned cardiac patches were developed by Miao et al. using integrated SLA and photolithography (Miao et al. 2018b). Human mesenchymal stem cells (hMSCs) actively grow along the formed micropatterns on the 4D scaffolds. This scaffold can act as a myogenic bioreactor with repeated self-folding and recovery (Fig. 9.3a).

Based on a biodegradable polymer, Montgomery and colleagues developed an elastic and microfabricated scaffold for delivering functional tissue (Montgomery et al. 2017). Cardiomyocyte viability and function were not affected by delivering cardiac patches through an orifice as small as 1 mm. When comparing vascularization, macrophage recruitment, and cell survival, injection of cardiac patches was comparable to open surgery in a subcutaneous syngeneic rat model. When compared

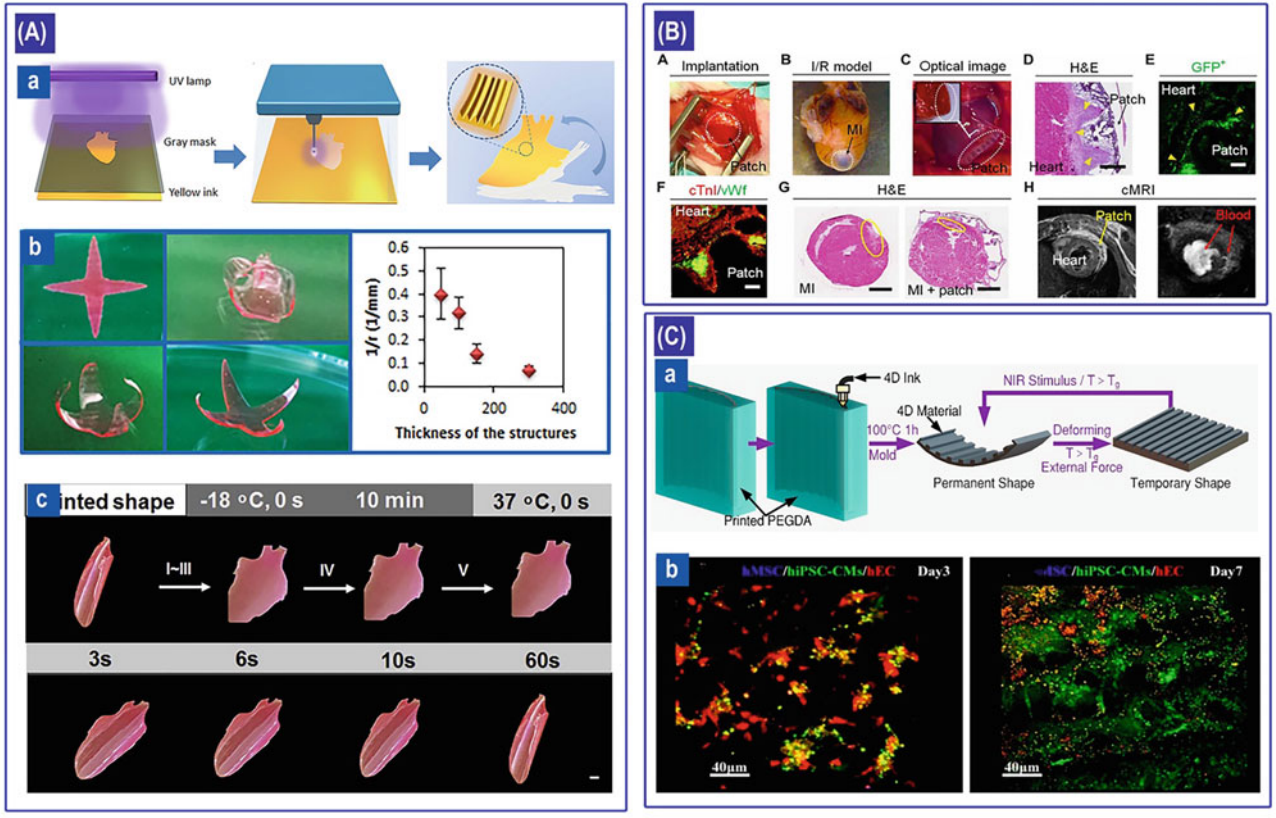

Fig. 9.3 4D-printed cardiac patches and valves. (**A**) Manufacturing of 4D smart scaffolds for enhanced stem cell cardiomyogenic differentiation. (a) Schematic illustration of the photolithographic-stereolithographic-tandem process. (b) The dynamic 4D shape change controlled by different thicknesses. (c) Illustration of the shape memory process with 4D-printed heart-shaped construct. When the flat heart-shaped construct was placed in a 37 °C environment, it gradually

with untreated controls, the patches greatly improved cardiac function in rats following myocardial infarction. It was successfully possible to deliver human cell-derived patches to the epicardium using a large animal model (porcine).

Using beam-scanning SLA, Cui et al. constructed a 4D self-morphing cardiac patch with biomechanical adaptability, as illustrated in Fig. 9.3b (Cui et al. 2020b). As a result of the printing process, the patch changed from a flat mesh design to a 3D wavy design after solvent-induced relaxation. By using a self-morphing 4D capability in conjunction with an expanding microstructure, the patch can enhance its dynamic integration with the beating heart and its biomechanical properties. Study results showed that hMSCs, human-induced pluripotent stem cell-derived cardiomyocytes (iPSC-CMs), and HUVECs promoted vascularization and cardiomyocyte differentiation in the patch with a wavy design.

Due to its noninvasiveness, high penetration, and ability to remotely control shape transformation, near-infrared (NIR) light has gained popularity as a creative and harmless stimulus for better performance in 4DP (Cui et al. 2019; Ma et al. 2020). To engineer cardiac tissue, Wang et al. used 4D inks to generate micropatterned nanocomposite structures, as shown in Fig. 9.3c (Wang et al. 2021b). The scaffold changed from flat to curved due to photothermal effects induced by NIR. The scaffold has also been used to grow human-induced pluripotent stem cell-derived cardiomyocytes (hiPSC-CMs), human bone marrow mesenchymal stem cells (hMSCs), and human umbilical vein endothelial cells (hECs). Even cell alignment and better myocardial maturation were observed on the curved scaffolds.

9.2.5 Muscle Tissue Regeneration

3DP has gained popularity in recent years as a tool for fabricating engineered muscles (Seyedmahmoud et al. 2019; Li et al. 2019). However, it is unable to exhibit

Fig. 9.3 (continued) recovered its rolling shape. Reproduced from Miao et al. (2018b) with permission from IOP Publishing, 2018. (**B**) In vivo implantation and long-term evaluation of 4D patches. (a) Optical image of surgical implantation of the patch. (b) Optical image of a heart I/R MI model after 4 months. (c) Optical image of the implanted cellularized patch at week 3, showing a firm adhesion. (d) H&E image of the cellularized patch at week 3, indicating the cell clusters with a high density, (e) Fluorescent image of (GFP+) iPSC-CMs on the patch at week 3, showing a high engraftment rate. (f) Immunostaining of cTnI (red) and vWf (green) on the cellularized patch at week 3. (g) H&E images of mouse MI hearts without treatment (MI) and with cellularized patch (MI + patch) at week 10. (h) Cardiac magnetic resonance imaging (cMRI) images of a mouse heart with patch at week 10. Reproduced from Cui et al. (2020b) with permission from *American Association for the Advancement of Science*, © 2020. (**C**) An aligned myofiber myocardial construct with adjustable curvature for myocardial regeneration using 4D printing. (a) A schematic of the printing process. (b) Coculture of hMSCs, hECs, and hiPSC-CMs on the 4D constructs on (i) day 3 and (ii) day 7, which were designed to create the cardiac tissue. Reproduced from Wang et al. (2021b) with permission of *American Chemical Society*, © 2021

any dynamic mechanical properties such as stretching or folding to respond to myogenic alignment and functional maturation. Thus, 4DP offers a solution. Using a unique photolithographic-stereolithographic-tandem strategy (PSTS), Miao et al. developed a hierarchical micropattern (Miao et al. 2018b). The results showed that hMSCs grew strongly and aligned along the micropattern. hMSCs grown on the scaffolds also showed cardiomyogenesis, indicating that these scaffolds could be used in future tissue and organ regeneration procedures.

A cell alignment and myogenic differentiation platform using electric field (EF)-assisted cell printing and 4DP has also been developed by Yang et al. (2020b). The electric field-induced cell alignment enhanced myotube formation, the formation of highly ordered myotubes, and cell maturation compared to the normally printed cell-laden structures. This process activates voltage-gated calcium channels similar to those that govern muscle contractions in vivo. Other tissues with a high degree of organization and anisotropy may benefit from these alignment methods. Therefore, EF-responsive 4D materials could be used to facilitate cell-cell interactions or provide physiologically relevant environments in 4D-printed scaffolds.

9.2.6 Trachea Regeneration

Known as the windpipe, the trachea connects the larynx and bronchi (Ahn et al. 2019). Repair of long segments of tracheal stenosis is almost impossible in the clinic. Artificial replacements can be constructed using tissue engineering to solve this clinical need. 4D-printed tracheas with C-shape folding ability are another vital application of this method (Greaney and Niklason 2021; Gao et al. 2017).

Based on DLP and photocurable silk fibroin (Sil-MA) hydrogel, Kim et al. developed a 4D bioprinting system that prints more than two cell types (Kim et al. 2020). By modulating the exterior and interior properties of 3D-printed bilayered Sil-MA hydrogels in physiological conditions, the shape changes were controlled. Through this 4D bioprinting procedure, they fabricated tissues that mimicked the trachea using two types of cells and transplanted them into a rabbit's damaged trachea for 8 weeks. Both epithelium and cartilage developed at the intended sites of the implants as they integrated with the host trachea organically.

These results indicate that 4DP can develop innovative biomedical tools, particularly in tissue engineering.

9.3 Implantable Devices

4DP technology has had a significant impact on implantable devices, and 4D-bioprinted dynamic implants are in high demand (Lai et al. 2021b). 4DP can be used to make dynamic biomedical implants, which can be deployed with

minimally invasive surgery. In situ reshaping allows implants to match the shape and size of the implant site.

9.3.1 Stents

Surgical stents are used to maintain or restore the patency of blood vessels, airways, and other lumens (Kang 2019; Scafa Udriște et al. 2021). In the biomedical literature, several studies have investigated the 4DP of stents. 4D-printed stents possess the inherent ability to change shape, allowing them to minimize the amount of invasiveness when deployed at target sites in humans (Bodaghi et al. 2016; van Manen et al. 2021). Most studies manipulate the shape memory effect induced by body temperature to alter the shape of stents, usually from closed temporary shapes to open ones.

Similarly, Morrison et al. and Zarek et al. have developed customizable tracheobronchial stents using 4DP (Morrison et al. 2015; Zarek et al. 2017). By implantation into the human body, open constructs could transform from temporary closed to permanent open. In this way, a minimally invasive implant and better stent fit would be possible. The device was embedded in the tracheobronchomalacia of a child. Weaning could be accomplished after 7 days via mechanical ventilation, which was no longer needed after 3 weeks. As time passes and tissues expand, static structures would not be able to support growing infants. Using the same strategy, Wan et al. developed 4DP flower-shaped intravascular stents based on direct ink writing (DIW) (Wan et al. 2019). As a result of heating, the stents self-expand from a closed deformed form to an expanded form (Fig. 9.4a).

SMPs with variable photo-cross-linkable allyl groups were developed by Boire et al. (2016). The SMPs maintained their shape and were mechanically strong at body temperature. The vascular compatibility of the 4D-printed stents was evaluated in a murine model of hindlimb ischemia. Following culture, the tubular structures cellularized without inflammatory responses, did not form fibrotic tissue, and did not form giant foreign body cells 2 weeks after culture. In addition, Wu et al. developed self-expanding vascular stents by using a 4D structural element with a negative Poisson's ratio (NPR) (Wu et al. 2018b). The radial and longitudinal dimensions of stents decreased upon crimping with NPR structures. The results say that stents that have a smaller diameter and thicker walls may have a better radial force if they have more surface area.

It usually requires surgery to deploy a bifurcated stent in narrowed or blocked branch vessels. Kim et al. used FDM to develop a polyurethane-based bifurcated stent inspired by kirigami (Kim et al. 2019a). While in its temporary programmed state, the stent could move efficiently through the vessel. A raised room temperature led to the vessel recovering its original Y shape. Kirigami has also been shown to be useful in fabricating cylindrical stents in other studies. Using kirigami structures, Kim et al. designed and constructed a bifurcated stent (Kim and Lee 2018). The 3D-printed kirigami bifurcated stent was folded into a compact form, allowing it to

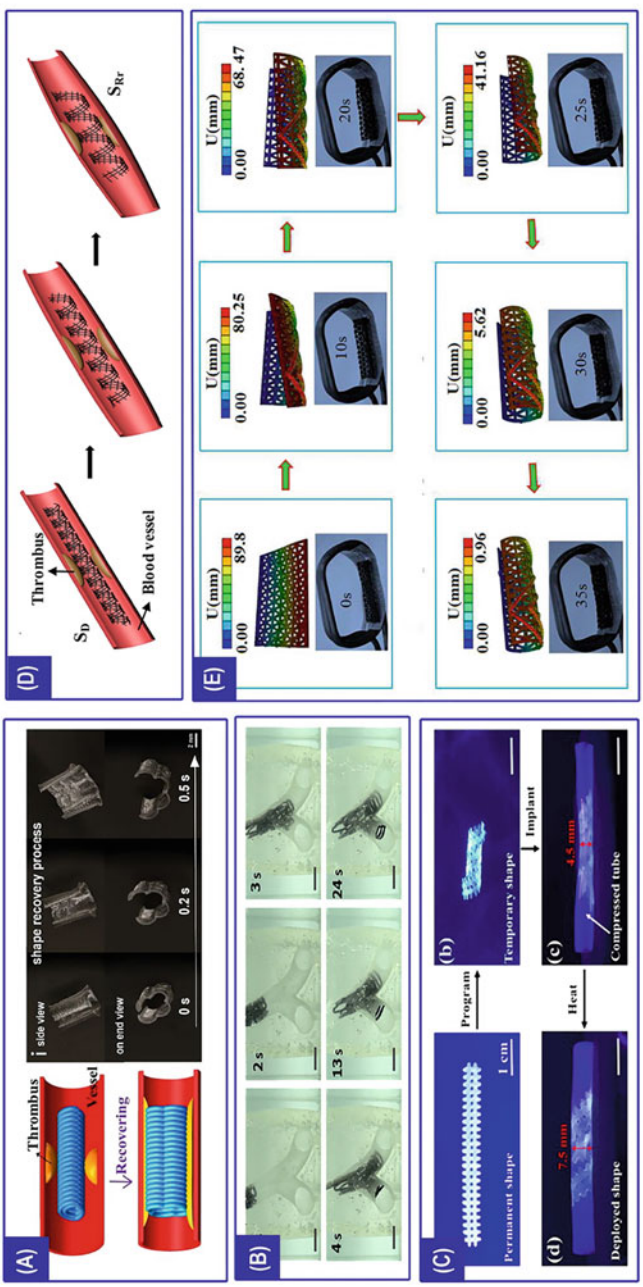

Fig. 9.4 4D-printed stents. (**A**) 4D-printed shape-changing 3D scaffolds using PLMC 1/6 ink. (a) Schematic diagram of restrictive shape recovery behavior exhibiting potential as an intravascular stent. (b) Macroscopic shape memory behavior of the scaffold within 0.5 s. Reproduced from Wan et al. (2019) with permission from Wiley Periodicals, Inc., 2019. (**B**) Shape-transformable bifurcated stents. A mock-up experiment of the whole process is shown in the figure. The branched vessels were created using a 3D-printed blood vessel as a mold. When inserted into the bifurcating point, the two branches were folded together. After the stent is heated by the surrounding medium, the tip of the folded dual branches begins to divide. The division is further accelerated by the operator pushing as each branch is inserted into its target vessel. Upon full entry, the cylindrical branch tubes expand to full size, and deployment is complete. Reproduced from Kim and Lee (2018) with permission from Nature Portfolio, 2018. (**C**) In vitro testing of a printed vascular stent. (a) A permanent form and (b) a temporary form. (c) The stent is implanted into a compressed silicone tube that simulates a narrowed blood vessel. (d) An enlarged tube diameter following

travel through the vessel without damaging the inner walls. The stent expanded automatically once it reached the target location, expanding the blocked or narrowed blood vessels (Fig. 9.4b). Although biocompatibility, biodegradability, and high Tg of SMP material have not been addressed, the study shows a noninvasive way to overcome the hindrances and obstructions of conventional stents. This is done by noninvasively inserting a thin structure to change its shape to that of a bifurcating vessel.

The improper transition temperature of SMPs makes implantation difficult and increases the risk of tissue or organ damage. In this respect, Zhang et al. recently developed SMP stents that are programmable at room temperature and adaptive to the physiological environment after implantation (Zhang et al. 2021a). Geometrical and mechanical adaptability of printed structures for biomedical implantation has been validated in vitro and in vivo (Fig. 9.4c).

As well as thermo-responsive materials, other stimuli-responsive 4D stents have been developed. A study reported 4DP of both shape memory nanoparticles (SMNPs) and shape memory nanocomposites (SMNCs) with remote actuated and magnetically guided behavior (Fig. 9.4d) (Wei et al. 2017). The remote actuation of the stent system allows for the design of 4D active vascular stents with the ability to change shape and function. Using FDM, Caberera et al. designed a 3D-printed self-expanding polymer stent for minimally invasive heart valve regeneration (Cabrera et al. 2017). Shin et al. successfully implanted a shape memory tube in a vessel less than 3 mm in diameter using in vivo validation and computational fluid dynamics modeling, thereby avoiding vascular stenosis (Shin et al. 2019).

The tracheal stent is a medical device that treats tracheal stenosis and tracheomalacia. Initially, it provides mechanical support to the tracheal wall. The tissue that grows along the scaffold is gradually degraded and expelled outside, preventing a second injury. Most tracheal stents are not biodegradable in clinical trials. Biodegradable tracheal stents are becoming the focus of more and more studies (Morrison et al. 2015; Huang et al. 2016).

The configuration of a tracheal stent and hole size are crucial. With the right size of holes, cells can attach and grow on the stent. Also, a reasonable structural design is critical to stent stability. An excellent tracheal stent must maintain structural integrity and stability after implanting in vivo, and it must provide sufficient force

Fig. 9.4 (continued) stent deployment. Reproduced from Zhang et al. (2021a) with permission from Elsevier Ltd., 2020. (**D**) Potential application of a 4D-printed c-PLA/Fe_3O_4 scaffold as an intravascular stent. SD and SRr represent the deformed and recovery shapes under restrictive conditions, respectively. Reproduced from Wei et al. (2017) with permission from American Chemical Society, 2016. (**E**) Photos showing shape recovery after 35 s of exposure to an alternating magnetic field of 30 kHz. The scaffolds were first expanded into a predetermined shape so that they could be wrapped easily around the trachea. Afterward, the magnetic field was imposed, and the scaffolds gradually returned to their initial form over time. Though the bioinspired tracheal scaffolds have been shown to almost fully recover their shape in 30 s, the last 5 s are needed to ensure the best fit with the geometry of the trachea. Reproduced from Zhao et al. (2019) with permission from Elsevier Ltd., 2019

to regenerate and degrade tissues. Two bioinspired irregular-shaped SMP tracheal stents were developed by Zhao et al. using a novel fabrication method (Zhao et al. 2019). In the experiment, both scaffolds proved tough enough to deform due to the deformation of the trachea. Furthermore, the stent provides reliable support for the trachea without compromising its rigidity. Both scaffolds recovered their initial shape after 35 s of exposure to an alternating magnetic field, which indicates that in vitro functionality was successfully verified (Fig. 9.4e).

Recently, a series of composite shape memory tracheal stents were developed by Zhang and colleagues (Zhang et al. 2021b). The temperature distribution during the shape recovery of stents was measured while they were placed in the magnetic field. This composite tracheal stent is well suited for application in the medical field, thanks to its excellent shape memory properties, reduced volume, and appropriate medical temperature.

9.3.2 Other Medical Devices

4DP technology has also been used to develop other smart medical devices. Using extrusion printing, Bon et al. prepared hollow cylindrical scaffolds for gastrointestinal anastomosis (Bittolo Bon et al. 2021). The porcine intestine was 140% more resistant to bursting than the manually sutured intestine in ex vivo tests.

Zhang et al. proposed an innovative 4DP technique that combines traditional 3D injection printing with origami-based magnetization (Zhang et al. 2021c). 4D magnetoactive soft materials (MASMs) were created using customized magnetization profiles. After being removed from the magnetic field, the object spontaneously reformed back into its original shape. Therefore, MASM-based 4D-printed beams can achieve complex geometries when magnetized strongly. In addition, as a proof of concept, the authors constructed MASM-based robots, which performed tasks such as playing rock-paper-scissors.

Additionally, using 4DP to create occlusion devices for treating cardiac diseases would be a great benefit (Huang et al. 2014). For instance, Lin et al. developed an adsorbable left atrial appendage occluder (LAAO) that was 4D printed (Lin et al. 2021). Using this medical device, left atrial appendage (LAA) blood clots are prevented from entering the bloodstream, thereby reducing stroke risks. Tests were performed on the structure that best fitted the stress-strain curve of the LAA tissue. As well as being durable, biocompatible, and biodegradable, the device's quick response to magnetic fields enables it to control its 4D transformation rapidly. LAAO was successfully deployed in a freshly isolated swine heart to confirm its feasibility.

Kuang et al. recently developed a 3D-printed complex structure for use in biomedical devices such as vascular repair devices (Kuang et al. 2018). They produced a semi-interpenetrating elastomer to make tubular structures via DIW printing. The tube's shape memory properties make insertion easier and allow it to

recover its original shape after heating, enabling it to adhere tightly to the inside surface of the vessel.

9.4 Soft Robots

Synergistic effects can be achieved by integrating 4DP and soft robotics (Whitesides 2018). Based on the inherent elastomeric properties of soft materials, soft robotics is concerned with developing soft robots that can perform complex tasks with minimal manipulation (Whitesides 2018; Polygerinos et al. 2015; Zolfagharian et al. 2020).

To print tubular geometries using DIW, Liu et al. combined passive, nonthermoresponsive inks with active, thermoresponsive inks (Liu et al. 2019b). Depending on whether ink is arranged horizontally or vertically, either linear or radial elongation occurs. As part of their research, they developed a tube-shaped structure with self-bending fingers that exhibits both uniaxial tube expansion and finger gripping, a feature derived from coral polyps. They could be used for soft-robotic endoscopy and vascular implants. Ilievski et al. presented a more conventional application of 4D soft robots with 3DP and mold casting (Ilievski et al. 2011). When compressed air is applied, starfish-like grippers morph into patterned channels. In view of the complexity of the human body, micro- or nano-sized soft grippers may perform better at inaccessible sites when they are mobile.

Using magnetic actuation, Kim et al. created ferromagnetic domains 3D printed in soft materials that can quickly transform 3D shapes (Kim et al. 2018). They showed diverse functions resulting from design changes, such as a soft robot that crawls, rolls, catches fast-moving objects, and can carry a pharmaceutical pill.

Remote actuation of 4D-printed magnetic soft robots in enclosed and confined spaces makes them a viable candidate for minimally invasive surgery. Kim et al. described a DIW-printed soft continuum robot capable of omnidirectional steering and navigation (Kim et al. 2019b). It was constructed from a polymer body combined with ferromagnetic microparticles evenly dispersed and an overlay of hydrogel skin. These features enabled the soft robot to navigate complicated and confined spaces, e.g., a cerebrovascular phantom with multiple aneurysms. This is done by using active, omnidirectional steering motions that are usually difficult to achieve with traditional robotic catheters or passive manual devices.

9.5 Drug Delivery

"Drug delivery" refers to formulations, manufacturing processes, storage systems, and technologies designed to carry pharmaceuticals to their target sites. As a replacement for traditional manufacturing methods with quick release, innovative delivery systems can improve drug effectiveness and minimize unwanted side effects. To ensure their optimal performance for drug release, drug delivery

instruments should be designed based on their specific applications (Goole and Amighi 2016; Vashist et al. 2016; Fu et al. 2019).

Due to the different pharmacokinetic characteristics among patients, the traditional healthcare model cannot generate accurate results when using "one-size-fits-all" criteria. Individual differences in health backgrounds, metabolisms, and genetics explain the variability of drug results. This means that different patients will react differently to prescribed medicines. The traditional method can also lead to overdosing or underdosing (Lui et al. 2019).

In recent years, the desire to develop drugs centered on the patient has grown. Progress in pharmacogenetics has enabled personalized medicine, a potential method of meeting the needs of individuals with specific medical conditions. Medicine will likely move away from mass production to a more personalized approach in the future. Therefore, a targeted group of patients can be given a customized dosage based on their metabolism homogeneity (Goyanes et al. 2015; Wang et al. 2021c). 4DP technology may be able to satisfy the patient-centric principle. So now it is possible to fabricate sophisticated devices previously impossible through conventional pharmaceutical manufacturing methods (Cui et al. 2021).

Applications of shape memory materials to drug delivery include both shape evolution and retention to provide maximum benefits, treat local diseases, reduce dosage frequency, and increase patient compliance (Bellinger et al. 2016; Babaee et al. 2019; Kirtane et al. 2018; Maroni et al. 2020). As a result of recent advances in 4DP, SMPs have been gaining interest in the pharmaceutical industry due to their ability to fabricate complex devices that shape-shift over time based on external nonmechanical stimuli (Firth et al. 2018; Durga Prasad Reddy and Sharma 2020). Using a chemically cross-linked PCL scaffold, Liu et al. have achieved in vivo controlled drug delivery (Liu et al. 2014). Growth factors were incorporated into compact shape memory porous constructs. When exposed to body temperature, the scaffolds regained their original shape by releasing growth factors. According to the authors, implants are likely to be successfully implanted in dynamically changing in vivo environments with little effect on drug delivery (Fig. 9.5a).

Many diseases could benefit from the extended release of drugs from stomach-retained systems. Gastroretentive devices can be swallowed in collapsed forms and expanded in situ to prevent voidance through the wide-open pylorus. Melocchi et al. proposed an expandable system for gastric retention (Melocchi et al. 2019a). As a result of exposure to 37 °C aqueous fluids, a variety of original configurations were created. Various temporary shapes, suitable for application, were created by manually deforming samples. In spite of being short-lived, the releases remained independent of their original shapes and were slowed down significantly by Eudragit® RS/RL-based coatings (Fig. 9.5b).

The control of acidification in cancerous and inflammatory areas has also been achieved by pH-responsive materials (Ashfaq et al. 2017; Senapati et al. 2018) to deliver controlled anticancer drugs. Larush designed and printed hydrogel tablets based on acrylic acid that release drugs at a high pH (Larush et al. 2017). In a similar way to Larush's work, Okwuosa et al. used composite materials for the core and shell of polyvinylpyrrolidone/methacrylic acid copolymer tablets (Okwuosa et al.

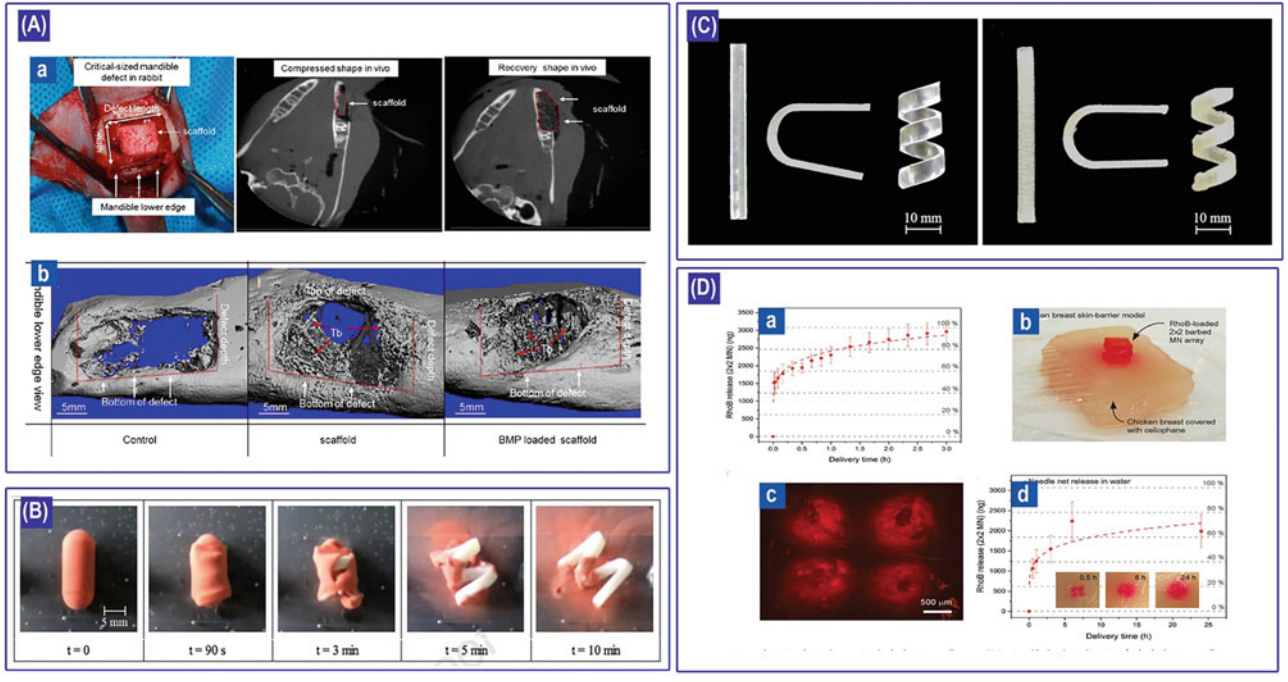

Fig. 9.5 4D-printed structures for drug delivery applications. (**A**) Delivering of growth factors through a smart porous nanocomposite scaffold to repair a mandibular bone defect. (a) In vivo shape memory recovery of the BMP-2-loaded SMP scaffold observed by cone beam computed tomography imaging. (b) 3D micro-CT images of the bone defect area. The red squares show the defect area, and the white arrows show the defect bottom. The BMP-2-loaded scaffold group had the most bone generation, and half of the defect area was filled with calcified structure. The SMP scaffold group had more neonatal bone than the control group. Reproduced from Liu et al. (2014) with permission from American Chemical Society, © 2014. (**B**) A shape memory polymer-based expandable drug delivery system for gastric retention. The images were taken during shape recovery of cylindrical and conical helix-shaped samples made from PVA05GLY-ALP, after programming of the temporary supercoiled shape. Reproduced from Melocchi et al. (2019a) with permission from Elsevier, © 2019. (**C**) 4D-printed

retentive device for intravenous drug delivery based on PVA shape memory. Images of original I-, U-, and helix-shaped samples produced by hot-melt extrusion (HME) and FDM. Reproduced from Melocchi et al. (2019b) with permission from Elsevier, © 2019. (**D**) In vitro and ex vivo drug release using barbed microneedle array. (a) In vitro RhoB release kinetics of a barbed microneedle array. (b) Photograph of an ex vivo drug release test with the chicken breast skin-barrier model. (c) A fluorescence microscope image of the chicken breast skin-barrier model treated with RhoB-loaded microneedle array at 0.5 h after insertion. (d) The amount of released RhoB from microneedle array into the chicken breast at different insertion times: 0.5, 1, 3, 6, and 24 h. Reproduced from Han et al. (2020a) with permission from WILEY-VCH Verlag GmbH & Co, © 2020

2017). In both studies, the tablets achieved gastric resistance characteristics and pH-responsive drug release, making them a viable method for gastrointestinal drug delivery. Enteric polymers with different grades were used by Goyanes and colleagues to delay and selectively release paracetamol for tablets containing hypromellose acetate succinate. These can be used to develop customized medicine dosages that are tailored to the needs of the patient (Goyanes et al. 2017).

The 4D bioprinting of drug delivery systems can also be performed using magnetically responsive materials (Lin et al. 2017). Miyashita and colleagues printed a device that moves at 3.8 body lengths per second in an external magnetic field to make origami robots (Miyashita et al. 2015). This miniature untethered robotic device is also capable of delivering drugs via heat stimulation in addition to its bioresorbability and self-folding ability.

Matrix metalloproteinases (MMPs) have been shown to be associated with certain types of tumor invasion and metastasis. Thus, MMP acts as a biological trigger to release anti-inflammatory drugs from negatively charged hydrogels in a targeted manner (Hu et al. 2014). Using this mechanism, drugs are delivered to specific body regions by degrading hydrogels. Additionally, Wang et al. and Ceylan et al. produced micro-robots for targeted drug delivery. These magnetically driven microrobotic devices were completely removed in the presence of collagenase (Wang et al. 2018a) and MMP2 enzymes (Ceylan et al. 2019) without any detectable toxic residues. With enzymatic degradation, they have been able to deal with issues such as non-degradable or cytotoxic by-products on AM-printed micro-robots.

A patch containing alginate (Alg) and pluronic F127 diacrylate macromer (F127DA) was created by extrusion printing (Wang et al. 2018b). The patch's permanent form was defined by the F127DA photo-cross-linked stable network, and a temporary folded shape was created by applying external stress. According to the results, the surface area and shape of temporary and recovered patches significantly affect drug release profiles.

Rather than modifying drug delivery devices' release profiles, 4DP has improved the devices' tissue retentiveness. By using hot-melt extrusion (HME) and FDM, Melocchi et al. fabricated retentive devices with diverse geometries for intravenous drug delivery systems (Melocchi et al. 2019b). By injecting a temporary shape into the bladder, the devices could remain in the bladder for a programmed period, and then dissolved/erosive substances are eliminated with urine. Along with the ability to restore the original shape, samples also released a tracer for a prolonged period, which was consistent with relevant thermo-mechanical properties (Fig. 9.5c).

To expedite patient care, pathogenic infections and drugs must be detected and released at the wound site. By developing a multifunctional dressing (GelDerm), Mirani et al. reported colorimetric pH measurement and antibiotic release (Mirani et al. 2017). GelDerm was found to be able to detect and eradicate bacteria in vitro and in vivo by releasing antibiotics over time. In a recent study, Han et al. created a miniature, 4D-printed hypodermic microneedle array with backward-facing barbs for better penetration into tissue (Han et al. 2020a). The microneedle array consisting of PEGDA was created by projection micro-stereolithography (PμSL). It was found that this new microneedle array stuck 18 times better than microneedles without

barbed tips. In addition, ex vivo research using the chicken breast skin barrier model has shown prolonged microneedle drug release (Fig. 9.5d).

9.6 Current Limitations and Future Outlook

Recent advancements in the field of 4DP, especially in biomedical applications, have been rapid and significant over the past several years. Despite this, 4DP technology is still at the very beginning of what it can do. The capabilities of 4D bioprinting to fabricate tissue-like structures have been demonstrated, but a number of challenges remain. These issues await the development of dynamically engineered tissues, soft robotics, and implantable drug delivery systems for minimally invasive surgery or patient-specific delivery. Moreover, the novel technique raises a number of concerns that should be addressed.

9.6.1 Design Limitations

Due to the complex nature of biological systems and the complexity of their feedback mechanisms, design-based limitations result. The oversimplification of engineered tissues and drug delivery systems can lead to problems. Furthermore, another design limitation is the unpredictability of stimuli-driven responses of shap mempry materials (SMMs) as well as their response times to those stimuli. For 4DP research to reach its ultimate potential, other issues will need to be addressed in the near future, including activation/deactivation of constructs, biocompatibility, amplitude, duration, and elimination of stimuli. By analyzing computational predictions as well as their behavior during morphing, we may be able to gain insight into energy transfer through materials (Agarwal et al. 2021c). The non-linear locomotion characteristics of linear rigid materials can make these predictions very useful. However, for soft stimuli-responsive materials, it can prove impossible to verify their behavior (Kim et al. 2021). But soon, the accumulation of experimental data and the outcome of these predictions will provide a significant database for the development of artificial intelligence (AI) systems for developing new smart materials.

9.6.2 Manufacturing Limitations

From a manufacturing perspective, 4DP is limited to only a few 3DP technologies as well as biocompatible smart materials. Though extrusion-based 4DP allows the printing of multiple materials and is cost-effective, the process has major limitations when compared to light-assisted printing in terms of speed and resolution. Alternatively, light-assisted printing technologies may offer faster print speeds and higher

print resolutions, but at the same time, they are expensive and do not support the printing of multiple materials.

9.6.3 Material Limitations

Considering the bioprinting method relies on viable cells, smart materials should be biocompatible and noncytotoxic. Stabilizing bioprinted structures should also utilize nontoxic crosslinkers. Biological constructs containing cells must be able to crosslink properly without releasing toxic substances. Furthermore, adding cells or tissue to the printed constructs should not alter the shape-changing properties of the constructs (Li et al. 2017). A suitable rheological property is also required to achieve both high cell viability and printability simultaneously. As explained above, the materials used for 4D bioprinting lack some of the desired qualities. It is necessary to optimize the use of biomaterials in hybrid structures in order to solve these problems. Moreover, there are only a limited number of smart materials suitable for biomedical applications. In the biomedical field, hydrogels and SMPs are currently the most common materials available for 4D bioprinting. A majority of these materials will only react to one stimulus, and 4D-printed constructs can only change shape in simple ways like folding, bending, curling, or opening and closing. Their potential applications in biomedicine are limited as they do not reflect the complex environment of the human body. It is imperative that innovative stimulus-responsive shape-changing materials be developed, including polymers, hydrogels, metals, ceramics, and composites/hybrids.

9.6.4 Sustainability

There are still a limited number of smart materials available for 4DP technology, and 3D printers are very expensive. These factors have put a damper on the sustainability of this technology in industries (Han et al. 2021). It is also noteworthy that there is a limited amount of literature available on how the 4DP technology will impact the environment. An example of this is the fact that one report found that SMP-based 4D-printed products had a reduction of up to 33.33% in energy consumption (Han et al. 2020b). It is imperative that a strong focus is placed on this research area, which will help to minimize energy consumption by adjusting printing parameters to match results.

9.6.5 FDA Regulation and Commercialization

Regulation of bioproducts and medical devices produced by 4DP or other technologies is governed by the FDA. The FDA created a working group to assess technical and regulatory considerations regarding the 3DP of medical devices. This was following the development of 3DP technology for biomedical applications. In terms of future commercialization of 4DP, a new market research report by Global Market Estimates predicts that the 4D bioprinting market will grow at a compound annual growth rate (CAGR) of 28.5% from 2020 to 2026. Although this technology has yet to realize tissue/organ manufacturing and implantable devices, it has the potential to address organ shortages, save lives, and extend life expectancy despite its complexity and challenges (Wang et al. 2021a).

9.7 Conclusions

4DP is a cutting-edge technology that combines 3DP and functional materials to develop products that change their shapes and characteristics when exposed to certain stimuli. Using 4DP technology, stimuli-responsive materials and additive manufacturing can combine to offer novel solutions in tissue engineering, medical devices, soft robotics, and drug delivery. 4DP for biomedical applications is an emerging research field with significant potential to develop the next generation of tissue engineering and biomedical devices. Even though a number of challenges still exist in this field, multidisciplinary collaboration can achieve success by advancing smart materials, printing, and 4D materials transformation strategies. Simultaneous research and breakthroughs in 3DP and 4DP will give rise to new technological avenues for pharmaceutical and biomedical applications. The majority of the reports analyzed in this review are proof of concept or potential application reports. However, technological advancements in both AM technologies and materials will soon allow these concepts to be realized in the near future. In other words, 4DP will not solely focus on shaping mechanisms but instead move from experimental evaluations to practical implementations of functional materials in real-world applications and multifunctional applications.

References

Agarwal T, Subramanian B, Maiti TK (2019) Liver tissue engineering: challenges and opportunities. ACS Biomater Sci Eng 5:4167–4182

Agarwal T, Tan S-A, Onesto V et al (2021a) Engineered herbal scaffolds for tissue repair and regeneration: recent trends and technologies. Biomed Eng Adv 2:100015. https://doi.org/10.1016/j.bea.2021.100015

Agarwal T, Chiesa I, Presutti D et al (2021b) Recent advances in bioprinting technologies for engineering different cartilage-based tissues. Mater Sci Eng C 123:112005
Agarwal T, Hann SY, Chiesa I et al (2021c) 4D printing in biomedical applications: emerging trends and technologies. J Mater Chem B 9:7608–7632
Ahmed AR, Gauntlett OC, Camci-Unal G (2021) Origami-inspired approaches for biomedical applications. ACS Omega 6:46–54
Ahn CB, Son KH, Yu YS et al (2019) Development of a flexible 3D printed scaffold with a cell-adhesive surface for artificial trachea. Biomed Mater 14:055001. https://doi.org/10.1088/1748-605X/ab2a6c
An J, Chua CK, Mironov V (2016) A perspective on 4D bioprinting. Int J Bioprinting 2:3–5. https://doi.org/10.18063/IJB.2016.01.003
Ashfaq UA, Riaz M, Yasmeen E, Yousaf M (2017) Recent advances in nanoparticle-based targeted drug-delivery systems against cancer and role of tumor microenvironment. Crit Rev Ther Drug Carrier Syst 34:317–353
Askari M, Afzali Naniz M, Kouhi M et al (2021) Recent progress in extrusion 3D bioprinting of hydrogel biomaterials for tissue regeneration: a comprehensive review with focus on advanced fabrication techniques. Biomater Sci 9:535–573
Azhar Z, Haque N, Ali S, et al (2019) Bioengineered cardiac patch scaffolds. In: Handbook of tissue engineering scaffolds: vol 1
Babaee S, Pajovic S, Kirtane AR et al (2019) Temperature-responsive biometamaterials for gastrointestinal applications. Sci Transl Med 11:eaau8581. https://doi.org/10.1126/scitranslmed.aau8581
Bajpai A, Baigent A, Raghav S et al (2020) 4D printing: materials, technologies, and future applications in the biomedical field. Sustainability 12:10628
Bakarich SE, Gorkin R, Panhuis MIH, Spinks GM (2015) 4D printing with mechanically robust, thermally actuating hydrogels. Macromol Rapid Commun 36:1211–1217. https://doi.org/10.1002/marc.201500079
Barabaschi GDG, Manoharan V, Li Q, Bertassoni LE (2015) Engineering pre-vascularized scaffolds for bone regeneration. In: Advances in experimental medicine and biology, vol 881, pp 79–94. https://doi.org/10.1007/978-3-319-22345-2_5
Bellinger AM, Jafari M, Grant TM et al (2016) Oral, ultra-long-lasting drug delivery: application toward malaria elimination goals. Sci Transl Med 8:365ra157. https://doi.org/10.1126/scitranslmed.aag2374
Bittolo Bon S, Chiesa I, Morselli D et al (2021) Printable smart 3D architectures of regenerated silk on poly(3-hydroxybutyrate-co-3-hydroxyvalerate). Mater Des 201:109492. https://doi.org/10.1016/j.matdes.2021.109492
Bodaghi M, Liao WH (2019) 4D printed tunable mechanical metamaterials with shape memory operations. Smart Mater Struct 28:045019. https://doi.org/10.1088/1361-665X/ab0b6b
Bodaghi M, Damanpack AR, Liao WH (2016) Self-expanding/shrinking structures by 4D printing. Smart Mater Struct 25:1–15. https://doi.org/10.1088/0964-1726/25/10/105034
Boire TC, Gupta MK, Zachman AL et al (2016) Reprint of: pendant allyl crosslinking as a tunable shape memory actuator for vascular applications. Acta Biomater 34:73–83. https://doi.org/10.1016/j.actbio.2016.03.021
Brassard JA, Nikolaev M, Hübscher T et al (2021) Recapitulating macro-scale tissue self-organization through organoid bioprinting. Nat Mater 20:2–3. https://doi.org/10.1038/s41563-020-00803-5
Budharaju H, Subramanian A, Sethuraman S (2021) Recent advancements in cardiovascular bioprinting and bioprinted cardiac constructs. Biomater Sci 9:1974–1994. https://doi.org/10.1039/d0bm01428a
Cabrera MS, Sanders B, Goor OJGM et al (2017) Computationally designed 3D printed self-expandable polymer stents with biodegradation capacity for minimally invasive heart valve implantation: a proof-of-concept study. 3D Print Addit Manuf 4:19–29. https://doi.org/10.1089/3dp.2016.0052

Ceylan H, Yasa IC, Yasa O et al (2019) 3D-printed biodegradable microswimmer for theranostic cargo delivery and release. ACS Nano 13:3353–3362. https://doi.org/10.1021/acsnano.8b09233
Chalissery D, Schönfeld D, Walter M et al (2022) Highly shrinkable objects as obtained from 4D printing. Macromol Mater Eng 307:2100619. https://doi.org/10.1002/mame.202100619
Champeau M, Heinze DA, Viana TN et al (2020) 4D printing of hydrogels: a review. Adv Funct Mater 30:1910606. https://doi.org/10.1002/adfm.201910606
Chen DXB (2019) Extrusion bioprinting of scaffolds: an introduction. In: Extrusion bioprinting of scaffolds for tissue engineering applications. Springer, pp 1–13. https://doi.org/10.1007/978-3-030-03460-3_1
Cheng CY, Xie H, Xu Z y et al (2020) 4D printing of shape memory aliphatic copolyester via UV-assisted FDM strategy for medical protective devices. Chem Eng J 396:25242. https://doi.org/10.1016/j.cej.2020.125242
Choi J, Kwon OC, Jo W et al (2015) 4D printing technology: a review. 3D Print Addit Manuf 2:159–167
Constante G, Apsite I, Alkhamis H et al (2021) 4D biofabrication using a combination of 3D printing and melt-electrowriting of shape-morphing polymers. ACS Appl Mater Interfaces 13:12767–12776
Cui H, Miao S, Esworthy T et al (2019) A novel near-infrared light responsive 4D printed nanoarchitecture with dynamically and remotely controllable transformation. Nano Res 12:1381–1388. https://doi.org/10.1007/s12274-019-2340-9
Cui C, Kim DO, Pack MY et al (2020a) 4D printing of self-folding and cell-encapsulating 3D microstructures as scaffolds for tissue-engineering applications. Biofabrication 12:045018. https://doi.org/10.1088/1758-5090/aba502
Cui H, Liu C, Esworthy T et al (2020b) 4D physiologically adaptable cardiac patch: a 4-month in vivo study for the treatment of myocardial infarction. Sci Adv 6:eabb5067. https://doi.org/10.1126/sciadv.abb5067
Cui M, Pan H, Su Y et al (2021) Opportunities and challenges of three-dimensional printing technology in pharmaceutical formulation development. Acta Pharm Sin B 11:2488–2504
Demirtaş TT, Irmak G, Gümüşderelioğlu M (2017) A bioprintable form of chitosan hydrogel for bone tissue engineering. Biofabrication 9:035003. https://doi.org/10.1088/1758-5090/aa7b1d
Devillard CD, Mandon CA, Lambert SA et al (2018) Bioinspired multi-activities 4D printing objects: a new approach toward complex tissue engineering. Biotechnol J 13:1800098. https://doi.org/10.1002/biot.201800098
Ding A, Lee SJ, Ayyagari S et al (2022) 4D biofabrication via instantly generated graded hydrogel scaffolds. Bioact Mater 7:324–332. https://doi.org/10.1016/j.bioactmat.2021.05.021
Durga Prasad Reddy R, Sharma V (2020) Additive manufacturing in drug delivery applications: a review. Int J Pharm 589:119820. https://doi.org/10.1016/j.ijpharm.2020.119820
Esworthy TJ, Miao S, Lee SJ et al (2019) Advanced 4D-bioprinting technologies for brain tissue modeling and study. Int J Smart Nano Mater 10:177–204. https://doi.org/10.1080/19475411.2019.1631899
Fang JH, Hsu HH, Hsu RS et al (2020) 4D printing of stretchable nanocookie@conduit material hosting biocues and magnetoelectric stimulation for neurite sprouting. NPG Asia Mater 12:61. https://doi.org/10.1038/s41427-020-00244-1
Firth J, Gaisford S, Basit AW (2018) A new dimension: 4D printing opportunities in pharmaceutics. In: AAPS Advances in the Pharmaceutical Sciences Series, pp 153–162. https://doi.org/10.1007/978-3-319-90755-0_8
Fu S, Du X, Zhu M et al (2019) 3D printing of layered mesoporous bioactive glass/sodium alginate-sodium alginate scaffolds with controllable dual-drug release behaviors. Biomed Mater 14:065011. https://doi.org/10.1088/1748-605X/ab4166
Gao B, Yang Q, Zhao X et al (2016) 4D bioprinting for biomedical applications. Trends Biotechnol 34:746–756

Gao M, Zhang H, Dong W et al (2017) Tissue-engineered trachea from a 3D-printed scaffold enhances whole-segment tracheal repair. Sci Rep 7:5246. https://doi.org/10.1038/s41598-017-05518-3

Genova T, Roato I, Carossa M et al (2020) Advances on bone substitutes through 3D bioprinting. Int J Mol Sci 21:1–28. https://doi.org/10.3390/ijms21197012

Goole J, Amighi K (2016) 3D printing in pharmaceutics: a new tool for designing customized drug delivery systems. Int J Pharm 499:376–394. https://doi.org/10.1016/j.ijpharm.2015.12.071

Goulart E, De Caires-Junior LC, Telles-Silva KA et al (2020) 3D bioprinting of liver spheroids derived from human induced pluripotent stem cells sustain liver function and viability in vitro. Biofabrication 12:015010. https://doi.org/10.1088/1758-5090/ab4a30

Goyanes A, Robles Martinez P, Buanz A et al (2015) Effect of geometry on drug release from 3D printed tablets. Int J Pharm 494:657–663. https://doi.org/10.1016/j.ijpharm.2015.04.069

Goyanes A, Fina F, Martorana A et al (2017) Development of modified release 3D printed tablets (printlets) with pharmaceutical excipients using additive manufacturing. Int J Pharm 527:21–30. https://doi.org/10.1016/j.ijpharm.2017.05.021

Greaney AM, Niklason LE (2021) The history of engineered tracheal replacements: interpreting the past and guiding the future. Tissue Eng - Part B Rev 27:341–352. https://doi.org/10.1089/ten.teb.2020.0238

Gungor-Ozkerim PS, Inci I, Zhang YS et al (2018) Bioinks for 3D bioprinting: an overview. Biomater Sci 6:915–946

Guo J, Zhang R, Zhang L, Cao X (2018) 4D printing of robust hydrogels consisted of agarose nanofibers and polyacrylamide. ACS Macro Lett 7:442–446. https://doi.org/10.1021/acsmacrolett.7b00957

Gupta D, Vashisth P, Bellare J (2021) Multiscale porosity in a 3D printed gellan–gelatin composite for bone tissue engineering. Biomed Mater 16:034103. https://doi.org/10.1088/1748-605X/abf1a7

Han D, Morde RS, Mariani S et al (2020a) 4D printing of a bioinspired microneedle array with backward-facing barbs for enhanced tissue adhesion. Adv Funct Mater 30:1909197. https://doi.org/10.1002/adfm.201909197

Han M, Yang Y, Li L (2020b) Energy consumption modeling of 4D printing thermal-responsive polymers with integrated compositional design for material. Addit Manuf 34:101223. https://doi.org/10.1016/j.addma.2020.101223

Han M, Yang Y, Li L (2021) Techno-economic modeling of 4D printing with thermo-responsive materials towards desired shape memory performance. IISE Trans 54:1047–1059. https://doi.org/10.1080/24725854.2021.1989093

Hendrikson WJ, Rouwkema J, Clementi F et al (2017) Towards 4D printed scaffolds for tissue engineering: exploiting 3D shape memory polymers to deliver time-controlled stimulus on cultured cells. Biofabrication 9:031001. https://doi.org/10.1088/1758-5090/aa8114

Hu Q, Katti PS, Gu Z (2014) Enzyme-responsive nanomaterials for controlled drug delivery. Nanoscale 6:12273–12286. https://doi.org/10.1039/c4nr04249b

Hu Y, Wang Z, Jin D et al (2020) Botanical-inspired 4D printing of hydrogel at the microscale. Adv Funct Mater 30:1907377. https://doi.org/10.1002/adfm.201907377

Huang Y, Kong JF, Venkatraman SS (2014) Biomaterials and design in occlusion devices for cardiac defects: a review. Acta Biomater 10:1088–1101. https://doi.org/10.1016/j.actbio.2013.12.003

Huang L, Wang L, He J et al (2016) Tracheal suspension by using 3-dimensional printed personalized scaffold in a patient with tracheomalacia. J Thorac Dis 8:3323. https://doi.org/10.21037/jtd.2016.10.53

Ilievski F, Mazzeo AD, Shepherd RF et al (2011) Soft robotics for chemists. Angew Chem Int Ed 50. https://doi.org/10.1002/anie.201006464

Inverardi N, Pandini S, Bignotti F et al (2020) Sequential motion of 4D printed photopolymers with broad glass transition. Macromol Mater Eng 305:1900370. https://doi.org/10.1002/mame.201900370

Ionov L (2013) Biomimetic hydrogel-based actuating systems. Adv Funct Mater 23:4555–4570. https://doi.org/10.1002/adfm.201203692

Ionov L (2018) 4D biofabrication: materials, methods, and applications. Adv Healthc Mater 7:1800412. https://doi.org/10.1002/adhm.201800412

Jacob J, More N, Kalia K, Kapusetti G (2018) Piezoelectric smart biomaterials for bone and cartilage tissue engineering. Inflamm Regen 38:2

Jamal M, Kadam SS, Xiao R et al (2013) Bio-origami hydrogel scaffolds composed of photocrosslinked PEG bilayers. Adv Healthc Mater 2:1142–1150. https://doi.org/10.1002/adhm.201200458

Javaid M, Haleem A (2020) Significant advancements of 4D printing in the field of orthopaedics. J Clin Orthop Trauma 11:S485–S490. https://doi.org/10.1016/j.jcot.2020.04.021

Ji Z, Yan C, Yu B et al (2019) 3D printing of hydrogel architectures with complex and controllable shape deformation. Adv Mater Technol 4:1800713. https://doi.org/10.1002/admt.201800713

Kang Y (2019) A review of self-expanding esophageal stents for the palliation therapy of inoperable esophageal malignancies. Biomed Res Int 2019. https://doi.org/10.1155/2019/9265017

Kang H, Hou Z, Qin QH (2018) Experimental study of time response of bending deformation of bone cantilevers in an electric field. J Mech Behav Biomed Mater 77:192–198. https://doi.org/10.1016/j.jmbbm.2017.09.017

Karageorgiou V, Kaplan D (2005) Porosity of 3D biomaterial scaffolds and osteogenesis. Biomaterials 26:5474–5491. https://doi.org/10.1016/j.biomaterials.2005.02.002

Khademhosseini A, Langer R (2016) A decade of progress in tissue engineering. Nat Protoc 11:1775–1781. https://doi.org/10.1038/nprot.2016.123

Khalid MY, Arif ZU, Ahmed W (2022) Four-dimensional (4D) printing: technological and manufacturing renaissance. Macromol Mater Eng 2200003. https://doi.org/10.1002/mame.202200003

Khoo ZX, Teoh JEM, Liu Y et al (2015) 3D printing of smart materials: a review on recent progresses in 4D printing. Virtual Phys Prototyp 10:103–122. https://doi.org/10.1080/17452759.2015.1097054

Kim T, Lee YG (2018) Shape transformable bifurcated stents. Sci Rep 8:13911. https://doi.org/10.1038/s41598-018-32129-3

Kim Y, Yuk H, Zhao R et al (2018) Printing ferromagnetic domains for untethered fast-transforming soft materials. Nature 558:274–279. https://doi.org/10.1038/s41586-018-0185-0

Kim D, Kim T, Lee YG (2019a) 4D printed bifurcated stents with Kirigami-inspired structures. J Vis Exp 2019. https://doi.org/10.3791/59746

Kim Y, Parada GA, Liu S, Zhao X (2019b) Ferromagnetic soft continuum robots. Sci Robot 4: eaax7329. https://doi.org/10.1126/SCIROBOTICS.AAX7329

Kim SH, Seo YB, Yeon YK et al (2020) 4D-bioprinted silk hydrogels for tissue engineering. Biomaterials 260:120281. https://doi.org/10.1016/j.biomaterials.2020.120281

Kim D, Kim SH, Kim T et al (2021) Review of machine learning methods in soft robotics. PLoS One 16:e0246102. https://doi.org/10.1371/journal.pone.0246102

Kirillova A, Maxson R, Stoychev G et al (2017) 4D biofabrication using shape-morphing hydrogels. Adv Mater 29:1703443. https://doi.org/10.1002/adma.201703443

Kirtane AR, Abouzid O, Minahan D et al (2018) Development of an oral once-weekly drug delivery system for HIV antiretroviral therapy. Nat Commun 9:2. https://doi.org/10.1038/s41467-017-02294-6

Ko H, Ratri MC, Kim K et al (2020) Formulation of sugar/hydrogel inks for rapid thermal response 4D architectures with sugar-derived macropores. Sci Rep 10:7527. https://doi.org/10.1038/s41598-020-64457-8

Kuang X, Chen K, Dunn CK et al (2018) 3D printing of highly stretchable, shape-memory, and self-healing elastomer toward novel 4D printing. ACS Appl Mater Interfaces 10:7381–7388. https://doi.org/10.1021/acsami.7b18265

Kuang X, Roach DJ, Wu J et al (2019) Advances in 4D printing: materials and applications. Adv Funct Mater 29:1805290

Kuribayashi-Shigetomi K, Onoe H, Takeuchi S (2012) Cell origami: self-folding of three-dimensional cell-laden microstructures driven by cell traction force. PLoS One 7:e51085. https://doi.org/10.1371/journal.pone.0051085

Lai J, Li J, Wang M (2020) 3D printed porous tissue engineering scaffolds with the self-folding ability and controlled release of growth factor. MRS Commun 10:579–586. https://doi.org/10.1557/mrc.2020.65

Lai J, Wang C, Wang M (2021a) 3D printing in biomedical engineering: processes, materials, and applications. Appl Phys Rev 8:021322

Lai J, Ye X, Liu J et al (2021b) 4D printing of highly printable and shape morphing hydrogels composed of alginate and methylcellulose. Mater Des 205:109699. https://doi.org/10.1016/j.matdes.2021.109699

Langford T, Mohammed A, Essa K et al (2021) 4D printing of origami structures for minimally invasive surgeries using functional scaffold. Appl Sci 11:332. https://doi.org/10.3390/app11010332

Larush L, Kaner I, Fluksman A et al (2017) 3D printing of responsive hydrogels for drug-delivery systems. J 3D Print Med 1:219–229. https://doi.org/10.2217/3dp-2017-0009

Le Fer G, Becker ML (2020) 4D printing of resorbable complex shape-memory poly(propylene fumarate) star scaffolds. ACS Appl Mater Interfaces 12:22444–22452. https://doi.org/10.1021/acsami.0c01444

Lee Ventola C (2014) Medical applications for 3D printing: current and projected uses. P T 39:704–711

Lee S-J, Esworthy T, Stake S et al (2018) Advances in 3D bioprinting for neural tissue engineering. Adv Biosyst 2:1700213. https://doi.org/10.1002/adbi.201700213

Lee YB, Jeon O, Lee SJ et al (2021) Induction of four-dimensional spatiotemporal geometric transformations in high cell density tissues via shape-changing hydrogels. Adv Funct Mater 31:2010104. https://doi.org/10.1002/adfm.202010104

Leist SK, Zhou J (2016) Current status of 4D printing technology and the potential of light-reactive smart materials as 4D printable materials. Virtual Phys Prototyp 11:249–262

Li J, Chen M, Fan X, Zhou H (2016) Recent advances in bioprinting techniques: approaches, applications and future prospects. J Transl Med 14:1–5. https://doi.org/10.1186/s12967-016-1028-0

Li YC, Zhang YS, Akpek A et al (2017) 4D bioprinting: the next-generation technology for biofabrication enabled by stimuli-responsive materials. Biofabrication 9:012001

Li X, Wang X, Chen H et al (2019) A comparative study of the behavior of neural progenitor cells in extrusion-based in vitro hydrogel models. Biomed Mater 14:65001

Lin G, Makarov D, Schmidt OG (2017) Magnetic sensing platform technologies for biomedical applications. Lab Chip 17:1884–1912

Lin C, Liu L, Liu Y, Leng J (2021) 4D printing of bioinspired absorbable left atrial appendage occluders: a proof-of-concept study. ACS Appl Mater Interfaces 13:12668–12678. https://doi.org/10.1021/acsami.0c17192

Liu X, Zhao K, Gong T et al (2014) Delivery of growth factors using a smart porous nanocomposite scaffold to repair a mandibular bone defect. Biomacromolecules 15:1019–1030. https://doi.org/10.1021/bm401911p

Liu JJ, He J, Liu JJ et al (2019a) Rapid 3D bioprinting of in vitro cardiac tissue models using human embryonic stem cell-derived cardiomyocytes. Bioprinting 13:1–15. https://doi.org/10.1016/j.bprint.2019.e00040.Rapid

Liu J, Erol O, Pantula A et al (2019b) Dual-gel 4D printing of bioinspired tubes. ACS Appl Mater Interfaces 11:8492–8498. https://doi.org/10.1021/acsami.8b17218

Lu L, Mende M, Yang X et al (2013) Design and validation of a bioreactor for simulating the cardiac niche: a system incorporating cyclic stretch, electrical stimulation, and constant perfusion. Tissue Eng - Part A 19:403–414. https://doi.org/10.1089/ten.tea.2012.0135

Lui YS, Sow WT, Tan LP et al (2019) 4D printing and stimuli-responsive materials in biomedical aspects. Acta Biomater 92:19–36

Luo Y, Lin X, Chen B, Wei X (2019) Cell-laden four-dimensional bioprinting using near-infrared-triggered shape-morphing alginate/polydopamine bioinks. Biofabrication 11:045019. https://doi.org/10.1088/1758-5090/ab39c5

Ma SQ, Zhang YP, Wang M et al (2020) Recent progress in 4D printing of stimuli-responsive polymeric materials. Sci China Technol Sci 63:532–544

Manero A, Smith P, Sparkman J et al (2019) Implementation of 3D printing technology in the field of prosthetics: past, present, and future. Int J Environ Res Public Health 16:1641. https://doi.org/10.3390/ijerph16091641

Maroni A, Melocchi A, Zema L et al (2020) Retentive drug delivery systems based on shape memory materials. J Appl Polym Sci 137:48798

Melocchi A, Uboldi M, Inverardi N et al (2019a) Expandable drug delivery system for gastric retention based on shape memory polymers: development via 4D printing and extrusion. Int J Pharm 571:118700. https://doi.org/10.1016/j.ijpharm.2019.118700

Melocchi A, Inverardi N, Uboldi M et al (2019b) Retentive device for intravesical drug delivery based on water-induced shape memory response of poly(vinyl alcohol): design concept and 4D printing feasibility. Int J Pharm 559:299–311. https://doi.org/10.1016/j.ijpharm.2019.01.045

Miao S, Zhu W, Castro NJ et al (2016a) 4D printing smart biomedical scaffolds with novel soybean oil epoxidized acrylate. Sci Rep 6:1–10. https://doi.org/10.1038/srep27226

Miao S, Zhu W, Castro NJ et al (2016b) Four-dimensional printing hierarchy scaffolds with highly biocompatible smart polymers for tissue engineering applications. Tissue Eng - Part C Methods 22:952–963. https://doi.org/10.1089/ten.tec.2015.0542

Miao S, Castro N, Nowicki M et al (2017) 4D printing of polymeric materials for tissue and organ regeneration. Mater Today 20:577–591

Miao S, Cui H, Nowicki M et al (2018a) Stereolithographic 4D bioprinting of multiresponsive architectures for neural engineering. Adv Biosyst 2:1800101. https://doi.org/10.1002/adbi.201800101

Miao S, Cui H, Nowicki M et al (2018b) Photolithographic-stereolithographic-tandem fabrication of 4D smart scaffolds for improved stem cell cardiomyogenic differentiation. Biofabrication 10:035007. https://doi.org/10.1088/1758-5090/aabe0b

Miao S, Nowicki M, Cui H et al (2019) 4D anisotropic skeletal muscle tissue constructs fabricated by staircase effect strategy. Biofabrication 11:035030. https://doi.org/10.1088/1758-5090/ab1d07

Miao S, Cui H, Esworthy T et al (2020) 4D self-morphing culture substrate for modulating cell differentiation. Adv Sci 7:1902403. https://doi.org/10.1002/advs.201902403

Mirani B, Pagan E, Currie B et al (2017) An advanced multifunctional hydrogel-based dressing for wound monitoring and drug delivery. Adv Healthc Mater 6:1700718. https://doi.org/10.1002/adhm.201700718

Miyashita S, Guitron S, Ludersdorfer M et al (2015) An untethered miniature origami robot that self-folds, walks, swims, and degrades. In: Proceedings - IEEE international conference on robotics and automation, pp 1490–1496

Montgomery M, Ahadian S, Davenport Huyer L et al (2017) Flexible shape-memory scaffold for minimally invasive delivery of functional tissues. Nat Mater 16:1038–1046. https://doi.org/10.1038/nmat4956

Morrison RJ, Hollister SJ, Niedner MF et al (2015) Mitigation of tracheobronchomalacia with 3D-printed personalized medical devices in pediatric patients. Sci Transl Med 7:285ra64. https://doi.org/10.1126/scitranslmed.3010825

Murphy SVSV, Atala A (2014) 3D bioprinting of tissues and organs. Nat Biotechnol 32:773–785. https://doi.org/10.1038/nbt.2958

Nafee N, Zewail M, Boraie N (2018) Alendronate-loaded, biodegradable smart hydrogel: a promising injectable depot formulation for osteoporosis. J Drug Target 26:563–575. https://doi.org/10.1080/1061186X.2017.1390670

Narupai B, Smith PT, Nelson A (2021) 4D printing of multi-stimuli responsive protein-based hydrogels for autonomous shape transformations. Adv Funct Mater 31:2011012. https://doi.org/10.1002/adfm.202011012

Ng WL, Lee JM, Yeong WY, Win Naing M (2017) Microvalve-based bioprinting-process, bio-inks and applications. Biomater Sci 5:632–647

Okolie O, Stachurek I, Kandasubramanian B, Njuguna J (2020) 3D printing for hip implant applications: a review. Polymers (Basel) 12:1–29. https://doi.org/10.3390/polym12112682

Okwuosa TC, Pereira BC, Arafat B et al (2017) Fabricating a shell-core delayed release tablet using dual FDM 3D printing for patient-centred therapy. Pharm Res 34:427–437. https://doi.org/10.1007/s11095-016-2073-3

Ong CS, Nam L, Ong K et al (2018) 3D and 4D bioprinting of the myocardium: current approaches, challenges, and future prospects. Biomed Res Int 2018

Park SA, Lee SJ, Lim KS et al (2015) In vivo evaluation and characterization of a bio-absorbable drug-coated stent fabricated using a 3D-printing system. Mater Lett 141:355–358. https://doi.org/10.1016/j.matlet.2014.11.119

Park G-S, Kim S-K, Heo S-J et al (2019) Effects of printing parameters on the fit of implant-supported 3D printing resin prosthetics. Materials (Basel) 12:2533. https://doi.org/10.3390/ma12162533

Patel DK, Sakhaei AH, Layani M et al (2017) Highly stretchable and UV curable elastomers for digital light processing based 3D printing. Adv Mater 29:1606000. https://doi.org/10.1002/adma.201606000

Ploszajski AR, Jackson R, Ransley M, Miodownik M (2019) 4D printing of magnetically functionalized chainmail for exoskeletal biomedical applications. In: MRS advances, vol 14, pp 361–366

Polley C, Distler T, Rüffer D et al (2019) 3D printing of smart materials for bone regeneration. Trans Addit Manuf Meets Med 1. https://doi.org/10.18416/AMMM.2019.1909S07T03

Polygerinos P, Wang Z, Galloway KC et al (2015) Soft robotic glove for combined assistance and at-home rehabilitation. In: Robotics and autonomous systems, vol 73, pp 135–143

Rider P, Kačarević ŽP, Alkildani S et al (2018) Bioprinting of tissue engineering scaffolds. J Tissue Eng 9:2041731418802090. https://doi.org/10.1177/2041731418802090

Saska S, Pilatti L, Blay A, Shibli JA (2021) Bioresorbable polymers: advanced materials and 4D printing for tissue engineering. Polymers (Basel) 13:563. https://doi.org/10.3390/polym13040563

Scafa Udriște A, Niculescu AG, Grumezescu AM, Bădilă E (2021) Cardiovascular stents: a review of past, current, and emerging devices. Materials (Basel) 14:2498

Senapati S, Mahanta AK, Kumar S, Maiti P (2018) Controlled drug delivery vehicles for cancer treatment and their performance. Signal Transduct Target Ther 3:7

Seo JW, Shin SR, Park YJ, Bae H (2020) Hydrogel production platform with dynamic movement using photo-crosslinkable/temperature reversible chitosan polymer and stereolithography 4D printing technology. Tissue Eng Regen Med 17:423–431. https://doi.org/10.1007/s13770-020-00264-6

Seyedmahmoud R, Celebi-Saltik B, Barros N et al (2019) Three-dimensional bioprinting of functional skeletal muscle tissue using gelatin methacryloyl-alginate bioinks. Micromachines 10:679

Shakibania S, Ghazanfari L, Raeeszadeh-Sarmazdeh M, Khakbiz M (2021) Medical application of biomimetic 4D printing. Drug Dev Ind Pharm 47:521–534

Shapira A, Noor N, Oved H, Dvir T (2020) Transparent support media for high resolution 3D printing of volumetric cell-containing ECM structures. Biomed Mater 15:045018. https://doi.org/10.1088/1748-605X/ab809f

Shin YC, Lee JB, Kim DH et al (2019) Development of a shape-memory tube to prevent vascular stenosis. Adv Mater 31:1904476. https://doi.org/10.1002/adma.201904476

Simińska-Stanny J, Nizioł M, Szymczyk-Ziółkowska P et al (2022) 4D printing of patterned multimaterial magnetic hydrogel actuators. Addit Manuf 49:102506. https://doi.org/10.1016/j.addma.2021.102506

Skylar-Scott MA, Uzel SGM, Nam LL et al (2019) Biomanufacturing of organ-specific tissues with high cellular density and embedded vascular channels. Sci Adv 5:eaaw2459. https://doi.org/10.1126/sciadv.aaw2459

Song Z, Ren L, Zhao C et al (2020) Biomimetic nonuniform, dual-stimuli self-morphing enabled by gradient four-dimensional printing. ACS Appl Mater Interfaces 12:6351–6361. https://doi.org/10.1021/acsami.9b17577

Stroganov V, Pant J, Stoychev G et al (2018) 4D biofabrication: 3D cell patterning using shape-changing films. Adv Funct Mater 28:1706248. https://doi.org/10.1002/adfm.201706248

Suntornnond R, An J, Chua CK (2017) Bioprinting of thermoresponsive hydrogels for next generation tissue engineering: a review. Macromol Mater Eng 302:1600266

Sydney Gladman A, Matsumoto EA, Nuzzo RG et al (2016) Biomimetic 4D printing. Nat Mater 15:413–418. https://doi.org/10.1038/nmat4544

Tamay DG, Usal TD, Alagoz AS et al (2019) 3D and 4D printing of polymers for tissue engineering applications. Front Bioeng Biotechnol 7:164

Tandon B, Blaker JJ, Cartmell SH (2018) Piezoelectric materials as stimulatory biomedical materials and scaffolds for bone repair. Acta Biomater 73:1–20

Topuz M, Dikici B, Gavgali M, Yilmazer H (2018) A review on the hydrogels used in 3D bio-printing. Int J 3D Print Technol Digit Ind 2:68–75

Uribe-Gomez J, Posada-Murcia A, Shukla A et al (2021) Shape-morphing fibrous hydrogel/elastomer bilayers fabricated by a combination of 3D printing and melt electrowriting for muscle tissue regeneration. ACS Appl Bio Mater 4:1720–1730. https://doi.org/10.1021/acsabm.0c01495

van Manen T, Janbaz S, Jansen KMB, Zadpoor AA (2021) 4D printing of reconfigurable metamaterials and devices. Commun Mater 2:56. https://doi.org/10.1038/s43246-021-00165-8

Vashist A, Kaushik A, Vashist A et al (2016) Recent trends on hydrogel based drug delivery systems for infectious diseases. Biomater, Sci, p 4

Wan X, Wei H, Zhang F et al (2019) 3D printing of shape memory poly(d,l-lactide-co-trimethylene carbonate) by direct ink writing for shape-changing structures. J Appl Polym Sci 136:48177. https://doi.org/10.1002/app.48177

Wan Z, Zhang P, Liu Y et al (2020) Four-dimensional bioprinting: current developments and applications in bone tissue engineering. Acta Biomater 101:26–42

Wang C, Zhou Y, Wang M (2017a) In situ delivery of rhBMP-2 in surface porous shape memory scaffolds developed through cryogenic 3D plotting. Mater Lett 189:140–143. https://doi.org/10.1016/j.matlet.2016.11.039

Wang C, Zhao Q, Wang M (2017b) Cryogenic 3D printing for producing hierarchical porous and rhBMP-2-loaded Ca-P/PLLA nanocomposite scaffolds for bone tissue engineering. Biofabrication 9:025031. https://doi.org/10.1088/1758-5090/aa71c9

Wang X, Qin XH, Hu C et al (2018a) 3D printed enzymatically biodegradable soft helical microswimmers. Adv Funct Mater 28:1804107. https://doi.org/10.1002/adfm.201804107

Wang Y, Miao Y, Zhang J et al (2018b) Three-dimensional printing of shape memory hydrogels with internal structure for drug delivery. Mater Sci Eng C 84:44–51. https://doi.org/10.1016/j.msec.2017.11.025

Wang YJ, Jeng US, Hsu SH (2018c) Biodegradable water-based polyurethane shape memory elastomers for bone tissue engineering. ACS Biomater Sci Eng 4:1397–1406. https://doi.org/10.1021/acsbiomaterials.8b00091

Wang C, Yue H, Liu J et al (2020) Advanced reconfigurable scaffolds fabricated by 4D printing for treating critical-size bone defects of irregular shapes. Biofabrication 12:045025. https://doi.org/10.1088/1758-5090/abab5b

Wang Y, Cui H, Esworthy T et al (2021a) Emerging 4D printing strategies for next-generation tissue regeneration and medical devices. Adv Mater 34:2109198. https://doi.org/10.1002/adma.202109198

Wang Y, Cui H, Wang Y et al (2021b) 4D printed cardiac construct with aligned myofibers and adjustable curvature for myocardial regeneration. ACS Appl Mater Interfaces 13

Wang J, Zhang Y, Aghda NH et al (2021c) Emerging 3D printing technologies for drug delivery devices: current status and future perspective. Adv Drug Deliv Rev 174:294–316

Wei H, Zhang Q, Yao Y et al (2017) Direct-write fabrication of 4D active shape-changing structures based on a shape memory polymer and its nanocomposite. ACS Appl Mater Interfaces 9:876–883. https://doi.org/10.1021/acsami.6b12824

Wen Y, Xun S, Haoye M et al (2017) 3D printed porous ceramic scaffolds for bone tissue engineering: a review. Biomater, Sci, p 5

Whitesides GM (2018) Soft Robotics Angew Chemie - Int Ed 57

Wu JJ, Huang LM, Zhao Q, Xie T (2018a) 4D printing: history and recent progress. Chinese J Polym Sci (English Ed. 36)

Wu Z, Zhao J, Wu W et al (2018b) Radial compressive property and the proof-of-concept study for realizing self-expansion of 3D printing polylactic acid vascular stents with negative Poisson's ratio structure. Materials (Basel) 11:1357. https://doi.org/10.3390/ma11081357

Yang GH, Yeo M, Koo YW, Kim GH (2019) 4D bioprinting: technological advances in biofabrication. Macromol Biosci 19:1800441

Yang Q, Gao B, Xu F (2020a) Recent advances in 4D bioprinting. Biotechnol J 15:1900086. https://doi.org/10.1002/biot.201900086

Yang GH, Kim W, Kim J, Kim GH (2020b) A skeleton muscle model using GelMA-based cell-aligned bioink processed with an electric-field assisted 3D/4D bioprinting. Theranostics 11:48. https://doi.org/10.7150/THNO.50794

Yang C, Luo J, Polunas M et al (2020c) 4D-printed transformable tube array for high-throughput 3D cell culture and histology. Adv Mater 32:2004285. https://doi.org/10.1002/adma.202004285

Yoo J, Park JH, Kwon YW et al (2020) Augmented peripheral nerve regeneration through elastic nerve guidance conduits prepared using a porous PLCL membrane with a 3D printed collagen hydrogel. Biomater Sci 8:6261–6271. https://doi.org/10.1039/d0bm00847h

You D, Chen G, Liu C et al (2021) 4D printing of multi-responsive membrane for accelerated in vivo bone healing via remote regulation of stem cell fate. Adv Funct Mater 31:2103920. https://doi.org/10.1002/adfm.202103920

Zarek M, Mansour N, Shapira S, Cohn D (2017) 4D printing of shape memory-based personalized endoluminal medical devices. Macromol Rapid Commun 38:1600628. https://doi.org/10.1002/marc.201600628

Zhang D, George OJ, Petersen KM et al (2014) A bioactive "self-fitting" shape memory polymer scaffold with potential to treat cranio-maxillo facial bone defects. Acta Biomater 10:4597–4605. https://doi.org/10.1016/j.actbio.2014.07.020

Zhang L, Yang G, Johnson BN, Jia X (2019) Three-dimensional (3D) printed scaffold and material selection for bone repair. Acta Biomater 84:16–33

Zhang L, Xiang Y, Zhang H et al (2020) A biomimetic 3D-self-forming approach for microvascular scaffolds. Adv Sci 7:1903553. https://doi.org/10.1002/advs.201903553

Zhang C, Cai D, Liao P et al (2021a) 4D printing of shape-memory polymeric scaffolds for adaptive biomedical implantation. Acta Biomater 122:101–110. https://doi.org/10.1016/j.actbio.2020.12.042

Zhang F, Wen N, Wang L et al (2021b) Design of 4D printed shape-changing tracheal stent and remote controlling actuation. Int J Smart Nano Mater 12:375–389. https://doi.org/10.1080/19475411.2021.1974972

Zhang Y, Wang Q, Yi S et al (2021c) 4D printing of magnetoactive soft materials for on-demand magnetic actuation transformation. ACS Appl Mater Interfaces 13. https://doi.org/10.1021/acsami.0c19280

Zhao Q, Qi HJ, Xie T (2015) Recent progress in shape memory polymer: new behavior, enabling materials, and mechanistic understanding. Prog Polym Sci 49:79–120

Zhao W, Zhang F, Leng J, Liu Y (2019) Personalized 4D printing of bioinspired tracheal scaffold concept based on magnetic stimulated shape memory composites. Compos Sci Technol 184:107866. https://doi.org/10.1016/j.compscitech.2019.107866

Zhao Y-D, Lai J-H, Wang M (2021) 4D printing of self-folding hydrogel tubes for potential tissue engineering applications. Nano Life 11:2141001. https://doi.org/10.1142/s1793984421410014

Zolfagharian A, Kaynak A, Bodaghi M et al (2020) Control-based 4D printing: adaptive 4D-printed systems. Appl Sci 10:3020. https://doi.org/10.3390/app10093020

Chapter 10
Lithography in Drug Delivery

Khanh T. M. Tran and Thanh D. Nguyen

Abstract Research on advanced formulations and manufacturing methods to create multifunctional drug delivery systems has been actively pursued to optimize treatment efficacies via the ability to tune release kinetics, precisely target diseased tissues/cells, accurately diagnose abnormality, and respond to environmental or external stimuli. Manufacturing methods for intelligent therapeutics and medicines have emerged to create nano- or micro-dimension systems that could mimic and harmoniously work with the body. However, there is a remaining limitation on the feasibility to create such systems with well-defined and consistent sizes, shapes, components, and functions. The application of lithographic technologies, adapted from the semiconductor industry, on pharmacy has resolved many of these problems and enabled innovative drug-delivery systems/devices for advanced disease treatment and diagnosis. This book chapter provides an overview of principles, working mechanisms, fundamental science/knowledge, and technical challenges of advanced lithography-based technologies recently used for important drug-delivery applications. Current issues in formulating drug delivery systems and essential contributions of nano/micro-lithography techniques for other biomedical applications are also discussed.

Keywords Drug delivery · Photolithography · Soft lithography · Flow lithography · Nanoimprint lithography · Drug particles · Microneedles · Implanted devices

K. T. M. Tran
Department of Biomedical Engineering, University of Connecticut, Storrs, CT, USA

T. D. Nguyen (✉)
Department of Biomedical Engineering, University of Connecticut, Storrs, CT, USA

Department of Mechanical Engineering, University of Connecticut, Storrs, CT, USA
e-mail: nguyentd@uconn.edu

D. Lamprou (ed.), *Nano- and Microfabrication Techniques in Drug Delivery*,
Advanced Clinical Pharmacy – Research, Development and Practical Applications 2,
https://doi.org/10.1007/978-3-031-26908-0_10

10.1 Introduction

Many therapeutic agents struggle with a significant challenge in achieving desired bioavailability because of their unfavorable physicochemical and biopharmaceutical properties leading to biodegradation and rapid systemic clearance. Along with the emergence of new biomaterials, designing compatible delivery systems that imitate and synergistically function with the nature of the human body presents an appealing approach to enhance overall treatment efficiencies. "Intelligent" therapeutics, created by new manufacturing methods, have emerged to provide unique release profiles and better systemic circulation of drugs, bypassing natural barriers, targeting desired cells/tissues, diagnosing diseases, and responding to environmental stimuli (Anselmo and Mitragotri 2016). Current attempts have involved using polymers and lipids with chemical moiety modification to form nanoparticles through cross-linking, emulsion-based, self-assembly, and dispersion methods. Nanoparticles with an extremely small volume and increased surface area have been known to improve penetration across different biological barriers and avoid rapid clearance by the phagocytic system, thus prolonging therapeutics circulation and persistence in the bloodstream. Additional surface-modified factors, including targeted ligands, ionic properties, pH, and temperature sensitivity, can modulate release mechanisms and provide these nanocarriers with controlled release and high specificity (Mitchell et al. 2021). Besides formulating nanotherapeutics, increasing trends in designing and manufacturing implantable drug delivery systems (DDSs) with micro- or nanochannels for controlled release have been observed, especially for delivering large macromolecules with high dosage (Martin and Grove 2001). Carriers' structural and functional design strongly impacts the fate of encapsulated prophylactic and therapeutic agents in the human body. However, the ability to create DDSs at small scales with desired morphologies, components, and functionalized properties remains a compelling challenge. The convergence of lithography-based methods used in the semiconductor industry and drug delivery field has offered exciting opportunities to achieve new DDSs with high controllability over the architecture and release kinetics, essential for therapeutic efficacy.

Lithography is a micro- and nano-fabrication technique to create precise and complex two- or three-dimensional structures at micro- or nanoscales. The technology originated from a planographic printing method using smooth surfaces of a plate or stone invented by Alois Senefelder, a Bavarian author, in 1976 (Senefelder 1911). Lithography plays an undeniable key role in the electronics field by enabling the mass production of complicated electronic components such as semiconductors and integrated circuits (Thompson 1983). Despite the great potential of patterning nano- and micro-sized structures, the early twentieth century has seen limited lithography applications in biomedicine and related fields. High cost, complex operation, and unique facility requirements prevented the accessibility of lithography to scientists. Later, increased access to fabrication tools and clean-room facilities in many research institutes has facilitated significant growth and applications of lithography. The progress became a vital driving force to expand lithography implementation,

especially in the biomedical areas with the introduction of bio-microelectromechanical systems (Bio-MEMS), nanoelectromechanical systems (NEMS), microfluidics, biophotonics, biooptics, and multifunctional implanted devices. The advanced techniques to create well-defined morphology and structures at small scales present unique opportunities to produce intelligent therapeutics. Subsequently, there is a rising interest to further explore lithography-based approaches' applications. This chapter will explore different lithography techniques and provide an overview of their basic principles, unique advancements, and broad applications in drug delivery.

10.2 Basic Principles, Challenges, and Different Lithography Technologies Applied in Drug Delivery Systems

10.2.1 Photolithography

10.2.1.1 Basic Principles of Photolithography

Photolithography is an optical lithography process that uses light exposed through an optical mask to transfer a pattern onto a solid substrate pre-coated with photosensitive polymeric materials called photoresists (Moreau 2012). The optical mask (photomask), which defines fabricated features, is typically composed of opaque patterns usually made from chrome or iron oxide and printed on a transparent support (quartz). Although fabrication protocol and materials may be altered to meet specific applications, photolithography largely includes a basic set of standard procedures (Fig. 10.1a). Since photolithography produces micro- and nano-sized structures, the operation requires an environmentally controlled clean-room facility that strictly regulates airborne particulates, temperature, air pressure, humidity, vibration, and lighting. To begin with, the surface of a solid substrate like silicon wafers must be free from contaminants, including solvent stains, atmospheric dust, microorganism, aerosol particles, etc. The ultraviolet (UV)-sensitive photoresist is then dispensed and uniformly spread onto the solid substrate using a spin coater. The thickness of the coated photoresist directly corresponds to the thickness of fabricated structures, which is determined by a function of its intrinsic viscosity, concentration, and spin speed. After spin coating, the substrate is soft-baked at 75–100 °C to eliminate solvents in the photoresist, reduce built-in stresses, and promote adhesion. Next, the combination of consecutive photomask alignments and light exposures forms complex, multilayered structures. Upon light exposure, the photoresist undergoes a radiation-induced solubility change or curing process, which is a fundamental principle to transfer micro- and nanoscale patterns to the substrate. A photoresist's solubility changes when exposed to UV light, which correlates to increased and decreased solubility for positive and negative photoresists, respectively. Hence, opaque patterns on the photomask will indicate remaining features on

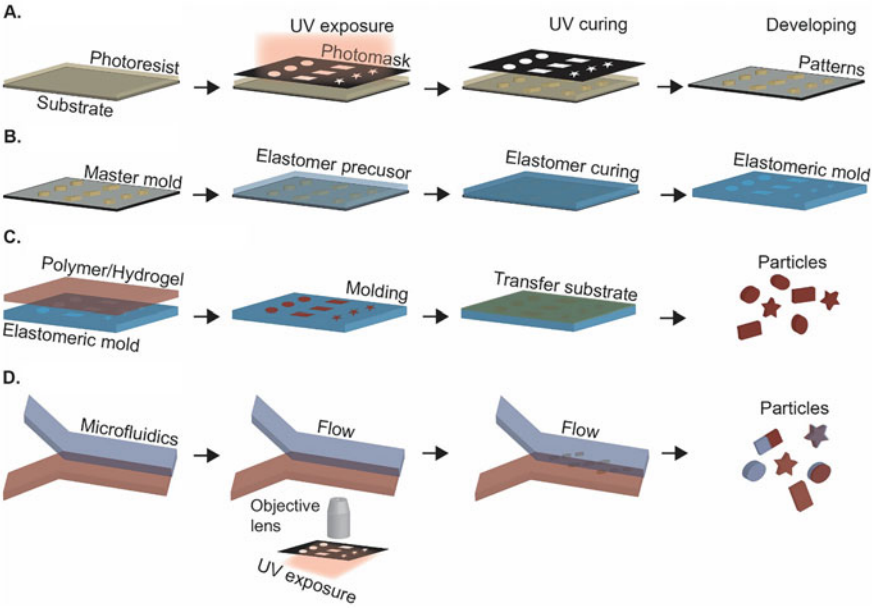

Fig. 10.1 Schematics of lithography-based technologies applied in drug delivery. (**a**) Photolithography, (**b**) soft lithography, (**c**) nanoimprint lithography, (**d**) flow lithography

the substrate for positive resists. For negative resists, on the other hand, clear patterns will be the remaining features. Post-exposure treatment is often necessary to ensure the initiated chemical reaction could run to the desired completion. This involves stopping the current reaction or inducing another one. Some usual methods are baking, flood exposure with other radiations, vacuum treatment, and reactive gas treatment. The developing process starts with selective photoresist removal using solvents (wet development), plasma (dry development), and gasses. Aqueous alkaline solutions containing diluted sodium hydroxide and potassium hydroxide or aqueous solutions containing free metal ions of organic TMAH (tetramethylammonium hydroxide) are generally used for both types of photoresists. After solvent development, an oxygen plasma treatment, an optional step, employs highly energetic oxygen ions to react and remove unwanted photoresist residuals. Finally, post-baking (hard baking) at approximately 120 °C enhances interfacial adhesion, hardens the structures, and, most importantly, removes trace solvents from previous steps.

Photolithography has rapidly matured with continuous improvements to realize higher feature resolution. Feature size can be controlled by scaling the wavelength of radiation. Reducing the wavelength of radiation could reduce the refraction limit and produce even smaller size features. To accommodate shorter wavelengths (e.g., deep UV light or soft X-rays), the challenge was to improve the absorption and sensitivity of photoresists as much as possible because of typically weak light sources. In the 1980s, IBM pioneered a revolutionary process named “chemical amplification” to

maximize photon use by introducing a small quantity of light-activated acid catalyst compounds into photoresists, thus enhancing the efficiency of light utilization (Ito 1997). However, the acid diffusion limits the resolution of the chemical amplification method to around 30 nm. Still, light-activated acid catalysts are present in most current standard photoresists because of the superior solubility contrast between exposed and unexposed areas. Studies on new resist materials and cross-linking mechanisms are actively under investigation (Bratton et al. 2006).

The search for new strategies to successfully pattern complex features on photoresists continues with the development of advanced exposure methods. Laser-based direct writing systems are particularly attractive for 3D microfabrication. Two-photon polymerization or two-photon lithography has built a reputation in constructing well-defined, free-standing 3D micro-nanostructures with a high spatial resolution (Harinarayana and Shin 2021). When exposing a material to ultrafast laser beams, high power density and short laser-matter interaction time result in rapid photon energy transfer, which generates nonlinear absorption effects and features beyond the diffraction limit. The resolution linearly correlates to scanning speed at a defined laser power range. This unique two-photon lithography method provides remarkable resolution and is highly applicable to various materials.

10.2.1.2 Challenges of Photolithography in Drug Delivery

Photolithography is a high-throughput manufacturing process that could produce small-scale patterns with high complexity and precision. Photolithography is the core technology for the field of electronics and becoming more popular in biomedical applications. In this approach, the desired structure is fabricated and utilized as a master mold. While holding those great values, the high cost of photolithography is a significant disadvantage. A high-end vibration-free alignment system, light sources, materials, and clean-room facilities are factors driving up the overall costs. Complicated structures may require extensive prototyping and designing. Additionally, the materials used for this technique are not suitable for direct applications in biological systems because of their toxicity and incompatibility. Photolithography has relatively little use for materials other than photoresists. Modification procedures involving the attachment of chromophores or adding photosensitizers are inconvenient and unfavorable. The rigid structure and substrate give little room for manipulating surface chemical properties and implementations on curved/nonplanar surfaces. Rigorous manufacturing steps such as cleaning, baking, and UV exposure are not favorable for biomaterials. Nevertheless, photolithography has established an essential foundation for further developing other advanced microfabrication methods, which will be discussed in the following sections.

10.2.2 Soft Lithography

10.2.2.1 Basic Principles of Soft Lithography

Photolithography has offered powerful tools to fabricate well-defined solid master templates/molds, which can be used to create replicable biomaterial nano- or microstructures for applications in drug delivery. To improve the compatibility with biomaterials, scientists have developed an alternative set of microfabrication methods to convert and adapt those rigid templates/molds for "soft-matter" (i.e., organic materials, polymers, complex biochemical agents, etc.) manufacture (Fig. 10.1b). The master mold/template structures patterned from lithographic methods, like photolithography and electron beam lithography or micromachining, will be replicated onto elastomeric materials by an essential soft lithography process known as micro-transfer molding (Xia and Whitesides 1998). This technology prepares an elastomeric stamp commonly made from polydimethylsiloxane (PDMS) by cast molding. The master is first exposed to a chemical vapor of chlorosilane in a process called silanization for enhancing surface hydrophobicity, which facilitates molding and release. A liquid prepolymer of the elastomer mixed with the curing agent is degassed and poured over the master. When heating at elevated temperatures, solidification occurs under cross-linking of elastomer via hydrosilylation reaction between vinyl and hydrosilane groups. Elastomers are excellent mold materials because they have conformal contact with most surfaces over relatively large areas and can also be easily released from a complex-rigid 3D master being molded. Based on soft lithography, some well-studied patterning techniques developed for biomaterials are solvent-assisted micromolding (SAMIM), microcontact printing (mCP), nanoskiving, replica molding (REM), phase-shifting edge lithography, and decal transfer lithography. Collectively, these techniques present powerful, scalable patterning capabilities and experimental simplicity, making them suitable for a wide range of applications.

10.2.2.2 Challenges of Soft Lithography in Drug Delivery

The main advantage of soft lithography is mass production. From one master template, hundreds or thousands of copies can be quickly replicated. Soft lithography possesses greater versatility in materials and processing approaches as compared to silicon-based microfabrication. The elastomer of PDMS used in the process has low surface interfacial energy in addition to good chemical and thermal stability. Thus, PDMS is compatible with many biomaterials since molded parts do not adhere or react and can be easily harvested. However, this technique is limited in the structural design of the master structure. Another main drawback is the PDMS mold/stamp deformation encountered during micro-transfer molding since PDMS is an elastic material. Similarly, the elastomer properties need optimization to make pattern transfer more accurate, especially for nano-size features. Moreover,

closed-loop or core-shell structures are not replicable by micro-transfer molding in a single step. Additional additive manufacturing and layer-by-layer fabrication approaches are needed to create those structures via micro-transfer molding. The ability to generate DDSs with multifunctional or complex chemistries remains a challenge for soft lithography.

10.2.3 Nanoimprint Lithography

10.2.3.1 Basic Principles of Nanoimprint Lithography

Nanoimprint lithography is a procedure to transfer nano-patterns from a rigid mold to other materials (Guo 2007). Most of the popular imprint techniques were based upon thermal induced mechanical deformation or a UV-curing process. There are two basic steps in nanoimprint lithography (Fig. 10.1c). In the first step, the prefabricated mold with an inverse of desired nanostructures is heat-pressed (thermal nanoimprint) onto a thermoplastic polymer at its glass transition temperature or dipped into a liquid photoresist (UV-based nanoimprint). For thermal nanoimprint, also known as hot embossing, when heating the polymer at elevated temperatures, it will become soft and enter a molten phase. With adequate applied pressure, the polymer can fill in empty cavities on the mold. As the temperature is lowered, the polymer returns to its solid stage. Followed by removing the mold, the structures are duplicated onto the polymeric film. The UV-based nanoimprint, which is carried out at room temperature and low pressure, employs a similar principle (Bender et al. 2000). The UV-transparent mold is imprinted onto the substrate coated with UV-curable resist. After exposure, the precursor resist cross-links and produces stable patterns. One needs to consider the compatibility of the mold material with microfabrication process or targeted applications, hardness, durability, and thermal expansion coefficient of the material. Some common candidates for the mold materials are Si, SiO_2, metals, silicon nitride, sapphire, etc. In the second step of nanoimprint, an anisotropic etching process (i.e., reactive ion etching) removes the residual materials in the compressed regions, which completes the pattern transfer. Chou et al. have demonstrated that imprint lithography can achieve nano-sized feature (25–70 nm) with high uniformity and reproducibility (Chou et al. 1996). Nanoimprint lithography contributes a versatile and cost-efficient solution to obtain high-quality and precise nanostructures and establish a foundation for the direct patterning of biomaterials.

Among several advanced nanoimprint lithography methods, particle replication in nonwetting templates (PRINT) offers a unique soft imprint lithography technology for mass production of shape- and size-specific micro- and nanoparticles (Merkel et al. 2010; Rolland et al. 2005). The key principle of PRINT is the implementation of a highly hydrophobic perfluorinated polyether elastomer (PFPE) as the mold material instead of PDMS (Rolland et al. 2004) to avoid any residual/scum layer after the nano-molding process. After imprinting on a solution or

a material of interest, the liquid material filled into the mold cavities is further converted into solid form through cross-linking or solvent evaporation. PRINT allows direct fabrication of monodisperse particles in the absence of a flash or residual scum layer. The array of molded particles can then be removed by transferring onto a dissolvable adhesive layer. The PRINT technique allows a great control over the shape, size, matrix, surface chemistry, and modulus of the molded drug nanoparticles, which are essential parameters for therapeutic design.

10.2.3.2 Challenges of Nanoimprint Lithography in Drug Delivery

Nanoimprint lithography has made essential contributions to the field of drug delivery with its simplicity, efficiency, high production rate, and low cost. Still, there are rooms for further technological improvements. Currently, the shape and size of particles heavily rely on expensive master templates. And it is not feasible to manufacture particles with various aspect ratios from the same nanoimprint templates. Although nanoimprints could produce billions of distinct particles in a single patterning step, their geometries are limited to 2D extrusions. Difficulty producing a sufficiently thin uniform precursor layer of material may result in an excessive residual layer on the mold surface, leading to interconnected particles. On the same note, using a low-surface-energy mold, removing particles after fabrication could be challenging, influencing overall fabrication yields.

10.2.4 Flow Lithography

10.2.4.1 Basic Principles of Flow Lithography

The demand for custom-shape colloidal micro- and nanoparticles remains high in the field of drug delivery. Particle shape strongly influences the dynamics and interaction with the biological environment. And by tuning colloid chemistry, different properties of drug particles such as release profile, responses to stimuli, targeting, and functionality can be engineered. With the development of high-throughput microfluidic-based technology, continuous flow lithography (CFL) has been investigated to synthesize monodisperse 2D microparticles (Dendukuri et al. 2006) (Fig. 10.2). CFL was constructed on a one-phase system containing a microscope projection photolithography and a microfluidic channel (Fig. 10.1d). As the oligomer solution carrying photoinitiator travels through the microfluidic channels, microparticles are formed by UV light cross-linking. The size, shape, and anisotropy of synthesized microparticles are precisely controlled using microscopic projection through the photomasks. Continuous laminar flow allows high-throughput production of complex, multifunctional, and chemically anisotropic microparticles. One disadvantage of this technology is particle deformation and restricted resolutions due to the high fluid flow rate.

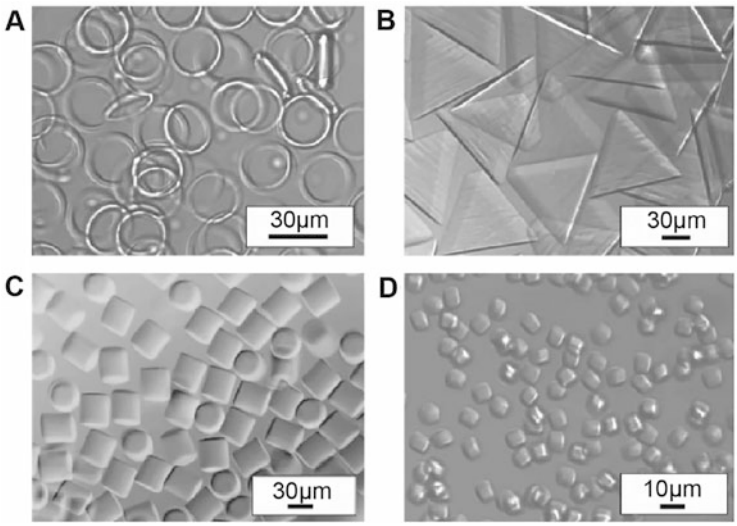

Fig. 10.2 Particles were generated using continuous flow lithography. (**a**) Rings formed using a 9.6-μm high channel and the ×20 objective. (**b**) Triangles formed in a 38-μm high channel using a triangular mask and the ×20 objective. (**c**) Cylinders synthesized using circular masks in 38-μm high channels using the ×20 objective. (**d**) Colloidal cuboids were synthesized using a square mask and the ×20 objective in a 9.6-μm high channel. Republished with permission from Springer Nature BV, from (Dendukuri et al. 2006); permission conveyed through Copyright Clearance Center, Inc.

On the basis of CFL, stop-flow lithography (SFL) was exploited as an automated semicontinuous process. The first SFL attempt was proposed by Doyle et al. to fabricate freely floating colloidal particles. In SFL, the flow of the oligomer stream is stopped by using a computer-controlled three-way solenoid valve. Then an array of particles is synthesized in the stopped oligomer stream by UV light exposure. After microparticles are formed, the three-way valve is opened. And particles are collected by being flushed out at a high flow rate. SFL has provided particles with sharper and more distinct interfaces between sections compared to CFL. Better resolution (down to 1 μm) and 1000 times higher throughput were also achieved. Yet most flow lithography methods are limited to 2D extruded shapes. Recent approaches have introduced a third dimension of geometric control. The Pisignano group has proposed a method integrating a highly localized two-photon lithography process to a CFL system (TP-CFL) (Laza et al. 2012).

10.2.4.2 Challenges of Flow Lithography in Drug Delivery

Since flow lithography relies on a projection photolithography technique, its fundamental limitation is governed by the optical resolution and the depth of field of the microscope objective. Synthesizing submicron-sized particles is still challenging due to the presence of an oxygen lubrication layer (about 1 μm) on the inner PDMS

channel, which only allows particle size around the micrometer range. Furthermore, the complexities of 3D microparticles are constrained by microfluidic channel topography and minimum printable feature size on the photomask. Although the TP-CFL technique allows 3D manufacturing, the fabrication rate is limited due to slow 3D positioning of the writing spots and constrained particle shapes generated by continuous laser scans. Another flow lithography technology known as inertial flow shaping provides a way of constructing 3D particles (Paulsen et al. 2015). Still, particle geometry depends on axial features, which must be extensively modeled and designed by complex microfluidic flow profiles. Current approaches require using UV-curable materials (some of which have unknown biological safety profiles) and permit a finite polymerization time. Consequently, future improvements in flow lithography are needed to realize micro- and nanoparticles with more controlled properties such as customized shapes, multifunctionalities, and applicability to wider materials/therapeutics of choice.

10.3 Applications of Lithography in Manufacturing Drug Delivery Systems

10.3.1 Fabricating Injectable Drug Particles

Particles ranging from a few nanometers to hundreds of microns have served many purposes in drug delivery. Besides encapsulating and delivering therapeutics, they could operate as intracellular biosensors or contrast agents for imaging. Key factors affecting the efficacies of these carriers are particle size, surface chemistry, mechanical properties, and permeability (Mitragotri and Lahann 2009). Petros and DeSimone have extensively discussed different strategies when designing nanotherapeutics (Petros and Desimone 2010). Conventional formulation techniques such as self-assembly, emulsion, spray drying, and grinding typically result in spherical particles with non-uniformity, large size distributions, and limited control over surface and mechanical properties. Thus, significant interests in creating particles of different anisotropic shapes have grown remarkably. Particle shape dictates transport and interaction of particles in the body by influencing particle dynamics, adhesion and diffusion to the blood vessel wall, and cellular uptake (Ilium et al. 1982). The particle shape also partially determines the degradation rate, the release profile of encapsulated agents, and targeted properties. Other unique advantages of modulating particle shape are to enhance (1) resistance to blood shear stress, (2) responses to external triggers, and (3) potential optical behaviors. Micro- and nanofabrication techniques have offered an exceptional solution to large-scale manufacturing of particles with high fidelity, diverse shapes, and multifunctionalities.

Projection photolithography techniques allow one to make particles with various shapes by altering the features on the photomask. Using photolithography, direct

patterning of biomaterials is feasible by adding a photoinitiator and a cross-linking agent into a monomer or reactive polymer precursor (Helgeson et al. 2011). Top-down microfabrication approaches such as photolithography, thin film deposition, photoablation, and etching can create porous silicon particles for drug delivery. Interests have been put on using these particles in the systemic administration of the cytotoxic drug for treating metastatic tumors (Wang et al. 2015). Besides containing pores for drug loading, such particles can be chemically modified with proteins, targeted ligands, and imaging modalities for multifunctional properties. However, particles with sizes ranging from 2 to 5 μm could accumulate in organs. Long-term safety effects remain to be further investigated (Ferrari 2005).

Soft lithography-based techniques have been widely studied to fabricate polymeric microparticles for drug delivery. These techniques are much more versatile than conventional methods in adjusting particle size and shape while being less expensive and requiring milder processing conditions than photolithography. They are also compatible with many materials and processing approaches. For example, Guan et al. have modified and implemented soft lithography methods to produce microparticles made from three different polymers: PLGA, chitosan, and poly (PEGMA-*co*-PEGDMA) (Guan et al. 2006). Based upon nanoimprint lithography, PRINT particles have been loaded with chemotherapeutics, magnetic resonance contrast agents, and fluorophores for cancer nanotheranostics (Fig. 10.3) (Perry et al. 2011). The surface properties of the particles can be functionalized with multiple moieties such as "stealth" poly(ethylene glycol) (PEG) chains to increase systemic circulation, targeting ligand for targeted delivery, or radiolabels for imaging, etc. Overall, these micro- and nanofabricated particles have demonstrated enormous potential for nanomedicine and diagnostics applications.

Flow lithography has introduced many attempts to produce shape- and size-specific particles with complicated matrix chemistry and multifunctionality. Researchers from the Doyle group have invented a new method named hydrodynamic focusing lithography, which harnesses flow focusing on generating stacked flows in several layered channels (Bong et al. 2010). In this method, monomer streams are combined in both y and z directions, resulting in complex dual-axis multilayer particles. The throughput of multifunctional particle synthesis has increased over 200 times compared to stop-flow lithography.

McHugh and Nguyen have introduced an additive manufacturing approach combining the technology used for computer chip fabrication with soft lithography and an aligned sintering process, termed StampEd Assembly of polymer Layers (SEAL), to produce small ($\leq$400 μm) polymeric structures (Mchugh et al. 2017). SEAL is a bottom-up, high-resolution technique to generate microdevices with complex geometries. It applies to broad commercially relevant biomaterials. Based on heat sintering and 3D assembly of different components, SEAL enables the fabrication of microstructures for thermoplastic materials without additional additives. By changing the properties of the polymer (i.e., molecular weight and composition), the degradation rate of the microparticle material can be adjusted; hence, the cargos in the internal reservoir can burst out at multiple desired times. SEAL has demonstrated great potential in delivering multiple vaccine doses by a single

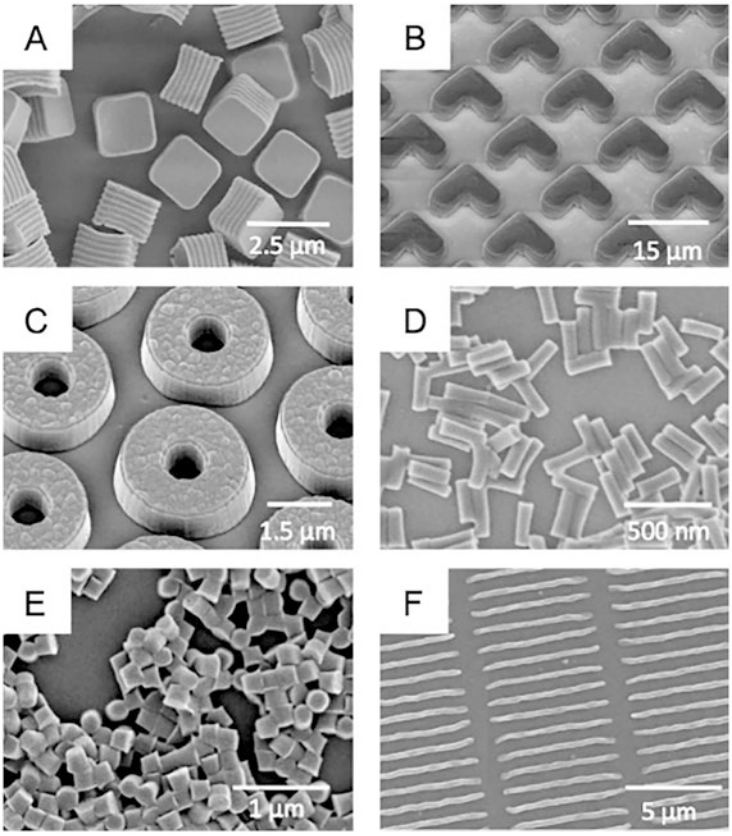

Fig. 10.3 Scanning electron micrograph images of particles fabricated using the PRINT method: (**a**) degradable 2-μm cubic particles; (**b**) 10-μm magnetic hydrogel boomerangs; (**c**) 3-μm hydrogel toroids; (**d**) 100 × 300 nm hydrogel rods; (**e**) 200-nm cylindrical hydrogel; (**f**) 80 × 2000 nm filamentous hydrogel particles. Reprinted with permission from Perry et al. (2011). Copyright 2011 American Chemical Society

administration, mimicking the immunogenic effect of multiple bolus injections in the traditional vaccination process. On the same note, the Langer group has discussed on characteristics and applications of micro-reservoir devices for drug delivery (Grayson et al. 2004).

The flexibility of lithography-based techniques has been employed to design DDSs to address several barriers related to oral drug uptake. Specifically, micro- and nanodevices with planar and asymmetric structures have enhanced adhesion and unidirectional drug release toward epithelial tissue, prolonging drug exposure and permeation. Additional surface modification, topography customization, permeation enhancers, pH-responsive release, and motion responses can further enhance uptake efficacy. Fox et al. have thoroughly reviewed current and developing technologies on these microfabricated platforms to increase the bioavailability of oral drugs and

biotherapeutics (Fox et al. 2015). Other noticeable strategies to produce small-sized drug particles by lithography for different applications are summarized in Table 10.1.

10.3.2 Fabricating Skin Microneedle Patch

The traditional hypodermic needle has provided a rapid way to directly inject almost any type of biomolecules into the human body. However, the hypodermic needle is not favorable in many means (Kim et al. 2012). It typically requires trained personnel to administer a dose. Patients either travel to the clinic or receive extensive training on injection methods, which also cause sharp biohazard wastes and other issues. Pain, discomfort, and poor compliance are limitations associated with hypodermic needles, especially for patients with needle phobia. Other needle and syringe-related safety problems such as needle reuse and the spread of blood-borne pathogens are significant concerns. Alternative delivery routes like oral administration, which could overcome these problems, are not applicable to many drugs due to poor absorption and drug degradation. Instead of avoiding needles, scientists have scaled their size and geometry to micron dimensions and introduced a revolutionized system known as microneedle (MN). As at a micron scale, the microneedle should be sufficiently large to deliver almost any drug formulations but still possess a sufficiently small penetration tip and overall structure to avoid any patient incompliances, related to the traditional hypodermic needles mentioned above. MN allows highly localized transport of drug molecules, macromolecules, proteins, and fluids to target not only the skin but also the eye, cell nucleus, gastrointestinal tract, and other mucosa walls.

MN technology has been recognized as a pioneering approach to effectively deliver therapeutics across the skin barrier. By piercing past the skin in a minimally invasive manner, MNs generate micro-dimensional pathways for drug diffusion through the viable epidermis to blood capillaries. On the other hand, transdermal delivery has been recognized as a promising delivery route for prophylactic and therapeutic agents. It could provide a steady drug concentration in plasma, bypass hepatic first-pass metabolism, limit systemic exposure, and potentially provide a direct drug application to an affected site in some instances (Prausnitz and Langer 2008). Yet the major challenge for transdermal delivery is the presence of the skin stratum corneum (SC) layer that protects and regulates foreign entry into the body. SC mainly permits access of lipophilic and low weight molecules. Conventional efforts focused on in situ topical formula, particularly gels and creams, suffer from inadequate drug retention and absorption, frequent dosing requirement, and cosmetic visibility on skin (Singh Malik et al. 2016).

Although being first conceptualized many decades ago, the field of microneedles has only begun to rapidly evolve in the mid-1990s with the accompany of the lithography technology. In 1998, Henry et al. reported the first MN production using a lithography-based method named deep reactive ion etching (Henry et al. 1998). Briefly, on a silicon wafer, arrays of circle dots made of a chromium masking

Table 10.1 Examples of therapeutic particles produced by lithography-based technologies

	Materials	Therapeutic cargo	Lithography methods	Size	Properties	References
1	Porous silicon particles (pSi)	Cancer therapeutic and immunotherapy	Porosification and photolithography	400 nm, nanopore sizes (5–150 nm), and 30–90% porosity	Diverse geometries, controlled porosity, modifiable surface functionalities	Savage et al. (2013)
2	Polystyrene beads and silica colloids	Cells and vesicles	Physical templating (via photolithography) and capillary forces	150 nm in diameter	Complex aggregates of monodispersed colloids with well-defined sizes, shapes, and structures	Yin et al. (2001)
3	Poly(ethylene glycol) diacrylate (PEGDA)	3D tissue constructs for drug delivery	Stop-flow lithography	100 μm	Continuously generate viable cell-laden hydrogel micro blocks	Panda et al. (2008)
4	PEGylated cationic hydrogels	Small interfering RNA (siRNA)	PRINT	200 × 200 nm cylindrical dimension	Size, shape, composition, surface chemistry, and modulus controls	Dunn et al. (2012)

material were deposited. The diameter of these dots was equal to the bases of patterned MNs. After loading the silicon wafer into a reactive ion etching system, fluorine/oxygen plasma was attentively applied to deeply etch high aspect ratio valleys into the wafer, which resulted in the formation of arrays of sharp MNs. In vitro testing of human skin using the Franz cell model showed a significant enhancement in calcein permeability across the skin by as much as 10,000-fold. Preliminary studies in human subjects demonstrated that the skin could be safely permeabilized and holes generated by MNs could be re-sealed without causing pain and irritation. The microfabrication method used here was considered to be simple, inexpensive, and suitable for mass production. Technological advancements in lithography have nourished the expansion of MN fabrications and applications in drug delivery. Photolithography, especially high-resolution two-photon, provides an excellent tool for a direct patterning of MNs with complex geometries or master templates for replication. A review by Gittard et al. described fabrications of in-plane MNs, out-of-plane MNs, and mosquito fascicle-shaped and rocket-shaped MNs out of polyethylene glycol diacrylate containing silver, gemcitabine, or quantum dots for antimicrobial treatment (Gittard et al. 2010). An effort to create MNs with sharp tips has been made by inclined UV lithography in which light is exposed on the photoresist-coated substrate at calculated angles (Sato et al. 2006). Another method called magnetorheological drawing lithography by Chen et al. offered a fast fabrication of solid MN arrays. In this work, a 3D structure was drawn in one step from the droplets of curable magnetorheological liquid and subsequently solidified to maintain its shape under an external magnetic field (Chen et al. 2019). Since MNs' role is to carry or transport therapeutic cargos which could be sensitive and delicate to handle, photolithographic and etching processes are not applicable in many cases. Soft lithography and imprint lithography have presented alternative solutions (Fig. 10.4) (Moga et al. 2013; Elahpour et al. 2021). In these approaches, the master MN structures are replicated onto elastomeric molds. Biomaterials are then solvent-casted or compression-molded followed by evaporation, cross-linking, or phase changes to form solid-state MNs ready for skin administration.

MNs are generally categorized into four groups: (1) solid MN for skin pretreatment (micropores forming) before therapeutics application, (2) coated MN with a layer of drug coated onto solid MN and dissolves off in the skin, (3) polymeric MN that encapsulates drugs in its matrix and fully degrades or dissolves in the skin, and (4) hollow MN for drug infusion from an external reservoir into the skin. To meet different delivery requirements, scientists have diversified MN designs from the above four main categories, besides altering drug formulations (Fig. 10.5). Yang et al. have reported statistical analysis on MN publications from 2010 to 2020 (Yang et al. 2021). Some noticeable applications of MN are described in Table 10.2.

MN has drawn remarkable interests in vaccine delivery and become one of the most widely studied subjects. The epidermal and dermal tissues on the skin contain a high number of immune cells, thus being good sites for immunizations (Mikszta and Laurent 2008). MN not only offers a reliable and simple method for vaccination via the skin but also could facilitate global vaccine distribution and administration.

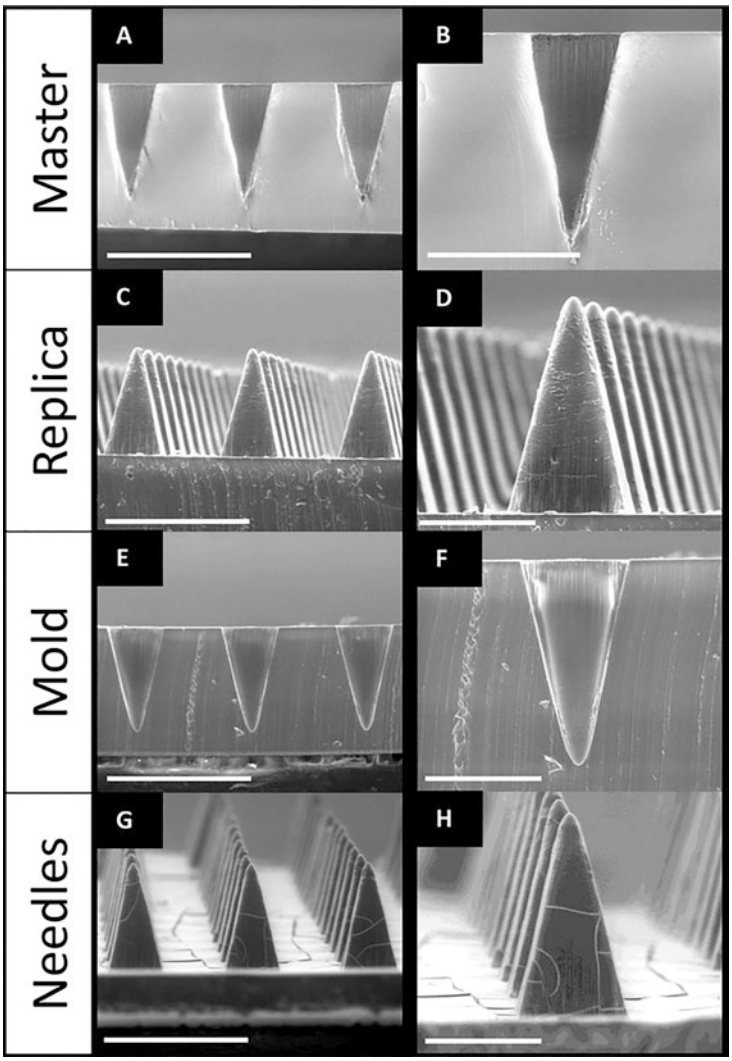

Fig. 10.4 Soft lithography and nanoimprint lithography processes. Scanning electron micrograph images of (**a**, **b**) SU-8 Master template, (**c**, **d**) PDMS template, (**e**, **f**) PFPE mold, and (**g**, **h**) PVP microneedles. Needles show comparable lengths and tip diameters. Scale bars for A, C, E, and G are 500 μm. Scale bars for B, D, F, and H are 200 μm. Republished with permission from John Wiley & Sons - Books, from Moga et al. (2013); permission conveyed through Copyright Clearance Center, Inc.

Multiple demonstrations have been conducted accordingly by investigating different types of MN for deliveries of diphtheria toxoid (Ding et al. 2009) and recombinant anthrax (Mikszta et al. 2005), hepatitis B (Qiu et al. 2016), rabies (Laurent et al. 2010), and influenza vaccines (Sullivan et al. 2010). Moreover, vaccines are

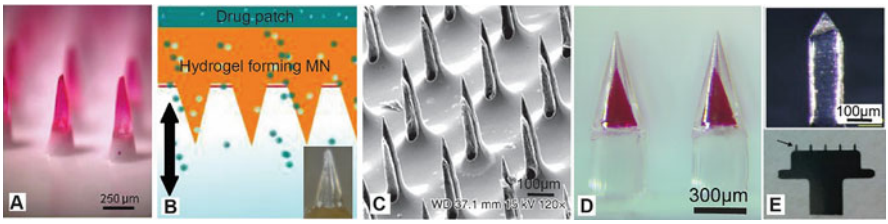

Fig. 10.5 Illustrations of different MN designs. (**a**) Dissolving MN patch for influenza vaccination. Republished with permission from Springer Nature BV, from Sullivan et al. (2010); permission conveyed through Copyright Clearance Center, Inc. (**b**) Hydrogel-forming MN with antimicrobial properties. Reprinted from Donnelly et al. (2013), Copyright (2013), with permission from Elsevier. (**c**) Hollow MN for minimally invasive diagnostics. Reprinted from Li et al. (2019), Copyright (2019), with permission from Springer Nature. (**d**) Core-shell MN for pulsatile release of vaccines. Republished with permission from Springer Nature BV, from Tran et al. (2021); permission conveyed through Copyright Clearance Center, Inc. (**e**) Stainless steel MN coated with a stabilized measles vaccine. Reprinted from Edens et al. (2013), Copyright (2013), with permission from Elsevier

typically given in multiple doses, which cause logistic burdens to medical facilities and low patient compliances (Hutin and Chen 1999). Most reported works on vaccine MN patches have been designed to perform an immediate delivery of vaccine antigens, which requires additional booster administrations. Hence, there is a need to develop a transdermal MN system for programmable multiple delayed burst releases over long periods of time to simulate the multiple bolus injections in the traditional vaccination process. This requires a manufacturing technology being capable of creating MNs with core-shell or reservoir-based microstructures, which provide pulsatile releases with desired lag times to mimic the pattern of multiple injections. To this end, Tran et al. have introduced an additive manufacturing procedure that combines different lithography-based methods to create a biodegradable polymeric core-shell MN structure for multi-dose vaccine delivery via a single administration (Tran et al. 2021). Moreover, increasing interests in using MN for mediating vaccine delivery through the oral mucosa have been noted lately (Creighton and Woodrow 2019).

Lithography has enabled MN fabrication from multiple materials for both local and systemic delivery of a wide range of drugs, vaccines, biotherapeutics, and theranostic agents (Prausnitz 2004). Many works are now transitioning from pre-clinical to clinical trials in human and have been extensively reviewed in literatures (Ingrole et al. 2021; Bhatnagar et al. 2017). Li et al. have recently summarized progresses of several clinical trials on MN (Li et al. 2021). Building off a strong technological foundation, MN is sought to advance further into clinical practice to serve several treatment purposes. MN is one of the most highlighted contributions of lithography technologies in biomedicine.

Table 10.2 Examples of MNs for a broad variety of biomedical applications

Route	Application	Features	MN type	Materials	Methods	References
Skin	Diabetes	On-demand delivery of antidiabetic drugs	Dissolving MN	Cu_7S_4 nanocrystals (NPs); lauric acid and polycaprolactone (LA/PCL); poly(vinyl alcohol) and polyvinylpyrrolidone (PVA/PVP)	Soft lithography	Zhang et al. (2018)
		Glucose-responsive MN for the delivery of antidiabetic drugs	Dissolving MN	Hypoxia-sensitive hyaluronic acid encapsulating insulin and glucose oxidase	Soft lithography	Yu et al. (2015)
	Skin interstitial fluid (ISF) and blood sampling	In vivo biomarker detections through fluorescence intensity	Dissolving MN	Photonic crystal (PhC) barcodes loaded with UV-curable PEG-PEGDA mixed solution	Dynamic ferrofluid-cast micromolding	Zhang et al. (2019)
		Extract ISF for bioanalysis	Swellable MN	Methacrylated hyaluronic acid (MeHA)	Soft lithography	Chang et al. (2017)
		Minimally invasive blood extraction	Hollow MN	Metal (nickel)	Drawing lithography technique and laser cutting	Li et al. (2013)
	Cancer	MN patch-assisted cancer immunotherapy	Dissolving MN	Hyaluronic acid integrated with pH-sensitive dextran nanoparticles (NPs) that encapsulate anti-PD-1 and glucose oxidase (GOx)	Soft lithography	Wang et al. (2016)
		Combination of chemotherapy and photothermal therapy	Coated MN	PEGylated gold nanorod-coated poly(l-lactide) MN and docetaxel-loaded mPEG-PDLLA micelles	Soft lithography	Hao et al. (2017)
Oral	Diabetes	Oral delivery of insulin and macromolecules	Dissolving MN on an ingestible capsule (luminal unfolding injector)	Polyvinylpyrrolidone (PVP)	Soft lithography	Abramson et al. (2019)
			Dynamic omnidirectional adhesive	Carbopol (outer layer); PCL (inner core)	Soft lithography, 3D printing	Chen et al. (2022)

			microneedle system (DOAMS)			
Ocular spaces	Model drugs, protein, and DNA	Delivery to intrascleral and intracorneal routes in a minimally invasive manner	Coated MN	Stainless steel MN	Laser cutting	Jiang et al. (2007)

10.3.3 Fabricating Other Microdevices for Drug Delivery

Advances in the field of drug delivery have yet to include a lot of other crucial classes of therapeutic agents. Large-molecule biopharmaceuticals and thermal/pH-sensitive drugs, for example, are challenging to formulate and deliver. Systemic administration of cancer drugs causes acute side effects and toxicities. Other useful properties such as local sensing and feedback mechanism remain to be explored. Therefore, implantable drug delivery systems simultaneously carrying sufficient doses, environmental sensors, and imaging/diagnostic agents with a triggered/targeted release may present ideal solutions to the aforementioned obstacles. Structural, mechanical, and electrical designs of these implantable devices at micro- and nano-dimensions are made feasible by technologies borrowed from the semiconductor industry. The general concept involves the implantation of microfabricated nanopores, nanochannels, or nanoreservoir-based devices, coupled with electronic sensory and actuation, for controlled delivery (Gardner 2006).

In 1999, Langer and Cima and their coworkers invented an implantable microchip containing one or more therapeutics with wirelessly on-demand dosage control (Santini et al. 1999). From this device, uniform and reproducible multiple pulsatile releases could be delivered in desirable manners. The fabrication process of the microchip is based upon a sequential microfabrication procedure that was comprised of UV photolithography, chemical vapor deposition, electron beam evaporation, and reactive ion etching. The microchip is designed to accommodate hundreds of individual drug reservoirs of approximately 25 nL etched into the silicon wafer. To seal the reservoir, 0.3-μm-thick gold membrane anode or layers of titanium and platinum are deposited on top. When the gold membranes dissolve in an electrochemical process triggered by wireless control, feedback control, or preprogrammed processors, the drugs will actively empty out from the reservoirs (Maloney et al. 2005).

Lithography allows the fabrication of different nanopore structures for controlling drug release rates. An implantable titanium pump cylinder (4×30 nm) containing potent molecules and enclosed with a nanopore membrane has been investigated for sustained (3–6 months) and zero-order release kinetics (Fig. 10.6). The drug diffusion rate from the implant is regulated by the pore size, length, and density of the membrane. Depending on the drug molecule size, the pore size could be tailored accordingly. The silicone membrane is patterned with top-down microfabrication techniques using photolithography, selective etching, and thin film deposition. Arrays of uniform nanochannels having dimensions as small as 7 nm can be achieved (Martin et al. 2005). On the similar trend, chambers with microfabricated nanopores known as nanocages have drawn attentions in the implantation of cell or tissue transplants (Desai et al. 1998). These nanoporous biocapsules constructed by lithography techniques consist of homogenous pores (7–20 nm) with modified surface chemistry and particular architectures. Using the nanocages, encapsulated islet cells such as allografts, xenografts, or engineered β-cells can stay hidden from the immune system or be immune-isolated, which mitigates the requirement for

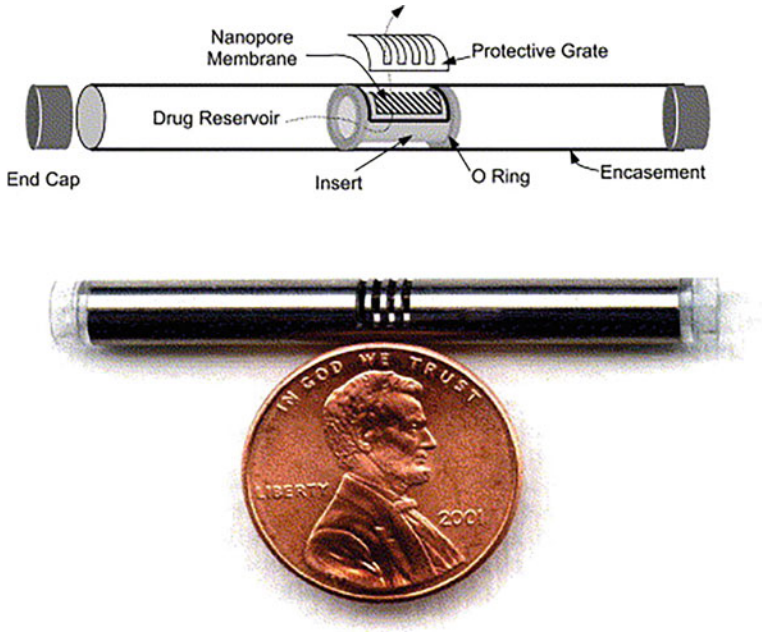

Fig. 10.6 Illustrations of the implant device fitted with nanopore membrane. Republished with permission from Elsevier Science & Technology Journals, from Martin et al. (2005); permission conveyed through Copyright Clearance Center, Inc.

immunosuppression. One major common drawback of these implantable devices is the need for retrieval surgery. Silicone, gold, titanium, etc., are some of the most common materials used due to their inert property. The search for biodegradable, compatible, and flexible materials for implanted devices continues to be actively pursued.

Besides, microfabrication has made important contributions in the field of medical microrobotics. These micro-sized robots fabricated by lithography techniques could gently interact and adapt with the biological environment. In order to perform multiple robotic duties including on-demand drug transport, cell manipulation, and traceability, the robots must be specifically designed and precisely fabricated. Two-photon lithography combined with smart materials provides an ultimate manufacturing strategy. More in-depth readings on this area can be found in many literatures (Rajabasadi et al. 2021; Nelson et al. 2010; Kim et al. 2013).

10.4 Conclusion

Lithography technologies have contributed a revolution to the field of drug and vaccine delivery. Given the wide range of fascinating systems that are actively evolving, it is anticipated that microfabrication will continue to better support the development of innovative therapeutics and diagnostic tools for disease treatments/prevention. The power of lithography technologies comes from the ability to fabricate reservoirs, pores, and channels in micro- and nano-dimension with high precision and complex geometries. Structural composition and surface chemistry can be additionally modulated to improve targetability and functionality. The capability of adding electrical components could help the systems to sense the internal conditions or be externally controlled. More importantly, lithography technologies offer the ease of scalability and uniformity for mass manufacture. Since traditional light exposure, lithographic etching, and photomask uses do not necessarily lend themselves to rapid prototyping and be suitable for a broad range of biomaterials, alternative microfabrication technologies such as soft lithography, molding, and imprinting are being studied. With the rapid movement of this field, more lithography-based products will soon be available for clinical applications, offering a significant impact on medicine in general and the area of drug delivery in particular.

Acknowledgment This project has been funded in whole or in part with federal funds from the Department of Health and Human Services, Office of the Assistant Secretary for Preparedness and Response, Biomedical Advanced Research and Development Authority, under Contract No. 75A50120C00162. We thank Nicole E. Nelson for proofreading this book chapter.

Conflict of Interest T.D.N. has a conflict of interest with PiezoBioMembrane Inc. and SingleTimeMicroneedles Inc.

References

Abramson A, Caffarel-Salvador E, Soares V, Minahan D, Tian RY, Lu X, Dellal D, Gao Y, Kim S, Wainer J (2019) A luminal unfolding microneedle injector for oral delivery of macromolecules. Nat Med 25:1512–1518

Anselmo AC, Mitragotri S (2016) Nanoparticles in the clinic. Bioeng Transl Med 1:10–29

Bender M, Otto M, Hadam B, Vratzov B, Spangenberg B, Kurz H (2000) Fabrication of nanostructures using A Uv-based imprint technique. Microelectron Eng 53:233–236

Bhatnagar S, Dave K, Venuganti VVK (2017) Microneedles in the clinic. J Control Release 260: 164–182

Bong KW, Bong KT, Pregibon DC, Doyle PS (2010) Hydrodynamic focusing lithography. Angew Chem 122:91–94

Bratton D, Yang D, Dai J, Ober CK (2006) Recent progress in high resolution lithography. Polym Adv Technol 17:94–103

Chang H, Zheng M, Yu X, Than A, Seeni RZ, Kang R, Tian J, Khanh DP, Liu L, Chen P (2017) A Swellable microneedle patch to rapidly extract skin interstitial fluid for timely metabolic analysis. Adv Mater 29:1702243

Chen Z, Ye R, Yang J, Lin Y, Lee W, Li J, Ren L, Liu B, Jiang L (2019) Rapidly fabricated microneedle arrays using magnetorheological drawing lithography for transdermal drug delivery. ACS Biomater Sci Eng 5:5506–5513

Chen W, Wainer J, Ryoo SW, Qi X, Chang R, Li J, Lee SH, Min S, Wentworth A, Collins JE (2022) Dynamic omnidirectional adhesive microneedle system for oral macromolecular drug delivery. Sci Adv 8:Eabk1792

Chou SY, Krauss PR, Renstrom PJ (1996) Nanoimprint lithography. J Vacuum Sci Technol B 14: 4129–4133

Creighton RL, Woodrow KA (2019) Microneedle-mediated vaccine delivery to the oral mucosa. Adv Healthc Mater 8:1801180

Dendukuri D, Pregibon DC, Collins J, Hatton TA, Doyle PS (2006) Continuous-flow lithography for high-throughput microparticle synthesis. Nat Mater 5:365–369

Desai TA, Chu WH, Tu JK, Beattie GM, Hayek A, Ferrari M (1998) Microfabricated immunoisolating biocapsules. Biotechnol Bioeng 57:118–120

Ding Z, Van Riet E, Romeijn S, Kersten G, Jiskoot W, Bouwstra J (2009) Immune modulation by adjuvants combined with diphtheria toxoid administered topically in Balb/C mice after microneedle array pretreatment. Pharm Res 26:1635–1643

Donnelly RF, Singh TRR, Alkilani AZ, Mccrudden MT, O'neill S, O'mahony C, Armstrong K, Mcloone N, Kole P, Woolfson AD (2013) Hydrogel-forming microneedle arrays exhibit antimicrobial properties: potential for enhanced patient safety. Int J Pharm 451:76–91

Dunn SS, Tian S, Blake S, Wang J, Galloway AL, Murphy A, Pohlhaus PD, Rolland JP, Napier ME, Desimone JM (2012) Reductively responsive siRNA-conjugated hydrogel nanoparticles for gene silencing. J Am Chem Soc 134:7423–7430

Edens C, Collins ML, Ayers J, Rota PA, Prausnitz MR (2013) Measles vaccination using a microneedle patch. Vaccine 31:3403–3409

Elahpour N, Pahlevanzadeh F, Kharaziha M, Bakhsheshi-Rad HR, Ramakrishna S, Berto F (2021) 3D printed microneedles for transdermal drug delivery: a brief review of two decades. Int J Pharm 597:120301

Ferrari M (2005) Cancer nanotechnology: opportunities and challenges. Nat Rev Cancer 5:161–171

Fox CB, Kim J, Le LV, Nemeth CL, Chirra HD, Desai TA (2015) Micro/nanofabricated platforms for oral drug delivery. J Control Release 219:431–444

Gardner P (2006) Microfabricated nanochannel implantable drug delivery devices: trends, limitations and possibilities. Expert Opin Drug Deliv 3:479–487

Gittard SD, Ovsianikov A, Chichkov BN, Doraiswamy A, Narayan RJ (2010) Two-photon polymerization of microneedles for transdermal drug delivery. Expert Opin Drug Deliv 7: 513–533

Grayson ACR, Cima MJ, Langer R (2004) Molecular release from A polymeric microreservoir device: influence of chemistry, polymer swelling, and loading on device performance. J Biomed Mater Res Part A 69:502–512

Guan J, Ferrell N, Lee LJ, Hansford DJ (2006) Fabrication of polymeric microparticles for drug delivery by soft lithography. Biomaterials 27:4034–4041

Guo LJ (2007) Nanoimprint lithography: methods and material requirements. Adv Mater 19:495–513

Hao Y, Dong M, Zhang T, Peng J, Jia Y, Cao Y, Qian Z (2017) Novel approach of using near-infrared responsive pegylated gold nanorod coated poly (L-Lactide) microneedles to enhance the antitumor efficiency of docetaxel-loaded mpeg-Pdlla micelles for treating an A431 tumor. ACS Appl Mater Interfaces 9:15317–15327

Harinarayana V, Shin Y (2021) Two-photon lithography for three-dimensional fabrication in micro/nanoscale regime: a comprehensive review. Opt Laser Technol 142:107180

Helgeson ME, Chapin SC, Doyle PS (2011) Hydrogel microparticles from lithographic processes: novel materials for fundamental and applied colloid science. Curr Opin Colloid Interface Sci 16: 106–117

Henry S, Mcallister DV, Allen MG, Prausnitz MR (1998) Microfabricated microneedles: a novel approach to transdermal drug delivery. J Pharm Sci 87:922–925

Hutin Y, Chen RT (1999) Injection safety: a global challenge. Bull World Health Organ 77:787

Ilium L, Davis S, Wilson C, Thomas N, Frier M, Hardy J (1982) Blood clearance and organ deposition of intravenously administered colloidal particles. The effects of particle size, nature and shape. Int J Pharm 12:135–146

Ingrole RS, Azizoglu E, Dul M, Birchall JC, Gill HS, Prausnitz MR (2021) Trends of microneedle technology in the scientific literature, patents, clinical trials and internet activity. Biomaterials 267:120491

Ito H (1997) Chemical amplification resists: history and development within IBM. IBM J Res Dev 41:119–130

Jiang J, Gill HS, Ghate D, Mccarey BE, Patel SR, Edelhauser HF, Prausnitz MR (2007) Coated microneedles for drug delivery to the eye. Invest Ophthalmol Vis Sci 48:4038–4043

Kim Y-C, Park J-H, Prausnitz MR (2012) Microneedles for drug and vaccine delivery. Adv Drug Deliv Rev 64:1547–1568

Kim S, Qiu F, Kim S, Ghanbari A, Moon C, Zhang L, Nelson BJ, Choi H (2013) Fabrication and characterization of magnetic microrobots for three-dimensional cell culture and targeted transportation. Adv Mater 25:5863–5868

Laurent PE, Bourhy H, Fantino M, Alchas P, Mikszta JA (2010) Safety and efficacy of novel dermal and epidermal microneedle delivery systems for rabies vaccination in healthy adults. Vaccine 28:5850–5856

Laza SC, Polo M, Neves AA, Cingolani R, Camposeo A, Pisignano D (2012) Two-photon continuous flow lithography. Adv Mater 24:1304–1308

Li CG, Lee CY, Lee K, Jung H (2013) An optimized hollow microneedle for minimally invasive blood extraction. Biomed Microdevices 15:17–25

Li Y, Zhang H, Yang R, Laffitte Y, Schmill U, Hu W, Kaddoura M, Blondeel EJ, Cui B (2019) Fabrication of sharp silicon hollow microneedles by deep-reactive ion etching towards minimally invasive diagnostics. Microsyst Nanoeng 5:1–11

Li D, Hu D, Xu H, Patra HK, Liu X, Zhou Z, Tang J, Slater N, Shen Y (2021) Progress and perspective of microneedle system for anti-cancer drug delivery. Biomaterials 264:120410

Maloney JM, Uhland SA, Polito BF, Sheppard NF Jr, Pelta CM, Santini JT Jr (2005) Electrothermally activated microchips for implantable drug delivery and biosensing. J Control Release 109: 244–255

Martin FJ, Grove C (2001) Microfabricated drug delivery systems: concepts to improve clinical benefit. Biomed Microdevices 3:97–108

Martin F, Walczak R, Boiarski A, Cohen M, West T, Cosentino C, Ferrari M (2005) Tailoring width of microfabricated nanochannels to solute size can be used to control diffusion kinetics. J Control Release 102:123–133

Mchugh KJ, Nguyen TD, Linehan AR, Yang D, Behrens AM, Rose S, Tochka ZL, Tzeng SY, Norman JJ, Anselmo AC (2017) Fabrication of fillable microparticles and other complex 3D microstructures. Science 357:1138–1142

Merkel TJ, Herlihy KP, Nunes J, Orgel RM, Rolland JP, Desimone JM (2010) Scalable, shape-specific, top-down fabrication methods for the synthesis of engineered colloidal particles. Langmuir 26:13086–13096

Mikszta JA, Laurent PE (2008) Cutaneous delivery of prophylactic and therapeutic vaccines: historical perspective and future outlook. Expert Rev Vaccines 7:1329–1339

Mikszta JA, Sullivan VJ, Dean C, Waterston AM, Alarcon JB, Dekker Iii JP, Brittingham JM, Huang J, Hwang CR, Ferriter M (2005) Protective immunization against inhalational anthrax: a comparison of minimally invasive delivery platforms. J Infect Dis 191:278–288

Mitchell MJ, Billingsley MM, Haley RM, Wechsler ME, Peppas NA, Langer R (2021) Engineering precision nanoparticles for drug delivery. Nat Rev Drug Discov 20:101–124
Mitragotri S, Lahann J (2009) Physical approaches to biomaterial design. Nat Mater 8:15–23
Moga KA, Bickford LR, Geil RD, Dunn SS, Pandya AA, Wang Y, Fain JH, Archuleta CF, O'neill AT, Desimone JM (2013) Rapidly–dissolvable microneedle patches via a highly scalable and reproducible soft lithography approach. Adv Mater 25:5060–5066
Moreau WM (2012) Semiconductor lithography: principles, practices, and materials. Springer Science & Business Media
Nelson BJ, Kaliakatsos IK, Abbott JJ (2010) Microrobots for minimally invasive medicine. Annu Rev Biomed Eng 12:55–85
Panda P, Ali S, Lo E, Chung BG, Hatton TA, Khademhosseini A, Doyle PS (2008) Stop-flow lithography to generate cell-laden microgel particles. Lab Chip 8:1056–1061
Paulsen KS, Di Carlo D, Chung AJ (2015) Optofluidic fabrication for 3D-shaped particles. Nat Commun 6:1–9
Perry JL, Herlihy KP, Napier ME, Desimone JM (2011) Print: a novel platform toward shape and size specific nanoparticle theranostics. Acc Chem Res 44:990–998
Petros RA, Desimone JM (2010) Strategies in the design of nanoparticles for therapeutic applications. Nat Rev Drug Discov 9:615–627
Prausnitz MR (2004) Microneedles for transdermal drug delivery. Adv Drug Deliv Rev 56:581–587
Prausnitz MR, Langer R (2008) Transdermal drug delivery. Nat Biotechnol 26:1261–1268
Qiu Y, Guo L, Zhang S, Xu B, Gao Y, Hu Y, Hou J, Bai B, Shen H, Mao P (2016) DNA-based vaccination against hepatitis B virus using dissolving microneedle arrays adjuvanted by cationic liposomes and CpG ODN. Drug Deliv 23:2391–2398
Rajabasadi F, Schwarz L, Medina-Sánchez M, Schmidt OG (2021) 3D and 4D lithography of untethered microrobots. Prog Mater Sci 120:100808
Rolland JP, Van Dam RM, Schorzman DA, Quake SR, Desimone JM (2004) Solvent-resistant photocurable "liquid Teflon" for microfluidic device fabrication. J Am Chem Soc 126:2322–2323
Rolland JP, Maynor BW, Euliss LE, Exner AE, Denison GM, Desimone JM (2005) Direct fabrication and harvesting of monodisperse, shape-specific nanobiomaterials. J Am Chem Soc 127:10096–10100
Santini JT, Cima MJ, Langer R (1999) A controlled-release microchip. Nature 397:335–338
Sato H, Yagyu D, Ito S, Shoji S (2006) Improved inclined multi-lithography using water as exposure medium and its 3D mixing microchannel application. Sensors Actuators A Phys 128:183–190
Savage DJ, Liu X, Curley SA, Ferrari M, Serda RE (2013) Porous silicon advances in drug delivery and immunotherapy. Curr Opin Pharmacol 13:834–841
Senefelder A (1911) The invention of lithography. Sun Chemical Corporation
Singh Malik D, Mital N, Kaur G (2016) Topical drug delivery systems: a patent review. Expert Opin Ther Pat 26:213–228
Sullivan SP, Koutsonanos DG, Del Pilar Martin M, Lee JW, Zarnitsyn V, Choi S-O, Murthy N, Compans RW, Skountzou I, Prausnitz MR (2010) Dissolving polymer microneedle patches for influenza vaccination. Nat Med 16:915–920
Thompson LF (1983) An introduction to lithography. Acs Publications
Tran K, Gavitt TD, Farrell NJ, Curry EJ, Mara AB, Patel A, Brown L, Kilpatrick S, Piotrowska R, Mishra N (2021) Transdermal microneedles for the programmable burst release of multiple vaccine payloads. Nat Biomed Eng 5:998–1007
Wang C-F, Sarparanta MP, Mäkilä EM, Hyvönen ML, Laakkonen PM, Salonen JJ, Hirvonen JT, Airaksinen AJ, Santos HA (2015) Multifunctional porous silicon nanoparticles for cancer theranostics. Biomaterials 48:108–118
Wang C, Ye Y, Hochu GM, Sadeghifar H, Gu Z (2016) Enhanced cancer immunotherapy by microneedle patch-assisted delivery of anti-Pd1 antibody. Nano Lett 16:2334–2340
Xia Y, Whitesides GM (1998) Soft lithography. Annu Rev Mater Sci 28:153–184

Yang J, Zhang H, Hu T, Xu C, Jiang L, Zhang YS, Xie M (2021) Recent advances of microneedles used towards stimuli-responsive drug delivery, disease theranostics, and bioinspired applications. Chem Eng J 426:130561

Yin Y, Lu Y, Gates B, Xia Y (2001) Template-assisted self-assembly: a practical route to complex aggregates of monodispersed colloids with well-defined sizes, shapes, and structures. J Am Chem Soc 123:8718–8729

Yu J, Zhang Y, Ye Y, Disanto R, Sun W, Ranson D, Ligler FS, Buse JB, Gu Z (2015) Microneedle-array patches loaded with hypoxia-sensitive vesicles provide fast glucose-responsive insulin delivery. Proc Natl Acad Sci 112:8260–8265

Zhang Y, Wang D, Gao M, Xu B, Zhu J, Yu W, Liu D, Jiang G (2018) Separable microneedles for near-infrared light-triggered transdermal delivery of metformin in diabetic rats. ACS Biomater Sci Eng 4:2879–2888

Zhang X, Chen G, Bian F, Cai L, Zhao Y (2019) Encoded microneedle arrays for detection of skin interstitial fluid biomarkers. Adv Mater 31:1902825

Chapter 11
Micro-molding and Its Application to Drug Delivery

Edina Vranić

Abstract Micro-molding techniques are used in many areas including pharmaceutical technology. Injection molding is the cyclic process of polymer processing. Most of them are thermoplastics. The procedure is performed by injecting a molten polymer of a certain viscosity from an injection unit into a tempered mold using heat and pressure. The workpiece hardens in the mold by cooling or by cross-linking. Hot embossing uses pressure. The template is pressed into a heated polymer. In this case, a thermo-softening polymer is placed between molds, heated, and later allowed to cool maintaining constant pressure. Casting is a process where the non-viscous polymer is poured into a tempered mold. The casting takes the shape of the mold cavity and is created in it by evaporating the solvent or dispersant, gelling, chemical reactions, or cross-linking. These techniques can also be applied to prepare solid dosage forms or controlled-release systems such as implants or vaginal rings among others. In this way, using these techniques results in precise medication. It is directly related to the patient's quality of life and successful treatment.

Keywords Micro-molding · Drug delivery · Biomedical application

11.1 Introduction

The application of new manufacturing techniques, generally derived from other industrial fields, is one of the most promising innovation tools in pharmaceutical technology. This may result in a reduction of costs for development and manufacturing and simplification of industrial scalability (Melocchi 2014).

Polymeric materials have experienced an important development. The technologies used in polymer microproduction can be divided into two groups: direct and

E. Vranić (✉)
Faculty of Pharmacy, Department of Pharmaceutical Technology, University of Sarajevo, Sarajevo, Bosnia and Herzegovina
e-mail: edina.vranic@ffsa.unsa.ba

D. Lamprou (ed.), *Nano- and Microfabrication Techniques in Drug Delivery*,
Advanced Clinical Pharmacy – Research, Development and Practical Applications 2,
https://doi.org/10.1007/978-3-031-26908-0_11

replication techniques (Yao 2008; Rotting et al. 2002). The direct methods that include lithography, laser ablation, and micro-milling have been used for prototyping purposes (Yao 2008).

The three most promising replication methods are microinjection molding, hot embossing, and casting. They were adapted from conventional polymer molding processes, so these replication methods are also named micro-molding (Yao 2008; Heckele and Schomburg 2004; Mekaru et al. 2004; Rotting et al. 2002).

Miniaturization is becoming a consistent trend in technological development, particularly in biomedicine, electronics, optics, and telecommunication. Innovative micro devices with better performance and functionality than their macro counterpart can be designed, utilizing the scaling benefits (Yao 2008).

So injection molding (IM) and micro-molding (μIM) were identified as very interesting techniques to be exploited in the pharmaceutical field. These techniques are commonly employed within the plastic industry for the fast production of objects with different sizes, shapes, and, potentially, many details (Melocchi 2014). Micro-molding applies to the manufacturing of parts of a few milligrams weight or with features where dimensions or dimension tolerances should be in the micrometer range, which is the potential scope of drug products (Melocchi 2014).

Micro-molding involves four primary steps: microfabrication of the mold containing a negative or inverse of the desired pattern geometry, introduction of the polymer material to the mold, curing or cooling of the polymer material, and release or separation of the molded polymer from the mold (Papautsky and Peterson 2008).

11.2 Micro-molding Techniques

11.2.1 Injection Molding

Injection molding (IM) is one of the most important techniques for manufacturing polymer products. It is a complex process, so it is very difficult to take into account all the changes taking place during the process. Also, proper input parameter setting is very important to enhance the efficiency of the process and to have consistent product quality. These input process parameters are melt temperature, mold temperature, injection pressure, injection speed, injection time, holding pressure, holding time, and cooling time. The responses/output process parameters may be mechanical properties; defects, e.g., warpage, shrinkage, sink mark, and residual thermal stress; and aesthetic requirement such as surface finish/roughnes (Farooque et al. 2021).

This technology is highly acceptable for industrial applications due to the low cost in the production of polymeric parts, especially for large quantities, versatile shapes, short cycle times, simple automation, and the possibility of simultaneous shaping of bulk and surface structures (Maghsoudi et al. 2017; Matschuk and Larsen 2012; Park et al. 2011; Matschuk et al. 2010).

Injection molding is the most important cyclic process of polymer processing, and according to the achieved technology, the most advanced. This process belongs to the primary processing of polymers, i.e., to the pre-forming of polymers, because the shape of the mold is obtained from the starting material that does not have a specific shape (granules, pieces, etc.). All polymers are formed by injection molding: duromers, elastomers, elastoplastomers. The processing of plastomeric materials is especially widespread (Čatić 2006). According to the processed quantities, the injection molding of polymers is behind the extrusion technology. Additionally, biomaterials, ceramic ones, and combinations of different material mixtures (e.g., thermoplastics, metals, and ceramics) are also processed by injection molding (Čatić 2006).

11.2.1.1 Injection Molding Materials

Almost all thermoplastic materials can be used in injection molding. All material producers are obliged to disclose, along with the material, process parameters, and conditions, where the given material is supposed to be used. These recommendations are further adjusted for each injection molding cycle in order to achieve the minimum required cycle with optimal performance and mold quality. Materials with lower viscosity are more suitable for this type of shaping due to the easier flow of the melt through the distribution channels and the orifice to the mold cavity. Due to the low viscosity of the material, less injection pressure is required (Čatić 2006).

Some thermoset materials can also be used for injection molding, but special conditions are required. It is necessary to keep the temperature in the cylinder low, and then the L/R ratio should be as small as possible and the cycle as fast as possible. The conditions of elastomer processing by injection molding are also significantly different from the conditions of thermoplastic processing and are closer to the conditions of thermoset processing (Čatić 2006).

11.2.1.2 Injection Molding Procedures

Injection molding is a cyclic process of primary molding (pre-forming) of a polymer that is performed by injecting a molten polymer of a certain viscosity from the injection unit into a tempered mold. The material in the mold hardens by cooling (in the case of thermoplastic materials) or cross-linking in the case of elastomers, elastoplastomers, and duromers. Injection molding is performed on special machines that consist of an injection unit, drive system, mold closing unit, mold tempering device, and control unit (Čatić 2006).

The injection molding process takes place in several stages. The three basic phases are as follows (Čatić 2006):

- In the first phase, the molten material is injected into the mold cavity through the inlet channels by axial movement of the auger. The rotation of the auger is

excluded, and its axial movement is achieved by a hydraulic cylinder (Čatić 2006).

- In the second phase, the workpiece is cooled with an intensive circulation of refrigerant through the tool cooling system. Thereby, the auger acts on the molten material by subsequent pressure in order to compensate the lack of material due to the shrinkage of the mold during cooling. After the cooling process of the mold is completed, at the end of the subsequent pressure action phase, the auger returns back, rotates, and draws in a new amount of granulate, melts it, and plasticizes it (Čatić 2006).
- The third phase involves opening the mold and ejecting the workpiece. The injection unit is pushed back, and the nozzle is closed by means of a valve. The opening of the mold is provided by an opening system that, depending on the drive, can be mechanical or hydraulic. The workpiece is ejected from the mold using an ejector. Extraction of excess material from the inflow sleeve is performed by an extractor (Čatić 2006).

Injection molding is suitable for the production of very complex workpieces with tolerances of several micrometers. Molds obtained with this technology can be multi-part and multi-colored, produced in combination with metal inserts. They can be rigid (solid) or in foam form. Their production can run continuously 24 h a day (Čatić 2006).

11.2.1.3 Injection Molding Tools

The tool is one of the basic elements of an injection molding system that directly shapes the mold. Each new workpiece requires a new tool. The injection mold is cooled in the mold after injection. Therefore, the tool must be connected to a tempering device. After the final hardening of the mold, it is opened and ejected with the help of an ejector (Čatić 2006).

Leftover extraction at the inflow system is performed by an extractor. The molds are placed on the appropriate tool housing plates. One half of the mold is attached to the movable plate of the machine and the other to the fixed one. Starting of the housing plates is provided by cylindrical guides. Housing plates can be rectangular or circular. The total compression force, which depends on the projection of the workpiece cluster and the polymer pressure, is transmitted via the plates to the closure system (Čatić 2006).

11.2.1.4 Injection Molding Cycle

The injection molding cycle is the time required to make one or more moldings if the tool contains several mold cavities. This is the time that elapses between the two phases of the same name in the injection molding process. The working cycle begins with the closing of the mold and ends with its opening. The time course of activity

during the injection molding of thermoplastic moldings contains the following phases (Čatić 2006):

- Closing of the mold, performed by the closing unit in a very short period of time.
- The injection unit is getting closer to the stationary plate; this phase ends with the nozzle leaning on the pouring sleeve.
- Injection of the molten mass into the mold cavity is the next stage. The required melting pressure is provided by the axial movement of the auger and hydraulic cylinder.
- The injection pressure depends on the type of polymer and ranges from 500 to 3000 bar. It provides a pressure in the mold around 1000 bar; the injection speed is 2 m/s.
- At the end of the injection phase, the mold-cooling phase begins. For some time, the pressure in the cylinder has a lower value than the injection pressure and represents subsequent pressure. Subsequent pressure provides an additional amount of melt in the mold cavity due to the shrinkage of the molding during the cooling process.
- The movement of the nozzle and the beginning of re-plasticization begin at the moment when the action of the subsequent pressure stops. Subsequently, the auger begins to rotate and draw in a new amount of granules.
- If the cooling of the mold is not completed, it continues during the additional cooling time.
- Opening and ejection of the mold are done after its complete hardening/cooling.
- At the end of the injection cycle, the mold is prepared for the next cycle, cleaned, and lubricated.

11.2.2 Hot Embossing

Hot embossing is a technique wherein thermoplastics, or polymers that become viscous liquids at elevated temperatures, are precisely shaped using a mold, pressure, and heat. Common thermoplastics used include cyclic olefin copolymer, polycarbonate, polymethyl methacrylate, and polyethylene terephthalate (Weerakoon-Ratnayake et al. 2017; Gale et al. 2018).

In this process, a thermoplastic film is placed between two mold inserts. Next, the mold chamber is evacuated, compressed, and heated, creating a cast of the mold. Finally, the mold is cooled and the cast is removed. Due to this technology's capacity for cost efficiency, precision, and high throughput, hot embossing has found widespread commercial adoption by microfluidic companies (Wu and Gu 2011).

Hot embossing has several advantages over injection molding. It requires the thermoplastic to flow a relatively small distance in comparison to injection molding. This significantly reduces the stress produced in the material (Heckele and Schomburg 2004).

Additionally, shrinkage of the cast is reduced, making this method effective in the fabrication of delicate designs (Heckele and Schomburg 2004). Limitations of the technology include a restriction to thermoplastics and difficulty in the fabrication of complex three-dimensional structures (Wu and Gu 2011).

Advances in molding technology have enabled the production of nanoscale devices. The draw to fabrication and research at this scale is directly related to the unique physical phenomena that occur only at the nanoscale. Scaling effects define a unique change in flow physics when moving from a macroscale to a microscale. Such a change in flow physics is also apparent when moving from the microscale to the nanoscale (Bocquet and Tabeling 2014).

Intermolecular forces and electrokinetic effects move from a relatively minor contributor to nearly dominating at the nanofluidic scale. It is interesting to note that most biological fluid processes function at the nanoscale (Bocquet and Tabeling 2014).

Current research continues to build upon prior knowledge by improving on effective, but limited, technologies. One key limitation of hot embossing is the time-consuming and expensive process of making molds. Using a unique modification of hot embossing known as hot intrusion embossing, Debono et al. created a one-step process for the fabrication of microfluidic channels containing complex three-dimensional structures in various thermoplastics (Debono et al. 2016).

Their use of a rapid template mold fabrication method enabled molding of sub-50 μm tapered posts, steps, and walls, as well as three-dimensional serpentine channels. The value of this technology is in its ability to reduce the cost of thermoplastic molding, making it more accessible to researchers and commercialization entities. Due to its capacity for high throughput, cost-efficient, and precise molding, hot embossing will likely continue to be an excellent option for commercial use (Weerakoon-Ratnayake et al. 2017).

11.2.3 Casting

Casting is the most popular of the three micro-molding methods (McDonald et al. 2000; Duffy et al. 1999; Papautsky and Peterson 2008). The polymer (elastomer precursor) and the curing agent are typically mixed at a specific ratio and poured over the mold (also called template or master). The system is thermally cured, allowing the elastomer to be peeled off once it sets. The most prominent elastomer is polydimethylsiloxane (PDMS), and the casting template can be fabricated with conventional micromachining techniques (Madou 2002; Papautsky and Peterson 2008). Micro-molding in capillaries (MIMIC) (Kim et al. 1995; Papautsky and Peterson 2008) is a popular variation of the technique, in which PDMS is cast on a mold containing a relief pattern, which is then released and used as the mold in a second step. The mold is formed by placing the PDMS casting in conformal contact with a substrate to create a network of channels, which are then filled with a liquid pre-polymer by capillary action or vacuum and cured. Once cured, the mold is

removed, leaving the microstructures. MIMIC has been used to produce complex microstructures in thermally and UV-curable polymers (Papautsky and Peterson 2008).

11.3 Application of Micro-molding

The advantages of the technique are lower production costs (no need for water or other solvents, continuous manufacturing, scalability, patentability) in the development process of drug products and improved technological/ biopharmaceutical characteristics of the molded items (versatility of the design and composition, possibility of obtaining solid molecular dispersions/solutions of the active ingredient) (Melocchi 2014).

Also micro-molding is a key process in the field of micro manufacturing especially in the production of medical devices (Heckele and Schomburg 2004; Giboz et al. 2007; Yao 2008; Mitchell et al. 2017). This technology involves the injection of the whole material with the result of a high degree of efficiency due to the material saving process. In comparison with conventional large injection molding, the volume of the material is very much reduced, and as a consequence, the flow and temperature profiles are considerably different to macro injection molding (Mitchell 2017).

11.3.1 Immediate-Release Solid Dosage Forms

Immediate-release solid dosage forms in the configuration of a tablet or capsule today are powder-based materials with porous bulk containing excipients and drug at the specified content (Blaesi 2014; Augsburger and Hoag 2008a, b, c).

The manufacturing procedure of solid dosage form of the size of a conventional tablet or capsule can be done, for example, by several processes that are also used for forming operations in the polymer production: injection molding, hot-melt extrusion, and melt casting. Injection molding using a multi-shot injection molding machine. It allows mixed API and excipient materials, as well as the coating material, both in powder form, to be fed into it, providing a coated finished product as an output. Plasticization of the pharmaceutical material to form the product and subsequent solidification of the material are done via phase change within the material, instead of addition and removal of a solvent. This process opens opportunities for manufacturing optimization by reducing the number of unit operations, process time, and material waste. Raw API and excipient are fed into a mixing unit that provides the required raw materials to be fed into the injection molding machine together with the coating formulation (Blaesi 2014).

Also, it has been shown that single and multicomponent injection molding to produce solid dosage forms can be done using commercially available equipment

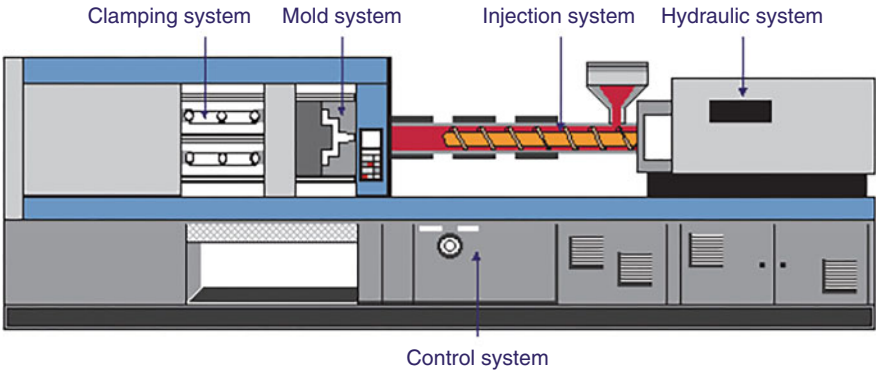

Fig. 11.1 Scheme of an injection molding machine with a hydraulic injection actuation system applicable for producing solid dosage forms (Blaesi 2014)

(Blaesi 2014; Zema et al. 2012; Quinten et al. 2009, 2011; Rothen-Weinhold et al. 1999). The injection molding process comprises solid material feeding, material plasticization, melt distribution, melt injection, melt solidification, and part ejection (Blaesi 2014).

All these individual steps are typically done in a time of 2–10 min using a conventional injection molding machine as shown in Fig. 11.1 (Blaesi 2014).

The most relevant parameter in injection molding is the rate at which a product can be produced, determined by the mold cycle time, *t*cycle, which is the sum of injection time, cooling time (i.e., solidification time), and mold resetting time (i.e., mold opening, part ejection, mold closing) (Blaesi 2014; Boothroyd et al. 2011; Osswald et al. 2008; Tadmor and Gogos 2006; Cuff and Raouf 1998).

11.3.2 Implants

Implants are generally rigid, millimeter-sized carriers in which a solid drug formulation is homogeneously distributed as a hydrophobic, biodegradable polymeric matrix (Novak et al. 2003).

Drug-loaded implants do not require a vehicle for delivery and can be positioned as a single unit at (or close to) the target site. The drug is homogenously entrapped in their polymer matrices, so implants can be used to attain sustained localized delivery of high-bioavailability drugs into the systemic circulation. This is achieved via slow, controlled release at the site of implantation (Maniruzzaman and Nokhodchi 2016).

Polymeric implantable drug delivery systems have remarkable potential for systemic delivery of various therapeutic agents. Generally, drug-loaded implants do not require a vehicle for delivery. They can be used to attain prolonged delivery into the systemic circulation of active pharmaceutical ingredients (APIs) with enhanced drug bioavailability. They can also provide drug release, ranging from

months to years. They improve patient compliance, especially for poorly bioavailable and rapidly metabolized compounds. Continuous manufacturing technology has been successfully employed to prepare drug-loaded single-unit polymeric implants. Employing heat and mechanical shear, such systems retain the stability of thermolabile therapeutics (e.g., proteins) in implants (Maniruzzaman and Nokhodchi 2016).

Implantable drug delivery systems (IDDSs) are particularly suitable means of drug administration where compliance with prescribed conventional drug delivery is impossible (Hoffman 2008; Martin et al. 2009; Shiah et al. 2011). IDDSs allow a drug to be delivered to or near the targeted site at a specific rate without regular patient/physician intervention. Two IDDS types are described: reservoir and matrix. In reservoir implants, the drug core is coated with a semipermeable polymeric membrane that controls the rate of drug release and is dependent on the rate of water influx into the system. Matrix implants deliver a uniformly distributed drug into the polymeric matrix (Koob 2004; Maniruzzaman and Nokhodchi 2016).

Depending on their polymer degradation properties, matrix implants can be of two types. The surface erosion type normally degrades only at the surface. In the bulk erosion type, slow uniform degradation in the implant bulk occurs. A matrix implant eliminates dose dumping and provides desirable drug release mediated by diffusion (Koob 2004; Maniruzzaman and Nokhodchi 2016). This type of drug release consists of a biphasic procedure in which a burst release is followed by a slow controlled release. To rapidly reach therapeutic concentration, initial burst release delivers the drug for large-volume distribution; controlled release maintains therapeutic concentrations for a prolonged period of time at a controlled rate (Dash and Cudworth 1998; Maniruzzaman and Nokhodchi 2016).

Polymeric carriers used in IDDSs can be classified as biodegradable and nonbiodegradable. They are summarized in Table 11.1 (Pizzi et al. 2004; Lyu and Untereker 2009; Maniruzzaman and Nokhodchi 2016).

Table 11.2 provides examples of various commercial implants using these polymeric systems (Wright et al. 2001, 2003; Rohloff et al. 2008; Kleiner et al. 2014; Maniruzzaman and Nokhodchi 2016).

The most widely clinically investigated polymeric materials in IDDS are the aliphatic polyesters based on lactic and glycolic acids. These materials have received considerable attention first as sutures, then as excipients for drug delivery, and finally as IDDSs. Their desirable features include biocompatibility (including the acceptability of degradation products), the ability of their degradation kinetics to be tuned, and ease of fabrication. Other important biodegradable polymers include polyanhydrides, poly(orthoesters), and poly(phosphoesters) (Ormiston and Serruys 2009).

Gliadel® wafer contains 7.7 mg of the anticancer drug carmustine; this completely biodegradable wafer is designed to be placed intracranially in the resection cavity. Gliadel® wafer circumvents the blood-brain barrier, reduces systemic toxicities, and provides direct, prolonged, and high dose of the alkylating drug to residual cancer cells (Abdelkader et al. 2021; Rudnick et al. 2020).

Table 11.1 Polymeric carriers used in IDDSs (Pizzi et al. 2004; Lyu and Untereker 2009; Maniruzzaman and Nokhodchi 2016)

Nondegradable carrier	
Poly(dimethyl siloxane)	Rate-controlling membrane for drug delivery, catheters, adhesives, tissue filling, and prosthesis
Polyethylene (PE)	Orthopedic parts, drug delivery rate-controlling membrane
Poly(ethylene-co-vinyl acetate) (PEVA)	Drug delivery coating, rate-controlling membrane (transdermal patch and ocular)
Poly(ethylene terephthalate) (PET)	Vascular graft, orthopedic, transdermal patch backing
Polyurethanes (PU)	Matrix for drug delivery devices, catheters, and structural components
Poly(methyl methacrylate) (PMMA)	Bone cement, drug delivery to the eye and bone investigated
Fluoropolymer (PTFE and PVDF and copolymers)	Coating for DES, transdermal patch liner, vascular graft
Biodegradable carrier	
Poly(lactide), stereoisomer forms and copolymers	Drug-loaded microparticles, sutures, structural components, orthopedic, coating, DES backbone
Polyanhydride	Monolithic delivery device matrix
Collagen	Tissue filling, tissue engineering scaffolds, drug delivery

Table 11.2 Commercial implants using polymeric systems (Wright et al. 2001, 2003; Rohloff et al. 2008; Kleiner et al. 2014; Maniruzzaman and Nokhodchi 2016)

Implants	Description	Application
Gliadel® wafer	Dime-sized biodegradable polyanhydride disks, 1.45 cm in diameter and 1.0 mm thick; delivers a chemotherapeutic drug, BCNU/carmustine, directly into the surgical cavity created after a tumor (high-grade malignant glioma) is surgically excised	Cancer treatment
Zoladex®	Sterile biodegradable; contains goserelin acetate (3.6 or 10.8 mg depending on the design); dispersed in PLGA matrix	Advanced prostate cancer, breast cancer, endometriosis
BioMatrix®	PLA—asymmetric abluminal coating	Anticancer
JACTAX®	PLA—microdots on the abluminal side	Anticancer
Ozurdex®	Intravitreal implant containing 0.7 mg dexamethasone; composed of PLGA (length, 6.5 mm; diameter, 0.45 mm)	Macular edema due to branch retinal vein or central retinal vein occlusion

The only local delivery implant approved by the FDA for the treatment of newly diagnosed or recurrent glioblastoma to date is the Gliadel® wafer. The 1,3-bis-(p-carboxphenoxy) propane (pCPP) and sebacic acid (SA) *co*-polymer is loaded with the anticancer drug (Bastiancich et al. 2021; Juratli et al. 2013). Patients receive up to eight wafers implanted into the tumor resection cavity, equivalent to a dose of 61 mg of carmustine/BCNU. Drug release should occur over a 3-week period, with in vivo studies observing that most of the drug is released in the first 3–7 days

(Bastiancich et al. 2021; Grossman et al. 1992). In terms of drug distribution, studies have reported high concentrations from 3 to 12 mm adjacent to the polymer site in animal models (Bastiancich et al. 2021; Bota et al. 2007; Fung et al. 1998; Grossman et al. 1992). When it was approved in the late 1990s, the efficacy was measured in terms of an improvement of median overall survival compared to radiotherapy alone (Bastiancich et al. 2021; Westphal et al. 2006; Westphal et al. 2003). Recently, a systematic literature review has analyzed the results of a series of small trials to evaluate the combination of Gliadel® wafers with the Stupp protocol for newly diagnosed GBM patients showing a benefit of this sequential combination (Bastiancich et al. 2021; Ashby et al. 2016). The Gliadel®-related side effects and complications (such as intracranial hypertension, meningitis, impaired neurosurgical wound healing, wafer migration, and seizures) as well as the technical difficulties experienced during the wafer implantation limit its clinical use (Bregy et al. 2013; Perry et al. 2007). So Gliadel® is a potentially effective drug delivery system (DDS) but requires additional improvements to overcome potential drawbacks. Important efforts have been made in the last decades incorporating a wide range of drugs into a variety of biodegradable DDSs (e.g., wafers, disks, soft gels, micro/nano-particle systems) to improve compatibility with the brain tissue, increase the antitumor efficacy, and reduce adverse effects (Bastiancich et al. 2016; Wolinsky et al. 2012).

Zoladex® contains goserelin acetate. It is used to treat prostate cancer and relieve the symptoms of advanced breast cancer and endometriosis. Goserelin is a synthetic decapeptide and a potent analog of LHRH (luteinizing hormone-releasing hormone). It uses PLGA or PLA as a carrier for the drug delivery system. The drug is dispersed in the polymer matrix using the hot-melt extrusion method, and the implant is distributed in the form of a prefilled syringe (Zhang et al. 2021).

Encapsulating peptides in biodegradable polymers can help protect peptides from thermal and shear stresses. Specifically, PLGAs and related polymers can extend the duration of a peptide's action by up to 6 months in a solid dosage form (Mohammadpour et al. 2019). Further, the ratio of lactic acid to glycolic acid in PLGA polymers dictates the glass transition temperature (which can range from 40 to 60 °C) and can be tuned to enable the hot-melt extrusion of peptides. The resulting composition, which encapsulates the 30% w/w goserelin within PLGA, forms thin rods for implantation without impacting the activity of the goserelin (Patel et al. 2010).

BioMatrix® is a 316L SS stent having struts of 120-μm thickness coated with a material composed of 1:1 PLLA and Biolimus A9 mix. This stent is the third-generation DES (drug-eluting stent) because it employs a biodegradable polymer instead of the durable polymer. This third-generation DES was developed to overcome the long-term adverse events observed with DESs comprising durable polymers. As the biodegradable polymer is coated on the abluminal surface of the stent, 40% of the coated drug is released in the initial burst release, and 6–9 months is required for complete drug release and polymer degradation. Biolimus shows an improved therapeutic efficacy even upon a weak systemic exposure, because the lipophilicity of the drug is more than ten times as that of sirolimus, causing easy penetration of the drug into the target cell membrane (Ostojic et al. 2011).

The JACTAX® HD stent represents a novel way to accomplish abluminal coating, with neither continuous polymer nor filled wells penetrating stent struts. Instead, a pre-crimped bare-metal stent is abluminally coated with a minimal amount of biodegradable polylactide polymer plus paclitaxel (nominally 9.2 μg of each per 16-mm stent) applied to the abluminal surface as 2750 discrete microdots/16-mm stent. The coating drops impact the stent at high velocity, allowing the low viscosity solution to spread in a thin layer and adhere to the stent surface. The biodegradable polymer is designed to fully release the drug in 60 days and resorb in 4 months, thereby eliminating chronic exposure to drug and polymer. The concept of the JACTAX® HD stent is thus to emulate a drug-eluting stent initially and then transition to a BMS (Bekmurzayevaa et al. 2018; Grube et al. 2010).

The dexamethasone intravitreal implant (Ozurdex®) is a sustained-release preparation of dexamethasone embedded in a bioerodible copolymer consisting of poly (lactic-co-glycolic acid) that has been approved by the FDA for the treatment of macular edema secondary to retinal vein occlusion, non-infectious posterior uveitis, and diabetic macular edema (Lee and Chan 2020). Ozurdex® has been reported to be effective in treating diabetic macular edema refractory to anti-vascular endothelial growth factor therapy (Busch et al. 2018). It consists of a solid rod-shaped polymer with a sustained-release delivery system that allows a gradual delivery of dexamethasone into the vitreous cavity (Lee and Chan 2020). The variability of the responses to Ozurdex® is due to multiple unique factors associated with individual patients and the underlying differing disease processes; the frequency of its insertion may range from every 2 to 6 months. Despite the beneficial therapeutic effects of Ozurdex®, there are reports of its migration into the anterior chamber in patients with an opening or a defect in the lens-iris diaphragm, causing vision loss primarily due to corneal toxicity (Lee and Chan 2020).

11.3.3 Vaginal Rings

Injection molding was also explored as an alternative technique for the preparation of intravaginal inserts (Gokhale et al. 2009; Rathbone et al. 2002), which are mostly manufactured by HME at present.

Vaginal rings are flexible, ring-shaped, silicone, or thermoplastic elastomers that provide long-term, sustainable, and controlled delivery of active substances to the vagina to achieve local or systemic effects. Simple vaginal rings contain an active substance that is homogeneously released within the polymer matrix. The active substance is released faster from the ring surface than the substance located inside the ring. In order to obtain a constant release of the active substance from the vaginal ring, sandwich, matrix, and reservoir ring types were made (Fig. 11.2) (Hussain and Ahsan 2005; Malcolm et al. 2012).

Vaginal rings are flexible drug delivery systems in the form of a torus. They provide a continuous and controlled release of the drug that lasts from a few weeks to several months. Vaginal rings are used for the localized delivery of

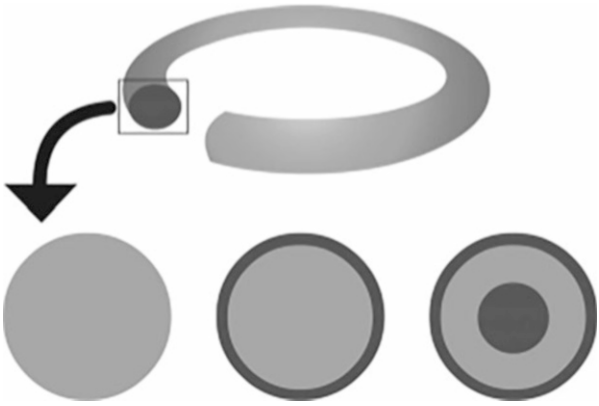

Fig. 11.2 Cross sections of three vaginal rings presenting different designs: matrix design (left), core or reservoir design (center), and sandwich or shell design (right). Light gray represents drug-polymer mixture, and dark gray represents polymer only (das Neves et al. 2008)

chemotherapeutics to the cervix (with the potential to reduce the need for surgery); preparations for the treatment of fungal, bacterial, and sexually transmitted infections; the delivery of contraceptives; and hormone replacement therapy (Ordikhani et al. 2016; Mesquita et al. 2019).

The technology of production of vaginal rings has improved in the last decade and seems to offer enough advantages for proper implantation and release of nanosystems. Local drug delivery performed by vaginal rings has made dose reduction possible and avoids influence of the first pass effect through the liver. The advantage of the rings is the practical application; it does not interfere with coitus and is not felt during daily activities. However, it can lead to bleeding and inflammation of the vagina (Osmałek et al. 2021; Mesquita et al. 2019).

To increase the efficiency of small interfering RNA (siRNA) delivery for the treatment of HIV infection and prevention of its transmission, Kim et al. (2018a, b) have designed an interesting polyurethane formulation that responds to changes in pH. In the study, polyethylene glycol-coated siRNA-filled polyaspartic acid nanoparticles were encapsulated in a polyurethane hydrogel, and the final formulation was physically cross-linked within the intravaginal ring. In vitro release profile showed that the release was close to zero at pH 4.2 and prolonged at pH 7.0. Modifications of physicochemical interactions of copolymer chains are the cause of pH-sensitive release. Deprotonation of 2,2-dimethylolpropionic acid at pH 7.0 creates a relatively weak intermolecular hydrophobic interaction. The space between the particles enabled the rapid release of nanoparticles. Moreover, a zeta potential value close to zero increased the penetration of nanoparticles into the mucosa. Nanoparticles did not show cytotoxicity, while hydrogel showed low cytotoxicity (Pandey et al. 2021).

Vaginal ring products have already reached the market. Each of them offers the release of one or more steroid molecules for estrogen replacement therapy (Estring® and Femring®), contraception (Nuvaring®, Progering® and Ornibel®) or hormone supplementation and pregnancy maintenance during in vitro fertilization (Fertiring®) (Wang et al. 2018; Brache et al. 2013; Friend 2011; Malcolm et al. 2015, 2012).

11.3.3.1 Vaginal Contraceptive Rings

The concept of contraceptive vaginal rings is based on a combination of two principles (Đekić and Primorac 2016):

- Slow release of hormones by constant rate diffusion through a biocompatible silicone elastomer
- The ability of the vaginal epithelium to rapidly absorb released steroid hormones from the vagina into the circulation

Numerous clinical studies have been published, examining different doses and different steroid hormones. Initially, only two contraceptive rings were developed to the level of a commercial pharmaceutical product: NuvaRing® vaginal ring for combined hormonal contraception with etonogestrel and ethinyl estradiol and Progering® vaginal ring (Laboratorios Silesia, SA, Chile) for progesterone contraception for breastfeeding women (Đekić and Primorac 2016).

For most vaginal rings, there is an initial rapid increase in plasma hormone levels. That is attributed to the migration and accumulation of some active substance on the ring surface during storage. The release of the substance at a constant rate, resulting in constant blood levels corresponding to minimum doses compared to daily fluctuations in steroid hormone concentrations that are present when oral contraceptives are in use. Additionally, steroids that are inactive when administered orally may be administered using a vaginal ring. The next advantage is that the position, i.e., the place in the vagina where the ring is placed, has no effect on its efficiency, since each part of the vaginal epithelium is equally permeable. As a result, no special adjustments or any special installation instructions are required, which gives the woman the option to start or stop use whenever she wants. It is extremely important that the contraceptive vaginal ring does not require daily placement, eliminating the possibility of forgetting the daily intake, which is the main reason for reducing the effectiveness of oral contraceptives in contraception (Filipović and Đekić 2017).

NuvaRing®, a sandwich-type vaginal ring, is made of EVA copolymer with 28% vinyl acetate (inside) and 9% vinyl acetate (outer layer). The ring contains 11.7 mg of etonogestrel and 2.7 mg of ethinyl estradiol. It continuously releases 120 μg of etonogestrel and 15 μg of ethinyl estradiol daily. The ring remains at the place of application for 3 weeks, and after a 1-week break, a new ring is placed. Combined rings (progestin + estrogen) have several advantages: estrogen increases the contraceptive effectiveness of progestin with a synergistic effect on ovulation inhibition. More importantly, estrogen maintains endometrial development and protects against heavy bleeding, which provides good control of the menstrual cycle with regular bleeding (Filipović and Đekić 2017). Systemic exposure to etonogestrel is similar between NuvaRing® and oral contraceptives containing 150 μg of desogestrel and 30 μg of ethinyl estradiol. The bioavailability of ethinyl estradiol from this vaginal ring was about 50% lower compared to the corresponding combined hormonal contraceptives for oral administration (Kerns and Darney 2011; Brache and Faundes 2010). The most common side effects are headache, nausea, and leukorrhea. The

incidence of estrogen-dependent side effects, such as breast swelling, headache, and nausea, was similar between NuvaRing® vaginal rings and appropriate oral contraceptives. Occasionally, there is discomfort at the site of application (foreign body sensation), ring loss, leukorrhea, and vaginitis (Filipović and Đekić 2017).

A new strategy in the development of vaginal rings for combined hormonal contraception is based on the appropriate replacement of ethinyl estradiol with less potent estrogens (estradiol). The aim of this approach was reducing the risk of venous thromboembolism, especially in obese women. Obesity in combination with ethinyl estradiol shows a synergistic effect in increasing the risk of venous thromboembolism. In the United States, clinical trials have been conducted on the vaginal ring that supplies nestoron (200 μg/24 h) and estradiol (10–40 μg/24 h) for 3 months (Brache et al. 2013).

The Progering® contraceptive vaginal ring with progesterone is effective during breastfeeding and is currently available in a number of South American markets. The ring is made of silicone elastomer and releases 10 mg/day of progesterone, continuously for 3 months, after which it should be replaced with a new ring. It can be used for up to 1 year continuously. Since it is a matrix-type therapeutic system, the highest concentration of progesterone in plasma is reached during the first week of use (33.7 nmol/l) and then decreases to 50% and 30% of this value in the ninth and 16th week of use, respectively. Although the effectiveness of the Progering® is lower than that of the NuvaRing®, the effectiveness of the progesterone vaginal ring in breastfeeding mothers is high (over 98.5%), because they already have a certain physiological level of protection against pregnancy. The advantage is that this vaginal ring does not contain an estrogenic component that can reduce lactation. However, in the period of weaning, it is necessary to use additional methods of contraception (Kerns and Darney 2011; Brache and Faundes 2010).

Progesterone has possible benefits for contraception during lactation because it is a natural hormone and is almost inactive when administered orally (the same is true in newborns, even when present in milk), and there are results of a subsequent study on the safe and effective use of this ring during extended use up to 4 months (instead of 3 months) (Filipović and Đekić 2017). In addition, this hormone prolongs lactational amenorrhea, which is an additional benefit for women with anemia, as it reduces bleeding and improves hemoglobin levels (Brache et al. 2013).

Ornibel® is composed of a core of polyurethane and an external membrane of ethylene vinyl acetate, containing 28% vinyl acetate. This different polymer composition allows the active ingredients in a concentration below the saturation limit. As consequence, the ring is more stable and the release of the hormones is more gradual on the first day of use, in contrast to the burst observed with other rings. An additional advantage to this phenomenon is that no special conditions for storage temperature are required (Jaime et al. 2017). It contains 11.00 mg of etonogestrel and 3.47 mg of ethinyl estradiol. The average hormonal release from both rings is 120 mg/day of etonogestrel and 15 mg/day of ethinyl estradiol (Jaime et al. 2017).

Both etonogestrel and ethinyl estradiol are well known and widely used active pharmaceutical ingredients in contraceptive products. Etonogestrel release in the vagina is well controlled and well absorbed, with plasma concentration levels

increasing during the first week to a maximum and then gradually decreasing until the end of the period of use. The maximum plasma concentrations of ethinyl estradiol occur 2–3 days after ring insertion, which is then followed by a gradual decrease in concentrations (Timmer and Mulders 2000; Rafiei et al. 2021).

11.3.3.2 Vaginal Rings for Hormone Replacement Therapy (HRT) for Postmenopausal Men

Continuous delivery of low doses of estrogen from vaginal rings has been recognized as a significant benefit from the aspect of postmenopausal HRT safety (Primorac et al. 2005). The Estring® (Pfizer, UK) vaginal ring is a commercially available pharmaceutical preparation containing 2.0 mg of estradiol hemihydrate (equivalent to 1.94 mg of estradiol) in a ring of silicone elastomers, liquid silicones, and barium sulfate. It releases 7.5 μg of hormone during 24 h, over a period of 3 months. The indication for the use of this vaginal ring is the alleviation of the symptoms of atrophic vaginitis due to estrogen deficiency in postmenopausal women (Filipović and Đekić 2017). The Femring® (Allergan, USA) vaginal ring releases 50 or 100 μg of estradiol per day for a period of 3 months, and the base of the ring consists of silicone elastomers. A higher daily amount of hormones also provides absorption through the vaginal mucosa, so in addition to alleviating urogenital symptoms, vasomotor symptoms (hot flashes) in the postmenopausal period are also regulated (Filipović and Đekić 2017).

References

Abdelkader H, Fathalla Z, Seyfoddin A, Farahani M, Thrimawithana T, Allahham A, Alani AWG, Al-Kinani AA, Alany G (2021) Polymeric long-acting drug delivery systems (LADDS) for treatment of chronic diseases: inserts, patches, wafers, and implants. Adv Drug Deliv Rev 177: 113957

Ashby LS, Smith KA, Stea B (2016) Gliadel wafer implantation combined with standard radiotherapy and concurrent followed by adjuvant temozolomide for treatment of newly diagnosed high-grade glioma: a systematic literature review. W J Surg Oncol 14:225

Augsburger LL, Hoag SW (2008a) Pharmaceutical dosage forms: tablets, Volume 1: Unit operations and mechanical properties, 3rd edn. Informa Healthcare, New York, NY

Augsburger LL, Hoag SW (2008b) Pharmaceutical dosage forms: tablets, volume 2: rational design and formulation, 3rd edn. Informa Healthcare, New York

Augsburger LL, Hoag SW (2008c) Pharmaceutical dosage forms: tablets, volume 3: manufacture and process control, 3rd edn. Informa Healthcare, New York

Bastiancich C, Danhier P, Preat V, Danhier F (2016) Anticancer drug-loaded hydrogels as drug delivery systems for the local treatment of glioblastoma. J Control Release 243:29–42

Bastiancich C, Bozzato E, Henley I, Newland B (2021) Does local drug delivery still hold therapeutic promise for brain cancer? A systematic review. J Control Release 337:296–305

Bekmurzayevaa A, Duncansond WJ, Azevedoc HS, Kanayevaf D (2018) Surface modification of stainless steel for biomedical applications: revisiting a century-old material. Mater Sci Eng C 93: 1073–1089

Blaesi AH (2014) The design and manufacture of immediate-release optimal solid dosage forms. Doctoral dissertation, Massachusetts Institute of Technology

Bocquet L, Tabeling P (2014) Physics and technological aspects of nanofluidics. Lab Chip 14: 3143–3158

Boothroyd G, Dewhurst P, Knight WA (2011) Design for injection molding. In: Boothroyd G, Dewhurst P, Knight WA (eds) Product design for manufacture and assembly, 3rd edn. CRC Press, Boca Raton

Bota DA, Desjardins A, Quinn JA, Affronti ML, Friedman HS (2007) Interstitial chemotherapy with biodegradable BCNU (Gliadel) wafers in the treatment of malignant gliomas. Ther Clin Risk Manag 3:707–715

Brache V, Faundes A (2010) Contraceptive vaginal rings: a review. Contraception 82:418–427

Brache V, Payáan LJ, Faundes A (2013) Current status of contraceptive vaginal rings. Contraception 87:264–272

Bregy A, Shah AH, Diaz MV, Pierce HE, Ames PL, Diaz D et al (2013) The role of Gliadel wafers in the treatment of high-grade gliomas. Expert Rev Anticancer Ther 13:1453–1461

Busch C, Zur D, Fraser-Bell S, Lains I, Santos AR, Lupidi M et al (2018) Shall we stay, or shall we switch? Continued antiVEGF therapy versus early switch to dexamethasone implant in refractory diabetic macular edema. Acta Diabetol 55:789–796

Čatić I (2006) Uvod u proizvodnju polimernih tvorevina. Biblioteka Polimerstvo, Zagreb, pp 1–9

Cuff G, Raouf F (1998) A preliminary evaluation of injection molding as a technology to produce tablets. Pharm Tech 22:96–106

das Neves J, Amaral MH, Bahia MF (2008) Vaginal drug delivery: vaginal drug delivery systems. In: Cox Gad S (ed) Pharmaceutical manufacturing handbook: production and processes. Wiley, Hoboken, pp 809–878

Dash A, Cudworth G (1998) Therapeutic applications of implantable drug delivery systems. J Pharmacol Toxicol Meth 40(1):1–12

Debono M, Voicu D, Pousti M, Safdar M, Young R, Kumacheva E, Greener J (2016) One-step fabrication of microchannels with integrated three dimensional features by hot intrusion embossing. Sensors 16:2023

Đekić L, Primorac M (2016) Farmaceutsko-tehnološki aspekti terapijskih sistema za hormonsku kontracepciju. Arh farm 66:217–238

Duffy DC, Schueller OJA, Brittain ST, Whitesides GM (1999) Rapid prototyping of microfluidic switches in poly(dimethylsiloxane) and their actuation by electro-osmotic flow. J Micromech Microeng 9:211

Farooque R, Asjad M, Rizvi SJA (2021) A current state of art applied to injection moulding manufacturing process – a review. Mater Today: Proc 43:441–446

Filipović M, Đekić L (2017) Karakteristike terapijskih sistema za vaginalnu primenu/characteristics of vaginal delivery systems. Arh farm 67:360–367

Friend DR (2011) Intravaginal rings: controlled release systems for contraception and prevention of transmission of sexually transmitted infections. Drug Deliv Transl Res 1:185–193

Fung LK, Ewend MG, Sills A, Sipos EP, Thompson R, Watts M et al (1998) Pharmacokinetics of interstitial delivery of carmustine, 4-hydroperoxycyclophosphamide, and paclitaxel from a biodegradable polymer implant in the monkey brain. Cancer Res 58:672–684

Gale BK, Jafek AR, Lambert CJ, Goenner BL, Moghimifam H, Nze UC, Kamarapu SK (2018) A review of current methods in microfluidic device fabrication and future commercialization prospects. Inventions 3:60

Giboz J, Copponnex T, Mélé P (2007) Microinjection molding of thermoplastic polymers: a review. J Micromech Microeng 17(6):96–109

Gokhale A, McConnell J, Loxley A, Mitchnick M (2009) Combination devices to protect women from sexual transmission of HIV. Drug Del Technol 9:18–21

Grossman SA, Reinhard C, Colvin OM, Chasin M, Brundrett R, Tamargo RJ et al (1992) The intracerebral distribution of BCNU delivered by surgically implanted biodegradable polymers. J Neurosurg 76:640–647

Grube E, Schofer J, Hauptmann KE, Nickenig G, Curzen N, Allocco DJ, Dawkins KD (2010) A novel paclitaxel-eluting stent with an ultrathin abluminal biodegradable polymer. JACC Cardiovasc Interv 3(4):431–438

Heckele M, Schomburg WK (2004) Review on micro molding of thermoplastic polymers. J Micromech Microeng 14:R1–R14

Hoffman AS (2008) The origins and evolution of "controlled" drug delivery systems. J Control Release 132(3):153–163

Hussain A, Ahsan F (2005) The vagina as a route for systemic drug delivery. J Control Release 103(2):301–313

Jaime A, Maria D, de Benito R, Lefebvre M, Sicard E, Furtado M et al (2017) Pharmacokinetic bioequivalence, safety and acceptability of Ornibel®, a new polymer composition contraceptive vaginal ring (etonogestrel/ethinylestradiol 11.00/3.474 mg) compared with Nuvaring ® (etonogestrel/ethinylestradiol 11.7/2.7 mg). Eur J Contracept Reprod Health Care 22(6): 429–438

Juratli TA, Schackert G, Krex D (2013) Current status of local therapy in malignant gliomas - a clinical review of three selected approaches. Pharmacol Ther 139:341–358

Kerns J, Darney P (2011) Vaginal ring contraception. Contraception 2011(83):107–115

Kim E, Xia Y, Whitesides GM (1995) Polymeric microstructures formed by moulding in capillaries. Nature 376:581–584

Kim S, Traore YL, Chen Y, Ho EA, Liu S (2018a) Switchable on-demand release of a nanocarrier from a segmented reservoir type intravaginal ring filled with a pH-responsive supramolecular polyurethane hydrogel. ACS Appl Biol Mater 1:652–662

Kim S, Traore YL, Ho EA, Shafiq M, Kim SH, Liu S (2018b) Design and development of pH-responsive polyurethane membranes for intravaginal release of nanomedicines. Acta Biomater 82:12–23

Kleiner LW, Wright JC, Wang Y (2014) Evolution of implantable and insertable drug delivery systems. J Control Release 181:1–10

Koob TJ (2004) Encyclopedia of biomaterials and biomedical engineering. Marcel Dekker, New York, p 335

Lee DH, Chan CK (2020) Modified insertion technique for a intravitreal implant (Ozurdex®). Am J Ophthalmol Case Rep 19:100725

Lyu S, Untereker D (2009) Degradability of polymers for implantable biomedical devices. Int J Mol Sci 10(9):4033–4065

Madou MJ (2002) Fundamentals of microfabrication: the science of miniaturization, 2nd edn. CRC Press, Boca Raton

Maghsoudi K, Jafari R, Momen G, Farzaneh M (2017) Micro-nanostructured polymer surfaces using injection molding: a review. Mater Today Commun 13:126–143

Malcolm RK, Fetherston SM, McCoy CF, Boyd P, Major I (2012) Vaginal rings for delivery of HIV microbicides. Int J Women's Health 4:595–605

Malcolm RK, Boyd PJ, McCoy CF, Murphy DJ (2015) Microbicide vaginal rings: technological challenges and clinical development. Adv Drug Deliv Rev 103:33–56

Maniruzzaman M, Nokhodchi A (2016) Advanced implantable drug delivery systems via continuous manufacturing. Crit Rev Ther Drug Carrier Syst 33(6):569–589

Martín del Valle EM, Galan MA, Carbonell RG (2009) Drug delivery technologies: the way forward in the new decade. Ind Eng Chem Res 48(5):2475–2486

Matschuk M, Larsen NB (2012) Injection molding of high aspect ratio sub −100 nm nanostructures. J Micromech Microeng 23(2):025003

Matschuk M, Bruus H, Larsen NB (2010) Nanostructures for all-polymer microfluidic systems. Microelectron Eng 87(5):1379–1382

McDonald JC, Duffy DC, Anderson JR, Chiu DT, Wu H, Schueller OJ, Whitesides GM (2000) Fabrication of microfluidic systems in poly(dimethylsiloxane). Electrophoresis 21:27

Mekaru H, Yamada T, Yan S, Hattori T (2004) Microfabrication by hot embossing and injection molding at LASTI. Microsyst Technol 10:682

Melocchi A (2014) Injection molding/micromolding applications to drug delivery, Doctoral dissertation. University of Milan, pp 8–30
Mesquita L, Galante J, Nunes R, Sarmento B, Neves J (2019) Pharmaceutical vehicles for vaginal and rectal administration of anti-HIV microbicide nanosystems. Pharmaceutics 11(3):1–20
Mitchell GR, Carreira P, Gomes S, Mateus A, Mohan S (2017) Morphology development during micro injection moulding of thermoplastics. Procedia Manufact 12:230–241
Mohammadpour F, Hadizadeh F, Tafaghodi M, Sadri K, Mohammadpour AH, Kalani MR et al (2019) Preparation, in vitro and in vivo evaluation of PLGA/chitosan based nanocomplex as a novel insulin delivery formulation. Int J Pharm 572:118710
Novak A, De la Loge C, Abetz L, Van der Meulen E (2003) The combined contraceptive vaginal ring, NuvaRing®: an international study of user acceptability. Contraception 67(3):187–194
Ordikhani F, Arslan ME, Marcelo R, Sahin I, Grigsby P, Schwarz J et al (2016) Drug delivery approaches for the treatment of cervical cancer. Pharmaceutics 8(23):1–15
Ormiston JA, Serruys PW (2009) Bioabsorbable coronary stents. Circ Cardiovasc Interventions 2(3):255–260
Osmałek T, Froelich A, Jadach B, Tatarek A, Gadziński P, Falana A (2021) Recent advances in polymer-based vaginal drug delivery systems. Pharmaceutics 13(6):1–49
Osswald T, Turng LS, Gramann P (2008) Injection molding handbook, 2nd edn. Carl Hanser, Munich
Ostojic MC, Perisic Z, Sagic D, Jung R, Zhang Y-L, Bendrick-Peart J et al (2011) The pharmacokinetics of Biolimus A9 after elution from the BioMatrix II stent in patients with coronary artery disease: the stealth PK study. Eur J Clin Pharmacol 67:389–398
Pandey M, Choudhury H, Abdul-Aziz A, Bhattamisra SK, Gorain B, Carine T et al (2021) Promising drug delivery approaches to treat microbial infections in the vagina: a recent update. Polymers 13(26):1–65
Papautsky I, Peterson ETK (2008) Micromolding. In: Li D (ed) Encyclopedia of microfluidics and nanofluidics. Springer, New York, pp 1256–1267
Park S, Lee W, Moon S, Yoo Y, Cho Y (2011) Injection molding micro patterns with high aspect ratio using a polymeric flexible stamper. eXPRESSPolym Lett 5(11):950–958
Patel CM, Patel MA, Patel NP, Prajapati P, Patel C (2010) Poly lactic glycolic acid (PLGA) as biodegradable polymer. Res J Pharmacy Technol 3:353–360
Perry J, Chambers A, Spithoff K, Laperriere N (2007) Gliadel wafers in the treatment of malignant glioma: a systematic review. Curr Oncol 14:189–194
Pizzi M, De Martiis O, Grasso V (2004) Fabrication of self assembled micro reservoirs for controlled drug release. Biomed Microdevices 6(2):155–158
Primorac M, Đorđević L, Vasiljević D (2005) Characteristics of novel pharmaceutical preparations for hormone replacement therapy in menopause/Karakteristike savremenih farmaceutskih preparata za terapijsku supstituciju hormona u menopauzi. Arh Farm 55:131–147
Quinten T, De Beer T, Vervaet C, Remon JP (2009) Evaluation of injection moulding as a pharmaceutical technology to produce matrix tablets. Eur J Pharm Biopharm 71:145–154
Quinten T, De Beer T, Onofre FO, Mendez-Montealvo G, Wang YJ, Remon JP, Vervaet C (2011) Sustained-release and swelling characteristics of xanthan gum/ethylcellulose-based injection moulded matrix tablets: in vitro and in vivo evaluation. J Pharm Sci 100:2858–2870
Rafiei F, Tabesh H, Farzad S, Farzaneh F, Rezaei M, Hosseinzade F et al (2021) Development of hormonal intravaginal rings: technology and challenges. Geburtsh Frauenheilk 81:789–806
Rathbone MJ, Bunt CR, Ogle CR, Burggraaf S, Macmillan KL, Pickering K (2002) Development of an injection molded poly(ε-caprolactone) intravaginal insert for the delivery of progesterone to cattle. J Control Release 85:61–71
Rohloff CM, Alessi TR, Yang B, Dahms J, Carr JP, Lautenbach SD (2008) DUROS® technology delivers peptides and proteins at consistent rate continuously for 3 to 12 months. J Diabetes Sci Technol 2(3):461–467

Rothen-Weinhold A, Besseghir K, Vuaridel E, Sublet E, Oudry N, Kubel F, Gurny R (1999) Injection-molding versus extrusion as manufacturing technique for the preparation of biodegradable implants. Eur J Pharm Biopharm 48:113–121

Rotting O, Ropke W, Becker H, Gartner C (2002) Polymer microfabrication technologies. Microsyst Technol 8:36–32

Rudnick JD, Sarmiento JM, Uy B, Nuno M, Wheeler CJ, Mazer MJ, Wang H, Hua JL, Chu RM, Phuphanich S, Black KL, Yu JS (2020) A phase I trial of surgical resection with Gliadel Wafer placement followed by vaccination with dendritic cells pulsed with tumor lysate for patients with malignant glioma. J Clin Neurosci 74:187–193

Shiah JG, Bhagat R, Blanda WM, Nivaggioli T, Peng L, Chou D, Weber DA (2011) Ocular implant made by a double extrusion process. French patent CA2576392 C 2011, July 12

Tadmor Z, Gogos CG (2006) Principles of polymer processing. Wiley, Hoboken, NJ

Timmer CJ, Mulders TMT (2000) Pharmacokinetics of etonogestrel and ethinylestradiol released from a combined contraceptive vaginal ring. Clin Pharmacokinet 39:233–242

Wang Y, Boyd P, Hunter A, Malcolm RK (2018) Intravaginal rings for continuous low-dose administration of cervical ripening agents. Int J Pharm 549:124–132

Weerakoon-Ratnayake KM, O'Neil CE, Uba FI, Soper SA (2017) Thermoplastic nanofluidic devices for biomedical applications. Lab Chip 17:362–381

Westphal M, Hilt DC, Bortey E, Delavault P, Olivares R, Warnke PC et al (2003) A phase 3 trial of local chemotherapy with biodegradable carmustine (BCNU) wafers (Gliadel wafers) in patients with primary malignant glioma. Neurooncology 5:79–88

Westphal M, Ram Z, Riddle V, Hilt D, Bortey E (2006) Gliadel wafer in initial surgery for malignant glioma: long-term follow-up of a multicenter controlled trial. Acta Neurochir 148: 269–275. (discussion 275)

Wolinsky JB, Colson YL, Grinstaff MW (2012) Local drug delivery strategies for cancer treatment: gels, nanoparticles, polymeric films, rods, and wafers. J Control Release 159:14–26

Wright JC, Leonard ST, Stevenson CL, Beck JC, Chen G, Jao RM, Johnson PA, Leonard J, Skowronski RJ (2001) An in vivo/in vitro comparison with a leuprolide osmotic implant for the treatment of prostate cancer. J Control Release 75(1):1–10

Wright J, Johnson R, Yum S (2003) DUROS® osmotic pharmaceutical systems for parenteral & site-directed therapy. Drug Deliv Technol 3(1):64–73

Wu J, Gu M (2011) Microfluidic sensing: state of the art fabrication and detection techniques. J Biomed 16:080901

Yao D (2008) Micromolding of polymers. In: Thomas S, Weimin Y (eds) Advances in polymer processing - from macro to nano scales. CRC Press, Washington, pp 552–578

Zema L, Loreti G, Melocchi A, Maroni A, Gazzaniga AA (2012) Injection molding and its application to drug delivery. J Control Release 159:324–331

Zhang Y, Davis DA, Aboul Fotouh K, Wang J, Williams D, Bhambhani A et al (2021) Novel formulations and drug delivery systems to administer biological solids. Adv Drug Deliv Rev 172:183–210

Chapter 12
Supercritical Fluids: A Promising Technique in Pharmaceutics

Vivek Trivedi and Adejumoke Lara Ajiboye

Abstract The unique properties of supercritical carbon dioxide provide numerous opportunities for developing environmentally friendly pharmaceutical processes. The applications of supercritical carbon dioxide range from particle engineering to encapsulation to biopolymeric scaffold manufacturing. Moreover, the tunable nature of supercritical carbon dioxide can also impart interesting properties in the final product that may not be possible via any other conventional process. This chapter aims to provide an overview of the available processes and techniques according to the role of supercritical carbon dioxide and how can those be applied in pharmaceutical research and development and manufacturing. The application of supercritical carbon dioxide as solvent, antisolvent and solute/additive is discussed along with examples to highlight advancements in this field and how pharmaceutical manufacturing could benefit from moving to a greener and cleaner processing technique that is environmentally sustainable.

Keywords Supercritical carbon dioxide · Drug delivery systems · Rapid Expansion of Supercritical Solutions (RESS) · Supercritical antisolvent (SAS) · Gas antisolvent (GAS) · Particles from gas-saturated solutions (PGSS) · Green processing

12.1 Introduction

The major goal of the pharmaceutical industry is to develop new molecules and formulations to produce novel treatments with improved therapeutic efficacy. However, this endeavour makes pharmaceutical research and development and manufacturing environmentally unsustainable partly due to the continuous need to employ organic solvents in these processes. The importance of sustainability in the development of drug delivery systems has led to the rising interest in the use of

V. Trivedi (✉) · A. L. Ajiboye
University of Kent, Kent, UK
e-mail: V.Trivedi@Kent.ac.uk; L.Ajiboye@kent.ac.uk

D. Lamprou (ed.), *Nano- and Microfabrication Techniques in Drug Delivery*,
Advanced Clinical Pharmacy – Research, Development and Practical Applications 2,
https://doi.org/10.1007/978-3-031-26908-0_12

Table 12.1 Density, viscosity and diffusivity comparison of fluids (Goodship and Oqur 2005; Mukhopadhyay 2000)

Phase	Density (g/cm^3)	Viscosity (Poise)	Diffusivity (cm^2/s)
Gas	0.001	$0.5–3.5 \times 10^{-4}$	0.01–1.00
SCF	0.2–0.9	$0.2–1.0 \times 10^{-3}$	$0.1–3.3 \times 10^{-4}$
Liquid	0.8–1.0	$0.3–2.4 \times 10^{-2}$	$0.5–2.0 \times 10^{-5}$

environmentally friendly alternatives such as ionic liquids and supercritical or dense phase fluids that can either remove the use of organic solvents completely or at least reduce their usage. The continuous advancements in this field including in the application of supercritical fluids (SCFs) have allowed the development of processes favourable to pharmaceutical manufacturing and analysis, which has been gaining significant interest lately (Kankala et al. 2017, 2021; Franco and de Marco 2021; Ahangari et al. 2021; Chen et al. 2021; Kai Bin et al. 2020).

An SCF can be defined as a substance above its critical pressure (P_c) and critical temperature (T_c) (Nic et al. 2014). SCFs exist as a single phase above their critical point with distinctive properties that are unlike those of either liquids or gases under standard conditions. The properties of an SCF are intermediate (Table 12.1) to those of liquids and gases; that is, gas-like viscosity and diffusivity with almost zero surface tension give SCF excellent transport properties, while liquid-like density provides higher and tunable solvent power.

The relationship between temperature, pressure and their effect on the phase behaviour of a substance can be easily explained using phase diagrams.

Figure 12.1 presents a phase diagram of carbon dioxide (CO_2) and indicates the transition between different phases including into supercritical state (Ginty et al. 2005). The melting (ABC) and boiling (ABD) curves in the phase diagram denote the transition between liquid, solid and vapour phases, whereas triple point at which CO_2 exists simultaneously as liquid, gas and solid is represented with point B and its conversion into the supercritical state is denoted by point D. A list of selected SCFs along with their T_c, P_c and critical densities is shown in Table 12.2.

It is important to remember that SCFs cannot be liquified above their P_c even with extreme pressures and similarly these cannot be converted into vapour with an increase in temperature above T_c. However, the properties of an SCF can be easily tuned by varying pressure and temperature, as opposed to conventional organic solvents that show minimal impact to changes in temperatures and pressures. CO_2 is one of the most commonly used SCFs due to its relatively low critical temperature and pressure ($T_c = 31.1$ and $P_c = 73.8$ bar), which is ideal for processing thermosensitive materials. The advantages of $scCO_2$ or SCF, in general, can be summarised as follows.

- SCFs with higher diffusivities and lower viscosities are desirable due to solvating power like organic solvents.
- The ability to rapidly vary density resulting in the change of solvent strength allows SCFs to be used as both solvent and antisolvent in many pharmaceutical operations.

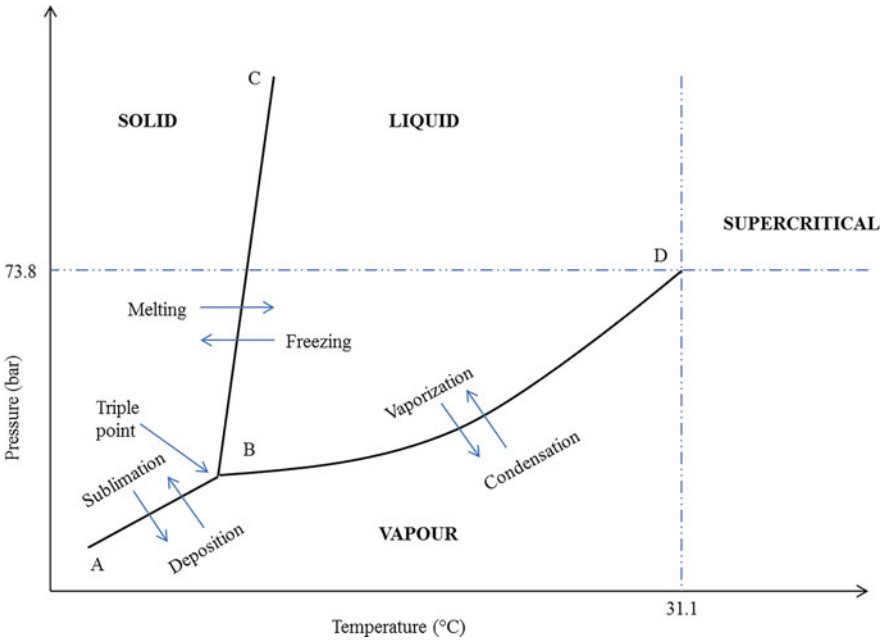

Fig. 12.1 Phase diagram of carbon dioxide

Table 12.2 A list of SCFs with T_c, P_c and critical densities (Lide and Haynes 2009)

SCF	Molecular weight (g/mol)	T_c (°C)	P_c (bar)	Critical density (g/cm^3)
Water	18.02	374.1	220.5	0.322
Ammonia	17.03	132.5	112.8	0.235
Methanol	32.04	239.4	81.0	0.272
Ethane	30.07	32.2	48.8	0.203
Ethanol	46.07	243.0	63.8	0.276
Nitrogen	28.01	−147.0	34.0	0.314
Dinitrogen monoxide	44.01	36.4	72.5	0.452
Acetone	58.08	235	46.9	0.278
Ethylene	28.05	9.2	50.4	0.215
Carbon dioxide	44.01	31.1	73.8	0.469

- SCFs are effective media for particle formation due to their easily tunable density and diffusivity.
- Commonly used SCFs (e.g. CO_2) are economical, safe, non-flammable and easily available.
- Unlike organic solvents, SCFs are environmentally benign and easy to dispose of and recycle.

The primary disadvantages of SCFs, such as $scCO_2$, include the necessity to work at high pressures and the complex thermodynamics of the fluid. This results in the initial high set-up costs that may act as a hindrance to its applicability on a wider scale (Girotra et al. 2013). Nonetheless, there are numerous applications of $scCO_2$ in the pharmaceutical industry with more advancements being reported on a regular basis. The applications of $scCO_2$ can be largely divided according to the role of the $scCO_2$ in the process, i.e. solvent, antisolvent and solute, which will be discussed in the forthcoming sections.

12.2 Applications of Supercritical Fluids

The applications of SCFs in the field of pharmaceuticals are varied (e.g. synthesis, modification, purification or particle formation) and based on the role of the SCF in the process, i.e. as a solvent, antisolvent and/or solute. SCFs can find applications in any aspect of the pharmaceutical industry, few of which are summarised in Fig. 12.2.

As mentioned earlier, CO_2 is the most commonly used SCFs in the pharmaceutical industry due to its safety profile and favourable operating conditions in comparison to many others. The versatility of CO_2 also makes it suitable for the processing of pharmaceutical actives and excipients since it can play different roles to produce micro/nanoparticles, controlled release drug delivery systems, polymeric scaffolds and amorphous materials, to name a few. A summary of various $scCO_2$-based techniques according to the role of SCF in the process is presented in Table 12.3.

This chapter aims to discuss the utilisation of $scCO_2$ as a solvent, antisolvent and solute or additive with examples to provide an overview of these processes and their applicability in pharmaceutical research and development.

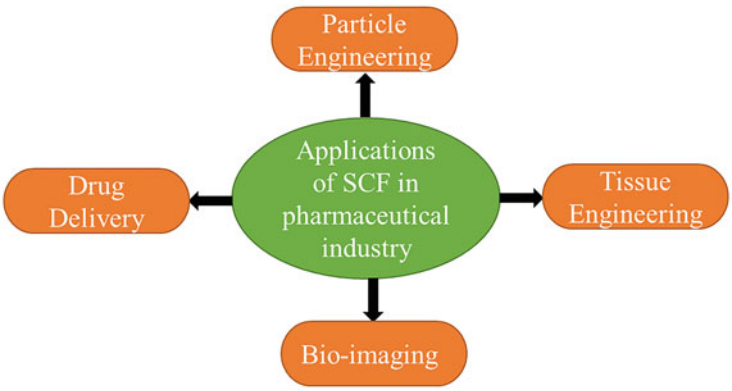

Fig. 12.2 Applications of SCFs in the pharmaceutical industry

Table 12.3 $scCO_2$-based methodologies, corresponding processes and acronyms (Padrela et al. 2018)

Role	Acronym	$scCO_2$ process
Solvent	RESS	Rapid expansion of supercritical solutions
	RESOLV	Rapid expansion of a supercritical solution into a liquid solvent
	RESSAS	Rapid expansion of a supercritical solution into an aqueous solvent
	RESS-N	Rapid expansion of supercritical solutions with a non-solvent
	RESS-SC	Rapid expansion of supercritical solutions with a solid co-solvent
	CSS	(Co)crystallisation from a supercritical solution
Antisolvent or co-antisolvent	SAS	Supercritical antisolvent crystallisation
	SAS-DEM	Supercritical antisolvent with drug-excipient mixing
	SAS-EM	Supercritical antisolvent with enhanced mass transfer
	SEDS	Solution-enhanced dispersion of solids
	SpEDS	Suspension-enhanced dispersion by $scCO_2$
	SEDS-PA	Solution-enhanced dispersion by supercritical fluids-prefilming atomisation
	ASES	Aerosol solvent extraction system
	ARISE	Atomised rapid injection for solvent extraction
	SFEE	Supercritical fluid extraction of emulsions
	ASAIS	Atomisation of supercritical antisolvent induced suspensions
	AAS	Atomisation and antisolvent crystallisation
	GAS	Gas antisolvent crystallisation
	GASR	Gas antisolvent recrystallisation
	GASP	Gas antisolvent precipitation
	PCA	Precipitation with a compressed fluid antisolvent
	ELAS	Expanded liquid antisolvent
Additive (solute, co-solute, co-solvent)	PGSS	Particles from gas-saturated solutions
	PGSS-drying	Particle formation from gas-saturated solutions and drying
	CPF	Concentrated powder form
	CPCSP	Continuous powder coating spraying process
	GAMA	Gas-assisted melting atomisation
	PPRGEL	Precipitation by pressure reduction of gas-expanded liquids
	CAN-BD	Carbon dioxide-assisted nebulisation with a bubble dryer
	SAILA	Supercritical-assisted injection in a liquid antisolvent
	SAA	Supercritical CO_2-assisted atomisation
	SASD	Supercritical-assisted spray drying

(continued)

Table 12.3 (continued)

Role	Acronym	$scCO_2$ process
	SAA-HCM	Supercritical-assisted atomisation-hydrodynamic cavitation mixer
	SEA	Supercritical-enhanced atomisation
	DELOS	Depressurisation of an expanded-liquid organic solution

12.2.1 $scCO_2$ Processes as Solvent

The solvating power of SCF is based on its thermophysical properties (density, viscosity, diffusivity and dielectric constant), which can be easily fine-tuned by varying the processing pressure and temperature, thus offering the possibility of customising an SCF to accommodate the specific needs of the system under investigation (Duarte et al. 2009; Bhomia et al. 2014a). The RESS was the first technique conceptualised by Krukonis in 1984 and has since established itself as a simple process for the generation of small particles with narrow distribution (Joshi 2011). This procedure utilises the solvating power of SCFs in the recrystallisation of solid materials with the intention of formulating uniform-sized fine particles. In the RESS process, a solute is originally dispersed or solubilised in SCF at high pressures, and then the saturated solution is expanded rapidly through a heated nozzle to a lower pressure chamber. This results in the formation of a super-saturated solution, which subsequently causes the rapid nucleation and precipitation of the solute into micro/nanoparticles (Fages et al. 2004; Fahim et al. 2014). Generally, the most used solvent in RESS is $scCO_2$ due to its mild operating conditions, inert properties and its ability to produce final products without any solvent residues (Fages et al. 2004; Knez et al. 2019).

The schematic representation of the RESS process is presented in Fig. 12.3.

The success of RESS in particle formation is largely dependent on the ability of $scCO_2$ to dissolve a solute to practical levels, which can be achieved by changes to the solvent density (i.e. by adjusting the working temperature and pressure) (Kopcak and Mohamed 2005). The solubility of a material in $scCO_2$ is also governed by the chemical properties of the solute. The presence of CO_2-philic moieties such as carbonyl groups in the molecule can facilitate the dissolution by promoting solute-solvent interactions between the carbon atom of CO_2 (Lewis acid) and the lone pairs on the oxygen of a carbonyl group (Lewis base) (Kilic et al. 2009; Peach and Eastoe 2014). However, these solute-CO_2 interactions can be weakened by the strong solute-solute interactions due to the presence of hydrogen-bonding functionalities in a molecule. In general, solubility in $scCO_2$ is said to be better for non-polar substances than polar materials because of the low dielectric constant and polarisability per volume of CO_2 (Peach and Eastoe 2014; Kajiya et al. 2008; Kanakubo et al. 2000; Zhang et al. 2002). The low solubility of CO_2-phobic compounds or polar substances in non-polar SCF solvents, like $scCO_2$, can serve as a limitation in the RESS process. This could lead to high consumption of CO_2,

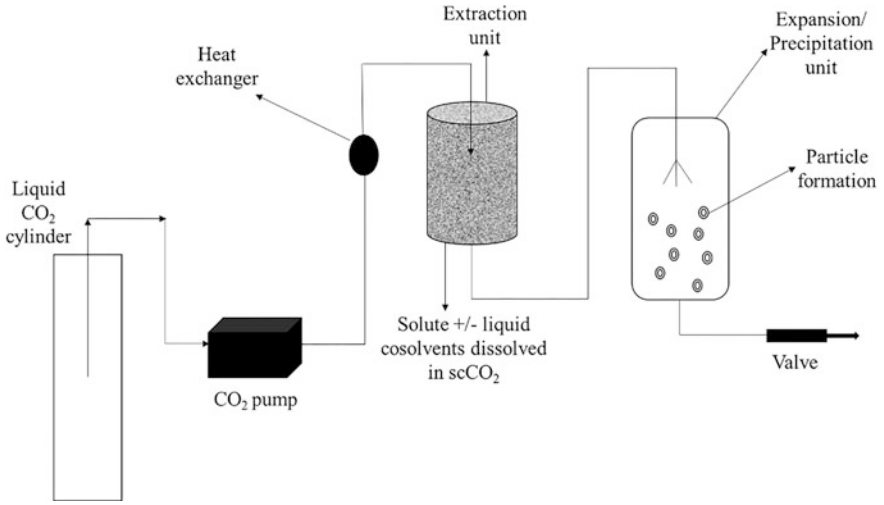

Fig. 12.3 Schematic diagram of the RESS process

which consequently may result in a significant increase in production costs. Furthermore, there is also a high tendency for insoluble particles to accumulate and block the expansion nozzle (Kopcak and Mohamed 2005; Zhang et al. 2002). Several modifications to the standard RESS technique have been introduced to overcome these limitations, but they are still governed by the same principle of RESS where solubility is the most important factor for it to be successfully applied. The modified techniques employ various strategies including the use of co-solvents or agents to enhance the solubility of the drug or excipient before they could be expanded to produce desirable particles. A brief summary of various RESS-based methods is presented in Table 12.4 (Padrela et al. 2018).

In general, the RESS and RESS-based methodologies with $scCO_2$ have been applied to process a wide range of organic and inorganic materials and even biologics, some of which are presented in Table 12.5.

In summary, the efficacy of $scCO_2$ as a solvent is reliant on the functional groups present in a solute and processing parameters (pressure and temperature) that govern the solubility of the material in the SCF and control nucleation and resulting morphology. Although there have been major improvements to the RESS processes, solubility remains the critical factor that limits their use, especially as many pharmaceutically important molecules tend to have limited or no solubility in $scCO_2$.

12.2.2 $scCO_2$ Processes as Antisolvent

As mentioned above, CO_2 is an excellent processing medium, but the relatively low solubilities of pharmaceuticals in $scCO_2$ pose an issue. The exploitation of $scCO_2$ as

Table 12.4 A brief description of RESS-based methods for particle formation

RESS-based method	Description
Rapid expansion of a supercritical solution into a liquid solvent (*RESOLV*) Rapid expansion of a supercritical solution into an aqueous solvent (*RESSAS*)	Expansion of a supercritical solution into an aqueous solution containing surfactant (s) or reducing agents. The presence of surfactants inhibits the formation of aggregates or agglomerates in the expansion jet and promotes stability within the final liquid suspension
Rapid expansion of supercritical solutions with a solid co-solvent (*RESS-SC*)	The RESS process that uses limited quantities of co-solvents to enhance solubilities and solute loading in the SCF. Ideally, the chosen co-solvent is inert, non-toxic and non-flammable and has substantial solubility in $scCO_2$ and high vapour pressure for easy removal
Rapid expansion of supercritical solutions with a non-solvent (*RESS-N*)	This technique is only used for encapsulating pre-formed solid materials within other substances. Firstly, the non-soluble solid particles are mixed with the coating substance that has been dissolved in a binary $scCO_2$/co-solvent system. The coating material nucleates and precipitates around the solid material to form encapsulated products following expansion to atmospheric pressure
Cocrystallisation from a supercritical solution (*CSS*)	Similar to the RESS process, supersaturation and nucleation of particles are induced by lowering the temperature and pressure to obtain cocrystals. However, in this method, the reduction rate is usually much slower and maintained at a steady rate. This gives better control over the particle size, shape and morphology of the final product

an antisolvent addresses this limitation wherein the solutes of interest (e.g. drugs, polymers or combinations) are dissolved in organic solvent/s of choice before introducing them to the SCF. Table 12.3 lists a number of antisolvent processes that primarily work on the principle of volume expansion of the liquid phase owing to the ability of a solvent to solubilise large quantities of gas/$scCO_2$. This volume expansion leads to the reduction in the solvent density leading to supersaturation and finally solute precipitation. The solvent is then removed from the product during depressurisation, which can be collected and recycled at the end of the process.

GAS was the first antisolvent process described by Gallagher et al. for the micronisation of explosives (Gallagher et al. 1989). GAS is a batch method that involves the controlled addition of pressurised CO_2 into a drug solution consisting of a CO_2-miscible solvent. The reduction in the solvency of a solvent due to its miscibility with CO_2 causes drug precipitation and micronisation. The supercritical antisolvent (SAS) process is a slightly modified version of GAS. SAS can be a continuous or semi-continuous process, and it involves spraying a solution into the SCF via a nozzle to produce micro/nanoparticles or encapsulates. Variations of SAS processes include SAS-DEM, SEDS, SAS-EM, SEDS-PA, SpEDS, SFEE and

Table 12.5 Examples of RESS/RESS-based methods for particle formation

Solute	T_{ext} (°C)	P_{ext} (bar)	T_{exp} (°C)	P_{exp} (bar)	Co-solvent/ additive	PS (μm)	Method	References
Ibuprofen/nicotinamide	50	300	–	–	–	< / > 10	RESS	Müllers et al. (2015)
Coumarin	40–60	150–420	–	10–50	–	19–61	RESS	Oliveira and Pinto (2017)
Gemfibrozil	25–55	100–250	35	Atm.	–	0.8–2.2	RESS	Baseri and Lotfollahi (2013)
Piroxicam	35–60	160–220	–	–	–	1.5–8.8	RESS	Zeinolabedini Hezave and Esmaeilzadeh (2012)
Ethosuximide	35	150–200	Pre: 30–70 Post: 0–30	Atm.	–	1.5–12.5	RESS	Lin et al. (2012)
Raloxifene	40–80	100–180	Pre: 100	–	–	0.02–0.14	RESS	Keshavarz et al. (2012)
Amoxicillin	40–60	150–210	–	–	–	1.08–5.72	RESS	Hezave and Esmaeilzadeh (2012)
Artemisinin	32–62	100–250	25–55	Atm.	–	0.55–2.1	RESS	Yu et al. (2012)
Naproxen	60 and 100	200–300	Pre: 60 and 100	–	Methanol	0.06–0.92	RESS	Montes et al. (2013)
Paracetamol Mefenamic acid Nabumetone Tolbutamide	55–75 55 35 50	250–300 150–300 150–250 150–300	Pre: 60–100 Pre: 60–110 Pre:	Pre: 250–300 Pre: 150–300 Pre:	– – – –	0.16–0.34 0.08–0.16 0.75–0.81 0.34–0.45	RESS	Türk and Bolten (2016)

(continued)

Table 12.5 (continued)

Solute	T_{ext} (°C)	P_{ext} (bar)	T_{exp} (°C)	P_{exp} (bar)	Co-solvent/ additive	PS (μm)	Method	References
			40–60 Pre: 60–100	150–250 Pre: 150–300				
Clobetasol propionate	55	200–260	Pre: 70–110	–	Menthol	0.09–0.32	RESS-SC	Keshmiri et al. (2015)
Letrozole	45–75	120–360	Pre: 80 Post: 0	–	Menthol	0.02–0.26	RESS-SC	Sodeifian and Sajadian (2018)
Beclomethasone dipropionate	–	200–260	Pre: 70–110	–	Menthol	0.06–0.29	RESS-SC	Hosseinpour et al. (2015)
Theophylline	35–65 40	140–180 220	Pre: 40–65 65	–	Menthol Vanillin	– 0.085–0.089	RESS-SC	Uchida et al. (2015)
Fenofibrate	60	100–200	–	Pre: 100–200	Tween 80 SDS PF-68 HPMC SA	0.5–5	RESOLV/ RESSAS	Sameer et al. (2013)
Amiodarone hydrochloride	35–65	120–270	65	1	– HPMC PVP	0.10–0.48 0.04–0.26	RESS RESOLV/ US- RESOLV	Sodeifian and Sajadian (2019)
Acetamidophenol Acetylsalicylic acid Flavone 3-Hydroxyflavone 1,3-Dimethylxanthine	–	–	Pre: 35	Pre: 100–250	PEG/PMMA/ PLLA/EC/PEG- PPG-PEG Methanol/etha- nol/1-propanol/ toluene	>6	RESS-N	Matsuyama et al. (2003)

Saccharin + theophylline/indomethacin/ carbamazepine/caffeine/sulfamethazine/ acetylsalicylic acid	50	200	–	–	Ethanol	–	CSS	Padrela et al. (2015)

T_{ext}: Extraction Temperature, P_{ext}: Extraction Pressure, T_{exp}: Expansion Temperature, P_{exp}: Expansion Pressure, PS: Particle size, Atm.: Atmospheric, RT: Room Temperature, SDS: Sodium dodecyl sulphate, PF-68: Pluronic F-68, HPMC: Hydroxypropyl methyl cellulose, SA: Sodium alginate, US-RESOLV: Ultrasonic-assisted RESOLV, PVP: Polyvinylpyrrolidone, PEG: Poly (ethylene glycol), PMMA: Poly (methyl methacrylate), PLLA: Poly (L-lactic acid), EC: Ethyl cellulose, PEG-PPG-PEG: PEG-poly (propylene glycol)-PEG

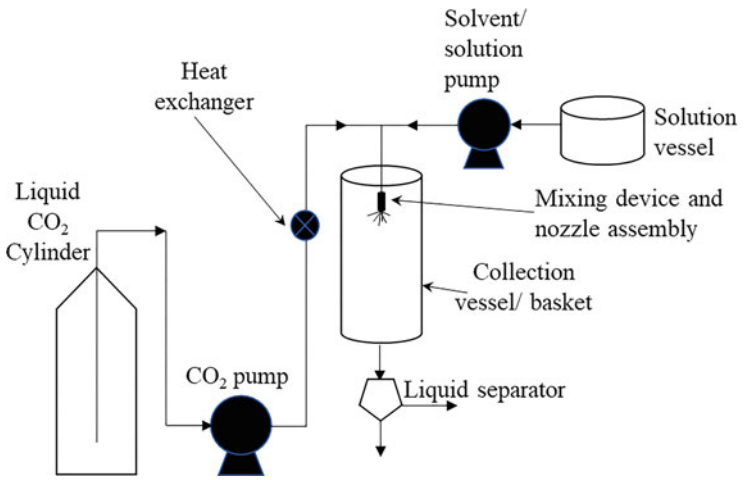

Fig. 12.4 Schematic diagram of the SAS process

ASES. All of these work using the same principles with slight variation in the operation.

The schematic representation of the SAS process is presented in Fig. 12.4.

The SAS process relies on the complete miscibility of the solvent with $scCO_2$ and insolubility of the solute in the $scCO_2$ or binary solvent mixture to be successfully applied into micronisation or micro/nano-encapsulation (Subramaniam et al. 1997). In general, a solution of drug/polymer or mixture is sprayed in a vessel filled with $scCO_2$ at a given pressure and temperature where the precipitation or coprecipitation of solute/s takes place due to the fast diffusion of CO_2 into the solvent followed by supersaturation and then precipitation. The properties of the resultant product from the SAS process depend on the solvent, solution concentration, flow rate, nozzle type and size along with the temperature and pressure of $scCO_2$ (Chen et al. 2020; Franco and de Marco 2020a).

The reduction in the particle size can be obtained using various techniques such as milling, grinding, spray drying, freeze drying, solvent evaporation, etc. However, there are numerous drawbacks associated with these conventional techniques including shear stress, use of organic solvent and the possibility of thermal or oxidative decomposition. $scCO_2$ antisolvent-based processes can avoid or minimise many of these shortcomings. A review containing a comparison between $scCO_2$-based processes and cryogenic spray-freezing technologies for the micronisation of actives that cannot be processed via conventional techniques was published by Rogers et al. (2001). They concluded that one of the advantages of using $scCO_2$-based processes was the ability to obtain dry powder in one step without the presence of any residual solvent. $scCO_2$-based antisolvent processes can also outperform conventional techniques in micro/nanonisation. A study by Park et al. showed that the SAS process produced 150 nm particles with increased surface area (56 m^2/g) of cefdinir in comparison to 2.3 μm particles with 35 m^2/g using spray drying (Park et al. 2010).

As expected, the reduced particle size and increased surface area resulted in a higher dissolution rate of cefdinir due to the improved contact with the dissolution media. Table 12.6 presents examples of actives processed by SAS.

Similar to micronisation or coprecipitation examples mentioned above, SAS processes can also be used to produce drug coprecipitates with polymers in the micro or nano range. In general, a solution of drug and polymer in a suitable solvent is atomised inside a pressurised vessel where the miscibility of the solvent with $scCO_2$ ensures the formation of polymeric spheres containing drug uniformly distributed within them. The choice of the polymer herein is governed by the final goal, i.e. hydrophilic polymers to improve the dissolution rate and hydrophobic polymers to produce sustained-release formulations. Various polymers have been studied for the preparation of drug/polymer coprecipitates, but PVP is undoubtedly one of the most commonly studied polymers to obtain regular, spherical and uniformly shaped microspheres using SAS. For example, Machmudah et al. reported the production of submicron curcumin-loaded PVP particles via SAS where they also showed the impact of temperature and polymer concentration on the particle morphology and size (Machmudah et al. 2020). The morphology and the particle size of the coprecipitate are governed by factors such as polymer type, polymer/drug ratio, pressure and temperature. A high polymer/drug ratio, in general, produces larger particles, but concentration plays an equally crucial role in the resulting morphology (Ozkan et al. 2019b; Chhouk et al. 2018). The operating pressure of a SAS process needs to be considered carefully as very high pressure can fail to break the liquid jet due to the dominant lack of surface tension, resulting in the failure of coprecipitation completely or the creation of nanoprecipitates of varying sizes (Kalani and Yunus 2011). Similarly, the temperature and its effect on the solubility of the drug and polymer in a solvent can also influence the particle size as shown by Franco et al. where an increase in temperature resulted in the reduction of the size of coprecipitates (Franco et al. 2019b).

12.2.3 $scCO_2$ Processes as a Solute

The ability of $scCO_2$ to act as a solute makes it highly attractive in nano/micro encapsulation and micronisation processes. The primary technique that utilises solute properties of the $scCO_2$ is known as particles from gas-saturated solutions (PGSS). PGSS is performed by solubilising an SCF into a solid, solution, suspension, emulsion, or molten material (Esfandiari 2015). The ability of dense gases such as CO_2 to solubilise in large quantities into a solid or liquid due to its low viscosity and high diffusivity makes it highly suitable for PGSS (Fages et al. 2004). Unlike other $scCO_2$ procedures, PGSS does not require the processing material to have sufficient solubility in CO_2, and there is typically no need for additional organic solvents. The advantages of the PGSS method also include low production cost, reduced working pressure and the use of small volumes of SCF (Kerc 1999; Hakuta et al. 2003).

Table 12.6 Examples of SAS processing of actives

Drug	P (bar)	T (° C)	Solvent/s	C (mg/mL)	PS (μm)	Process	References
Hydrochlorothiazide	150	42	DMF, NMP, DMSO, THF, AC, 2-BT	20	0.05–0.2	CP	Park et al. (2017)
Telmisartan	120	45	EtOH/ DCM	25	700–750	SD	Park et al. (2013)
Moxifloxacin	150	40	DMSO, DMF, MeOH, AA	1–50	0.3–8	Mic	Kudryashova et al. (2017)
Theophylline, diclofenac sodium	90–150	40	DMSO	20–40	0.1–8	CP	Franco and de Marco (2020b)
Paracetamol	100	40	MeOH	NR	4–5	CC	Hiendrawan et al. (2016)
Ampicillin, amoxicillin	90	40–50	DMSO	20	0.2–20	CP	Franco et al. (2019a)
Dexamethasone, prednisolone, budesonide	90–150	40	EtOH	20	1.8–3.6	CP	Prosapio et al. (2016)
5-Fluorouracil	150–180	40–50	DMSO, DMSO/ DCM	10–20	0.2–0.7	Mic	Cuadra et al. (2019)
Diflunisal	85–150	35–40	AC, AC/DCM	20–40	0.21–0.23	CP	Zahran et al. (2014)
Paclitaxel (Taxol)	100–250	35–68	EtOH	2.5	0.15–2	Mic	Zhao et al. (2012)
Curcumin	90–120	40	EtOH, AC, AC/EtOH	2–20	0.14–327	CP	Matos et al. (2019, 2020)
Mangiferin	100–200	35–59	NMP	5–60	0.53–0.98	Mic	Liu et al. (2020)
Resveratrol	150	40	MeOH, EtOH, MeOH/ DCM, EtOH/ DCM	~30	0.17–0.5	Mic	Ha et al. (2020)
Fisetin	100	45	EtOH/ DCM	1	0.07–0.35	CP	Chen et al. (2020)
Folic acid	90–150	35–40	DMSO		0.05–3.8	CP	Prosapio et al. (2015a)
Quercetin	80–250	35–65	EtOH, DMSO, EtAc	8–25	0.15–10	Mic	Fernández-Ponce et al. (2015), Ozkan et al. (2019a), Montes et al. (2015)
Rutin	80–200	40–60	DMSO, DMSO/ EtOH	20–85	0.3–2	Mic	Ozkan et al. (2019a), Montes et al. (2016)

(continued)

Table 12.6 (continued)

Drug	P (bar)	T (° C)	Solvent/s	C (mg/mL)	PS (μm)	Process	References
			DMSO/ AC				
β-Carotene	85	40	AC/EtOH	4–8	4–250	CP	Prosapio et al. (2015b)
Vitexin	150–300	40–70	DMSO	1–2.5	0.13	Mic	Zu et al. (2012)
Sulfathiazole	100	40	AC, ACN, THF, AA	0.19–6	0.3–100	Mic/ poly	Clercq et al. (2018)

P: Pressure, T: Temperature, C: Concentration, PS: Particle size, CP: Coprecipitation, Mic: Micronisation, SD: Solid dispersion, CC: Cocrystallisation, Poly: Polymorph formation. AA: Acetic acid, AC: Acetone, ACN: Acetonitrile, 2-BT: 2-Butanone, DMF: Dimethylformamide, DMSO: Dimethylsulfoxide, DCM: Dichloromethane, EtOH: Ethanol, EtAc: Ethyl acetate, MeOH: Methanol, NMP: N-methyl-2-pyrrolidone

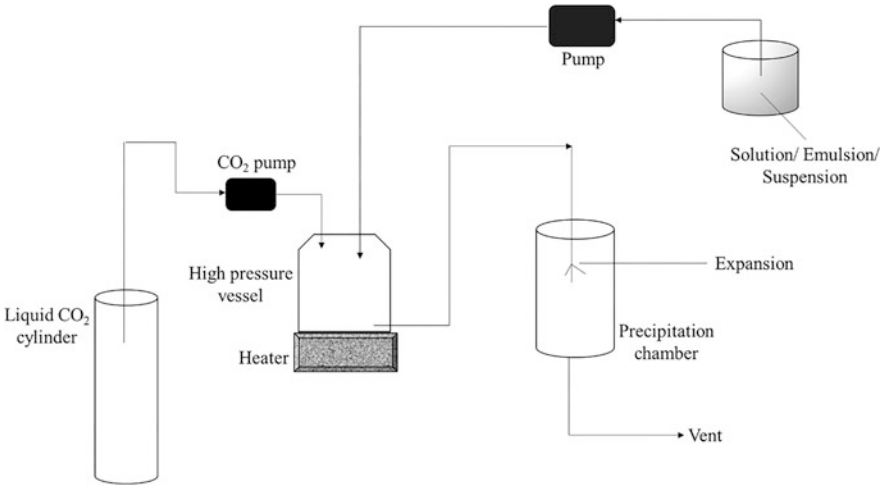

Fig. 12.5 Schematic diagram of the PGSS process

A schematic diagram of the PGSS process is presented in Fig. 12.5.

During the PGSS procedure, compressed CO_2 is diffused or solubilised in the material of interest at a fixed temperature in a high-pressure vessel to form a gas-saturated solution. Afterwards, the CO_2-saturated solution is rapidly depressurised and expanded through a heated nozzle into the precipitation chamber. As a result of the Joule-Thomson effect and gas evaporation, the expanded solution cools down, which leads to precipitation and the formation of fine particles (Hakuta et al. 2003; Jung and Perrut 2001). The PGSS process is suitable for the micronisation of substances that can absorb CO_2 at high concentrations such as polymers. Also, the physicochemical properties of polymers including viscosity, melting point and glass transition temperature can be modified as a result of this

process. For polymeric systems where a third component has been previously dispersed or solubilised, the expansion step during PGSS can lead to the formation of loaded polymeric/lipidic microspheres (Fages et al. 2004; Martín and Cocero 2008). The PGSS process is also suitable for drying of materials without causing any thermal degradation or product contamination. During the PGSS-drying process, the drug/polymer solution is brought in contact with CO_2 at a relatively high temperature and pressure. Then, the $scCO_2$-rich solution is sprayed into a vessel at lower working conditions, which causes drying as the result of the expansion and subsequent Joule-Thomson cooling effect (Sheth et al. 2012). Similarly, PGSS-related techniques can be employed in the micronisation of fats, drugs and excipients using a process known as scMM (supercritical melt micronisation) (Soh and Lee 2019). A few examples of PGSS processing of materials from literature are presented in Table 12.7.

The favourable diffusivity of CO_2 especially in polymeric matrices is commonly utilised in the production of microporous biopolymeric structures via CO_2 foaming. The diffusion of CO_2 into polymers is not only beneficial in generating microporous structures but depression in melting and/or glass transition of polymers due to the dissolution of CO_2 within the matrix also allows processing at lower temperatures (Bhomia et al. 2014b). In general, a solution of polymer with $scCO_2$ is formed at a given pressure and temperature, which upon depressurisation leads to polymer vitrification due to the removal of CO_2, resulting in the porous structure formation. The significance of such porous structures in the pharmaceutical and biomedical industries is immense. Moreover, CO_2 foaming also avoids or minimises the use of organic solvent/s during the processes, resulting in zero or minimal residual solvent in the resultant product. The pore size and morphology of the foams can be regulated by operating parameters such as temperature, pressure, depressurisation rate and the nature of the selected polymer (e.g. functional groups and molecular weight). It is also possible to encapsulate active ingredients during the foaming process. The impregnation of actives is usually a two-step process, but it is possible to achieve encapsulation and foaming at the same time (Satpayeva et al. 2022; Nie et al. 2008; Cabezas et al. 2013). Examples of foaming and encapsulation of actives via CO_2 foaming are presented in Table 12.8.

The application of $scCO_2$ as a solute can also be used in the preparation of drug-cyclodextrin (drug-CD) complexes in an organic solvent-free environment through supercritical solvent impregnation (SSI). The mechanism involved in drug-CD complexation is thought to be due to the displacement of the naturally included water molecules in CD by a less polar guest molecule if the drug is soluble in $scCO_2$ (van Hees et al. 1999). However, melting point depression in both the drug and CD caused by the dissolution of $scCO_2$ can also be used to prepare complexes in the melt state at comparatively lower temperatures. For example, the melting point of MβCD decreases from 110 °C to 70 °C at 80 bar in $scCO_2$ and reaches to 25 °C at 190 bar (He 2009). Similarly, there are numerous drugs (ibuprofen, naproxen, piroxicam etc.) that also melt at lower temperatures in $scCO_2$ (Türk and Kraska 2009; Türk et al. 2007; Grandelli et al. 2012). This depression in melting point can be utilised to prepare drug-CD complexes at comparatively lower temperatures as the molten state

Table 12.7 Examples of PGSS-based methods for processing of actives

Material(s)	P (bar)	T (°C)	PS (μm)	Process	References
Theophylline + HPO	120–180	86	2–3	ES	Rodrigues et al. (2004)
Ibuprofen + PEG 6000	200	60	0.02–0.5	NS	Chen et al. (2013)
Lavandin + PEG 9000/OSA-modified starches	50–90 90–124	76–84 100–130	30–100 20–200	ES ES/PD	Varona et al. (2010)
Ibuprofen + Gelucire®/Pluronic/GMS	100–200	37–62	50–200	ES	Fraile et al. (2013)
Coenzyme Q_{10} + PEG 6000	100–250	65–80	0.2	NS	Hu et al. (2011)
Caffeine + GMS	130	62	2–24	ES/LP	Sampaio de Sousa et al. (2007)
Ribonuclease A/lysozyme/insulin/calcitonin + P($_{DL}$LA)	320	35	10–300	ES	Whitaker et al. (2005)
YNS3107 + PEG and Pluronic	80–300	55–85	27–32	MZ/SD	Brion et al. (2009)
Trans-chalcone + Precirol® +/− Gelucire®	120	42–52	2–7	MZ/LP	Sampaio de Sousa et al. (2009)
Fenofibrate + Gelucire®	80–240	50–80	9–782	SD	Pestieau et al. (2015)
PEG 6000/10000	120–220	55–75	200–357	MZ	Nalawade et al. (2007)
Cydia pomonella granulovirus/palm oil-based fat	100	65	20–80	ES	Pemsel et al. (2010)
Tristearate	115–215	54–70	10–30	MZ	Mandžuka et al. (2010)
Polybutylene terephthalate, Polybutylene terephthalate/ZnO, Polybutylene terephthalate/bentonite	50–410	230–320	100–300	MZ	Pollak et al. (2010)
hgH/PLGA/PLA	76	32	25–100	ES	Jordan et al. (2010)
Shellac	300	40	180–300	MZ	Labuschagne et al. (2016)
Salmon oil/PEG 6000	250	50	65–165	ES	Haq and Chun (2018)
Limonene, modified starch	100–120	50–60	2–9	ES	Machado et al. (2016)
Coffee oil/PEG 8000	200–300	40–50	78	ES	Getachew and Chun (2016)
β-Carotene/soy lecithin	80–100	102–113	10–500	ES/PD	de Paz et al. (2012a)

(continued)

Table 12.7 (continued)

Material(s)	P (bar)	T (°C)	PS (μm)	Process	References
β-Carotene/poly-(ε-caprolactone)	110–150	70	270–650	ES	de Paz et al. (2012b)

P: Pressure, T: Temperature, PS: Particle size, HPO: Hydrogenated palm oil, PEG: Polyethylene glycol, GMS: Glyceryl monostearate, OSA: n-Octenyl succinic anhydride, ES: Encapsulation, NS: Nanosizing, LP: Lipid particles, P($_{DL}$LA): Poly ($_{DL}$-lactic acid), MZ: Micronisation, SD: Solid dispersion, PD: PGSS drying

Table 12.8 Examples of foaming and encapsulation using CO_2 as a foaming agent

Polymer	Active	P (Bar)	T (°C)	Pore size (μm)	References
PLA/PLGA	5-Fluorouracil	180	40	100–360	Cabezas et al. (2013)
PLGA/chitosan	DNA	120	70	20–60	Nie et al. (2008)
PLGA	Gemcitabine	120–200	25–40	85–160	Álvarez et al. (2020)
PCL	Quercetin	150–300	35–60	NS	García-Casas et al. (2019)
PCL	*Usnea* extracts	150	35	150–340	Fanovich et al. (2013)
PLA/PLGA	Indomethacin	180	40	60–410	Cabezas et al. (2012)
PCL	Ibuprofen	150–200	35–40	NS	Yoganathan et al. (2010)
Silk fibroin aerogel/PCL	Dexamethasone	140	37	37–95	Goimil et al. (2019)
PCL	Nimesulide	150–200	35–60	700–800	Campardelli et al. (2019)
PCL/silica	Dexamethasone	140–250	35	200–900	de Matos et al. (2013)
PCL/starch	Growth factors	100	37	0.32–0.57	Diaz-Gomez et al. (2016)
PCL/chitosan	Vancomycin	140	40	0.17–0.54	García-González et al. (2018)

PLA: Polylactic acid, PLGA: Poly($_{D,L}$-lactic-co-glycolic acid), PCL: Polycaprolactone, NS: Not specified

of at least one component upon $scCO_2$ treatment is considered sufficient for the successful inclusion of a drug in the cyclodextrin (Bandi et al. 2004). The complexes prepared in the molten state in $scCO_2$ were found to be either comparable to or better performing than the complexes prepared via conventional methods with respect to the drug dissolution and complexation efficiency (He 2009, 2010; Bandi et al. 2004; Banchero et al. 2013; He and Li 2009; Rudrangi et al. 2015a, b, 2016).

In summary, CO_2 as a solute can be effectively utilised to generate nano/micro-particles of varying physical properties such as morphology, size and crystallinity. These product characteristics can be controlled by altering the operating parameters including temperature, pressure and nozzle diameter. Also, the composition of the

starting material plays a role in the type of formulated particles (Mishima 2008). Similarly, the application of $scCO_2$ in developing porous matrix is also of great interest where the foaming properties of CO_2 can impart extremely attractive properties. The possibility to prepare drug-CD complexes without the need of an organic solvent is also highly desirable. The suitability of the CO_2 for the applications discussed in this section is undebatable, but the success of these techniques can sometimes be limited by issues such as particle aggregation and nozzle blockage, especially in large-scale operations (Pilcer and Amighi 2010).

12.3 Conclusions and Future Perspectives

The favourable and tunable properties of $scCO_2$ permit its utilisation in various ways and make it extremely attractive especially for particle engineering, micronisation, amorphisation and microencapsulation. The use of $scCO_2$ in minimising or avoiding the use of organic solvent/s makes it highly suitable as a processing technique in the pharmaceutical, food and biomedical industries. The versatile nature of $scCO_2$ allows the selection of processes dependent on the properties (e.g. solubility, hydrophobicity, molecular weight, glass transition temperatures, crystallinity, etc.) of the active ingredient or coating material. For example, the micronisation and formation of amorphous drug particles can be easily achieved via the RESS and/or SAS methods based on drugs or excipients' solubility or miscibility with the supercritical fluid. Whereas the alternatives such as the PGSS technique can be used to process a range of polymers including PCL, PLGA, PHBV, etc., that cannot be processed via SAS or RESS due to their limited solubility in $scCO_2$. The continuous advancements in this field such as the ability to combine fluidisation coating with SAS or $scCO_2$-based drying methods offer further opportunities to develop novel drug delivery systems. The ability of $scCO_2$ to act as a solute in foaming results in the production of well-defined three-dimensional microporous structures with the drugs encapsulated within to be able to offer controlled drug release from scaffolds and implantable materials. The melting point depression caused by $scCO_2$ can be utilised in micronisation, implant production, preparation of solid dispersions and drug-CD complexation.

It is evident from the available literature that there is sufficient understanding of the mechanisms and configurations of $scCO_2$ processes providing a rich database for both thermodynamic (density, viscosity, solubility at different temperatures, pressure conditions, etc.) and fluid dynamic behaviour (jet break-up, mass transfer, etc.). However, the major hesitation in implanting $scCO_2$-based methods as conventional techniques in the pharmaceutical industry is the fact that many of the discussed methods in this chapter are considered batch processes. The current advancements are aiming to address this, but we must develop integrated processing strategies to combine multiple pharmaceutical processing steps for the industry to adopt $scCO_2$ processes freely. The greener and cleaner credentials of $scCO_2$ along with its versatility can be used in particle formation, encapsulation, purification, extraction,

sterilisation and recovery of organic solvents from formulations. Hence, further developments in this field while keeping pharmaceutical manufacturing practices in mind that include the health and safety guidelines and economic considerations would be necessary to achieve the full potential of supercritical fluid-based processing techniques in the pharmaceutical industry.

References

Ahangari H, King JW, Ehsani A, Yousefi M (2021) Supercritical fluid extraction of seed oils – a short review of current trends. Trends Food Sci Technol 111:249–260

Álvarez I, Gutiérrez C, Rodríguez JF, de Lucas A, García MT (2020) Production of drug-releasing biodegradable microporous scaffold impregnated with gemcitabine using a CO2 foaming process. J CO2 Util 41

Banchero M, Ronchetti S, Manna L (2013) Characterization of ketoprofen/methyl-β-cyclodextrin complexes prepared using supercritical carbon dioxide. J Chem 2013:1

Bandi N, Wei W, Roberts CB, Kotra LP, Kompella UB (2004) Preparation of budesonide- and indomethacin-hydroxypropyl-beta-cyclodextrin (HPBCD) complexes using a single-step, organic-solvent-free supercritical fluid process. Eur J Pharm Sci 23(2):159

Baseri H, Lotfollahi MN (2013) Formation of gemfibrozil with narrow particle size distribution via rapid expansion of supercritical solution process (RESS). Powder Technol 235:677–684

Bhomia R, Trivedi V, Mitchell JC, Coleman NJ, Snowden MJ (2014a) Effect of pressure on the melting point of pluronics in pressurized carbon dioxide. Ind Eng Chem Res 53(26): 10820–10825

Bhomia R, Trivedi V, Mitchell JC, Coleman NJ, Snowden MJ (2014b) Effect of pressure on the melting point of pluronics in pressurized carbon dioxide. Ind Eng Chem Res 53(26):10820

Brion M, Jaspart S, Perrone L, Piel G, Evrard B (2009) The supercritical micronization of solid dispersions by particles from gas saturated solutions using experimental design. J Supercrit Fluids 51(1):50–56

Cabezas LI, Fernández V, Mazarro R, Gracia I, de Lucas A, Rodríguez JF (2012) Production of biodegradable porous scaffolds impregnated with indomethacin in supercritical CO_2. J Supercrit Fluids 63:155

Cabezas LI, Gracia I, García MT, de Lucas A, Rodríguez JF (2013) Production of biodegradable porous scaffolds impregnated with 5-fluorouracil in supercritical CO2. J Supercrit Fluids 80:1

Campardelli R, Franco P, Reverchon E, de Marco I (2019) Polycaprolactone/nimesulide patches obtained by a one-step supercritical foaming + impregnation process. J Supercrit Fluids 146:47

Chen W, Hu X, Hong Y, Su Y, Wang H, Li J (2013) Ibuprofen nanoparticles prepared by a PGSS™-based method. Powder Technol 245:241–250

Chen LF, Xu PY, Fu CP, Kankala RK, Chen AZ, Wang S (2020) Fabrication of supercritical antisolvent (SAS) process-assisted fisetin-encapsulated poly (vinyl pyrrolidone) (PVP) nanocomposites for improved anticancer therapy. Nano 10(2)

Chen L, Dean B, Liang X (2021) A technical overview of supercritical fluid chromatography-mass spectrometry (SFC-MS) and its recent applications in pharmaceutical research and development. Drug Discov Today Technol 40:69–75

Chhouk K, Wahyudiono KH, Kawasaki SI, Goto M (2018) Micronization of curcumin with biodegradable polymer by supercritical anti-solvent using micro swirl mixer. Front Chem Sci Eng 12(1):184

Clercq S, Mouahid A, Gérard P, Badens E (2018) Investigation of crystallization mechanisms for polymorphic and habit control from the supercritical antisolvent process. J Supercrit Fluids 141: 29–38

Cuadra IA, Zahran F, Martín D, Cabañas A, Pando C (2019) Preparation of 5-fluorouracil microparticles and 5-fluorouracil/poly(l-lactide) composites by a supercritical CO2 antisolvent process. J Supercrit Fluids 143:64–71

de Matos MBC, Piedade AP, Alvarez-Lorenzo C, Concheiro A, Braga MEM, de Sousa HC (2013) Dexamethasone-loaded poly(É-caprolactone)/silica nanoparticles composites prepared by supercritical CO2 foaming/mixing and deposition. Int J Pharm 456(2):269

de Paz E, Martín Á, Cocero MJ (2012a) Formulation of β-carotene with soybean lecithin by PGSS (particles from gas saturated solutions)-drying. J Supercrit Fluids 72

de Paz E, Martín Á, Duarte CMM, Cocero MJ (2012b) Formulation of β-carotene with poly-(ε-caprolactones) by PGSS process. Powder Technol 217

Diaz-Gomez L, Concheiro A, Alvarez-Lorenzo C, García-González CA (2016) Growth factors delivery from hybrid PCL-starch scaffolds processed using supercritical fluid technology. Carbohydr Polym 142:282

Duarte ARC, Mano JF, Reis RL (2009) Supercritical fluids in biomedical and tissue engineering applications: a review. Int Mater Rev 54(4):214–222

Esfandiari N (2015) Production of micro and nano particles of pharmaceutical by supercritical carbon dioxide. J Supercrit Fluids 100:129–141

Fages J, Lochard H, Letourneau JJ, Sauceau M, Rodier E (2004) Particle generation for pharmaceutical applications using supercritical fluid technology. Powder Technol 141(3):219–226

Fahim TK, Zaidul ISM, Abu Bakar MR, Salim UM, Awang MB, Sahena F et al (2014) Particle formation and micronization using non-conventional techniques- review. Chem Eng Process Process Intensif 86:47–52

Fanovich MA, Ivanovic J, Misic D, Alvarez M, Jaeger P, Zizovic I et al (2013) Development of polycaprolactone scaffold with antibacterial activity by an integrated supercritical extraction and impregnation process. J Supercrit Fluids 78

Fernández-Ponce MT, Masmoudi Y, Djerafi R, Casas L, Mantell C, de la Ossa EM et al (2015) Particle design applied to quercetin using supercritical anti-solvent techniques. J Supercrit Fluids 105:119–127

Fraile M, Martín Y, Deodato D, Rodriguez-Rojo S, Nogueira ID, Simplício AL et al (2013) Production of new hybrid systems for drug delivery by PGSS (particles from gas saturated solutions) process. J Supercrit Fluids 81:226–235

Franco P, de Marco I (2020a) Supercritical antisolvent process for pharmaceutical applications: a review. PRO 8(8)

Franco P, de Marco I (2020b) Eudragit: a novel carrier for controlled drug delivery in supercritical antisolvent coprecipitation. Polymers (Basel) 12(1)

Franco P, de Marco I (2021) Nanoparticles and nanocrystals by supercritical CO2-assisted techniques for pharmaceutical applications: a review. Appl Sci (Switzerland) 11(4)

Franco P, Reverchon E, de Marco I (2019a) Production of zein/antibiotic microparticles by supercritical antisolvent coprecipitation. J Supercrit Fluids 145:31–38

Franco P, Reverchon E, de Marco I (2019b) Production of zein/antibiotic microparticles by supercritical antisolvent coprecipitation. J Supercrit Fluids 145:31

Gallagher PM, Coffey MP, Krukonis VJ, Klasutis N (1989) Gas antisolvent recrystallization: new process to recrystallize compounds insoluble in supercritical fluids

García-Casas I, Montes A, Valor D, Pereyra C, de la Ossa EJM (2019) Foaming of polycaprolactone and its impregnation with quercetin using supercritical CO2. Polymers (Basel). 11(9)

García-González CA, Barros J, Rey-Rico A, Redondo P, Gómez-Amoza JL, Concheiro A et al (2018) Antimicrobial properties and osteogenicity of vancomycin-loaded synthetic scaffolds obtained by supercritical foaming. ACS Appl Mater Interfaces 10(4):3349

Getachew AT, Chun BS (2016) Optimization of coffee oil flavor encapsulation using response surface methodology. LWT Food Sci Technol 70:126

Ginty PJ, Whitaker MJ, Shakesheff KM, Howdle SM (2005) Drug delivery goes supercritical. Mater Today 8(Suppl 8):42

Girotra P, Singh SK, Nagpal K (2013) Supercritical fluid technology: a promising approach in pharmaceutical research. Pharm Dev Technol 18:22

Goimil L, Santos-Rosales V, Delgado A, Évora C, Reyes R, Lozano-Pérez AA et al (2019) ScCO2-foamed silk fibroin aerogel/poly(ϵ-caprolactone) scaffolds containing dexamethasone for bone regeneration. J CO2 Util:31

Goodship V, Oqur E (2005) Polymer processing with supercritical fluids, Rapra review reports, vol 15, 8th edn. Rapra Technology Ltd, Shawbury, pp 148–150

Grandelli HE, Hassler JC, Whittington A, Kiran E (2012) Melting point depression of Piroxicam in carbon dioxide + co-solvent mixtures and inclusion complex formation with β-cyclodextrin. J Supercrit Fluids 71:19

Ha ES, Park H, Lee SK, Sim WY, Jeong JS, Baek IH et al (2020) Pure trans-resveratrol nanoparticles prepared by a supercritical antisolvent process using alcohol and dichloromethane mixtures: effect of particle size on dissolution and bioavailability in rats. Antioxidants 9(4)

Hakuta Y, Hayashi H, Arai K (2003) Fine particle formation using supercritical fluids. Curr Opinion Solid State Mater Sci 7(4–5):341–351

Haq M, Chun BS (2018) Microencapsulation of omega-3 polyunsaturated fatty acids and astaxanthin-rich salmon oil using particles from gas saturated solutions (PGSS) process. LWT 92

He J (2009) Complex of shikonin and β-cyclodextrins by using supercritical carbon dioxide. J Incl Phenom Macrocycl Chem 63(3–4)

He J (2010) Complex between modified β-cyclodextrins and three components of traditional Chinese medicine in supercritical carbon dioxide medium. J Incl Phenom Macrocycl Chem 68(3–4)

He J, Li W (2009) Preparation of borneol-methyl-β-cyclodextrin inclusion complex by supercritical carbon dioxide processing. J Incl Phenom Macrocycl Chem 65(3):249

Hezave AZ, Esmaeilzadeh F (2012) Fabrication of micron level particles of amoxicillin by rapid expansion of supercritical solution. J Dispers Sci Technol 33(10):1419–1428

Hiendrawan S, Veriansyah EWB, Soewandhi SN, Wikarsa S, Tjandrawinata RR (2016) Simultaneous cocrystallization and micronization of paracetamol and dipicolinic acid cocrystals by supercritical antisolvent (SAS). Int J Pharmacy Pharmaceutical Sci [Internet] [cited 2022 Mar 6];8(2):89–99. Available from: https://innovareacademics.in/journals/index.php/ijpps/article/view/9121

Hosseinpour M, Vatanara A, Zarghami R (2015) Formation and characterization of beclomethasone dipropionate nanoparticles using rapid expansion of supercritical solution. Adv Pharmaceutical Bull 5(3):343–349

Hu X, Guo Y, Wang L, Hua D, Hong Y, Li J (2011) Coenzyme Q10 nanoparticles prepared by a supercritical fluid-based method. J Supercrit Fluids 57(1):66–72

Jordan F, Naylor A, Kelly CA, Howdle SM, Lewis A, Illum L (2010) Sustained release hGH microsphere formulation produced by a novel supercritical fluid technology: in vivo studies. J Control Release 141(2):153

Joshi J (2011) A review on micronization techniques. Pharmaceut Sci Technol 651–681

Jung J, Perrut M (2001) Particle design using supercritical fluids: literature and patent survey. J Supercrit Fluids 20(3):179–219

Kai Bin L, Janakiraman AK, Razak FSA, Uddin ABMH, Sarker MZI, Ming LC et al (2020) Supercritical fluid technology and its pharmaceutical applications: a revisit with two decades of progress. Indian J Pharmaceut Educ Res 54:s1

Kajiya D, Mouri Y, Saitow K (2008) Difference of solute−solvent interactions of *cis*- and *trans*-1,2-Dichloroethylene in supercritical CO_2 investigated by Raman spectroscopy. J Phys Chem B 112(27):7980–7983

Kalani M, Yunus R (2011) Application of supercritical antisolvent method in drug encapsulation: a review. Int J Nanomedicine 6

Kanakubo M, Aizawa T, Kawakami T, Sato O, Ikushima Y, Hatakeda K et al (2000) Studies on solute−solvent interactions in gaseous and supercritical carbon dioxide by high-pressure ^{1} H NMR spectroscopy. J Phys Chem B 104(12):2749–2758

Kankala RK, Zhang YS, Wang S, Lee CH, Chen AZ (2017) Supercritical fluid technology: an emphasis on drug delivery and related biomedical applications. Adv Healthcare Mater 6

Kankala RK, Xu PY, Chen BQ, Wang S, bin, Chen AZ. (2021) Supercritical fluid (SCF)-assisted fabrication of carrier-free drugs: an eco-friendly welcome to active pharmaceutical ingredients (APIs). Adv Drug Deliv Rev 176:113846

Kerc J (1999) Micronization of drugs using supercritical carbon dioxide. Int J Pharm 182(1):33–39

Keshavarz A, Karimi-Sabet J, Fattahi A, Golzary A, Rafiee-Tehrani M, Dorkoosh FA (2012) Preparation and characterization of raloxifene nanoparticles using rapid expansion of supercritical solution (RESS). J Supercrit Fluids 63:169–179

Keshmiri K, Vatanara A, Tavakoli O, Manafi N (2015) Production of ultrafine clobetasol propionate via rapid expansion of supercritical solution (RESS): full factorial approach. J Supercrit Fluids 101:176–183

Kilic S, Wang Y, Johnson JK, Beckman EJ, Enick RM (2009) Influence of tert-amine groups on the solubility of polymers in CO2. Polymer (Guildf) 50(11):2436–2444

Knez Ž, Pantić M, Cör D, Novak Z, Knez HM (2019) Are supercritical fluids solvents for the future? Chem Eng Process Process Intensification [Internet] 141:107532. https://linkinghub.elsevier.com/retrieve/pii/S0255270118315721

Kopcak U, Mohamed RS (2005) Caffeine solubility in supercritical carbon dioxide/co-solvent mixtures. J Supercrit Fluids [Internet] 34(2):209–214. https://linkinghub.elsevier.com/retrieve/pii/S0896844604002931

Kudryashova E, Sukhoverkov K, Deygen IM, Vorobei AM, Pokrovskiy OI, Parenago OO et al (2017) Moxifloxacin micronization via supercritical antisolvent precipitation. Russ J Phys Chem B 11(7):1153

Labuschagne PW, Naicker B, Kalombo L (2016) Micronization, characterization and in-vitro dissolution of shellac from PGSS supercritical CO2 technique. Int J Pharm 499(1–2)

Lide DR, Haynes W (2009) CRC handbook of chemistry and physics, 90th edn. CRC Press, New York

Lin PC, Su CS, Tang M, Chen YP (2012) Micronization of ethosuximide using the rapid expansion of supercritical solution (RESS) process. J Supercrit Fluids 72:84–89

Liu M, Liu Y, Ge Y, Zhong Z, Wang Z, Wu T et al (2020) Solubility, antioxidation, and oral bioavailability improvement of mangiferin microparticles prepared using the supercritical antisolvent method. Pharmaceutics 12(2)

Machado LC, Pelegati VB, Oliveira AL (2016) Study of simple microparticles formation of limonene in modified starch using PGSS - particles from gas-saturated suspensions. J Supercrit Fluids 107:260

Machmudah S, Winardi S, Wahyudiono KH, Goto M (2020) Formation of fine particles from curcumin/PVP by the supercritical Antisolvent process with a coaxial nozzle. ACS Omega 5(12)

Mandžuka Z, Škerget M, Knez Ž (2010) High pressure micronization of tristearate. J Am Oil Chem Soc 87(2):119

Martín A, Cocero MJ (2008) Micronization processes with supercritical fluids: fundamentals and mechanisms. Adv Drug Deliv Rev 60(3):339–350

Matos RL, Lu T, Prosapio V, McConville C, Leeke G, Ingram A (2019) Coprecipitation of curcumin/PVP with enhanced dissolution properties by the supercritical antisolvent process. J CO2 Util 30:48–62

Matos RL, Lu T, Leeke G, Prosapio V, McConville C, Ingram A (2020) Single-step coprecipitation and coating to prepare curcumin formulations by supercritical fluid technology. J Supercrit Fluids 159:104758

Matsuyama K, Mishima K, Hayashi KI, Ishikawa H, Matsuyama H, Harada T (2003) Formation of microcapsules of medicines by the rapid expansion of a supercritical solution with a nonsolvent. J Appl Polym Sci 89(3):742–752

Mishima K (2008) Biodegradable particle formation for drug and gene delivery using supercritical fluid and dense gas. Adv Drug Deliv Rev 60(3):411–432
Montes A, Bendel A, Kürti R, Gordillo MD, Pereyra C, Martínez de la Ossa EJ (2013) Processing naproxen with supercritical CO2. J Supercrit Fluids 75:21–29
Montes A, Pereyra C, de La Ossa EJM (2015) Screening design of experiment applied to the supercritical antisolvent precipitation of quercetin. J Supercrit Fluids 104:10–18
Montes A, Wehner L, Pereyra C, Martínez de la Ossa EJ (2016) Precipitation of submicron particles of rutin using supercritical antisolvent process. J Supercrit Fluids 118:1–10
Mukhopadhyay M (2000) Natural extracts using supercritical carbon dioxide. CRC Press, Boca Raton
Müllers KC, Paisana M, Wahl MA (2015) Simultaneous formation and micronization of pharmaceutical cocrystals by rapid expansion of supercritical solutions (RESS). Pharm Res 32(2): 702–713
Nalawade SP, Picchioni F, Janssen LPBM (2007) Batch production of micron size particles from poly(ethylene glycol) using supercritical CO2 as a processing solvent. Chem Eng Sci 62(6): 1712–1720
Nic M, Jirat J, Kosatu B (eds) (2014) Compendium of chemical terminology. Int Union Pure Appl Chem, pp 1486–1487
Nie H, Lee LY, Tong H, Wang CH (2008) PLGA/chitosan composites from a combination of spray drying and supercritical fluid foaming techniques: new carriers for DNA delivery. J Control Release 129(3):207
Oliveira GE, Pinto JF (2017) Evaluation of the potential use of laminar Extrudates on stabilizing micronized Coumarin particles by supercritical fluids (RESS)—study of different RESS processing variables and mode of operation. AAPS PharmSciTech 18(7):2792–2807
Ozkan G, Franco P, Capanoglu E, de Marco I (2019a) PVP/flavonoid coprecipitation by supercritical antisolvent process. Chem Eng Process Process Intensification 146:107689
Ozkan G, Franco P, Capanoglu E, de Marco I (2019b) PVP/flavonoid coprecipitation by supercritical antisolvent process. Chem Eng Process Process Intensification 146
Padrela L, Rodrigues MA, Tiago J, Velaga SP, Matos HA, de Azevedo EG (2015) Insight into the mechanisms of Cocrystallization of Pharmaceuticals in Supercritical Solvents. Cryst Growth Des 15(7):3175–3181
Padrela L, Rodrigues MA, Duarte A, Dias AMA, Braga MEM, de Sousa HC (2018) Supercritical carbon dioxide-based technologies for the production of drug nanoparticles/nanocrystals – a comprehensive review. Adv Drug Deliv Rev 131:22–78
Park J, Park HJ, Cho W, Cha KH, Kang YS, Hwang SJ (2010) Preparation and pharmaceutical characterization of amorphous cefdinir using spray-drying and SAS-process. Int J Pharm 396(1–2)
Park J, Cho W, Cha KH, Ahn J, Han K, Hwang SJ (2013) Solubilization of the poorly water soluble drug, telmisartan, using supercritical anti-solvent (SAS) process. Int J Pharm 441(1–2):50–55
Park HJ, Yoon TJ, Kwon DE, Yu K, Lee YW (2017) Coprecipitation of hydrochlorothiazide/PVP for the dissolution rate improvement by precipitation with compressed fluid antisolvent process. J Supercrit Fluids 126:37–46
Peach J, Eastoe J (2014) Supercritical carbon dioxide: a solvent like no other. Beilstein J Org Chem 10:1878–1895
Pemsel M, Schwab S, Scheurer A, Freitag D, Schatz R, Schlücker E (2010) Advanced PGSS process for the encapsulation of the biopesticide Cydia pomonella granulovirus. J Supercrit Fluids 53(1–3)
Pestieau A, Krier F, Lebrun P, Brouwers A, Streel B, Evrard B (2015) Optimization of a PGSS (particles from gas saturated solutions) process for a fenofibrate lipid-based solid dispersion formulation. Int J Pharm 485(1–2):295–305
Pilcer G, Amighi K (2010) Formulation strategy and use of excipients in pulmonary drug delivery. Int J Pharm 392(1–2):1–19

Pollak S, Petermann M, Kareth S, Kilzer A (2010) Manufacturing of pulverised nanocomposites-dosing and dispersion of additives by the use of supercritical carbon dioxide. J Supercrit Fluids 53(1–3)

Prosapio V, de Marco I, Scognamiglio M, Reverchon E (2015a) Folic acid–PVP nanostructured composite microparticles by supercritical antisolvent precipitation. Chem Eng J 277:286–294

Prosapio V, Reverchon E, de Marco I (2015b) Coprecipitation of Polyvinylpyrrolidone/β-carotene by supercritical antisolvent processing. Ind Eng Chem Res 54(46):11568

Prosapio V, de Marco I, Reverchon E (2016) PVP/corticosteroid microspheres produced by supercritical antisolvent coprecipitation. Chem Eng J 292:264–275

Rodrigues M, Peiriço N, Matos H, Gomes De Azevedo E, Lobato MR, Almeida AJ (2004) Microcomposites theophylline/hydrogenated palm oil from a PGSS process for controlled drug delivery systems. J Supercrit Fluids 29(1–2)

Rogers TL, Johnston KP, Williams RO (2001) Solution-based particle formation of pharmaceutical powders by supercritical or compressed fluid CO2 and cryogenic spray-freezing technologies. Drug Dev Ind Pharm 27:1003

Rudrangi SRS, Trivedi V, Mitchell JC, Wicks SR, Alexander BD (2015a) Preparation of olanzapine and methyl-β-cyclodextrin complexes using a single-step, organic solvent-free supercritical fluid process: an approach to enhance the solubility and dissolution properties. Int J Pharm 494(1):408

Rudrangi SRS, Bhomia R, Trivedi V, Vine GJ, Mitchell JC, Alexander BD et al (2015b) Influence of the preparation method on the physicochemical properties of indomethacin and methyl-β-cyclodextrin complexes. Int J Pharm 479(2):381

Rudrangi SRS, Kaialy W, Ghori MU, Trivedi V, Snowden MJ, Alexander BD (2016) Solid-state flurbiprofen and methyl-β-cyclodextrin inclusion complexes prepared using a single-step, organic solvent-free supercritical fluid process. Eur J Pharm Biopharm 104:164

Sameer D, Azad MA, Dave R (2013) Precipitation and stabilization of ultrafine particles of Fenofibrate in aqueous suspensions by RESOLV. Powder Technol 236:75–84

Sampaio de Sousa AR, Simplício AL, de Sousa HC, Duarte CMM (2007) Preparation of glyceryl monostearate-based particles by PGSS®—application to caffeine. J Supercrit Fluids 43(1): 120–125

Sampaio de Sousa AR, Silva R, Tay FH, Simplício AL, Kazarian SG, Duarte CMM (2009) Solubility enhancement of trans-chalcone using lipid carriers and supercritical CO2 processing. J Supercrit Fluids 48(2):120–125

Satpayeva A, Rojas A, Tyrka M, Ksepko E, Galotto MJ, Zizovic I (2022) Supercritical foaming and impregnation of Polycaprolactone and Polycaprolactone-hydroxyapatite composites with Carvacrol. PRO 10(3)

Sheth P, Sandhu H, Singhal D, Malick W, Shah N, Serpil KM (2012) Nanoparticles in the pharmaceutical industry and the use of supercritical fluid technologies for nanoparticle production. Curr Drug Deliv 9(3):269–284

Sodeifian G, Sajadian SA (2018) Solubility measurement and preparation of nanoparticles of an anticancer drug (Letrozole) using rapid expansion of supercritical solutions with solid cosolvent (RESS-SC). J Supercrit Fluids 133:239–252

Sodeifian G, Sajadian SA (2019) Utilization of ultrasonic-assisted RESOLV (US-RESOLV) with polymeric stabilizers for production of amiodarone hydrochloride nanoparticles: optimization of the process parameters. Chem Eng Res Des 142:268–284

Soh SH, Lee LY (2019) Microencapsulation and nanoencapsulation using supercritical fluid (SCF) techniques. Pharmaceutics 11

Subramaniam B, Rajewski RA, Snavely K (1997) Pharmaceutical processing with supercritical carbon dioxide. J Pharm Sci 86(8):885

Türk M, Bolten D (2016) Polymorphic properties of micronized mefenamic acid, nabumetone, paracetamol and tolbutamide produced by rapid expansion of supercritical solutions (RESS). J Supercrit Fluids 116:239–250

Türk M, Kraska T (2009) Experimental and theoretical investigation of the phase behavior of naproxen in supercritical CO_2. J Chem Eng Data 54(5):1592

Türk M, Upper G, Steurenthaler M, Hussein K, Wahl MA (2007) Complex formation of Ibuprofen and β-Cyclodextrin by controlled particle deposition (CPD) using SC-CO2. J Supercrit Fluids 39(3):435

Uchida H, Nishijima M, Sano K, Demoto K, Sakabe J, Shimoyama Y (2015) Production of theophylline nanoparticles using rapid expansion of supercritical solutions with a solid cosolvent (RESS-SC) technique. J Supercrit Fluids 105:128–135

van Hees T, Piel G, Evrard B, Otte X, Thunus L, Delattre L (1999) Application of supercritical carbon dioxide for the preparation of a piroxicam-β-cyclodextrin inclusion compound. Pharm Res 16(12):1864

Varona S, Kareth S, Martín Á, Cocero MJ (2010) Formulation of lavandin essential oil with biopolymers by PGSS for application as biocide in ecological agriculture. J Supercrit Fluids 54(3):369–377

Whitaker MJ, Hao J, Davies OR, Serhatkulu G, Stolnik-Trenkic S, Howdle SM et al (2005) The production of protein-loaded microparticles by supercritical fluid enhanced mixing and spraying. J Control Release 101(1–3):85–92

Yoganathan R, Mammucari R, Foster NR (2010) Impregnation of ibuprofen into Polycaprolactone using supercritical carbon dioxide. J Phys Conf Ser 215

Yu H, Zhao X, Zu Y, Zhang X, Zu B, Zhang X (2012) Preparation and characterization of micronized artemisinin via a rapid expansion of supercritical solutions (RESS) method. Int J Mol Sci 13(4):5060–5073

Zahran F, Cabañas A, Cheda JAR, Renuncio JAR, Pando C (2014) Dissolution rate enhancement of the anti-inflammatory drug diflunisal by coprecipitation with a biocompatible polymer using carbon dioxide as a supercritical fluid antisolvent. J Supercrit Fluids 88:56–65

Zeinolabedini Hezave A, Esmaeilzadeh F (2012) Precipitation of micronized Piroxicam particles via RESS. J Dispers Sci Technol 33(7):990–999

Zhang X, Han B, Hou Z, Zhang J, Liu Z, Jiang T et al (2002) Why do co-solvents enhance the solubility of solutes in supercritical fluids? New evidence and opinion. Chem Eur J 8(22): 5107–5111

Zhao X, Chen X, Zu Y, Jiang R, Zhao D (2012) Recrystallization and micronization of taxol using the supercritical antisolvent (SAS) process. Ind Eng Chem Res 51(28):9591

Zu Y, Zhang Q, Zhao X, Wang D, Li W, Sui X et al (2012) Preparation and characterization of vitexin powder micronized by a supercritical antisolvent (SAS) process. Powder Technol 228: 47–55

Chapter 13
Microfluidics as a Tool for the Synthesis of Advanced Drug Delivery Systems

João P. Martins and Hélder A. Santos

Abstract Advanced drug delivery systems hold great potential for the diagnosis and treatment of several diseases, and the benefits of nanomedicine-based products in healthcare have recently started to crystallize. Yet, their translation into clinical applications is still considered to be slow, mainly due to high batch-to-batch variation, complexity of preparation, high costs, and compromised scale-up feasibility. Considering the impact that mixing kinetics play on the properties of nanomedicines, microfluidics emerged as a technique to foster the preparation of micro- and nanoparticles with precisely controlled features, such as narrow size distribution, high homogeneity and reproducibility, high drug encapsulation efficiency, and enhanced scale-up feasibility. This chapter provides an overview on recent advances in microfluidic-assisted particle production. The basic principles of flow patterns and regimes are reviewed, as well as the materials and geometries used for the preparation of microfluidic devices. The impact of different parameters of the microfluidic setup on the physicochemical properties of the formulations is also discussed, and some of the most relevant micro- and nanoparticle technologies are reviewed. Possibilities for scale-up and the introduction of microfluidics in industrial settings are also briefly addressed.

Keywords Microfluidics · Nanotechnology · Nanoparticles · Microparticles · Droplets

J. P. Martins
Drug Research Program, Division of Pharmaceutical Chemistry and Technology, Faculty of Pharmacy, University of Helsinki, Helsinki, Finland

H. A. Santos (✉)
Drug Research Program, Division of Pharmaceutical Chemistry and Technology, Faculty of Pharmacy, University of Helsinki, Helsinki, Finland

Department of Biomedical Engineering, W.J. Kolff Institute for Biomedical Engineering and Materials Science, University Medical Center Groningen, University of Groningen, AV, Groningen, The Netherlands
e-mail: h.a.santos@umcg.nl

D. Lamprou (ed.), *Nano- and Microfabrication Techniques in Drug Delivery*,
Advanced Clinical Pharmacy – Research, Development and Practical Applications 2,
https://doi.org/10.1007/978-3-031-26908-0_13

13.1 Introduction

Nanotechnology emerged as a new field of research after Richard P. Feynman has postulated the existence of an unexplored "staggeringly small world" in the 1950s and predicted that one day we would be making things at the atomic level (Feynman 1960). Ever since, the awakened interest of many scientists and their gathered efforts led to an exponential introduction of nanotechnology-based operations into our daily lives. Nanotechnology consists of the design, production, characterization, and application of structures, devices, and systems at the nanometer scale, which thereby present novel or superior characteristics and properties (Stylios 2013).

Nowadays, the benefits of miniaturization to the nanoscale are well established in the fields of, for example, engineering, computing, communication, and materials science. Concomitantly, nanotechnology has become highly relevant in healthcare, due to its fairly predictable potential to revolutionize also medicine (Farokhzad and Langer 2009). Over the years, the exploration of nanotechnology has resulted in the development of nanosized devices like prostheses and implants, which are expected to reach the forefront of diagnostic, medical monitoring, and biological technologies (Wujcik and Monty 2013; Wallace et al. 2012). Also importantly, nanotechnology has opened the doors to groundbreaking solutions in the diagnosis and treatment of several diseases through the use of advanced drug delivery systems (Veiseh et al. 2015; Anselmo and Mitragotri 2016). Indeed, nanosized formulations with precisely controlled features have shown to offer multiple advantages over their macro-sized counterparts, including improved drug encapsulation, controlled and/or targeted drug release, enhanced cellular uptake, improved bioavailability, and reduced side effects (Sanjay et al. 2018; Hui et al. 2019; Park 2007).

The application of nanotechnology into medicine, eventually named "nanomedicine," is now a paramount field of research in academia and industry, in which thinking big and working small is the key for success. Currently, there are over 50 nanomedicines in the market, and another estimated 100 undergoing clinical trials (Anselmo and Mitragotri 2019; Martins et al. 2020). The benefits of nanomedicine-based products in healthcare have started to crystallize, and the recent implementation of a worldwide vaccination process against COVID-19 using lipid-based nanocarriers comes as further categorical evidence of that (Fig. 13.1) (Batty et al. 2021).

Based on their size, nanomedicine-based particles can be divided into nanoparticles (NPs) and microparticles (MPs). Yet, their successful translation into the clinic greatly depends on the reproducibility and scalability of their manufacturing processes. Advanced drug delivery systems are generally manufactured by two main methods: (i) "top-down," when starting from bulk counterparts that are leached out until the generation of fine particles, and (ii) "bottom-up," consisting of the coalescence or assembly of atoms or molecules towards the generation of particles (Martins et al. 2020). "Top-down" approaches include methods like lithography, anodization, milling, and etching, whereas "bottom-up" approaches include emulsions, self-assembly, nanoprecipitation, desolvation, and spray-drying, among

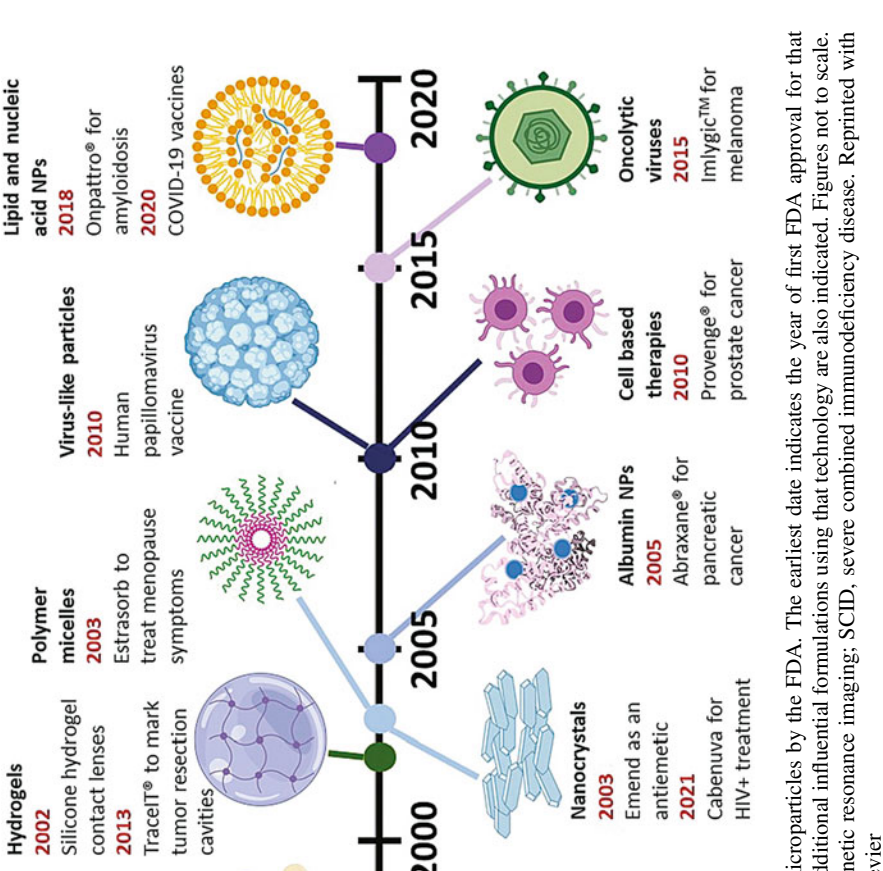

Fig. 13.1 Timeline of the approval of therapeutic nano- and microparticles by the FDA. The earliest date indicates the year of first FDA approval for that formulation, with respective commercial name and indication. Additional influential formulations using that technology are also indicated. Figures not to scale. Abbreviation: COVID-19, coronavirus disease 2019; MRI, magnetic resonance imaging; SCID, severe combined immunodeficiency disease. Reprinted with permission from ref. (Batty et al. 2021). Copyright © 2021, Elsevier

others (Martins et al. 2020; Krishnamoorthy and Mahalingam 2015; Quintanar-Guerrero et al. 1998). Despite the relative success of these techniques, they are often pointed out as one of the main reasons behind the slow translation of NPs and MPs from bench to bedside (Tomeh and Zhao 2020). Therefore, it is necessary to invest on the development of techniques that can overcome the limitations of conventional manufacturing processes, and which can lead to the preparation of drug delivery systems with well-defined properties, in a reproducible manner, and easy to scale-up for mass production when moving into an industrial setting.

The search for alternative and innovative techniques has led to the appearance of "lab-on-a-chip" (LOC) platforms, which allow the integration of several components and laboratory functions into single microdevices (Riahi et al. 2015). The underlying concept for LOC technologies is microfluidics: the science of manipulating small amounts of fluids (10^{-9} to 10^{-18} L) inside of submillimeter channels (Whitesides 2006). The continued refinement and sophistication of microfluidics has turned it into a valuable tool for the production of advanced drug delivery systems, but also for the implementation of 3D cell cultures, cell/molecule isolation and purification, single cell analysis, organ-on-chip and body fluidic stream simulation (Whitesides 2006; Beebe et al. 2002; Sackmann et al. 2014; Liu et al. 2020).

In this chapter, we focus on recent advances in the use of microfluidics for the synthesis of drug delivery systems. Firstly, we review the basic principles of flow patterns and regimes, as they represent theoretical background of relevance for the rational design of microfluidic platforms. Then, we summarize the materials used for the fabrication of microfluidic devices and their geometries. Subsequently, we describe how microfluidics can be finely tuned to control the physicochemical properties of the produced formulations. Finally, we review some of the most relevant drug delivery systems prepared by microfluidics and their therapeutic applications. The introduction of microfluidics in industrial settings and the associated challenges are also briefly addressed.

13.2 Main Advantages of Microfluidics for the Synthesis of Drug Delivery Systems

The materials, flow patterns and regimes, and devices and device geometries used in microfluidic technologies allow for the implementation of a wide variety of platforms and, consequently, enable infinite possibilities when generating drug delivery systems. With microfluidics, the hitherto limited control over the mixing rates between solvent and non-solvent phases can be tackled, and thereby, high-throughput platforms can be established for the synthesis, screening, and optimization of drug nanocarriers (Ahadian et al. 2020; Ding et al. 2016). Besides enhanced controllability, microfluidics also provides improved reproducibility of single or multicomponent drug carriers when compared to bulk production methods (Tomeh and Zhao 2020; Leung and Shen 2018; Chen et al. 2012). For example, the rapid

mixing time ensured by microfluidics leads to the fabrication of NPs with a narrower size distribution when compared to that of similar formulations prepared by traditional nanoprecipitation methods (Leung and Shen 2018).

As the microfluidic processes take place inside of channels with dimension of tens of micrometers, the consumption of samples and reagents can be substantially reduced, resulting in an overall reduction of the manufacturing costs (Liu et al. 2017a). Moreover, the materials used for the fabrication of microfluidic channels can be suitably adapted to withstand different types of fluids, and their parallelization can be used to achieve an industrial-scale production of drug formulations (Romanowsky et al. 2012; Eggersdorfer et al. 2017). No less important, the possibilities for integration and automation of microfluidics can decrease human intervention in the production of drug delivery systems, and therefore, the associated human error (Rahil Hasan et al. 2021).

Altogether, microfluidic platforms enable a rapid sample processing toward the preparation of highly homogenous and monodisperse colloids of varying chemical compositions, which can load different cargos, such as therapeutics, targeting moieties and imaging modalities (Liu et al. 2014; Duncanson et al. 2012; Yang et al. 2012; Zhao et al. 2011; Amstad et al. 2012). Over the past decades, a vast number of studies relying on microfluidic technologies led to the development of a myriad of formulations, with different physicochemical properties and for varying purposes. The increasing exploratory research in the field is also testimony of the growing interest and pursuit of ameliorated fabrication techniques for bringing nanomedicines into the clinic.

13.3 Microfluidic Flow Patterns and Regimes

The success of microfluidics largely depends on the efficiency of the mixing. Mixing is a transport process for species, temperature, and phases to reduce inhomogeneity, which leads to secondary effects like reaction and alteration of properties (Nguyen 2012). In the context of microfluidics, mixing is the process of achieving uniformity of concentration of, for example, solutes, solvents or suspended particles, depending on the intended application. Microfluidics enables a thorough and rapid mixing of several mutually soluble fluids inside of microchannels/capillaries (Liu et al. 2018a). The submillimeter length scale of these channels enhances the surface-to-volume ratio and, therefore, increases the effect of surface tension and the fluid viscous forces (Liu et al. 2018a).

13.3.1 Flow Patterns

The physical properties of the fluids and their mixing patterns are extremely important when aiming at the production of advanced drug delivery systems (Martins et al.

2018a). For example, mixing has a great impact on the size and monodispersity, composition, surface properties, drug loading, and release of the developed nanocarriers, (Karnik et al. 2008; Liu et al. 2015a; Stepanyan et al. 2012) as later discussed in this chapter. The action of molecules within the fluid and the characteristics of the fluid flow can be characterized by two dimensionless parameters: Reynolds number (*Re*) and Péclet number (*Pe*). *Re* is used to predict flow patterns (Stroock et al. 2002) and can be calculated according to Eq. 13.1:

$$Re = \frac{\rho \upsilon L}{\mu} \tag{13.1}$$

where ρ corresponds to the density of the fluid (kg/m^3), υ is the velocity of the fluid (m/s), L is the characteristic linear dimension (m), and μ is the dynamic viscosity of the fluid (Pa·s or N·s/m^2 or kg/[m·s]) (Liu et al. 2018a; Stroock et al. 2002). High *Re* (usually considered to be >2300) can therefore be achieved either by increasing the density and/or flow rate of the fluid or by decreasing its viscosity. High *Re* generates a flow pattern named as turbulent flow, which is characterized by chaotic changes in the fluid motion and no distinct streamlines (Fig. 13.2a) (Sharp and Adrian 2004). On the contrary, low *Re* (usually considered to be <1800) generates a laminar flow, in which distinct streamlines flow in parallel to the direction of the fluid (Fig. 13.2b) (Sharp and Adrian 2004). In this case, since the fluid flows in parallel layers without disruption, it is possible to manipulate the fluids and molecules with high precision and sensitivity and thereby obtain controllable and monodisperse droplets (Liu et al. 2017a). In line with this, the empirical transition between laminar and turbulent flow is expected to occur at *Re* between ~1800 and 2000 (Sharp and Adrian 2004).

The *Pe* is also an important parameter to consider when operating microfluidic technologies, as it reflects the diffusion and convection of molecules. Diffusion

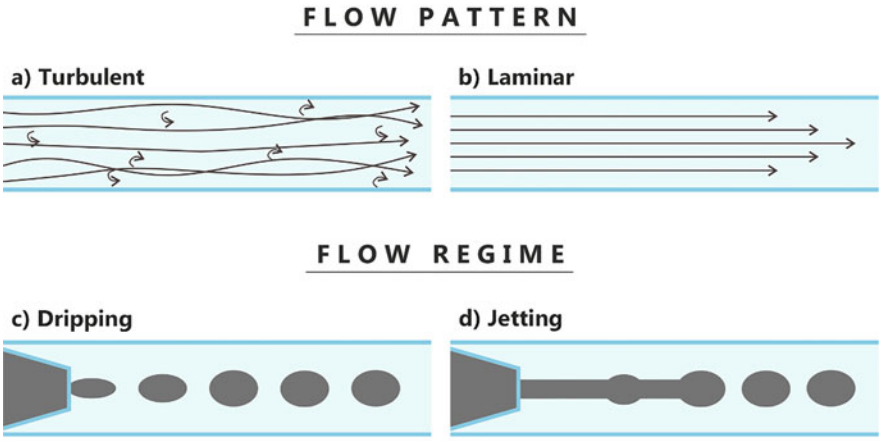

Fig. 13.2 Microfluidic flow patterns and flow regimes. Schematic illustration of (**a**) turbulent flow and (**b**) laminar flow, (**c**) dripping regime, and (**d**) jetting regime

refers to the random thermal motion of molecules within their surrounding environment, whereas convection refers to the transport that results from the bulk motion of a fluid (Atencia and Beebe 2005). The *Pe* can be determined according to Eq. 13.2:

$$Pe = \frac{U_a H}{D} \tag{13.2}$$

where U_a corresponds to the average velocity of the flow, H is the length of the system perpendicular to the direction of the flow, and D is the mass diffusion coefficient of the particle/molecule of interest (Atencia and Beebe 2005). In droplet microfluidics, the use of small volumes and of a laminar flow pattern leads to a slow transfer of molecules, which occurs mainly through diffusion instead of convection (Liu et al. 2017a). The minimized transfer of molecules from the dispersed to the continuous phase enables thus the high encapsulation efficiency of the payloads into the droplets (Beebe et al. 2002).

13.3.2 Flow Regimes

The formation of drops inside microfluidic channels is known to be the result of fluid instabilities (Nunes et al. 2013). When the free surface instabilities between the two phases are large enough, the droplets are formed and, through the creation of a dragging force higher than the viscosity force, the droplets break off from the dispersed phase (Liu et al. 2017a; Martins et al. 2018a). The large volume of the continuous phase plays a crucial role in stabilizing the droplets and in preventing them from merging with each other.

When one immiscible fluid is introduced into another, one of the two events generally occurs: (i) the formation of droplets or (ii) the formation of a continuous jet (Nunes et al. 2013). In the first case, known as dripping regime, the formation of drops is the result of a balance between surface tension forces and the pulling viscous drag (Fig. 13.2c) (Liu et al. 2017a; Nunes et al. 2013). For the second scenario to occur, i.e., the jetting regime, the flow rate of both phases needs to be higher than in the dripping regime (Manshadi et al. 2021). However, the dispersed phase must have a lower flow rate than the continuous phase. This leads to the creation of a jet of the dispersed phase, which becomes unstable due to forces of surface tension that seek to minimize the interfacial area (Rayleigh–Plateau instability). Consequently, the droplets start to separate only at the end of the jet (Fig. 13.2d) (Nunes et al. 2013; Manshadi et al. 2021). The pinch-off of the drops is driven by the balance between the surface tension that is pulling the fluid away and the viscous drag of the fluid that resists the flow (Liu et al. 2017a). Overall, it is the balance between the tension and viscous forces that determines whether, under a given set of conditions, droplets or jets are formed (Nunes et al. 2013).

Hence, the formation of droplets is an extremely dynamic process, as it is affected by the average velocity of both fluids and their viscosities, densities, surface tension,

and surface chemistry (Utada et al. 2007a). The understanding of these parameters is thus a valuable tool for the rational design of microfluidic devices, and thereby, for the development of drug delivery systems with an exquisite control over the manufacturing parameters.

13.4 Microfluidic Devices: Materials and Geometries

13.4.1 Materials for the Fabrication of Microfluidic Devices

The fabrication of microfluidic devices demands for special attention to the choice of materials, as they will determine the inherent properties of the channels, and thereby, also the applicable microfabrication techniques. Materials should thus be selected and/or adapted to meet the requirements that are necessary to produce a certain formulation. The first-generation microfluidic devices were made of silicon and glass (Ren et al. 2013). Nonetheless, as new technological advances occurred, other materials have been explored for their preparation, including polydimethylsiloxane (PDMS) (Friend and Yeo 2010; Thu et al. 2016; Sia and Whitesides 2003), hydrogel molds (Yao et al. 2009; Nge et al. 2013; Hatch et al. 2006; Cheng et al. 2007), polystyrene (Pentecost and Martin 2015; Li et al. 2012a), fused silica (He et al. 2010; Bings et al. 1999; Grosse et al. 2001), polytetrafluoroethylene (Lizotte 2008), polycarbonate (PC) (Ogończyk et al. 2010), poly(methyl methacrylate) (PMMA) (Chen et al. 2008; Muck et al. 2004), and paper, (Gong and Sinton 2017; Li and Steckl 2019), among others. Moreover, these materials have been explored alone or in combination, leading to the generation of hybrid microfluidic devices made of, for example, PC and PMMA (Wabuyele et al. 2001) or PC and PDMS (Chang et al. 2014). A summary of the most used materials for the fabrication of microfluidic channels is presented in Table 13.1.

Silicon has been a dominant material in the fabrication of microfluidic devices for decades owing to its semiconducting properties (Nielsen et al. 2020). Also, the thoroughly characterized modification of the surface properties of silicon based on the silanol group, together with its chemical resistance, excellent thermal stability, and design flexibility turn it into a particularly desirable material for the creation of devices (Nielsen et al. 2020; Zhang et al. 2015). However, these devices are opaque to visible and ultraviolet light and, therefore, have limited application for direct fluid imaging or fluorescence-based detection imaging (Nielsen et al. 2020). Silicon is also expensive and fragile, and its high elastic modulus (150 GPa) turns the incorporation of active components like valves and pumps into the devices more intricate (Zhang et al. 2015; Grover et al. 2003; Grover et al. 2006).

Soon after the exploration of silicon for the production of microfluidic platforms, glass became also widely adopted, due to its stable electroosmotic flow, excellent optical transparency, low fluorescence background, and surface stability (Nielsen et al. 2020). Glass is chemically resistant to organic solvents, which makes it especially suitable for the development of drug delivery systems. Moreover, glass

Table 13.1 Common materials used in the production of microfluidic devices. Adapted with permission from refs (Vladisavljević et al. 2013; Fontana et al. 2019).

Materials	Fabrication methods	Inherent surface affinity	Refs.
Surface-oxidized silicon	Anisotropic wet etching, chemical dry etching	Hydrophilic	Kawakatsu et al. (1997); Kobayashi et al. (2002)
Silicon nitride	Chemical dry etching followed by anisotropic wet etching	Hydrophilic	Kuiper et al. (1998)
Soda lime glass, Pyrex glass, Photo-etchable glass	Isotropic wet etching	Hydrophilic	Lin et al. (2001); Okushima et al. (2004); Kim and Kwon (2006)
Fused silica glass	Chemical dry etching	Hydrophilic	Nisisako et al. (2012)
Glass capillaries	Micropipette pulling, microforge, manual sanding of orifice, gluing to glass slide	Hydrophilic, with modifications hydrophobic	Liu et al. (2015a); Martins et al. (2018b); Utada et al. (2007b); Liu et al. (2015b)
Stainless steel platform for glass capillaries	Micropipette pulling, microforge, manual sanding of orifice	Hydrophilic, with modifications hydrophobic	Herranz-Blanco et al. (2017)
PDMS	Soft lithography	Hydrophobic, can be hydrophilic by plasma oxidation, sol–gel coating with silica or titania, layer-by-layer deposition of polyelectrolytes, UV polymerization of acrylic acid, UV irradiation, chemical vapor deposition, antifouling coatings	Whitesides (2006); Zhou et al. (2010); Zhang and Chiao (2015); Xia and Whitesides (1998)
COP	Hot embossing, injection molding, nanoimprint lithography, laser ablation	Hydrophobic	Jena et al. (2012); Nunes et al. (2010)
Polyurethane	Soft lithography	Hydrophobic	Nie et al. (2005); Thorsen et al. (2001)
PMMA	Hot embossing lithography, injection molding, mechanical cutting, laser ablation, stereolithography	Hydrophobic	Eusner et al. (2010); Liu et al. (2005); Yeh et al. (2009); Morimoto et al. (2009)
Nickel	LIGA process	Hydrophobic	Kim and Lee (2007)
Stainless steel	Mechanical cutting	Hydrophilic	Tong et al. (2001)
Paper	Cutting, wax printing, inkjet printing, photolithography, DLP printing	Hydrophilic, with modifications hydrophobic	Akyazi et al. (2018); Park et al. (2018)

COP cyclic olefin copolymer, *DLP* digital light projector, *PDMS* polydimethylsiloxane, *PMMA* poly(methyl methacrylate)

microfluidic platforms allow the execution of experiments under high pressure (Nielsen et al. 2020). Glass is cheap, robust yet easily modifiable, and compatible with biological samples, resists to high temperature, and can be used in the additive manufacturing of devices (Nielsen et al. 2020; Zhang et al. 2015).

Glass microfluidic devices are generally prepared by (i) the assembly of glass capillaries or patterned coverslips on microscope glass slides (Martins et al. 2018b; Costa et al. 2020; Deng et al. 2011) or (ii) wet chemical etching of channels on glass plates (McCreedy 2001). Glass capillary microfluidic devices can be prepared by simultaneously heating and pulling a circular capillary using a pipette puller, thereby creating a tapered geometry, which culminates in a fine orifice (Shah et al. 2008). The precisely pulled circular capillary is then slid and coaxially aligned into another circular or a square capillary, forming a simple microfluidic device. The coaxial alignment of both inner and outer capillaries is achieved by choosing capillaries in such way that the outer diameter of the inner capillary is the same as the inner diameter of the outer capillary (Shah et al. 2008). The disposition in which these capillaries are assembled dictates the geometry of the device (Martins et al. 2018a). Moreover, their inner surfaces can be chemically modified and turned into hydrophilic or hydrophobic, for example, to suit an intended application (Shah et al. 2008; Fontana et al. 2016). Typically, glass capillary and patterned coverslip devices can be prepared in general laboratories. However, they require skilled manual operation, which may reduce the efficiency of preparation, and the precision of their dimensions and overall features (Zhang et al. 2015). Wet chemical etching combined with photolithography, in turn, enables a flexible designing of microchannels and with high precision, reducing the need for intricate manual operation (Bein et al. 2018). In order to help overcoming some of the limitations associated with the fabrication of glass-based microfluidic devices, a number of companies have recently started to make them commercially available (e.g., MicroLab devices, Microflexis, and Schott) (Nielsen et al. 2020).

Over the years, PDMS has become one of the most popular materials used in microfluidic devices. Briefly, the production of PDMS devices relies on soft lithography methods and consists in pouring a mixture of PDMS (liquid) and a cross-linking agent (to cure it) into a master mold, followed by heating at high temperature (Qin et al. 2010). Once the polymer has hardened, the replica can be taken off the mold. The microfluidic device completion is achieved by the generation of the fluids' inputs and outputs, using a PDMS puncher with the same size as the future connection tubes. The polymer replica is then bound to either another PDMS slab or a different planar material to seal the channels (Nielsen et al. 2020). The replica can adhere and seal the channels either reversibly or, after oxidation, irreversibly to many different types of substrates (Qin et al. 2010). Alternatively, PDMS devices can be prepared by 3D printing (Chande et al. 2020) or hydrogel molding (Odera et al. 2014).

PDMS has become a staple of microfluidics research by virtue of its simple fabrication process and material attributes (Regehr et al. 2009). PDMS is optically transparent, facilitating the observation of the fluids inside of the channels with the help of a microscope, and has low autofluorescence (Regehr et al. 2009; Piruska

et al. 2005). It is flexible and easy to mold, gas permeable, and inexpensive compared to other previously used materials (Herranz-Blanco et al. 2017). Nonetheless, PDMS chips are often considered less suitable for the development of advanced drug delivery systems, particularly due to their reactivity with organic solvents, low capacity to withstand high pressures, and absorption of small inorganic molecules (Bein et al. 2018; Vladisavljević et al. 2013; Fontana et al. 2019). Moreover, PDMS is soft and must be handled delicately to avoid tearing (Nielsen et al. 2020), and PDMS-based devices often need to be prepared in clean rooms, adding to the complexity of the manufacturing process, and reducing its widespread availability for a broader scientific community (Herranz-Blanco et al. 2017).

13.4.2 Devices for the Synthesis of Drug Delivery Systems

When it comes to the synthesis of drug delivery systems, the most commonly used microfluidic devices are microchannels and microcapillaries (Khan et al. 2015). Microchannel-based devices can be obtained through different microfabrication techniques, such as lithography, micromilling, micromachining, or mold replication, using materials like glass, silicon, metal, or polymers (Khan et al. 2015). In these devices, spontaneous droplet formation occurs as a result of interfacial area minimization. Thus, as long as the flow rate of the oil phase is maintained within a certain range, the droplet size depends only on the geometry of the microchannel (van Dijke et al. 2009). Microchannel-based devices offer some advantages over capillary-based systems, since it is possible to obtain channel widths with sizes as low as few tens of microns (Serra and Chang 2008). Also, mask lithography techniques enable a perfect alignment of the channels and the creation of complex microstructures (Serra and Chang 2008). Moreover, upstream and downstream functionalities (e.g., flow distribution, droplet scission, fusion, and selective droplets) can be easily implemented (Serra and Chang 2008). Finally, the chips can be designed with multiple microstructures, and the devices can be paralleled to achieve large yields (Khan et al. 2015; Serra and Chang 2008). Nonetheless, the production of microchannel-based systems can be costly and time-consuming. Also, in these systems, the dispersed phase is in direct contact with the wall of the device before being emulsified by the continuous phase. Such feature demands for particular attention to the choice of the materials used in the fabrication of the devices in order to avoid phase inversion. Briefly, phase inversion occurs when the dispersed phase has greater affinity for the material (preferentially wetting the walls) than for the continuous phase (Serra and Chang 2008). Consequently, the continuous phase becomes emulsified by the dispersed phase, leading to the formation of droplets of the continuous phase. Choosing the right material (e.g., hydrophilic material to produce hydrophobic droplets) or modifying the properties of the material specifically at the location where the droplet formation takes place can help overcoming this limitation. Yet, such modification requires additional steps in the microfabrication process.

Microcapillary-based devices are generally assembled by the use of capillaries (mostly made out of glass) and tubes, and can be prepared from cheap and commercially available parts, typically in less time than microchannel-based systems (Khan et al. 2015; Wang et al. 2011). On such devices, the fluids are manipulated by the use of capillary effects (also known as capillary action or capillary force), which are governed both by the surface tension of a liquid and the geometry and surface chemistry of its solid support (Olanrewaju et al. 2018). Microcapillary-based systems are ideal for working under aggressive chemical conditions (Wang et al. 2011), and can be used to deliver the dispersed phase in the centerline of the continuous phase flow, avoiding the negative impact of the contact between the droplets and the walls of the device (Serra and Chang 2008). Yet, aligning the capillaries and placing them in parallel can be challenging. Capillary-based devices can also solve the clogging issues commonly associated with the use of microchannel-based devices and can even be used to obtain, for instance, oil-in-water (O/W) or water-in-oil (W/O) emulsions with a single device (Serra and Chang 2008). Overall, depending on the desired drug delivery system, microchannels and microcapillaries can be engineered to have a suitable geometry, so that, together with a precise control over the flow rates of the fluids, highly stable, uniform, and monodispersed particles can be obtained (Niculescu et al. 2021).

13.4.3 Device Geometries for Droplet Microfluidics

One subdivision of microfluidics is droplet-based microfluidics, consisting of the manipulation of discrete droplets inside microdevices, and through which nano- and micro-meter-sized monodisperse particles can be produced (Sohrabi et al. 2020). The formation of these droplets relies on the use of two immiscible phases: (i) the dispersed phase (droplet base) and (ii) the continuous phase (medium in which droplets are generated and where they flow). At the microscale, the high surface area-to-volume ratio, the shorter heat and mass transfer times, and shorter diffusing distances lead to faster reaction times (Sohrabi et al. 2020). Also, the flow rates of the two phases and their ratios, the interfacial tension between them, and the geometry of the device will dictate the properties of the generated droplets (Dendukuri et al. 2005).

In general, methods for droplet generation can be classified as passive or active (Zhu and Wang 2017). Passive methods generate droplets without external actuation, whereas active methods rely on the use of additional energy inputs (e.g., electric, magnetic, thermal, centrifugal) by external elements (Zhu and Wang 2017). Active methods have been reported to add another level of controllability over the produced droplets (Zhu and Wang 2017). Yet, passive methods are generally more common, since they lead to similar results with simpler device designs.

As already mentioned above, droplet formation is governed by Rayleigh–Plateau instabilities and occurs as a result of the interfacial tension between the dispersed phase and the continuous phase (Martins et al. 2018a). The application of shear

stress on a droplet promotes its elongation and, subsequently, its rupture. The physical mechanisms behind this process are strongly associated with the geometry of the microfluidic devices, which can be suitably engineered to produce single emulsions, double emulsions, or Janus particles (Fig. 13.3) (Lizotte 2008).

Emulsions consist of droplets of one liquid dispersed in another, with these liquids being immiscible (Atencia and Beebe 2005). Single emulsions can be (i) W/O, when water is dispersed in an oil phase, or (ii) O/W, when the oil phase is dispersed in water (Martins et al. 2018a). Single emulsions can be prepared by three main device geometries (flow focusing, co-flow, and T-junction) and are usually passive droplet formation methods. In the flow-focusing geometry, both the continuous and the dispersed phase flow through two opposite sides of the channel, meeting at the entrance of the narrow orifice of the inner capillary, where the droplets are formed (Fig. 13.3a) (Zhu and Wang 2017). The physical mechanisms behind this geometry are complex, and both jetting and dripping regimes can be used (Liu et al. 2017a). The co-flow geometry relies on the flow of the continuous and dispersed phase in parallel streamlines (Fig. 13.3b). However, the fluids flow through separate channels: usually, the dispersed phase flows through an inner capillary of defined dimension, whereas the continuous phase flows from an outer capillary, in the same direction, with the droplets forming when both phases meet (Liu et al. 2017a). While most of the geometries lead to the formation of micrometer-sized particles, the co-flow geometry is often used to prepare particles at the nanoscale (Rondeau and Cooper-White 2008). The polydispersity of the droplets depends on the flow conditions used: droplets prepared in dripping more are usually monodisperse, while those prepared in jetting mode are polydisperse (Zhu and Wang 2017). T-junction microfluidic devices are commonly used for their simplicity. Briefly, the continuous phase flows through a main channel, whereas the dispersed phase is supplied through side channels, reaching the main channel through cross flow (Fig. 13.3c) (Garstecki et al. 2006). When the stream of the dispersed phase penetrates into the main channel, the droplets start to grow. Droplets prepared by T-junction devices are usually highly monodisperse (Liu et al. 2017a).

Droplet-based microfluidics is often used to prepare also double and multiple emulsions. This process relies on the combined use of two geometries. Double emulsions can be classified as water-in-oil-in-water (W/O/W) or oil-in-water-in-oil (O/W/O) and are particularly attractive as drug delivery systems. A common microfluidic device for the preparation of double emulsions consists of two inner capillaries, coaxially aligned, and oppositely inserted (orifices facing each other) into a bigger outer capillary (Liu et al. 2017a). Generally, the inner phase flows through an inner capillary, while the middle and outer phases flow through the outer capillary. When the middle and outer phases flow in opposite directions, a co-flow combining flow-focusing configuration is obtained (Fig. 13.3d). Double emulsions are formed when the three fluids enter the inner capillary that is oppositely facing the inner capillary through which the dispersed phase is flowing, and which also serves as a collecting tube (Liu et al. 2017a). Double emulsions can also be obtained by simultaneously introducing two inner fluids in the inner capillary (Fig. 13.3e). Moreover, the inner capillary can be inserted into a middle capillary that, in turn,

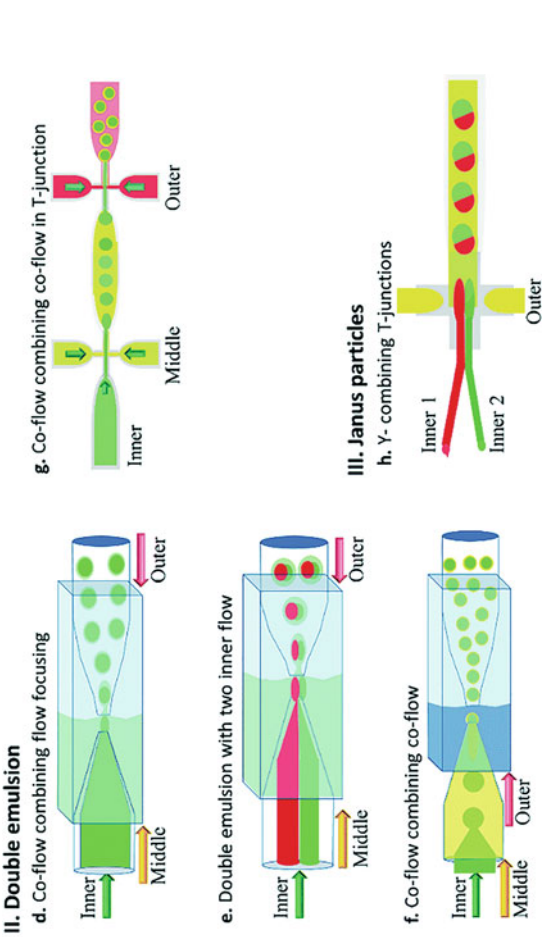

Fig. 13.3 Device geometries for droplet microfluidics. Single emulsions can be prepared using (**a**) flow-focusing, (**b**) co-flow, and (**c**) T-junction geometries. Double emulsions can be prepared using combined geometries, such as co-flow combining flow focusing with (**d**) one inner fluid or (**e**) two inner fluids, (**f**) sequential co-flows to produce thin shell capsules, and (**g**) sequential T-junction geometries. (**h**) Janus particles can be prepared by Y- combining T-junctions, with two parallel inner flows. Reprinted with permission from ref. (Liu et al. 2017a); Copyright © 2017, Royal Society of Chemistry

is inserted into an outer capillary. Even though the inner, middle, and outer fluids flow through different channels, they flow in the same direction, originating a co-flow combining co-flow geometry (Fig. 13.3f), and which has been reported to enable the preparation of double emulsions with ultrathin shells (Kim et al. 2011). Additionally, double emulsions can be prepared by a two-stage process on a T-junction configuration. In this case, the inner fluid is firstly encapsulated by a middle fluid, forming a single emulsion, which then flows through a second droplet maker, and encapsulated again by an outer fluid (Fig. 13.3g).

Janus particles can also be prepared using droplet-based microfluidics. In this case, two separate streams are co-flowed through the same inner channel of a T-junction microfluidic device (Fig. 13.3h) (Chen et al. 2009). The solidification of Janus droplets leads to the formation of a unique class of particles, with two distinct sides, which can be anisotropic in composition and surface features (Le et al. 2019). Their asymmetric structure enables the compartmentalization of materials that can have opposite or complementary features and that impart a different functionality. Janus particles have shown successful applicability for combined therapy (e.g., chemo-photothermal therapy, cellular targeting, and multimodal imaging), and for dual drug release (Garbuzenko et al. 2014).

13.5 Microfluidics to Control the Properties of Advanced Drug Delivery Systems

Microfluidics is mostly known for providing an exquisite degree of control over the properties of advanced drug delivery systems, and therefore, it is gaining increasing popularity in the field of nanomedicine. The possibility to control different parameters within a certain microfluidic setup enables the fine modulation of micro- and nano-particulate drug delivery systems in terms of size, morphology, surface engineering, and mechanical properties, and these features dictate the success of the formulation.

13.5.1 Size

It is widely established that the uniformity of size and reproducibility of a drug formulation are essential for its pharmaceutical application (Tomeh and Zhao 2020). For example, large-sized nanocarriers have low permeability to stromal-rich tumors and therefore fail to efficiently deliver drugs (Lin et al. 2013; Matsumura and Maeda 1986; Cabral et al. 2011). In turn, formulations with small and precisely controlled size can provide size-selective targeting of such tumors (Kimura et al. 2018). Other studies indicate that there is an optimal NP size for efficient endocytosis, regardless

of the materials used in their composition, and that, under similar conditions, smaller NPs are more likely to cause cytotoxicity (Shang et al. 2014).

In a typical synthesis of drug carriers by microfluidics, the particle formation process is based on "bottom-up" approaches and can be explained by the classical crystallization theory (Capretto et al. 2013). Obtaining a desirable size depends, thus, on controlling the molecular assembly and particle growth (Tomeh and Zhao 2020). In this context, it has been reported that the nucleation time depends on the concentration of the precursor used for the preparation of the formulation, while the particle growth is governed by the *Re*, total flow rate (TFR), and flow rate ratio (FRR) between the aqueous and the organic phase (Tomeh and Zhao 2020). To obtain batches of drug delivery systems with narrow size distribution, it is necessary to make sure that the nucleation occurs in a shorter period compared to the growth phase and that a homogenous environment in terms of temperature and concentration of species is ensured (Capretto et al. 2013). Such requirements have been facilitated by the use of microfluidic platforms. Jahn et al. proved that they could control the size of liposomes by altering the FRR of the side channels in relation to that of the main inlet channel on a T-junction microfluidic device (Jahn et al. 2004). When increasing the FRR, the shear stresses applied to the liposomes during their self-assembly also increased, resulting in a reduction of both mean particle size and polydispersity (Fig. 13.4a). Moreover, this microfluidic technique resulted in the production of more monodisperse liposomes when compared to those prepared by bulk methods (Jahn et al. 2004). Later, the same authors reported that the geometry of the microfluidic device and the use of hydrodynamic flow focusing (HFF) also have a strong impact on the size distribution of a formulation (Jahn et al. 2010). In fact, such parameters served as a coarse method to control the size of liposomes, while the TFR allowed its fine-tuning under certain focusing regimes (Jahn et al. 2010). Overall, increasing the FRR led to a reduction of the mixing time, and thereby to a reduction in the size of the particles (Fig. 13.4b) (Jahn et al. 2010).

Other studies have investigated the impact of the FRR and the device geometry in the size of the prepared formulations. For example, in 2017, Ghazal et al. combined HFF microfluidics with synchrotron small-angle X-ray scattering (SAXS) to monitor the early dynamic structural features occurring during the continuous production of multilamellar vesicles (MLVs) (Ghazal et al. 2017). The authors observed that changes in the TFR had a less pronounced impact on the size of the vesicles than changes in the FRR. For example, increasing the FRR from 10 to 50 for a determined TFR (100 μL/min) generated a significant reduction both on the size of MLVs (from 224 nm to 175 nm) and on their polydispersity (from 0.26 to 0.19) (Fig. 13.4c) (Ghazal et al. 2017). Channel widths and geometries also showed to affect the size characteristics of the vesicles, with a relatively long serpentine channel leading to the formation of MLVs with narrower size distribution and eliminating the formation of lipid aggregates (Fig. 13.4d) (Ghazal et al. 2017). In this study, the integration of postproduction processes and analytical techniques into a single microfluidic platform provided even better control of the produced formulation, highlighting the potential of such technique.

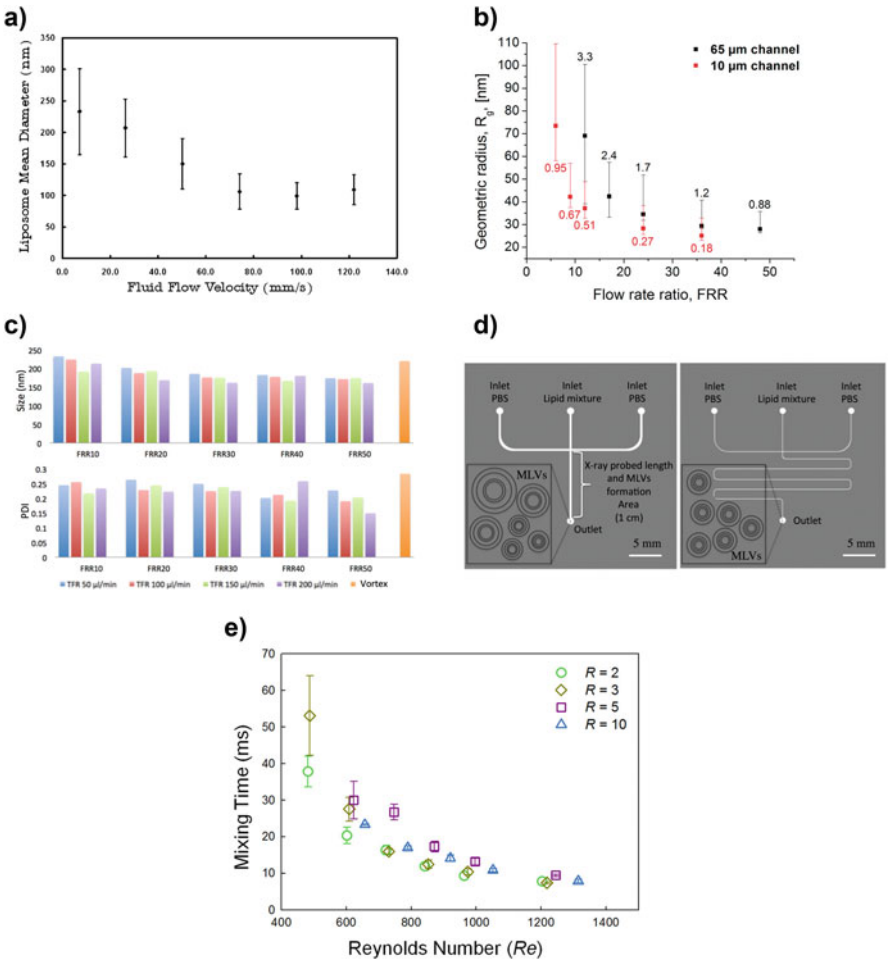

Fig. 13.4 Effects of different parameters on the size of drug delivery systems. (**a**) Decrease of the liposome mean diameter by tuning the flow rates in the microfluidic channel. (**b**) Liposome size distribution as a function of FRR for two channel geometries. (**c**) Effects of FRR and TFR on the size and size distribution of the produced MLVs using a polyimide-based microfluidic chip. (**d**) Schematic representation of two different microfluidic chip designs and geometries for the production of MLVs. (**e**) Mixing time as a function of *Re* when the coaxial turbulent jet mixer is operated in turbulent jet regime. (**a**) Reprinted with permission from ref. Jahn et al. (2004); Copyright © 2004, American Chemical Society. (**b**) Reprinted with permission from ref. Jahn et al. (2010); Copyright © 2010, American Chemical Society. (**c**, **d**) Reprinted with permission from ref. Ghazal et al. (2017); Copyright © 2016, American Chemical Society. (**e**) Reprinted with permission from ref. Lim et al. (2014); Copyright © 2014, American Chemical Society

The *Re* can also play a crucial role on the size of microfluidic-based drug delivery systems. Lim et al. reported a coaxial turbulent jet mixer that can synthesize various types of NPs (PLGA–PEG NPs, lipid vesicles, iron oxide NPs, polystyrene NPs, and

siRNA/PEI polyplex NPs) (Lim et al. 2014). Overall, the size of the particles prepared by this jet mixer was smaller than those prepared by bulk methods, and the size distribution was narrower. This effect was attributed to the fact that the mixing inside the jet mixer is more controlled than in the bulk synthesis, and the mixing time is shorter than the aggregation time (Fig. 13.4e) (Lim et al. 2014). Importantly, the size of the NPs was shown to be controllable, in a reproducible manner, by applying changes in the *Re*. In summary, NPs of varying types and compositions were consistently produced with smaller sizes upon increasing the *Re* (Lim et al. 2014). Beyond a certain *Re*, the influence of the mixing time on the size of the NPs plateaued, suggesting that the formulations had reached a size that corresponds to the limit of rapid mixing.

13.5.2 Shape

Shape is another critical parameter when developing advanced drug delivery systems, and it has an equally significant impact on their performance. The shape of a drug carrier is known to affect, for example, its diffusivity and adhesion to cells (Toy et al. 2013). It has been reported that spherical NPs are more efficiently internalized by cells for being symmetrical and having a constant contact angle, while NPs with more intricate shapes depend on a specific orientation for successful cellular internalization (Toy et al. 2013). The shape can also impact the loading and release of a drug from a formulation. For example, a better design of mesoporous silica nanoparticles in terms of pore size has led to an enhanced loading capacity of genes (Fujiwara et al. 2005). On a different study, particles with larger pore size have shown increased cellular uptake and faster intracellular release of doxorubicin in multidrug-resistant cancer cells (Gao et al. 2011).

In 2018, Hao et al. established a PDMS spiral-shaped microfluidic channel with two inlets and one outlet for the synthesis of mesoporous silica nanofibers (Fig. 13.5a) (Hao et al. 2018). The authors investigated the formation mechanisms and tunability of these fibers by altering a series of parameters in the microfluidic process. Transmission electron microscopy (TEM) images depicted marked changes in the morphology of the fibers by varying the flow rates and the concentrations of the reactants (Fig. 13.5b). In summary, increasing the flow rate of inlet II led to a reduction in the aspect ratios of the fibers until they became spherical (Fig. 13.5b **[A]**), while decreasing the flow rate of this inlet increased their aspect ratios (Fig. 13.5b **[B]**). Increasing the concentration of reactants in inlet II but maintaining its flow rate led to an increase in the size and aspect ratio of the silica products (Fig. 13.5b **[C, D]**). Increasing the flow rate of inlet I, in turn, raised the aspect ratios of silica fibers (Fig. 13.5b **[E]**), whereas decreasing the flow rate of this inlet reduced the aspect ratios and yielded the formation of nanospheres (Fig. 13.5b **[F]**). Similarly, increasing the concentration of reactants in inlet I and maintaining the flow rate led to an increase in the aspect ratios of silica nanostructures (Fig. 13.5b **[G, H]**). The concentration of ammonia used in the microfluidic process regulated the hydrolysis

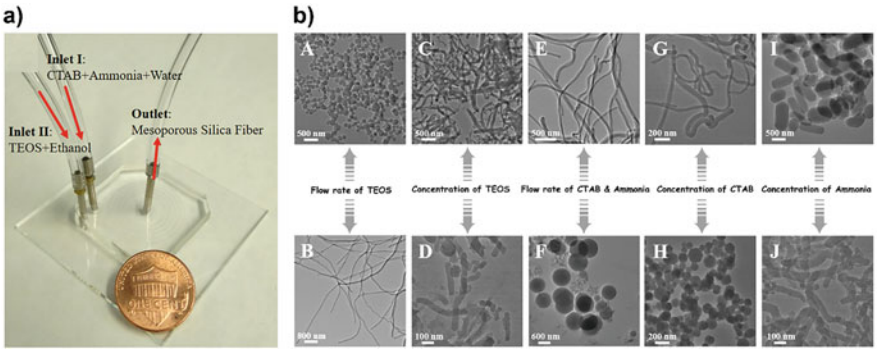

Fig. 13.5 Effects of different parameters on the shape of drug delivery systems. (**a**) Experimental setup for the microfluidic synthesis of mesoporous silica nanofibers. (**b**) Effect of reaction conditions on the shape of the fibers, including changes in [A, B] flow rate of inlet II, [C, D] concentration of reactants in inlet II, [E, F] flow rate of inlet I, and [G–J] concentration of reactants in inlet I. Reprinted with permission from ref. Hao et al. (2018); Copyright © 2017, American Chemical Society

of silica precursor and its condensation rates and therefore also played a crucial role in controlling the diameter and shape of the fibers (Fig. 13.5b **[I, J]**) (Hao et al. 2018).

On another study, Dashtimoghadam et al. designed a cross-junction microfluidic channel to create a HFF device and explored the possibility of rapid and tunable mixing to control the characteristics of self-assembled hydrophobically modified chitosan (HMC) NPs (Dashtimoghadam et al. 2013). The microfluidic technique applied in this study enabled the production of NPs with defined size and narrow size distribution, high drug loading capacity, and controlled compactness. Importantly, this study suggested that shorter mixing times resulted in the formation of smaller and more compact NPs, consisting of lower number of HMC chains. The compactness of the NPs, in turn, had a strong impact on the drug loading and release, with NPs produced in the rapid mixing regime presenting higher encapsulation efficiencies than those prepared by conventional methods (Dashtimoghadam et al. 2013). Overall, NPs prepared by this microfluidic platform presented homogenous and spherical shapes, whereas the corresponding bulk-synthesized particles presented visible deviations from the spherical shape and a broader size distribution (Dashtimoghadam et al. 2013).

13.5.3 Surface Properties

Surface properties directly affect the dispersibility and stability of drug delivery systems in aqueous media. Moreover, surface properties affect drug entrapment, and the way a formulation interacts with biological systems. Generally, a strong surface charge (either positive or negative) guarantees improved colloidal stability (Araújo

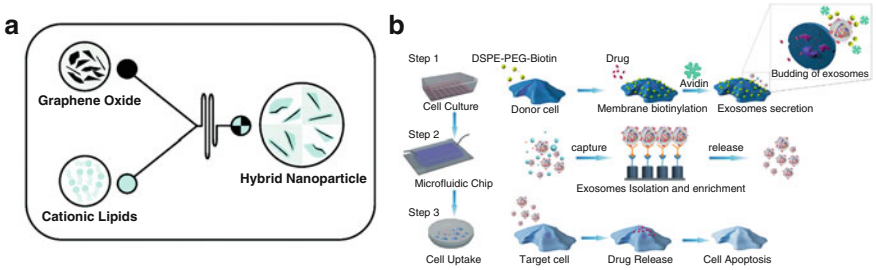

Fig. 13.6 Effects of different parameters on the surface properties of drug delivery systems. (**a**) Schematic representation of a microfluidic system used for the preparation of graphene oxide NPs coated with a double layer of cationic lipids. (**b**) Schematic illustration of microfluidic chip isolation of exosomes secreted from engineered donor cells and application to active targeted drug delivery. (**a**) Reprinted with permission from ref. (Di Santo et al. 2019); Copyright © 2019, Royal Society of Chemistry. (**b**) Reprinted with permission from ref. Wang et al. (2017); Copyright © 2017, American Chemical Society

et al. 2017). Positively charged particles are generally more efficiently internalized by cells, while particles with a neutral charge are reported to avoid nonspecific interactions in vivo (Cho et al. 2009; Verma and Stellacci 2010). Exploring the surface properties of drug delivery systems provides exciting opportunities also in terms of targeting. Targeting ligands, such as antibodies and peptides, have the ability to direct micro- and nanoparticles for selective and/or specific recognition by molecules or sites, such as cells or pathogenic tissues (Friedman et al. 2013). These strategies hold thus a tremendous potential to increase the local drug concentration at the target site, as well as to minimize side effects on healthy tissues (Friedman et al. 2013).

In a recent study, Di Santo et al. developed hybrid NPs made of graphene oxide and coated with cationic lipids by microfluidic mixing (Di Santo et al. 2019). The microfluidic platform used in this study (Nanoassemblr™ Benchtop; Precision Nanosystems, Inc., Vancouver, Canada) relies on the use of two syringe pumps to mix two different solutions (graphene oxide and cationic lipids) into channels of the same cartridge (Fig. 13.6a). This platform provides a high degree of control over the mixing parameters, such as flow rate and flow ratio. The hybrid NPs presented adequate size (<150 nm) and surface charge (ξ = +15 mV) for the intended application. Also importantly, the particles presented a uniformly coated surface with a double layer of cationic lipids, making the system suitable for gene delivery (Di Santo et al. 2019).

Recently, Wang et al. reported the use of a 3D nanostructured microfluidic chip in a new strategy to chemically modify exosomes, toward enhanced targeting efficiency and delivery of a chemotherapeutic drug to tumor cells (Fig. 13.6b) (Wang et al. 2017). Briefly, donor cells (human umbilical vein endothelial cells [HUVECs]) were firstly labeled with biotin, and anti-tumor drugs were encapsulated in their cytosol. Then, the cells were further labeled with avidin for targeting purposes. When these donor cells started to secrete exosomes, they had inherited the ligands

and the drugs and, thus, were chemically modified. Then, the culture media collected from the donor cells and containing the exosomes were subjected to a microfluidic chip. The chip consisted of a series of micropillars functionalized with multiwall carbon nanotubes, which allowed to isolate and recover intact exosomes with high purity for further targeted drug delivery (Fig. 13.6b) (Wang et al. 2017). The efficiency of exosome capturing was optimized by investigating parameters such as micropillar height, spacing distances, and flow rates.

13.5.4 Mechanical Properties

Mechanical properties refer to the behavior of materials under loads and include, for example, elasticity, stiffness, rigidity, strength, and hardness (Hui et al. 2019). Among these, elasticity and stiffness have been widely used to explore the properties of drug delivery systems. Elasticity is, by definition, the ability of an object to withstand deformation when subjected to stress and to return to its original state when the stress is removed (Hui et al. 2019). Stiffness, in turn, refers to the extent to which an object resists deformation when subjected to a loading. Recent studies suggest that mechanical properties like elasticity and stiffness affect the biological performance of drug carriers (Hui et al. 2019).

In 2014, Sun et al. implemented a two-stage microfluidic platform: the first stage comprising three inlets and a straight synthesis microchannel and the second stage comprising one centered inlet and a spiral mixing channel (Fig. 13.7) (Sun et al. 2015). This microfluidic platform was then used to assemble, in a single step, lipid-covered PLGA NPs. By tuning the amounts of interfacial water between the PLGA core and the lipid shell, it was possible to obtain NPs of the same size, but varying rigidity. This was achieved by altering the order of injection of the solutions in the microfluidic chip (Fig. 13.7a, b). Results suggested that rigidity can dramatically impact the cellular uptake efficiency, and particularly, more rigid NPs can move more easily through membranes (Sun et al. 2015).

13.6 Microfluidics for the Preparation of Advanced Drug Delivery Systems and Their Applications

Microfluidics is a multidisciplinary technology, and microfluidic devices have proven to be suitable for a variety of applications in healthcare, including the development of homogenous and reproducible drug delivery systems, cell-free protein synthesis and the establishment of cell-, organ-, and human-on-a-chip platforms for rapid and sensitive drug screening, which could partially replace animals in research (Damiati et al. 2018). This section focuses solely on the unique advantages of microfluidics for the preparation of drug delivery systems, with

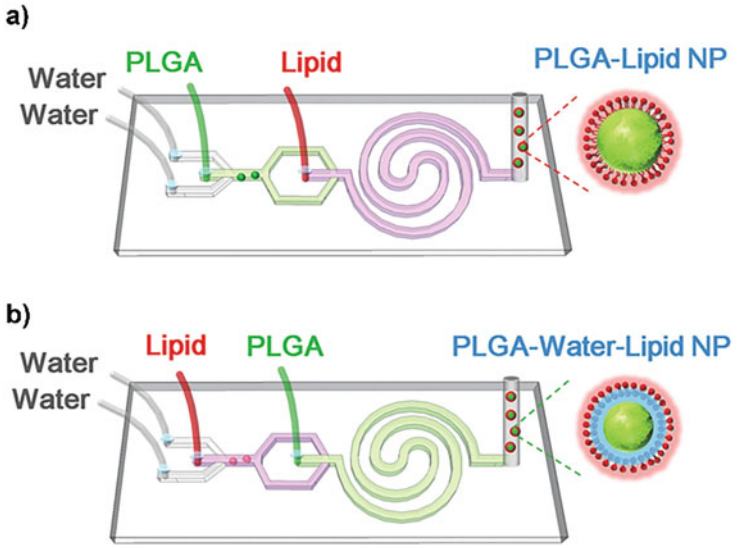

Fig. 13.7 Effects of different parameters on the rigidity of drug delivery systems. Two-stage microfluidic platform for assembling lipid-coated PLGA NPs with varying amounts of water. (**a**) NPs composed of a lipid shell and a PLGA core by injecting the PLGA solution in the first stage and the lipid–PEG solution in the second stage; (**b**) NPs composed of a lipid shell, an interfacial water layer, and a PLGA core by injecting the lipid–PEG solution in the first stage and the PLGA solution in the second stage. Reprinted with permission from ref. Sun et al. (2015); Copyright © 2014, Wiley-VCH Verlag GmbH & Co. KGaA

particular emphasis to lipid-based particles, polymeric and hybrid particles, and emulsions. Other applications of microfluidics are out of the scope of this chapter and can be found extensively reviewed elsewhere (Vladisavljević et al. 2013; Damiati et al. 2018; Li et al. 2012b; Wu et al. 2010).

13.6.1 Lipid-Based Particles

Lipid nanoparticles (LNPs) usually consist of vesicular structures formed by phospholipids, surrounding one or more internal aqueous compartments (Mitchell et al. 2021). The most common subclasses of LNPs are solid-lipid NPs (SLNs), liposomes, and micelles. LNPs have shown tremendous potential in clinical applications, particularly after the FDA approval of Onpattro® (used in the treatment of amyloidosis) and COVID-19 vaccines (Ali et al. 2021).

Over the years, microfluidics has been providing solutions for the successful preparation of LNPs, paving the way of these drug delivery systems to the market (Samaridou et al. 2020; Arduino et al. 2021a, b). On a study from Prof. Cullis' research group, the authors showed that microfluidic mixing using a simple

staggered herringbone micromixer (SHM) device enabled the routine and reliable production of LNP small interfering RNA (siRNA) systems (Belliveau et al. 2012). For this purpose, lipids were dispersed in ethanol, while siRNA was dispersed in an aqueous solution. Both phases were pumped into separate inlets of the microfluidic device using a syringe pump (Fig. 13.8a **[A]**). The mixing channels had dimensions of 200 × 79 μm, and the herringbone structures were 31 μm high and 50 μm thick (Belliveau et al. 2012). The presence of herringbone structures induced chaotic advection of the laminar streams, causing the rapid mixing of both phases, and consequently of the rapid polarity of the lipid solution. At a critical polarity, the precipitates turn into LNPs (Belliveau et al. 2012). This microfluidic platform enabled the production of LNP siRNA in the size range 20–100 nm while offering multiple advantages over previous formulation processes, such as high loading efficiency (~100%; Fig. 13.8a **[B]**), low polydispersity, and improved or equivalent gene silencing potency. Furthermore, the ease of design and parallelization of the devices enabled a successful scale-up of the formulation while ensuring the maintenance of its properties (Belliveau et al. 2012).

Koh et al. reported the use of a microfluidic approach to produce lipopolyplex NPs (Koh et al. 2010). Lipopolyplexes are core–shell structures consisting of nucleic acids, polycations, and lipids (Chen et al. 2016). The authors used a five-inlet PMMA microfluidic HFF system (Fig. 13.8b **[A–C]**), through which they were able to obtain lipopolyplexes of lipid–polymer–DNA. The fact that the flow is strictly laminar inside the channels allowed the well-defined mixing to be controlled exclusively by interfacial diffusion between the multiple flow streams. By optimizing the flow conditions and mixing process of the reagents inside the microfluidic channels, it was possible to produce lipopolyplex NPs with a smaller size, narrower size distribution, and enhanced delivery of the payload to cancer cells than those prepared by conventional bulk mixing methods (Fig. 13.8b **[D, E]**) (Koh et al. 2010).

Recently, Costa et al. explored the use of glass capillary microfluidics for the preparation of a liposome-based nano-in-micro composite system (Costa et al. 2020). For this purpose, a two-stage microfluidic platform was established (Fig. 13.8c **[A]**). On the first stage, lipids and cholesterol, previously dissolved in ethanol, were pumped through the inner capillary, whereas an insulin solution was pumped through the outer capillary, in the same direction. When both phases meet, insulin-encapsulated liposomes are formed via nanoprecipitation (Costa et al. 2020). After being collected, the liposomes were coated with chitosan by physical mixture under stirring. On the second stage, chitosan-coated, insulin-encapsulated liposomes were dispersed in a polymeric solution (hydroxypropyl methylcellulose acetate succinate (HPMCAS)) and pumped through a second glass capillary microfluidic device. This time, the particle dispersion was pumped from the outer end, which is opposed to the inner glass capillary, and this, in turn, served as collection tube. An outer fluid was simultaneously pumped from the opposite end of the outer capillary, and, via a double emulsion technique, the final microcarrier system was formed (Fig. 13.8c **[A]**). For the optimization of the size of the liposomes, the authors explored changes in the FRR, TFR, and initial lipid concentration. Overall, increasing the FRR reduced the size of the liposomes (Fig. 13.8c **[B]**). When maintaining

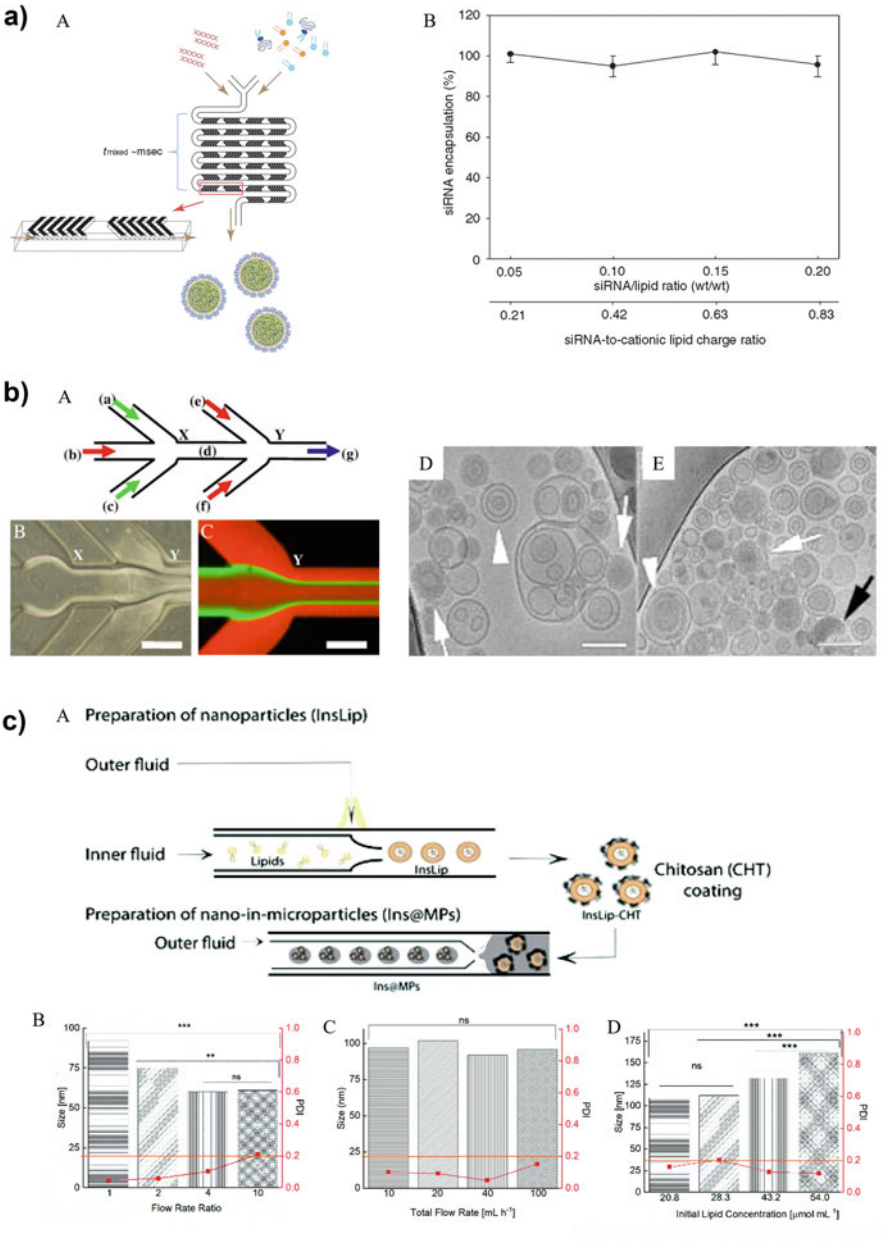

Fig. 13.8 Microfluidics for the preparation of lipid-based NPs. (**a**) Preparation of LNP siRNA employing an SHM device; [A] schematic representation of the microfluidic device; [B] the ~100% encapsulation efficiency of the prepared formulations over a wide range of siRNA-to-cationic charge ratios. (**b**) Five-inlet PMMA microfluidic device for the preparation of lipopolyplex NPs; [A] schematic representation of the device; [B] optical micrograph of the flow pattern at the two junctions (X and Y); and [C] fluorescence micrograph of flow pattern at junction Y; scale bar = 250 μm. Cryo-TEM images of lipopolyplex NPs prepared by [D] bulk methods and

the FRR, but varying the TFR, no significant changes were observed on the size of the liposomes (Fig. 13.8c **[C]**). Ultimately, when maintaining both the FRR and TFR, an increase in the lipid concentration led to an increase in the size of the liposomes (Fig. 13.8c **[D]**) (Costa et al. 2020). In summary, a multistage drug delivery system was successfully developed using a two-stage microfluidic platform, with potential application in the oral delivery of insulin.

13.6.2 Polymeric and Hybrid Particles

Polymeric NPs are colloidal particles with sizes ranging between 1 and 1000 nm and can be synthesized from monomers and natural, synthetic, or pre-formed polymers (Suriya Prabha et al. 2020; Zielińska et al. 2020). Over the years, polymeric NPs have attracted considerable interest due to their small size, and capability to load different drugs, biomolecules, and genes (Conniot et al. 2014). Moreover, they can be formulated to have a variety of structures and properties, to protect drugs against harsh physiological environments, improving their bioavailability and therapeutic index (Zielińska et al. 2020). Polymeric NPs usually present high biocompatibility and biodegradability, and moderate toxicity (Conniot et al. 2014). Their most common forms include nanocapsules and nanospheres, which can be subdivided into polymersomes, micelles, and dendrimers (Conniot et al. 2014). A number of polymeric NPs have also made their way into the clinic after being approved by the FDA (Mitchell et al. 2021). Importantly, the combined use of, for example, two polymers, polymer and lipids, or even polymers and inorganic materials has led to the development of hybrid systems, which often display advantageous properties over single-material systems, such as improved circulation time, stability, encapsulation rate, controlled release, and release kinetics (Ferreira Soares et al. 2020).

Microfluidics has also been widely used to control the mixing and, subsequently, the physicochemical properties of polymeric NPs. For example, Karnik et al. synthesized PLGA–PEG NPs in a Y-shaped, PDMS-based microfluidic device using HFF (Karnik et al. 2008). In this platform, the polymers in solution flowed along the central channel, meeting two adjacent streams that flow at higher flow rates (Fig. 13.9a **[A]**). Using a low *Re*, the central stream containing the polymers was squeezed into a narrow stream. Thus, the narrow width of the focused stream

Fig. 13.8 (continued) [E] microfluidics; scale bar = 100 μm. (**c**) Microfluidic platform for the preparation of an insulin-loaded, liposome-based nano-in-microparticle; [A] schematic representation of the two-stage microfluidic platform; size and size distribution variation of liposomes upon changes on the [B] FRR, [C] TFR, and [D] initial lipid concentration. (**a**) Reprinted with permission from ref. Belliveau et al. (2012); Attribution-NonCommercial-NoDerivs 3.0 Unported (CC BY-NC-ND 3.0); (**b**) Reprinted with permission from ref. Koh et al. (2010); Copyright © 2010, Elsevier. (**c**) Reprinted with permission from ref. Costa et al. (2020); Attribution-NonCommercial 3.0 Unported (CC BY-NC 3.0)

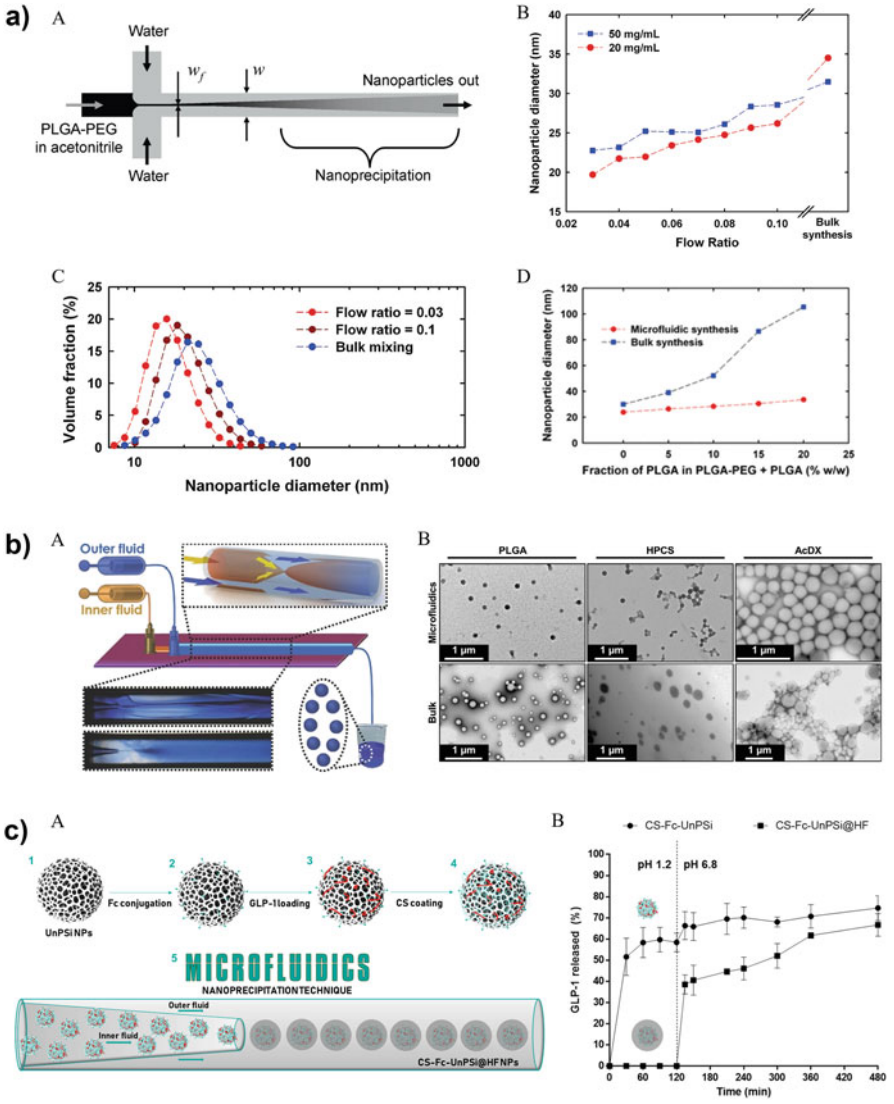

Fig. 13.9 Microfluidics for the preparation of polymeric and hybrid NPs. (**a**) Microfluidic fabrication of PLGA–PEG NPs; [A] microfluidic device using HFF, where the polymer stream is focused into a thin stream between two water streams with higher flow rates; [B] effect of flow ratio on NP size; [C] effect of flow ratio on the homogeneity of the NPs; [D] effect of polymer composition on the size of the NPs. (**b**) High-throughput synthesis of NPs through a controlled mixing microfluidic process; [A] glass capillary co-flow microfluidic nanoprecipitation platform; [B] TEM images of PLGA, HPCS, and AcDX NPs prepared by microfluidics and conventional bulk methods; scale bar = 1 μm; (**c**) Microfluidic nanoassembly of NPs for oral drug delivery; [A] schematic representation of the preparation of Fc-functionalized, chitosan-coated porous silicon NPs, entrapped into HPMC via glass capillary microfluidics; [B] release profile of an antidiabetic drug from HPMC-encapsulated and non-encapsulated NPs in different physiological conditions. (**a**) Reprinted with permission from ref. (Karnik et al. 2008); Copyright © 2008, American Chemical

allowed the rapid mixing through diffusion (Karnik et al. 2008). The authors demonstrated that by applying changes in the flow rates, polymer composition and polymer concentration, it was possible to optimize the size, polydispersity, drug loading, and release from the NPs. Briefly, the size of the NPs decreased upon decreasing the flow ratio and increasing the mixing rate (Fig. 13.9a **[B]**). Increasing the mixing rate, in turn, increased the homogeneity of the formed NPs (Fig. 13.9a **[C]**). Moreover, the size of the NPs remained relatively unchanged upon addition of hydrophobic $PLGA_{100K}$ to the initial particle precursors ($PLGA_{15K}$–$PEG_{3.4K}$) (Fig. 13.9a **[D]**). The addition of this hydrophobic PLGA to the formulation nearly doubled the drug loading and encapsulation efficiency (Karnik et al. 2008).

In 2015, Liu et al. proposed the use of a microfluidic co-flow glass capillary device for the preparation of three different types of polymeric NPs: PLGA, hydrophobic chitosan (HPCS), and acetalated dextran (AcDX) NPs (Liu et al. 2015a). The microfluidic device consisted of two glass capillaries, with a smaller tapered glass capillary being inserted and coaxially aligned into a bigger cylindrical capillary. In this co-flow geometry, the inner fluid (aqueous solution and stabilizers) and the outer fluid (particle precursors) flow in the same direction, resulting in a 3D coaxial flow, with the latter streaming in between the inner and outer capillaries (Fig. 13.9b **[A]**). Controlled nanoprecipitation provided by the controlled mixing time ensured a homogenous environment for NP nucleation and growth and, therefore, enabled the preparation of NPs of different nature with homogeneous size distribution and efficient drug encapsulation (Liu et al. 2015a). Overall, this microfluidic platform enabled a more successful synthesis of polymeric NPs when compared to conventional bulk methods (Fig. 13.9b **[B]**).

Recently, our research group has reported the microfluidic nanoassembly of a hybrid NP system for oral delivery of an antidiabetic peptide, which consisted of Fc-functionalized, chitosan-coated porous silicon NPs encapsulated into HPMC (Martins et al. 2018b). For this purpose, a tapered borosilicate glass capillary was inserted through the left end of an outer capillary and coaxially aligned (Fig. 13.9c **[A]**). The inner phase (NPs dispersed in a HPMC solution) and the outer phase (aqueous solution with stabilizer) were injected into the microfluidic channels at constant flow rates, in the same direction, resulting in a coaxial flow (Martins et al. 2018b). When both phases met, HPMC spherical matrices entrapped the core porous silicon NPs by nanoprecipitation, resulting in the formation of NPs with a controlled size and narrow size distribution. The presence of HPMC in the formulation was essential for preserving the integrity of the peptide loaded into the core NPs in the harsh conditions of the stomach, enabling a controlled release of the drug in conditions that mimicked the intestine (Fig. 13.9c **[B]**). These results highlighted the potential of microfluidics for the preparation of stimuli-responsive platforms for

Fig. 13.9 (continued) Society; (**b**) Reprinted with permission from ref. (Liu et al. 2015a); Copyright © 2015, Wiley-VCH Verlag GmbH & Co. KGaA; (**c**) Reprinted with permission from ref. (Martins et al. 2018b); Copyright © 2018, American Chemical Society

oral drug delivery in ahighly reliable, efficient, and reproducible manner (Martins et al. 2018b).

13.6.3 Single and Double Emulsions

As already mentioned above, emulsions consist of stable mixtures of two or more immiscible liquids and can be classified as single (W/O and O/W) or double emulsions (W/O/W and O/W/O) (Martins et al. 2018a; Atencia and Beebe 2005). As a result of the natural tendency for a liquid/liquid interface to separate, emulsions are thermodynamically unstable, as droplets coalesce to minimize the Gibbs free energy of the system (Jenjob et al. 2019). Nonetheless, surfactants and stabilizers can be used to counteract this effect. Emulsions are particularly relevant for drug delivery purposes, mostly due to their high encapsulation efficiency of payloads (Jenjob et al. 2019). Microfluidic devices offer a versatile route to produce both single and double emulsions (Liu et al. 2014; Bertoni et al. 2018; Zhang et al. 2022).

In 2016, Herranz-Blanco et al. presented a simple and reusable platform for creating microfluidic devices within minutes and in a flexible and easy way, which they used for the preparation of MPs via double emulsion (Fig. 13.10a **[A]**) (Herranz-Blanco et al. 2017). The components of the microfluidic device (base and injection chambers) were designed with a 3D modeling software, and 3D printed in stainless steel. The tightening systems consisted of metal screws and wing nuts, and the sealing systems consisted of rubber rings, which were assembled around the injection chambers (Fig. 13.10a **[A]**). The different modules were assembled manually, formed by a base connected through a hinge-like joint to the injection component, with the help of a guide that enabled angular and horizontal adjustment of the modules (Fig. 13.10a **[A]**). For the preparation of MPs via double emulsion, two tapered glass capillaries were inserted through opposite ends of an outer glass capillary (Fig. 13.10a **[B]**). The inner phase consisted of an aqueous solution with a surfactant, and it was injected through the left inner capillary. The middle phase consisted of 1% w/v SPAN™ 80 in octanol, being injected in between the inner and outer capillary, in the same direction. The outer phase had the same composition as the inner phase; however, it was injected in between the inner and outer capillary, in opposite direction to the inner and middle phases, focusing them, thereby forcing the formation of W/O/W droplets (Fig. 13.10a **[B]**) (Herranz-Blanco et al. 2017). This platform ensured robustness, durability, and high chemical compatibility of the device, along with the reproducible production of MPs via a double emulsion technique (Fig. 13.10a **[C, D]**).

Hollow core–shell MPs have great potential for the controlled capture/release of molecules, for protecting them from harsh physiological environments, confined cell culture, and microsphere classification/separation, and to serve as microreactors for catalysis (Hyuk Im et al. 2005; De Rose et al. 2008; Wang et al. 2013). Wang et al. used a capillary microfluidic device to prepare W/O/W emulsions with NP-containing inner drops (Wang et al. 2013). The devices consisted of three

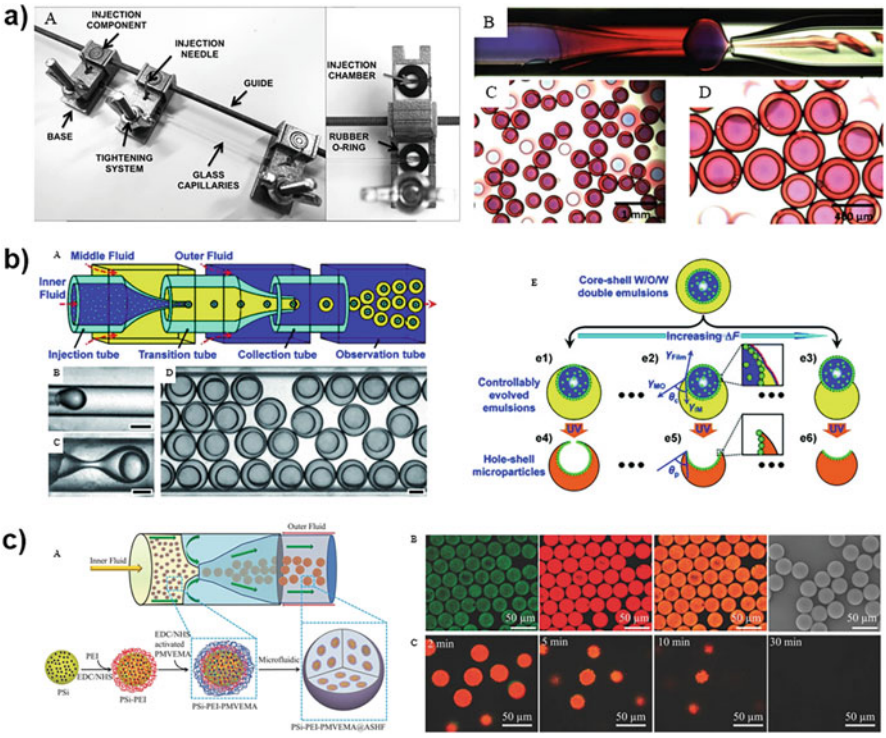

Fig. 13.10 Microfluidics for the preparation of single and double emulsions. (**a**) Production of double emulsion droplets; [A] components of a microfluidic platform for the flexible assembly of glass capillaries; [B] glass capillary setup to produce double emulsion droplets by a flow-focusing approach; [C, D] examples of the W/O/W drops obtained; scale bars = 1 mm and 400 μm, respectively. (**b**) Production of hole–shell MPs from W/O/W emulsions; [A] schematic representation of the microfluidic device; optical micrographs of the [B] inner drops and [C, D] core–shell W/O/W emulsions; scale bar = 100 μm; [E] synthesis of hole–shell microparticles from templated W/O/W emulsions. (**c**) Flow-focusing microfluidic preparation of an O/W emulsion; [A] schematic representation of the microfluidic device; [B] monodispersity of the composites by confocal microscopy and scanning election microscopy (SEM); scale bar = 50 μm; [C] dissolution behavior of the composites at pH 7.4 from 2 to 30 min by confocal microscopy; scale bar = 50 μm. (**a**) Reprinted with permission from ref. (Herranz-Blanco et al. 2017); Copyright © 2016, Elsevier; (**b**) Reprinted with permission from ref. (Wang et al. 2013); Copyright © 2013, Wiley-VCH Verlag GmbH & Co. KGaA; (**c**) Reprinted with permission from ref. (Zhang et al. 2014); Copyright © 2014, Wiley-VCH Verlag GmbH & Co. KGaA

cylindrical capillaries, which were used as injection, transition, and collection tubes, respectively. These capillaries were coaxially aligned inside square capillaries (Fig. 13.10b **[A]**). The ends of both the injection and transition tubes were tapered using a micropuller and then adjusted using a microforge. Finally, another square capillary was connected to the collection tube for observing the flowing of the emulsions. An aqueous solution containing nanogels was used as the inner fluid,

whereas a monomer and a photoinitiator served as middle fluid. Pluronic 127 and glycerol were used as outer fluid (Wang et al. 2013). Briefly, drops of the inner fluid were first generated inside of the transition tube, with nanogels absorbing at the surface of the drop for stabilization (Fig. 13.10b **[B]**). When flowing out of the orifice of the transition tube and meeting the outer fluid, these drops were encapsulated in the oil shell of the middle fluid, forming core–shell W/O/W emulsions (Fig. 13.10b **[C]**). The authors observed that, after collection, the inner drops were drawn to the top of the shell, due to a mismatch in the densities of the inner and middle fluids (Fig. 13.10b **[D]**) (Wang et al. 2013). Since it has been reported that the addition of holes to a shell can facilitate mass transport, and thus provide more versatility to the particles, UV irradiation was used for the polymerization of the eccentric core–shell emulsions, resulting in the production of fishbowl-shaped MPs, with a large hollow core and a small, single hole in the shell (Fig. 13.10b **[E]**). Overall, this microfluidic platform enabled the successful preparation of highly controlled W/O/W double emulsions, which served as templates for hole–shell MPs (Wang et al. 2013).

Zhang et al. explored the use of microfluidics for the preparation of single emulsions for oral delivery of anticancer drugs (Zhang et al. 2014). The proposed system consisted of porous silicon NPs, serving as drug nanocarrier, surface functionalized with a mucoadhesive polymer. Subsequently, these NPs were encapsulated into a pH-responsive polymer using microfluidics, to protect the drugs from the harsh stomach environment and avoid their premature release. For this purpose, the authors used a flow-focusing glass capillary microfluidic device, in which a tapered inner capillary was inserted from the right end of an outer cylindrical capillary (Fig. 13.10c **[A]**) (Zhang et al. 2014). The core porous silicon NPs, together with the pH-responsive polymer in ethyl acetate, served as inner fluid and were injected through the left end of the outer capillary. An aqueous solution with a stabilizer was used as outer fluid, and injected from the right end of the chip, in between the inner and outer capillaries. The particles were formed at the orifice of the inner capillary, which then served as collection tube (Fig. 13.10c **[A]**). By changing the flow rates in the two channels of the microfluidic device, it was possible to optimize the particle size and size distribution. Confocal microscopy and scanning election microscopy (SEM) images showed the successful preparation of highly monodisperse, smooth, and spherical MPs (Fig. 13.10c **[B]**) (Zhang et al. 2014). Moreover, these pH-responsive polymeric capsules were shown to start dissolving immediately after 2 min at pH 7.4, and to be fully collapsed within 30 min, making the system suitable for oral drug delivery applications (Fig. 13.10c **[C]**) (Zhang et al. 2014).

13.6.4 Other Types of Drug Delivery Systems

The myriad of possibilities offered by the miniaturization of fluidic operations turn the microfluidic synthesis of advanced drug delivery systems as broad as human

creativity. Consequently, microfluidics has been used for the fabrication of a wide range of micro- and nanoparticles that go far beyond the examples described above. Grigsby et al. used a microfluidic cross-flow droplet generator chip to prepare polyplexes loaded with either plasmid DNA or messenger RNA (Grigsby et al. 2013). Fontana et al. used glass capillary microfluidics to produce the initial two layers of a nanovaccine with immunostimulatory properties via nanoprecipitation (Fontana et al. 2017). Inspired by the fact that, when disturbed, cephalopods release dark ink containing melanin NPs, Wang et al. used a co-flow glass capillary microfluidic device for the superfast and controllable preparation of monodisperse melanin-like NPs (Wang et al. 2020).

In order to tackle the low solubility of hydrophobic drugs in biological fluids, and subsequently, low bioavailability, microfluidics has also been used to prepare nanosuspensions. Drug nanosuspensions consist of dispersions of nanocrystals in aqueous media (KianvashRad et al. 2019). Ali et al. applied the controlled liquid antisolvent precipitation technology to produce a hydrocortisone nanosuspension for ophthalmic delivery using a Y-junction microfluidic reactor (Ali et al. 2011). Panagiotou et al., in turn, reported the successful preparation of norfloxacin nanosuspensions using an impinging jet reactor-based microfluidic system (Panagiotou et al. 2009).

Microfluidics is also a promising technology for the synthesis of inorganic drug carriers. For example, several microfluidic platforms have shown to enable the effective preparation of quantum dots (Nightingale and de Mello 2010), and gold NPs with varying size (Jamal et al. 2012; Ftouni et al. 2012; Wagner et al. 2008) and shape (Wagner and Köhler 2005; Boleininger et al. 2006; Köhler et al. 2007; Weng et al. 2008). Silver (Silvestrini et al. 2013), magnetic (e.g., cobalt) (Song et al. 2006), and silica NPs (Khan et al. 2004) are further examples of inorganic drug delivery systems that have been successfully synthesized via microfluidic-assisted approaches.

Niosomes are synthetic bilayer nanovesicles, typically formed by the self-assembly of nonionic surfactants in aqueous media (Hong et al. 2009). Over the past decade, microfluidics has enabled the rapid and reliable preparation of niosomes, with high degree of reproducibility, and for a variety of therapeutic purposes (Ag Seleci et al. 2019; Obeid et al. 2019).

As already mentioned above, the shape affects the performance of drug delivery systems in vivo, in aspects like biodistribution, blood circulation time, and cellular uptake (Toy et al. 2013; Fujiwara et al. 2005; Gao et al. 2011; Mathaes et al. 2015). Despite being more common to prepare spherical particles, microfluidics has also been used to generate nonspherical drug carriers. In fact, there are several strategies to obtain nonspherical NPs via microfluidics, including flow lithography, self-assembly of spherical building blocks, or stretching and deforming droplets in confined channels before or during solidification (Wang et al. 2009a; Studart et al. 2009; Annabi et al. 2014). For example, droplets can be confined to microchannels, and, if the droplet volume is larger than the largest sphere that is accommodated in the channel, ellipsoids, disks, or rods can be obtained (Dendukuri et al. 2005; Damiati et al. 2018; Xu et al. 2005).

One of the biggest challenges in nanomedicine is the preparation of nanoformulations that can diagnose, image, monitor, target, and treat diseases simultaneously (Wagner et al. 2006). Even though the design and development of multicomponent nanocarriers that can respond to these demands is still a hard task, microfluidics has been providing a number of solutions. Liu et al. produced a nanohybrid system consisting of AcDX NPs encapsulating dextranilated porous silicon NPs and gold NPs using microfluidic mixing in a co-flow capillary microtube (Liu et al. 2018b). This system revealed to be promising for liver regeneration and acute liver failure theranostics (Liu et al. 2018b). Valencia et al. applied microfluidic rapid mixing using HFF in combination with passive mixing structures for the single-step synthesis of lipid–polymer or lipid-quantum dot NPs (Valencia et al. 2010). These systems showed potential both for imaging and drug delivery applications. In turn, Russo et al. used a quartz microfluidic device for the synthesis of PEGylated cross-linked hyaluronic acid NPs encapsulating a magnetic resonance imaging contrast agent and a dye for multimodal imaging purposes (Russo et al. 2017).

13.7 Scale-Up and Industrial Application

The concept behind microfluidics is based on solid principles, and the widespread investigation of this technology is increasingly influencing the way pharmaceutical research and development is conducted. While the pharmaceutical industry is adapting to the use of microfluidics, continued progress in the field keeps unveiling the enormous advantages of this technology over traditional approaches (Zhao and Middelberg 2016).

Indeed, microfluidics can help overcoming the challenges that are persistently hindering the clinical translation of advanced drug delivery systems, and therefore, their mass commercialization. Yet, the translation of a benchtop microfluidic instrument to an industrial setting is not straightforward, as pharmaceutical industries look for technologies that can generate products on-demand, in a rapid, cost-effective, and sustainable manner, while complying with good manufacturing practices (GMPs) (Tomeh and Zhao 2020; Jensen 2017; Webb et al. 2020).

Different strategies have been investigated to prove the added value of microfluidics in industrial settings and to foster their implementation for mass-scale production of micro- and nanoparticles. One of the most feasible approaches to consistently produce materials on the gram-to-kilogram scale is to increase the number of identical devices using parallel and stackable microfluidic systems at the same fluid velocity (Nisisako et al. 2012; Jahn et al. 2007; Yu et al. 2009; Zook and Vreeland 2010; Mulligan and Rothstein 2012). Nisisako and Torii developed a production module consisting of a glass microfluidic chip with 16–256 droplet-formation units and a palm-sized holder with several layers for supplying liquids into the inlets of the chip (Nisisako and Torii 2008). This platform enabled the production of uniform droplets and microspheres at a throughput of 320 mL/h and 0.3 kg/h,

respectively. Romanowsky et al., in turn, reported the development of microfluidic devices incorporating up to 15 droplet-formation units, in a 2D and 3D array, which enabled the production of single-core double emulsion drops at rates over 1 kg/day, and displaying diameter variations of less than 6% (Romanowsky et al. 2012). Nightingale et al. reported the establishment of a multichannel microfluidic droplet reactor for the large-scale fabrication of different nanocrystals (Nightingale et al. 2013). A five-way level parallelization of this microfluidic reactor enabled a production rate of 145 g/day. The authors foresee that, with only minimal changes to the reactor architecture, it should be feasible to achieve a production rate of 1 kg/day (Nightingale et al. 2013).

In addition to the parallelization of devices, other strategies have been explored for obtaining high production rates of nanocarrier systems. For example, Wang et al. developed a microporous tube-in-tube microfluidic reactor for the preparation of barium sulfate NPs and achieved a throughput of 9 L/min (Wang et al. 2009b). Also interestingly, by using a superfast sequential nanoprecipitation glass capillary microfluidic platform, Liu et al. generated core–shell nanocomposites at a production rate of ~700 g/day (Liu et al. 2017b).

The use of multiple pressure sources (e.g., pumps) for each microfluidic device can provide a higher level of control over the preparation process, and thus, a more uniform particle size distribution; however, this is a more costly approach (Tomeh and Zhao 2020). Therefore, using a single pressure source for distributing a uniform flow is more practical and convenient for industrial applications (Capretto et al. 2012; Amador et al. 2004; Ying et al. 2008).

Recently, the NanoAssemblr® GMP system has be proposed by Precision NanoSystems, Inc. as a continuous flow microfluidic platform for the rapid, reproducible, and scalable manufacturing of NPs under current GMP conditions (Webb et al. 2020). The system contains a semi-disposable cartridge, which contains the mixing elements, and it is compatible with a variety of solvents (Tomeh and Zhao 2020). This cartridge can have different designs and be easily replaced for ensuring mixing quality and sterility (Tomeh and Zhao 2020; Webb et al. 2020). Established in 2005, Dolomite has been designing and developing innovative microfluidic devices and components for a variety of applications, from drug delivery to food and cosmetics. This company provides reusable microfluidic chips made of quartz, glass, or platinum, with hundreds of different designs and different channel sizes and junction geometries suitable for droplet generation and the preparation of drug nanocarriers (Damiati et al. 2020). These systems also offer good optical transparency, chemical compatibility, and thermal characteristics, and the surface of the channels can be modified to provide customized solutions.

The past decades brought a revolutionary progress in the design, development, and optimization of microfluidic platforms, with several approaches demonstrating capability to yield industrial-scale production of micro- and nanoparticles. Hence, knowing the potential of microfluidics for the preparation of advanced formulations for therapeutic and diagnostic applications, researchers and private companies must, more than ever, keep channeling efforts toward the mainstream application of this technology.

13.8 Conclusions and Future Perspectives

The current clinical landscape, and particularly the COVID-19 pandemic, reminds us that high-value flexible solutions are permanently needed to meet urgent clinical needs. Over the last decades, nanomedicine has been providing unique delivery and diagnostic technologies to tackle complex medical challenges. Microfluidic technologies, in turn, are paving the way for accelerating the translation of these nanomedicine-based formulations into the clinic. The versatility of microfluidics is attributed to the wide range of materials, technologies, flow patterns and regimes, and devices and device geometries that can be explored to produce advanced drug delivery systems. Moreover, manipulating the mixing and the overall production parameters in a microfluidic setup extends the range of possibilities provided by this technique. Emulsions, lipid-based and polymeric particles, among many others, have been successfully fabricated via microfluidics, exhibiting physicochemical properties and functionalities that outperform their bulk-synthesized counterparts. Moreover, microfluidics enables a significant reduction in manufacturing costs, and the scale-up of micro- and nanoparticles to a larger commercial scale. A myriad of proof-of-concept studies, academic publications, and startup companies are testimony of the success of microfluidics.

As in any other technology, there are also limiting factors to the widespread implementation of microfluidics. For example, certain geometry and mixing parameters are usually optimized and calibrated for producing a certain formulation, not being necessarily suitable to obtain other types of drug delivery systems. Also, many formulations cannot be assembled in one single step, requiring more advanced protocols and mixing conditions. The formation of aggregates and impurities inside the submicron-sized channels and capillaries can also be challenging. Recent studies have highlighted the potential of real-time characterization of particles inside of microfluidic devices. However, further investigation is also needed to improve the current designs and, thereby, to obtain more accurate on-chip data about the drug delivery systems during microfabrication.

With this, the future of microfluidics depends on the design and development of easy-to-use, less instrument-demanding, reliable, cost-effective, and industrial-oriented platforms. The successful incorporation of strategies for the characterization of multiple properties of the produced formulations would turn microfluidics into a more complete technology, and most certainly make it even more appealing for the industry. Hence, investing in the pursuit of ameliorated microfluidic technologies and their widespread implementation seem to be the key for a future in which microfluidics and pharmaceutical manufacturing go hand in hand.

Acknowledgements Financial support from the Sigrid Jusélius Foundation and the Academy of Finland (Grant No. 331151) is acknowledged.

Conflict of Interest The authors declare no conflict of interest.

References

Ag Seleci D, Maurer V, Stahl F, Scheper T, Garnweitner G (2019) Rapid microfluidic preparation of niosomes for targeted drug delivery. Int J Mol Sci 20:4696

Ahadian S, Finbloom JA, Mofidfar M, Diltemiz SE, Nasrollahi F, Davoodi E, Hosseini V, Mylonaki I, Sangabathuni S, Montazerian H, Fetah K, Nasiri R, Dokmeci MR, Stevens MM, Desai TA, Khademhosseini A (2020) Micro and nanoscale technologies in oral drug delivery. Adv Drug Deliv Rev 157:37–62

Akyazi T, Basabe-Desmonts L, Benito-Lopez F (2018) Review on microfluidic paper-based analytical devices towards commercialisation. Anal Chim Acta 1001:1–17

Ali HSM, York P, Ali AMA, Blagden N (2011) Hydrocortisone nanosuspensions for ophthalmic delivery: a comparative study between microfluidic nanoprecipitation and wet milling. J Control Release 149:175–181

Ali MS, Hooshmand N, El-Sayed M, Labouta HI (2021) Microfluidics for development of lipid nanoparticles: paving the way for nucleic acids to the clinic. ACS Appl Bio Mater

Amador C, Gavriilidis A, Angeli P (2004) Flow distribution in different microreactor scale-out geometries and the effect of manufacturing tolerances and channel blockage. Chem Eng J 101: 379–390

Amstad E, Kim SH, Weitz DA (2012) Photo- and thermoresponsive polymersomes for triggered release. Angew Chem Int Ed Engl 51:12499–12503

Annabi N, Tamayol A, Uquillas JA, Akbari M, Bertassoni LE, Cha C, Camci-Unal G, Dokmeci MR, Peppas NA, Khademhosseini A (2014) 25th anniversary article: rational design and applications of hydrogels in regenerative medicine. Adv Mater 26:85–124

Anselmo AC, Mitragotri S (2016) Nanoparticles in the clinic. Bioeng Transl Med 1:10–29

Anselmo AC, Mitragotri S (2019) Nanoparticles in the clinic: an update. Bioeng Transl Med 4: e10143

Araújo F, das Neves J, Martins JP, Granja PL, Santos HA, Sarmento B (2017) Functionalized materials for multistage platforms in the oral delivery of biopharmaceuticals. Prog Mater Sci 89: 306–344

Arduino I, Liu Z, Iacobazzi RM, Lopedota AA, Lopalco A, Cutrignelli A, Laquintana V, Porcelli L, Azzariti A, Franco M, Santos HA, Denora N (2021a) Microfluidic preparation and in vitro evaluation of iRGD-functionalized solid lipid nanoparticles for targeted delivery of paclitaxel to tumor cells. Int J Pharm 610:121246

Arduino I, Liu Z, Rahikkala A, Figueiredo P, Correia A, Cutrignelli A, Denora N, Santos HA (2021b) Preparation of cetyl palmitate-based PEGylated solid lipid nanoparticles by microfluidic technique. Acta Biomater 121:566–578

Atencia J, Beebe DJ (2005) Controlled microfluidic interfaces. Nature 437:648–655

Batty CJ, Bachelder EM, Ainslie KM (2021) Historical perspective of clinical nano and microparticle formulations for delivery of therapeutics. Trends Mol Med 27:516–519

Beebe DJ, Mensing GA, Walker GM (2002) Physics and applications of microfluidics in biology. Annu Rev Biomed Eng 4:261–286

Bein A, Shin W, Jalili-Firoozinezhad S, Park MH, Sontheimer-Phelps A, Tovaglieri A, Chalkiadaki A, Kim HJ, Ingber DE (2018) Microfluidic organ-on-a-chip models of human intestine. Cell Mol Gastroenterol Hepatol 5:659–668

Belliveau NM, Huft J, Lin PJC, Chen S, Leung AKK, Leaver TJ, Wild AW, Lee JB, Taylor RJ, Tam YK, Hansen CL, Cullis PR (2012) Microfluidic synthesis of highly potent limit-size lipid nanoparticles for in vivo delivery of siRNA. Mol Ther Nucleic Acids 1:e37

Bertoni S, Liu Z, Correia A, Martins JP, Rahikkala A, Fontana F, Kemell M, Liu D, Albertini B, Passerini N, Li W, Santos HA (2018) pH and reactive oxygen species-sequential responsive nano-in-micro composite for targeted therapy of inflammatory bowel disease. Adv Funct Mater 28:1806175

Bings NH, Wang C, Skinner CD, Colyer CL, Thibault P, Harrison DJ (1999) Microfluidic devices connected to fused-silica capillaries with minimal dead volume. Anal Chem 71:3292–3296

Boleininger J, Kurz A, Reuss V, Sönnichsen C (2006) Microfluidic continuous flow synthesis of rod-shaped gold and silver nanocrystals. Phys Chem Chem Phys 8:3824–3827
Cabral H, Matsumoto Y, Mizuno K, Chen Q, Murakami M, Kimura M, Terada Y, Kano MR, Miyazono K, Uesaka M, Nishiyama N, Kataoka K (2011) Accumulation of sub-100 nm polymeric micelles in poorly permeable tumours depends on size. Nat Nanotechnol 6:815–823
Capretto L, Carugo D, Mazzitelli S, Nastruzzi C, Zhang X (2013) Microfluidic and lab-on-a-chip preparation routes for organic nanoparticles and vesicular systems for nanomedicine applications. Adv Drug Deliv Rev 65:1496–1532
Capretto L, Mazzitelli S, Brognara E, Lampronti I, Carugo D, Hill M, Zhang X, Gambari R, Nastruzzi C (2012) Mithramycin encapsulated in polymeric micelles by microfluidic technology as novel therapeutic protocol for beta-thalassemia. Int J Nanomedicine 7:307–324
Chande C, Riaz N, Harbour V, Noor H, Torralba M, Cheng Y-H, Li Z, Tong A, Voronov R, Basuray S (2020) Universal method for fabricating PDMS microfluidic device using SU8, 3D printing and soft lithography. Technology 08:50–57
Chang CW, Cheng YJ, Tu M, Chen YH, Peng CC, Liao WH, Tung YC (2014) A polydimethylsiloxane-polycarbonate hybrid microfluidic device capable of generating perpendicular chemical and oxygen gradients for cell culture studies. Lab Chip 14:3762–3772
Chen C-H, Shah RK, Abate AR, Weitz DA (2009) Janus particles templated from double emulsion droplets generated using microfluidics. Langmuir 25:4320–4323
Chen D, Love KT, Chen Y, Eltoukhy AA, Kastrup C, Sahay G, Jeon A, Dong Y, Whitehead KA, Anderson DG (2012) Rapid discovery of potent siRNA-containing lipid nanoparticles enabled by controlled microfluidic formulation. J Am Chem Soc 134:6948–6951
Chen W, Li H, Liu Z, Yuan W (2016) Lipopolyplex for therapeutic gene delivery and its application for the treatment of Parkinson's disease. Front Aging Neurosci 8
Chen Y, Zhang L, Chen G (2008) Fabrication, modification, and application of poly(methyl methacrylate) microfluidic chips. Electrophoresis 29:1801–1814
Cheng S-Y, Heilman S, Wasserman M, Archer S, Shuler ML, Wu M (2007) A hydrogel-based microfluidic device for the studies of directed cell migration. Lab Chip 7:763–769
Cho EC, Xie J, Wurm PA, Xia Y (2009) Understanding the role of surface charges in cellular adsorption versus internalization by selectively removing gold nanoparticles on the cell surface with a I2/KI etchant. Nano Lett 9:1080–1084
Conniot J, Silva JM, Fernandes JG, Silva LC, Gaspar R, Brocchini S, Florindo HF, Barata TS (2014) Cancer immunotherapy: nanodelivery approaches for immune cell targeting and tracking. Front Chem 2
Costa C, Liu Z, Martins JP, Correia A, Figueiredo P, Rahikkala A, Li W, Seitsonen J, Ruokolainen J, Hirvonen S-P, Aguiar-Ricardo A, Corvo ML, Santos HA (2020) All-in-one microfluidic assembly of insulin-loaded pH-responsive nano-in-microparticles for oral insulin delivery. Biomater Sci 8:3270–3277
Damiati S, Kompella UB, Damiati SA, Kodzius R (2018) Microfluidic devices for drug delivery systems and drug screening. Genes 9:103
Damiati SA, Rossi D, Joensson HN, Damiati S (2020) Artificial intelligence application for rapid fabrication of size-tunable PLGA microparticles in microfluidics. Sci Rep 10:19517
Dashtimoghadam E, Mirzadeh H, Taromi FA, Nyström B (2013) Microfluidic self-assembly of polymeric nanoparticles with tunable compactness for controlled drug delivery. Polymer 54: 4972–4979
De Rose R, Zelikin AN, Johnston APR, Sexton A, Chong S-F, Cortez C, Mulholland W, Caruso F, Kent SJ (2008) Binding, internalization, and antigen presentation of vaccine-loaded nanoengineered capsules in blood. Adv Mater 20:4698–4703
Dendukuri D, Tsoi K, Hatton TA, Doyle PS (2005) Controlled synthesis of nonspherical microparticles using microfluidics. Langmuir 21:2113–2116
Deng N-N, Meng Z-J, Xie R, Ju X-J, Mou C-L, Wang W, Chu L-Y (2011) Simple and cheap microfluidic devices for the preparation of monodisperse emulsions. Lab Chip 11:3963–3969

Di Santo R, Digiacomo L, Palchetti S, Palmieri V, Perini G, Pozzi D, Papi M, Caracciolo G (2019) Microfluidic manufacturing of surface-functionalized graphene oxide nanoflakes for gene delivery. Nanoscale 11:2733–2741

van Dijke K, Veldhuis G, Schroën K, Boom R (2009) Parallelized EDGE-based droplet generation (EDGE) devices. Lab Chip 9:2824–2830

Ding S, Anton N, Vandamme TF, Serra CA (2016) Microfluidic nanoprecipitation systems for preparing pure drug or polymeric drug loaded nanoparticles: an overview. Expert Opin Drug Deliv 13:1447–1460

Duncanson WJ, Lin T, Abate AR, Seiffert S, Shah RK, Weitz DA (2012) Microfluidic synthesis of advanced microparticles for encapsulation and controlled release. Lab Chip 12:2135–2145

Eggersdorfer ML, Zheng W, Nawar S, Mercandetti C, Ofner A, Leibacher I, Koehler S, Weitz DA (2017) Tandem emulsification for high-throughput production of double emulsions. Lab Chip 17:936–942

Eusner T, Hale M, Hardt DE (2010) Process robustness of hot embossing microfluidic devices. J Manuf Sci Eng 132

Farokhzad OC, Langer R (2009) Impact of nanotechnology on drug delivery. ACS Nano 3:16–20

Ferreira Soares DC, Domingues SC, Viana DB, Tebaldi ML (2020) Polymer-hybrid nanoparticles: current advances in biomedical applications. Biomed Pharmacother 131:110695

Feynman RP (1960) There's plenty of room at the bottom. An invitation to enter a new field of physics. Eng Sci 23:22–36

Fontana F, Ferreira MPA, Correia A, Hirvonen J, Santos HA (2016) Microfluidics as a cutting-edge technique for drug delivery applications. J Drug Deliv Sci Technol 34:76–87

Fontana F, Martins JP, Torrieri G, Santos HA (2019) Nuts and bolts: microfluidics for the production of biomaterials. Adv Mater Technol 4:1800611

Fontana F, Shahbazi M-A, Liu D, Zhang H, Mäkilä E, Salonen J, Hirvonen JT, Santos HA (2017) Multistaged nanovaccines based on porous silicon@acetalated dextran@cancer cell membrane for cancer immunotherapy. Adv Mater 29:1603239

Friedman AD, Claypool SE, Liu R (2013) The smart targeting of nanoparticles. Curr Pharm Des 19: 6315–6329

Friend J, Yeo L (2010) Fabrication of microfluidic devices using polydimethylsiloxane. Biomicrofluidics 4:026502

Ftouni J, Penhoat M, Addad A, Payen E, Rolando C, Girardon J-S (2012) Highly controlled synthesis of nanometric gold particles by citrate reduction using the short mixing, heating and quenching times achievable in a microfluidic device. Nanoscale 4:4450–4454

Fujiwara M, Yamamoto F, Okamoto K, Shiokawa K, Nomura R (2005) Adsorption of duplex DNA on mesoporous silicas: possibility of inclusion of DNA into their mesopores. Anal Chem 77: 8138–8145

Gao Y, Chen Y, Ji X, He X, Yin Q, Zhang Z, Shi J, Li Y (2011) Controlled intracellular release of doxorubicin in multidrug-resistant cancer cells by tuning the shell-pore sizes of mesoporous silica nanoparticles. ACS Nano 5:9788–9798

Garbuzenko OB, Winkler J, Tomassone MS, Minko T (2014) Biodegradable Janus nanoparticles for local pulmonary delivery of hydrophilic and hydrophobic molecules to the lungs. Langmuir 30:12941–12949

Garstecki P, Fuerstman MJ, Stone HA, Whitesides GM (2006) Formation of droplets and bubbles in a microfluidic T-junction—scaling and mechanism of break-up. Lab Chip 6:437–446

Ghazal A, Gontsarik M, Kutter JP, Lafleur JP, Ahmadvand D, Labrador A, Salentinig S, Yaghmur A (2017) Microfluidic platform for the continuous production and characterization of multilamellar vesicles: a synchrotron small-angle X-ray scattering (SAXS) study. J Phys Chem Lett 8:73–79

Gong MM, Sinton D (2017) Turning the page: advancing paper-based microfluidics for broad diagnostic application. Chem Rev 117:8447–8480

Grigsby CL, Ho Y-P, Lin C, Engbersen JFJ, Leong KW (2013) Microfluidic preparation of polymer-nucleic acid nanocomplexes improves nonviral gene transfer. Sci Rep 3:3155

Grosse A, Grewe M, Fouckhardt H (2001) Deep wet etching of fused silica glass for hollow capillary optical leaky waveguides in microfluidic devices. J Micromech Microeng 11:257–262
Grover WH, Ivester RH, Jensen EC, Mathies RA (2006) Development and multiplexed control of latching pneumatic valves using microfluidic logical structures. Lab Chip 6:623–631
Grover WH, Skelley AM, Liu CN, Lagally ET, Mathies RA (2003) Monolithic membrane valves and diaphragm pumps for practical large-scale integration into glass microfluidic devices. Sens Actuators B Chem 89:315–323
Hao N, Nie Y, Zhang JXJ (2018) Microfluidic flow synthesis of functional mesoporous silica nanofibers with tunable aspect ratios. ACS Sustain Chem Eng 6:1522–1526
Hatch AV, Herr AE, Throckmorton DJ, Brennan JS, Singh AK (2006) Integrated preconcentration SDS-PAGE of proteins in microchips using photopatterned cross-linked polyacrylamide gels. Anal Chem 78:4976–4984
He F, Cheng Y, Xu Z, Liao Y, Xu J, Sun H, Wang C, Zhou Z, Sugioka K, Midorikawa K, Xu Y, Chen X (2010) Direct fabrication of homogeneous microfluidic channels embedded in fused silica using a femtosecond laser. Opt Lett 35:282–284
Herranz-Blanco B, Ginestar E, Zhang H, Hirvonen J, Santos HA (2017) Microfluidics platform for glass capillaries and its application in droplet and nanoparticle fabrication. Int J Pharm 516:100–105
Hong M, Zhu S, Jiang Y, Tang G, Pei Y (2009) Efficient tumor targeting of hydroxycamptothecin loaded PEGylated niosomes modified with transferrin. J Control Release 133:96–102
Hui Y, Yi X, Hou F, Wibowo D, Zhang F, Zhao D, Gao H, Zhao C-X (2019) Role of nanoparticle mechanical properties in cancer drug delivery. ACS Nano 13:7410–7424
Hyuk Im S, Jeong U, Xia Y (2005) Polymer hollow particles with controllable holes in their surfaces. Nat Mater 4:671–675
Jahn A, Stavis SM, Hong JS, Vreeland WN, DeVoe DL, Gaitan M (2010) Microfluidic mixing and the formation of nanoscale lipid vesicles. ACS Nano 4:2077–2087
Jahn A, Vreeland WN, DeVoe DL, Locascio LE, Gaitan M (2007) Microfluidic directed formation of liposomes of controlled size. Langmuir 23:6289–6293
Jahn A, Vreeland WN, Gaitan M, Locascio LE (2004) Controlled vesicle self-assembly in microfluidic channels with hydrodynamic focusing. J Am Chem Soc 126:2674–2675
Jamal F, Jean-Sébastien G, Maël P, Edmond P, Christian R (2012) Gold nanoparticle synthesis in microfluidic systems and immobilisation in microreactors designed for the catalysis of fine organic reactions. Microsyst Technol 18:151–158
Jena RK, Yue CY, Lam YC (2012) Micro fabrication of cyclic olefin copolymer (COC) based microfluidic devices. Microsyst Technol 18:159–166
Jenjob R, Phakkeeree T, Seidi F, Theerasilp M, Crespy D (2019) Emulsion techniques for the production of pharmacological nanoparticles. Macromol Biosci 19:e1900063
Jensen KF (2017) Flow chemistry—microreaction technology comes of age. AICHE J 63:858–869
Karnik R, Gu F, Basto P, Cannizzaro C, Dean L, Kyei-Manu W, Langer R, Farokhzad OC (2008) Microfluidic platform for controlled synthesis of polymeric nanoparticles. Nano Lett 8:2906–2912
Kawakatsu T, Kikuchi Y, Nakajima M (1997) Regular-sized cell creation in microchannel emulsification by visual microprocessing method. J Amer Oil Chem Soc 74:317–321
Khan IU, Serra CA, Anton N, Vandamme TF (2015) Production of nanoparticle drug delivery systems with microfluidics tools. Expert Opin Drug Deliv 12:547–562
Khan SA, Günther A, Schmidt MA, Jensen KF (2004) Microfluidic synthesis of colloidal silica. Langmuir 20:8604–8611
KianvashRad N, Barkhordari E, Mostafavi SH, Aghajani M (2019) Optimizing microfluidic preparation parameters of nanosuspension to evaluate stability in nanoprecipitation of stable-iodine (127I). SN Appl Sci 1:1054
Kim K, Lee J-B (2007) High aspect ratio tapered hollow metallic microneedle arrays with microfluidic interconnector. Microsyst Technol 13:231–235

Kim S-H, Kim JW, Cho J-C, Weitz DA (2011) Double-emulsion drops with ultra-thin shells for capsule templates. Lab Chip 11:3162–3166

Kim T, Kwon S (2006) Design, fabrication and testing of a catalytic microreactor for hydrogen production. J Micromech Microeng 16:1752–1760

Kimura N, Maeki M, Sato Y, Note Y, Ishida A, Tani H, Harashima H, Tokeshi M (2018) Development of the iLiNP device: fine tuning the lipid nanoparticle size within 10 nm for drug delivery. ACS Omega 3:5044–5051

Kobayashi I, Nakajima M, Chun K, Kikuchi Y, Fujita H (2002) Silicon array of elongated through-holes for monodisperse emulsion droplets. AICHE J 48:1639–1644

Koh CG, Zhang X, Liu S, Golan S, Yu B, Yang X, Guan J, Jin Y, Talmon Y, Muthusamy N, Chan KK, Byrd JC, Lee RJ, Marcucci G, Lee LJ (2010) Delivery of antisense oligodeoxyribonucleotide lipopolyplex nanoparticles assembled by microfluidic hydrodynamic focusing. J Control Release 141:62–69

Köhler JM, Romanus H, Hübner U, Wagner J (2007) Formation of star-like and core-shell AuAg nanoparticles during two- and three-step preparation in batch and in microfluidic systems. J Nanomater 2007:098134

Krishnamoorthy K, Mahalingam M (2015) Selection of a suitable method for the preparation of polymeric nanoparticles: multi-criteria decision making approach. Adv Pharm Bull 5:57–67

Kuiper S, van Rijn CJM, Nijdam W, Elwenspoek MC (1998) Development and applications of very high flux microfiltration membranes. J Membr Sci 150:1–8

Le TC, Zhai J, Chiu W-H, Tran PA, Tran N (2019) Janus particles: recent advances in the biomedical applications. Int J Nanomedicine 14:6749–6777

Leung MHM, Shen AQ (2018) Microfluidic assisted nanoprecipitation of PLGA nanoparticles for curcumin delivery to leukemia Jurkat cells. Langmuir 34:3961–3970

Li H, Fan Y, Kodzius R, Foulds IG (2012a) Fabrication of polystyrene microfluidic devices using a pulsed CO2 laser system. Microsyst Technol 18:373–379

Li H, Steckl AJ (2019) Paper microfluidics for point-of-care blood-based analysis and diagnostics. Anal Chem 91:352–371

Li XJ, Valadez AV, Zuo P, Nie Z (2012b) Microfluidic 3D cell culture: potential application for tissue-based bioassays. Bioanalysis 4:1509–1525

Lim J-M, Swami A, Gilson LM, Chopra S, Choi S, Wu J, Langer R, Karnik R, Farokhzad OC (2014) Ultra-high throughput synthesis of nanoparticles with homogeneous size distribution using a coaxial turbulent jet mixer. ACS Nano 8:6056–6065

Lin C-H, Lee G-B, Lin Y-H, Chang G-L (2001) A fast prototyping process for fabrication of microfluidic systems on soda-lime glass. J Micromech Microeng 11:726–732

Lin Q, Chen J, Zhang Z, Zheng G (2013) Lipid-based nanoparticles in the systemic delivery of siRNA. Nanomedicine 9:105–120

Liu D, Cito S, Zhang Y, Wang C-F, Sikanen TM, Santos HA (2015a) A versatile and robust microfluidic platform toward high throughput synthesis of homogeneous nanoparticles with tunable properties. Adv Mater 27:2298–2304

Liu D, Zhang H, Cito S, Fan J, Mäkilä E, Salonen J, Hirvonen J, Sikanen TM, Weitz DA, Santos HA (2017b) Core/Shell nanocomposites produced by superfast sequential microfluidic nanoprecipitation. Nano Lett 17:606–614

Liu D, Zhang H, Fontana F, Hirvonen JT, Santos HA (2017a) Microfluidic-assisted fabrication of carriers for controlled drug delivery. Lab Chip 17:1856–1883

Liu D, Zhang H, Fontana F, Hirvonen JT, Santos HA (2018a) Current developments and applications of microfluidic technology toward clinical translation of nanomedicines. Adv Drug Deliv Rev 128:54–83

Liu D, Zhang H, Herranz-Blanco B, Mäkilä E, Lehto V-P, Salonen J, Hirvonen J, Santos HA (2014) Microfluidic assembly of monodisperse multistage pH-responsive polymer/porous silicon composites for precisely controlled multi-drug delivery. Small 10:2029–2038

Liu D, Zhang H, Mäkilä E, Fan J, Herranz-Blanco B, Wang C-F, Rosa R, Ribeiro AJ, Salonen J, Hirvonen J, Santos HA (2015b) Microfluidic assisted one-step fabrication of porous

silicon@acetalated dextran nanocomposites for precisely controlled combination chemotherapy. Biomaterials 39:249–259
Liu H, Nakajima M, Nishi T, Kimura T (2005) Effect of channel structure on preparation of a water-in-oil emulsion by polymer microchannels. Eur J Lipid Sci Technol 107:481–487
Liu Z, Fontana F, Python A, Hirvonen JT, Santos HA (2020) Microfluidics for production of particles: mechanism, methodology, and applications. Small 16:1904673
Liu Z, Li Y, Li W, Xiao C, Liu D, Dong C, Zhang M, Mäkilä E, Kemell M, Salonen J, Hirvonen JT, Zhang H, Zhou D, Deng X, Santos HA (2018b) Multifunctional nanohybrid based on porous silicon nanoparticles, gold nanoparticles, and acetalated dextran for liver regeneration and acute liver failure theranostics. Adv Mater 30:1703393
Lizotte T (2008) Vacuum isostatic micro molding of microfluidic structures into polytetrafluoroethylene (PTFE) materials paper presented at the SPIE Photonics Europe, Strasbourg, France
Manshadi MKD, Khojasteh D, Abdelrehim O, Gholami M, Sanati-Nezhad A (2021) In: Rahimpour MR, Kamali R, Amin Makarem M, Manshadi MKD (eds) Advances in bioenergy and microfluidic applications. Elsevier, pp 387–406
Martins JP, das Neves J, de la Fuente M, Celia C, Florindo H, Günday-Türeli N, Popat A, Santos JL, Sousa F, Schmid R, Wolfram J, Sarmento B, Santos HA (2020) The solid progress of nanomedicine. *Drug Deliv*. Transl Res 10:726–729
Martins JP, Liu D, Fontana F, Ferreira MPA, Correia A, Valentino S, Kemell M, Moslova K, Mäkilä E, Salonen J, Hirvonen J, Sarmento B, Santos HA (2018b) Microfluidic nanoassembly of bioengineered chitosan-modified FcRn-targeted porous silicon nanoparticles @ hypromellose acetate succinate for oral delivery of antidiabetic peptides. ACS Appl Mater Interfaces 10:44354–44367
Martins JP, Torrieri G, Santos HA (2018a) The importance of microfluidics for the preparation of nanoparticles as advanced drug delivery systems. Expert Opin Drug Deliv 15:469–479
Mathaes R, Winter G, Besheer A, Engert J (2015) Non-spherical micro- and nanoparticles: fabrication, characterization and drug delivery applications. Expert Opin Drug Deliv 12:481–492
Matsumura Y, Maeda H (1986) A new concept for macromolecular therapeutics in cancer chemotherapy: mechanism of tumoritropic accumulation of proteins and the antitumor agent smancs. Cancer Res 46:6387–6392
McCreedy T (2001) Rapid prototyping of glass and PDMS microstructures for micro total analytical systems and micro chemical reactors by microfabrication in the general laboratory. Anal Chim Acta 427:39–43
Mitchell MJ, Billingsley MM, Haley RM, Wechsler ME, Peppas NA, Langer R (2021) Engineering precision nanoparticles for drug delivery. Nat Rev Drug Discov 20:101–124
Morimoto Y, Tan W-H, Tsuda Y, Takeuchi S (2009) Monodisperse semi-permeable microcapsules for continuous observation of cells. Lab Chip 9:2217–2223
Muck A, Wang J, Jacobs M, Chen G, Chatrathi MP, Jurka V, Výborný Z, Spillman SD, Sridharan G, Schöning MJ (2004) Fabrication of poly(methyl methacrylate) microfluidic chips by atmospheric molding. Anal Chem 76:2290–2297
Mulligan MK, Rothstein JP (2012) Scale-up and control of droplet production in coupled microfluidic flow-focusing geometries. Microfluid Nanofluid 13:65–73
Nge PN, Rogers CI, Woolley AT (2013) Advances in microfluidic materials, functions, integration, and applications. Chem Rev 113:2550–2583
Nguyen N-T (2012) In: Nguyen N-T (ed) Micromixers (second edition). William Andrew Publishing, Oxford, pp 1–8
Niculescu A-G, Chircov C, Bîrcă AC, Grumezescu AM (2021) Nanomaterials synthesis through microfluidic methods: an updated overview. Nano 11
Nie Z, Xu S, Seo M, Lewis PC, Kumacheva E (2005) Polymer particles with various shapes and morphologies produced in continuous microfluidic reactors. J Am Chem Soc 127:8058–8063

Nielsen JB, Hanson RL, Almughamsi HM, Pang C, Fish TR, Woolley AT (2020) Microfluidics: innovations in materials and their fabrication and functionalization. Anal Chem 92:150–168

Nightingale AM, Bannock JH, Krishnadasan SH, O'Mahony FTF, Haque SA, Sloan J, Drury C, McIntyre R, deMello JC (2013) Large-scale synthesis of nanocrystals in a multichannel droplet reactor. J Mater Chem A 1:4067–4076

Nightingale AM, de Mello JC (2010) Microscale synthesis of quantum dots. J Mater Chem 20: 8454–8463

Nisisako T, Ando T, Hatsuzawa T (2012) High-volume production of single and compound emulsions in a microfluidic parallelization arrangement coupled with coaxial annular world-to-chip interfaces. Lab Chip 12:3426–3435

Nisisako T, Torii T (2008) Microfluidic large-scale integration on a chip for mass production of monodisperse droplets and particles. Lab Chip 8:287–293

Nunes JK, Tsai SSH, Wan J, Stone HA (2013) Dripping and jetting in microfluidic multiphase flows applied to particle and fiber synthesis. J Phys D Appl Phys 46:114002

Nunes PS, Ohlsson PD, Ordeig O, Kutter JP (2010) Cyclic olefin polymers: emerging materials for lab-on-a-chip applications. Microfluid Nanofluid 9:145–161

Obeid MA, Khadra I, Albaloushi A, Mullin M, Alyamani H, Ferro VA (2019) Microfluidic manufacturing of different niosomes nanoparticles for curcumin encapsulation: physical characteristics, encapsulation efficacy, and drug release. Beilstein J Nanotechnol 10:1826–1832

Odera T, Hirama H, Kuroda J, Moriguchi H, Torii T (2014) Droplet formation behavior in a microfluidic device fabricated by hydrogel molding. Microfluid Nanofluid 17:469–476

Ogończyk D, Węgrzyn J, Jankowski P, Dąbrowski B, Garstecki P (2010) Bonding of microfluidic devices fabricated in polycarbonate. Lab Chip 10:1324–1327

Okushima S, Nisisako T, Torii T, Higuchi T (2004) Controlled production of monodisperse double emulsions by two-step droplet breakup in microfluidic devices. Langmuir 20:9905–9908

Olanrewaju A, Beaugrand M, Yafia M, Juncker D (2018) Capillary microfluidics in microchannels: from microfluidic networks to capillaric circuits. Lab Chip 18:2323–2347

Panagiotou T, Mesite SV, Fisher RJ (2009) Production of norfloxacin nanosuspensions using microfluidics reaction technology through solvent/antisolvent crystallization. Ind Eng Chem Res 48:1761–1771

Papi M, Pozzi D, Palmieri V, Caracciolo G (2022) Principles for optimization and validation of mRNA lipid nanoparticle vaccines against COVID-19 using 3D bioprinting. Nano Today 43: 101403

Park C, Han YD, Kim HV, Lee J, Yoon HC, Park S (2018) Double-sided 3D printing on paper towards mass production of three-dimensional paper-based microfluidic analytical devices (3D-μPADs). Lab Chip 18:1533–1538

Park K (2007) Nanotechnology: what it can do for drug delivery. J Control Release 120:1–3

Pentecost AM, Martin RS (2015) Fabrication and characterization of all-polystyrene microfluidic devices with integrated electrodes and tubing. Anal Methods 7:2968–2976

Piruska A, Nikcevic I, Lee SH, Ahn C, Heineman WR, Limbach PA, Seliskar CJ (2005) The autofluorescence of plastic materials and chips measured under laser irradiation. Lab Chip 5: 1348–1354

Qin D, Xia Y, Whitesides GM (2010) Soft lithography for micro- and nanoscale patterning. Nat Protoc 5:491–502

Quintanar-Guerrero D, Allémann E, Fessi H, Doelker E (1998) Preparation techniques and mechanisms of formation of biodegradable nanoparticles from preformed polymers. Drug Dev Ind Pharm 24:1113–1128

Rahil Hasan M, Anzar N, Tyagi M, Yadav N, Narang J (2021) In: Hussain CM, Shukla SK, Joshi GM (eds) Functionalized nanomaterials based devices for environmental applications. Elsevier, pp 175–198

Regehr KJ, Domenech M, Koepsel JT, Carver KC, Ellison-Zelski SJ, Murphy WL, Schuler LA, Alarid ET, Beebe DJ (2009) Biological implications of polydimethylsiloxane-based microfluidic cell culture. Lab Chip 9:2132–2139

Ren K, Zhou J, Wu H (2013) Materials for microfluidic chip fabrication. Acc Chem Res 46:2396–2406

Riahi R, Tamayol A, Shaegh SAM, Ghaemmaghami AM, Dokmeci MR, Khademhosseini A (2015) Microfluidics for advanced drug delivery systems. Curr Opin Chem Eng 7:101–112

Romanowsky MB, Abate AR, Rotem A, Holtze C, Weitz DA (2012) High throughput production of single core double emulsions in a parallelized microfluidic device. Lab Chip 12:802–807

Rondeau E, Cooper-White JJ (2008) Biopolymer microparticle and nanoparticle formation within a microfluidic device. Langmuir 24:6937–6945

Russo M, Grimaldi AM, Bevilacqua P, Tammaro O, Netti PA, Torino E (2017) PEGylated crosslinked hyaluronic acid nanoparticles designed through a microfluidic platform for nanomedicine. Nanomedicine 12:2211–2222

Sackmann EK, Fulton AL, Beebe DJ (2014) The present and future role of microfluidics in biomedical research. Nature 507:181–189

Samaridou E, Heyes J, Lutwyche P (2020) Lipid nanoparticles for nucleic acid delivery: current perspectives. Adv Drug Deliv Rev 154-155:37–63

Sanjay ST, Zhou W, Dou M, Tavakoli H, Ma L, Xu F, Li X (2018) Recent advances of controlled drug delivery using microfluidic platforms. Adv Drug Deliv Rev 128:3–28

Serra CA, Chang Z (2008) Microfluidic-assisted synthesis of polymer particles. Chem Eng Technol 31:1099–1115

Shah RK, Shum HC, Rowat AC, Lee D, Agresti JJ, Utada AS, Chu L-Y, Kim J-W, Fernandez-Nieves A, Martinez CJ, Weitz DA (2008) Designer emulsions using microfluidics. Mater Today 11:18–27

Shang L, Nienhaus K, Nienhaus GU (2014) Engineered nanoparticles interacting with cells: size matters. J Nanobiotechnol 12:5

Sharp KV, Adrian RJ (2004) Transition from laminar to turbulent flow in liquid filled microtubes. Exp Fluids 36:741–747

Sia SK, Whitesides GM (2003) Microfluidic devices fabricated in poly(dimethylsiloxane) for biological studies. Electrophoresis 24:3563–3576

Silvestrini S, Carofiglio T, Maggini M (2013) Shape-selective growth of silver nanoparticles under continuous flow photochemical conditions. Chem Commun 49:84–86

Sohrabi S, Kassir N, Keshavarz Moraveji M (2020) Droplet microfluidics: fundamentals and its advanced applications. RSC Adv 10:27560–27574

Song Y, Modrow H, Henry LL, Saw CK, Doomes EE, Palshin V, Hormes J, Kumar CSSR (2006) Microfluidic synthesis of cobalt nanoparticles. Chem Mater 18:2817–2827

Stepanyan R, Lebouille JG, Slot JJ, Tuinier R, Stuart MA (2012) Controlled nanoparticle formation by diffusion limited coalescence. Phys Rev Lett 109:138301

Stroock AD, Dertinger SK, Ajdari A, Mezic I, Stone HA, Whitesides GM (2002) Chaotic mixer for microchannels. Science 295:647–651

Studart AR, Shum HC, Weitz DA (2009) Arrested coalescence of particle-coated droplets into nonspherical supracolloidal structures. J Phys Chem B 113:3914–3919

Stylios GK (2013) There is plenty of room at the bottom, R.P. Feynman. Int J Cloth Sci Technol 25

Sun J, Zhang L, Wang J, Feng Q, Liu D, Yin Q, Xu D, Wei Y, Ding B, Shi X, Jiang X (2015) Tunable rigidity of (polymeric core)–(lipid shell) nanoparticles for regulated cellular uptake. Adv Mater 27:1402–1407

Suriya Prabha A, Dorothy R, Jancirani S, Rajendran S, Singh G, Senthil Kumaran S (2020) In: Rajendran S, Mukherjee A, Nguyen TA, Godugu C, Shukla RK (eds) Nanotoxicity. Elsevier, pp 143–165

Thorsen T, Roberts RW, Arnold FH, Quake SR (2001) Dynamic pattern formation in a vesicle-generating microfluidic device. Phys Rev Lett 86:4163–4166

Thu VT, Mai AN, Le The T, Van Trung H, Thu PT, Tien BQ, Thuat NT, Lam TD (2016) Fabrication of PDMS-based microfluidic devices: application for synthesis of magnetic nanoparticles. J Electron Mater 45:2576–2581

Tomeh MA, Zhao X (2020) Recent advances in microfluidics for the preparation of drug and gene delivery systems. Mol Pharm 17:4421–4434

Tong J, Nakajima M, Nabetani H, Kikuchi Y, Maruta Y (2001) Production of oil-in-water microspheres using a stainless steel microchannel. J Colloid Interface Sci 237:239–248

Toy R, Peiris PM, Ghaghada KB, Karathanasis E (2013) Shaping cancer nanomedicine: the effect of particle shape on the in vivo journey of nanoparticles. Nanomedicine 9:121–134

Utada AS, Chu LY, Fernandez-Nieves A, Link DR, Holtze C, Weitz DA (2007b) Dripping, jetting, drops, and wetting: The magic of microfluidics. MRS Bull 32:702–708

Utada AS, Fernandez-Nieves A, Stone HA, Weitz DA (2007a) Dripping to jetting transitions in coflowing liquid streams. Phys Rev Lett 99:094502

Valencia PM, Basto PA, Zhang L, Rhee M, Langer R, Farokhzad OC, Karnik R (2010) Single-step assembly of homogenous lipid-polymeric and lipid-quantum dot nanoparticles enabled by microfluidic rapid mixing. ACS Nano 4:1671–1679

Veiseh O, Tang BC, Whitehead KA, Anderson DG, Langer R (2015) Managing diabetes with nanomedicine: challenges and opportunities. Nat Rev Drug Discov 14:45–57

Verma A, Stellacci F (2010) Effect of surface properties on nanoparticle-cell interactions. Small 6: 12–21

Vladisavljević GT, Khalid N, Neves MA, Kuroiwa T, Nakajima M, Uemura K, Ichikawa S, Kobayashi I (2013) Industrial lab-on-a-chip: design, applications and scale-up for drug discovery and delivery. Adv Drug Deliv Rev 65:1626–1663

Wabuyele MB, Ford SM, Stryjewski W, Barrow J, Soper SA (2001) Single molecule detection of double-stranded DNA in poly(methylmethacrylate) and polycarbonate microfluidic devices. Electrophoresis 22:3939–3948

Wagner J, Köhler JM (2005) Continuous synthesis of gold nanoparticles in a microreactor. Nano Lett 5:685–691

Wagner J, Tshikhudo TR, Köhler JM (2008) Microfluidic generation of metal nanoparticles by borohydride reduction. Chem Eng J 135:S104–S109

Wagner V, Dullaart A, Bock A-K, Zweck A (2006) The emerging nanomedicine landscape. Nat Biotechnol 24:1211–1217

Wallace GG, Higgins MJ, Moulton SE, Wang C (2012) Nanobionics: the impact of nanotechnology on implantable medical bionic devices. Nanoscale 4:4327–4347

Wang B, Shum HC, Weitz DA (2009a) Fabrication of monodisperse toroidal particles by polymer solidification in microfluidics. ChemPhysChem 10:641–645

Wang J, Li W, Zhang L, Ban L, Chen P, Du W, Feng X, Liu B-F (2017) Chemically edited exosomes with dual ligand purified by microfluidic device for active targeted drug delivery to tumor cells. ACS Appl Mater Interfaces 9:27441–27452

Wang JT, Wang J, Han JJ (2011) Fabrication of advanced particles and particle-based materials assisted by droplet-based microfluidics. Small 7:1728–1754

Wang Q-A, Wang J-X, Li M, Shao L, Chen J-F, Gu L, An Y-T (2009b) Large-scale preparation of barium sulphate nanoparticles in a high-throughput tube-in-tube microchannel reactor. Chem Eng J 149:473–478

Wang S, Wannasarit S, Figueiredo P, Li J, Correia A, Xia B, Wiwattanapatapee R, Hirvonen J, Liu D, Li W, Santos HA (2020) Superfast and controllable microfluidic inking of anti-inflammatory melanin-like nanoparticles inspired by cephalopods. Mater Horiz 7:1573–1580

Wang W, Zhang M-J, Xie R, Ju X-J, Yang C, Mou C-L, Weitz DA, Chu L-Y (2013) Hole–shell microparticles from controllably evolved double emulsions. Angew Chem Int Ed 52:8084–8087

Webb C, Forbes N, Roces CB, Anderluzzi G, Lou G, Abraham S, Ingalls L, Marshall K, Leaver TJ, Watts JA, Aylott JW, Perrie Y (2020) Using microfluidics for scalable manufacturing of nanomedicines from bench to GMP: a case study using protein-loaded liposomes. Int J Pharm 582:119266

Weng C-H, Huang C-C, Yeh C-S, Lei H-Y, Lee G-B (2008) Synthesis of hexagonal gold nanoparticles using a microfluidic reaction system. J Micromech Microeng 18:035019

Whitesides GM (2006) The origins and the future of microfluidics. Nature 442:368–373

Wu M-H, Huang S-B, Lee G-B (2010) Microfluidic cell culture systems for drug research. Lab Chip 10:939–956

Wujcik EK, Monty CN (2013) Nanotechnology for implantable sensors: carbon nanotubes and graphene in medicine. Wiley Interdiscip Rev Nanomed Nanobiotechnol 5:233–249

Xia Y, Whitesides GM (1998) Soft lithography. Angew Chem Int Ed Engl 37:550–575

Xu S, Nie Z, Seo M, Lewis P, Kumacheva E, Stone HA, Garstecki P, Weibel DB, Gitlin I, Whitesides GM (2005) Generation of monodisperse particles by using microfluidics: control over size, shape, and composition. Angew Chem Int Ed Engl 44:724–728

Yang S, Guo F, Kiraly B, Mao X, Lu M, Leong KW, Huang TJ (2012) Microfluidic synthesis of multifunctional Janus particles for biomedical applications. Lab Chip 12:2097–2102

Yao X, Chen Z, Chen G (2009) Fabrication of PMMA microfluidic chips using disposable agar hydrogel templates. Electrophoresis 30:4225–4229

Yeh C-H, Lin P-W, Lin Y-C (2009) Chitosan microfiber fabrication using a microfluidic chip and its application to cell cultures. Microfluid Nanofluid 8:115

Ying Y, Chen G, Zhao Y, Li S, Yuan Q (2008) A high throughput methodology for continuous preparation of monodispersed nanocrystals in microfluidic reactors. Chem Eng J 135:209–215

Yu B, Lee RJ, Lee LJ (2009) Microfluidic methods for production of liposomes. Methods Enzymol 465:129–141

Zhang H, Chiao M (2015) Anti-fouling coatings of poly(dimethylsiloxane) devices for biological and biomedical applications. J Med Biol Eng 35:143–155

Zhang H, Liu D, Shahbazi M-A, Mäkilä E, Herranz-Blanco B, Salonen J, Hirvonen J, Santos HA (2014) Fabrication of a multifunctional nano-in-micro drug delivery platform by microfluidic templated encapsulation of porous silicon in polymer matrix. Adv Mater 26:4497–4503

Zhang L, Wang W, Ju X-J, Xie R, Liu Z, Chu L-Y (2015) Fabrication of glass-based microfluidic devices with dry film photoresists as pattern transfer masks for wet etching. RSC Adv 5:5638–5646

Zhang P, Du C, Huang T, Hu S, Bai Y, Li C, Feng G, Gao Y, Li Z, Wang B, Hirvonen JT, Fan J, Santos HA, Liu D (2022) Surface adsorption-mediated ultrahigh efficient peptide encapsulation with a precise ratiometric control for type 1 and 2 diabetic therapy. Small:2200449

Zhao C-X, Middelberg APJ (2016) In: Aliofkhazraei M (ed) Handbook of nanoparticles. Springer International Publishing, Cham, pp 455–473

Zhao Y, Shum HC, Chen H, Adams LL, Gu Z, Weitz DA (2011) Microfluidic generation of multifunctional quantum dot barcode particles. J Am Chem Soc 133:8790–8793

Zhou J, Ellis AV, Voelcker NH (2010) Recent developments in PDMS surface modification for microfluidic devices. Electrophoresis 31:2–16

Zhu P, Wang L (2017) Passive and active droplet generation with microfluidics: a review. Lab Chip 17:34–75

Zielińska A, Carreiró F, Oliveira AM, Neves A, Pires B, Venkatesh DN, Durazzo A, Lucarini M, Eder P, Silva AM, Santini A, Souto EB (2020) Polymeric nanoparticles: production, characterization, toxicology and ecotoxicology. Molecules 25:3731

Zook JM, Vreeland WN (2010) Effects of temperature, acyl chain length, and flow-rate ratio on liposome formation and size in a microfluidic hydrodynamic focusing device. Soft Matter 6: 1352–1360

Chapter 14
Nanofluidic Technologies for Drug Screening and Drug Delivery

Yutaka Kazoe, Kenji Sueyoshi, Sasikarn Seetasang, and Yan Xu

Abstract Recently, nanofluidics exploiting 10–1000 nm spaces has developed and suggested a potential of novel analytical methods for pharmaceutical studies such as monitoring drug response of rare targets (extracellular vesicles, single cell, etc.) and ultrahigh-sensitivity assays of the diverse biological samples. A platform of nanofluidic device, where a network of micro- and nanochannels are fabricated on a substrate, allows analyses with minimal volumes (aL, fL, and pL) and a short

Y. Kazoe (✉)
Department of System Design Engineering, Faculty of Science and Technology, Keio University, Yokohama, Kanagawa, Japan
e-mail: kazoe@sd.keio.ac.jp

K. Sueyoshi
Department of Applied Chemistry, Graduate School of Engineering, Osaka Metropolitan University, Sakai, Osaka, Japan

Japan Science and Technology Agency (JST), PRESTO, Saitama, Japan

Japan Science and Technology Agency (JST), CREST, Saitama, Japan
e-mail: sueyoshi@omu.ac.jp

S. Seetasang
Department of Chemical Engineering, Graduate School of Engineering, Osaka Prefecture University, Sakai, Osaka, Japan

National Nanotechnology Center (NANOTEC), National Science and Technology Development Agency, Pathum Thani, Thailand
e-mail: sseetasang@chemeng.osakafu-u.ac.jp

Y. Xu
Japan Science and Technology Agency (JST), PRESTO, Saitama, Japan

Department of Chemical Engineering, Graduate School of Engineering, Osaka Prefecture University, Sakai, Osaka, Japan

Department of Chemical Engineering, Graduate School of Engineering, Osaka Metropolitan University, Sakai, Osaka, Japan

Japan Science and Technology Agency (JST), CREST, Saitama, Japan
e-mail: xuy@omu.ac.jp

D. Lamprou (ed.), *Nano- and Microfabrication Techniques in Drug Delivery*,
Advanced Clinical Pharmacy – Research, Development and Practical Applications 2,
https://doi.org/10.1007/978-3-031-26908-0_14

analysis time (ms to min) by integrating chemical operations. In this chapter, fundamental methods and technologies of nanofluidics including device fabrication by top-down and bottom-up technologies, ultrasmall fluid manipulation by valves and liquid/liquid and gas/liquid interfaces, separation for biomolecules and nanoparticles, detection by electrical methods and optical methods and using analytical instruments, and high-throughput screening by an array of nanostructures in multi-nanofluidic channels are introduced. Applications of nanofluidics to single-cell analysis and shotgun proteomics, which are important for drug discovery and development to identify specific cellular responses to drug treatments, are presented.

Keywords Nanofluidics · Nanochannel · Fabrication · Manipulation · Separation · Detection · High-throughput screening · Single-cell analysis · Shotgun proteomics

14.1 Introduction

Drug delivery systems are based on transporting active pharmaceutical ingredients and delivering them precisely where they act. Thus, the delivery carriers such as nanoparticles containing drug components affect the essential and desired tissues, and they have to minimize any unwanted effects in the health organs. Of course, monitoring biological responses to drug administration is extremely important, and numerous researchers have continued to work on the development of analytical techniques for this purpose. Over the past few decades, lab-on-a-chip technologies, which is demonstrated by integrating various chemical operations into a microscale platform, have shown remarkable progress as powerful tools for controlled synthesis of drug delivery systems, precisely controlled drug release, and real-time observation of drug delivery to the desired location at the desired rate (Forigua et al. 2021; Dispas et al. 2021; Staicu et al. 2021; Shepherd et al. 2021; Liu et al. 2021; Sato et al. 2022). These technologies are also applicable to the assessment of nano-drug delivery systems, nanomedicine (Ejeta 2021; Jaradat et al. 2021).

Nanomedicine, which uses nanotechnologies such as the manipulation and fabrication of materials and devices with 1–100 nanometers in diameter, is a branch of medicine that prevents, images, diagnoses, monitors, treats, repairs, and regenerates biological systems for diseases. Nanoparticle-based drug delivery has been discovered to effectively affect nanomedicine due to their small size, large surface-to-volume ratio, and tunable characteristics of surface and components. Since early times, animal models have traditionally been widely used to monitor the drug responses for evaluating nanomedicines. In current in vitro studies, nanomedicine is most commonly tested in 2D and 3D cell culture models to mimic in vivo interactions between the cells. In the static 2D and 3D methods, however, nanomaterials for nanomedicine settle out quickly due to low diffusion rates in the static culture model, which can subsequently lead to significant changes in transport rates and nanoparticle interactions. More recently, there have been remarkable advances in microfluidic devices related to organ-on-a-chips (Chen et al. 2021; Kang et al. 2021; Gonçalves et al. 2022). An organ-on-a-chip is a microfluidic cell

culture device developed by microchip-manufacturing methods, which contains a continuous perfusion chamber in which living cells are cultured and arranged to simulate tissue-level or organ-level physiology. A variety of devices and technologies have been developed for culturing, maintaining, analyzing, and experimenting with cells in dynamic microscale systems and have been widely applied in cell biology. One of the most obvious advantages of using the organ-on-a-chip for nanomedicine assessment is its ability to accurately evaluate the transport and migration of nanomedicine at the tissue-tissue interface under in vivo-relevant shear flow, a major difference compared to conventional methods. The advantages of organ-on-a-chip for pharmacokinetic analysis on biological tissues without sacrificing animals have also led to its application and commercialization, especially in the field of nanomedicine.

Microfluidic devices including organ-on-a-chip are one of the most useful tools to deal with biological samples because these devices can effectively handle them owing to their advantages, e.g., small consumption of reagents, integration ability of experimental procedures, large specific surface area, short diffusion length, and so on. In the past decades, the microfluidic devices have continued to play a very important role in measuring diverse and rare targets in body fluids such as whole blood, plasma, saliva, urine, tissues, and so on, from a living body (Manz et al. 1990; Vilkner et al. 2004; Dittrich et al. 2006; West et al. 2008; Kovarik et al. 2013; Culbertson et al. 2014; Patabadige et al. 2016). Additionally, the bioanalytical targets are becoming smaller in scale, such as single-cell analysis, assessment of extracellular vesicles (EVs) including exosomes, evaluation of functions of single molecules, and so on. Among them, isolation of exosomes and analysis of nucleic acids and proteins contained in exosomes have been actively studied in recent years as important analytical techniques that lead to elucidation of not only nanomedicine but also intercellular communication and cancer metastasis mechanisms (Zhao et al. 2021; Alzhrani et al. 2021; Soliman et al. 2021; Yu et al. 2022). However, conventional microfluidic devices sometimes face difficulties in the measurement of them as the targets become smaller.

Recently, advances in nano- and microfabrication technologies have enabled the fabrication of more sophisticated, precise, and integrated devices for the analysis of extremely few amounts of sample solutions. Various experimental operations such as mixing, extraction, reaction, separation, detection, and so on can be successfully integrated on nano- and microdevice, providing rapid, simple, and sensitive measurements in many fields (Xu et al. 2010a, b, 2015b; Yamamoto et al. 2021). Nowadays, nanofluidics are one of the most exciting technologies of the last few decades and are novel and promising fields of research, and the nanofluidic devices have attracted significant attention as a method for precise analysis of minute and complex biological/pharmaceutical samples. Especially in pharmaceutical studies, it is often difficult to invasively collect large amounts of sample solutions containing rate targets from participants. Additionally, the more participants, the greater the number of samples, thus the longer time for their analyses. Furthermore, molecular sizes, concentrations, and chemical/physical characteristics of the components are greatly different for each individual. Thus, analytical methods of minimal-volume

samples containing rare targets with a short analysis time (high-throughput analysis) have been desired for assays of the diverse biological samples (Chantipmanee and Xu 2023a, b). The advantages of nanofluidic and microfluidic devices, as described above, are also highly useful for drug delivery systems in the field of nanomedicine. Therefore, the application of nano- and microtechnologies in the medical and pharmaceutical fields would be an encouraging step. Nowadays, many nano- and microtechnology applications have been reported, including in vivo and in vitro diagnosis, assessment of drug delivery systems, evaluation of nanomedicine, and so on (Ejeta 2021; Rahimnejad et al. 2021; Jaradat et al. 2021).

In this chapter, recent advances in fabrications and operations related to nanofluidic devices and technologies will be presented with special focus because there are many reviews on microfluidics for biological, medical, and pharmaceutical assays, but few reviews on nanofluidics. Fabrication of nanofluidic devices, manipulation technologies in nanoscale, separation technologies based on nano- and microfluidics, novel detection strategies in nanospace, high-throughput measurement in nanoscale arrays, and applications based on nanotechnologies are described in the following sections.

14.2 Fabrication Technologies

14.2.1 Top-Down Fabrication of Nanofluidic Device

Nanoscale fabrication technologies are fundamental for nanofluidics. To fabricate nanofluidic devices for miniaturization and integration of various chemical operations, top-down fabrication technologies have been employed rather than bottom-up fabrication technologies for platforms such as carbon nanotubes and mesoporous silica. Figure 14.1 illustrates representative top-down fabrication process and conceptual structure of nanofluidic device (Mawatari et al. 2014). Nanochannels with controlled dimensions are fabricated on a substrate, which are connected to microchannels as an interface between the nanochannels and bulk space for injection of samples and reagents with accurate fluidic control (Hibara et al. 2002; Tsukahara et al. 2008). Due to mechanical rigidity to construct nanochannels and chemical resistance, glasses are often used as the material of device.

A typical fabrication procedure for nanochannels consists of lithography and etching, as illustrated in Fig. 14.1. For fabricating nanochannels of micrometer-width and nanometer-depth, photolithography and plasma etching have been employed. For fabricating nanochannels of nanometer-width and nanometer-depth, instead of photolithography, patterns of nanochannels are depicted by electron beam (EB) lithography. In EB lithography, an electron beam resist is spin coated onto a glass substrate, and the channel pattern is depicted by irradiating an electron beam. After developing the resist, plasma etching (e.g., reactive-ion etching) is performed

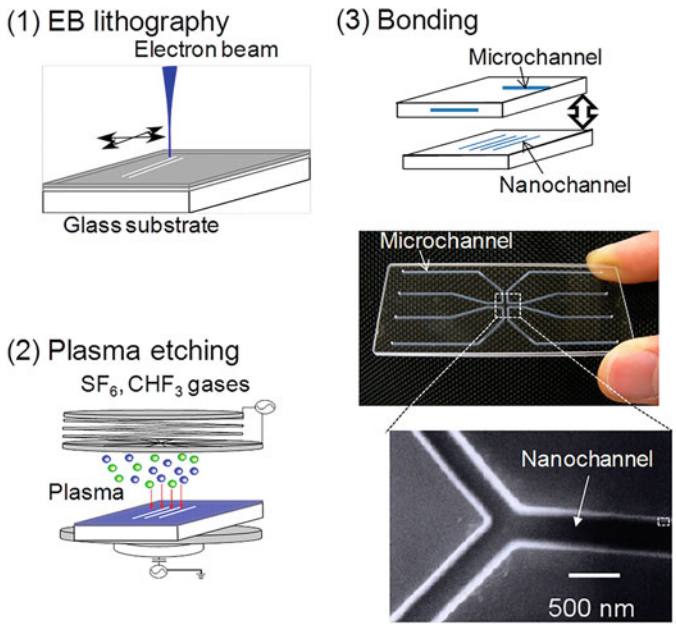

Fig. 14.1 Top-down fabrication process and conceptual structure of nanofluidic device. (Reprinted with permission from (Mawatari et al. 2014). Copyright 2022 American Chemical Society)

to fabricate nanometer-deep channels using a mixture of gaseous compounds such as CHF_3 and SF_6 in case of glass etching. When fabricating deep nanochannels (deeper than 500 nm), a metal layer like chromium is preliminarily sputtered on the substrate before spin coating the resist to enhance the etching resistance. For nanochannels with high aspect ratios (depth/width > 5), planar-type neutral loop discharge (NLD) etching has been employed (Kaji et al. 2004). Based on these procedures, geometrically controlled 50 nm square nanochannels were realized in minimum size by optimizing the conditions, and the nanochannels were successfully connected to microchannels, as shown in Fig. 14.2 (Morikawa et al. 2020).

Other fabrication procedures for nanochannels have been reported. For example, although relatively long fabrication time is required, a direct patterning and etching of nanochannels by focused ion beam (FIB) has been reported (Menard et al. 2012). Although the material is limited to plastic polymers, such as polymethyl methacrylate and polycarbonate, with relatively weak chemical resistance compared to glasses, fabrication procedures by molding process (nanoimprint lithography) were realized, which have advantages in producing nanochannels in large quantities and simple fabrication process (Thamdrup et al. 2008; Zhang et al. 2008).

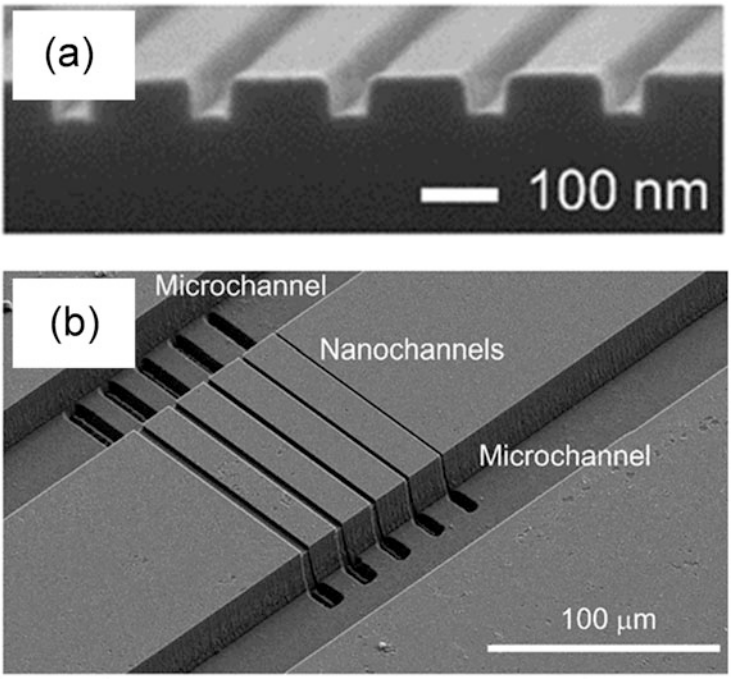

Fig. 14.2 Scanning electron microscope images of (**a**) square-shaped 50 nm nanochannels and (**b**) nanochannels connected to microchannels. (Morikawa et al. (2020) with permission from MDPI)

14.2.2 Nano-in-Nano Integration for Fabrication of Functional Nanofluidic Devices

Nanodevices have been shown potential in supporting researches in drug delivery field such as to mimic organ or cell environments (Pearce and Williams 2006; Wang et al. 2016; Zierold et al. 2020), prepare samples (Moghadam et al. 2006; Vilchis et al. 2007; Aminorroaya and Dippenaar 2008), and prepare sensor (Greve et al. 2007; Nam 2012; Spira and Hai 2013; Dong et al. 2021), which are all important for microscopic analysis to gain more understanding insight properties both in quality and quantity. The fabrication of nanodevices can be accomplished either by breaking down bulk substrates to obtain nanostructures (top-down approach) or by building up materials from nanoscales to form larger structures (bottom-up approach). Recently, by the combination of top-down and bottom-up approaches, new approach called nano-in-nano integration technology has been developed to fabricate functional nanofluidic devices (Fig. 14.3). The concept of the nano-in-nano integration technology is to fabricate nanopatterns in nanofluidic channels using top-down approach. After that, the functions of the nanopatterns can be activated by self-assembling (bottom-up approach).

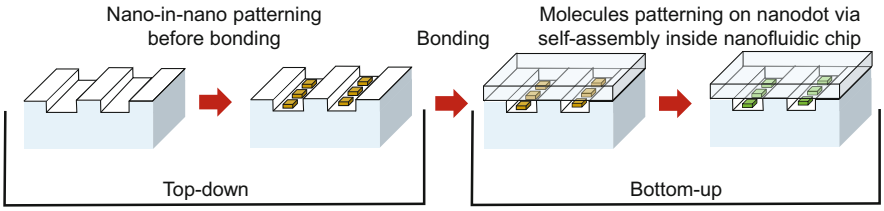

Fig. 14.3 The conceptual schematic of nano-in-nano integration technology including top-down and bottom-up processes

In fabrication of nano-in-nano integration structures, multiple steps of electron beam (EB) lithography are required. Therefore, the key strategy to accomplish the fabrication is to precisely control drawing positions in the second or more EB lithography. Briefly, the first EB lithography fabricating the nanochannels can be done by common steps including resist spin coating, dry etching, resist lifting off, and metal deposition. In the second EB lithography, the key step to successfully create the nanopatterns inside the nanofluidic channels is the placement control technique. This step can be accomplished with the assistance from a pair of pre-deposited gold reference marks (Xu et al. 2015a, d). Using this strategy, the second or more replications of EB lithography can be performed and nano-in-nano or even nano-in-nano-in-nano structures with high precision can be fabricated. Furthermore, nano-in-nano structures with ultrasmall sizes in the order of tens nanometers can be further achieved by optimizing thickness of the resist and dry etching time (Kamai and Xu 2021). Figure 14.4 confirms the achievement of the precise placement control for the multiple replications of EB lithography to fabricate nano-in-nano structures with varying sizes and shapes. Specific distances and high-density array of nanostructures were also successfully fabricated by using the developed placement control technique. Notably, further adding the alignment and EB lithography processes, the fabrication of nano-in-nano-in-nano structures was accomplished (Figs. 14.4i–j) (Xu and Matsumoto 2015). Not only EB lithography but also focused ion beam (FIB) milling with multiple replications can also fabricate nano-in-nano structures as shown in Fig. 14.5 (Xu and Matsumoto 2015).

Finally, the nanopatterns can be used as molecular capture, valve, needle, probe, etc. by self-assembling with other materials such as polymers, drugs, cellular matters, and biomolecules on the nanopatterns (Xu et al. 2015a, d, 2016; Kawagishi et al. 2021, 2023). This intelligent development facilitates the handling and studying in nanoscale targets using ultrasmall volume of fluid, which is suitable for the development in drug delivery field such as used for drug/cell reaction and restriction and drug screening test.

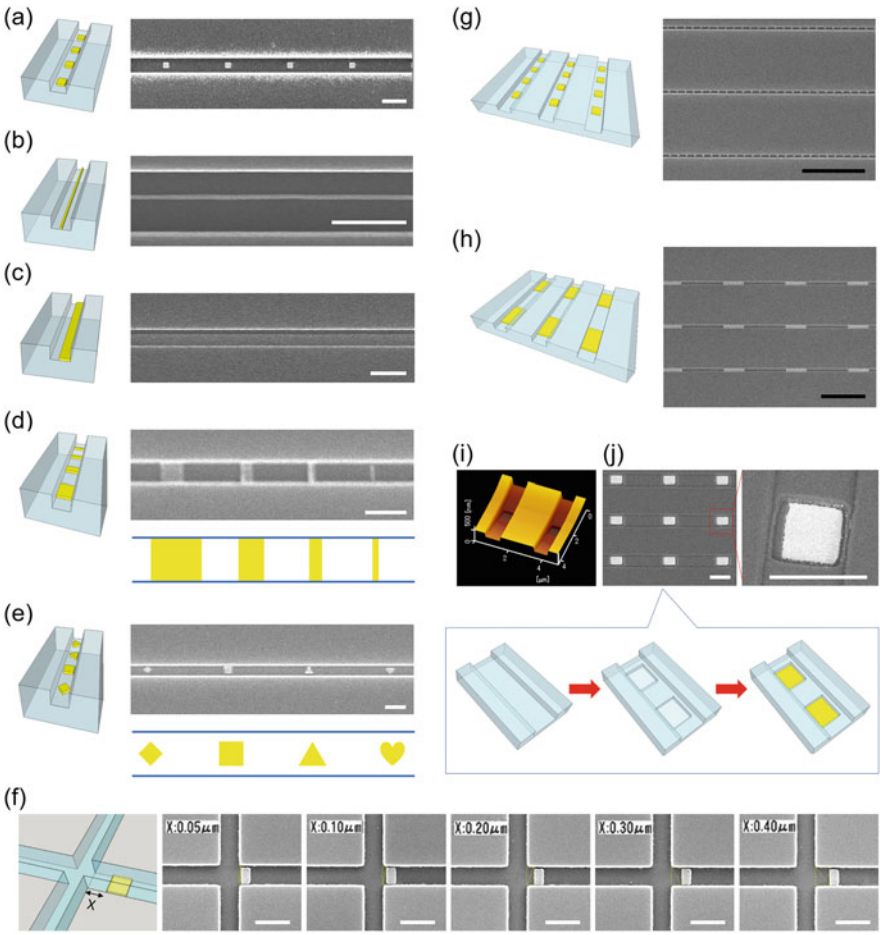

Fig. 14.4 Schematic and SEM images of nano-in-nano integration having (**a**–**e**) different nanopatterns, i.e., nanodots, nanowires, nanostrips, gradient nanorectangles, and different nanogeometrics in single-glass nanofluidic channels, (**f**) specific positions along *X*-axis, and (**g**–**h**) array of nanopatterns in multiple nanofluidic channels. (**i**, **j**) Schematic and SEM images of nano-in-nano-in-nano integration. White scale bar is 1 μm and black scale bar is 10 μm (Reprinted with permission from Xu et al. (2015a). Copyright 2015 the Royal Society of Chemistry)

14.2.3 Bonding Technologies for Chip-Based Nanofluidic Devices

To enable functions of nanofluidic devices, the key technology is chip bonding to create closed spaces for flowing fluids. Bonding technologies can be divided into two types: (1) indirect bonding which demands an adhesive medium between cover substrate and nanomanufacturing substrate and (2) direct bonding which normally requires high temperature (~1000 °C) and vacuum conditions, especially for fusion

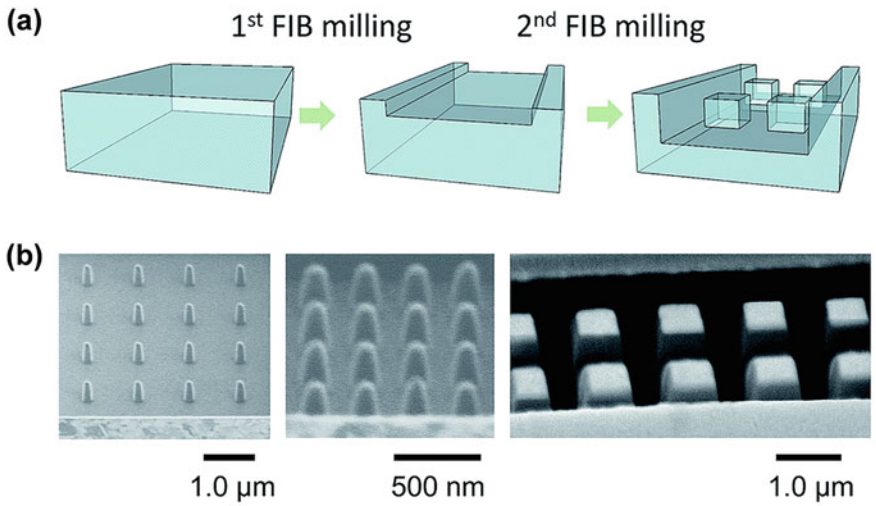

Fig. 14.5 (**a**) Schematic drawing of focus ion beam (FIB) milling with multiple replications for nano-in-nano fabrication and (**b**) SEM images of nano-in-nano structures fabricated. Reprinted with permission from Xu and Matsumoto (2015). Copyright 2015 the Royal Society of Chemistry)

bonding of glass substrates. These extreme conditions cause several disadvantages such as expensive instruments, high-energy consumption, and long bonding time, and the most critical issue is the high temperature is not friendly for pre-modified materials that have melting points lower than the bonding temperature. Therefore, mild bonding conditions at low temperatures are necessary to overcome these technical bottleneck problems in nanofluidic fields.

Low-temperature bonding technology can be accomplished at around 200 °C in ambient environment based on two-step plasma surface activations. First is to remove dust and reactivate native oxides on surfaces by O_2 reactive-ion etching. Second is to further generate chemically reactive surfaces by N_2 radicals (Xu et al. 2012b). Moreover, there is a "step-forward" bonding technology that becomes more friendly for wider ranges of materials. This technology successfully bonds glass substrates together at room temperature (~25 °C) with an assistance from mixture plasma of O_2/CF_4 gases to treat the glass surface before bonding (Fig. 14.6) (Xu et al. 2013). These two technologies can bond the substrates with high strength, maintaining the functions of nanofluidic chips. The nanofluidic chips can work under a high-pressure introduction of 2.5 MPa.

The low-temperature and room-temperature bonding technologies provide possibility to integrate wider range of functional elements such as sensors, electrodes, optical and thermal conductive units, and more importantly biological entities into the nanofluidic devices, which usually cannot tolerate high temperature (~1000 °C) (Xu et al. 2015c). The integration will open a path for wider applications in drug delivery field.

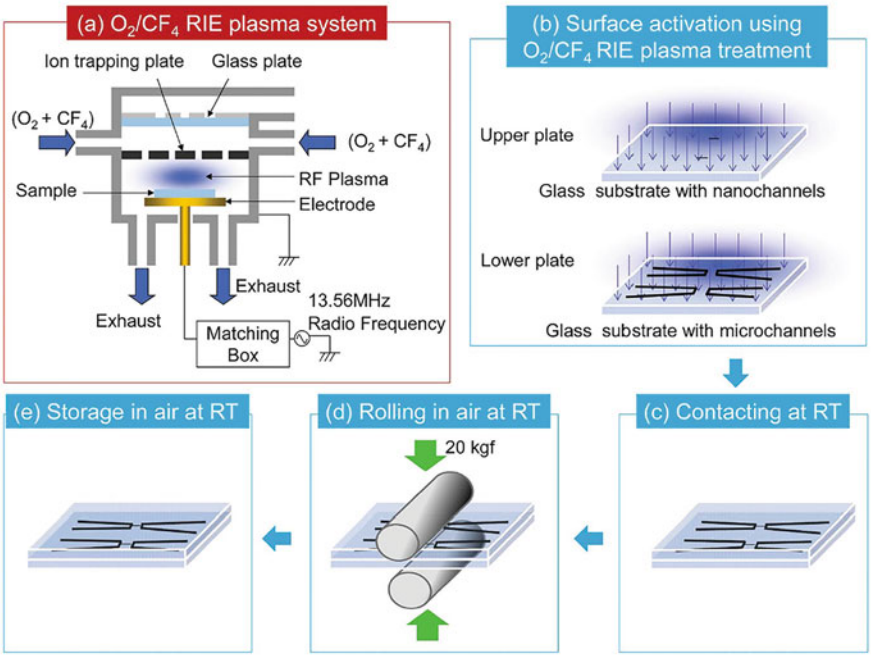

Fig. 14.6 Schematic process of room temperature (RT) bonding of fused silica glass nanofluidic devices based on the surface activation using the O_2/CF_4 gas mixture plasma treatment; (**a**) the fused silica glass substrates were placed in a plasma chamber equipped with an reactive-ion etching (RIE) plasma source, (**b**) O_2 with small amount of CF_4 were introduced into the plasma chamber for surface activation, (**c**) the activated surfaces were preliminarily bonded at RT by hand-applied pressure, (**d**) the preliminary bonded substrates were further rolled from the center of the substrate to the left and right side to remove the trapped air across the interface, and (**e**) the bonded device was stored in ambient air at RT. (Reprinted with permission from Xu et al. (2013). Copyright 2013 the Royal Society of Chemistry)

14.2.4 Surface Modification of Nanochannels

To realize various functions in nanofluidic devices, surface modification technologies for nanochannels have been developed. Since glass, which is a typical material of nanofluidic device, has silanol groups (-SiOH) on the surface, silane coupling agents have been often used to form self-assembled monolayer on the glass surface. For example, to achieve reversed-phase chromatography with ultrahigh separation efficiency utilizing a nanochannel as a separation column, the nanochannel surface was modified by octadecylsilane (ODS) (Smirnova et al. 2015).

Structural deficiencies or functional abnormalities of the nanofluidic channels due to the accumulation of biological entities on the surface are critical issues in drug delivery developments. The biofouling can bring diverse problems such as decreasing analytical performances, increasing drug degradation, and bringing about adverse interactions. To suppress nonspecific biological adsorption, surface

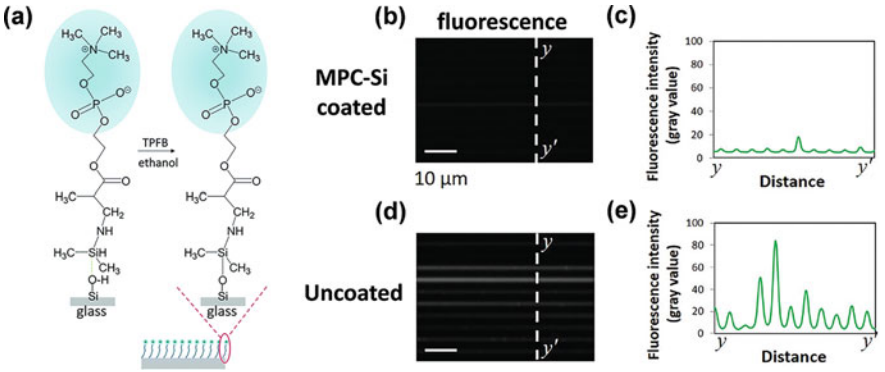

Fig. 14.7 (**a**) Formation of MPC-Si coating on glass surface inside nanofluidic channels. Fluorescence microscopic images and corresponding line profiles of the fluorescence intensity along y-y' lines on (**b, c**) MPC-Si coated and (**d**, **e**) uncoated nanofluidic channels after protein absorption experiment by flowing bovine serum albumin conjugated with fluorescein isothiocyanate (BSA-FITC) through the nanofluidic channels. (Reprinted with permission from Fukuda and Xu (2022). Copyright 2022 the Royal Society of Chemistry)

coating is an effective way. Many coating methodologies using varieties of advanced materials, in particular polymers, have been reported (Xu et al. 2007, 2010c; Xu 2018; Lee et al. 2020). However, almost all reported methodologies focused on the surface modification by polymers in open-/closed-microscale spaces or open-nanoscale surfaces, which may no longer satisfy for closed-nanoscale spaces like nanofluidic chips. The reason is that nanofluidic channels generally have equivalent length scales to the dimensions of polymers, consequently increasing the risk of clogging. Therefore, well-regulated short chain polymers or monomers can be the effective strategies for the surface modification of the closed-nanoscale spaces. One of famous materials to suppress the nonspecific adsorption is 2-methacryloyloxyethyl phosphorylcholine (MPC), which has zwitterionic phosphorylcholine (PC) head groups. The PC group has been proven to be the key component for suppression of the biofouling (Xu et al. 2009a, b, 2021; Seetasang and Xu 2022). The methacrylate group of MPC was functionalized by a hydrosilane group via Michael addition reaction (MPC-Si). The surface modification was simply achieved by introducing the MPC-Si solution into nanofluidic channels to form Si-O-Si covalent bond between MPC-Si and silanol group (Si-OH) of glass surface (Fig. 14.7a). Figure 14.7b, c show the accomplishment in suppression of nonspecific adsorption of a fluorescence-labeled protein when using the nanochannels coated by MPC-Si monomers. There is almost no fluorescence detected in the coated nanochannels, while the fluorescence is detected in the uncoated nanochannels (Fig. 14.7d, e) (Fukuda and Xu 2022). This surface coating approach using MPC monomers was introduced for the first time, which can open up new road for the development of drug delivery systems and drug screening test using nanofluidic devices.

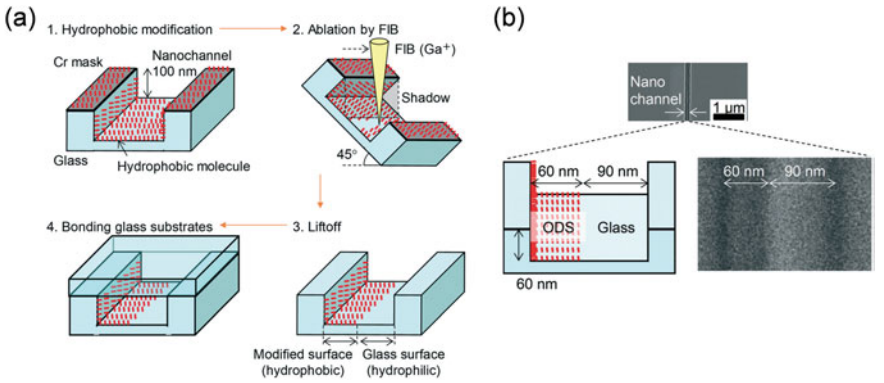

Fig. 14.8 (**a**) A method for nanoscale partial surface modification of a nanochannel utilizing FIB. (**b**) A schematic and field emission scanning electron microscope images of a nanochannel following partial hydrophobic surface modification. (Reproduced from Kazoe et al. (2019b) with permission from the Royal Society of Chemistry)

An approach to the integration of multiple functions into nanofluidic devices is to partially modify nanofluidic channels. For example, a method of antibody patterning in a nanochannel has been developed providing the achievement in immunoassay by nanofluidics (Shirai et al. 2014, 2018). For introducing functional groups for antibody immobilization, first, the entire surface of a fused silica substrate is modified with aminopropyltriethoxysilane (APTES). Then, vacuum ultraviolet light is irradiated through a photomask for partially decomposing APTES for patterning. After bonding the substrate with another substrate containing a nanochannel, antibodies are chemically immobilized with the amino groups of patterned APTES. Accordingly, pattern of antibodies with a width ranging from 100 μm to 3 mm was formed in a nanochannel. However, optical patterning methods cannot achieve nanoscale surface patterning due to the diffraction limit and difficulty of the alignment of the optical mask. To overcome the subject, a method of nanoscale partial surface modification utilizing FIB has been developed, as shown in Fig. 14.8 (Kazoe et al. 2019b). A nanochannel itself, which is fabricated on a glass substrate with a sputtered chromium layer, is used as a mask. In case of fabricating hydrophilic and hydrophobic areas patterned side by side along the nanochannel, after modifying the entire surface by ODS, the substrate is inclined to produce a shadowed area used as a mask of FIB. Then, FIB is irradiated to remove ODS. After lift off by removing the chromium layer, the substrate is bonded to another substrate to seal the nanochannel. This method allows precise nanoscale surface patterning of a nanochannel with high reproducibility and was applied to formation of aqueous/organic parallel two-phase flow for fL ultrafast solvent extraction as described in Sect. 14.3.2.

Another approach that offers an achievement in partial surface modification is additive approach associating with nano-in-nano integration technology. High precision and partial surface modification, which enable to create hydrophobic/

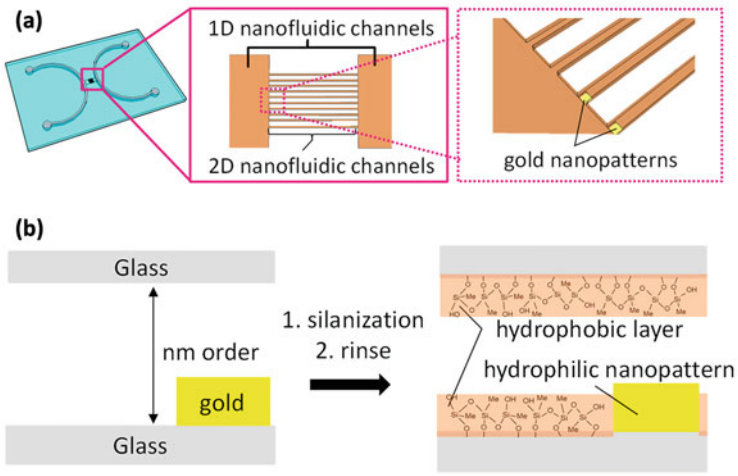

Fig. 14.9 Schematic images of (**a**) the nanofluidic devices consisting of multiple nanofluidic channels and gold nanopatterns fabricated using nano-in-nano integration technology, and (**b**) partial surface modification by additive approach to obtain hydrophobic/hydrophilic surface inside nanofluidic device. (Reprinted with permission from Kawagishi et al. (2021). Copyright 2021 American Chemical Society)

hydrophilic surface in nanofluidic channels, is an example (Kawagishi et al. 2021). The procedures started with fabrication of 1D and 2D nanofluidic channels before precisely depositing gold nanopatterns at the entrance of 2D nanofluidic channels as displayed in Fig. 14.9a. The modification is based on additive approach by flowing a solution of trichloromethylsilane, which is a hydrophobic molecule, through the nanofluidic channels. The hydrophobic molecules can strongly bind with silanol groups on glass substrate while attributing to nonspecific physical adsorption on the gold nanopatterns. Therefore, after special rising with toluene, trichloromethylsilane was removed from the gold nanopatterns leading to hydrophilic surface being recovered. While the hydrophobic molecules still remained on glass surface, the hydrophobic surface was obtained as illustrated in Fig. 14.9b. This developed partial hydrophobic/hydrophilic surface was used in nanoscale gas-liquid interface application, which was addressed in Sect. 14.3.2.

14.3 Ultrasmall Fluid Manipulation Methods

A technical challenge existing in nanofluidic manipulation is to directly control and contact liquid inside nanochannels in the very small volume at aL, fL, and pL levels. The fact is that their tiny and closed spaces bring difficulty in the fabrication of a proper tool to function at such ultrasmall spaces, which is important for the researches focusing on nanoscopic species like drug delivery and drug screening

systems. So far, most of the publications reported indirect approaches to control the fluid inside nanochannels via tools in microfluidic channels that were connected with the nanofluidic channels. Such approaches are difficult to consider as the nanofluidic manipulations. Hence, the methodology for the creation of the nanocomponents inside the nanofluidic channels needs to be established in order to overcome the critical challenge.

14.3.1 Nanochannel Valves

A valve is one of the essential components that has been commonly employed in fluidic experiments to precisely control molecules/cells for synthesis, analysis, isolation, confining, releasing, switching, and partitioning inside nanofluidic channels by opening/closing a valve. As mention above, most of the valves are fabricated in microchannels such as valves utilizing channel deformation (Unger et al. 2000), hydrogel structures (Beebe et al. 2000), and wettability patterns (Takei et al. 2007). However, employing valves in nanochannels is challenging owing to the smallness of nanospace. Recently, several types of nanochannel open/close valve have been reported.

Valves utilizing channel deformations have the most overall usability. Although the nanofluidic devices are usually made of glasses with mechanical rigidity to construct nanostructures, even tiny elastic deformation of glass materials can close nanoscale channels. Therefore, recent studies have developed a nanochannel open/close valve utilizing nanoscale elastic glass deformation (Kazoe et al. 2019a; Sano et al. 2020). This developed valve is considered to be an active valve because the nanofluidic manipulation is directly dependent on the changes of the elastic glass nanovalves triggered by external force. Figure 14.10a illustrates a schematic structure of the nanofluidic valve. A four-stepped shallow circular valve chamber of fL volume, in which the shape of a chamber approximately corresponds to that of the glass deflection curve, is located between nanochannels for stopping fluid flows by the valve closing. By adding a force by an actuator, the glass is deflected and the valve is closed. The thickness of the glass is designed based on the material mechanics to avoid breaking of glass at the valve closing with the stress over the breaking stress. Figure 14.10b, c shows a valve fabricated in a nanofluidic device and its demonstration. The open/close operation of the nanochannel was successful with a pressure resistance higher than 500 kPa, a response time of 0.06 s, and durability over 100,000 operations, which are sufficient performances for nanofluidic chemical analyses. Flow switching and flow rate control in the nanochannel utilizing the valve were also achieved.

The active nanovalves can be alternatively fabricated by grafting polymers inside nanofluidic channels. These polymers can be sensitive to electrical fields (Ouyang et al. 2010), temperatures (Zuo et al. 2016; Xu et al. 2016), etc., which allow reversible opening and closing many times. Nano-in-nano integration technology also plays a role in the fabrication of the active nanovalves by using poly

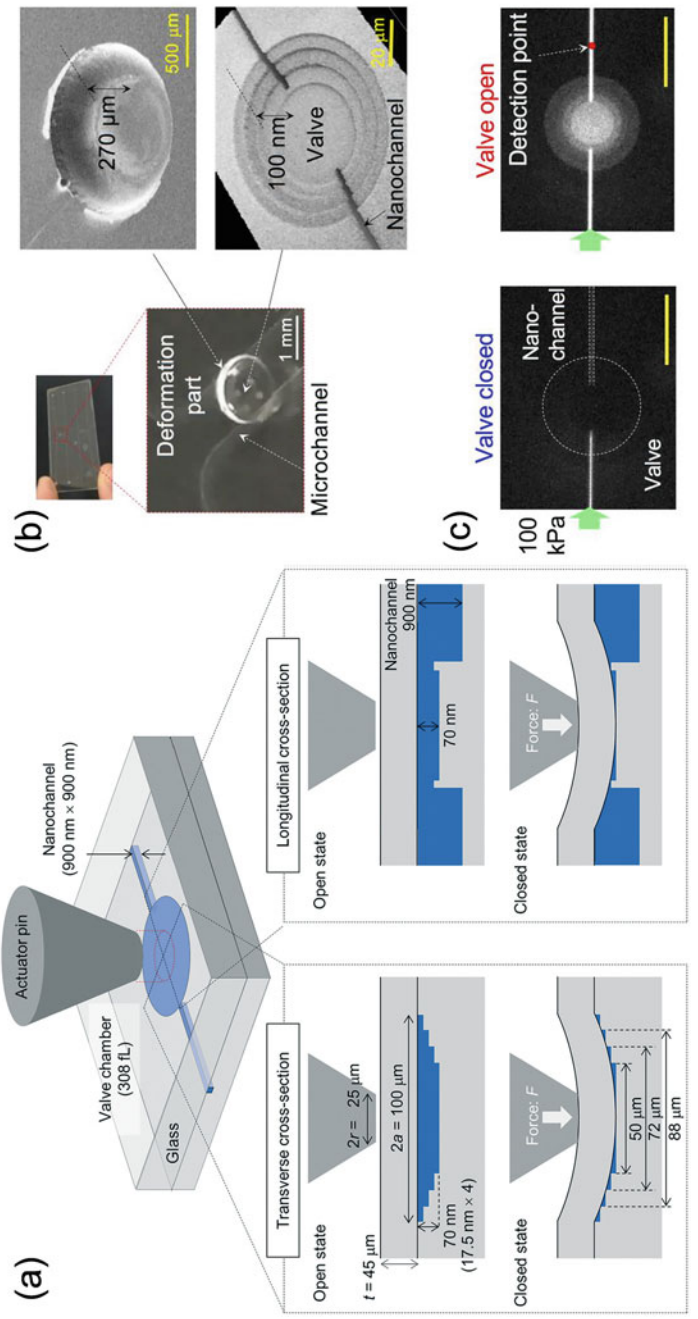

Fig. 14.10 (**a**) Conceptual design of a nanochannel open/close valve made of glass. Cross-sectional views show the valve operation under applied force by the actuator. Noted that the vertical and horizontal scales are different. (Reproduced from Kazoe et al. (2019a) with permission from the Royal Society of Chemistry.) (**b**) A nanofluidic device containing a valve with a glass deformation part of a 30 μm thickness. (**c**) An open/close operation of a nanochannel. (Reproduced from Sano et al. (2020) with permission from Springer Nature)

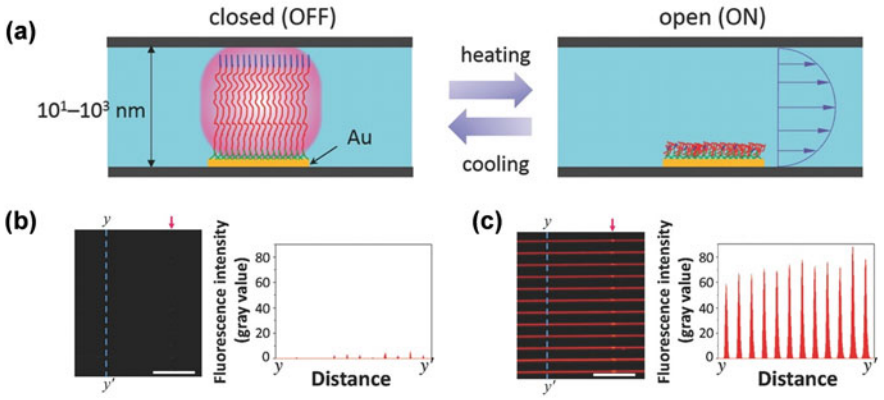

Fig. 14.11 (**a**) Conceptual image of the nanovalve by using thermosensitive TTC-*t*-PNIPAM polymer which can be swollen or shrunken when temperature changes, and fluorescence images and fluorescence intensity at y-y' position of the nanofluidic channel when introducing sulforhodamine B solution (**b**) before and (**c**) after heating nanofluidic device with thermoplate at 45 °C in order to close or open the nanovalve, respectively. (Reprinted with permission from Xu et al. (2016). Copyright 2016 Wiley-VCH)

(N-isopropylacrylamide) (PNIPAM) terminated with a trithiocarbonate (TTC) group at one end (TTC-*t*-PNIPAM), which can specifically bind with gold nanopatterns embedded in nanochannels via thiol groups. The change of temperatures affected the swelling/shrinking behaviors of this polymer, which can actively block/allow nanofluidic flow (Fig. 14.11a) (Xu et al. 2016). Figure 14.11b, c demonstrates the successful closing/opening of the nanovalves (pink arrows) before and after heating at 45 °C, respectively. More recently, Xu et al. has reported a flexible glass-based active nanofluidic valve that can precisely block, open, and direct the flow of single small molecules in nanochannels. The flexible valve and approach open an avenue for not only understanding the original behavior of individual molecules in their natural forms, but also developing single-molecule regulated chemical and biological processes (Kawagishi et al. 2023). The aforementioned examples are tools that can directly manipulate nanofluidic flows and molecules inside nanochannels, which may play a potential role in drug delivery field for drug dilution, incubation, releasing, etc.

Another type of nanovalve is a passive valve, in which the nanofluid is regulated by the change of the environment inside the nanofluidic channels. For example, a Laplace nanovalve having nanopillar arrays as wetting boundary can trap liquid and resist the Laplace pressure at the liquid surface. This valve can be opened or closed by changing its pressures. Furthermore, the Laplace valve can generate a droplet at femtoliter levels for the first time (Mawatari et al. 2012; Nakao et al. 2020). The Laplace valve is considered to be a passive valve because the fluid was not controlled by the changes of the valves, but the changes of the pressures. Other examples of passive valves are nano-bubble valves operated by changing temperatures (Furukawa et al. 2021), and nano-electrokinetic valve worked by applying voltages (Eberle et al. 2018), etc.

14.3.2 Multiphase Fluid Manipulations in Nanochannels

Control of multiphase fluids with immiscible liquid/liquid or gas/liquid interfaces is important for chemical operations such as reaction, extraction, purification, and preconcentration. In the bulk scale, multiphase fluid manipulations by shaking with dominant gravity effect have been utilized. In contrast, in the microscale, since the surface tension is dominant compared with the gravity, parallel multiphase flows (Aota et al. 2009; Mawatari et al. 2011) and droplet/plug flows in microchannels (Khan et al. 2004; Larrea et al. 2015) have been utilized for multiphase chemical operations. By optimizing channel geometry and flow conditions, parallel flows and droplet/plug flows can be generated on demand under the dominant surface tension effects. Expanding such approaches to nanofluidics allows multiphase chemical operations with ultrasmall volumes (aL, fL, and pL) and high efficiency.

Previously, formation of aL-fL volume droplets in nano-/microchannels has been reported, which is applicable to synthesize functional nanoparticles and for drug delivery (Malloggi et al. 2010) and single-enzyme analysis (Shui et al. 2011; Arayanarakool et al. 2013). As shown in Fig. 14.12, ultrasmall monodisperse droplets with defined diameters were generated utilizing flow focusing by a

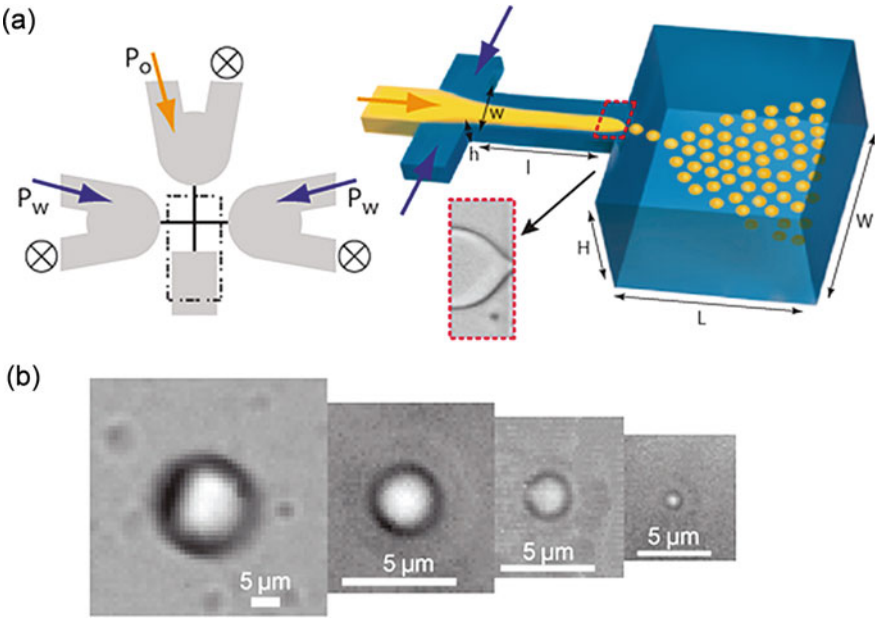

Fig. 14.12 (**a**) Schematic of a micro-/nanofluidic device for droplet generation by pressure-driven flow focusing. Typical dimensions of the experiment are $H = 10$ μm, $L = 5000$ μm, W = 40–100 μm, $h = 420$ nm-1 μm, $L = 50$ μm, and $W = 5$–10 μm. (**b**) Microscopic images of individual oil droplets generated in the device. (Reprinted with permission from Malloggi et al. (2010). Copyright 2022 American Chemical Society)

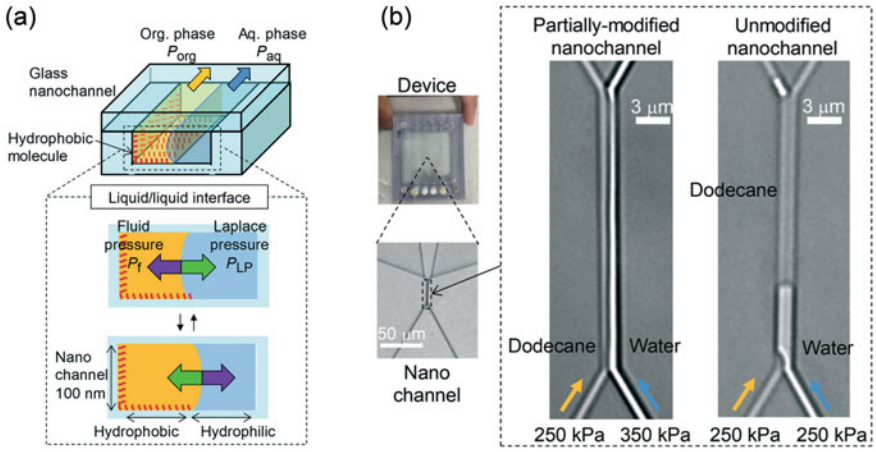

Fig. 14.13 (**a**) Schematic of the method of formation of aqueous/organic parallel two-phase flow in a nanochannel with partial hydrophobic surface modification. (**b**) Microscopic images of water/dodecane two-phase flow in nanochannels. Parallel two-phase flow in a nanochannel with partial hydrophobic surface modification with external pressures of 250 and 350 kPa applied to the organic and aqueous phases, and a plug flow in an unmodified glass nanochannel at external pressures of 250 and 250 kPa. (Reproduced from Kazoe et al. (2019b) with permission from the Royal Society of Chemistry)

continuous phase and instabilities of interfaces. On the other hand, to form parallel multiphase flows, it is necessary to balance the fluid pressure and Laplace pressure derived from the surface tension to maintain the liquid/liquid or gas/liquid interfaces along the nanochannel. However, since the Laplace pressure is inversely proportional to the space size, it becomes 100–1000 kPa in nanospaces and multiphase fluid manipulations by controlling the interfaces are challenging. For this issue, a method to form aqueous/organic parallel two-phase flow in a nanochannel was developed based on a nanoscale partial surface modification as described in Sect. 14.2.4 (Kazoe et al. 2019b). As illustrated in Fig. 14.13a, in a partially hydrophobic nanochannel, the high Laplace pressure works to stabilize the parallel two-phase flow by maintaining an aqueous/organic phase interface at a boundary between the hydrophobic and hydrophilic region. By this method, water/dodecane parallel two-phase flow was successfully formed in a partially ODS-modified nanochannel (width, 1500 nm; depth, 890 nm), while a plug flow was formed in an unmodified glass nanochannel (Fig. 14.13b). Utilizing the parallel two-phase flow, solvent extraction of a lipid according to the Bligh-Dyer method, which is a broadly used pretreatment process in lipidomics, was realized with a sample volume of 4 fL (250 times smaller than the volume of single cell) and an ultrafast processing time of 1 ms, by integrating chemical operations of phase confluence, extraction, and phase separation.

Another interesting example using multiphase flow for fluid manipulation in nanochannels is gas-liquid interfaces (GLIs). The GLIs, a unique region allowing molecules across from one state to another, have been recently downscaled to the

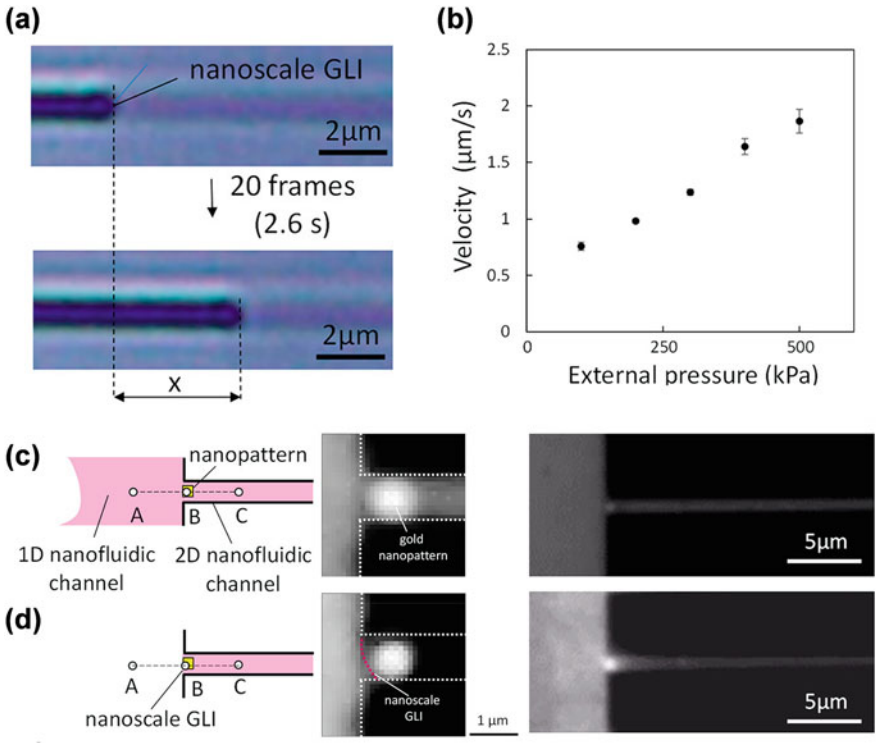

Fig. 14.14 (**a**) Microscopic images of moving nanoscale GLIs in the nanofluidic channels, (**b**) different applied pressures provide different velocities of the nanoscale generated GLIs. Schematic and microscopic images of the nanofluidic channels (**c**) before and (**d**) after the generation of GLIs at hydrophobic/hydrophilic surface

nanoscales using nanofluidics. The nanoscale GLIs were developed to be uniform, array able, stable, and transportable inside nanofluidic channels (Kawagishi et al. 2021). The nanofluidic channels consisting of (1) hydrophobic 1D/2D nanochannels and (2) hydrophilic gold nanopatterns were prepared as described in Sect. 14.2.4. The formation of GLIs can be induced by physicochemical effects and optimized nanofluidic operations and occurred at the region between hydrophobic wall of 1D/2D nanochannels and hydrophilic gold nanopatterns. The generated nanoscale GLIs were moveable and varied depending on applied pressures (Fig. 14.14a, b). The nanoscale GLIs could enrich targeted molecules (Fig. 14.14c, d). This feature is important and useful for drug screening tests that have to deal with low concentration of samples in the future.

14.4 Separation

14.4.1 Separation Technologies for Biomolecules/Fine Particles in a Living Body

As described in Sect. 14.1, separation technologies are one of the key technologies for the accurate analyses of diverse biological samples. In nano- and microfluidics, various devices and methods have been developed to realize the effective separation of biomolecules and fine particles. In Sect. 14.4.2, recent advances in nano- and microfluidic devices for separation assays of biomolecules are introduced and summarized. The separations of the microparticles such as blood cells, circulating tumor cells, microvesicles, and so on in the samples have been employed for decades to analyze solid and liquid components individually. Recently, the analysis of the dynamics of nanoparticles (NPs) in living bodies is of great importance not only in drug delivery systems but also in the entire field of life sciences because there are various extracellular vesicles (EVs), microparticles, and NPs in the body (Zhao et al. 2021; Rai et al. 2021; Yu et al. 2022). Especially exosomes, a class of small EVs with sizes typically in the range of 30–150 nm, have been also attracting a great deal of interest because it has been clarified that exosomes play important roles in intercellular communications. Other NPs in the body are also important targets, especially in pharmaceutical/clinical diagnosis and drug delivery systems (DDS). Therefore, effective separation or isolation of exosomes and NPs from other EVs in the biological samples is attracting attention in life science as a great challenge to reveal their dynamics. In bulk scale procedures, NPs and EVs have been separated/isolated mainly by filtration, centrifugation, and affinity interaction, owing to their differences in sizes, densities, and surface characteristics (Wang et al. 2021a; Wu et al. 2021; Tzaridis et al. 2021; Chen et al. 2022). However, there still remain many issues such as complex and labor-intensive manipulations, requirement of large sample consumption, and longtime protocols. In nano- and microfluidic devices, various devices have been developed for separation/isolation of NPs/EVs because of the characteristics related to miniaturization above described (Salafi et al. 2016; Ding et al. 2021; Hassanpour Tamrin et al. 2021). Furthermore, different separation/isolation mechanisms could be integrated in the devices, providing the specific separation/isolation of NPs/EVs that the bulk scale methods cannot provide. In Sect. 14.4.3, recent advances in nano- and microfabricated devices for separation/isolation of NPs/EVs are introduced and summarized.

14.4.2 Separation of Biomolecules Based on Microfluidic/Nanofluidic Technologies

Since the early times, nano- and microstructures have been used for the separation of various molecules. For example, nanopore structures of the hydrogels have been

employed for the separation of proteins and nucleic acids (Bae and Soane 1993). Microparticles have been used for various separations due to their large surface areas (Xie et al. 2005). Monolithic structures have a serially linked microscale skeleton structure with a large surface/volume ratio, which provides highly effective separation especially in chromatography (Bedair and El Rassi 2004). However, these conventional materials have random nano- and microstructures, which limited their separation performance. As discussed above, nano- and microfluidic devices have great advantages, e.g., small consumption of reagents, integration ability of experimental procedures, large specific surface area, and short diffusion length. In addition to the above characteristics, the precisely regulated nano- and microstructures allow for separation that cannot be achieved by the conventional methods. In Sect. 14.4.2, recent advances in nano- and microfluidic devices for separation of various biomolecules are described, considering their advantages.

Nano- and micropillar arrays are typical structures for separation based on nano- and microfabrication technologies (Kaji et al. 2004; Yasui et al. 2011, 2012, 2013; Rahong et al. 2014, 2015a, b). It has a regulated structure of nano- or micropillars aligned in the microfluidic channels. The first report of the micropillar array device for the electrophoretic separation of biomolecules was from Kaji et al. (2004) and Yasui et al. (2011, 2013), reporting various devices with different sizes and structures and finally providing rapid and fine separation of nucleic acids. However, the sub-micrometer-order pillar arrays with finely regulated structures are often difficult to fabricate. Thus, analyses using such devices are expensive, making it hard to apply them in practical use. To overcome the issue, Yasui et al. reported other approaches to fabricate nanopatterns using nanowire (Yasui et al. 2013; Rahong et al. 2014, 2015a, b). The various nanowires of different lengths, thicknesses, spacing, and materials were fabricated in the microfluidic devices (Fig. 14.15).

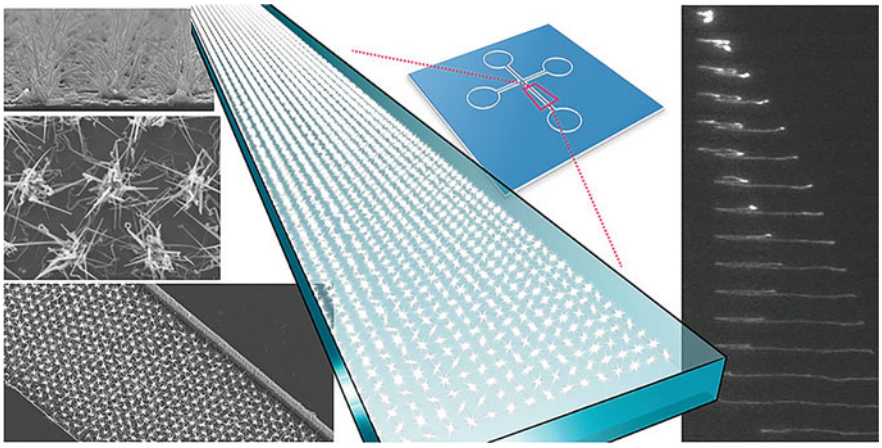

Fig. 14.15 Schematic illustration and scanning electron microscope images of 3D nanowire network structure in microfluidic channel and time-course observations of a T4-DNA molecule in the nanowire spot-array structure under the applied electric field of 10 V/cm (Yasui et al. (2013) with permission from American Chemical Society)

The multistep growth of nanowires has been also employed, resulting in the dense nanowire patterns like a tree. These nanowire devices could be easily fabricated and could perform the same as or better than the nanopillar arrayed devices, which is advantageous for commercialization.

Nano- and micropillar arrayed devices are also used as the separation column in chromatography (He et al. 1998; De Malsche et al. 2007, 2012; Vangelooven et al. 2010; Aoyama et al. 2010; Song et al. 2013; Nys et al. 2019). As compared to the conventional columns such as microbeads-packed column and monolithic column, the finely regulated pillar arrays suppress the band broadening due to the random walking of the analytes. From the first report related to the micropatterned column (He et al. 1998), various innovations have been reported. De Malsche (De Malsche et al. 2007) reported on reversed-phase liquid chromatography using surface-modified micropatterned column. Vangelooven (Vangelooven et al. 2010) investigated the effect of micropatterned structures on flow distributions. De Malsche (De Malsche et al. 2012) also fabricated the longer micropatterned column, providing highly effective separation with 1,000,000 theoretical plates. Aoyama (Aoyama et al. 2010) and Song (Song et al. 2013) reported on low-dispersion turn structure to realize longer column without reducing resolution due to skewing at curved channels (Fig. 14.16). Nys (Nys et al. 2019) combined a micropillar array column device with

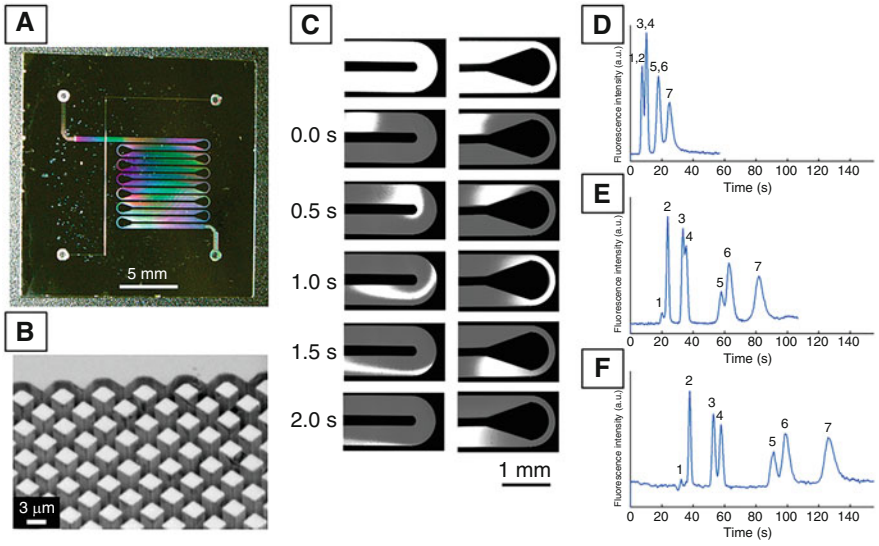

Fig. 14.16 Pillar array column for chromatographic separation. (**A**) Overview of fabricated microchip with low-dispersion turns. (**B**) SEM images of the fabricated pillar array structure. (**C**) Movement of flat sample bands through (left column) constant radius turns and (right column) low-dispersion turns under nonretained conditions. The top two rows of the images show the separation channel filled with the fluorescent solution. Subsequent images were recorded every 0.5 s. Chromatograms are obtained from fluorescently labeled amino acid solution on the microchip with low-dispersion turns. Detection of NBD-labeled amino acids was carried out at various points just before the (**D**) first turn, (**E**) third turn, and (**F**) fifth turn (Aoyama et al. (2010), Images are reconstructed with permission from American Chemical Society)

ion mobility mass spectrometry for proteomic researches. These studies allow the fine separation with shorter analysis time, smaller amount of the samples, and high resolution as compared to the conventional chromatography columns.

Chromatographic separation using inner surfaces of a hollow column, which is also used in conventional methods, has been studied to improve the analysis time and consumption of the samples. Generally, the surface/volume ratio increases upon decreasing the scale of the device and the higher ratio provides better resolution. Thus, everyone can easily imagine the idea of fabricating the smaller channels below micrometer scale for the better separation, but it was often difficult to achieve it because it requires both accurate nanofabrication technologies and precise nanomanipulations.

Recently, one of the most impressive chromatographic separation technologies using nanofluidic device was first reported by Ishibashi (Ishibashi et al. 2012). The developed nanochromatography device can separate a fL-order volume of sample within 4 s with high separation efficiency (440,000 plates/m). Shimizu (Shimizu et al. 2016) improved the nanochromatography system, resulting in higher theoretical plate (140,000 plate/89 mm column) for 35 fL samples with good repeatability (Fig. 14.17). Tsuyama (Tsuyama et al. 2020) achieved the nanochromatographic separation of 1.8-fL samples, and the limit of detection was 5.4 zmol (3300 molecules in the detection volume) by the noble label-free detection method of

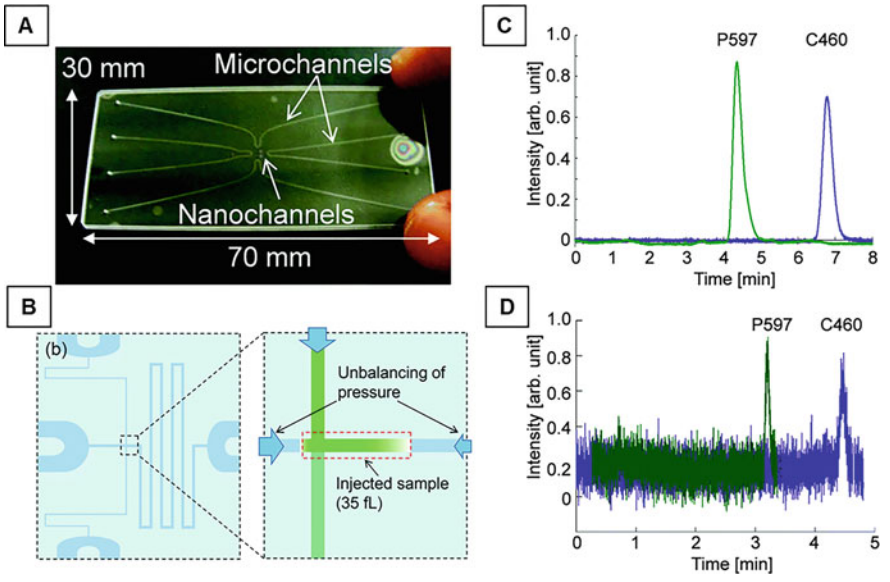

Fig. 14.17 Overview of nanochromatography device. (**A**): Photograph of fused silica chip. (**B**) Illustration of the sample loading state before the pinched injection. Unbalancing pressure and injection volume of 35 fL. Chromatograms of P597 and C460 by (**C**) HPLC and (**D**) extended-nanochromatography (Shimizu et al. (2016), Images are reconstructed with permission from The Royal Society of Chemistry)

photothermal optical diffraction. Tsuyama (Tsuyama et al. 2021) also developed a nanochromatography device with a depth below 100 nm. In the device, the limit of detection was 7.5 molecules in the detection volume of 7 aL. Yamamoto (Yamamoto et al. 2022) integrated nanochromatography with an enzyme reactor channel, an injector, and a valve structure. As a typical result, 1 pL of enzyme reaction products was well separated within 120 s by the developed device. Amarasekara (Amarasekara et al. 2020) developed a nanoelectrochromatography device made from poly(methyl methacrylate). The separation of oligonucleotides could be demonstrated within 1 s by an effective column length of 60 μm (100 nm × 100 nm, depth and width).

In the future, this type of integrated device will be applicable to single-cell analysis of which sample volumes are approximately 1 pL.

14.4.3 Separation of NPs/EVs in Nano- and Microfluidic Devices

In the analyses of NPs/EVs, one of the approaches that microfluidic/nanofluidic devices are most adept at is size-based separation/isolation. Filtration by integrated nanoporous membranes or nanofluidic channels, sorting by hydrodynamic force, and deterministic lateral displacement (DLD) have been intensively developed for mainly size-based separations/isolations of NPs/exosomes from other microparticles/other EVs with micrometer scale. Field-flow fractionation combined with acoustic fractionation, electrophoresis, dielectrophoresis, magnetophoresis, and other technologies can separate/isolate the particles by the differences in the density, permittivity, and other physical properties of NPs/EVs, in addition to their different sizes. In this section, recent studies of the size-based separation/isolation of NPs/EVs using nano- and microfluidic technologies are explained with introduction of recent progresses.

Filtration is the simplest size-based separation/isolation of NPs/EVs by integrating nanostructures with microfluidic devices (Davies et al. 2012; Yukawa et al. 2021; Ren et al. 2022). Larger NPs/EVs than nanopores/nanochannels cannot pass through, whereas the smaller one can. Although the microfluidic devices integrated with membranes or nanochannels progress in fabrication technologies for the uniform nanoporous membranes and nanochannels, accuracy of the separation/isolation of NPs/EVs has been greatly improved. These membrane devices allow the fine separation based on the pore sizes as a threshold (Fig. 14.18A-C) (Sundaram et al. 2020; Casadei et al. 2021; Kim et al. 2021a, b). In other words, the desired separation/isolation needs the fabrication of the membranes/nanochannels with appropriate pores/channel sizes, which is sometimes disadvantageous due to the requirement of complex fabrication processes. Recently, Fujiwara (Fujiwara et al. 2020) developed a microfluidic/nanofluidic device with tunable gates for size-based classification of NPs/EVs. The device made of quartz and its inner surfaces are

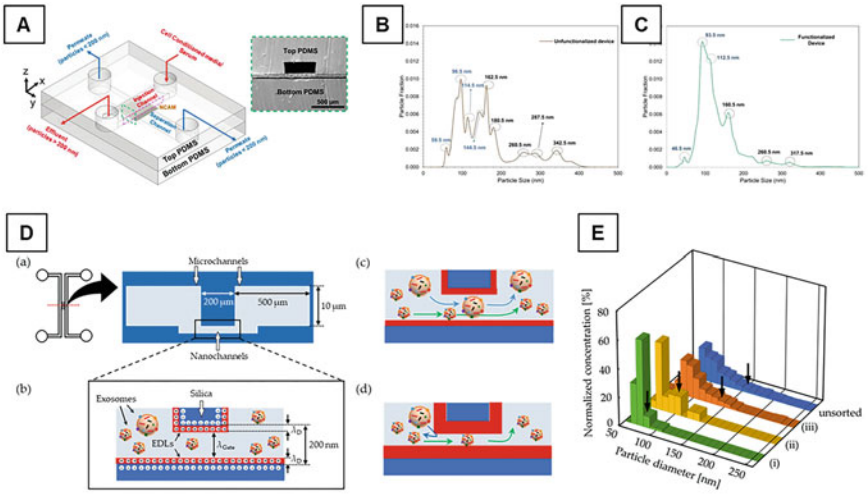

Fig. 14.18 (**A**) Schematic of the microfluidic channels (each 500 μm wide and 150 μm high) separated by a nanocapillary array membrane. Size distribution according to the particle fraction obtained by NTA for (**B**) EV isolated using the micro-nanofluidic device with the separation channel not functionalized with anti-CD63 antibody and (**C**): EV isolated using the micro-nanofluidic device with the separation channel functionalized with anti-CD63 antibody ((Casadei et al. 2021), illustrations are reconstructed with permission from WILEY). (**D**) Schematic illustration of the proposed size sorting of exosomes. (a) Channel configuration and cross-sectional view of the developed micro-nanofluidic device. (b) Schematic of electric double layers (EDLs) formed on the inner surface of the nanochannels. (c, d) Schematic illustrations of the size sorting of exosomes by tuning the thicknesses of EDLs by employing background electrolytes at (c) high and (d) low concentrations. (**E**) Distribution of exosome sizes before and after sorting (Fujiwara et al. (2020), illustrations are reconstructed with permission from MDPI)

negatively charged by proton desorption from silanol groups, which form the electric double layer (EDL). Under the experimental conditions, negatively charged NPs/EVs cannot approach the EDL by electrostatic repulsion. The thickness of the EDL in nanochannels connecting two parallel microchannels is easily controlled by the ionic strength of background solutions, which allow to tune the gate sizes that NPs/EVs located in the microchannel can pass through. As a typical result, the developed device achieved the fine separation/isolation of EVs at least 30 nm units (Fig. 14.18D, E). This precise separation/isolation is very difficult for other methods/devices, except the disadvantage that the applicable sizes of NPs/EVs are limited to about 200 nm or less.

Hydrodynamic force in microfluidic devices has been used for the alignment, sorting, and isolation of the microparticles with different sizes (Yamada et al. 2004; Yamada and Seki 2005, 2006; Kawamata et al. 2008; Maenaka et al. 2008; Aoki et al. 2008; Morijiri et al. 2011; Shin et al. 2017; Ozawa et al. 2019). In pinched flow fractionation (PFF) reported by Yamada et al. (2004), Kawamata et al. (2008), Maenaka et al. (2008), and Morijiri et al. (2011), a pressurized flow shows a parabolic profile that is fastest near the center and slows down as it nears the

edges in the microfluidic devices. The particles are pinched to one side of the microchannels by a sheath flow, resulting in the difference in the position and velocity of the particles due to their sizes because the smaller particles can get closer to the wall than the larger ones. After reaching the pinched particles to the broadened channel, the particles were sorted by the position in the pinched segment owing to their sizes. Shin (Shin et al. 2017) reported tunable PFF devices by the addition of the magnification channel (Fig. 14.19A). As a typical result, the developed device enables to control the size-based classification of nano- and microparticles, which allows isolation of nano-EVs from cancer cell culture broth. This approach allows

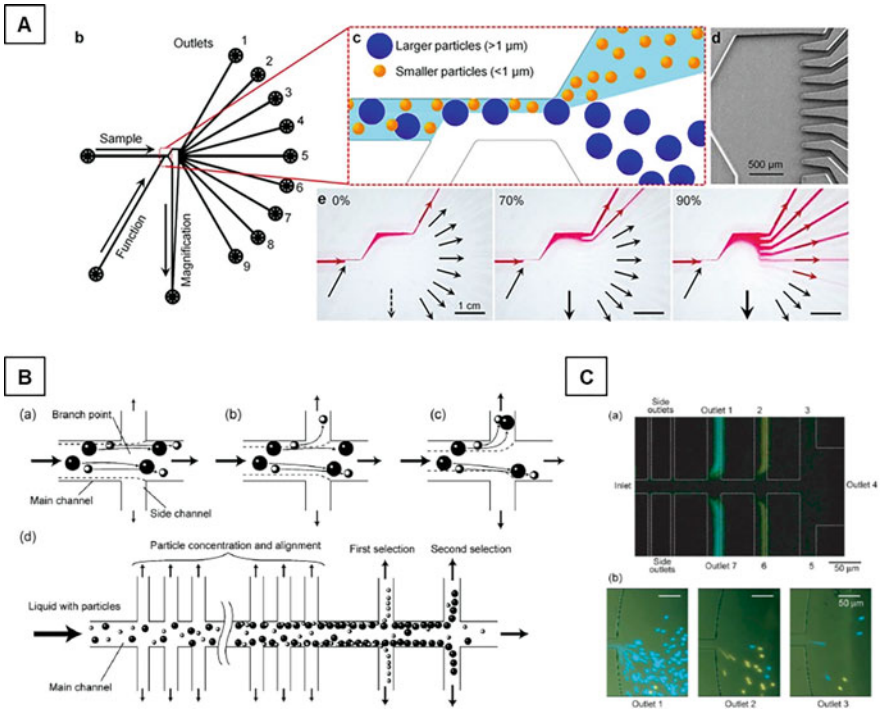

Fig. 14.19 Microfluidic chip design and operational conditions. (**A**) (b) Microchannel design consisting of two inlets (sample and function channels), nine outlets, and a magnification channel that withdraw the flow. (c) Schematic diagram of size separation of nano-vesicles and microparticles at the core region of microfluidic device (not to scale). (d) Scanning electron microscopy of the core part of the chip. (e) Pictures of sophisticated control of sample flow using the magnification channel. ((Shin et al. 2017), illustration is reconstructed with permission from Springer Nature) (**B**) Schematic diagrams showing particle behavior at a branch point; (a) the relative flow rates distributed into side channels are low, (b) medium, and (c) high. Broken lines show the virtual boundaries of the flows distributed into side and main channels. (d) Schematic diagram showing particle concentration and classification in a microchannel having multiple branch points and side channels. (**C**) Particle behavior in the microdevice. The diameters of blue and red (seen as yellow) particles were 2.1 and 3.0 mm, respectively. (a) Concentrated and separated particles at branch points connected to each outlet. (b) Particles flowing into each outlet (Yamada and Seki (2005); illustrations are reconstructed with permission from The Royal Society of Chemistry)

easy and continuous size-based sorting of the microparticles and isolation of the NPs from various samples, while the separation/sorting of different sizes of NPs is often difficult because of the limitation of the flow balance of the sample and sheath solutions at the pinched segment. The hydrodynamic filtration (HDF) was also developed by Yamada (Yamada and Seki 2005, 2006; Yamada et al. 2007), Aoki (Aoki et al. 2008), and Ozawa (Ozawa et al. 2019) demonstrated the highly effective and successive sorting of microparticles, which is also applicable for the isolation of NPs from sample mixtures. In HDF, a main microchannel is accompanied by several side branch channels that repeatedly withdraw small amounts of liquid from the main stream. As a result, particles in a main flow channel are concentrated and aligned onto the sidewalls. Then the concentrated and aligned particles can be collected according to the size through other side channels downstream the microchannel, providing both particle concentration and classification simultaneously (Yamada and Seki 2005), Fig. 14.19B, C). As in PFF, HDF enables the fine classification of microparticles, and good isolation of NPs from the mixture with microparticles. However, the concentration/classification of different sizes of NPs requires the sophisticated nano- and microfabrication technologies, which makes it difficult to have continuous classification of different sizes of NPs with good resolution to obtain the subpopulation of exosomes.

Deterministic lateral displacement (DLD) is one of the most impressive size-based separation and classification technologies for micro- and nanoparticles. In DLD devices, specifically regulated nano- or micropillar patterns are fabricated in the microfluidic channel. When the particles hydrodynamically introduced into the device pass through the DND channel, the particles collide with the patterned pillars and change their position perpendicular to the flow. The variation of the position depends on both the size of the particles and patterned pillars, resulting in the successive separation/isolation of the particles at the outlet side of the channel (Huang et al. 2004). In DLD, the size range of the separable particles depends on the critical size which is determined by the pillar displacement angle and distance between the pillars. Recent advances in the fabrication processes provide the smaller patterns in the device, which allows the separation/isolation of the smaller NPs/EVs (McGrath et al. 2014; Smith et al. 2018; Salafi et al. 2019; Hochstetter et al. 2020; Razaulla et al. 2022). Tayebi (Tayebi et al. 2021) developed the deterministic sorting device combined dielectrophoretic and acoustic field classification technologies to realize tunable sorting. As a typical result, submicron-order fine sorting of particles is successfully demonstrated by tuning the applied voltages and acoustic pressures. It was also confirmed that the developed device was also applicable to deterministic sorting of EVs with exosome purity and recovery rates higher than 95 and 81%, respectively. However, the hydrodynamic flow by the applied pressure is sometimes disadvantageous because the pressure-driven nano- and microfluidic devices often need high pressure. To simplify the experimental setup without high-pressure pumps, Hattori (Hattori et al. 2019) also developed a DLD device employed by applying voltages to generate electroosmotic flow (Fig. 14.20). The DLD methods are very well suited for separating particles that are larger than the threshold from those that are smaller. On the other hand, it is difficult to sort particles with similar

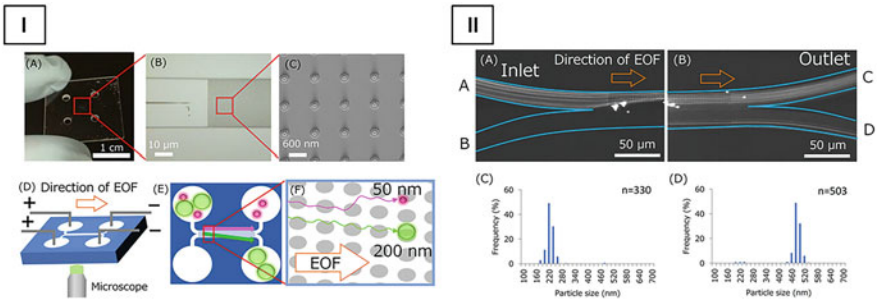

Fig. 14.20 I: Micro- and nanopillar chip for EOF-driven DLD. (**A**) Photo of the nanopillar chip. (**B**) Magnified optical microscopy image and (**C**) scanning electron microscopy image. (**D**–**F**) Working principle of the nanopillar chip. EOF transports nm-scale objects in a bumping mode (200 nm green beads) or a zigzag mode (50 nm red beads) based on the angle of the nanopillar array. II: Separation of the 200 and 500 nm fluorescent bead mixture by the micropillar chip. (**A**) Fluorescence images upstream and (**B**) downstream of the micropillar array. The samples were loaded from reservoir A, and then separated samples were collected from reservoirs **C** and **D**, followed by analysis via FE-SEM, as shown in (**C**) and (**D**), respectively (Hattori et al. (2019), permission from American Chemical Society)

sizes to the threshold value. Wunsch (Wunsch et al. 2016) demonstrated the clear separation of 50 and 110 nm NPs, while the device cannot change the distribution of the sizes of exosomes remarkably. In the near future, the fine size-based separation of exosome subclasses to analyze their characteristics based on their different sizes will be achieved through further optimization of the device using more sophisticated fabrication technologies.

Field-flow fractionation (FFF) is a flow-based separation and sorting method for various mixtures, which is also applicable to the continuous separation/classification of the nano- and microparticles (Zattoni et al. 2014; Quattrini et al. 2021; Plavchak et al. 2021; Lespes and De Carsalade Du Pont 2022; Ventouri et al. 2022). To separate/sort the molecules/particles, the liquid suspension is introduced into the microchannel in which the external field perpendicular to the direction of suspension flow is applied. As a result, the particles are sorted not only by their hydrodynamic properties but also by other properties affected by the external field. Various external fields have been applied to FFF (Fig. 14.21): DC electric field for electrophoretic separation based on charge density of the particles (Johann et al. 2015), AC electric field for dielectrophoretic separation based on the difference in the polarization property (Waheed et al. 2021), magnetic field for magnetic particles (Rogers et al. 2015), and acoustic waves for the separation based on the difference in the material properties (Hwang et al. 2019). Asymmetric-flow field-flow fractionation is a very powerful technique for the size-based analysis and separation of NPs (Marioli and Kok 2020; Nickel et al. 2021; Mildner et al. 2021). These FFF technologies have been applied to the analysis of exosomes (Petersen et al. 2018), providing fine separation of NPs and EVs from various samples.

Regarding the surface of the NPs/EVs, they have different properties such as various functional groups and molecules. In EVs, various membrane proteins are located on/in their membranes. NPs for nanoDDS also have some biofunctionalized

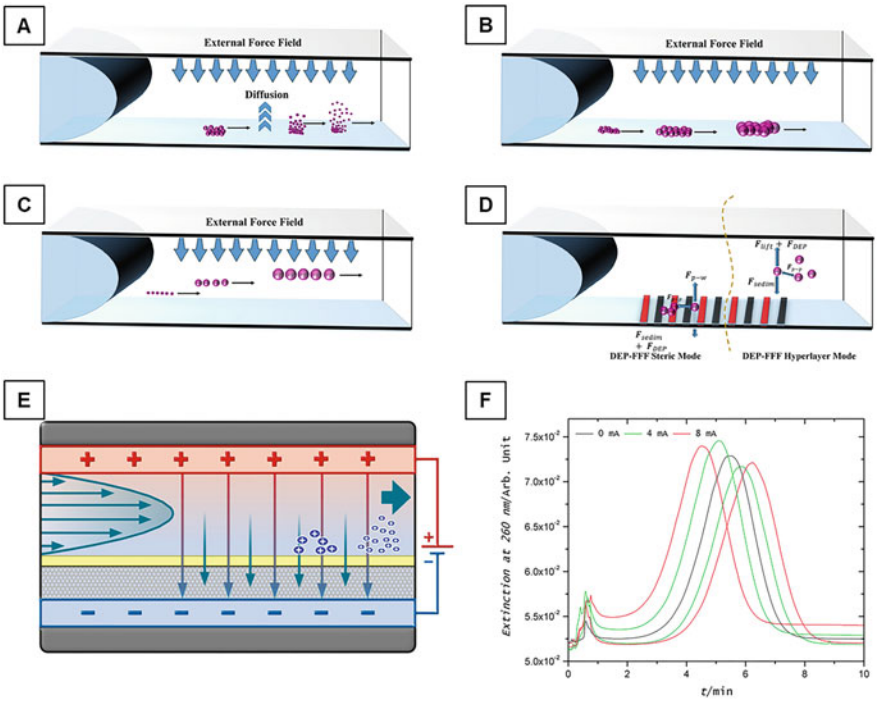

Fig. 14.21 Schematic diagrams of (**A**) normal; (**B**) steric; (**C**) hyper-layer FFF elution; and (**D**) dielectrophoretic separation modes. The particles are being transported from left to right. ((Waheed et al. 2021), illustrations are reconstructed with permission from Elsevier). (**E**) Scheme of the channel construction used for the electrical asymmetrical flow-FFF experiments. (**F**) Fractograms of sulfate stabilized spherical polystyrene latex particles (46 nm), with (red and green) and without (black) electric field (Johann et al. (2015), permission from American Chemical Society)

modules for recognizing target cells/organs. Therefore, the NPs/EVs can be separated/isolated based on the difference in the surface characteristics. The surface-based separation/isolation technologies of NPs/EVs were mainly employed by affinity interactions using various ligands such as antibody for antigens (Hung et al. 2014; Hisey et al. 2018; Brambilla et al. 2021; Zhang et al. 2021; Gwak et al. 2021; Sung et al. 2021; Wang et al. 2021b; Yu et al. 2021), lectin for glycoproteins/glycans (Konoshenko et al. 2018; Choi et al. 2021), aptamers mainly for membrane proteins (Liu et al. 2019), and so on (Kato et al. 2022). Many conventional isolations/separations of NPs/EVs have used the microbeads immobilizing the affinity ligands appropriate for the surface property of targets (affinity beads) because the target particles captured by the affinity beads can be easily gathered by centrifugation or magnetic fields. In the microfluidic devices, mainly two approaches have been studied: one is a microfluidic device of which inner surfaces were modified with affinity ligands due to their large surface/volume ratio (Hisey et al. 2018) and the other is an isolation of the affinity beads capturing NPs/EVs by the particle separation technologies based on microfluidics (Fig. 14.22)

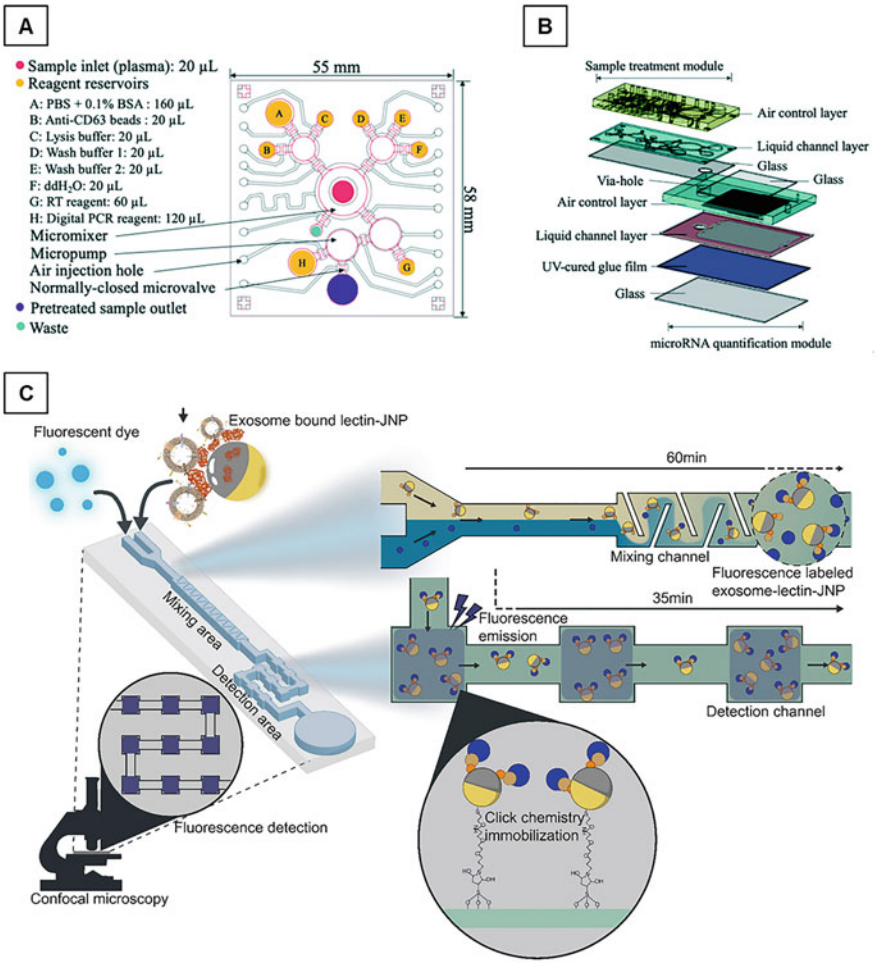

Fig. 14.22 The schematic illustrations of (**A**) the sample treatment module and (**B**) exploded view of the integrated chip for immunoaffinity assay of EVs ((Sung et al. 2021), illustrations are reconstructed with permission from the Royal Society of Chemistry). (**C**) The schematic illustration of the exo-chip system. Each sample is introduced onto the exo-chip with Janus nanoparticles (JNPs) and is then subjected to fluorescence imaging and analysis. JNPs conjugated with lectin mediate the interaction between exosomes and the substrate of the chip through the selective preference of lectins for glycans that attract exosomes and carry out click reactions (maleimide-functionalized JNPs and thiol-functionalized substrate) that bind the substrate in a laminar flow system (Choi et al. (2021), Illustration is reconstructed with permission from Elsevier)

(Hung et al. 2014; Choi et al. 2021; Gwak et al. 2021; Sung et al. 2021; Yu et al. 2021). Both strategies allow the effective affinity separation/isolation of target NPs/EVs from complex samples based on their surface properties with minimal consumption of the sample volume and shorter time compared to conventional bulk methods.

Recently, it was reported that inorganic nanowire devices are also appropriate for the surface characteristic-based separation/isolation of NPs/EVs owing to the extremely large surface/volume ratio. Wang (Wang et al. 2013) reported a nanowire-modified micropillar device that provides good isolation of exosomes. Yasui (Yasui et al. 2017; Takahashi et al. 2021) and Suwatthanarak (Suwatthanarak et al. 2021) developed dense nanowire devices for capturing exosomes in biological samples. The device has ZnO nanowires densely anchored on the bottom side of the PDMS microchannel and microfluidic herringbone structures fabricated on the top side of the channel. Effective capture of exosomes in urinary samples was achieved by utilizing both the effective mixing through the herringbone structures and the large surface/volume ratio of nanowires (Yasui et al. 2017). The investigation into the effect of the surface material of the nanowire showed that ZnO-coated nanowires with a positive zeta potential efficiently capture the exosomes with negatively charged membranes. They also studied the surface modification of nanowires with the designed bifunctional peptide, consisting of a ZnO-binding site, a linker, and an exosome-binding site for capturing and releasing exosomes (Fig. 14.23) (Suwatthanarak et al. 2021). As a typical result, effective capturing of exosomes from a cultured cell-suspended medium and downstream analysis of the miRNAs in the released exosomes were successfully demonstrated, which indicates the great potential to be applied in microfluidic platforms for exosome-based diagnostics and therapeutics.

14.5 Detection in Nanofluidic Devices

14.5.1 In Situ Detection of Electrokinetic Phenomena in a Single Nanochannel

Due to the similar dimensions with most of biomolecules, nanofluidic channels show capability to better restrict and separate the targeted biomolecules in a highly closed space than in a bulk solution space. The transparent substrates of nanofluidic devices allow optical methods for directly observing phenomena inside the closed nanospaces. However, the direct monitoring is difficult to be performed with other detection principles such as electrochemistry, atomic force microscopy, and scanning electron microscopy (SEM). This is the challenge to apply such technologies to direct contact with targeted analytes especially when the experiments or applications are conducted in closed nanoscale spaces. Recently, the in situ measurement of electrokinetic phenomenon, i.e., streaming current (I_{str}), inside a single nanofluidic channels was accomplished by employing the nano-in-nano integration technologies (Xu et al. 2015d). A pair of gold nanoelectrodes was precisely embedded inside the nanofluidic channel, where the water flowing through the nanofluidic channel by different pressure introductions and streaming currents was generated (Fig. 5.1.1(a)–(b)). The nanoelectrodes were connected using an electrometer for measuring

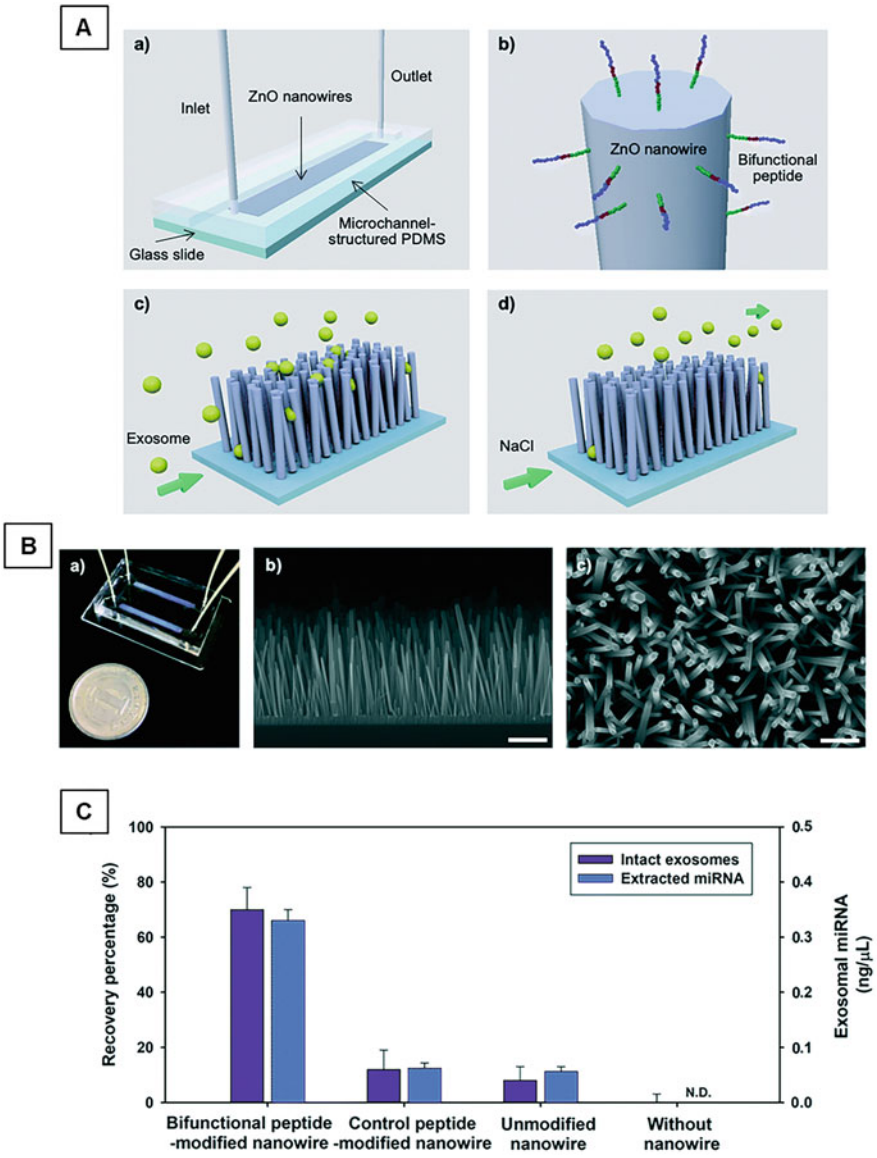

Fig. 14.23 (**A**) Schematic illustrations of the peptide-nanowire interface within a microfluidic channel for capture and release of cancer-derived exosomes. (a) The platform configuration. PDMS, polydimethylsiloxane. (b) Modification of ZnO nanowire surface with a bifunctional peptide, consisting of a ZnO-binding site (green), a linker (red), and an exosome-binding site (blue). (c) Capture of exosomes by the peptide-modified nanowire interface. (d) Release of the captured exosomes from the nanowire interface using a NaCl solution. (**B**) An image of the double-channel platform relative to a one Japanese yen coin (1.5 cm in diameter). One channel was used for one experiment. (b and c) FESEM images of the ZnO nanowires, hydrothermally grown on a glass substrate. Scale bar, 500 nm. (**C**): NTA-based exosome recovery percentage and quantification of exosomal miRNA in the released exosome suspensions. N.D., not detected. (Suwatthanarak et al. (2021), illustrations are reconstructed with permission from the Royal Society of Chemistry)

streaming currents. The results revealed that the changes of streaming current depend on the applied pressure (ΔP). However, the obtained results were significantly distinctive from the theoretical Smoluchowski values (Fig. 14.24c), indicating that the theory of bulk area may be no longer applicable for an explanation in the cases at nanospaces. This work permitted the monitoring insight phenomena in nanofluidic channels, where it used to be an "untouchable" area because of their tiny and closed spaces. The nanoelectrodes inside nanofluidic channels are a promising example in nanofluidic technology that may provide positive solutions for further studies of electrokinetic phenomena of biomolecules/drugs confined in nanospaces.

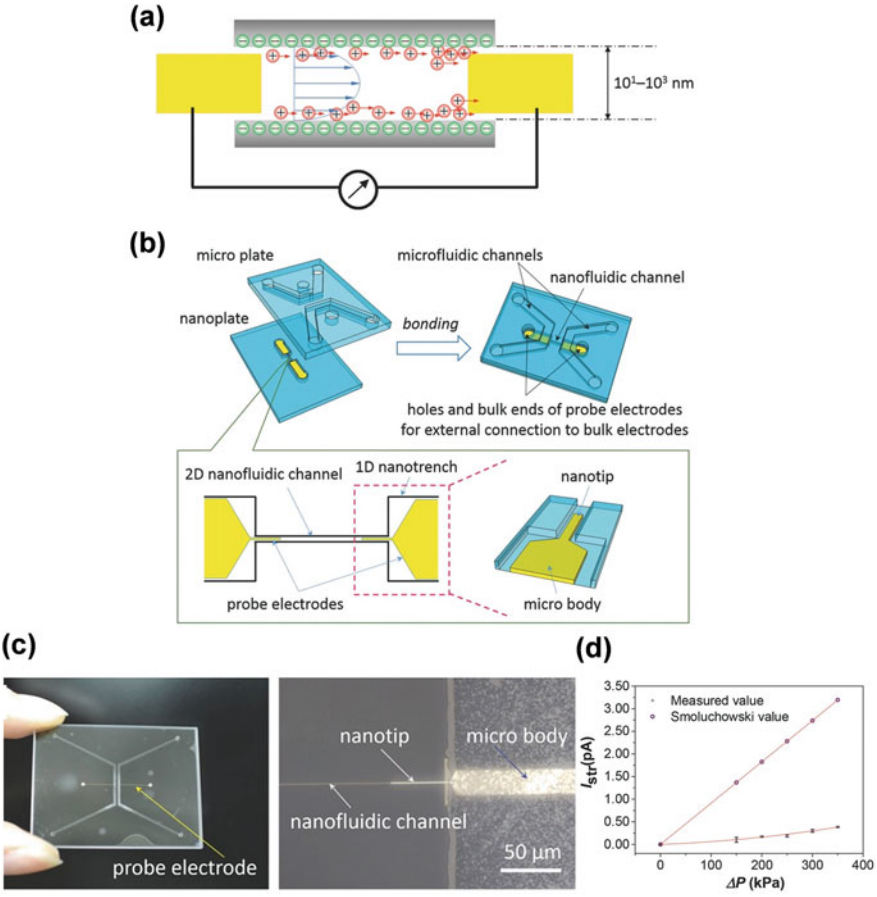

Fig. 14.24 Schematic drawing of (**a**) in situ measurement of streaming currents using (**b**) nanoelectrodes embedded in a single 2D nanochannels. (**c**) Picture of the nanofluidic device and microscopic image of nanoelectrode embedded in the single nanofluidic channel. (**d**) A comparison of the measured streaming current values with the Smoluchowski values. (Reprinted with permission from Xu et al. (2015d). Copyright 2015 Wiley-VCH)

14.5.2 Optical Detection for Nonfluorescent Molecules

Optical detection methods are important for nanofluidics because they allow simple and noninvasive measurements in confined small spaces. However, the detection of target molecules in nanochannels is challenging. Due to limited number of molecules and extremely short optical path lengths, which is often shorter than the light wavelength, the signal from target molecules is much lower than that obtained by measurements in the bulk space. Laser-induced fluorescence (LIF) has been widely utilized for nanofluidics to realize single molecule detection (Stavis et al. 2005; Fernandez-Cuesta et al. 2019). Since only the analyte emits fluorescence, high signal-to-background ratio can be easily achieved, but the analyte molecules should be labeled fluorescently or inherently fluorescent (in rare cases). The majority of molecules are nonfluorescent, and thus, optical detection of nonfluorescent molecules is required.

Several optical detection methods for nonfluorescent molecules/particles in nanochannels utilizing specific nanostructures have been reported, such as detection utilizing nanochannel arrays as diffraction gratings and surface-enhanced Raman spectroscopy and surface-enhanced infrared absorption spectroscopy utilizing metal nanostructures. These methods allowed real-time monitoring of DNA amplification (Yasui et al. 2016), tracing conformational transition of β-amyloid peptide for studies on Alzheimer's disease (Chou et al. 2008), and characterization of water structure confined in nanospaces (Le et al. 2018). However, necessity of specific nanostructures often makes fabrication and operability of nanofluidic devices difficult.

On the other hand, detection methods without any specific nanostructures have been developed. These methods allow background-free detections, in which the signal during the measurement of a blank sample is significantly reduced, in order to detect limited number of analyte molecules in a nanochannel. For characterizing viruses and nanoparticles, a method for detection of elastically scattered light from single nanoparticle utilizing a differential heterodyne interferometer was developed (Mitra et al. 2010). For measuring the absorbance of molecules, a photothermal detection method, called differential interference contrast thermal lens microscopy (DIC-TLM) or photothermal optical phase shift (POPS), has been developed (Shimizu et al. 2010; Le et al. 2020). The principle is based on the detection of a change in refractive index of the medium due to heat produced from the analyte molecules by subsequent nonradiative relaxation process with optical absorption. To detect the change of refractive index in a nanochannel, which is often smaller than light wavelengths, the principle of wave optics is employed, as illustrated in Fig. 14.25a. The photothermal effect produces a phase shift and it is detected through an interference. By this method, the limit of detection (LOD) of 390 molecules in a 500 nm nanochannel was achieved (Fig. 14.25b). In addition, by utilizing an ultraviolet laser as an excitation light for biomolecules with absorbance at 257 nm, detection of ~30 protein molecules in a nanochannel was realized (Shimizu et al. 2020).

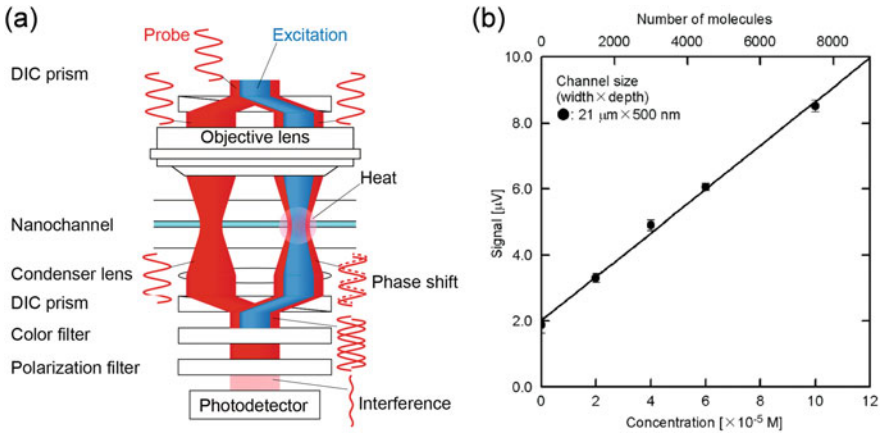

Fig. 14.25 (**a**) Principle of DIC-TLM. A probe beam (red) is separated by a DIC prism and integrated by another DIC prism. An excitation beam (blue) is not separated and induces photothermal effect. A phase shift induced by the photothermal effect is detected through an interference. (Le et al. 2020) (**b**) Calibration curve of DIC-TLM for determination of nonfluorescent dye, Sunset Yellow FCF (SY). (Reprinted with permission from Shimizu et al. (2010). Copyright 2022 American Chemical Society)

14.5.3 Method for Detection Utilizing Analytical Instruments

Currently, most of detection methods for nanofluidics is restricted to in situ and online detection of analyte molecules in nanochannels. In contrast, utilizing analytical instruments such as mass spectrometers and DNA sequencers would greatly expand applications of nanofluidic device. However, an interface to transport fL samples, containing ultrasmall amount of analyte molecules, from a nanochannel to the instruments without dispersion or dilution, is challenging.

To realize the sample transport, a micro-/nanofluidic droplet shooter utilizing two-step flow focusing by gas-phase laminar flows was developed (Kazoe et al. 2021a; Takagi et al. 2021). As illustrated in Fig. 14.26a, a liquid sample is detached from side walls of a sample channel at the first confluence point, converted to uniform droplets at the second confluence point, and shot to a deeper microchannel with trajectory control by streamlines of laminar flows. Figure 14.26b, c shows an example of a device with a 10-μm sample channel prepared by top-down glass fabrication (described in Sect. 14.2.1) and generation of droplets floating in gas phase (droplet size, 28.7 μm; droplet volume, 12.3 pL; frequency, 6.77 kHz) for ejection. By decreasing the size of sample channel to 3000 nm and utilizing Rayleigh instabilities of gas-liquid interface, generation of fL droplets (size, 11.0 μm; volume, 704 fL) was achieved.

Utilizing the micro-/nanofluidic droplet shooter, an interface for mass spectrometry (MS) was developed for transporting a sample from a nanofluidic device to a mass spectrometer, as illustrated in Fig. 14.27a (Kazoe et al. 2021b).

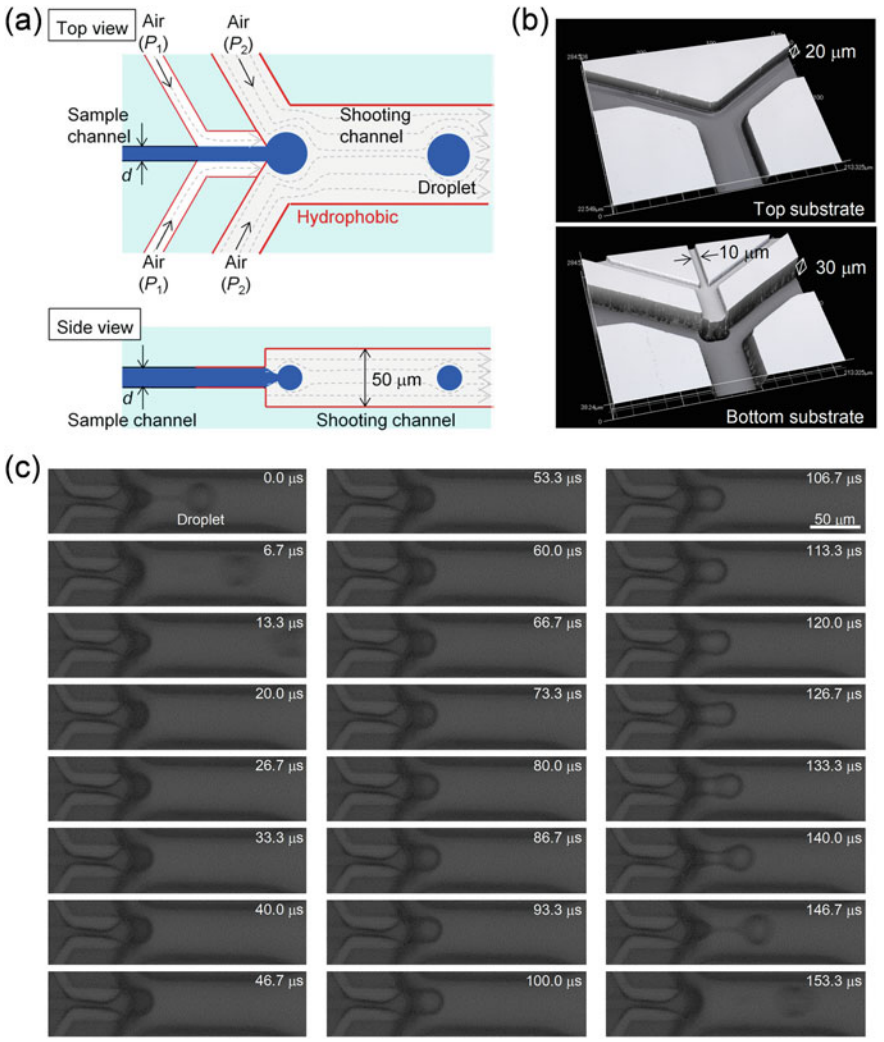

Fig. 14.26 (**a**) Schematics of micro-/nanofluidic droplet shooter utilizing two-step gas-phase flow focusing. (Reproduced from Takagi et al. (2021) with permission from Springer Nature.) (**b**) Laser scanning microscopy images of top and bottom substrates for constructing a device with a 10-μm sample channel and (**c**) droplet generation observed by a high-speed CMOS camera. A sample flow rate was 5 μm/min, and air pressures were $P_1 = 80$ kPa and $P_2 = 40$ kPa. (Reproduced from Kazoe et al. (2021a) with permission from Elsevier)

Conventionally, electrospray ionization (ESI) has been used for an MS interface. Applying a high voltage, the sample is electrically sprayed and vaporized for ionization, and analyte ions injected into a mass spectrometer are detected. However, owing to spraying, the sample injection rate into the mass spectrometer is only several percent, which causes limited sensitivity. In contrast, in the proposed

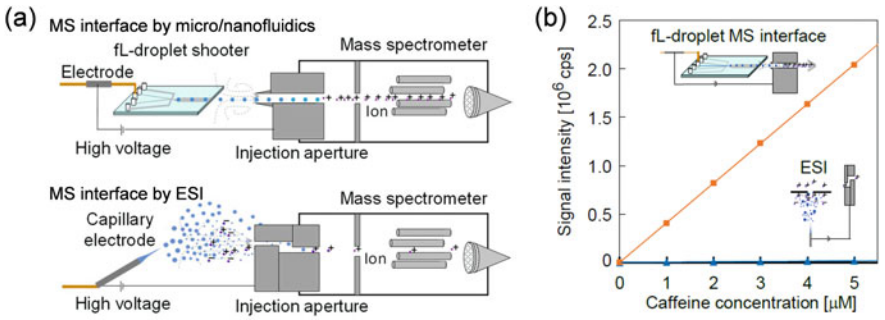

Fig. 14.27 (**a**) Comparison of an MS interface by micro-/nanofluidic droplet shooter and that by ESI. (**b**) Calibration curve for determination of caffeine contained in an aqueous solution with 0.1% formic acid at a flow rate of 1 μm/min and an applied voltage of 3 kV. (Reproduced from Kazoe et al. (2021b) with permission from the Chemical and Biological Microsystems Society (CBMS). Copyright 2022 CBMS.)

method, after applying a high voltage, the sample is ejected from a nanochannel as uniform fL droplets, and whole droplets are injected into the mass spectrometer with trajectory control, vaporized for ionization, and detected. Therefore, ultrahigh sensitivity can be achieved by 100% sample injection. As shown in Fig. 14.27(b), a 290 times higher sensitivity of caffeine ions was achieved by the proposed MS interface, compared with an MS interface utilizing ESI. The method will greatly contribute to novel applications of nanofluidics in the fields of biology, medicine, and drug screening.

14.6 Nanofluidic Devices for High-Throughput Screening

Due to the dimensions of nanofluidic devices equivalent to the sizes of biomolecules and drugs, it provides an advantage in a restriction of those molecules with better stability leading to easier observation than huge spaces like in a bulk solution. In addition, due to the ultrasmall sample volumes used in nanofluidic devices, the backgrounds can be reduced. These advantages bring the nanofluidic devices to suitably serve the researches in microscopic levels. Currently, most nanofluidic devices are having only bare nanofluidic channels with no internally functional component, which provide several limitations, in particular achieving site-specific immobilization. The site-specific immobilization is necessary in order to prevent confusion between the specific sensing and nonspecific absorption, especially when dealing with complex and numerous analyses of drug screening test. Using nano-in-nano technology is a good strategy to accomplish site-specific modification in nanofluidic channels due to its site-specific nanopatterning feature. The EB lithography with the precise placement control allows us to precisely pattern high-density array of gold nanodots inside nanofluidic channels enabling site-specific interaction

between the gold surface and other molecules via molecular self-assembly (Fig. 14.28a). Therefore, the fabricated nanofluidic devices are considered to be one of the potential platforms for the high-throughput detection and analysis of numerous biomolecules/drugs with highly site-specific immobilization. Figure 14.28b displays array of fluorescence molecules after conventional nanofluidic operation steps including sample introduction, reaction, and washing. The results show the strong fluorescence intensity at the designed locations, where gold nanoarray was precisely located, indicating its potential capability for high-throughput analysis with high specificity (Xu et al. 2015a). By using appropriate modification, other biomolecules and drugs that are important for drug studies can be detected and analyzed in the same way. Different molecules with different interaction with gold surface are simultaneously attached at the desired position before being analyzed at the same time. This is another excellent example that could promote and accelerate the utilization of nanofluidic devices for the research and applications in drug screening.

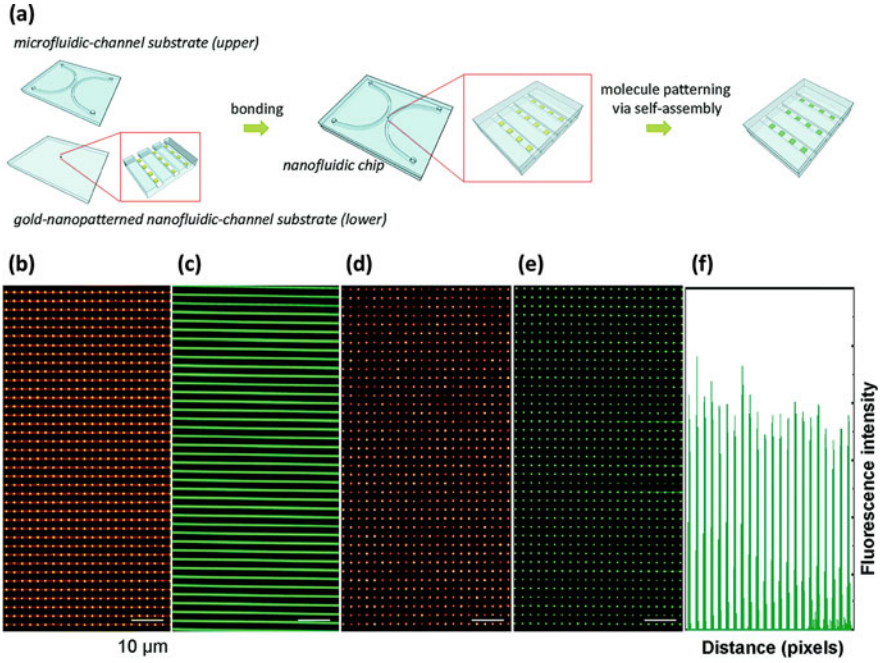

Fig. 14.28 (**a**) Schematic of the fabrication of nanofluidic device containing the array of gold nanodots in multi-nanofluidic channels used as molecule capture via self-assembly. (**b**) A bright-field microscopic image of the gold nanopatterns in nanofluidic devices before introducing liquid, and (**c**) the nanofluidic channels after filling with fluorescein solution. (**d**) A bright-field image and (**e**) a fluorescence image of the fluorescent molecules self-assembled on array of gold nanopatterns with (**f**) a fluorescence intensity of the first row of (**e**). (Reprinted with permission from Xu et al. (2015a). Copyright 2015 the Royal Society of Chemistry)

14.7 Applications

14.7.1 Single-Cell Protein Analysis

Recently, single-cell analyses have become increasingly important in the fields of biology and medicine. For example, analysis of proteins released from living single cells is indispensable to examine gene expression, cell-cell communication, and cytopathology. In drug screening, monitoring of response, resistance, and insensitivity of individual cells toward a drug is required. However, such analyses are challenging due to ultrasmall volume of single cell (pL) and ultrasmall amount of analyte molecules.

Single-cell analysis targeting nucleic acids has been achieved because nucleic acids are amplifiable by the polymerase chain reaction even if the sample volume is only pL (Shalek et al. 2013; Shapiro et al. 2013). In contrast, single-cell analysis targeting proteins is difficult. Proteins are not amplifiable and require complex chemical processing such as western blotting or enzyme-linked immunosorbent assay (ELISA). Previously, single-cell protein analyses using nL to μL wells have been reported (Tarkowski et al. 1984; Ma et al. 2011), but due to the volume of wells much larger than single cell (pL), the analyte is diluted and the sensitivity is significantly decreased. Currently, single-cell protein analyses are limited to a few approaches even for analysis of cell lysate (Eyer et al. 2012; Hughes et al. 2014). The subject is comprehensive integration of chemical processing of single-cell analysis into spaces smaller than pL to prevent dispersion-associated analyte loss.

To solve the subject, a single-cell protein analysis device based on micro-/nanofluidic was proposed and developed (Nakao et al. 2019). Chemical processing of single cell is conducted in microchannels (pL scale), and after sampling the analyte molecules produced from the single cell, chemical processing of analyte proteins is conducted in nanochannels (fL scale). As illustrated in Fig. 14.29a, according to a flowchart describing the single-cell protein analysis, chemical processing was broken down into 13-unit operations. The unit operations in cellular and molecular processing were converted into micro-unit operations (MUOs) and nano-unit operations (NUOs), respectively, which were connected by a network of micro- and nanochannels. In the analysis, (1) a living single cell is selected by an optical tweezers and captured into a pL-single cell chamber (Morikawa et al. 2021), and after (2)–(4) stimulation, (5) the supernatant is sampled by fL-volumetric pipette and (6) transported to pL flask (Nakao et al. 2020), after (7) dilution, (8) and (9) protein molecules contained in the supernatant are separated and (10)–(13) quantified by ELISA with detection of colored substrate using a high-sensitivity optical detector utilizing photothermal effect, called DIC-TLM (described in Sect. 14.5.2) (Shirai et al. 2018). Based on surface modification technologies as described in Sect. 14.2.3, hydrophilic (silanol), hydrophobic (ODS), antibody-modified, and blocking (polyethylene glycol) surfaces were incorporated into the channels to generate functions required for MUOs and NUOs. Utilizing a fabricated device as shown in Fig. 14.29b, interleukin-6 (IL-6) secreted from living single B cell was determined.

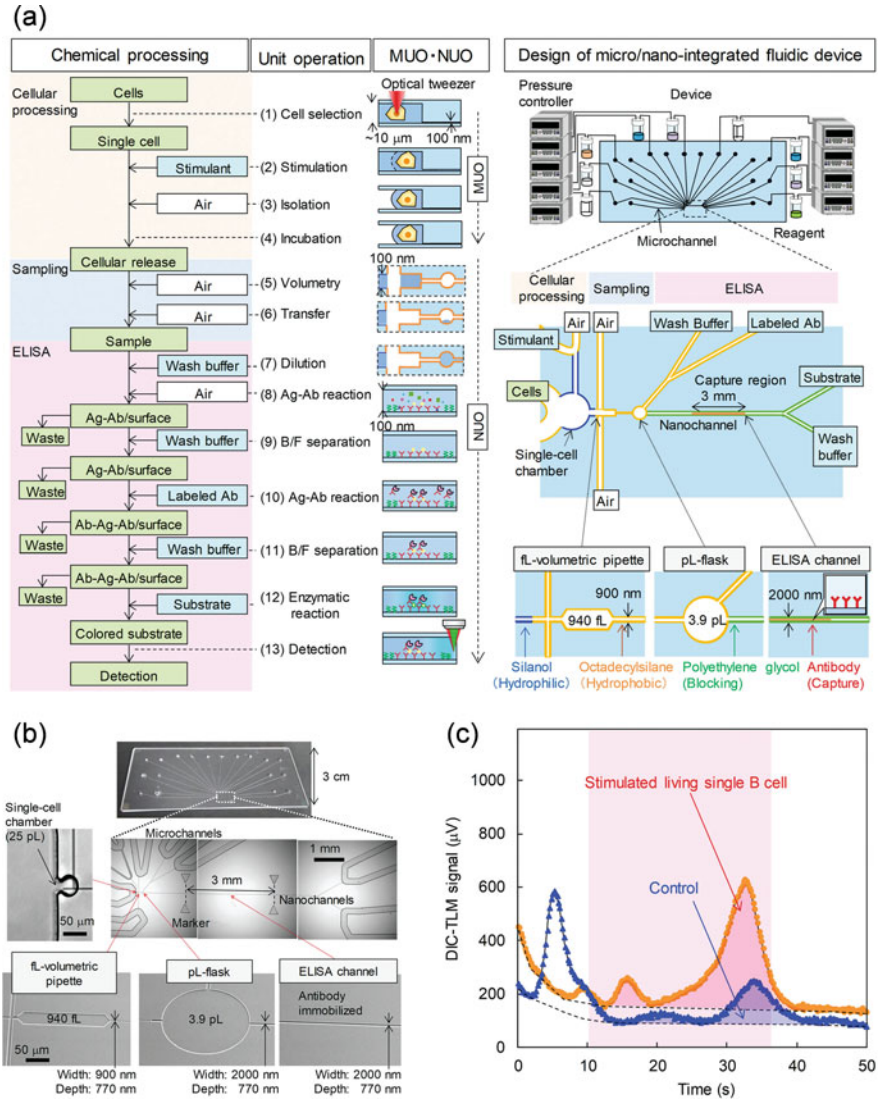

Fig. 14.29 (**a**) Design of living single-cell protein analysis device. Chemical processing is composed of four MUOs and nine NUOs, which are connected in series in micro- and nanochannels. (**b**) Fabricated micro-/nanofluidic device for living single-cell analysis. (**c**) Signals for a stimulated and unstimulated (control) living single B cells. The signals of colored substrate with ELISA detected by DIC-TLM correspond to 183 IL-6 molecules for stimulated B cell and 87.6 IL-6 molecules for unstimulated B cell. (Reproduced from Nakao et al. (2019) with permission from the Royal Society of Chemistry)

The result as shown in Fig. 14.29c indicated that the living single B cell under stimulation for 6 hours secretes 3.09×10^3 IL-6 molecules (108 ag), whereas that without stimulation (control) secretes 1.86×10^3 IL-6 molecules (64.9 ag). The developed device enabled the analysis of even a countable number of protein

molecules secreted by a living single cell, with 10^2 times higher sensitivity than previous approaches using nL to μL wells, and allows clear discrimination between pathogenic and nonpathogenic cells for identification of a therapeutic target.

14.7.2 Ultrafast Protein Digestion and Separation for Shotgun Proteomics

In drug discovery and development, proteome profiling is important to identify specific cellular responses to drug treatments (Kikuchi and Carbone 2007; Kreutz et al. 2017). Shotgun proteomics, in which the sample is digested into peptides and separated by chromatography, electrophoresis, etc., and detected by MS, is a powerful method for such purpose. However, conventionally, the digestion and separation processes often take up to a day and time consuming. Thus, analytical throughput is limited.

On the other hand, recently, an ultrafast pL enzyme reactor utilizing a nanochannel has been developed, which can greatly accelerate protein digestion (Yamamoto et al. 2020). Based on surface modification technologies as described in Sect. 14.2.3, trypsinogen, which is activated to trypsin by enterokinase, was immobilized to the nanochannel surface. Due to a 36 times higher apparent enzyme concentration by an extremely high surface-to-volume ratio compared with the bulk reactor, the enzyme reaction was accelerated 25 times. In addition, as described in Sect. 14.4.2, fL chromatography utilizing a nanochannel as a separation column has been developed to realize 100 times faster separation with ten times higher efficiency (Ishibashi et al. 2012; Smirnova et al. 2015).

Based on these NUOs, a nanofluidic device for ultrafast protein digestion and separation was developed (Yamamoto et al. 2022). As shown in Fig. 14.30a, an enzyme reactor and a separation column were integrated on a nanofluidic device. After the enzyme reaction, a sample solution is transported into an injector channel with a volume of 1 pL by opening a nanofluidic valve utilizing glass deformation (described in Sect. 14.3.1), and then driven to a separation channel. Figure 14.30b, c shows results of digestion, separation, and detection of cytochrome C. Noted that the peptide derived from cytochrome C was detected by DIC-TLM (also called POPS, described in Sect. 14.5.2). The results suggested that the digestion time of 30 min is sufficient for cytochrome C to be converted to peptide fragments, while the digestion time of 12 h was required in case of the bulk reactor. In the future, ultrafast comprehensive protein analysis by shotgun proteomics will be achieved by integrating the developed nanofluidic device and an MS interface utilizing microfluidic droplet shooter (described in Sect. 14.5.3).

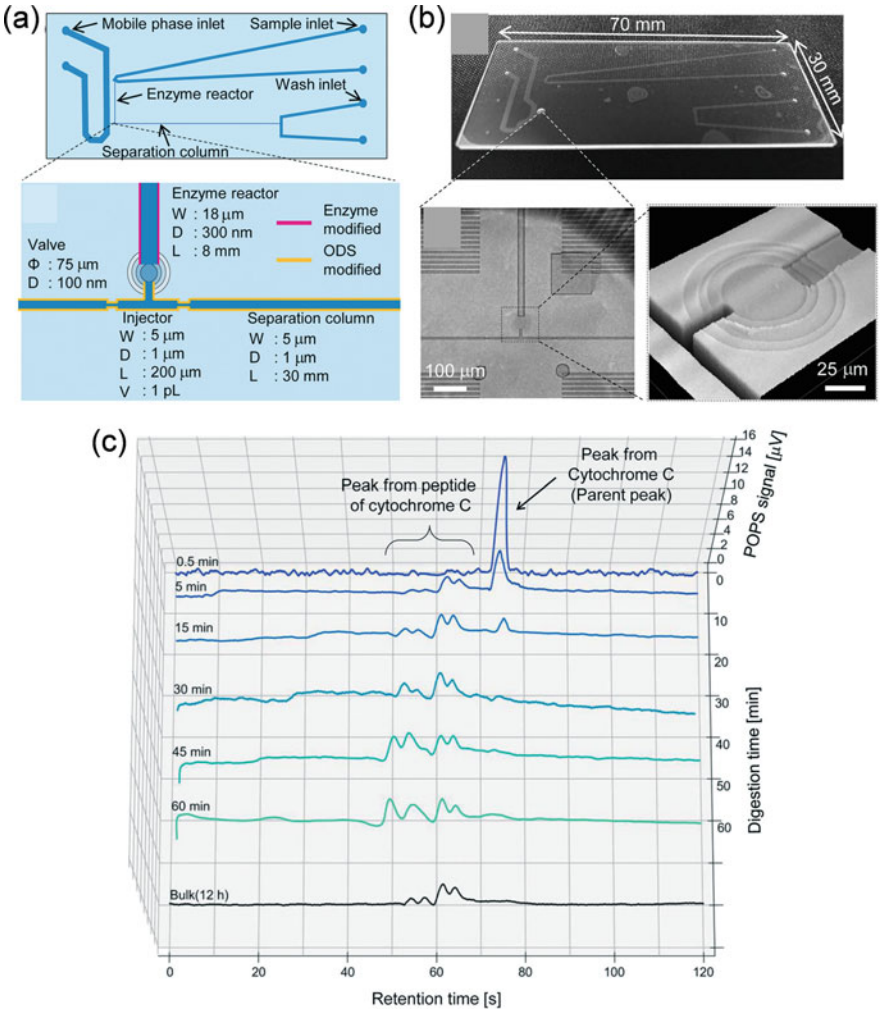

Fig. 14.30 (**a**) Design of protein digestion and separation device. An enzyme reactor and an injector of separation column are connected by a nanochannel open/close valve utilizing glass deformation. (**b**) Fabricated nanofluidic device. (**c**) Chromatogram obtained by digestion and separation of cytochrome C. (Reproduced from Yamamoto et al. (2022) with permission from the Royal Society of Chemistry)

14.8 Summary and Perspectives

We have seen a significant growth of nanotechnologies for fabricating nanofluidic devices over the past decades with varieties of fundamental studies reported by many research groups. Several applications attractive to the fields of drug discovery and development such as single-cell analysis and shotgun proteomics, which allow

analyses of rare samples with ultrasmall volumes (aL, fL, and pL) and ultrahigh sensitivity (even countable number of molecules), have been reported. Even though the nanotechnologies allow the researchers to precisely fabricate nanofluidic devices as their desired designs, size, and functions, the complicated and time-consuming procedures and high cost of the fabrications are still being obstacles to widely expand the utilization of nanofluidic devices covering multidisciplinary applications, which also include drug delivery system. Therefore, the developments to gain simpler, faster, and cheaper methodologies for the fabrication of nanofluidic devices are important and waiting to be taken actions by the researchers. The accomplishment will trigger the utilization of nanofluidic devices in wider ranges of applications, in particular the researches that focus on microscopic analysis like drug screening and drug delivery systems because nanofluidic devices have suitable spaces for handling and studying nanoscale targets such as drugs, cells, virus, exosome, and other biological entitles with the requirement of ultrasmall sample volumes. For example, sub-single cellular studies are expected to be performed (Xu et al. 2012a; Yang and Xu 2022; Chantipmanee and Xu 2023a). Furthermore, the improvement of other features such as being user friendly by developing an automated system coupling with the nanofluidic devices is interesting not only to perform experiments by a few operation steps or clicks but also to reduce possible errors from individually experimental skills of researchers which affect the reproducible results. High-throughput analysis is crucial feature of nanofluidic devices for time-limited researches, such as drug development and screening for pandemic and epidemic diseases. This not only saves time but also reduces cost of the analysis. There are many remaining features of the nanofluidic devices that are waiting to be explored by researchers to serve the needs of drug screening and drug delivery, and to discover new phenomena/reactions that are unachievable in the bulk and microscale experiments.

References

Alzhrani GN, Alanazi ST, Alsharif SY et al (2021) Exosomes: isolation, characterization, and biomedical applications. Cell Biol Int 45:1807–1831. https://doi.org/10.1002/CBIN.11620

Amarasekara CA, Athapattu US, Rathnayaka C et al (2020) Open-tubular nanoelectrochromatography (OT-NEC): gel-free separation of single stranded DNAs (ssDNAs) in thermoplastic nanochannels. Electrophoresis 41:1627–1640. https://doi.org/10.1002/ELPS.202000109

Aminorroaya S, Dippenaar R (2008) TEM analysis of centreline sulphide precipitates modified by titanium additions to low carbon steel. J Microsc 232:123–129. https://doi.org/10.1111/J.1365-2818.2008.02085.X

Aoki R, Yamada M, Yasuda M, Seki M (2008) In-channel focusing of flowing microparticles utilizing hydrodynamic filtration. Microfluid Nanofluidics 64(6):571–576. https://doi.org/10.1007/S10404-008-0334-0

Aota A, Mawatari K, Kitamori T (2009) Parallel multiphase microflows: fundamental physics, stabilization methods and applications. Lab Chip 9:2470–2476. https://doi.org/10.1039/B904430M

Aoyama C, Saeki A, Noguchi M et al (2010) Use of folded micromachined pillar Array column with low-dispersion turns for pressure-driven liquid chromatography. Anal Chem 82:1420–1426. https://doi.org/10.1021/AC902491X

Arayanarakool R, Shui L, Kengen SWM et al (2013) Single-enzyme analysis in a droplet-based micro- and nanofluidic system. Lab Chip 13:1955–1962. https://doi.org/10.1039/C3LC41100A

Bae YC, Soane D (1993) Polymeric separation media for electrophoresis: cross-linked systems or entangled solutions. J Chromatogr A 652:17–22. https://doi.org/10.1016/0021-9673(93)80640-T

Bedair M, El Rassi Z (2004) Recent advances in polymeric monolithic stationary phases for electrochromatography in capillaries and chips. Electrophoresis 25:4110–4119. https://doi.org/10.1002/ELPS.200406136

Beebe DJ, Moore JS, Bauer JM et al (2000) Functional hydrogel structures for autonomous flow control inside microfluidic channels. Nat 4046778(404):588–590. https://doi.org/10.1038/35007047

Brambilla D, Sola L, Ferretti AM et al (2021) EV separation: release of intact extracellular vesicles immunocaptured on magnetic particles. Anal Chem 93:5476–5483. https://doi.org/10.1021/ACS.ANALCHEM.0C05194/SUPPL_FILE/AC0C05194_SI_001.PDF

Casadei L, Choudhury A, Sarchet P et al (2021) Cross-flow microfiltration for isolation, selective capture and release of liposarcoma extracellular vesicles. J Extracell Vesicles 10:e12062. https://doi.org/10.1002/JEV2.12062

Chantipmanee N, Xu Y (2023a) Toward nanofluidics-based mass spectrometry for exploring the unknown complex and heterogeneous subcellular worlds. View 4:20220036. https://doi.org/10.1002/VIW.20220036

Chantipmanee N, Xu Y (2023b) Nanofluidics for chemical and biological dynamics in solution at the single molecular level. Trends Anal Chem 158:116877. https://doi.org/10.1016/j.trac.2022.116877

Chen J, Li P, Zhang T et al (2022) Review on strategies and technologies for exosome isolation and purification. Front Bioeng Biotechnol 9:1378. https://doi.org/10.3389/FBIOE.2021.811971/BIBTEX

Chen X, Zhang YS, Zhang X, Liu C (2021) Organ-on-a-chip platforms for accelerating the evaluation of nanomedicine. Bioact Mater 6:1012–1027. https://doi.org/10.1016/J.BIOACTMAT.2020.09.022

Choi Y, Park U, Koo HJ et al (2021) Exosome-mediated diagnosis of pancreatic cancer using lectin-conjugated nanoparticles bound to selective glycans. Biosens Bioelectron 177:112980. https://doi.org/10.1016/J.BIOS.2021.112980

Chou IH, Benford M, Beier HT et al (2008) Nanofluidic biosensing for β-amyloid detection using surface enhanced raman spectroscopy. Nano Lett 8:1729–1735. https://doi.org/10.1021/NL0808132/SUPPL_FILE/NL0808132-FILE002.PDF

Culbertson CT, Mickleburgh TG, Stewart-James SA et al (2014) Micro total analysis systems: fundamental advances and biological applications. Anal Chem 86:95–118. https://doi.org/10.1021/AC403688G/ASSET/IMAGES/AC403688G.SOCIAL.JPEG_V03

Davies RT, Kim J, Jang SC et al (2012) Microfluidic filtration system to isolate extracellular vesicles from blood. Lab Chip 12:5202–5210. https://doi.org/10.1039/C2LC41006K

De Malsche W, Eghbali H, Clicq D et al (2007) Pressure-driven reverse-phase liquid chromatography separations in ordered nonporous pillar Array columns. Anal Chem 79:5915–5926. https://doi.org/10.1021/AC070352P

De Malsche W, Op De Beeck J, De Bruyne S et al (2012) Realization of 1 × 10 6 theoretical plates in liquid chromatography using very long pillar array columns. Anal Chem 84:1214–1219. https://doi.org/10.1021/AC203048N/ASSET/IMAGES/AC203048N.SOCIAL.JPEG_V03

Ding L, Yang X, Gao Z et al (2021) A holistic review of the state-of-the-art microfluidics for exosome separation: an overview of the current status, existing obstacles, and future outlook. Small 17:2007174. https://doi.org/10.1002/SMLL.202007174

Dispas A, Emonts P, Fillet M (2021) Microchip electrophoresis: a suitable analytical technique for pharmaceuticals quality control? A critical review. TrAC Trends Anal Chem 139:116266. https://doi.org/10.1016/J.TRAC.2021.116266

Dittrich PS, Tachikawa K, Manz A (2006) Micro total analysis systems. latest advancements and trends. Anal Chem 78:3887–3907. https://doi.org/10.1021/AC0605602

Dong Y, Wang S, Zhao L et al (2021) Some frontier technologies for aptamers in medical applications. Aptamers Med Appl:375–403. https://doi.org/10.1007/978-981-33-4838-7_13

Eberle P, Höller C, Müller P et al (2018) Single entity resolution valving of nanoscopic species in liquids. Nat Nanotechnol 137(13):578–582. https://doi.org/10.1038/s41565-018-0150-y

Ejeta F (2021) Recent advances of microfluidic platforms for controlled drug delivery in nanomedicine. Drug Des Devel Ther 15:3881. https://doi.org/10.2147/DDDT.S324580

Eyer K, Kuhn P, Hanke C, Dittrich PS (2012) A microchamber array for single cell isolation and analysis of intracellular biomolecules. Lab Chip 12:765–772. https://doi.org/10.1039/C2LC20876H

Fernandez-Cuesta I, West MM, Montinaro E et al (2019) A nanochannel through a plasmonic antenna gap: an integrated device for single particle counting. Lab Chip 19:2394–2403. https://doi.org/10.1039/C9LC00186G

Forigua A, Kirsch RL, Willerth SM, Elvira KS (2021) Recent advances in the design of microfluidic technologies for the manufacture of drug releasing particles. J Control Release 333:258–268. https://doi.org/10.1016/J.JCONREL.2021.03.019

Fujiwara S, Morikawa K, Endo T et al (2020) Size sorting of exosomes by tuning the thicknesses of the electric double layers on a micro-nanofluidic device. Micromachines 11:458. https://doi.org/10.3390/MI11050458

Fukuda S, Xu Y (2022) A biomimetic anti-biofouling coating in nanofluidic channels. J Mater Chem B 10:2481–2489. https://doi.org/10.1039/D1TB02627E

Furukawa S, Mawatari K, Tsuyama Y et al (2021) Nano-bubble valve. Microfluid Nanofluidics 25:1–8. https://doi.org/10.1007/S10404-021-02429-8/FIGURES/9

Gonçalves IM, Carvalho V, Rodrigues RO et al (2022) Organ-on-a-Chip platforms for drug screening and delivery in tumor cells: a systematic review. Cancers 14:935. https://doi.org/10.3390/CANCERS14040935

Greve F, Frerker S, Bittermann AG et al (2007) Molecular design and characterization of the neuron–microelectrode array interface. Biomaterials 28:5246–5258. https://doi.org/10.1016/J.BIOMATERIALS.2007.08.010

Gwak H, Park S, Kim J et al (2021) Microfluidic chip for rapid and selective isolation of tumor-derived extracellular vesicles for early diagnosis and metastatic risk evaluation of breast cancer. Biosens Bioelectron 192:113495. https://doi.org/10.1016/J.BIOS.2021.113495

Hassanpour Tamrin S, Sanati Nezhad A, Sen A (2021) Label-free isolation of exosomes using microfluidic technologies. ACS Nano 15:17047–17079. https://doi.org/10.1021/ACSNANO.1C03469/ASSET/IMAGES/ACSNANO.1C03469.SOCIAL.JPEG_V03

Hattori Y, Shimada T, Yasui T et al (2019) Micro- and nanopillar chips for continuous separation of extracellular vesicles. Anal Chem 91:6514–6521. https://doi.org/10.1021/ACS.ANALCHEM.8B05538/SUPPL_FILE/AC8B05538_SI_002.MPG

He B, Tait N, Regnier F (1998) Fabrication of nanocolumns for liquid chromatography. Anal Chem 70:3790–3797. https://doi.org/10.1021/AC980028H

Hibara A, Saito T, Kim HB et al (2002) Nanochannels on a fused-silica microchip and liquid properties investigation by time-resolved fluorescence measurements. Anal Chem 74:6170–6176. https://doi.org/10.1021/AC025808B

Hisey CL, Dorayappan KDP, Cohn DE et al (2018) Microfluidic affinity separation chip for selective capture and release of label-free ovarian cancer exosomes. Lab Chip 18:3144–3153. https://doi.org/10.1039/C8LC00834E

Hochstetter A, Vernekar R, Austin RH et al (2020) Deterministic lateral displacement: challenges and perspectives. ACS Nano 14:10784–10795. https://doi.org/10.1021/ACSNANO.0C05186/ASSET/IMAGES/ACSNANO.0C05186.SOCIAL.JPEG_V03

Huang LR, Cox EC, Austin RH, Sturm JC (2004) Continuous particle separation through deterministic lateral displacement. Science (80-) 304:987–990. https://doi.org/10.1126/SCIENCE.1094567/SUPPL_FILE/HUANG.SOM.PDF

Hughes AJ, Spelke DP, Xu Z et al (2014) Single-cell western blotting. Nat Methods 117(11): 749–755. https://doi.org/10.1038/nmeth.2992

Hung LY, Chang JC, Tsai YC et al (2014) Magnetic nanoparticle-based immunoassay for rapid detection of influenza infections by using an integrated microfluidic system. Nanomed Nanotechnol Biol Med 10:819–829. https://doi.org/10.1016/J.NANO.2013.11.009

Hwang JY, Youn S, Yang IH (2019) Gravitational field flow fractionation: enhancing the resolution power by using an acoustic force field. Anal Chim Acta 1047:238–247. https://doi.org/10.1016/J.ACA.2018.09.056

Ishibashi R, Mawatari K, Kitamori T (2012) Highly efficient and ultra-small volume separation by pressure-driven liquid chromatography in extended nanochannels. Small 8:1237–1242. https://doi.org/10.1002/SMLL.201102420

Jaradat E, Weaver E, Meziane A, Lamprou DA (2021) Microfluidics technology for the design and formulation of nanomedicines. Nano 11:3440. https://doi.org/10.3390/NANO11123440

Johann C, Elsenberg S, Schuch H, Rösch U (2015) Instrument and method to determine the electrophoretic mobility of nanoparticles and proteins by combining electrical and flow field-flow fractionation. Anal Chem 87:4292–4298. https://doi.org/10.1021/AC504712N/SUPPL_FILE/AC504712N_SI_001.PDF

Kaji N, Tezuka Y, Takamura Y et al (2004) Separation of long DNA molecules by quartz nanopillar chips under a direct current electric field. Anal Chem 76:15–22. https://doi.org/10.1021/AC030303M/SUPPL_FILE/AC030303M.AVI

Kamai H, Xu Y (2021) Fabrication of ultranarrow nanochannels with ultrasmall nanocomponents in glass substrates. Micromachines 12:775. https://doi.org/10.3390/MI12070775

Kang S, Park SE, Huh DD (2021) Organ-on-a-chip technology for nanoparticle research. Nano Converg 81(8):1–15. https://doi.org/10.1186/S40580-021-00270-X

Kato M, Yamaguchi M, Morita T et al (2022) A method for purifying nanoparticles using cationic modified monoliths and aqueous elution. J Chromatogr A 1664:462802. https://doi.org/10.1016/J.CHROMA.2021.462802

Kawagishi H, Kawamata S, Xu Y (2021) Fabrication of nanoscale gas–liquid interfaces in hydrophilic/hydrophobic nanopatterned nanofluidic channels. Nano Lett 21:10555–10561. https://doi.org/10.1021/acs.nanolett.1c02871

Kawagishi H, Funano S, Tanaka Y, Xu Y (2023) Flexible glass-based hybrid nanofluidic device to enable the active regulation of single-molecule flows. Nano Lett. https://doi.org/10.1021/acs.nanolett.2c04807

Kawamata T, Yamada M, Yasuda M, Seki M (2008) Continuous and precise particle separation by electroosmotic flow control in microfluidic devices. Electrophoresis 29:1423–1430. https://doi.org/10.1002/ELPS.200700658

Kazoe Y, Pihosh Y, Takahashi H et al (2019a) Femtoliter nanofluidic valve utilizing glass deformation. Lab Chip 19:1686–1694. https://doi.org/10.1039/C8LC01340C

Kazoe Y, Shimizu Y, Morikawa K et al (2021a) Development of microfluidic droplet shooter and its application to interface for mass spectrometry. Sensors Actuators B Chem 340:129957. https://doi.org/10.1016/J.SNB.2021.129957

Kazoe Y, Takagi Y, Morikawa K (2021b) High-sensitivity detection by an interface of mass spectrometry utilizing femtoliter-droplet nanofluidics. In: The 25th International Conference on Miniaturized Systems for Chemistry and Life Sciences. Palm Springs Convention Center and Online, Palm Springs, pp 59–60

Kazoe Y, Ugajin T, Ohta R et al (2019b) Parallel multiphase nanofluidics utilizing nanochannels with partial hydrophobic surface modification and application to femtoliter solvent extraction. Lab Chip 19:3844–3852. https://doi.org/10.1039/C9LC00793H

Khan SA, Günther A, Schmidt MA, Jensen KF (2004) Microfluidic synthesis of colloidal silica. Langmuir 20:8604–8611. https://doi.org/10.1021/LA0499012/ASSET/IMAGES/LA0499012.SOCIAL.JPEG_V03

Kikuchi T, Carbone DP (2007) Proteomics analysis in lung cancer: challenges and opportunities. Respirology 12:22–28. https://doi.org/10.1111/J.1440-1843.2006.00957.X

Kim G, Park MC, Jang S et al (2021a) Diffusion-based separation of extracellular vesicles by nanoporous membrane chip. Biosens 11:347. https://doi.org/10.3390/BIOS11090347

Kim K, Park J, Jung JH et al (2021b) Cyclic tangential flow filtration system for isolation of extracellular vesicles. APL Bioeng 5:016103. https://doi.org/10.1063/5.0037768

Konoshenko MY, Lekchnov EA, Vlassov AV, Laktionov PP (2018) Isolation of extracellular vesicles: general methodologies and latest trends. Biomed Res Int 2018. https://doi.org/10.1155/2018/8545347

Kovarik ML, Ornoff DM, Melvin AT et al (2013) Micro total analysis systems: fundamental advances and applications in the laboratory, clinic, and field. Anal Chem 85:451–472. https://doi.org/10.1021/AC3031543/ASSET/IMAGES/AC3031543.SOCIAL.JPEG_V03

Kreutz D, Bileck A, Plessl K et al (2017) Response profiling using shotgun proteomics enables global metallodrug mechanisms of action to be established. Chem – A Eur J 23:1881–1890. https://doi.org/10.1002/CHEM.201604516

Larrea A, Sebastian V, Ibarra A et al (2015) Gas slug microfluidics: a unique tool for ultrafast, highly controlled growth of iron oxide nanostructures. Chem Mater 27:4254–4260. https://doi.org/10.1021/ACS.CHEMMATER.5B00284/SUPPL_FILE/CM5B00284_SI_001.PDF

Le THH, Morita A, Mawatari K et al (2018) Metamaterials-enhanced infrared spectroscopic study of nanoconfined molecules by plasmonics-nanofluidics hybrid device. ACS Photonics 5:3179–3188. https://doi.org/10.1021/ACSPHOTONICS.8B00398/SUPPL_FILE/PH8B00398_SI_001.PDF

Le THH, Shimizu H, Morikawa K (2020) Advances in label-free detections for nanofluidic analytical devices. Micromachines 11:885. https://doi.org/10.3390/MI11100885

Lee D, Park K, Seo J (2020) Recent advances in anti-inflammatory strategies for implantable biosensors and medical implants. Biochip J 14:48–62. https://doi.org/10.1007/S13206-020-4105-7/FIGURES/4

Lespes G, De Carsalade Du Pont V (2022) Field-flow fractionation for nanoparticle characterization. J Sep Sci 45:347–368. https://doi.org/10.1002/JSSC.202100595

Liu C, Zhao J, Tian F et al (2019) I-DNA- and aptamer-mediated sorting and analysis of extracellular vesicles. J Am Chem Soc 141:3817–3821. https://doi.org/10.1021/JACS.9B00007/SUPPL_FILE/JA9B00007_SI_001.PDF

Liu Y, Sun L, Zhang H et al (2021) Microfluidics for drug development: from synthesis to evaluation. Chem Rev 121:7468–7529. https://doi.org/10.1021/ACS.CHEMREV.0C01289/ASSET/IMAGES/ACS.CHEMREV.0C01289.SOCIAL.JPEG_V03

Ma C, Fan R, Ahmad H et al (2011) A clinical microchip for evaluation of single immune cells reveals high functional heterogeneity in phenotypically similar T cells. Nat Med 176(17):738–743. https://doi.org/10.1038/nm.2375

Maenaka H, Yamada M, Yasuda M, Seki M (2008) Continuous and size-dependent sorting of emulsion droplets using hydrodynamics in pinched microchannels. Langmuir 24:4405–4410. https://doi.org/10.1021/LA703581J/SUPPL_FILE/LA703581J-FILE002.AVI

Malloggi F, Pannacci N, Attia R et al (2010) Monodisperse colloids synthesized with nanofluidic technology. Langmuir 26:2369–2373. https://doi.org/10.1021/LA9028047/SUPPL_FILE/LA9028047_SI_002.PDF

Manz A, Graber N, Widmer HM (1990) Miniaturized total chemical analysis systems: a novel concept for chemical sensing. Sensors Actuators B Chem 1:244–248. https://doi.org/10.1016/0925-4005(90)80209-I

Marioli M, Kok WT (2020) Continuous asymmetrical flow field-flow fractionation for the purification of proteins and nanoparticles. Sep Purif Technol 242:116744. https://doi.org/10.1016/J.SEPPUR.2020.116744

Mawatari K, Kazoe Y, Aota A et al (2011) Microflow systems for chemical synthesis and analysis: approaches to full integration of chemical process. J Flow Chem 11(1):3–12. https://doi.org/10.1556/JFCHEM.2011.00003

Mawatari K, Kazoe Y, Shimizu H et al (2014) Extended-nanofluidics: fundamental technologies, unique liquid properties, and application in chemical and bio analysis methods and devices. Anal Chem 86:4068–4077. https://doi.org/10.1021/AC4026303

Mawatari K, Kubota S, Xu Y et al (2012) Femtoliter droplet handling in nanofluidic channels: a Laplace Nanovalve. Anal Chem 84:10812–10816. https://doi.org/10.1021/AC3028905

McGrath J, Jimenez M, Bridle H (2014) Deterministic lateral displacement for particle separation: a review. Lab Chip 14:4139–4158. https://doi.org/10.1039/C4LC00939H

Menard LD, Mair CE, Woodson ME et al (2012) A device for performing lateral conductance measurements on individual double-stranded DNA molecules. ACS Nano 6:9087–9094. https://doi.org/10.1021/NN303322R/ASSET/IMAGES/NN303322R.SOCIAL.JPEG_V03

Mildner R, Hak S, Parot J et al (2021) Improved multidetector asymmetrical-flow field-flow fractionation method for particle sizing and concentration measurements of lipid-based nanocarriers for RNA delivery. Eur J Pharm Biopharm 163:252–265. https://doi.org/10.1016/J.EJPB.2021.03.004

Mitra A, Deutsch B, Ignatovich F et al (2010) Nano-optofluidic detection of single viruses and nanoparticles. ACS Nano 4:1305–1312. https://doi.org/10.1021/NN901889V/SUPPL_FILE/NN901889V_SI_001.PDF

Moghadam SH, Dinarvand R, Cartilier LH (2006) The focused ion beam technique: a useful tool for pharmaceutical characterization. Int J Pharm 321:50–55. https://doi.org/10.1016/J.IJPHARM.2006.05.006

Morijiri T, Sunahiro S, Senaha M et al (2011) Sedimentation pinched-flow fractionation for size- and density-based particle sorting in microchannels. Microfluid Nanofluidics 111(11):105–110. https://doi.org/10.1007/S10404-011-0785-6

Morikawa K, Kazoe Y, Takagi Y et al (2020) Advanced top-down fabrication for a fused silica nanofluidic device. Micromachines 11:995. https://doi.org/10.3390/MI11110995

Morikawa K, Murata SI, Kazoe Y et al (2021) Picoliter liquid handling at gas/liquid interface by surface and geometry control in a micro-nanofluidic device. J Micromechanics Microengineering 32:024001. https://doi.org/10.1088/1361-6439/AC4006

Nakao T, Kazoe Y, Mori E et al (2019) Cytokine analysis on a countable number of molecules from living single cells on nanofluidic devices. Analyst 144:7200–7208. https://doi.org/10.1039/C9AN01702J

Nakao T, Kazoe Y, Morikawa K et al (2020) Femtoliter volumetric pipette and flask utilizing nanofluidics. Analyst 145:2669–2675. https://doi.org/10.1039/C9AN02258A

Nam Y (2012) Material considerations for in vitro neural interface technology. MRS Bull 376(37):566–572. https://doi.org/10.1557/MRS.2012.98

Nickel C, Scherer C, Noskov S et al (2021) Observation of interaction forces by investigation of the influence of eluent additives on the retention behavior of aqueous nanoparticle dispersions in asymmetrical flow field-flow fractionation. J Chromatogr A 1637:461840. https://doi.org/10.1016/J.CHROMA.2020.461840

Nys G, Cobraiville G, Fillet M (2019) Multidimensional performance assessment of micro pillar array column chromatography combined to ion mobility-mass spectrometry for proteome research. Anal Chim Acta 1086:1–13. https://doi.org/10.1016/J.ACA.2019.08.068

Ouyang H, Xia Z, Zhe J (2010) Voltage-controlled flow regulating in nanofluidic channels with charged polymer brushes. Microfluid Nanofluidics 9:915–922. https://doi.org/10.1007/S10404-010-0614-3/FIGURES/7

Ozawa R, Iwadate H, Toyoda H et al (2019) A numbering-up strategy of hydrodynamic microfluidic filters for continuous-flow high-throughput cell sorting. Lab Chip 19:1828–1837. https://doi.org/10.1039/C9LC00053D

Patabadige DEW, Jia S, Sibbitts J et al (2016) Micro Total analysis systems: fundamental advances and applications. Anal Chem 88:320–338. https://doi.org/10.1021/ACS.ANALCHEM.5B04310/ASSET/IMAGES/ACS.ANALCHEM.5B04310.SOCIAL.JPEG_V03

Pearce TM, Williams JC (2006) Microtechnology: meet neurobiology. Lab Chip 7:30–40. https://doi.org/10.1039/B612856B

Petersen KE, Shiri F, White T et al (2018) Exosome isolation: cyclical electrical field flow fractionation in low-ionic-strength fluids. Anal Chem 90:12783–12790. https://doi.org/10.1021/ACS.ANALCHEM.8B03146/SUPPL_FILE/AC8B03146_SI_001.PDF

Plavchak CL, Smith WC, Bria CRM, Williams SKR (2021) New advances and applications in field-flow fractionation. 14:257–279. https://doi.org/10.1146/ANNUREV-ANCHEM-091520-052742

Quattrini F, Berrecoso G, Crecente-Campo J, Alonso MJ (2021) Asymmetric flow field-flow fractionation as a multifunctional technique for the characterization of polymeric nanocarriers. Drug Deliv Transl Res 11:373–395. https://doi.org/10.1007/S13346-021-00918-5/FIGURES/6

Rahimnejad M, Rabiee N, Ahmadi S et al (2021) Emerging phospholipid nanobiomaterials for biomedical applications to Lab-on-a-Chip, drug delivery, and cellular engineering. ACS Appl Bio Mater. https://doi.org/10.1021/ACSABM.1C00932

Rahong S, Yasui T, Yanagida T et al (2014) Ultrafast and wide range analysis of DNA molecules using rigid network structure of solid nanowires. Sci Rep 41(4):1–8. https://doi.org/10.1038/srep05252

Rahong S, Yasui T, Yanagida T et al (2015a) Self-assembled nanowire arrays as three-dimensional nanopores for filtration of DNA molecules. Anal Sci 31:153–157. https://doi.org/10.2116/ANALSCI.31.153

Rahong S, Yasui T, Yanagida T et al (2015b) Three-dimensional nanowire structures for ultra-fast separation of DNA, Protein and RNA Molecules. Sci Rep 51(5):1–9. https://doi.org/10.1038/srep10584

Rai PK, Kumar V, Sonne C et al (2021) Progress, prospects, and challenges in standardization of sampling and analysis of micro- and nano-plastics in the environment. J Clean Prod 325:129321. https://doi.org/10.1016/J.JCLEPRO.2021.129321

Razaulla TM, Young OM, Alsharhan A et al (2022) Deterministic lateral displacement using hexagonally arranged, bottom-up-inspired micropost arrays. Anal Chem 94:1949–1957. https://doi.org/10.1021/ACS.ANALCHEM.1C03035/SUPPL_FILE/AC1C03035_SI_001.PDF

Ren Y, Ge K, Sun D et al (2022) Rapid enrichment and sensitive detection of extracellular vesicles through measuring the phospholipids and transmembrane protein in a microfluidic chip. Biosens Bioelectron 199:113870. https://doi.org/10.1016/J.BIOS.2021.113870

Rogers HB, Anani T, Choi YS et al (2015) Exploiting size-dependent drag and magnetic forces for size-specific separation of magnetic nanoparticles. Int J Mol Sci 16:20001–20019. https://doi.org/10.3390/IJMS160820001

Salafi T, Zeming KK, Zhang Y (2016) Advancements in microfluidics for nanoparticle separation. Lab Chip 17:11–33. https://doi.org/10.1039/C6LC01045H

Salafi T, Zhang Y, Zhang Y (2019) A review on deterministic lateral displacement for particle separation and detection. Nano-Micro Lett 111(11):1–33. https://doi.org/10.1007/S40820-019-0308-7

Sano H, Kazoe Y, Morikawa K, Kitamori T (2020) Implementation of a nanochannel open/close valve into a glass nanofluidic device. Microfluid Nanofluidics 24:1–11. https://doi.org/10.1007/S10404-020-02383-X/FIGURES/7

Sato Y, Bettini R, Ma Z et al (2022) Recent development of drug delivery systems through microfluidics: from synthesis to evaluation. Pharm 14:434. https://doi.org/10.3390/PHARMACEUTICS14020434

Seetasang S, Xu Y (2022) Recent progress and perspectives in applications of 2-methacryloyloxyethyl phosphorylcholine polymers in biodevices at small scales. J Mater Chem B 10:2323–2337. https://doi.org/10.1039/D1TB02675E

Shalek AK, Satija R, Adiconis X et al (2013) Single-cell transcriptomics reveals bimodality in expression and splicing in immune cells. Nat 4987453(498):236–240. https://doi.org/10.1038/nature12172

Shapiro E, Biezuner T, Linnarsson S (2013) Single-cell sequencing-based technologies will revolutionize whole-organism science. Nat Rev Genet 149(14):618–630. https://doi.org/10.1038/nrg3542

Shepherd SJ, Issadore D, Mitchell MJ (2021) Microfluidic formulation of nanoparticles for biomedical applications. Biomaterials 274:120826. https://doi.org/10.1016/J.BIOMATERIALS.2021.120826

Shimizu H, Mawatari K, Kitamori T (2010) Sensitive determination of concentration of nonfluorescent species in an extended-nano channel by differential interference contrast thermal lens microscope. Anal Chem 82:7479–7484. https://doi.org/10.1021/AC1017088

Shimizu H, Morikawa K, Liu Y et al (2016) Femtoliter high-performance liquid chromatography using extended-nano channels. Analyst 141:6068–6072. https://doi.org/10.1039/C6AN01195K

Shimizu H, Takeda S, Mawatari K, Kitamori T (2020) Ultrasensitive detection of nonlabelled bovine serum albumin using photothermal optical phase shift detection with UV excitation. Analyst 145:2580–2585. https://doi.org/10.1039/D0AN00037J

Shin S, Han D, Park MC et al (2017) Separation of extracellular nanovesicles and apoptotic bodies from cancer cell culture broth using tunable microfluidic systems. Sci Rep 71(7):1–8. https://doi.org/10.1038/s41598-017-08826-w

Shirai K, Mawatari K, Kitamori T (2014) Extended nanofluidic immunochemical reaction with femtoliter sample volumes. Small 10:1514–1522. https://doi.org/10.1002/SMLL.201302709

Shirai K, Mawatari K, Ohta R et al (2018) A single-molecule ELISA device utilizing nanofluidics. Analyst 143:943–948. https://doi.org/10.1039/C7AN01144J

Shui L, Van Den Berg A, Eijkel JCT (2011) Scalable attoliter monodisperse droplet formation using multiphase nano-microfluidics. Microfluid Nanofluidics 11:87–92. https://doi.org/10.1007/S10404-011-0776-7/FIGURES/5

Smirnova A, Shimizu H, Mawatari K, Kitamori T (2015) Reversed-phase chromatography in extended-nano space for the separation of amino acids. J Chromatogr A 1418:224–227. https://doi.org/10.1016/J.CHROMA.2015.09.022

Smith JT, Wunsch BH, Dogra N et al (2018) Integrated nanoscale deterministic lateral displacement arrays for separation of extracellular vesicles from clinically-relevant volumes of biological samples. Lab Chip 18:3913–3925. https://doi.org/10.1039/C8LC01017J

Soliman HM, Ghonaim GA, Gharib SM et al (2021) Exosomes in Alzheimer's disease: from being pathological players to potential diagnostics and therapeutics. Int J Mol Sci 22:10794. https://doi.org/10.3390/IJMS221910794

Song Y, Takatsuki K, Isokawa M et al (2013) Fast and quantitative analysis of branched-chain amino acids in biological samples using a pillar array column. Anal Bioanal Chem 40525(405):7993–7999. https://doi.org/10.1007/S00216-013-7034-7

Spira ME, Hai A (2013) Multi-electrode array technologies for neuroscience and cardiology. Nat Nanotechnol 82(8):83–94. https://doi.org/10.1038/nnano.2012.265

Staicu CE, Jipa F, Axente E et al (2021) Lab-on-a-Chip platforms as tools for drug screening in neuropathologies associated with blood–brain barrier alterations. Biomol Ther 11:916. https://doi.org/10.3390/BIOM11060916

Stavis SM, Edel JB, Samiee KT, Craighead HG (2005) Single molecule studies of quantum dot conjugates in a submicrometer fluidic channel. Lab Chip 5:337–343. https://doi.org/10.1039/B416161K

Sundaram PM, Casadei L, Lopez G et al (2020) Multi-layer micro-nanofluidic device for isolation and capture of extracellular vesicles derived from liposarcoma cell conditioned media. J Microelectromech Syst 29:776. https://doi.org/10.1109/JMEMS.2020.3006786

Sung CY, Huang CC, Chen YS et al (2021) Isolation and quantification of extracellular vesicle-encapsulated microRNA on an integrated microfluidic platform. Lab Chip 21:4660–4671. https://doi.org/10.1039/D1LC00663K

Suwatthanarak T, Thiodorus IA, Tanaka M et al (2021) Microfluidic-based capture and release of cancer-derived exosomes via peptide–nanowire hybrid interface. Lab Chip 21:597–607. https://doi.org/10.1039/D0LC00899K

Takagi Y, Kazoe Y, Kitamori T (2021) Generation of femtoliter liquid droplets in gas phase by microfluidic droplet shooter. Microfluid Nanofluidics 25:1–8. https://doi.org/10.1007/S10404-021-02474-3/FIGURES/10

Takahashi H, Baba Y, Yasui T (2021) Oxide nanowire microfluidics addressing previously-unattainable analytical methods for biomolecules towards liquid biopsy. Chem Commun 57:13234–13245. https://doi.org/10.1039/D1CC05096F

Takei G, Nonogi M, Hibara A et al (2007) Tuning microchannel wettability and fabrication of multiple-step Laplace valves. Lab Chip 7:596–602. https://doi.org/10.1039/B618851F

Tarkowski A, Czerkinsky C, Nilsson LÅ et al (1984) Solid-phase enzyme-linked immunospot (ELISPOT) assay for enumeration of IgG rheumatoid factor-secreting cells. J Immunol Methods 72:451–459. https://doi.org/10.1016/0022-1759(84)90013-9

Tayebi M, Yang D, Collins DJ, Ai Y (2021) Deterministic sorting of submicrometer particles and extracellular vesicles using a combined electric and acoustic field. Nano Lett 21:6835–6842. https://doi.org/10.1021/ACS.NANOLETT.1C01827/SUPPL_FILE/NL1C01827_SI_006.MP4

Thamdrup LH, Klukowska A, Kristensen A (2008) Stretching DNA in polymer nanochannels fabricated by thermal imprint in PMMA. Nanotechnology 19:125301. https://doi.org/10.1088/0957-4484/19/12/125301

Tsukahara T, Mawatari K, Hibara A, Kitamori T (2008) Development of a pressure-driven nanofluidic control system and its application to an enzymatic reaction. Anal Bioanal Chem 391:2745–2752. https://doi.org/10.1007/S00216-008-2198-2/FIGURES/6

Tsuyama Y, Morikawa K, Mawatari K (2020) Nanochannel chromatography and photothermal optical diffraction: femtoliter sample separation and label-free zeptomole detection. J Chromatogr A 1624:461265. https://doi.org/10.1016/J.CHROMA.2020.461265

Tsuyama Y, Morikawa K, Mawatari K (2021) Integration of sequential analytical processes into sub-100 nm channels: volumetric sampling, chromatographic separation, and label-free molecule detection. Nanoscale 13:8855–8863. https://doi.org/10.1039/D0NR08385B

Tzaridis T, Bachurski D, Liu S et al (2021) Extracellular vesicle separation techniques impact results from human blood samples: considerations for diagnostic applications. Int J Mol Sci 22:9211. https://doi.org/10.3390/IJMS22179211

Unger MA, Chou HP, Thorsen T et al (2000) Monolithic microfabricated valves and pumps by multilayer soft lithography. Science (80-) 288:113–116. https://doi.org/10.1126/SCIENCE.288.5463.113/ASSET/B92DF262-1777-4B31-B723-D0727EA2448E/ASSETS/GRAPHIC/SE1108400004.JPEG

Vangelooven J, Schlautman S, Detobel F et al (2010) Experimental optimization of flow distributors for pressure-driven separations and reactions in flat-rectangular microchannels. Anal Chem 83:467–477. https://doi.org/10.1021/AC101304P

Ventouri IK, Loeber S, Somsen GW et al (2022) Field-flow fractionation for molecular-interaction studies of labile and complex systems: a critical review. Anal Chim Acta 1193:339396. https://doi.org/10.1016/J.ACA.2021.339396

Vilchis RJS, Hotta Y, Yamamoto K (2007) Examination of enamel-adhesive interface with focused ion beam and scanning electron microscopy. Am J Orthod Dentofac Orthop 131:646–650. https://doi.org/10.1016/J.AJODO.2006.11.017

Vilkner T, Janasek D, Manz A (2004) Micro Total analysis systems. recent developments. Anal Chem 76:3373–3386. https://doi.org/10.1021/AC040063Q

Waheed W, Sharaf OZ, Alazzam A, Abu-Nada E (2021) Dielectrophoresis-field flow fractionation for separation of particles: a critical review. J Chromatogr A 1637:461799. https://doi.org/10.1016/J.CHROMA.2020.461799

Wang L, Pan MM, Xu L et al (2021a) Recent advances of emerging microfluidic chips for exosome mediated cancer diagnosis. Smart Mater Med 2:158–171. https://doi.org/10.1016/J.SMAIM.2021.06.001

Wang YT, Di CM, Sun LL, Hua RN (2021b) A rapid and facile separation-detection integrated strategy for exosome profiling based on boronic acid-directed coupling immunoaffinity. Anal Chem 93:16059–16067. https://doi.org/10.1021/ACS.ANALCHEM.1C03643/SUPPL_FILE/AC1C03643_SI_001.PDF

Wang Z, Samanipour R, Kim K (2016) Organ-on-a-Chip platforms for drug screening and tissue engineering. Biomed Eng Front Res Converging Technol 9:209–233. https://doi.org/10.1007/978-3-319-21813-7_10

Wang Z, Wu HJ, Fine D et al (2013) Ciliated micropillars for the microfluidic-based isolation of nanoscale lipid vesicles. Lab Chip 13:2879–2882. https://doi.org/10.1039/C3LC41343H

West J, Becker M, Tombrink S, Manz A (2008) Micro total analysis systems: latest achievements. Anal Chem 80:4403–4419. https://doi.org/10.1021/AC800680J

Wu P, Zhang B, Ocansey DKW et al (2021) Extracellular vesicles: a bright star of nanomedicine. Biomaterials 269:120467. https://doi.org/10.1016/J.BIOMATERIALS.2020.120467

Wunsch BH, Smith JT, Gifford SM et al (2016) Nanoscale lateral displacement arrays for the separation of exosomes and colloids down to 20 nm. Nat Nanotechnol 1111(11):936–940. https://doi.org/10.1038/nnano.2016.134

Xie J, Miao Y, Shih J et al (2005) Microfluidic platform for liquid chromatography−tandem mass spectrometry analyses of complex peptide mixtures. Anal Chem 77:6947–6953. https://doi.org/10.1021/AC0510888

Xu Y (2018) Nanofluidics: a new arena for materials science. Adv Mater 30:1702419. https://doi.org/10.1002/ADMA.201702419

Xu Y, Jang K, Konno T et al (2010a) The biological performance of cell-containing phospholipid polymer hydrogels in bulk and microscale form. Biomaterials 31:8839–8846. https://doi.org/10.1016/J.BIOMATERIALS.2010.07.106

Xu Y, Jang K, Yamashita T et al (2012a) Microchip-based cellular biochemical systems for practical applications and fundamental research: from microfluidics to nanofluidics. Anal Bioanal Chem 402:99–107. https://doi.org/10.1007/S00216-011-5296-5/FIGURES/6

Xu Y, Matsumoto N (2015) Flexible and in situ fabrication of nanochannels with high aspect ratios and nanopillar arrays in fused silica substrates utilizing focused ion beam. RSC Adv 5:50638–50643. https://doi.org/10.1039/C5RA06306J

Xu Y, Matsumoto N, Wu Q et al (2015a) Site-specific nanopatterning of functional metallic and molecular arbitrary features in nanofluidic channels. Lab Chip 15:1989–1993. https://doi.org/10.1039/C5LC00190K

Xu Y, Mawatari K, Konno T et al (2015b) Spontaneous packaging and hypothermic storage of mammalian cells with a cell-membrane-mimetic polymer hydrogel in a microchip. ACS Appl Mater Interfaces 7:23089–23097. https://doi.org/10.1021/ACSAMI.5B06796

Xu Y, Sato K, Mawatari K et al (2010b) A microfluidic hydrogel capable of cell preservation without perfusion culture under cell-based assay conditions. Adv Mater 22:3017–3021. https://doi.org/10.1002/ADMA.201000006

Xu Y, Shinomiya M, Harada A (2016) Soft matter-regulated active nanovalves locally self-assembled in femtoliter nanofluidic channels. Adv Mater 28:2209–2216. https://doi.org/10.1002/ADMA.201505132

Xu Y, Takai M, Ishihara K (2009a) Suppression of protein adsorption on a charged phospholipid polymer interface. Biomacromolecules 10:267–274. https://doi.org/10.1021/bm801279y

Xu Y, Takai M, Ishihara K (2009b) Protein adsorption and cell adhesion on cationic, neutral, and anionic 2-methacryloyloxyethyl phosphorylcholine copolymer surfaces. Biomaterials 30:4930–4938. https://doi.org/10.1016/J.BIOMATERIALS.2009.06.005

Xu Y, Takai M, Ishihara K (2010c) Phospholipid polymer biointerfaces for Lab-on-a-Chip devices. Ann Biomed Eng 386(38):1938–1953. https://doi.org/10.1007/S10439-010-0025-3

Xu Y, Takai M, Ishihara K (2021) Functional coatings for lab-on-a-chip systems based on phospholipid polymers. In: Handbook of Modern Coating Technologies. Elsevier, pp 555–595

Xu Y, Takai M, Konno T, Ishihara K (2007) Microfluidic flow control on charged phospholipid polymer interface. Lab Chip 7:199–206. https://doi.org/10.1039/B616851P

Xu Y, Wang C, Dong Y et al (2012b) Low-temperature direct bonding of glass nanofluidic chips using a two-step plasma surface activation process. Anal Bioanal Chem 402:1011–1018. https://doi.org/10.1007/S00216-011-5574-2/FIGURES/6

Xu Y, Wang C, Li L et al (2013) Bonding of glass nanofluidic chips at room temperature by a one-step surface activation using an O2/CF4 plasma treatment. Lab Chip 13:1048–1052. https://doi.org/10.1039/C3LC41345D

Xu Y, Wu Q, Shimatani Y, Yamaguchi K (2015c) Regeneration of glass nanofluidic chips through a multiple-step sequential thermochemical decomposition process at high temperatures. Lab Chip 15:3856–3861. https://doi.org/10.1039/C5LC00604J

Xu Y, Xu B, Xu Y, Xu B (2015d) An integrated glass nanofluidic device enabling in-situ electrokinetic probing of water confined in a single nanochannel under pressure-driven flow conditions. Small 11:6165–6171. https://doi.org/10.1002/SMLL.201502125

Yamada M, Kano K, Tsuda Y et al (2007) Microfluidic devices for size-dependent separation of liver cells. Biomed Microdevices 95(9):637–645. https://doi.org/10.1007/S10544-007-9055-5

Yamada M, Nakashima M, Seki M (2004) Pinched flow fractionation: continuous size separation of particles utilizing a laminar flow profile in a pinched microchannel. Anal Chem 76:5465–5471. https://doi.org/10.1021/AC049863R/SUPPL_FILE/AC049863RSI20040123_054437.AVI

Yamada M, Seki M (2005) Hydrodynamic filtration for on-chip particle concentration and classification utilizing microfluidics. Lab Chip 5:1233–1239. https://doi.org/10.1039/B509386D

Yamada M, Seki M (2006) Microfluidic particle sorter employing flow splitting and recombining. Anal Chem 78:1357–1362. https://doi.org/10.1021/AC0520083/SUPPL_FILE/AC0520083SI20051111_023259.PDF

Yamamoto K, Morikawa K, Imanaka H et al (2020) Picoliter enzyme reactor on a nanofluidic device exceeding the bulk reaction rate. Analyst 145:5801–5807. https://doi.org/10.1039/D0AN00998A

Yamamoto K, Morikawa K, Shimizu H et al (2022) Accelerated protein digestion and separation with picoliter volume utilizing nanofluidics. Lab Chip 22:1162–1170. https://doi.org/10.1039/D1LC00923K

Yamamoto K, Ota N, Tanaka Y (2021) Nanofluidic devices and applications for biological analyses. Anal Chem 93:332–349. https://doi.org/10.1021/ACS.ANALCHEM.0C03868/ASSET/IMAGES/ACS.ANALCHEM.0C03868.SOCIAL.JPEG_V03

Yang J, Xu Y (2022) Nanofluidics for sub-single cellular studies: nascent progress, critical technologies, and future perspectives. Chinese Chem Lett 33:2799–2806. https://doi.org/10.1016/J.CCLET.2021.09.066

Yasui T, Kaji N, Ogawa R et al (2011) DNA separation in nanowall array chips. Anal Chem 83:6635–6640. https://doi.org/10.1021/AC201184T/SUPPL_FILE/AC201184T_SI_002.AVI

Yasui T, Kaji N, Okamoto Y et al (2012) Nanopillar array chip integrated with on-line stacking for fast DNA separation with high sensitivity and high resolution. Microfluid Nanofluidics 146(14):961–967. https://doi.org/10.1007/S10404-012-1103-7

Yasui T, Ogawa K, Kaji N et al (2016) Label-free detection of real-time DNA amplification using a nanofluidic diffraction grating. Sci Rep 61(6):1–8. https://doi.org/10.1038/srep31642

Yasui T, Rahong S, Motoyama K et al (2013) DNA manipulation and separation in sublithographic-scale nanowire array. ACS Nano 7:3029–3035. https://doi.org/10.1021/NN4002424/SUPPL_FILE/NN4002424_SI_005.AVI

Yasui T, Yanagida T, Ito S et al (2017) Unveiling massive numbers of cancer-related urinary-microRNA candidates via nanowires. Sci Adv 3. https://doi.org/10.1126/SCIADV.1701133/SUPPL_FILE/1701133_SM.PDF

Yu D, Li Y, Wang M et al (2022) Exosomes as a new frontier of cancer liquid biopsy. Mol Cancer 21:1–33. https://doi.org/10.1186/S12943-022-01509-9/TABLES/4

Yu Z, Lin S, Xia F et al (2021) ExoSD chips for high-purity immunomagnetic separation and high-sensitivity detection of gastric cancer cell-derived exosomes. Biosens Bioelectron 194:113594. https://doi.org/10.1016/J.BIOS.2021.113594

Yukawa H, Yamazaki S, Aoki K et al (2021) Co-continuous structural effect of size-controlled macro-porous glass membrane on extracellular vesicle collection for the analysis of miRNA. Sci Rep 111(11):1–13. https://doi.org/10.1038/s41598-021-87986-2

Zattoni A, Roda B, Borghi F et al (2014) Flow field-flow fractionation for the analysis of nanoparticles used in drug delivery. J Pharm Biomed Anal 87:53–61. https://doi.org/10.1016/J.JPBA.2013.08.018

Zhang J, Nguyen LTH, Hickey R et al (2021) Immunomagnetic sequential ultrafiltration (iSUF) platform for enrichment and purification of extracellular vesicles from biofluids. Sci Rep 111(11):1–17. https://doi.org/10.1038/s41598-021-86910-y

Zhang L, Gu F, Tong L, Yin X (2008) Simple and cost-effective fabrication of two-dimensional plastic nanochannels from silica nanowire templates. Microfluid Nanofluidics 5:727–732. https://doi.org/10.1007/S10404-008-0314-4/FIGURES/6

Zhao Y, Liu P, Tan H et al (2021) Exosomes as smart nanoplatforms for diagnosis and therapy of cancer. Front Oncol 11:3364. https://doi.org/10.3389/FONC.2021.743189/BIBTEX

Zierold R, Harberts J, Fendler C et al (2020) Toward brain-on-a-chip: human induced pluripotent stem cell-derived guided neuronal networks in tailor-made 3d nanoprinted microscaffolds. ACS Nano 14:13091–13102. https://doi.org/10.1021/ACSNANO.0C04640/SUPPL_FILE/NN0C04640_SI_003.MP4

Zuo Y, Wang G, Yu Y et al (2016) Smart nanovalves with thermoresponsive amphiphilic triblock copolymer brushes. 56:26–38. https://doi.org/10.1080/00222348.2016.1254563

Chapter 15
Nanoparticles at the Stage of Clinical Trials

Konstantin Osetrov, Svetlana Morozkina, Petr Snetkov, and Mayya Uspenskaya

Abstract The search of new therapeutic tools and more intensive development of old ones are required to ensure effective treatment of various diseases. The usage of nanoparticles opens up future prospects for their involvement in the formulations of newly created biomaterials. They are widely applied for the targeted drug delivery, solving the diagnostic and therapeutic tasks. Nanoparticles have a significant set of factors that ensure their superiority over the conventional methods of the treatment. Among them are the ability to bypass biological barriers, a variety of pharmacokinetic profiles, and accurate delivery to the target tissue. This review discusses the current and future research of lipid, polymer, organic, and viral nanoparticles. In addition, the aspects related to the pharmacokinetics of nanoparticles during the application in vitro and their potential toxicity are considered in the area of clinical trials.

Keywords Diagnostics · Nanoparticles · Nanomedicine · Theranostic · Clinical use

The last decades show extensive interest growth in the field of nanoparticle (NP) application and development. The great attention usually concentrates on the usage of nanomedicines for therapeutic and diagnostic objectives. The widespread involvement of researchers on this topic is due to the unique properties that allow to solve particular problems. Some of the most widely distributed tasks (but not limited to) are target delivery of drug molecules to organs (Najahi-Missaoui et al. 2021), cancer immunotherapy (Nasirmoghadas et al. 2021), and diagnostic (Baetke et al. 2015).

The perspectives of nanosized molecules may include the improvement of drug pharmacokinetic properties without the modification of its structure, high-sensitive targeting on molecules/cells/organs, unique ability to overcome biological

K. Osetrov · S. Morozkina · P. Snetkov · M. Uspenskaya (✉)
Chemical Engineering Centre, ITMO University, St. Petersburg, Russia

D. Lamprou (ed.), *Nano- and Microfabrication Techniques in Drug Delivery*,
Advanced Clinical Pharmacy – Research, Development and Practical Applications 2,
https://doi.org/10.1007/978-3-031-26908-0_15

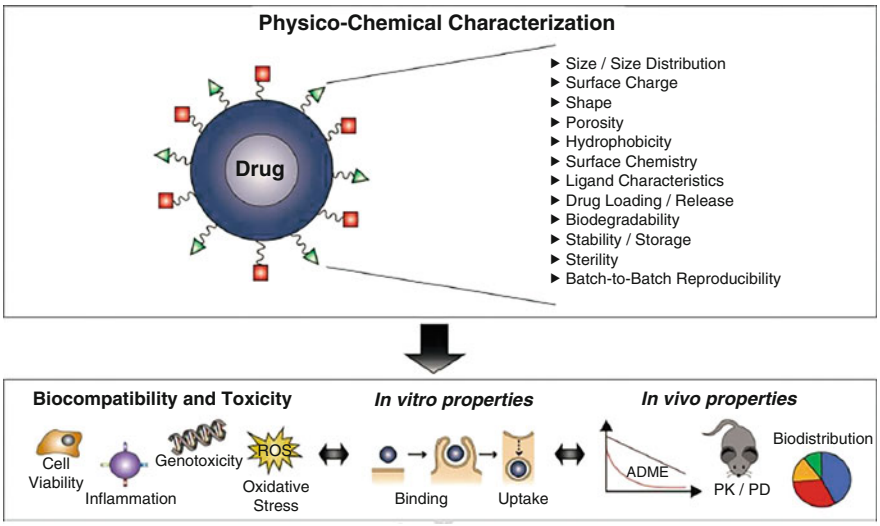

Fig. 15.1 Nanoparticle properties under controllable conditions (Wicki et al. 2015)

concerned restrictions, great availability of a drug at the end point, and possibility to deliver substances having different chemical nature (Mukherjee et al. 2019).

However, there are a number of factors restricting the common use of NPs in the clinical practice. Among them are long-term clinical studies, the complexity of providing the required profile of pharmacokinetics and particle capacity, the potential toxicity, and the necessary for biodegradation/isolation (Swartzwelter et al. 2020). Because of enormous parameters, NPs need to be controlled during synthesis: reproducibility, distribution of size, and monodispersity of particles at the end (Fig. 15.1). Thus, the researcher faces a complex multifactorial task that requires an integrated approach to achieve these goals.

There is a set of possible delivery locations for therapeutic molecules carried by NPs. Once it assembles in the bloodstream, nanomedicine could be absorbed in the liver, spleen, kidneys, and brain (Fig. 15.2). The transport mechanism to the human body could vary by structure-related properties of the substance and desired pharmacokinetic profile. The ways responsible for providing NPs' open access to the blood system are dermal, parenteral, pulmonary, and gastrointestinal. Of course, various physiological systems have different bioavailabilities regarding the usage of current drugs and their carriers.

A wide range of the applied NPs are developed in the current time. Roughly, they could be divided into several categories with the following properties shown in Table 15.1. However, only a few formulations were accepted for clinical use. Mostly it is regarded for the difficulties in achieving an appropriate pharmacokinetic properties and the development of reproducible NP synthesis. Also, the confirmation of drug safety in clinical studies is quiet a durable process, concerned with long-term approval by the medical regulatory agencies.

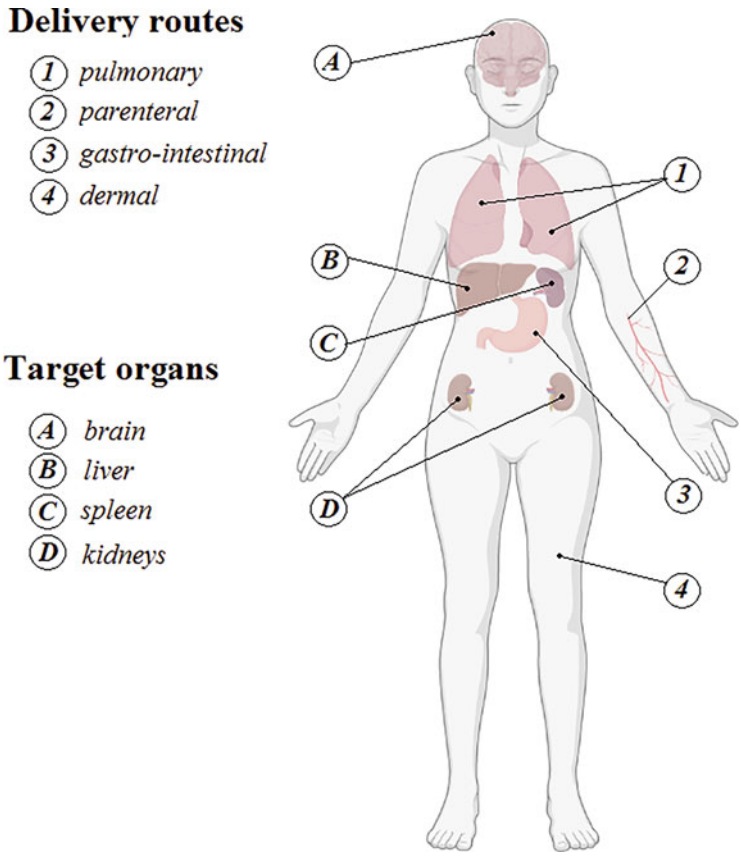

Fig. 15.2 The ways of NP release in the human body and delivery to available organs (created with BioRender.com)

All these classes have specific fields of application depending on their structures and properties (Zylberberg et al. 2017). Thus, lipid NPs greatly spread to deliver protein drugs to specific cells and concerned with the creation of dual-targeting systems, where several receptors or enzymes are targeted. Polymer NPs show well-controlled synthesis and wide versatility as the carrier choice, as well as provide controlled release. Inorganic NPs are extensively used for radio/magnetic diagnostic, therapeutic, and theranostic purposes. Viral NPs could provide an opportunity for specific interactions by biological cell mechanisms. The use of an appropriate drug carrier among various classes of nanoparticles mainly depends on physicochemical characteristics of the drug, targeted organ/cell type, and the desired pharmacokinetic profile.

Nowadays, researches related to the use of nanoparticles in clinical practice are at a new stage of development. More and more new nanomaterials are included each

Table 15.1 Main classes of nanoparticles and their properties

NPs depending on its nature:	Brief characteristic	Main representatives	Examples approved for clinical practice	Ref.
Lipid	The dispersal of lipid in water with two or more bilayers	Poly(d,l-lactide)-b-polyethylene glycol-methoxy, polylactic acid, polyester, cholesterol, phospholipids	Genexol-PM, Vyxeos, Doxil, Myocet, AmBisome, DaunoXome, Oncaspar, Visudyne	(Zhao et al. 2018)
Polymer	The polymeric-drug conjugated structures	Polysaccharides, polyethylene glycol, N-(2-hydroxypropyl) methacrylamide, proteins	Pegamotecan, Mureletecan, Pegasys, ProLindac, Delimotecan	(Plucinski et al. 2021)
Inorganic	Individual particles preliminary in view of oxides	Zinc, gold, titanium, iron, silver, carbon dotes	NanoTherm	(Al-Hashedi et al. 2019)
Viral	The home tumor viruses express therapeutic proteins	Modified pox, herpes, adenoviruses	Mylotarg, Adcetris, Kadcyla, Zevalin, Bexxar	(Wicki et al. 2015)

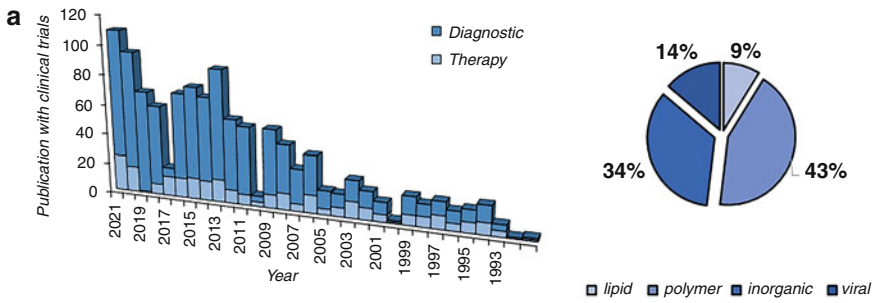

Fig. 15.3 The publications with the clinical trials of NPs: (**a**) with therapeutic and diagnostic purposes by year, (**b**) by type of a carrier from 2011 to 2021 (search in Pubmed database on 07.06.2022 with keywords: nanoparticle, organic/inorganic/metal/polymer/drug-conjugated/viral/lipid)

year in human trials (Fig. 15.3a). The tendency of the significant growth in the publications related to clinical trials of NPs is obviously tracked in the last 10 years.

According to many studies, the most investigated class of NPs (Fig. 15.3b) is polymer nanoparticles. Cutlip et al. effectively used the stents with nanothin layer of Polyzene-F for the examination of coronary artery lesions (Cutlip et al. 2017), which have reduced inflammation, neointimal hyperplasia, and thrombogenicity. This provides performing intervention processes in a more acceptable form and safe way. The polymer magnetic nanoparticles on the base of functionalized polyethylene

glycol, polylactide, and polycaprolactone found their application in the delivery of temozolomide for glioblastoma treatment (Young et al. 2018). On animal model, it demonstrated an appropriate delivery rate and an accurate targeting of the tumor. The polyethylene glycol-polyaspartate micelles with the epirubicin prodrug conjugate for the treatment of advanced or recurrent malignant solid tumors were developed (Mukai et al. 2017). The proposed NPs showed better safety profile compared to the conventional anthracycline therapy. Combination of cyclodextrin and camptothecin (Duska et al. 2021) demonstrated better efficacy of the treatment in recurrent or persistent epithelial ovarian, fallopian tube, or primary peritoneal cancer and provided lower toxicity compared with the conventional therapy. The authors also supposed to widen their use for the treatment of other oncological diseases. The polymer nanoparticles showed high reproducibility and reliability in the long term, coupled with the great variation of the accessible monomer types.

The research works of lipid NPs were concentrated on the punctual delivery of RNA modifications to the certain targets. This problem is of significant interest with the growing risks of oncology treatments. Also lipids with a nucleoside-modified mRNA is found to be greatly useful in the prevention of COVID-19 (Roncati and Corsi 2021). The used formulation demonstrated the formation of specific cellular immune response with tolerated doses and high efficiencies. Another study showed successful example of drug delivery for the treatment of hereditary transthyretin-mediated amyloidosis (Zhang et al. 2020). It was found out that the prolonged administration of patisiran for 3 weeks was appropriate to reach a therapeutic effect for this disease.

Apart from the conventional usage of iron oxide NPs in diagnostic current, inorganic NPs found their application in many more fields of medicine. Silver nanoparticles were productively used for the creation of an antibacterial middle ear prosthesis to replace the damaged ossicles (Ziąbka and Malec 2019). The proposed decision to this major problem allowed to avoid the rejection of the prosthesis and to bring the required suppression of bacterial growth in so-hard-to-reach area. The nanocrystalline magnesium phosphate gel was developed for the decontamination of organic wastes from titan implant surface, thereby preventing corrosion (Ashwaq et al. 2019). The implant-paste demonstrated high cleanability against bacteria, which could form biofilm on dental implants.

Because of the SARS-CoV-2 epidemic, viral NPs' clinical trials have shown a significant growth in the last years. Most of publications described vaccine assays for this disease. Only a few are dedicated to fight with other viruses. Shinde et al. proposed a vaccine against influenza: the quadrivalent recombinant hemagglutinin nanoparticle influenza vaccine (Shinde et al. 2021). The research showed high tolerance and formation of resistant antibodies in the recipients. Interesting studies on vaccine against Ebola virus were performed with the use of EBOV glycoprotein nanoparticle (Fries et al. 2000). The antibodies were formed and remained in the body after one year of the study.

The great question concerned with the nanomedicine application in clinical practice is pharmacokinetics. That is one of the key points when a researcher is projecting the future synthesis of NP delivery system. The drug release rate mainly

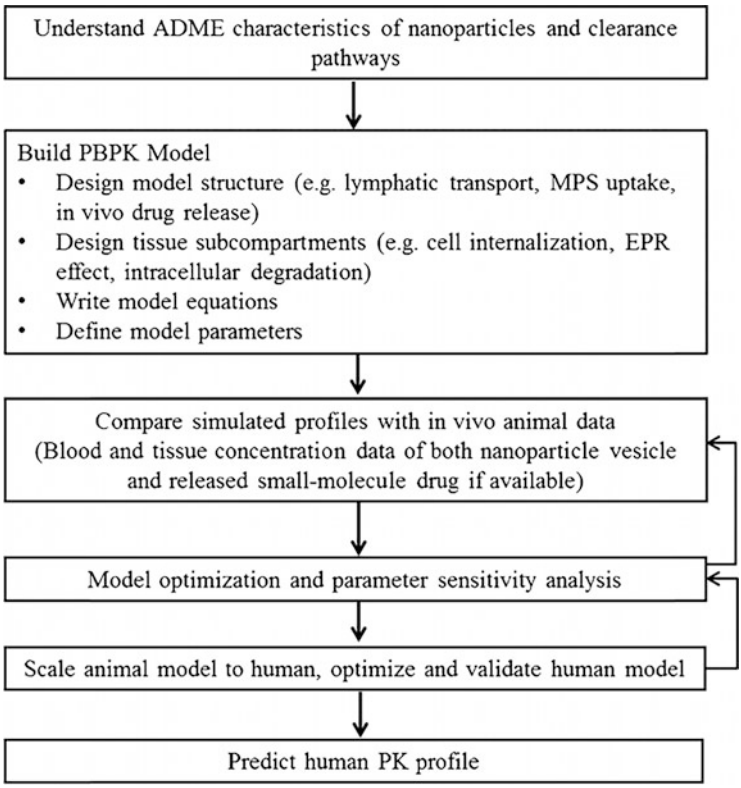

Fig. 15.4 The diagram explaining physiologically based pharmacokinetic model (Li et al. 2017)

depends on the solubility of the drugs, desorption rate of the adsorbed drug, diffusion of the drug, degradation or the erosion of the nanoparticle, and the combination of the diffusion and the erosion processes (Zahin et al. 2020). The medicine is distributed all along the nanoparticle and released following matrix erosion or diffusion. Also, the drug is another major factor relating to the delivery. The drug characteristics, which have an effect on kinetics, are structure, shape, size, distribution in NP, solubility, surface charge, and encapsulation efficiency of NP.

The pharmacokinetic models are usually considered from the two approaches: compartmental and non-compartmental (Rodallec et al. 2018). The compartmental approach is based on the mass balance law for the drug transport and is often used in the differential form. The non-compartmental approach is based on the strict dependence of the concentration on time. Another interesting intensive trend is physiologically based pharmacokinetic models. They are based on the anatomical structure of a living system, with important organs or tissues listed as individual compartments interconnected through the mass transportation described by mathematical equations (Li et al. 2017). Such approach allows to describe and predict drug kinetics in certain organs, physiological systems, and mediums (Fig. 15.4). Mainly, it

considers absorption, distribution, metabolism, and excretion (ADME), which have especially great significance to study both biodegradability and toxicity.

The high-drug loading nanoparticles (>10% wt.) were greatly discussed previously (Liu et al. 2020). The review describes a plethora of various drug delivery profiles and strategies for the drug loading (pre-/co-/post-loading). The authors concluded that the pre-loading approach represents a new and promising strategy for making core-shell nanoparticles with high-drug loading. The formation of core-shell structures has several advantages—separate engineering possibilities of the core and shell materials for the controlled release and the targeting delivery. However, this approach is approved only for hydrophobic drugs, but there are still prospects for further expansion in the field of hydrophilic molecules. The barriers for therapeutics release of siRNA were reviewed to cure cancer (Subhan and Torchilin 2019). The delivery of drugs is quite difficult and experiences a lot of limitations (medium influence, autoimmune response, and other factors) in these cases. The interesting summary of the research on inhaled medicines was performed by Guo et al. (Guo et al. 2021). They concluded that the endogenous lipid-based formulations and drug-lipid conjugates have a great potential for clinical applications in the current time. It demonstrated that the pulmonary way could successfully be used to treat not only lung but also systemic diseases. Future formulations have to overcome lung diseases for that purpose. Another promising research direction focused on smart drug release. It could reduce cytotoxicity, raise narrow focused delivery, and enhance therapeutic index (Kalaydina et al. 2018). More and more accurate targeting is one of the most extensive trends in NP application. It has to be dependent on the microbiota specific of the target organ (Ladaycia et al. 2021). The bacterial flora, mediums, and anatomic factors are necessary to take into account during the development of novel nanoparticles (Saquib Nanoparticles 2018).

Another problem is concerned with the toxicity of NPs. In the case of the use of metal nanoparticles, particular attention has to be paid to an appropriate encapsulation or coating of NPs for the prevention of nontarget/healthy organ poisoning (Jiang et al. 2019). Such nanoparticles could activate the damage of DNA, inflammation, and oxidative stress in humans without the cautious application (Roy et al. 2019). The nanotoxicity observed is not only from the NP core but also from the synergistic-additive influence of NPs mixed with coexisting species. Most of these behaviors and effects are not well-understood and remain to be topics of interest (Deng et al. 2018).

15.1 Conclusions and Future Perspectives

Nanoparticles take a major part in clinical practice nowadays. However, in this novel field, many uncertainties still remain. These are potential problems regarded with the precise targeting of cells/organs, mechanism of delivery, possible toxicity of some particles, and achievement of appropriate pharmacokinetic profile. The mentioned concerns have to be fully solved at the end of clinical studies. The nanoparticles

being developed can become a solution to a number of most important tasks facing medical practice nowadays.

References

Al-Hashedi AA, Laurenti M, Amine Mezour M, Basiri T, Touazine H, Jahazi M, Tamimi F (2019) Advanced inorganic nanocomposite for decontaminating titanium dental implants. J Biomed Mater Res–Part B Appl Biomater 107(3):761–772. https://doi.org/10.1002/jbm.b.34170

Baetke SC, Lammers T, Kiessling F (2015) Applications of nanoparticles for diagnosis and therapy of cancer. Br J Radiol 88(1054):20150207. https://doi.org/10.1259/bjr.20150207

Cutlip DE, Garratt KN, Novack V, Barakat M, Meraj P, Maillard L, Erglis A, Jauhar R, Popma JJ, Stoler R, Silber S, Cutlip D, Allaqaband S, Caputo R, Beohar N, Brown D, Garratt K, Jauhar R, George J, Varghese V, Huth M, Larrain G, Lee T, Malik A, Martin S, McGarry T, Phillips C, Shah A, Stoler R, Ball M, Price RJ, Rossi J, Taylor C, Tolleson T, Nicholson W, Kesanakurthy S, Shoukfeh M, Finn A, Devireddy C, Shoultz C, Robbins M, Kiesz R, Menon P, Weilenmann D, Sievert H, Stankovic G, Berland J, Delarche N, Hirsch JL, Maillard L, Shayne J, Serra A, Fernandez-Ortiz A, Monassier JP, Silber S (2017) 9-month clinical and angiographic outcomes of the COBRA Polyzene-F NanoCoated coronary stent system. JACC Cardiovasc Interv 10(2):160–167. https://doi.org/10.1016/j.jcin.2016.10.037

Deng H, Zhang Y, Yu H (2018) Nanoparticles considered as mixtures for toxicological research. J Environ Sci Heal–Part C Environ Carcinog Ecotoxicol Rev 36(1):1–20. https://doi.org/10.1080/10590501.2018.1418792

Duska LR, Krasner CN, O'Malley DM, Hays JL, Modesitt SC, Mathews CA, Moore KN, Thaker PH, Miller A, Purdy C, Zamboni WC, Lucas AT, Supko JG, Schilder RJ (2021) A phase Ib/II and pharmacokinetic study of EP0057 (formerly CRLX101) in combination with weekly paclitaxel in patients with recurrent or persistent epithelial ovarian, fallopian tube, or primary peritoneal cancer. Gynecol Oncol 160(3):688–695. https://doi.org/10.1016/j.ygyno.2020.12.025

Fries L, Cho I, Krähling V, Fehling SK, Strecker T, Hooper JW, Kwilas SA, Agrawal S, Wen J, Fix A, Thomas N, Flyer D, Smith G, Glenn G (2000) Randomized, blinded, dose-ranging trial of an Ebola virus glycoprotein nanoparticle vaccine with matrix-M adjuvant in healthy adults. J Infect Dis 222(4):572–582. https://doi.org/10.1093/infdis/jiz518

Guo Y, Bera H, Shi C, Zhang L, Cun D, Yang M (2021) Pharmaceutical strategies to extend pulmonary exposure of inhaled medicines. Acta Pharm Sin B 11(8):2565–2584. https://doi.org/10.1016/j.apsb.2021.05.015

Jiang Z, Shan K, Song J, Liu J, Rajendran S, Pugazhendhi A, Jacob JA, Chen B (2019) Toxic effects of magnetic nanoparticles on normal cells and organs. Life Sci 220:156–161. https://doi.org/10.1016/j.lfs.2019.01.056

Kalaydina RV, Bajwa K, Qorri B, Decarlo A, Szewczuk MR (2018) Recent advances in "smart" delivery systems for extended drug release in cancer therapy. Int J Nanomedicine 13:4727–4745. https://doi.org/10.2147/IJN.S168053

Ladaycia A, Passirani C, Lepeltier E (2021) Microbiota and nanoparticles: description and interactions. Eur J Pharm Biopharm 169:220–240. https://doi.org/10.1016/j.ejpb.2021.10.015

Li M, Zou P, Tyner K, Lee S (2017) Physiologically based pharmacokinetic (PBPK) modeling of pharmaceutical Nanoparticles. AAPS J 19(1):26–42. https://doi.org/10.1208/s12248-016-0010-3

Liu Y, Yang G, Jin S, Xu L, Zhao CX (2020) Development of high-drug-loading nanoparticles. Chempluschem 85(9):2143–2157. https://doi.org/10.1002/cplu.202000496

Mukai H, Kogawa T, Matsubara N, Naito Y, Sasaki M, Hosono A (2017) A first-in-human phase 1 study of epirubicin-conjugated polymer micelles (K-912/NC-6300) in patients with advanced

or recurrent solid tumors. Investig New Drugs 35(3):307–314. https://doi.org/10.1007/s10637-016-0422-z

Mukherjee A, Waters AK, Kalyan P, Achrol AS, Kesari S, Yenugonda VM (2019) Lipid-polymer hybrid nanoparticles as a next generation drug delivery platform: state of the art, emerging technologies, and perspectives. Int J Nanomedicine 14:1937–1952. https://doi.org/10.2147/IJN.S198353

Najahi-Missaoui W, Arnold RD, Cummings BS (2021) Safe nanoparticles: are we there yet? Int J Mol Sci 22(1):1–22. https://doi.org/10.3390/ijms22010385

Nasirmoghadas P, Mousakhani A, Behzad F, Beheshtkhoo N, Hassanzadeh A, Nikoo M, Mehrabi M, Kouhbanani MAJ (2021) Nanoparticles in cancer immunotherapies: an innovative strategy. Biotechnol Prog 37(2):e3070. https://doi.org/10.1002/btpr.3070

Plucinski A, Lyu Z, Schmidt BVKJ (2021) Polysaccharide nanoparticles: from fabrication to applications. J Mater Chem B 9(35):7030–7062. https://doi.org/10.1039/d1tb00628b

Rodallec A, Benzekry S, Lacarelle B, Ciccolini J, Fanciullino R (2018) Pharmacokinetics variability: why nanoparticles are not just magic-bullets in oncology. Crit Rev Oncol Hematol 129:1–12. https://doi.org/10.1016/j.critrevonc.2018.06.008

Roncati L, Corsi L (2021) Nucleoside-modified messenger RNA COVID-19 vaccine platform. J Med Virol 93(7):4054–4057. https://doi.org/10.1002/jmv.26924

Roy S, Liu Z, Sun X, Gharib M, Yan H, Huang Y, Megahed S, Schnabel M, Zhu D, Feliu N, Chakraborty I, Sanchez-Cano C, Alkilany AM, Parak WJ (2019) Assembly and degradation of inorganic Nanoparticles in biological environments. Bioconjug Chem 30(11):2751–2762. https://doi.org/10.1021/acs.bioconjchem.9b00645

Saquib Nanoparticles T (2018) Overview, T. Transmucosal Nanoparticles, Toxicological Overview

Shinde V, Cai R, Plested J, Cho I, Fiske J, Pham X, Zhu M, Cloney-Clark S, Wang N, Zhou H, Zhou B, Patel N, Massare MJ, Fix A, Spindler M, Thomas DN, Smith G, Fries L, Glenn GM (2021) Induction of cross-reactive Hemagglutination inhibiting antibody and Polyfunctional CD4+ T-cell responses by a recombinant matrix-M-Adjuvanted hemagglutinin nanoparticle influenza vaccine. Clin Infect Dis 73(11):4278–4287. https://doi.org/10.1093/cid/ciaa1673

Subhan MA, Torchilin VP (2019) Efficient nanocarriers of siRNA therapeutics for cancer treatment. Transl Res 214:62–91. https://doi.org/10.1016/j.trsl.2019.07.006

Swartzwelter BJ, Fux AC, Johnson L, Swart E, Hofer S, Hofstätter N, Geppert M, Italiani P, Boraschi D, Duschl A, Himly M (2020) The impact of nanoparticles on innate immune activation by live bacteria. Int J Mol Sci 21(24):1–22. https://doi.org/10.3390/ijms21249695

Wicki A, Witzigmann D, Balasubramanian V, Huwyler J (2015) Nanomedicine in cancer therapy: challenges, opportunities, and clinical applications. J Control Release 200:138–157. https://doi.org/10.1016/j.jconrel.2014.12.030

Young JS, Bernal G, Polster SP, Nunez L, Larsen GF, Mansour N, Podell M, Yamini B (2018) Convection-enhanced delivery of polymeric Nanoparticles encapsulating chemotherapy in canines with spontaneous Supratentorial tumors. World Neurosurg 117:698–704. https://doi.org/10.1016/j.wneu.2018.06.114

Zahin N, Anwar R, Tewari D, Kabir MT, Sajid A, Mathew B, Uddin MS, Aleya L, Abdel-Daim MM (2020) Nanoparticles and its biomedical applications in health and diseases: special focus on drug delivery. Environ Sci Pollut Res 27(16):19151–19168. https://doi.org/10.1007/s11356-019-05211-0

Zhang X, Goel V, Attarwala H, Sweetser MT, Clausen VA, Robbie GJ (2020) Patisiran pharmacokinetics, pharmacodynamics, and exposure-response analyses in the phase 3 APOLLO trial in patients with hereditary transthyretin-mediated (hATTR) amyloidosis. J Clin Pharmacol 60(1): 37–49. https://doi.org/10.1002/jcph.1480

Zhao J, Weng G, Li J, Zhu J, Zhao J (2018) Polyester-based nanoparticles for nucleic acid delivery. Mater Sci Eng C 92(11):983–994. https://doi.org/10.1016/j.msec.2018.07.027

Ziąbka M, Malec K (2019) Polymeric middle ear prosthesis enriched with silver nanoparticles–first clinical results. Expert Rev Med Devices 16(4):325–331. https://doi.org/10.1080/17434440.2019.1596796

Zylberberg C, Gaskill K, Pasley S, Matosevic S (2017) Engineering liposomal nanoparticles for targeted gene therapy. Gene Ther 24(8):441–452. https://doi.org/10.1038/gt.2017.41

Chapter 16
Nasal Drug Delivery Systems for the Treatment of Diseases of the Central Nervous System and Tuberculosis

Thi Hong Nhung Vu, Svetlana Morozkina, Petr Snetkov, and Mayya Uspenskaya

Abstract Nasal drug delivery is a current drug delivery trend that is gaining attraction, especially for respiratory and central nervous system (CNS) diseases. This delivery pathway avoids the undesirable effects of systemic drug delivery, such as excessive dosing, damage to non-diseased organs, or drug destruction before reaching the therapeutic target. Inhaled drugs have been used for therapeutic and recreational purposes since ancient times. The development of modern inhalers for drug delivery has increased the use of intranasal drugs. More than ever, the development of drug-integrated intranasal formulations is extremely promising, providing hope for the treatment of diseases previously thought to be difficult to treat, such as tuberculosis or central nervous system diseases. Numerous investigations of intranasal formulations have been studied and published by pharmacologists over the years. The majority of research products are nanocapsules such as nanoparticles, micelles, liposomes, sol-gels, emulsions, and microspheres. Targeted drug formulations are created based on the features of the disease, the cell's characteristics, the nature of the cell environment, and the biochemical barriers that the drug has to overcome. Preclinical and clinical assays of drug formulations help to determine their applicability in patients by the examination of their physicochemical properties, drug release, and pharmacokinetics. In this review, we focus on the factors that influence the nasal drug delivery, as well as drug release in the studies of tuberculosis and CNS formulations.

Keywords Central nervous system (CNS) diseases · Tuberculosis · Drug delivery system · Targeted drug delivery · Intranasal drug delivery · Nanoparticles · In vitro · In vivo · Clinical application

T. H. Nhung Vu · S. Morozkina · P. Snetkov · M. Uspenskaya (✉)
Chemical Engineering Centre, ITMO University, St. Petersburg, Russia

D. Lamprou (ed.), *Nano- and Microfabrication Techniques in Drug Delivery*,
Advanced Clinical Pharmacy – Research, Development and Practical Applications 2,
https://doi.org/10.1007/978-3-031-26908-0_16

Abbreviations

AUC	Area under the curve
CF	5(6)-Carboxyfluorescein
C_{max}	Maximum drug concentration
CNS	Central nervous system
CS	Chitosan
DDPC	Dipalmitoyl phosphatidylcholine
DH	Diphenhydramine hydrochloride
DMPC	Dimilystoylphosphatidylcholine
DOPE	1,2-Dioleoyl-sn-glycero3-phosphoethanolamine
DOTAP	1,2-Dioleoyl-3-trimethylammonium-propane
DSC	Differential scanning calorimetry
EE	Encapsulation efficiency
EPC	Egg phosphatidylcholine
FTIR	Fourier-transform infrared
HA	Hyaluronic acid
HPLC	High-performance liquid chromatography
INU/pArg	Inulin/polyarginine
LC	Loading capacity
LE	Licorice extract
MC	Mannosylated chitosan
MMDA	Mass median aerodynamic diameter
OZ	Olanzapine
PBS	Phosphate-buffered solution
PDI	Polydispersity index
PLGA	Poly(lactic-co-glycolic acid)
PVA	Poly(vinyl alcohol)
TC	Thiolated chitosan
TFM	Teriflunomide
T_{max}	Time required to reach maximum drug concentration
WGA	Wheat germ agglutinin
XRD	X-ray diffraction
ZP	Zeta potential

16.1 Introduction

For pharmacologists, central nervous system (CNS) diseases and tuberculosis have been and continue to be serious global problems and challenges. These diseases are also responsible for billions of deaths and active cases over the world.

Central nervous system diseases are a spectrum of neurological disorders related to the structure or function of the spinal cord or brain (Nervous System Diseases

2022; Cacabelos et al. 2016). Alzheimer's disease, Bell's palsy, cerebral palsy, epilepsy, motor neurone disease, multiple sclerosis, neurofibromatosis Parkinson's disease, and so on are the most frequent CNS disorders (Nervous System Diseases 2022). The nervous system is the part that controls all the functions of the body, so any damage or abnormality in the nervous system can lead to symptoms in different parts of the body. A peripheral nervous system injury quickly activates a fascinating repair process that allows the injured nerve to regenerate and repair the function. However, as there is no such repair process in the CNS, injuries frequently result in the permanent damage (Vaquié et al. 2019).

Tuberculosis is an airborne infection caused mostly by *Mycobacterium tuberculosis*, a rod-shaped bacteria. This infectious disease existed three million years ago (Daniel 2006). Tuberculosis can affect any region of the body, including the skin, bones, kidneys, central nervous system, and so on. Tuberculosis is a disease that primarily affects people in developing countries, but it can also be seen in developed nations. Isoniazid, the first oral antituberculous drug, was introduced in 1952, and rifamycins were introduced in 1957. Despite considerable effort and expense, no new formulation has been accepted to date (Daniel 2006). Despite decades of numerous treatment programs and potentially effective tuberculosis drugs, the disease's prevalence has not decreased (Zumla et al. 2013). Antituberculosis therapy is becoming increasingly complicated as drug-resistant strains emerge and patients experience adverse drug reactions. Aside from discovery work, the improvement of the delivery of existing antituberculosis drugs is being investigated.

Currently, traditional approaches for drug delivery through the mouth or injection into the blood circulation system are the mainstays of the treatment for these disorders. These are systemic drug delivery systems. Unfortunately, in many cases, the high doses required to achieve the required concentrations at the treatment destination, that can lead to undesirable effects. Such drug administrations also have negative side effects to healthy tissues and cells. In chemotherapy, for example, only around 1% of a drug is administered to the tumor site, while the remaining 99% is transferred to other tissues of the body, causing serious side effects in healthy organs (Trafton 2009). Furthermore, due to the advent of multidrug-resistant and extremely drug-resistant bacteria, as well as the combination of these diseases with other complicated conditions such as HIV, diabetes, etc., the treatment of these diseases is becoming increasingly challenging. Additionally, drug breakdown in the gastrointestinal tract, liver, kidneys, and other tissues, particularly the limitation of drug penetration thorugh the blood-brain barrier as well as by blood-cerebrospinal fluid, is a serious obstacle for the drug delivery systems to the therapeutic targets.

Drug delivery across the blood-brain barrier and blood-cerebrospinal fluid is the main problem in CNS diseases. The blood-brain barrier consists of the system of capillary wall endothelial cells, capillary-enveloping astrocyte terminals, and pericytes embedded in the capillary basement membrane (Ballabh et al. 2004). The system enables for passive diffusion of some small molecules as well as selective and active transport of nutrients, ions, organic anions, and macromolecules including glucose and amino acids that are essential for the brain functions (Gupta et al. 2019). Only low-molecular-weight drugs can pass through the blood-brain

barrier under normal circumstances, while almost all high-molecular-weight compounds are severely restricted. High-molecular-weight drugs working through a peripheral mechanism are the only examples approved for the clinical use for the treatment of neurological disorders (e.g., type I interferons) (Lochhead and Thorne 2012). Many high-molecular-weight compounds have demonstrated great promises for the treatment of CNS diseases in vitro and in vivo studies. The issue of drug delivery techniques that overcome the challenges of the blood-brain barrier and blood and cerebrospinal fluid to reach the disease sites, on the other hand, is a different matter.

Targeted drug delivery systems for the treatment of tuberculosis could be a potentially useful approach for the development of clinically accepted treatment modalities. The active targeting drug delivery utilizes a purpose-built targeting agent to deliver the chemically conjugated drug(s) to *Mycobacterium tuberculosis*. These are nanoparticles made from organic and inorganic materials that can be incorporated in macrophages to eliminate tuberculosis bacilli. In the other directions, these nanoparticles reach and release the drug at the tuberculosis infection sites in and out of the lungs (Mazlan et al. 2021).

Intranasal drug delivery systems, which have recently been identified as a non-invasive route for CNS drugs and tuberculosis treatment, are also a reliable alternative to oral and intravenous drugs. Along with its large surface area, high blood flow, porous endothelial membrane, ability to prevent first-pass metabolism via the liver, and availability, the nasal mucosa is considered as an important target tissue for drug delivery (Jadhav et al. 2007; Suman 2013). Furthermore, the nasal cavity is an appealing route for systemic drug delivery and needle-free vaccination, particularly once efficacy and absorption are critical (Djupesland et al. 2001). To achieve the targeted drug delivery, the following criteria have to be considered: the disease, the pathway considered for drug delivery, the drug's characteristics, potential adverse side effects, and the targeted organ. There are two types of the targeted drug delivery: passive targeting and active targeting. In nasal passive targeting drug delivery, drug molecules are directed to the target site in the airways by the modification of the drug dosage, size of the droplets (e.g., aerosol), timing of the injection of the aerosolized drugs, inhalation flow rate (breathing pattern), and inhaled gas density (Djupesland et al. 2001; Dolovich and Dhand 2011; Bakke et al. 2006; Moffa et al. 2019; Wofford et al. 2015). In the implementation of active targeting drug delivery, methods associated with chemical and biological factors are used (Galvin et al. 2012; Vasir et al. 2005). Magnetic (Häfeli 2004; Liu et al. 2019), electric (Bologa and Bologa 2001; Xi et al. 2015), and acoustic fields (Ballantine et al. 1960; Xi et al. 2017; Farnoud et al. 2020) are also the examples of physical and environmental resources that can be used as a triggering agent to actively deliver the drug to a specific site. The combination of active and passive targeted drug delivery will improve the outcomes for the treatment of diseases by an intranasal drug.

However, within the scope of this review, only the active nasal drug delivery studies using chemopreventive factors will be considered.

16.2 Characteristics of Nasal Drug Delivery

Intranasal drug delivery systems could be used for either topical or systemic delivery. The intranasal route is appropriate for drugs that require rapid action (e.g., for acute pain, nausea, erectile dysfunction, or Parkinson's disease), as well as for conditions requiring multiple doses or drugs which are difficult to deliver via other routes, such as proteins, peptides, or vaccines. Intranasal administration may be especially appealing for the therapies that require chronic dosing. For many drugs, intranasal administration is a good alternative to the invasiveness of injections and oral administration, which may be associated with the issues such as poor bioavailability and the possibility of gastrointestinal side effects.

16.2.1 Characteristics and Factors Influencing the Permeability of the Nasal Cavity

There is relatively large surface area (150–160 cm^2) in the nasal cavity (Arora et al. 2002; Merkel and Popp 2022). It is divided into five anatomical regions: the nasal vestibule, respiratory area, atrium, nasopharynx, and olfactory region. The permeability of each region is influenced by the factors such as blood flow, density, surface area, number of cells present, amount of nasal secretions, and cell type. So, the nasal vestibule has the least permeability due to the keratinized cells; the atrium is less permeable because it has small surface area and stratified cells anteriorly; the respiratory area is the most permeable region due to its large surface area and rich vasculature; the olfactory region directly accesses the cerebrospinal fluid; and the nasopharynx receives nasal cavity drainage (Arora et al. 2002). The septal wall separates the two nasal cavities, which are dominated by three turbinates that are primarily responsible for the warming and moistening of the nasal cavity (Ugwoke et al. 2010). The area available for the drug permeation is greatly increased by microvilli on cells (400 microvilli per cell). The total volume of nasal secretions is 15 ml per day under normal physiological conditions (Arora et al. 2002).

A number of barriers, including the mucosal layer, the epithelial membrane, and related barriers, have to be crossed before drugs can reach the capillaries below the mucosal layer. Nasal mucus has the role of being the enzymatic barrier for drug delivery due to the presence of a huge number of enzymes, including oxidative and conjugative enzymes, peptidases, and proteases. These enzymes in the nasal mucosa are responsible for the degradation of the drug (Arora et al. 2002; Dahl and Lewis 1993; Krishnamoorthy and Mitra 1998). However, because the nasal mucus is only a few micrometers thick (about 5μm), it may not provide a potent diffusion barrier (Arora et al. 2002; Costantino et al. 2007).

The exact mechanisms responsible for the transport of the drug from the nose to the brain are currently unclear. Nevertheless, various evidences show that the

trigeminal, olfactory, and systemic pathways are the major contributing forces in the drug delivery from the nose to the brain.

- The olfactory pathway: The olfactory region contains olfactory neural cells that are constantly turned over, giving the nasal barrier an open environment for the drug delivery from the nose to the brain. Drugs can cross the olfactory epithelium via two main mechanisms: extracellular and intracellular (Arora et al. 2002; Cassano et al. 2021).
- The extracellular pathway is the predominant mechanism of external drug transport into the perineural space. The extracellular pathway includes paracellular and transcellular mechanisms. The transcellular pathway is responsible for the transport of drugs of lipophilic nature via endocytosis or via passive diffusion. Paracellular drug transport is slower and involves tight junctions and/or clefts surrounding sustentacular and olfactory neural cells (Merkel and Popp 2022; Cassano et al. 2021).
- The intracellular mechanism involves the internalization of the drug via endocytosis or pinocytosis into olfactory neural cells, followed by the intracellular axonal transport into the nervous central system. The intracellular mechanism is a really slow and inefficient process that takes 24 hours to reach the CNS (Cassano et al. 2021; Pardeshi and Belgamwar 2013; Illum 2010).
- The trigeminal pathway: The trigeminal nerve is the largest of the 12 cranial nerves and is divided into ophthalmic, maxillary, and mandibular branches that transfer sensory information to the CNS from the nasal cavity, ocular mucosa, and oral cavity. Among them, the ophthalmic and maxillary branches are the most involved in the nose-to-brain route, because they innervate the nasal mucosa, whereas the mandibular branch just primarily innervates the oral cavity. Drug delivery via the trigeminal route, like the olfactory pathway, can occur via the extracellular pathways or intra-axonal transport (Cassano et al. 2021; Schaefer et al. 2002; Mittal et al. 2014; Simonato et al. 2013).
- Other nerves, such as the facial nerve, in addition to the trigeminal and olfactory routes may have a role in the drug delivery to the brain from the nose (Mittal et al. 2014).

The following factors influence the drug permeability through the nasal mucosa:

- Nasal secretion viscosity: The viscous surface layer inhibits the ciliary beating because the mucus sol layer is too thin; the mucociliary clearance is hampered because contact with cilia is lost because the sol layer is too thick. Mucociliary clearance impairment or modification affects the drug permeation by altering the time of drug-mucosa contact (Mortazavi and Smart 2011).
- Drug solubility in nasal secretions: A drug's physicochemical properties have to be appropriate for the dissolution in nasal secretions. Nasal secretions composed of approximately 90% water (Lansley 1993), 2% mucin, 1% salts, 1% protein (primarily albumin, lactoferrin, immunoglobulins, lysozyme, and so on), and lipids (Kaliner et al. 1984).

- Diurnal variation: Circadian rhythms influence nasal secretions during the day. Several studies have revealed the reduction of the secretion and the clearance rates during nighttime, altering the drug permeation. In these cases, the pattern and the rate of drug permeation will be determined by chronokinetics (Passàli and Bellussi 1988; Mygind and Thomsen 1976).
- pH of nasal cavity: Greater drug permeation is usually achieved at a nasal pH lower than the drug's pKa because the penetrant molecules exist as unionized species under such conditions (Huang et al. 1985). The nasal cavity has a pH in the range from 5.5–6.5 in adults to 5.0–7.0 in infants. The nature of the drug may change the mucus pH, which can affect the ionization, thus increasing or decreasing the drug permeation. The pH of the formulation is dependent on the pH of the nasal cavity, and the ideal formulation should have a pH between 4.5 and 6.5, with a buffering capacity if possible (Arora et al. 2002; Costantino et al. 2007; Gibson and Olanoff 1987; Corbo et al. 1989; Yang and Mitra 2001).

When the drug is delivered via the nasopharynx, the mucociliary clearance is approximately 21 min from the nasal cavity (Marttin et al. 1998). The reduced mucociliary clearance prolongs the time the drug spends in contact with the mucus membrane, which improves the drug permeation. Mucociliary clearance and drug permeability have been documented to be affected by a variety of medicines, hormonal shifts, medical conditions, environmental factors, and formulation factors (Cornaz 1994).

Attempts to modify the structural and mechanistic features of the nasal mucosa in order to increase the permeability are not recommended due to the risk of undesirable side effects and pathological consequences.

16.2.2 Characteristics and Factors Affecting the Permeability of the Intranasal Drugs

Intranasal drugs are typically administered in the form of an intranasal spray or powder. Powder sprays can easily irritate the mucosa (Ishikawa et al. 2001). Nasal drops are the most convenient, but they are difficult to accurately measure, which often leads to overdose, and they also cause rapid nasal drainage (Patel and McGarry 2001). For epy precise drug delivery, solution and suspension sprays, gels, emulsions, microspheres, liposomes, proliposomes, membranes, and niosomes are being developed. The volume of epy solution used in the nasal cavity is limited to 0.05–0.15 ml (Park et al. 2002; Abe et al. 1995).

Physical properties of drugs such as solubility, lipophilicity, molecular weight, stability, viscosity, and dosage are essential not just for the route of delivery selection but also for the selection of an effective drug delivery system.

A drug's solubility is the key determinant in its absorption via biological membranes (Rutkowska et al. 2013). Although nasal secretions are more aqueous in nature (Arora et al. 2002), nasal mucosa is predominantly lipophilic, and the lipid

domain is important in the barrier function of such membranes (Corbo et al. 1990). Therefore, drug's water and fatty solubility should be appropriate to allow for faster dissolution.

Basically, according to the pH partitioning theory, the non-ionized particles are better absorbed than the ionized ones. In general, drugs that are lipophilic or have a high partitioning coefficient tend to have better absorption through the nasal mucosa (Sakane et al. 1991). However, there are other transport routes for hydrophilic drugs (Huang et al. 1985). The drugs can be absorbed passively via the paracellular route, and in the case of the transcellular route, it may be absorbed both passively and actively, depending on their lipophilicity, when administered through the nasal cavity. Lipophilic drugs penetrate the nasal tissue transcellularly, while hydrophilic drugs penetrate the nasal tissue paracellularly (Arora et al. 2002; Costantino et al. 2007).

Many lipophilic drugs with low molecular weight (<1000 Da) administered nasally transport relatively efficiently across the mucosal membrane compared to larger lipophilic drugs. For polar drugs transported via the paracellular route, molecular weight is the important factor of the rate and the transportation. There is an inverse relationship between the proportion of the dose absorbed and the molecular weight for water-soluble hydrophilic compounds. High-molecular-weight drugs, such as peptides and proteins, can be delivered intranasally; however, systemic bioavailability is highly dependent on the presence of the permeation enhancers (Costantino et al. 2007).

The drug's absorption is affected by osmolarity. Osmotic regulators (such as sodium chloride, sorbitol, etc.) in the drug's formulation can affect nasal epithelial lining shrinkage (Ohwaki et al. 1987; Ohwaki et al. 1985), thereby altering the duration and permeability of drugs. Isotonic solutions are often preferred as the osmotic regulators (Ohwaki et al. 1989).

The higher viscosity of the formulation extends the time of the drug's contact with the nasal mucosa, resulting in a longer permeation time. Simultaneously, highly viscous formulations disrupt normal functions such as the ciliary beating or the mucociliary clearance, altering the drug permeability (Arora et al. 2002).

The biological, chemical, and physical stability of drugs is critical throughout the absorption process. Because the nasal cavity environment has a defensive enzymatic mechanism, the drug can be metabolized and its biostability reduced through the nasal passage. Many drugs, on the other hand, can be chemically unstable as a result of hydrolysis, oxidation, isomerization, photochemical degradation, or polymerization. Various strategies, such as the application of precursors and enzyme inhibitors, are being developed to overcome these difficulties (Pires et al. 2009).

16.3 Evaluation of Intranasal Drug Delivery Activity

Nasal drug delivery systems are designed based on the type of disease to be treated and the location of drug delivery. Liposomes, hydrogels, nanoparticles, nanoemulsions, microemulsions, micelles, and other formulations are commonly used.

Before being used, efficacy and safety standards of drug formulations have to be assured, so they have to pass via numerous preclinical and clinical trials.

16.3.1 Experiments to Evaluate the Biological Activity of a Formulation

* Preclinical trials:

- Evaluation of physical-chemical properties: Size, morphology, shape, crystallinity, solubility, chemical bonding, thermal properties, stability, osmolality, polydispersity index (PDI), zeta potential (ZP), encapsulation efficiency (EE) and loading capacity (LC), surface charge, type of lipids and emulsifiers, drug location in the nanoparticles/nanodroplets, and partition coefficient are some of the intranasal formulation properties which have to be evaluated. Among them, size, PDI, ZP, and EE are critical quality attributes to be considered.
- The size of the intranasal nanocarriers has to be less than 200 nm, according to the studies (Sabir et al. 2020; Cunha et al. 2020; Costa et al. 2021).
- The polydispersity index (PDI) indicates that the particle size distribution in the formula spans from 0 (monodisperse distribution) to 1 (polydisperse distribution). Intranasal nanocarriers often have the polydispersity values of less than 0.3 (Cunha et al. 2020; Pires and Santos 2018; Khosa et al. 2018; Danaei et al. 2018).
- The zeta potential (ZP), which corresponds to the surface charge of the nanoparticles/nanoparticles, forecasts the formulation's long-term physical stability and is affected by the factors such as pH and ionic strength. At the around ±30 mV, the zeta potential of intranasal nanocarriers is stable in the medium (Cunha et al. 2020; Costa et al. 2021; Khosa et al. 2018; Haider et al. 2020).
- Encapsulation efficiency (EE) quantifies the amount of the drug encapsulated in nanoparticles/nanodroplets and is used to confirm the nanocarrier suitability for the drug incorporation. Encapsulation efficiency has to be more than 80% for the transnasal lipid-based nanocarriers in general (Costa et al. 2021; Das et al. 2012).
- In vitro testing: studies of the drug release and activity in various environments at the anatomical model, cultured cell, cultured tissue, and so on. Determine whether or not to perform the in vivo test based on the results of the in vitro test.

In vitro experimental forms are built based on the type of formulation that has been designed. Typically, these experiments include the evaluation of the drug release, permeability ability, anti-pathogen activity, and protection of healthy cells

in buffer solutions with pH similar to that of a living organism's body or the simulated environment of the organ to be treated. Experiments and control samples are commonly conducted simultaneously, with the results recorded at regular intervals.

Furthermore, many researchers use the in vitro assessment of dry powders for inhalation (DPI) aerodynamic performance for the targeted delivery to the lungs. Aerodynamic evaluation combines particle size, morphology, density, intercellular interactions, crystallinity, in vitro solubility, in vitro permeability, in vitro aerodynamics (Andersen cascade impactor), and in silico aerodynamics (stochastic lung model) (Ignjatović et al. 2021). The visual fit of a straight line to data manually plotted on log-probability paper yields the mass median aerodynamic diameter (MMAD) and the geometric standard deviation (GSD). Because particles larger than about 10μm normally deposit in the extrathoracic regions, MMAD 10μm is commonly used as a rough measure of the mass that may enter the lungs (Finlay and Darquenne 2020).

– In vivo testing: On animals, the drug's therapeutic ability, safety, and side effects are evaluated. Animals that are used to test the drug delivery and activity include mice, dogs, rabbits, sheep, and others. Although the nose structure of other animals, particularly rats, differs from that of a human nose, mice are still the most commonly used due to their low cost and consistency with toxicity assessments (Erdő et al. 2018). Large animals, such as rabbits and dogs, are better suited to pharmacokinetic and pharmacodynamic research (Ugwoke et al. 2010; Costa et al. 2021; Erdő et al. 2018).

In vivo studies can predict the pharmacokinetic, pharmacodynamic, and absorption profiles of an intranasally administered drugs in humans (Erdő et al. 2018). Pharmacokinetics describes the effects of a drug on the body, such as absorption, distribution, metabolism, and elimination, whereas pharmacodynamics describes the effects of the drug on the body (Finlay and Darquenne 2020; Erdő et al. 2018; Meibohm 2006). Pharmacokinetic data report drug concentrations in the brain and plasma, which are calculated by measuring drug concentrations at the predetermined time intervals. These studies also assessed the drug's therapeutic effect and toxicity at the target site (Costa et al. 2021; Meibohm 2006).

Various parameters were evaluated in in vivo studies, such as C_{max} (maximum drug concentration), T_{max} (time required to reach maximum drug concentration), AUC (area under the curve), mean retention time of the formulation in each organ or by organ/blood ratio (i.e., drug bioavailability in specific organs), drug-targeting efficacy (DTE), and targeting potential drug consumption (DTP) (Ahmad et al. 2018a, b; Pardeshi and Belgamwar 2020; Youssef et al. 2018; Pires and Santos 2018; Alavian and Shams 2020).

A clinical trial: Test on humans to determine the safety of the drug, look for the side effects, determine the appropriate dose, and determine the drug's effectiveness. A clinical trial compares the activity of drugs to that of a clinically approved drug for the disease treatment or to a *placebo* (Costa et al. 2021).

16.3.2 Some Studies on Drug Release from the Preparations for the Treatment of CNS Disease and Tuberculosis

Researchers designed the trials to study drug properties and release based on an assessment of disease characteristics and drug formulation. A summary of some of the published reports is listed in Tables 16.1 and 16.2 to provide a rough overview of the research process for drug quality assessment and drug delivery from preparations.

The nasal drug delivery system is the trend nowadays, and many scientists are interested in this new and safe targeted system. Preparations are designed in various forms and ingredients based on the characteristics of the agent, cause, manifestation, location of disease onset, and impact of each disease on the patient. Formulators are increasingly developing experimental strategies to study the drug release and pharmacokinetics. The diversity of diseases and their causes, the variety of preparations, and the interference and interplay of biological cycles, the cell cycles, and the immune system against therapeutic agents make the drug research both fascinating and challenging. As a result, drug ingredients, drug forms, and the system for analyzing and evaluating drug quality are all constantly improving. This quantity also makes it difficult for researchers to choose an appropriate quality control method for the preparations.

After the selection of the ingredients and successfully obtaining the preparations, the products have to be evaluated for their physicochemical properties in order to provide the appropriate options for in vitro research and then ex vitro and in vivo for the preclinical assessments. In the evaluation of physicochemical properties, the morphology, size, ZP, PDI, EE, LC, as well as the changes in chemical structure (using FTIR, DSC, and XRD) are of most interest. For dry powder inhalation preparations for the delivery to the lungs, a mass median aerodynamic diameter (MMAD), $< 10\mu m$ is an important factor. The evaluation of drug resolution, cytotoxicity, and especially membrane permeability for intranasal drugs in in vitro experiments is of particular concern. In the in vivo evaluation, a successful preparation, in addition to its ability to target and cure diseases effectively compared with negative and positive controls, has to be nontoxic to the body and not accumulate in the liver, kidney, and other organs.

Currently, nasal drug delivery preparations are currently available in the form of drops, suspensions, emulsions, particles, and powders that are dripped or sprayed into the nose. As drug delivery systems have improved, the effectiveness of passive targeting has increased significantly and the amount of medicine lost owing to the entry to the gastrointestinal tract has decreased.

Even so, while developing nasal drug delivery systems for the treatment of tuberculosis or central nervous system disorders, scientists have to pay attention to research on nanofiber-based nasal drug delivery. The incorporation of a new carbon nanofiber-modified carbon electrode with a human nasal epithelial mucosa to achieve real-time quantitative monitoring of nasal administration in vitro (Gholizadeh et al. 2021), as well as the design of a self-assembled nanofiber vaccine

Table 16.1 Some studies on the activity of preparations for the treatment of CNS disorders

Drug formulations				
Preparation	*Components*	*Physicochemical properties*	In vitro test	In vivo *test*
Nanoparticles (Seju et al. 2011)	*Drug:* Olanzapine (OZ) *Polymers:* Poly(lactic-*co*-glycolic acid) (PLGA); S*tabilizer:* Poloxamer 407	*Optimum formulation:* 50 mg of PLGA and 6.25 mg of OZ in 2 ml acetonitrile and 10 ml Poloxamer 407 0.25% w/v solution *Nanoparticle properties:* – *EE:* 68.91 ± 2.31%, – *LC:* 8.613 ± 0.288% – *Size:* 91.2 ± 5.2 nm, – *PDI:* 0.120 ± 0.018 – *ZP:* −23.7 ± 2.1 mV. * ***XRD, DSC*:** The nanoparticles' thermogram revealed a broadening of the characteristic endothermic peak corresponding to OZ, while the PLGA peak shifted from 59.69 to 52.73 °C, indicating the decrease in its Tg. Physical interactions, such as hydrogen bonding between the carbonyl group of PLGA and the amino group of OZ, can explain this negative deviation. A decrease in the number and intensity of OZ peaks in diffractogram was observed in OZ-loaded nanoparticles,	*1.* In vitro *drug release studies* The OZ release experiment was carried out in a dialysis bag immersed in the receptor compartment containing methanolic PBS (pH 6.4) (the stirring speed of 100 rpm, 37 ± 2 °C). The solution was withdrawn at the regular intervals and analyzed at 259 nm. Within 7 h, the drug solution released 90.23 ± 0.817% of the drug, whereas nanoparticles released only 25.69 ± 0.361%, reaching 43.26 ± 0.156% after 120 h, indicating sustained release *2.* Ex vivo *diffusion studies* Freshly excised sheep nasal mucosa (diameter of 10 mm and thickness of 0.20 mm) in phosphate buffer (pH 6.4) in both donor and acceptor compartments. Solution from both compartments was removed, and the acceptor compartment was filled with 25 ml of fresh phosphate buffer (pH 6.4) – Ex vivo diffusion of	

		indicating a decrease in OZ crystallinity or amorphization.	pure drug: 1.0 ml of drug solution (2 mg/ml) was placed onto the stabilized sheep nasal mucosal membrane placed in the donor compartment and stirred slowly on a magnetic stirrer – Ex vivo diffusion of nanoparticles: Nanoparticles or lyophilized OZ-loaded nanoparticles (equivalent amount of 2 mg drug/1 ml phosphate buffer (pH 6.4)) were used. At the regular intervals, the samples from the receptor phase were taken, filtered through 0.45-μm nylon filter paper, and analyzed at 259 nm. Each sample then was replaced with an equal volume of the diffusion medium. Ex vivo diffusion of OZ from the drug solution and nanoparticles revealed that the drug diffusion through the nasal mucosa was rapid from the drug solution. No burst or biphasic release behavior was seen in any of the samples *3. Histopathological studies* The freshly isolated sheep nasal mucosa was cut into four	

(continued)

Table 16.1 (continued)

Drug formulations		*Physicochemical properties*	In vitro test	In vivo *test*
Preparation	*Components*			
			pieces. Each piece was treated with the nanoparticle suspension containing OZ at 2 mg/ml, drug solution (2 mg/ml) in PBS pH 6.4, PBS pH 6.4 (negative control), and isopropyl alcohol (positive control), respectively. After 2 h of the treatment, all samples were washed with distilled water, sectioned, and stained with hematoxylin and eosin. The mucosa was then dissected out and examined on optical microscope. The nanoparticulate formulation had no significant harmful effect on the microscopic structure of the nasal mucosa	
Liposome (Iwanaga et al. 2000)	*Drug:* Diphenhydramine hydrochloride (DH); 5(6)-carboxyfluorescein (CF) *Polymers:* Dipalmitoylphosphatidylcholine (DDPC) *Surfactant*: Dimyristoylphosphatidylcholine (DMPC) Cholesterol	– *Diameter:* 348 ÷ 411 nm – $EE_{(CF)}$*:* 34 ± 8% – $EE_{(DH)}$*:* 16 ± 6%		*Animal:* Male Wistar rats (280–320 g) *1.* In situ *nasal experiment (method Hirai)* Intranasal solutions: 20μl/per nostril (equivalent of 2μmol phospholipids +40 nmol CF). At the predetermined times, the femoral vein blood samples were centrifuged for 4 min at 10,000 rpm. The "absorbed

				fraction" of CF is determined by applying moment analysis. After 1 h, the "washable fraction" of CF was determined in the amount of nasal irrigation with PBS (flow rate; 0.2 ml/min) for 10 min. The "adhering fraction" of CF was obtained from the decapitated nasal mucosal lavage in 20 ml PBS. The liposomes increased the amount of CF adhered to the nasal mucosa 20 to 28 times compared with that in PBS *2. Antihistaminic effect (method of Kaise)* – Intranasal solution: 0.2% diphenhydramine hydrochloride (DH), an antihistamine (80μg/rat) – Allergic solution: Histamine dissolved in PBS (250 mg/ml). At the predetermined times, immediately after the perfusion of the histamine solution, 10 mm mucolytic agent dithiothreitol in PBS was perfused for 15 min. The pharmacological effect of DH was determined using the amount of protein leaking by the

(continued)

Table 16.1 (continued)

Drug formulations		*Physicochemical properties*	In vitro test	In vivo *test*
Preparation	*Components*			
				modified method of Bensadoun. The liposomes prolonged diphenhydramine hydrochloride's antihistaminic effects, indicating that liposomes can adhere to the nasal mucosa and slowly release diphenhydramine hydrochloride
Nanoparticles (Arisoy et al. 2020)	*Drug:* Levodopa *Polymers:* Resomer® RG 502 H (poly (D, L-lactide-co-glycolide) acid Wheat germ agglutinin (WGA) S*tabilizer:* Poly(vinyl alcohol) (PVA); Poloxamer 188	* *The effect of outer aqueous phases (S2)* As the PVA molecular weight increased, the particle size increased. Because smaller nanodroplets have a larger surface area, more surfactant may be required to stabilize the emulsion nanodroplet. To achieve high entrapment efficiency and smaller particle size, a large amount of Poloxamer was required to form nanoparticles. * *Determination of the optimal formulation*: – *S1:* HCl 20 mM, 0.125% levodopa – *S2:* PVA; 13,000–23,000 Da; 5%	*1. Cell viability in PC-12 neural-like cells (MTT assay)* The PC-12 neural-like cells were seeded in culture flasks and treated with 100-50-25-12.5-6.25 μg/mL of levodopa, F1-1, and WGA-F1-1 (corresponding to 100-50-25-12.5-6.25 μg/mL of levodopa concentration) and levodopa-free F1-1 and WGA-F1-1 (in the same amount of polymer and WGA with F1-1 and WGA-F1-1), separately. For comparison, well-contained cells and media were used as positive controls, and DMSO was used as the negative control. After 24 h of the incubation, cell viability	*Animal:* Male CD57/BL6 mice highly sensitive to the selected Parkinson's disease model. The acute Parkinson's disease model in mice with four two-hour-interval injection doses of 1-methyl-4-phenyl-1,2,3,6-tetrahydropyridine was employed to all of the animals (20 mg/kg; total dose 80 mg/kg/day). A week after the injections, the animals were evaluated for motor performance to approve the development of Parkinson's disease and allocated to the following groups: Oral levodopa treatment group (16 mg/kg levodopa/day); intranasal levodopa treatment group (16 mg/kg

		– *Volume:* 75 mL – *Oil phase:* Dichloromethane – *Evaporation condition:* 20 m, 40 °C, evaporator – *Size:* 329.0 ± 188.3 nm – *ZP:* −4.47 ± 0.576 mV – *PDI*: 0.384 ± 0.113 – *EE:* 72.95% ***DSC, FTIR analysis*:** The active substance did not bind to the carboxylic acid group and is thus suitable for nanoparticle surface modification. The DSC shows that the active substance in the formulation becomes amorphous or irregularly crystalline, becomes trapped in the polymer, and is partially adsorbed on the surface.	was determined by MTT assay – results show that no significant cell death was observed after the exposure to all agents at the doses ranging from 6.25 to 100 g/mL when compared to the control. The nanoparticles (F1-1) reduced levodopa toxicity at the higher doses by maintaining the cell viability. The cell viability of WGA-grafted and non-grafted F1-1 nanoparticles was comparable, indicating that WGA-conjugated nanoparticles were the safe carrier system for the delivery to the brain *2. Drug release and dissolution* The nanoparticles suspended in the buffer solution were placed in a dialysis bag and tied at both ends. The dialysis bag was suspended in 50 mL buffer solution with pH 4.5 (endolysosomal compartment pH) and pH 7.4 (brain pH) and kept at 37 0.5 °C. To compensate levodopa's low solubility, 2% Tween 80 was added to the buffer solutions. At the predetermined time intervals, 1 mL aliquots were sampled	levodopa/day; intranasal); intranasal levodopa loaded nanoparticle (F1-1) treatment group (equivalent of 16 mg/kg levodopa/day); and intranasa WGA-grafted levodopa loaded nanoparticle (WGA-F1-1) treatment group (equivalent of 16 mg/kg levodopa/day). The nanoparticles and the drug were dissolved in distilled water to obtain the same ratio of 1.0 mg/1.0 ml w:v. The maximum volume solution/ suspension was 20μL/nostril/ time. The treatments were continued for 7 days ***Experimental animal model for Parkinson's disease*** After the last day of the 7-day treatment period, motor activity tests were repeated at 30, 60, and 120 min, and the animals were sacrificed by cervical dislocation. Blood and brain tissue samples were obtained to measure DA level and stored at -80°C until the day of analysis *Motor tests* All of the animals developed Parkinson's disease as the

(continued)

Table 16.1 (continued)

Drug formulations				
Preparation	*Components*	*Physicochemical properties*	In vitro test	In vivo *test*
			and replaced with 1 mL of fresh pH 4.5 and pH 7.4 phosphate-buffered solutions. HPLC was used to determine the drug concentrations. At the different pH levels, the polymeric formulations demonstrated similar release profile. The release of the active substance is closer to the surface resulting in its rapid release in the first hours, and then the release of the active substance began from the PLGA polymer in the inner regions. Over 9 h, the F1-1 formulation released 96% of the drug at pH 4.5 and pH 7.4 *3. Surface modification with WGA* Formulation F1-1 was incubated with cross-linker NHS/EDAC and F-WGA. In the formulation F1-1a (WGA-F1-1), 86.44% F-WGA were conjugated to the surface of the nanoparticles – The conjugation ratio of WGA to the nanoparticles increased when the incubation	result of the used 1-methyl-4-phenyl-1,2,3,6-tetrahydropyridine, and all measurements of spontaneous and locomotor activity showed the impaired motor function. WGA-F1-1 nanoparticles significantly improved spontaneous and locomotor activity at all measurement points after the drug application, making them comparable to healthy animals *Determination of blood and tissue dopamine levels by ELISA* Dopamine levels in the brain tissue and blood are measured to compare the concentrations achieved after treatment with various pharmaceutical formulations and passage routes. In the intranasal levodopa group, the drug concentration was significantly higher than in the blood level. The highest concentration in the brain accompanied by the lowest blood

			time of WGA was increased independent of the incubation time with the cross-linker – The conjugated amount of WGA increased significantly, but the WGA/nanoparticle ratio decreased when the nanoparticle amount was increased from 6.5 mg to 20.0 mg, but the WGA/nanoparticle ratio decreased – The binding constant decreased significantly with the decrease of the incubation time of the cross-linking agents with the nanoparticles – After the binding of the nanoparticles with WGA, their size and PDI value increased. The drug release from the nanoparticles was still pH independent and burst release disappeared	concentration is measured in WGA-F1-1 nanoparticle group
Nanostructured lipid carriers (Gadhave and Kokare 2019)	*Drug:* Teriflunomide (TFM) *Lipid:* Compritol 888 ATO; maisine 35-1 Glyceryl monostearate; stearic acid *Surfactant*: Tween 20; Tween 80;	– *Size:* 99.82 ± 1.36 nm – *ZP:* − 22.29 ± 1.8 mV – *LC:* 6.68 ± 0.24% – *EE:* 83.39 ± 1.24% * ***XRD, DSC, FTIR analysis***	*1.* Ex vivo *mucoadhesive strength* Texture Pro CT V 1.8 Build 29 was used to determine the mucoadhesive strength of the optimized TFM mucoadhesive nanostructured lipid carrier formulation. The mucoadhesive polymers	*Animal:* Male Wistar rats (age 21 days, weight 50–100 g) *1. Cuprizone-induced microglia activation rat demyelination model* The elevated plus-maze study performed during the period of the regular supplemented 0.6% cuprizone via the oral route.

(continued)

Table 16.1 (continued)

Drug formulations				
Preparation	*Components*	*Physicochemical properties*	In vitro test	In vivo *test*
	Cremophor RH-40 *Stabilizers:* Gelucire 44/14; Poloxamer 407 *Mucoadhesive agents:* Carbopol 974P; chitosan; HPMC K4M		help to improve the adhesion of the formulation in the nasal cavity; hence, the adhesion time of formulation could be enhanced 2. In vitro *drug release of nanoparticles* The drug release of the optimized TFM nanostructured lipid carriers and TFM mucoadhesive nanostructured lipid carrier formulations was studied using a dialysis membrane in a Franz diffusion cell with simulated nasal electrolyte solution for 8 h at 34.5 ± 0.5 °C. The withdrawn and replenished aliquots of the simulated nasal electrolyte solution in the receiver compartment at the predefined time intervals were 0.1 mL. These dilutions were analyzed for % drug release using HPLC method. The % cumulative TFM release of the optimized TFM nanostructured lipid carriers and TFM mucoadhesive	The TFM-mucoadhesive nanostructured lipid carrier and TFM nanostructured lipid carrier formulations were administered through intranasal and oral routes after 15, 20, 25, and 30 days. There were four animal groups: – Group I (normal control – without cuprizone) – Group II (negative control – without TFM treatment) – Group III (orally treated by 100μg/mL solution of TFM nanostructured lipid carriers); – Group IV (intranasally treated by 50μg/mL of TFM mucoadhesive nanostructured lipid carriers) *Result:* Animals infected with cuprizone often enter, move, or fall into open compartments due to the abnormal movement. Group II animals did not improve clinically, but group III and IV animals with normal behaviors even reduced the number of entries and movements in the open

			nanostructured lipid carriers were found to be 75.11 ± 0.58% and 96.44 ± 0.73% within time frame of 8 h *3.* Ex vivo *permeation of nanoparticles* The permeation of the optimized TFM nanostructured lipid carriers and TFM mucoadhesive nanostructured lipid carrier formulations was studied using freshly dissected clean nasal mucosa in a Franz diffusion cell with the simulated nasal electrolyte solution for 8 h at 34 ± 1 °C. The withdrawn and replenished aliquots of the simulated nasal electrolyte solution in the receiver compartment at the predefined time intervals were 0.1 mL. These dilutions were diluted with methanol and centrifuged. The supernatants were separated and analyzed for % drug release using HPLC method. Permeation of TFM nanostructured lipid carriers: 65.13 ± 0.86% (651 ± 9.8μg/cm^2). Permeation of TFM	compartment (compared to the negative control). TFM mucoadhesive nanostructured lipid carrier intranasal formulation showed the significant effect on demyelination compared to the TFM nanostructured lipid carrier oral delivery. Hence, the intranasal administration of TFM was more effective in multiple sclerosis than the oral administration because direct delivery to the brain was achieved *2.* In vivo *subacute toxicity evaluation* Four groups of animals were treated via intranasal route with the doses of TFM mucoadhesive nanostructured lipid carriers 0, 1, 2, and 4 mg/kg, respectively. During 28 days, animals were observed for gross pathology, subacute toxicity, and body weight change. Then, animals were anesthetized and the blood samples in anticoagulant EDTA-coated tubes were collected at day 14 and day 28, and biomarker screening was performed for the

(continued)

Table 16.1 (continued)

Drug formulations				
Preparation	*Components*	*Physicochemical properties*	In vitro test	In vivo *test*
			mucoadhesive nanostructured lipid carriers: 83.01 ± 0.69% (830 ± 7.6μg/cm^2). The steady-state flux (Jss) of TFM mucoadhesive nanostructured lipid carriers was around 2.0 folds more than the TFM nanostructured lipid carriers *4. Assessment of nasal ciliotoxicity* The nasal ciliotoxicity study was carried out on sheep nasal mucosa for 8 h. Negative controls were mucosa sections treated with TFM nanostructured lipid carriers and TFM mucoadhesive nanostructured lipid carriers, while positive controls were untreated mucosa sections. These sections were stored in 10% formalin solution, paraffin-fixed, and stained with the staining agents (hematoxylin and eosin). Microscopic examinations of stained mucosa sections were performed to demonstrate the safety as well as structural changes by pathological studies.	estimation of TFM-induced hepatotoxicity Result: TFM exhibited satisfactory effect on demyelinating disorder like multiple sclerosis. The intranasal formulation decreased the number of activated immune responses including the proliferation of activated lymphocytes (T and B cells), astrocytes, and microglia cells and even block the synthesis of cytokines. The control group of animals did not reflect any changes in hepatic and renal biomarker levels. The TFM-MNLC formulation-treated (low and medium dose) groups did not show any significant changes in biomarkers for 14 and 28 days. But high-dose (4.0 mg/kg) group showed nonsignificant changes in the hepatic biomarker level. The TFM-MNLC formulation was found in less amount in the liver and kidney due to the

			The optimized TFM nanostructured lipid carrier and TFM mucoadhesive nanostructured lipid carrier formulations did not reflect any ciliotoxicity and structural changes; thus, the formulations were safe for nasal administration	mucoadhesive agent; however, the final TFM-MNLC formulation was found to be safe and effective for long-term therapy of multiple sclerosis via intranasal route

Table 16.2 Some studies on the activity of tuberculosis treatment preparations

Drug formulations				
Preparation	*Components*	Physicochemical properties	In vitro test	In vivo test
Dry powder inhalers (Mukhtar et al. 2021)	*Drug:* Isoniazid *Polymers:* Chitosan (CS), thiolated chitosan (TC), and mannosylated chitosan (MC) were used individually in the conjugation with hyaluronic acid (HA); Inhalac®400	***Freeze-dried particles:*** – *Morphology*: Not perfectly spherical and smooth – *Size:* 198 ÷ 316 nm – *ZP:* + 14÷ 25 – *PDI*: 0.112 ÷ 0.398 – *EE:* 61 ÷ 75% ***Spray-dried particles:*** – *Morphology*: Smooth- and majorly rough-surfaced. – *Size:* 300 nm÷342 nm – *ZP:* + 31 ÷ 34 – *PDI*: 0.199÷ 0.211 – *EE:* 90 ÷ 91% * ***XRD, DSC, FTIR analysis*:** – All the formulations were physicochemically compatible – The drug changed to the amorphous state after the entrapment inside the freeze-dried nanoparticles. However, in the case of CS-based spray-dried samples using mannitol, a mannitol's XRD peak at 10° remained	*1.* In vitro *release:* In the simulated lung fluid, 100% of unmodified isoniazid was released over 5 h. As the composition changed from CS to MC, the percentage release of isoniazid slowed (63–40%) *2.* In vitro *permeability:* The trend in the increased permeation of isoniazid was seen from CS to MC *3.* In vitro-in silico *aerodynamic deposition*: Regardless of the drying technique, the majority of the dry nanopowders were deposited in the alveolar region (MMDA <4.5μm) *4. Cell viability assay*: The MTT assay demonstrated that all of polymeric hybrid nanopowders were safe for animal use	
Microspheres (Vishwa et al. 2021)	*Drug:* Moxifloxacin *Polymer:* Poly (lactic-co-glycolic) (PLGA)	*Size:* 3.16μm *EE:* 78.0% *Drug loading:* 21.98% *XRD, DSC, FTIR analysis*: There	*1. Release study:* Moxifloxacin-Moxifloxacin-PLGA-microsphere showed a biphasic release pattern and their in vitro release	*Animals:* Male Swiss albino mice *1. Pharmacokinetics study:* – PLGA microspheres could

		were no remarkable changes, confirming the absence of drug-polymer interaction	pattern was nearly identical in phosphate buffer (pH 7.4) and acetate buffer (pH 4.4) *2. Testing bioactivity:* Microplate Alamar blue assay confirms that the drug maintains residence time in the lungs up to 24 h after inhalation	maintain higher drug concentrations in the lungs for prolonged period, up to 24 h – The mean residence time of moxifloxacin-PLGA-microsphere 277.39 ± 12.21 h and that of drug was 22.42 ± 0.76 h. – There was a twofold increase in the area under the curve AUC0–24 h in the lungs for moxifloxacin-PLGA-microsphere compared with the AUC0–24 h of the drug *2. Bio-distribution study:* After 30 min, the accumulation of moxifloxacin and moxifloxacin-PLGA-microsphere in the lungs was 78.1 ± 2.42% and 84.21 ± 2.59%, respectively. After 24 h, the accumulation of moxifloxacin and moxifloxacin-PLGA-microsphere in the lungs was 27.63% and 78.26 ± 2.19% of the dose, respectively
Nanocapsules (Diego-González et al. 2020)	*Drug:* Imiquimod *Polymers:* Chitosan (CS) or inulin/polyarginine (INU/pArg); ESAT-6/CFP-10 fusion protein	*Nanocapsules CS* – *Size:* 145± 14 nm – *ZP:* +28 ± 4.5 – *PDI*: ≤ 0.2 – *EE:* 60 ± 4%	*1. Cytocompatibility of the polymeric nanocapsules* – *Cell lines:* Two macrophage (RAW 264.7, PMA-differentiated THP-1) and	*Animals:* Female C57BL/6 mice (8–12 weeks old) *Systemic immune response against the ESAT-6/CFP-10 fusion protein*

(continued)

Table 16.2 (continued)

Drug formulations				
Preparation	*Components*	Physicochemical properties	In vitro test	In vivo test
	(ECH) *Oil:* Miglyol, linoleic acid, glycerin *Surfactant*:18:0 PE-PEG1000	*Nanocapsules CS:Ag* – *Size:* 152 ± 15 nm – *ZP:* +8 ± 10 – *PDI*: ≤ 0.2 – *Drug loading*: 60 ± 6% *Nanocapsules INU* – *Size:* 158 ± 7 nm – *ZP:* −37 ± 4 – *PDI*: ≤ 0.2 – *EE:* 69 ± 6% *Nanocapsules INU:Ag* – *Size:* 136 ± 7 nm – *ZP:* −36 ± 6 – *PDI*: ≤ 0.2 *Nanocapsules INU/pArg* – *Size:* 158± 22 – *ZP:* +20 ± 1 – *PDI*: ≤ 0.2 *Nanocapsules* INU:Ag:pArg – *Size:* 151± 11 – *ZP:* +27 ± 8 – *PDI*: ≤ 0.2 – *Drug loading*: 55 ± 5% *Nanocapsules INU:pArg:Ag* – *Size:* 158 ± 12 – *ZP:* +31 ± 7 – *PDI*: ≤ 0.2 – *Drug loading*: 30 ± 10%	two pulmonary epithelial (NCI-H460, A549) – At low-intermediate concentrations (<100μg/mL), CS and INU/pArg nanocapsules were cytocompatible with all cell lines tested, but at the high concentrations, they were toxic *2. Reactive oxygen species' release in HL-60 cells* After 6 h of the incubation, CS nanocapsules produced low levels of ROS at the concentration of 200 g/mL. After 14 h of the incubation, CS induced the release of ROS at the concentrations of 50 g/mL and 200 g/mL and INU/pArg NCs at 100 g/mL, respectively *3. Complement activation in human plasma* Only CS nanocapsules (200μg/mL) induce the activation of the complement system similar to zymosan (1.0 mg/mL) *4. Cytokine release* The polymeric nanocapsules induced low levels of TNF-α, GM-CSF, IL-6, and IL-10 and	*1. Characterization of specific IgG and IgA antibodies against ESAT-6/CFP-10* – Only the INU:pArg:Ag prototype produced specific IgA antibodies against the ESAT-6 antigen. When the antigen (INU:pArg:Ag) was on the nanocapsule surface, antibody levels were higher than when this antigen was shielded by the polymeric shell of the nanocapsules – Prior priming with the BCG vaccination resulted in equal or even higher antibody titers for the CS:Ag nanocapsule prototype, whereas lowered the antigenicity of the INU:pArg:Ag and INU:Ag:pArg prototypes *2. Characterization of the cellular immune response in splenocytes* The antigen recall caused the highest IFN-γ or IL-17 concentration in animals after their priming with the BCG vaccine and immunizing with the

			undetectable or very low levels of all the other cytokines tested	INU/pArg prototypes or the CS:Ag NCs. TNF-α was not found in any of the groups studied
Liposomal dry powder (Viswanathan et al. 2019)	*Drug:* Licorice extract (LE) *Polymers:* Cholesterol *Surfactant*: Soybean phosphatidylcholine (Lipoid S100)	– *Size:* 210 nm – *EE:* 75% – *ZP:* – 27.1 ÷ – 32.5 mV – *MMAD:* 4.29 ± 1.23μm – *Drug loading:* 1.5–2.0 % – *The moisture:* 7.98 ± 0.11% w/w	*1. Lung deposition studies using twin-stage impinger* The dosage values were about 100% recovered in all batches. The emitted dose for all of the batches was greater than 80%, showing that the Lupihaler® device had minimal retention. The percent fine particle fraction of the dry powder for inhalation batches ranged from 14 to 25%, indicating considerable dry powder for the inhalation deposition in the lungs *2. Lung deposition studies using Andersen cascade impactor:* All the formulations showed MMAD close to 5 ± 1.2μm. The fine particle fraction of batches LP-B, LP-C, and LP-D (drug/lipid weight ratio 1:9, 1:7, 1:6, respectively) were 54.68, 41.37, and 43.33, respectively, indicating higher deep lung deposition of the powder. Formulation LP-B (drug/lipid weight ratio 1:9) with a MMAD of 4.29 ± 1.23μm and fine	*1. Lung deposition studies* *Animals:* Healthy Swiss albino mice (weight range of 20–25 g; 6–7 weeks old). The drug retention in the rat lungs following the single dosage injection was measured over 24-h period. Approximately 46% of the drug administered in the formulations was deposited within the lungs *2. Pharmacodynamic evaluation* *Animals:* BALB/c mice infected with *Mycobacterium tuberculosis* H37Rv. Group 1: Control untreated Group 2: Treated with the Formulations (equivalent of 100μg drug) Group 3: Treated with the formulations (equivalent of 60μg of drug); Group 4: Treated with isoniazid (5 mg/kg body weight) and rifampicin (10 mg/kg body weight) Dosing began on day 29 after

(continued)

Table 16.2 (continued)

Drug formulations		Physicochemical properties	In vitro test	In vivo test
Preparation	*Components*			
			particle fraction of 54.68% was selected for further studies as the results were the most favorable	the animals were infected and lasted for 8 weeks (56 doses). The mice were sacrificed 4 days following their last dose. The lungs and spleen were excised aseptically and used for subjective evaluation as well as colony-forming unit estimation in homogenates. Formulation containing licorice extract is able to produce statistically significant, dose-dependent reduction in colony-forming units in lungs as well as the spleen when compared to the untreated control
Core-shell nanoparticles (Najafi et al. 2021)	*Drug:* PPE17 protein; class B CpG ODN *Polymers:* Chitosan, alginate	*Chitosan nanoparticle* – *Size:* 278 ± 4.5 nm – *ZP:* + 29 ± 2.2 mV – *PDI*: 0.33 ± 0.2 *Alginate-chitosan nanoparticle* – *Size:* 365 ± 6.3 nm – *ZP:* −36 ± 2.7 mV – *PDI*: 0.31 ± 0.1 *Alginate-chitosan CpG-PPE17 nanoparticle* – *Size:* 427 ± 8.6 nm – *ZP:* −37 ± 5.1 mV	*Release study* The released antigen was determined at the different time points of 6, 12, 24, 72, 96, 120, and 144 h. At each time point, nanoparticle suspension (1.0 ml) was centrifuged at 14,000 g for 20 min. The supernatant was replaced with fresh PBS (1.0 ml), pH 7.4). The released radiolabeled PPE17 was investigated by radiometric assay with gamma counter instrument.	*Animals:* Male BALB/c mice (6–0.8 weeks old) The study was performed on 11 groups of vaccinated and control animals, in which, in addition to one group injected with one dose of BCG on day 0, there were five groups injected intranasally and five groups injected subcutaneously three times on days 0, 14, and 28. Nanoparticles with or without alginate

		– *PDI*: 0.39 ± 0.2 – *EE:* 11%	The release experiments indicated that alginate-coated chitosan nanospheres improved the nanosphere's stability in PBS and changed the antigen release behavior	containing medicines, blank nanoparticles, or phosphate buffer were delivered to five binary subcutaneous and intranasal groups *1. Serum antibody titers* Two weeks after latest dosages, the blood samples were taken by orbital sinus puncturing and centrifuged to separate the serum for antibody evaluation in blood samples. The level of IgG1 and IgG2a in serum was elevated in subcutaneous groups. Only protein+ CpG group has the elicited IgG2a response in the case of intranasal route *2. Cytokines assay* After 2 weeks of the final immunization, the cytokine assay was performed in the spleens of mice. The level of cytokines IFN-γ, IL-4, IL-17, and TGF-β from spleen tissue were analyzed. Intranasal delivery of chitosan nanoparticles induces strong Th1- and Th17-associated cytokines and antibody responses in the animal model

(continued)

Table 16.2 (continued)

Drug formulations				
Preparation	*Components*	Physicochemical properties	In vitro test	In vivo test
Liposome cation (Rosada et al. 2008)	*Drug:* DNA-hsp65 vaccine *Polymers:* Egg phosphatidylcholine (EPC), 1,2-dioleoyl-sn-glycero-3-phosphoethanolamine (DOPE), and 1,2-dioleoyl-3-trimethylammonium-propane (DOTAP)	* *Emty liposome* – *Diameter:* 247.47 ± 86.26 (93.96) 862.92 ± 140.78 (6.04) *-ZP:* +26.9 ± 2.4 mV **Entrapping-hsp65 (ENTR-hsp65)* – *Diameter:* 244.53 ± 64.05 nm (93.21%) 985.92 ± 229.12 nm (6.79%). *-ZP:* +32.8 ± 4.0 mV * *Compexing-hsp65 (COMP-hsp65)* – *Diameter:* 616.73 ± 152.35 nm (93.4%) 2749.56 ± 774.90 nm (7.53%) – *ZP:* 23.7 ± 2.3 mV	*Cytotoxicity assay* The standard MTT colorimetric cytotoxicity assay was used for J774-macrophage cells. J774 cells were transfected with each of the liposome formulations (ENTR-hsp65 or COMP-hsp65) or with naked hsp65 showing more than 60% of cell viability even with high concentrations of DNA (200μg/mL, corresponding to 400μL of liposome)	Animals: BALB/c mice Mice were divided into four groups: BCG immunization group, naked DNA vaccination group, intranasal liposome group, and control group. Serum was collected 30 days after the last dose of each immunization scheme *1. Evaluation of antibody production* The presence of two subtypes of anti-hsp65 antibodies in the serum of BALB/c mice was examined 30 days after the injection with four doses of naked DNA or the single dose of liposomes. It was discovered that the immunization with liposomes containing DNA-hsp65 induces Th1 antibody production *2. Evaluation of route and dose of immunization* Intramuscular route: Two intramuscular doses of liposomes showed a slight colony forming-unit reduction, but overall it was not effective

				Intranasal route: COMP-hsp65 was delivered intranasally in single dose (25μg of DNA). The higher protection was observed, with the significant reduction of 1.97 ± 0.23 log in the bacterial load between the saline group and COMP-hsp65. This colony-forming unit reduction was similar to four doses (400μg of total DNA) of naked hsp65 and bacilli *Calmette-Guérin* *3. Histological examination* – Saline-treated lung sections revealed tissue damage caused by severe inflammation, with few lymphocyte infiltrations and the high number of foamy macrophages. In contrast, mice immunized with COMP-hsp65 had smaller pneumonic areas with a cell infiltrate dominated by lymphocytes and macrophages – In the saline control group, 70% of the lungs was damaged, whereas in mice immunized with COMP-hsp65, lung damage was reduced to 30%. These liposome immunization effects were comparable to

(continued)

Table 16.2 (continued)

Drug formulations		Physicochemical properties	In vitro test	In vivo test
Preparation	*Components*			
				those induced by naked hsp65 and bacilli *Calmette-Guérin* *4. The pattern of cytokine production* When mice were attacked with *M. tuberculosis*, a Th1 cytokine pattern was observed, with an increase in IFN-, IL-12, and IL-10 production compared to the uninfected animals. However, compared to the saline control mice, immunization with naked hsp65 and COMP-hsp65 induced the significant increase in IFN- and the significant decrease in IL-10. These immunization protocols had no effect on IL-12 expression

in the nose to support immunity against bacteria and fungi (Si et al. 2020), has recently been published with success. However, the development of a drug delivery system based on nanofibers for the treatment of tuberculosis or central nervous system diseases in particular has not yet received significant attention.

16.4 Conclusion

After many years of development, the nasal drug delivery system is gradually proving to be superior in the targeted drug delivery because of its low cost and simple and economical advantages. Scientists are interested in improving and working to improve the imprecise dosing limitations and the difficulty of accessing deep within the nasal cavity. However, the blood-brain barrier, blood-cerebrospinal fluid, and mucosal clearances in CNS diseases still pose significant challenges. As a result, research on nanoparticles, nanocapsules, cell-penetrating peptides, and other new drug delivery systems has gradually increased in recent years. Their advancement has positive implications for drug penetration, delivery of low osmolarity molecules, controlled release, and many other functions that are being discovered and researched. More detailed and in-depth research, as well as clinical trials, are required to determine the long-term clinical efficacy of nasal preparations.

References

Abe K, Irie T, Uekama K (1995) Enhanced nasal delivery of luteinizing hormone releasing hormone agonist Buserelin by oleic acid solubilized and stabilized in Hydroxy propyl-β-Cyclodextrin. Chem Pharm Bull 43:2232–2237. https://doi.org/10.1248/cpb.43.2232

Ahmad N, Ahmad R, Alam MA et al (2018b) Retracted article: impact of Ultrasonication techniques on the preparation of novel Amiloride-Nanoemulsion used for intranasal delivery in the treatment of epilepsy. Artif Cells Nanomed Biotechnol 46:S192–S207. https://doi.org/10.1080/21691401.2018.1489826

Ahmad N, Ahmad R, Naqvi AA et al (2018a) Retracted article: intranasal delivery of quercetin-loaded Mucoadhesive Nanoemulsion for treatment of cerebral Ischaemia. Artif Cells Nanomed Biotechnol 46:717–729. https://doi.org/10.1080/21691401.2017.1337024

Alavian F, Shams N (2020) Oral and intra-nasal Administration of Nanoparticles in the cerebral ischemia treatment in animal experiments: considering its advantages and disadvantages. Curr Clin Pharmacol 15:20–29. https://doi.org/10.2174/1574884714666190704115345

Arisoy S, Sayiner O, Comoglu T et al (2020) In vitro and in vivo evaluation of levodopa-loaded nanoparticles for nose to brain delivery. Pharm Dev Technol 25:735–747. https://doi.org/10.1080/10837450.2020.1740257

Arora P, Sharma S, Garg S (2002) Permeability issues in nasal drug delivery. Drug Discov Today 7:967–975. https://doi.org/10.1016/S1359-6446(02)02452-2

Bakke H, Samdal HH, Holst J et al (2006) Oral spray immunization may be an alternative to intranasal vaccine delivery to induce systemic antibodies but not nasal mucosal or cellular immunity. Scand J Immunol 63:223–231. https://doi.org/10.1111/j.1365-3083.2006.01730.x

Ballabh P, Braun A, Nedergaard M (2004) The blood–brain barrier: an overview. Neurobiol Dis 16: 1–13. https://doi.org/10.1016/j.nbd.2003.12.016

Ballantine HT, Bell E, Manlapaz J (1960) Progress and problems in the neurological applications of focused ultrasound. J Neurosurg 17:858–876. https://doi.org/10.3171/jns.1960.17.5.0858

Bologa A, Bologa A (2001) Electrohydrodynamic instability of droplets as an influencing factor for aerosol space charge generation. J Electrost 51–52:470–475. https://doi.org/10.1016/S0304-3886(01)00123-1

Cornaz A-L, Buri P (1994) Nasal mucosa as an absorption barrier. Eur J Pharm Biopharm 40:261–270

Cacabelos R, Torrellas C, Fernández-Novoa L et al (2016) Histamine and immune biomarkers in CNS disorders. Mediat Inflamm 2016:1–10. https://doi.org/10.1155/2016/1924603

Cassano R, Servidio C, Trombino S (2021) Biomaterials for drugs nose–brain transport: a new therapeutic approach for neurological diseases. Materials 14:1802. https://doi.org/10.3390/ma14071802

Corbo DC, Liu J, Chien YW (1989) Drug absorption through mucosal membranes: effect of mucosal route and penetrant hydrophilicity. Pharm Res 06:848–852. https://doi.org/10.1023/A:1015952320372

Corbo DC, Liu J-C, Chienx YW (1990) Characterization of the barrier properties of mucosal membranes. J Pharm Sci 79:202–206. https://doi.org/10.1002/jps.2600790304

Costa CP, Moreira JN, Sousa Lobo JM et al (2021) Intranasal delivery of nanostructured lipid carriers, solid lipid nanoparticles and Nanoemulsions: a current overview of in vivo studies. Acta Pharm Sin B 11:925–940. https://doi.org/10.1016/j.apsb.2021.02.012

Costantino HR, Illum L, Brandt G et al (2007) Intranasal delivery: physicochemical and therapeutic aspects. Int J Pharm 337:1–24. https://doi.org/10.1016/j.ijpharm.2007.03.025

Cunha S, Costa CP, Loureiro JA et al (2020) Double optimization of Rivastigmine-loaded nanostructured lipid carriers (NLC) for nose-to-brain delivery using the quality by design (QbD) approach: formulation variables and instrumental parameters. Pharmaceutics 12:599. https://doi.org/10.3390/pharmaceutics12070599

Dahl AR, Lewis JL (1993) Respiratory tract uptake of inhalants and metabolism of Xenobiotics. Annu Rev Pharmacol Toxicol 33:383–407. https://doi.org/10.1146/annurev.pa.33.040193.002123

Danaei M, Dehghankhold M, Ataei S et al (2018) Impact of particle size and polydispersity index on the clinical applications of lipidic nanocarrier systems. Pharmaceutics 10:57. https://doi.org/10.3390/pharmaceutics10020057

Daniel TM (2006) The history of tuberculosis. Respir Med 100:1862–1870. https://doi.org/10.1016/j.rmed.2006.08.006

Das S, Ng WK, Tan RBH (2012) Are nanostructured lipid carriers (NLCs) better than solid lipid nanoparticles (SLNs): development, characterizations and comparative evaluations of Clotrimazole-loaded SLNs and NLCs? Eur J Pharm Sci 47:139–151. https://doi.org/10.1016/j.ejps.2012.05.010

Diego-González L, Crecente-Campo J, Paul MJ et al (2020) Design of polymeric Nanocapsules for intranasal vaccination against mycobacterium tuberculosis: influence of the polymeric Shell and antigen positioning. Pharmaceutics 12:489. https://doi.org/10.3390/pharmaceutics12060489

Djupesland PG, Skatvedt O, Borgersen AK (2001) Dichotomous physiological effects of nocturnal external nasal dilation in heavy snorers: the answer to a Rhinologic controversy? Am J Rhinol 15:95–104. https://doi.org/10.2500/105065801781543745

Dolovich MB, Dhand R (2011) Aerosol drug delivery: developments in device design and clinical use. Lancet 377:1032–1045. https://doi.org/10.1016/S0140-6736(10)60926-9

Erdő F, Bors LA, Farkas D et al (2018) Evaluation of intranasal delivery route of drug administration for brain targeting. Brain Res Bull 143:155–170. https://doi.org/10.1016/j.brainresbull.2018.10.009

Farnoud A, Baumann I, Rashidi MM et al (2020) Simulation of patient-specific bi-directional pulsating nasal aerosol dispersion and deposition with clockwise 45° and 90° nosepieces. Comput Biol Med 123:103816. https://doi.org/10.1016/j.compbiomed.2020.103816

Finlay WH, Darquenne C (2020) Particle size distributions. J Aerosol Med Pulm Drug Deliv 33: 178–180. https://doi.org/10.1089/jamp.2020.29028.whf

Gadhave DG, Kokare CR (2019) Nanostructured lipid carriers engineered for intranasal delivery of Teriflunomide in multiple sclerosis: optimization and in vivo studies. Drug Dev Ind Pharm 45: 839–851. https://doi.org/10.1080/03639045.2019.1576724

Galvin P, Thompson D, Ryan KB et al (2012) Nanoparticle-based drug delivery: case studies for cancer and cardiovascular applications. Cell Mol Life Sci 69:389–404. https://doi.org/10.1007/s00018-011-0856-6

Gholizadeh H, Ong HX, Bradbury P et al (2021) Real-time quantitative monitoring of in vitro nasal drug delivery by a nasal epithelial mucosa-on-a-chip model. Expert Opin Drug Deliv 18:803–818. https://doi.org/10.1080/17425247.2021.1873274

Gibson RE, Olanoff LS (1987) Physicochemical determinants of nasal drug absorption. J Control Release 6:361–366. https://doi.org/10.1016/0168-3659(87)90089-7

Gupta S, Dhanda S, Sandhir R (2019) Anatomy and physiology of blood-brain barrier. In: Brain targeted drug delivery system. Elsevier, pp 7–31

Häfeli UO (2004) Magnetically modulated therapeutic systems. Int J Pharm 277:19–24. https://doi.org/10.1016/j.ijpharm.2003.03.002

Haider M, Abdin SM, Kamal L et al (2020) Nanostructured lipid carriers for delivery of chemotherapeutics: a review. Pharmaceutics 12:288. https://doi.org/10.3390/pharmaceutics12030288

Huang CH, Kimura R, Nassar RB et al (1985) Mechanism of nasal absorption of drugs I: physicochemical parameters influencing the rate of in situ nasal absorption of drugs in rats. J Pharm Sci 74:608–611. https://doi.org/10.1002/jps.2600740605

Ignjatović J, Šušteršič T, Bodić A et al (2021) Comparative assessment of in vitro and in Silico methods for aerodynamic characterization of powders for inhalation. Pharmaceutics 13:1831. https://doi.org/10.3390/pharmaceutics13111831

Illum L (2010) Is nose-to-brain transport of drugs in man a reality? J Pharm Pharmacol 56:3–17. https://doi.org/10.1211/0022357022539

Ishikawa F, Katsura M, Tamai I et al (2001) Improved nasal bioavailability of Elcatonin by insoluble powder formulation. Int J Pharm 224:105–114. https://doi.org/10.1016/S0378-5173(01)00736-0

Iwanaga K, Matsumoto S, Morimoto K et al (2000) Usefulness of liposomes as an intranasal dosage formulation for topical drug application. Biol Pharm Bull 23:323–326. https://doi.org/10.1248/bpb.23.323

Jadhav K, Gambhire M, Shaikh I et al (2007) Nasal drug delivery system-factors affecting and applications. Curr Drug Ther 2:27–38. https://doi.org/10.2174/157488507779422374

Kaliner M, Marom Z, Patow C et al (1984) Human respiratory mucus. J Allergy Clin Immunol 73: 318–323. https://doi.org/10.1016/0091-6749(84)90403-2

Khosa A, Reddi S, Saha RN (2018) Nanostructured lipid carriers for site-specific drug delivery. Biomed Pharmacother 103:598–613. https://doi.org/10.1016/j.biopha.2018.04.055

Krishnamoorthy R, Mitra AK (1998) Prodrugs for Nasal drug delivery. Adv Drug Deliv Rev 29: 135–146. https://doi.org/10.1016/S0169-409X(97)00065-3

Lansley AB (1993) Mucociliary clearance and drug delivery via the respiratory tract. Adv Drug Deliv Rev 11:299–327. https://doi.org/10.1016/0169-409X(93)90014-U

Liu Y-L, Chen D, Shang P et al (2019) A review of magnet systems for targeted drug delivery. J Control Release 302:90–104. https://doi.org/10.1016/j.jconrel.2019.03.031

Lochhead JJ, Thorne RG (2012) Intranasal delivery of biologics to the central nervous system. Adv Drug Deliv Rev 64:614–628. https://doi.org/10.1016/j.addr.2011.11.002

Marttin E, Schipper NGM, Verhoef JC et al (1998) Nasal Mucociliary clearance as a factor in nasal drug delivery. Adv Drug Deliv Rev 29:13–38. https://doi.org/10.1016/S0169-409X(97)00059-8

Mazlan MKN, Mohd Tazizi MHD, Ahmad R et al (2021) Antituberculosis targeted drug delivery as a potential future treatment approach. Antibiotics 10:908. https://doi.org/10.3390/antibiotics10080908

Meibohm B (2006) The role of pharmacokinetics and pharmacodynamics in the development of biotech drugs. In: Pharmacokinetics and pharmacodynamics of biotech drugs. Wiley-VCH Verlag GmbH & Co. KGaA, Weinheim, Germany, pp 1–13

Keller L-A, Merkel O, Popp A (2022) Intranasal drug delivery: opportunities and Toxicologic challenges during drug development. Drug Deliv Transl Res 12:735–757. https://doi.org/10.1007/s13346-020-00891-5

Mittal D, Ali A, Md S et al (2014) Insights into direct nose to brain delivery: current status and future perspective. Drug Deliv 21:75–86. https://doi.org/10.3109/10717544.2013.838713

Moffa A, Costantino A, Rinaldi V et al (2019) Nasal delivery devices: a comparative study on cadaver model. Biomed Res Int 2019:1–6. https://doi.org/10.1155/2019/4602651

Mortazavi SA, Smart JD (2011) Factors influencing gel-strengthening at the Mucoadhesive-mucus Interface. J Pharm Pharmacol 46:86–90. https://doi.org/10.1111/j.2042-7158.1994.tb03746.x

Mukhtar M, Szakonyi Z, Farkas Á et al (2021) Freeze-dried vs spray-dried Nanoplex DPIs based on chitosan and its derivatives conjugated with hyaluronic acid for tuberculosis: in vitro aerodynamic and in Silico deposition profiles. Eur Polym J 160:110775. https://doi.org/10.1016/j.eurpolymj.2021.110775

Mygind N, Thomsen J (1976) Diurnal variation of nasal protein concentration. Acta Otolaryngol 82:219–221. https://doi.org/10.3109/00016487609120888

Najafi A, Ghazvini K, Sankian M et al (2021) T helper type 1 biased immune responses by PPE17 loaded Core-Shell alginate-chitosan nanoparticles after subcutaneous and intranasal administration. Life Sci 282:119806. https://doi.org/10.1016/j.lfs.2021.119806

Nervous System Diseases. Available online: https://www.healthdirect.gov.au/nervous-system-diseases. Accessed on 3 June 2022

Ohwaki T, Ando H, Kakimoto F et al (1987) Effects of dose, PH, and Osmolarity on nasal absorption of secretin in rats II: histological aspects of the nasal mucosa in relation to the absorption variation due to the effects of Ph and Osmolarity. J Pharm Sci 76:695–698. https://doi.org/10.1002/jps.2600760905

Ohwaki T, Ando H, Watanabe S et al (1985) Effects of dose, PH, and Osmolarity on nasal absorption of secretin in rats. J Pharm Sci 74:550–552. https://doi.org/10.1002/jps.2600740511

Ohwaki T, Ishii M, Aok S et al (1989) Effect of dose, PH, and Osmolarity on Nasal absorption of secretin in rats: III: In Vitro membrane permeation test and determination of apparent partition coefficient of secretin. Chem Pharm Bull 37:3359–3362. https://doi.org/10.1248/cpb.37.3359

Pardeshi CV, Belgamwar VS (2013) Direct nose to brain drug delivery via integrated nerve pathways bypassing the blood–brain barrier: an excellent platform for brain targeting. Expert Opin Drug Deliv 10:957–972. https://doi.org/10.1517/17425247.2013.790887

Pardeshi CV, Belgamwar VS (2020) Improved brain pharmacokinetics following intranasal Administration of N,N,N-Trimethyl chitosan tailored Mucoadhesive NLCs. Mater Technol 35:249–266. https://doi.org/10.1080/10667857.2019.1674522

Park J-S, Oh Y-K, Yoon H et al (2002) In situ gelling and Mucoadhesive polymer vehicles for controlled intranasal delivery of plasmid DNA. J Biomed Mater Res 59:144–151. https://doi.org/10.1002/jbm.1227

Passàli D, Bellussi L (1988) Circadian changes in the secretory activity of nasal mucosa. Acta Otolaryngol 106:281–285. https://doi.org/10.3109/00016488809106437

Patel RS, McGarry GW (2001) Most patients overdose on topical nasal corticosteroid drops: an accurate delivery device is required. J Lar Otol 115:633–635. https://doi.org/10.1258/0022215011908694

Pires A, Fortuna A, Alves G et al (2009) Intranasal drug delivery: how, why and what for? J Pharm Pharm Sci 12:288. https://doi.org/10.18433/J3NC79

Pires PC, Santos AO (2018) Nanosystems in nose-to-brain drug delivery: a review of non-clinical brain targeting studies. J Control Release 270:89–100. https://doi.org/10.1016/j.jconrel.2017.11.047

Rosada RS, Torre LG, Frantz FG et al (2008) Protection against tuberculosis by a single intranasal administration of DNA-Hsp65 vaccine complexed with cationic liposomes. BMC Immunol 9:38. https://doi.org/10.1186/1471-2172-9-38

Rutkowska E, Pająk K, Jóźwiak K (2013) Lipophilicity–methods of determination and its role in medicinal chemistry. Acta Pol Pharm 70(1):3–18

Sabir F, Ismail R, Csoka I (2020) Nose-to-brain delivery of Antiglioblastoma drugs embedded into lipid Nanocarrier systems: status quo and outlook. Drug Discov Today 25:185–194. https://doi.org/10.1016/j.drudis.2019.10.005

Sakane T, Akizuki M, Yamashita S et al (1991) The transport of a drug to the cerebrospinal fluid directly from the nasal cavity: the relation to the Lipophilicity of the drug. Chem Pharm Bull 39:2456–2458. https://doi.org/10.1248/cpb.39.2456

Schaefer ML, Böttger B, Silver WL et al (2002) Trigeminal collaterals in the nasal epithelium and olfactory bulb: a potential route for direct modulation of olfactory information by trigeminal stimuli. J Comp Neurol 444:221–226. https://doi.org/10.1002/cne.10143

Seju U, Kumar A, Sawant KK (2011) Development and evaluation of olanzapine-loaded PLGA nanoparticles for nose-to-brain delivery: in vitro and in vivo studies. Acta Biomater 7:4169–4176. https://doi.org/10.1016/j.actbio.2011.07.025

Si Y, Tian Q, Zhao F et al (2020) Adjuvant-free nanofiber vaccine induces in situ lung dendritic cell activation and T_H 17 responses. Sci Adv 6(32):eaba0995. https://doi.org/10.1126/sciadv.aba0995

Simonato M, Bennett J, Boulis NM et al (2013) Progress in gene therapy for neurological disorders. Nat Rev Neurol 9:277–291. https://doi.org/10.1038/nrneurol.2013.56

Suman JD (2013) Current understanding of nasal morphology and physiology as a drug delivery target. Drug Deliv Transl Res 3:4–15. https://doi.org/10.1007/s13346-012-0121-z

Anne Trafton (2009) Targeting tumors using tiny gold particles. https://news.mit.edu/2009/gold-cancer-0504. Accessed on 11 August 2022

Ugwoke MI, Verbeke N, Kinget R (2010) The biopharmaceutical aspects of nasal Mucoadhesive drug delivery. J Pharm Pharmacol 53:3–21. https://doi.org/10.1211/0022357011775145

Vaquié A, Sauvain A, Duman M et al (2019) Injured axons instruct Schwann cells to build constricting actin spheres to accelerate axonal disintegration. Cell Rep 27:3152–3166.e7. https://doi.org/10.1016/j.celrep.2019.05.060

Vasir J, Reddy M, Labhasetwar V (2005) Nanosystems in drug targeting: opportunities and challenges. Curr Nanosci 1:47–64. https://doi.org/10.2174/1573413052953110

Vishwa B, Moin A, Gowda DV et al (2021) Pulmonary targeting of inhalable Moxifloxacin microspheres for effective Management of Tuberculosis. Pharmaceutics 13:79. https://doi.org/10.3390/pharmaceutics13010079

Viswanathan V, Pharande R, Bannalikar A et al (2019) Inhalable liposomes of Glycyrrhiza Glabra extract for use in tuberculosis: formulation, in vitro characterization, in vivo lung deposition, and in vivo Pharmacodynamic studies. Drug Dev Ind Pharm 45:11–20. https://doi.org/10.1080/03639045.2018.1513025

Wofford MR, Kimbell JS, Frank-Ito DO et al (2015) Computational study of functional endoscopic sinus surgery and maxillary sinus drug delivery. Rhinology 53:41–49. https://doi.org/10.4193/Rhin13.065

Xi J, Si XA, Peters S et al (2017) Understanding the mechanisms underlying pulsating aerosol delivery to the maxillary sinus: in vitro tests and computational simulations. Int J Pharm 520:254–266. https://doi.org/10.1016/j.ijpharm.2017.02.017

Xi J, Zhang Z, Si X (2015) Improving intranasal delivery of neurological Nanomedicine to the olfactory region using Magnetophoretic guidance of microsphere carriers. Int J Nanomedicine 2015(10):1211. https://doi.org/10.2147/IJN.S77520

Yang C, Mitra AK (2001) Nasal absorption of tyrosine-linked model compounds. J Pharm Sci 90: 340–347. https://doi.org/10.1002/1520-6017(200103)90:3<340:AID-JPS9>3.0.CO;2-F

Youssef NAHA, Kassem AA, Farid RM et al (2018) A novel nasal Almotriptan loaded solid lipid nanoparticles in Mucoadhesive in situ gel formulation for brain targeting: preparation, characterization and in vivo evaluation. Int J Pharm 548:609–624. https://doi.org/10.1016/j.ijpharm.2018.07.014

Zumla A, Raviglione M, Hafner R et al (2013) Tuberculosis. N Engl J Med 368:745–755. https://doi.org/10.1056/NEJMra1200894

Chapter 17
Regulatory Aspects and Barriers in Using Groundbreaking Technologies

Paola Minghetti, Umberto M. Musazzi, and Paolo Rocco

Abstract New scientific discoveries and technological applications have been deeply influencing both the R&D and manufacturing of healthcare products, stressing the need for upgrading the regulatory framework, in order to overcome existing regulatory barriers for high-innovation products and to ensure proper quality standards able to preserve public health. In this light, groundbreaking technologies in the pharmaceutical field can be classified as innovation-in-product or innovation-in-process. In the former case, although the existing regulatory pathways can be also applicable to the marketing of high-innovation products, the benefit/risk assessment should be redesigned case-by-case based on the specific features of innovative products. In the latter case, existing technical and regulatory frameworks, which have been designed to meet the need of conventional pharmaceutical production, may not be able to cover all the intrinsic complexity of innovative manufacturing processes (e.g., additive manufacturing). This chapter aims to discuss the critical issues, from a regulatory point of view, in the development of high-innovation products and processes. Nanomedicine products, combination products, and additive manufacturing are reported as case studies of innovative products and processes to highlighting the critical issues in the regulatory pathways for placing them on the market.

Keywords Regulatory science · Nanomedicine products · Combination products · Additive manufacturing · Innovation-in-process · Innovation-in-product

P. Minghetti (✉) · U. M. Musazzi · P. Rocco
Department of Pharmaceutical Sciences, Università degli Studi di Milano, Milan, Italy
e-mail: paola.minghetti@unimi.it

D. Lamprou (ed.), *Nano- and Microfabrication Techniques in Drug Delivery*,
Advanced Clinical Pharmacy – Research, Development and Practical Applications 2,
https://doi.org/10.1007/978-3-031-26908-0_17

17.1 Introduction

A new era for the pharmaceutical and biomedical sectors has opened following the scientific and technological progress of the twenty-first century. New scientific discoveries and technological applications have been deeply influencing both the R&D and manufacturing of healthcare products, stressing the need for upgrading the regulatory framework in order to overcome existing regulatory barriers for high-innovation products and to ensure proper quality standards able to preserve public health. On the one hand, if innovation is mainly related to the product itself, the regulatory pathways applied to assess the benefit/risk balance and to identify a product's critical quality attributes (CQAs) should be reviewed based on up-to-date scientific knowledge. In this context, correct product classification and proper definition of its target profile are essential. In most developed countries, products intended to be used for medical purposes fall generally under either the regulatory frameworks of medicinal products or medical devices, based on their primary mechanism of action. It is noteworthy that such regulations have proved robust enough to sustain the current technological innovation. The existing regulatory pathways can be also applicable to the marketing of high-innovation products. Evidently, the benefit/risk assessment should be evaluated case-by-case from the competent authorities, based not only on existing regulatory standards but also on novel information available in the literature. In this field, a strong and early cooperation between the scientific and the regulatory communities is crucial to sustain the success rate of such products. On the other hand, if scientific innovation is focused on developing processes and technologies applied in manufacturing medicinal products and medical devices, the aim of innovation is not about changing the features of the final product, but overcoming the limitations of consolidated and well-known manufacturing processes in order to meet clinical needs of specific patients and/or populations (e.g., therapy personalization). The target product profile and CQAs may not be influenced by innovations introduced in the production process; as a consequence, innovative processes may be allowed to produce drug delivery systems and devices with biopharmaceutical and technological features superimposable to those prepared by well-established technologies and methodologies. From a regulatory point of view, the existing regulatory framework on product manufacturing, quality control, and assurance (e.g., GMP or ISO guidelines) may be a critical barrier to the implementation of innovative processes by manufacturers. Indeed, existing technical frameworks, which have been designed to meet the need of conventional pharmaceutical production, are not able to cover the intrinsic complexity of innovative manufacturing processes, particularly when groundbreaking technologies are adopted (e.g., additive manufacturing). This chapter aims to discuss the critical issues, from a regulatory point of view, in the development of high-innovation products (paragraph 2) and processes (paragraph 3).

17.2 Innovation in Product

The proper administrative classification of high-innovative products has a strong impact on the regulatory pathways manufacturers have to fulfill to place them on the market. As a consequence, a wrong classification of a high-innovation product may result in critical issues and barriers that can slow down their development and marketing. In the European Union, products designed and marketed for medical purposes (i.e., treating, diagnosing, or preventing a disease in human beings) can fall into two administrative classes: medicinal products and medical devices. The regulatory frameworks of the two categories differ considerably both in philosophy and implementation. To avoid any overlap between the two categories, orthogonal definitions have been devised. A medicinal product is defined as "(a) Any substance or combination of substances presented as having properties for treating or preventing disease in human beings; or (b) Any substance or combination of substances which may be used in or administered to human beings either with a view to restoring, correcting or modifying physiological functions by exerting a pharmacological, immunological or metabolic action, or to making a medical diagnosis" (European Parliament and Council 2001; European Parliament and Council 2017).

On the other hand, a medical device can be a substance, but more in general "any instrument, apparatus, appliance, software, implant, reagent, material or other article" (European Parliament and Council 2001; European Parliament and Council 2017) to be used for human beings for specific medical purposes, including the diagnosis, monitoring, and treatment of disease, injury, or disability or the prevention of disease. A discriminating feature of medical devices lies in the principal mode of action, which is, as opposed to medicinal products, not by pharmacological, immunological, or metabolic means, but typically by mechanical/physical means.

Identifying the principal mechanism of action is thus a prerequisite for correct classification of a high-innovation product, and it represents the first step in determining the applicable regulation and competent authority. This aspect is particularly relevant in the EU where, unlike the USA where the Federal Food and Drug Administration (FDA) regulates both medicinal products and medical devices, different competent authorities are involved. In this light, providing a proper regulatory classification is crucial from the early stages of the development of a product or process to get appropriate scientific and regulatory advice. However, it can be challenging especially for innovative products of increasing complexity or those designed to be marketed as products combining a medicinal product and a medical device (Fig. 17.1).

The goal of the regulatory frameworks of both medical devices and medicinal products is to assure that only products with a favorable benefit-risk balance reach the market and avoid those products with a therapeutic, prophylactic, or diagnostic effect from escaping the strict requirements provided by the relevant legislation. In the case of medicinal products, this translates to an assurance that quality, safety, and efficacy are reached. For products either prepared industrially or manufactured by a method involving an industrial process, quality, safety and efficacy are demonstrated through a system based on preventive authorizations to be obtained by companies

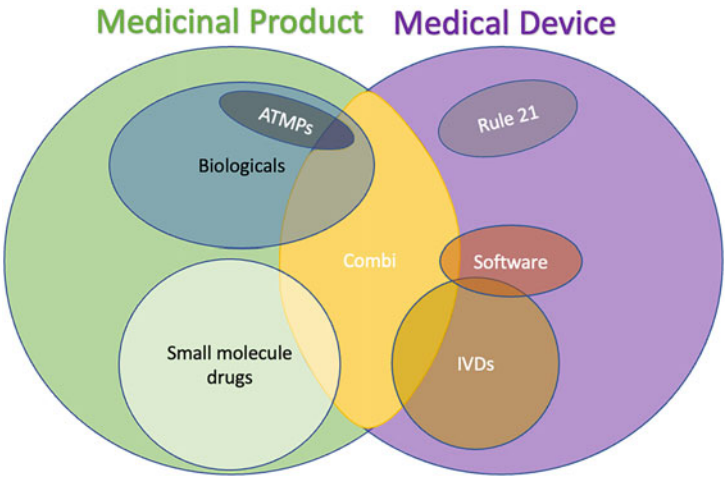

Fig. 17.1 Venn diagram representing sets and subsets of medicinal products and medical devices. *ATMPs* advanced therapy medicinal products, *IVDs* in vitro diagnostics, *Combi* products combining a medicinal product and a medical device

to both manufacture (manufacturing authorization) and place on the market (marketing authorization) a medicinal product. The manufacturing authorization, managed and issued by the national competent authority for medicinal products (MP-NCA), certifies compliance to the current Good Manufacturing Practice (cGMP). The GMP inspection and the issuing of a manufacturing authorization by and MP-NCA is an assurance of the quality of the process and the product. Such standardized regulatory pattern is not influenced by the grade of innovation of the manufactured products. The marketing authorization, on the other hand, is managed and issued by different regulatory authorites through different pathways.

17.2.1 Regulatory Pathways for Marketing Authorization of a Medicinal Product

To apply for a marketing authorization, a company submits a technical dossier, based on standardized format, the Common Technical Document (CTD), which contains all the analytical, biological, nonclinical, and clinical data supporting the quality, safety, and efficacy of the medicinal product. The nature and extent of the data to be included in the dossier depend on the type of medicinal product and can be influenced by the degree of innovation of the product itself. On this basis, different types of submission dossiers may result: a full dossier, in case of new active substances; a simplified dossier (as in case of generics), where the results from clinical trials may be replaced by the demonstration of bioequivalence; or a partial dossier in case of medicinal products the active substance of which is not new, for which the simplified dossier is not relevant, e.g., because generic approach is not

applicable. The latter scenario includes the case of biosimilars (biosimilar application), i.e., copies of biological medicinal products (European Parliament and Council 2004). Alongside biosimilars, other copies may fall under the partial dossier, as in the case of follow-on nonbiologic complex drugs (NBCDs) (Klein et al. 2019). NBCDs share their synthetic origin with small molecule drugs, and their complexity with biological drugs. In particular, their quality depends heavily on the manufacturing process. The complexity of NBCDs may arise from the active substance or from other sources, such as the formulation (e.g., nanomedicine products) or the (complex) combination with a medical device. Moreover, NBCDs may be difficult or impossible to characterize thoroughly using current analytical methods, and bioequivalence may not be sufficient to guarantee therapeutic equivalence as the pharmacodynamics can be different.

Focusing on innovative products intended to be marketed as medicinal products, the same regulatory pathways to obtain the marketing authorization for "conventional" medicinal products are applicable. In general, no specific regulatory pathways have been established for products characterized by a high technological innovation both in the EU and the USA. However, as previously discussed, regulatory authorities require applicants to integrate the data in the authorization dossier with additional data based on the type of innovative product/process, and its features. For a first-in-human medicinal product, a full dossier must be submitted to a regulatory agency. In the USA, the procedure to be followed is the New Drug Application (NDA), while in the EU, the procedure may be centralized or not (decentralized, mutual recognition, or national procedures). The centralized procedure can always be invoked in case of medicinal products that contain a new active substance (i.e., not authorized in the Union before 20 May 2004) or that constitute a significant therapeutic, scientific, or technical innovation (or for which a centralized authorization is in the interest of patients' health) (European Parliament and Council 2004). As a consequence, highly innovative medicinal products should be authorized by the European Medicines Agency (EMA), following a centralized procedure; however, this is not always the case, and many nanomedicine products and their follow-on products have been marketed following other regulatory pathways (e.g., decentralized, national). The dossier should include a full description of the quality, safety, and efficacy profile of the proposed drug product, and only if its benefit/risk balance results to be favorable after regulatory assessment, the applicant can obtain the marketing authorization. Thus, the pharmaceutical development of the drug product and the validation of the manufacturing process should be fully carried out taking into consideration the additional requirements stated in existing product guidelines (please refer to the following paragraphs) (European Medicines Agency 2017). In addition, specific CQAs can be identified based on the intended use and route of administration of the final product. If the product can be classified as a combination product in the benefit/risk assessment, the additional information provided in the application dossier on the medical device should be also taken into consideration. The suitability of the device should be discussed and justified by the applicant. When the innovative product is intended to be a device that, when placed on the market or put into service, incorporate, as an integral part, viable tissues or

cells of human origin or their derivatives, the specific regulatory framework on advanced therapy medicinal product (ATMP) should be taken also in consideration (European Parliament and Council 2007; FDA 2022a, b).

If the innovative drug product is a follow-on product of an already authorized one or contains a drug substance already used in human, the information regarding its efficacy or safety profile may be derived from information available in literature or provided by medicinal products already on the market. In this context, the strategies for obtaining the marketing authorization varies based on the complexity of the product and the demonstration of its therapeutic equivalence with respect to the reference. In this light, the assessment of therapeutic equivalence of a follow-on NBCD is challenging since bioequivalence studies are not necessarily enough. Consequently, an Abbreviated New Drug Application (ANDA; USA) or generic application (EU) cannot be applicable in most cases. More frequently, an abridged application can be followed. Such regulatory pathways are generally used when a) the new product has not the same qualitative and qualitative composition with respect to an originator (e.g., changes in active substance, strength, pharmaceutical form), b) the bioequivalence cannot be considered as a surrogate of the therapeutic equivalence (e.g., locally applied and locally acting drug products), and c) the therapeutic indications, pharmacokinetic profile or route of administration have changed with respect to the reference product. In the EU, these conditions fall in the "hybrid" procedure described by Article 10(3) of Directive 2001/83/EC. In the USA, it can be for the 505(b)(2) NDA application, which is a similar approach to the European hybrid procedure ("eCFR: 21 CFR Part 314 Subpart B—Applications" 2022). In both cases, although the preclinical and clinical data are generally less than those required for a first-in-human drug product, the authorization dossier should contain the proper data to demonstrate that quality product profile safety and efficacy data. For specific categories of innovative products (e.g., nanomedicine products), both EMA and FDA have made explicit the required additional data in specific regulatory guidelines (see the following paragraphs).

17.2.2 Nanomedicine Products: A First Case Study

Among innovative products classified as NBCDs, nanosystems represent one of the most interesting and groundbreaking technologies in the biomedical fields of the last decades. Indeed, due to their peculiar features, nanomaterials and nanotechnologies show new and innovative magnetic, optical, mechanical, and biological properties in comparison to bulk materials and conventional technologies. Consequently, the prevalence on the market of healthcare products—cosmetics, medical devices, and medicinal products—containing nanomaterials have been increasing in the last decades (Wagner et al. 2006). The interest in nanotechnology applications to medicine has increased so significantly that the term "nanomedicine" has been introduced to identified products designed with nanotechnology to have a therapeutic application. Indeed, as defined in EMA's reflection paper on nanotechnology-

based medicinal products for human use, nanomedicine is "the application of nanotechnology in view of making a medical diagnosis or treating or preventing diseases. It exploits the improved and often novel physical, chemical and biological properties of materials at nanometre scale" (European Medicines Agency 2006).

Different nanotechnology-based products, including nanocrystals, nanoemulsions, liposomes, protein nanoparticles, polymer-drug conjugates, polymeric micelles, and iron nanoparticles, were authorized and marketed in Europe and the USA for nanomedicine applications (Allen and Cullis 2013; Đorđević et al. 2022; Lee et al. 2015) and have been developed and marketed for treating or diagnosing several human diseases. Recently, nanotechnologies were also adopted in the design of COVID-19 vaccines as carriers of mRNA (Schoenmaker et al. 2021). However, in parallel to the huge scientific interest in finding novel applications of nanoscale technologies, their intrinsic complexity reveals potential toxic effects on humans and the environment (Domb et al. 2021; Saleh 2020). Indeed, nanosystems can disrupt the physiological functionality of cells and tissues and induction of inflammation processes for their peculiar ability to react with intra- and extracellular targets, thus causing changes of metabolic pathways and alteration of redox balance (Domb et al. 2021; Du et al. 2013; Zielińska et al. 2020).

In this light, national and international regulatory agencies started to improve their efforts in guiding the benefit/risk balance assessment of nanotechnology products for marketing authorization. Unfortunately, due to the lack of harmonized definitions and robust characterization techniques (Đorđević et al. 2022), the actions of different regulatory authorities have been not fully harmonized and, in most cases, they are still based on a case-by-case approach. In the EU, several definitions, mainly specific for a nanomaterial type, application, or industrial sector, have been available since before 2011 (Musazzi et al. 2017). However, most of them classify nanomaterials based on their physical dimensions (1–100 nm range). Unlike Europe, the USA took advantage of the existence of a unique regulatory agency, the FDA, for food, cosmetic, medicinal products, and medical devices and released specific guidance for healthcare products in 2014 (Food and Drug Administration (FDA) 2014). Although similar to the European approach in many aspects, from the beginning, the FDA's initiative has provided a holistic approach to the definition of nanomaterials, based on their biological properties.

Besides such general critical issues still on the ground, the development of nanotechnology-based products is difficult due to the high intrinsic complexity of such systems. This makes the definition of CQAs more difficult, as well as a proper assessment of process parameters that can impact the quality and, therefore, efficacy and safety profiles of the products (Colombo et al. 2018; European Medicines Agency 2017; Halamoda-Kenzaoui et al. 2019). Despite the huge scientific and industrial efforts in developing innovative nanomedicines, the success rate in terms of products reaching the market is particularly low (not more than 10%) due to quality failures (e.g., in developing a robust manufacturing process) and not satisfactory results of nonclinical and clinical studies (Colombo et al. 2018; Hay et al. 2014).

The expiration of patents on first nanomedicine products stimulated regulatory authorities to publish reflection papers of guidelines providing indications on the information that should be included in the CTD. Focusing on the European regulatory framework, between 2012 and 2015, EMA released five documents containing the agency position on specific modification of a nanomedicine product (e.g., surface coating) (European Medicines Agency (EMA) 2013a) or on developing a specific type of nanomedicine or its follow-on products (e.g., liposomal systems, micelles, and coated iron nanoparticles) (European Medicines Agency 2012; European Medicines Agency (EMA) 2015, 2013b, c). The general approach adopted by the EMA for assessing follow-on nanomedicine products is close to that of biosimilars (Minghetti et al. 2012). In addition to all data generally required for the authorization of a copy of a product containing a small-chemical entity, the EMA asks applicants to perform in-depth analyses of the CQAs and process parameters and how they influence the safety and efficacy profile of the nanomedicine. Indeed, although in most of the EU countries copies of nanomedicine products have been considered as generic products (Sofia et al. 2021), it is a current opinion among regulatory experts and scientists that therapeutic equivalence of copy versus nanomedicine originator should be supported by appropriate comparability studies since a bioequivalence study/biowaiver is not sensitive enough to assess the complex interaction between a nanomedicine product and a living body (Gaspar et al. 2020; Hafner et al. 2014). The additional data required by the EMA for different types of nanomedicine products are reported in Table 17.1.

17.2.2.1 Additional Data Required for Different Types of Nanomedicines

So far, EMA's regulatory guidance has focused on three classes of nanomedicine products: micellar systems, iron core nanoparticles, and liposomal systems (European Medicines Agency 2012; European Medicines Agency (EMA) 2015, 2013b, c).

Micellar systems are the simplest nanosystems for which the EMA released guidance (European Medicines Agency 2012, 2013b). They are generally used in medicinal products to ensure reproducibility in dose administration and to improve the biopharmaceutical performance of low-soluble drugs. Since micellar systems are designed to disassemble after distribution in blood, nonclinical and clinical additional data, if required, are focused on assessing the impact of infusion parameters on the breakdown of micelles and determining the risk of adverse reactions (e.g., hemolysis). For copies, biowaiver studies cannot be applied due to the complexity of the dosage forms, except for micellar systems where the composition is identical/similar (i.e., same surfactant) to the originator. However, if the micellar system is designed to be biopersistant, e.g., block copolymer micellar systems, a more complete assessment of quality, safety, and efficacy profiles is required, which may include clinical trials (Table 17.1) (European Medicines Agency (EMA) 2013b).

Table 17.1 Additional quality, nonclinical, and clinical studies required for Common Technical Document (CTD) of nanomedicine products according to EMA's reflection papers (Musazzi et al. 2017)

Nanomedicine products	Additional studies that should be included in the CTD	
Coated nanomedicine products (EMA/325027/2013)	*Quality studies*	– Complete characterization of coating materials – Definition of physicochemical nature of surface to which the coating adheres – Complete validation of coating steps, including detailed analyses of the chemistry beyond – Additional information (e.g., conformational state, protein consistency) are required for complex ligands (e.g., protein or antibody) intended to active targeting – Coating stability during storage and in use – Premature detachment and release of coated ligands and/or their degradation
	Nonclinical studies	– Impact of surface coverage heterogeneity and coating physicochemical stability on safety and efficacy of drug product – In vivo impact of different coating materials/surface coverage on pharmacokinetics and biodistribution of drug product – Biodistribution and metabolism of coating ligands
Micellar systems (EMA/CHMP/QWP/799402/2011)	*Quality studies*	– Physicochemical characterization of active substance (e.g., lipophilicity, pH solubility, pH stability, Log*P*, and Log*D*) – Physicochemical characterization of excipients (e.g., surfactant polydispersity, purity) – Impact of pH and ionic strength on micelle properties – Critical micelle concentration (CMC) in model of reconstitution vehicles – Carrier solubility capacity – Physical stability in diluted infusion solutions at different temperatures – Compatibility with the common injection and infusion devices – Mean size and distribution of dispersed micelles – Estimation of micelle concentration – Determination of entrapped/free drug factions
	Nonclinical studies	– In vitro studies for investigating the influence of infusion on the breakdown of micelles in plasma-based models – In vivo studies for determining the risk of persistence of micelles in animal models

(continued)

Table 17.1 (continued)

Nanomedicine products	Additional studies that should be included in the CTD	
	Clinical studies	– Determination of time and condition of infusion, for excluding risk of adverse effects (e.g., hemolysis) – Tracking of micelles in plasma to investigate their loss of integrity and their distribution – Biowaiver or bioequivalence studies (only for generic products)
Block copolymer micellar systems (bPMS) (EMA/CHMP/13099/2013)	*Quality studies*	– Complete characterization of all bPMS components (e.g., active substance, block copolymer, stabilizing agent) – Content of block copolymer and active substances in final drug product – Determination of unloaded/loaded drug in bPMS – Complete characterization of polymers used in the synthesis of block copolymer – Impact of copolymer modification of morphological properties of bPMS – Impact of micellar systems (e.g., osmolality, drug fraction adsorbed on the micellar surface) on the drug release – Validation of manufacturing process and identification of the key steps, including block copolymer synthesis – Accurate control of raw materials and intermediates – Physical stability of bPMS – Chemical stability of drug and block copolymer – Degradation profile of bPMS in physiological fluids
	Nonclinical studies	– Pharmacological profiles of placebo bPMS – Influence of bPMS on the drug pharmacokinetics (e.g., rate of clearance, distribution, interaction with plasma proteins) – Pharmacodynamics studies for investigating the impact of chemical composition and physicochemical properties of bPMS on its mechanism of action using in vitro and in vivo models – Full toxicity characterization of bPMS, including toxicokinetic investigation in circulating fluids, target tissues, and toxic relevant organs
Liposomal systems (EMA/CHMP/806058/2009/rev.02)	*Quality studies*	– Complete characterization of all liposome components, including the quality and the purity of lipids – Morphological properties of liposomal systems

(continued)

Table 17.1 (continued)

Nanomedicine products	Additional studies that should be included in the CTD	
		– Drug fraction encapsulated and its distribution in liposome – Determination of lipid bilayer phase transition behavior – pH of internal compartments (only for pH-gradient loaded liposome) – Stability in physiological fluids (e.g., plasma) – In vitro drug release from the liposome in physiologically/clinically relevant media – Full characterization of ligand should be carried out according to guideline on coated nanomedicine products, if liposome is functionalized – Stress tests for determining physical and chemical degradation profiles (comparative studies for generic products) – Identification of the key steps of manufacturing process – Stability of drug, lipids, and other critical excipients in the finished product – Stability of liposomal systems during storage and in-use conditions – Robustness of reconstitution process
	Nonclinical studies	– Comparative studies of pharmacokinetics, toxicology, and pharmacodynamics (only for generic products) – Interaction between liposome and cellular lines that are pharmacologically and toxicologically relevant – In vitro or in vivo immune reactogenicity assays – CARPA tests – Organ function tests
	Clinical studies	– Comparative pharmacokinetic studies for assessing the equivalence of generic and originator products (e.g., systemic exposure of total, unencapsulated, and encapsulated drug, similar distribution and elimination profiles)
Iron core nanoparticles (EMA/CHMP/SWP/100094/2011; EMA/CHMP/SWP/620008/2012)	*Quality studies*	– Complete characterization of physicochemical properties of raw materials (e.g., carbohydrate characterization, polymorphism of iron core) – Morphological properties of iron core and iron-carbohydrate complexes – Ratio between bound carbohydrate and iron – Impact of physicochemical properties of carbohydrate matrix on the nanoparticle stability during storage

(continued)

Table 17.1 (continued)

Nanomedicine products	Additional studies that should be included in the CTD	
		– Impact of physicochemical properties of carbohydrate matrix in vivo pharmacokinetics and toxicokinetics – Amount of labile iron released from the product when administered – Impurities (e.g., ratio of iron-(II) and iron (III)) – Degradation profiles – Measurement of amount of iron-(III) released by the systems – Stress tests for determining physical and chemical degradation profiles (comparative studies for generic products)
	Nonclinical studies	– Biodistribution studies on compartments involved in pharmacological action (e.g., plasma, RES, spleen) and in therapeutic (e.g., bone marrow) and toxic target tissues (e.g., kidney, liver, lungs, heart)
	Clinical studies	– Bioequivalence studies (only for generic products)

Moving to more complex nanosystems, such as iron core nanoparticles, the number of nonclinical and clinical studies required by the EMA increases (European Medicines Agency (EMA) 2015). Indeed, for follow-on products, in addition to comparative qualitative and quantitative physicochemical characterization and plasma pharmacokinetic studies in humans, the EMA requires nonclinical studies to compare the biodistribution in specific tissues/organs (e.g., RES, spleen, bone marrow, kidney, liver, lungs, heart) and toxicity between the nanosimilar and the innovator in animal models. If differences between copy and reference emerge from the physicochemical characterization, nonclinical biodistribution, or human pharmacokinetic studies, a further therapeutic equivalence study is required to demonstrate comparable efficacy and safety with the reference product.

Finally, liposomes are lipid-based nanosystems composed of one or more phospholipid bilayers enclosing aqueous compartments. In parallel to the expiration of the Doxil® patent in 2010, regulatory agencies started to work toward identifying supportive information for liposomal systems: they can be retrieved from the reflection paper released by the EMA (European Medicines Agency (EMA) 2013c); similar information is available also in FDA guidance (Food and Drug Administration (FDA) 2018). From Doxil® (doxorubicin-loaded PEGylated liposome approved in 1995), several liposomal products have been authorized as medicinal products both in the EU and the USA (Đorđević et al. 2022). For developing a follow-on liposomal product, both the EMA and FDA require a full and detailed characterization of the liposomal systems and their functionality-related excipients (e.g., lipids) (Table 17.1). In particular, the formulative studies should investigate in-depth all parameters that can influence the physicochemical quality of

liposomes and their stability in both vehicles and physiological environments. The assessment of the quality of lipids used in the formulation has been particularly stressed since small changes in their physicochemical properties or purity have a huge impact on the technological and biopharmaceutical performances of the liposomal systems. Focusing on safety and efficacy data for follow-on products, nonclinical and clinical requirements include extensive comparative in vitro and in vivo studies for demonstrating superimposable biopharmaceutics' and toxicological profiles between the generic and originator liposomal product. Considering that acute hypersensitivity infusion reactions are common for such nanomedicine systems (Alberts and Garcia 1997), appropriate toxicological studies [e.g., in vitro or in vivo immune reactogenicity assays and complement activation-related pseudoallergy CARPA) tests] are mandatory to exclude potential risks of adverse effects.

17.2.2.2 Functionality-Related Modifications of a Nanomedicine Product

Currently, the only functionality-related modification of nanosystems addressed by EMA guidelines is the coating of the surface (European Medicines Agency (EMA) 2013a). From a regulatory point of view, a "coated nanomedicine product" is a product with surface properties modified in order to alter its interactions with the biological environment after administration. The coating function may improve nanomedicine stability or impact the targeting and the pharmacological mechanism of action. The former case comprise the reduction of physical aggregation (e.g., coated iron nanoparticles for treating anemia) or improving the half-life, by reducing the interactions with circulating proteins or the clearance of reticuloendothelial system (RES) and macrophages. In the latter case, surface modifications can impact significantly the biodistribution of the nanosystems and their interactions with cellular targets, which are therapeutically and toxicologically relevant. Based on the nature of the attached ligand, the complexity of the coating process and the quality control vary; thus, additional data have to be provided. Therefore, developers of coated nanomedicine products should provide to the regulatory agency additional quality/nonclinical/clinical data to determine the impact of coating on product stability, pharmacokinetic, and pharmacodynamic profile (Table 17.1). Moreover, from a quality point of view, the coating process and the coated materials should be fully characterized to ensure batch-to-batch reproducibility and predict its impact on the nanomedicine pharmacokinetic profile. If premature detachment or any degradation of coating has been reasonably expended within the nanomedicine presence in the body, additional in vitro and in vivo studies have been required to assess the in vivo fate of detached/degraded moieties (e.g., biodistribution, metabolism).

17.2.3 Combination Products: A Second Case Study

In the EU, products combining a medical device (MD) and either a medicinal product (MP) or a substance that, if used separately, would be considered a medicinal product (from now on "medicinal substance") are defined and classified in the context of the regulatory frameworks of both medical devices and medicinal products (European Commission 2015; European Medicines Agency (EMA) 2021a). In the MD regulatory framework, such products were initially classified in the MEDDEV on Borderline products (European Commission 2015) released following Directive 93/42/CE, and now in the provisions of Regulation (EU) No. 2017/745 (Medical Devices Regulation, MDR), and related guidelines (i.e., MDCG guidance). Examples include prefilled syringes, nebulizers pre-charged with a specific medicine, or catheters coated with heparin. The classification and regulation of such products represent a challenge as they combine products—MPs and MDs—which follow very different regulatory pathways, which affect all aspects of product development, from preclinical testing to marketing to reimbursement policies.

The 2019 EMA draft "Guideline on the quality requirements for drug-device combinations" introduced the term "drug-device combination products" to mean "medicinal product(s) with integral and/or non-integral medical device/device component(s) necessary for administration, correct dosing or use of the medicinal product" (European Medicines Agency 2019). This term was later excised in the final EMA "Guideline on quality documentation for medicinal products when used with a medical device" (from now on, "MP + MD guideline") (European Medicines Agency (EMA) 2021b), which superseded the draft of 2019 (European Medicines Agency 2019). In the MP + MD guideline, these products are referred to as "medicinal products for use with a medical device, or device part" and assigned specific names according to the medicine/device configuration. The new nomenclature removed a possible source of confusion with "fixed combination medicinal products" as defined in Annex I, Section 5 of Directive 2001/83/CE.

The classification of products combining a medicinal product or substance and a medical device may be based on the principal mode of action (Fig. 17.2): products where the action of the medicinal product is primary and not ancillary to that of the device, or products where the action of the medicinal substance (i.e., substance that, if used separately, would be considered a medicinal product) is ancillary to that of the device (European Parliament and Council 2001; European Parliament and Council 2017).

For products where the action of the medicinal product is primary, an assessment of the suitability of the device for its intended purpose should be performed. A full evaluation of the impact of the device on the quality target product profile, CQAs, and overall control strategy of the medicinal product should be included in the dossier. An MP competent authority (national or, where applicable, the EMA) is involved in the assessment of the overall benefit-risk balance. The manufacturer or, where applicable, the notified body (NB) assesses the relevant General Safety and

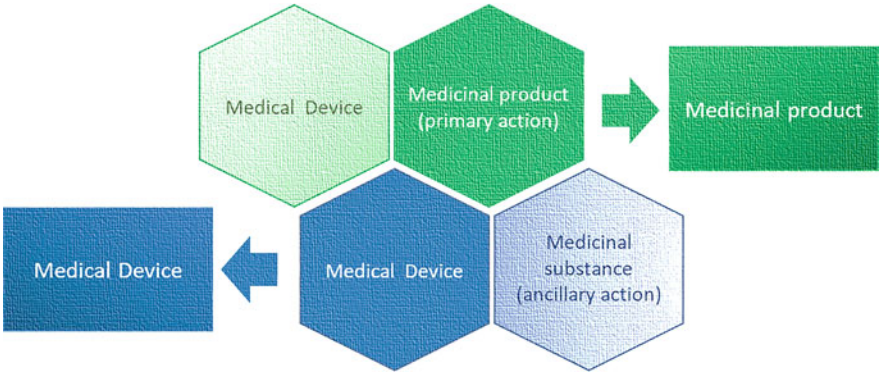

Fig. 17.2 Classification of products combining a medicinal or product or substance and a medical device

Performance Requirements (GSPRs) of the device. (European Medicines Agency (EMA) 2021b) These products are divided into three categories, depending on the configuration: integral medicinal products, where the MD and MP form an integral product where the MD is not reusable; medicinal products with co-packaged devices, where the MP and MD are developed separately but packaged together; and medicinal products with referenced devices, where the product information of the MP refers to a specific MD to be used.

Examples of integral medicinal products include single-dose prefilled syringes, pens, and injectors or dry powder inhalers preassembled with the MP, which are not intended to be refilled or reused and medicinal products with an embedded sensor, where the sensor is a medical device and has an action ancillary to the medicinal products (European Medicines Agency (EMA) 2021b). These products are regulated under Directive 2001/83/EC read in conjunction with Regulation (EC) No 726/2004 (if applicable). The marketing authorization application should include additional information, e.g., an assessment of the compatibility between all materials in contact with the drug product and a discussion and justification of the suitability of the device and the results of the assessment of the conformity of the device with the relevant GSPRs, i.e., the EU Declaration of Conformity or the relevant EU certificate issued by a Notified Body (NB). If the application dossier does not contain these results and where the conformity assessment of the device, if used separately, requires the involvement of a NB, a notified body opinion (NBOp) on the conformity of the device with the relevant GSPRs should be provided. In specific cases, evidence of usability ("usability studies") is required (European Parliament and Council 2001; European Parliament and Council 2017).

Examples of medical devices co-packaged with, or referenced by, medicinal products include oral administration devices (such as spoons or syringes); injection needles; refillable pens and injectors, such as the ones using cartridges; reusable dry powder inhalers; spacers for inhalation sprays; nebulizers; vaporizers; pumps for medicinal product delivery; or electronic tablet dispensers. The medical device part

must be CE marked, while the medicinal product is regulated under Directive 2001/83/EC read in conjunction with Regulation (EC) No 726/2004 (if applicable) (European Medicines Agency (EMA) 2021b).

On the other hand, products where the action of the medicinal substance is ancillary to that of the device fall under the scope of Regulation (EU) 2017/745 (Medical Devices Regulation, MDR) (Rule 14) and must be CE marked (European Parliament and Council 2001; European Parliament and Council 2017). These MDs are codified as class III medical devices. The NB, before issuing a CE certificate, must seek a scientific opinion on the quality and safety of the ancillary substance from the MP competent authority.

There are other classes for which both the medicinal product and the medical device legislations and competent authority must be taken into consideration. These are companion diagnostics, which are in vitro diagnostics tests that support the safe and effective use of a specific medicinal product by identifying suitable and unsuitable patients, and MDs that are composed of substances or of combinations of substances that are intended to be applied to the skin and that are absorbed by or locally dispersed in the human body.

The former fall under the scope of the in vitro diagnostic regulation (European Parliament and Council 2017), but the NB must seek a scientific opinion from the EMA or a national competent authority on the suitability of the companion diagnostics to the medicinal product concerned. The latter fall within the scope of the MDR (Rule 21), but the NB must seek a scientific opinion from the EMA or a national competent authority on the compliance of the substance with the requirements of Annex I to Directive 2001/83/EC (European Parliament and Council 2001; European Parliament and Council 2017).

17.3 Innovation in Process

The technological and digital progress of the latest decades influenced also the pharmaceutical manufacturing systems pushing researchers to find novel ways to implement conventional manufacturing processes. Their aim has been optimizing the production of medicinal products and medical devices with a lower risk of quality failures and/or overcoming the limitation of current pharmaceutical manufacturing systems to allow therapy and dose personalization on patient's physiological features and/or clinical needs. In this field, innovation in manufacturing processes can be classified into two categories: (a) finding innovative approach for optimizing/rationalizing manufacturing processes constituted of well-known technological operations and (b) developing groundbreaking technologies constituted by technological operations never applied in the pharmaceutical field. Continuous manufacturing and process analytical technologies (PAT) are clear examples of innovative approaches that are revolutionizing the manufacturing and quality control of medicinal products, by upgrading conventional processes with technologies able to improve the production efficiency and robustness, reducing wastes and risks of quality failures (Coffman et al. 2021; Sacher et al. 2022; Velez et al. 2022). For these

innovative approaches, the development of regulatory standards and guidelines is facilitated by the existence of a consolidated scientific knowledge on the CQAs and process parameters that should be investigated for each technological operations involved in product manufacturing. On the other hand, electrospinning (Luraghi et al. 2021) and additive manufacturing technologies fall in the second category. Due to the groundbreaking nature of such technologies, the development of regulatory standards and guidelines is slowed down by the lack of current scientific knowledge. For an example, the application of additive manufacturing processes, widely known as 3D printing, to the pharmaceutical field is forcing the scientific and regulatory communities to reconsider the conventional standard for assessing the quality of medicinal products and medical devices. In 2015, the first 3D printed medicinal product (Spritam®), a fast-dissolving tablet manufactured by binder jetting, was approved by the FDA for the treatment of seizures in children affected by epilepsy (FDA 2015). However, the 3D printing universe is constituted by a range of different technologies, which have in common the capability of fabricating, by adding subsequent layers of solid 3D objects starting from their digital model (i.e., CAD files). In this respect, the main 3D printing techniques studied and applied so far in the drug delivery area are reported in Table 17.2 (Elbadawi et al. 2021). The huge interest for investigating their application potential found its rationale in the possibility 3D printing would provide toward customization and personalization of the medicinal products/medical devices based on the peculiar needs of each subject to be treated. Indeed, by intervening on the raw material composition and the dosage form design, it is possible to obtain printed products with different strengths, shapes, and release performances.

Due to the versatility of 3D printing technologies, complex delivery systems and fixed-dose combination products can be obtained with high accuracy, precision, and cost-effectiveness (Maroni et al. 2017; Musazzi et al. 2018, 2021). In parallel, also 3D printed medical devices, including hearing aids, dental crowns, bone tether plates, skull plates, hip cups, spinal cages, knee trays, and other implantable items, have been manufactured to meet patients' need (Morrison et al. 2015; Rahman et al. 2018).

Although 3D printed medicinal products often seem to mimic the shape of a conventional dosage form (e.g., tablets, capsules), the application of additive manufacturing, especially for product personalization, entails several challenging aspects, starting from the identification of CQAs and critical process parameters. Indeed, all of them might impact on the reproducibility of the manufacturing process and on the physical technological characteristics as well as the in vitro/vivo performance of the product. Due to the complexity of the pharmaceutical development and of the manufacturing process involved, the conventional trial-and-error and quality-by-testing approaches would not be applicable neither in development stage nor during actual manufacturing (Elbadawi et al. 2021). Several approaches, such as those based on design of experiments (DoE), finite element analysis (FEA), computational fluid dynamics, and mechanistic modeling, have been applied to improve the production of 3D printed products and relevant quality (Morrison et al. 2015). In addition, novel analytical tools including artificial intelligence and machine learning have started to be considered. Since a fully customizable 3D printing process

Table 17.2. An overview of pharmaceutical 3D printing technologies (Elbadawi et al. 2021)

3D printing technology	Material	Mode of fusion	Advantages	Limitations
Material extrusion fused deposition modeling (FDM)	Thermoplastic polymers	Heat	– Ease of use – Inexpensive – Different materials can be printed together	– Not suitable for heat-labile molecules – Relatively low resolution – Complex structures require support
Direct powder extrusion (DPE)	Thermoplastic polymers	Heat	– Ease of use – Inexpensive – Different materials can be printed together – Single-step process	– Relatively low resolution – Complex structures require support
Semi-solid extrusion (SSE)	Gels, pastes	–	– Suitable for heat-labile drugs, and biomaterials – Conducted at room temperature	– Relatively low resolution – Requires post-processing steps
VAT photopolymerization stereolithography (SLA)	Liquid photopolymer	Laser beam	– High resolution – Relatively fast – Suitable for heat-labile drugs	– No FDA-approved excipient suitable for oral delivery applications – Post-processing (curing) necessary – Overhangs require support
Digital light processing (DLP)	Liquid photopolymer	Light	– High resolution – Smooth finishing – Relatively fast – Suitable for heat-labile drugs	– No FDA-approved excipient suitable for oral delivery applications – Overhangs require support – Post-processing required
Continuous liquid Interface production (CLIP)	Liquid photopolymer	Light and oxygen	– High resolution – Objects can be easily removed – Fast – Suitable for heat-labile drugs	– Expensive. – No FDA-approved excipient suitable for oral delivery applications

(continued)

Table 17.2. (continued)

3D printing technology	Material	Mode of fusion	Advantages	Limitations
Material jetting inkjet printing (IJP)	Liquid solvent	Evaporation, UV curing, reactive jetting	– High resolution – Suitable for heat-labile drugs (only for piezoelectric inkjet printers)	– Performance dependent on formulation properties – Chemical stability of drugs in solvent
Powder bed fusion selective laser sintering (SLS)	Thermoplastic polymer, metal, and ceramic	Laser beam	– Does not require supports – High resolution – Feed material can be recycled and reused – Able to confer rapid disintegration	– Potential thermal degradation of drug due to short-term exposure to heat – Objects can be too friable
Binder jetting	Polymer powder	Liquid binder	– Does not require support – Suitable for heat-labile drugs	– Potential drug hydrolysis due to presence of solvent – Time consuming

requires the definition of a clear design/process space, taking into account formulations differing significantly in terms of starting materials and relevant composition, design (e.g., shape and dimensions) of the product, and operating parameters (e.g., speed, temperature), application of artificial intelligence could support the operator or the expert compounder in identifying, from an innumerable number of options, the most suitable formulation, in optimizing the printing process, and in predicting the in vitro/vivo performance (Elbadawi et al. 2021).

Consequently, the regulatory provisions aimed at marketing 3D printed medicinal products require additional data, to demonstrate the quality profile of final products, that of raw materials and of the process itself. However, due to the number of 3D printing technologies currently available, the identification of standards and suitable approaches for providing quality control may be challenging and complex. The update of quality standards for 3D printed products starts from the need for more accurate characterization of physicochemical properties of function-related excipients. Indeed, based on the adopted 3D printing technology, raw materials should be characterized more in depth, especially in terms of physical properties mostly affecting the printing processes, such as morphological properties (e.g., particle size distribution, surface area, shape, surface charge, porosity), flow properties, viscoelastic properties, melting point, glass transition point, thermal conductivity, viscosity, impurities, degradation properties, solid state, and moisture (Mirza and Iqbal 2019).

Regarding the final 3D printed products, characterization methods for assessing their physicochemical, technological, and release performance properties should be reconsidered. Indeed, quality control of conventional dosage forms is currently based on consolidated methods (e.g., pharmacopoeias, ISO standards). However, such quality controls should be implemented by specific ones based on the peculiarities of adopted 3D printing methods. Indeed, quality defects peculiar of 3D printed products are elephant's foot, irregular corners, warping, Z-layer separation, shrinkage, balling, stringing, oozing, blobs, shifting, leading, banding, and collapsing (Parhi 2021). Most of them are correlated to failures in the physical properties of raw materials and/or technological properties of pre-made materials used in the printing process (e.g., mechanical properties), or to unoptimized set up of process parameters. The maintenance of suitable mechanical strengths of materials through the printing process results particularly critical in all fused deposition-based 3D technologies to avoid collapses in the 3D structure and ensure to obtain objects with high reproducibility and accuracy. However, the characterization of raw materials/pre-made materials for 3D printing is challenging as well, since conventional characterization methods cannot always be applicable. For example, mechanical strength tests conventionally adopted to check the hardness of a dosage form (e.g., a tablet) are not sensitive enough to be applied to a 3D printed one, which requires a texture analyzer for providing a proper characterization of the system.

Focusing on the validation of the manufacturing process, the principles of current FDA and EMA guidelines can also be enforced onto 3D printing. However, a particularly critical aspect is the validation of the software used for designing the final product and controlling the printing process itself. Indeed, the former aspect is strongly influenced by the capability of the printer to precisely execute the geometric design and the process parameter defined by the software. It is evident that an in-depth validation of hardware and software are mandatory for ensuring the quality throughout the manufacturing process. Moreover, 3D printing manufacturing processes required a continuous monitoring of the CQAs and process parameters. The adoption of online and nondestructive methods is especially critical for personalized productions due to the limited size of batches. PAT can also be adapted to 3D printing to control quality attributes and process parameters online enabling real-time approval of printed products, especially for preparing small batches (Elbadawi et al. 2021). The development of nondestructive tests [e.g., vibrational spectroscopy technologies, such as Raman or near-infrared (NIR) spectroscopy] is required for performing online controls without damaging the integrity of the final product, as well as requiring minimal sample preparation.

The stability assessment of 3D printed products shows some peculiarities as well. The current regulatory framework on substance/product stability is focused on assessing the maintenance of the quality critical attributes throughout the entire shelf-life of drug products and drug substances following the provisions reported in the ICH Q1A (R2) guideline. However, most of the printed products have been designed specifically for a patient's treatment and to be used at the bedside or within a few months from the preparations. In this context, long-term stability data are not

so necessary for 3D printed products, but they are essential for assessing the quality of pre-made materials used for the preparation.

Despite the complexity of the production processes and the heterogeneity of technologies that can be adopted, a few specific improvements have been proposed by regulatory authorities especially in the case of medicinal products or medical devices. In this field, FDA has actively supported the manufacturing of 3D printing since its early stage of development by the Emerging Technology Program (ETP) of the Center for Drug Evaluation and Research (CDER) (FDA 2022a, b). Taking advantages from the expertise gained during the approval of the first printed medicine (Spritam®), the program aims to discuss, identify, and resolve potential technical and regulatory issues regarding the development of the implementation of a 3D printing process before the regulatory submission. On the other side, regulations are more advanced in the case of medical devices. The Center for Devices and Radiological Health (CDRH) is in charge of supporting and regulating the marketing of 3D printed medical devices. In 2017, CDRH released a guidance on technical considerations for additive manufactured medical devices, including provisions for validating software and processes and controlling and characterizing raw materials. The same regulatory pathways can be applicable also to 3D printed products (FDA 2017). For example, many of them have been marketed in the USA after obtaining the clearance under the 510(k) Premarket notification. Following this pathway, the applicant has to demonstrate that the safety and efficacy of the 3D printed device are substantially equivalent to a legally marketed one that is not subject to premarket approval. It is out of doubts that European authorities appears less proactive in the 3D printing innovation than FDA. From a European perspective, the 3D printed products fall within the scope of the specific EU product legislation based on the specific intended needs. In the case of 3D printed medicines, Directive 2001/83/CE, Regulation (CE) No. 726/04 and guidelines issued by the European Medicines Agency (EMA) should be followed. Although specific supporting programs on 3D printing have not been activated, the EMA as well as FDA provides scientific and regulatory support and advise to all developers of innovative products, including 3D printed products. On the contrary, provisions of Regulation (EU) No. 2017/745 are the reference legal framework for medical devices. In April 2020, the European Commission released FAQs to support the production of 3D printed devices for fighting the COVID-19 outbreak (European Commission 2020). 3D printers should fulfill the requirement reported by the Directives 2006/42/CE (Machinery Directive), 2014/30/EC (Electromagnetic Compatibility Directive), and the EU legislation on chemicals (e.g., REACH 1907/2006/EU). Additional ISO standards are reported in the documents for specific 3D printed devices. Unlike FDA, the European authorities have not release specific guidance of technical requirements 3D printed products should follow to be marketed as medical devices. Indeed, the 3D printed products should follow the same conformity assessment procedures of other medical devices to obtain the EU declaration of conformity and CE marking, regardless if the printed device is a custom-made or mass-produced device.

Such regulatory challenges in developing and manufacturing 3D printed products overlap with uncertainty on which regulatory requirement should be followed for the preparation of on-demand personalized medicines in small batches (Rahman et al. 2018). Indeed, unlike industrial 3D printing that should be performed in GMP compliance, the preparation of personalized medicines has been carried out under the responsibility of a pharmacist in facilities authorized based on the compounding regulation in force in a specific country (e.g., hospital pharmacies, community pharmacies, outsourcing facilities). However, the 3D printing revolution is pushing regulators to reflect on how to integrate 3D printed products into the existing regulations and healthcare systems. This is particularly relevant considering that 3D printing technologies may allow, in the future, to prepare on-demand products in settings outside compounding facilities (e.g., patient's home, doctor's office) (Trenfield et al. 2018). In this light, there is plenty of room for implementing current regulatory pathways and guidelines in order to provide a clear reference for the manufacturing of pre-materials and 3D printers. Moreover, a proper quality management system applicable to on-demand/at bedside preparation of 3D printed products should be defined as well. In this context, the translation of the current GMP to the 3D printing at patient's bedside will be one of the most challenging iissues that should be addressed, since several aspects which are conventionally part of the validation of manufacturing process in pharmaceutical industries (e.g., definition of in-process quality tests, process controls, cleaning procedures) may not be easily adapted to preparation of small-batches.

References

Alberts DS, Garcia DJ (1997) Safety aspects of pegylated liposomal doxorubicin in patients with cancer. Drugs 54(Suppl 4):30–35. https://doi.org/10.2165/00003495-199700544-00007

Allen TM, Cullis PR (2013) Liposomal drug delivery systems: from concept to clinical applications. Adv Drug Deliv Rev 65(1):36–48. https://doi.org/10.1016/j.addr.2012.09.037

Coffman J, Brower M, Connell-Crowley L, Deldari S, Farid SS, Horowski B, Patil U, Pollard D, Qadan M, Rose S, Schaefer E, Shultz J (2021) A common framework for integrated and continuous biomanufacturing. Biotechnol Bioeng 118(4):1735–1749. https://doi.org/10.1002/bit.27690

Colombo S, Beck-Broichsitter M, Bøtker JP, Malmsten M, Rantanen J, Bohr A (2018) Transforming nanomedicine manufacturing toward quality by design and microfluidics. Adv Drug Deliv Rev 128:115–131. https://doi.org/10.1016/j.addr.2018.04.004

Domb AJ, Sharifzadeh G, Nahum V, Hosseinkhani H (2021) Safety evaluation of nanotechnology products. Pharmaceutics 13(10):1615. https://doi.org/10.3390/pharmaceutics13101615

Đorđević S, Gonzalez MM, Conejos-Sánchez I, Carreira B, Pozzi S, Acúrcio RC, Satchi-Fainaro R, Florindo HF, Vicent MJ (2022) Current hurdles to the translation of nanomedicines from bench to the clinic. Drug Deliv Transl Res 12(3):500–525. https://doi.org/10.1007/s13346-021-01024-2

Du J, Wang S, You H, Zhao X (2013) Understanding the toxicity of carbon nanotubes in the environment is crucial to the control of nanomaterials in producing and processing and the assessment of health risk for human: a review. Environ Toxicol Pharmacol 36(2):451–462. https://doi.org/10.1016/j.etap.2013.05.007

eCFR: 21 CFR Part 314 Subpart B–Applications [WWW Document] (2022). URL https://www.ecfr.gov/current/title-21/part-314/subpart-B. Accessed on 21 March 2022

Elbadawi M, McCoubrey LE, Gavins FKH, Ong JJ, Goyanes A, Gaisford S, Basit AW (2021) Harnessing artificial intelligence for the next generation of 3D printed medicines. Adv Drug Deliv Rev 175:113805. https://doi.org/10.1016/j.addr.2021.05.015

European Commission (2020) Conformity assessment procedures for 3D printing and 3D printed products to be used in a medical context for COVID-19 [WWW Document]. URL https://ec.europa.eu/health/system/files/2020-09/md_mdcg_qa_3d_ppp_covid-19_en_0.pdf. Accessed on 14 March 2022

European Commission (2015) MEDDEV 2.1/3 rev. 3–Borderline products, drug-delivery products and medical devices incorporating, as an integral part, an ancillary medicinal substance or an ancillary human blood derivative (MEDDEV 2.1/3 rev 3)

European Medicines Agency (2019) Guideline on the quality requirements for drug-device combinations (draft)

European Medicines Agency (2017) ICH guideline Q8 (R2) on pharmaceutical development

European Medicines Agency (2012) Reflection paper on the pharmaceutical development of intravenous medicinal products containing active substances solubilised in micellar systems

European Medicines Agency (2006) Reflection paper on nanotechnology-based medicinal products for Human Use

European Medicines Agency (EMA) (2021a) Questions & Answers for applicants, marketing authorisation holders of medicinal products and notified bodies with respect to the implementation of the Medical Devices and In Vitro Diagnostic Medical Devices Regulations ((EU) 2017/745 and (EU) 2017/746)

European Medicines Agency (EMA) (2021b) Guideline on quality documentation for medicinal products when used with a medical device

European Medicines Agency (EMA) (2015) Reflection paper on the data requirements for intravenous iron-based nano-colloidal products developed with reference to an innovator medicinal product

European Medicines Agency (EMA) (2013a) Reflection paper on surface coatings: general issues for consideration regarding parenteral administration of coated nanomedicine products

European Medicines Agency (EMA) (2013b) Joint MHLW/EMA reflection paper on the development of block copolymer micelle medicinal products

European Medicines Agency (EMA) (2013c) Reflection paper on the data requirements for intravenous liposomal products developed with reference to an innovator liposomal product

European Parliament and Council (2017) Regulation (EU) 2017/746 of 5 April 2017 on in vitro diagnostic medical devices and repealing Directive 98/79/EC and Commission Decision 2010/227/EU

European Parliament and Council (2007) Regulation (EC) No 1394/2007 of 13 November 2007 on advanced therapy medicinal products and amending Directive 2001/83/EC and Regulation (EC) No 726/2004 (Text with EEA relevance)

European Parliament and Council (2004) Regulation (EC) No 726/2004 of 31 march 2004 laying down Community procedures for the authorization and supervision of medicinal products for human and veterinary use and establishing a European Medicines Agency

European Parliament and Council (2001) Directive 2001/83/EC of 6 November 2001 on the Community code relating to medicinal products for human use [WWW Document]. URL https://eur-lex.europa.eu/legal-content/EN/TXT/HTML/?uri=CELEX:02001L0083-20190726&from=EN. Accessed on 9 Jan 2022

European Parliament and Council (2017) Regulation (EU) 2017/745 of 5 April 2017 on medical devices, amending Directive 2001/83/EC, Regulation (EC) No 178/2002 and Regulation (EC) No 1223/2009 and repealing Council Directives 90/385/EEC and 93/42/EEC [WWW Document]. URL https://eur-lex.europa.eu/legal-content/EN/ALL/?uri=CELEX:02017R0745-20170505. Accessed on 9 Feb 2022

FDA (2017) Technical considerations for additive manufactured medical devices guidance for industry and food and drug administration staff preface public comment
FDA (2015) SPRITAM (levetiracetam) Tablets [WWW Document]. URL https://www.accessdata.fda.gov/drugsatfda_docs/nda/2015/207958Orig1s000TOC.cfm. Accessed on 14 March 2022
FDA (2022a) Cellular & gene therapy products [WWW Document]. URL https://www.fda.gov/vaccines-bloodbiologics/cellular-gene-therapy-products. Accessed on 21 March 2022
FDA (2022b) Emerging technology program [WWW Document]. URL https://www.fda.gov/about-fda/center-drug-evaluationand-research-cder/emerging-technology-program. Accessed on 14 March 2022
Food and Drug Administration (FDA) (2018) Liposome drug products chemistry, manufacturing, and controls; human pharmacokinetics and bioavailability; and labeling documentation
Food and Drug Administration (FDA) (2014) Guidance for industry considering whether an FDA-regulated product involves the application of nanotechnology contains nonbinding recommendations
Gaspar RS, Silva-Lima B, Magro F, Alcobia A, da Costa FL, Feio J (2020) Non-biological complex drugs (NBCDs): complex Pharmaceuticals in Need of individual robust clinical assessment before any therapeutic equivalence decision. Front Med 7:590527. https://doi.org/10.3389/fmed.2020.590527
Hafner A, Lovrić J, Lak GP, Pepić I (2014) Nanotherapeutics in the EU: an overview on current state and future directions. Int J Nanomedicine 9:1005–1023. https://doi.org/10.2147/IJN.S55359
Halamoda-Kenzaoui B, Baconnier S, Bastogne T, Bazile D, Boisseau P, Borchard G, Borgos SE, Calzolai L, Cederbrant K, di Felice G, di Francesco T, Dobrovolskaia MA, Gaspar R, Gracia B, Hackley VA, Leyens L, Liptrott N, Park M, Patri A, Roebben G, Roesslein M, Thürmer R, Urbán P, Zuang V, Bremer-Hoffmann S (2019) Bridging communities in the field of nanomedicine. Regul Toxicol Pharmacol 106:187–196. https://doi.org/10.1016/j.yrtph.2019.04.011
Hay M, Thomas DW, Craighead JL, Economides C, Rosenthal J (2014) Clinical development success rates for investigational drugs. Nat Biotechnol 32:40–51. https://doi.org/10.1038/nbt.2786
Klein K, Stolk P, de Bruin ML, Leufkens HGM, Crommelin DJA, de Vlieger JSB (2019) The EU regulatory landscape of non-biological complex drugs (NBCDs) follow-on products: observations and recommendations. Eur J Pharm Sci 133:228–235. https://doi.org/10.1016/j.ejps.2019.03.029
Lee N, Yoo D, Ling D, Cho MH, Hyeon T, Cheon J (2015) Iron oxide based nanoparticles for multimodal imaging and Magnetoresponsive therapy. Chem Rev 115(19):10637–10689. https://doi.org/10.1021/acs.chemrev.5b00112
Luraghi A, Peri F, Moroni L (2021) Electrospinning for drug delivery applications: a review. J Control Release 334:463–484. https://doi.org/10.1016/j.jconrel.2021.03.033
Maroni A, Melocchi A, Parietti F, Foppoli A, Zema L, Gazzaniga A (2017) 3D printed multi-compartment capsular devices for two-pulse oral drug delivery. J Control Release 268:10–18. https://doi.org/10.1016/J.JCONREL.2017.10.008
Minghetti P, Rocco P, Cilurzo F, del Vecchio L, Locatelli F (2012) The regulatory framework of biosimilars in the European Union. Drug Discov Today 17:63–70. https://doi.org/10.1016/j.drudis.2011.08.001
Mirza MA, Iqbal Z (2019) 3D printing in pharmaceuticals: regulatory perspective. Curr Pharm Des 24:5081–5083. https://doi.org/10.2174/1381612825666181130163027
Morrison RJ, Kashlan KN, Flanangan CL, Wright JK, Green GE, Hollister SJ, Weatherwax KJ (2015) Regulatory considerations in the design and manufacturing of implantable 3D-printed medical devices. Clin Transl Sci 8:594–600. https://doi.org/10.1111/CTS.12315
Musazzi UM, Gennari CGM, Franzè S, Minghetti P, Cilurzo F (2021) Printing of cutaneous patches loaded with propranolol for the treatment of infantile haemangiomas. J Drug Delivery Sci Technol 66:102767. https://doi.org/10.1016/j.jddst.2021.102767

Musazzi UM, Marini V, Casiraghi A, Minghetti P (2017) Is the European regulatory framework sufficient to assure the safety of citizens using health products containing nanomaterials? Drug Discov Today 22:870–882. https://doi.org/10.1016/j.drudis.2017.01.016

Musazzi UM, Selmin F, Ortenzi MA, Mohammed GK, Franzé S, Minghetti P, Cilurzo F (2018) Personalized orodispersible films by hot melt ram extrusion 3D printing. Int J Pharm 551:52–59. https://doi.org/10.1016/j.ijpharm.2018.09.013

Parhi R (2021) A review of three-dimensional printing for pharmaceutical applications: quality control, risk assessment and future perspectives. J Drug Delivery Sci Technol 64:102571. https://doi.org/10.1016/j.jddst.2021.102571

Rahman Z, Barakh Ali SF, Ozkan T, Charoo NA, Reddy IK, Khan MA (2018) Additive manufacturing with 3D printing: Progress from bench to bedside. AAPS J 20(6):101. https://doi.org/10.1208/s12248-018-0225-6

Sacher S, Poms J, Rehrl J, Khinast JG (2022) PAT implementation for advanced process control in solid dosage manufacturing–a practical guide. Int J Pharm 613:121408. https://doi.org/10.1016/j.ijpharm.2021.121408

Saleh TA (2020) Nanomaterials: classification, properties, and environmental toxicities. Environ Technol Innov 20:101067. https://doi.org/10.1016/j.eti.2020.101067

Schoenmaker L, Witzigmann D, Kulkarni JA, Verbeke R, Kersten G, Jiskoot W, Crommelin DJA (2021) mRNA-lipid nanoparticle COVID-19 vaccines: structure and stability. Int J Pharm 601:120586. https://doi.org/10.1016/j.ijpharm.2021.120586

Sofia N, Mühlebach S, Musazzi UM, Khatib R, Martinez Sesmero JM, Lipp H, Surugue J, di Francesco T, Flühmann B (2021) How do Hospital pharmacists approach substitution of Nanomedicines? Insights from a qualitative pilot study and a quantitative market research analysis in five European countries. Pharmaceutics 13:1010. https://doi.org/10.3390/pharmaceutics13071010

Trenfield SJ, Awad A, Goyanes A, Gaisford S, Basit AW (2018) 3D printing pharmaceuticals: drug development to frontline care. Trends Pharmacol Sci 39(5):440–451. https://doi.org/10.1016/j.tips.2018.02.006

Velez NL, Drennen JK, Anderson CA (2022) Challenges, opportunities and recent advances in near infrared spectroscopy applications for monitoring blend uniformity in the continuous manufacturing of solid oral dosage forms. Int J Pharm 615:121462. https://doi.org/10.1016/j.ijpharm.2022.121462

Wagner V, Dullaart A, Bock AK, Zweck A (2006) The emerging nanomedicine landscape. Nat Biotechnol 24(10):1211–1217. https://doi.org/10.1038/nbt1006-1211

Zielińska A, Costa B, Ferreira M, Miguéis D, Louros JMS, Durazzo A, Lucarini M, Eder P, Chaud M, Morsink M, Willemen N, Severino P, Santini A, Souto EB (2020) Nanotoxicology and nanosafety: safety-by-design and testing at a glance. Int J Environ Res Public Health 17(13):4657. https://doi.org/10.3390/ijerph17134657